

Государственное образовательное учреждение
высшего профессионального образования
**«Томский государственный университет
систем управления и радиоэлектроники»**

ТЕМАТИЧЕСКИЙ РЕФЕРАТИВНЫЙ СБОРНИК № 4-2/3

**“Radar Remote Sensing”
(«Дистанционное зондирование в радиолокации»)**

Публикации в трудах конференций

Источник: *Digital Library IEEEExplore*

Язык: *английский*

Глубина поиска: *2005 – 2006 гг.*

Дата формирования: *март 2011 г.*

Составитель: *В.И. Карнышев*

Томск – 2011

ТЕМАТИЧЕСКИЙ РЕФЕРАТИВНЫЙ СБОРНИК № 4-2/3

"Radar Remote Sensing"

(«Дистанционное зондирование в радиолокации»)

Публикации в трудах конференций

"Man Made Target Detection in a Forest with a Subspace Detector SAR Processor"

This paper deals with the capability of a SAR processor based on a subspace detector to get better performance than a classical SAR processor for Man Made Target (MMT) detection in a forest. The new algorithm aims at using new models, different from the isotropic point one commonly used in SAR processors. The implementation of the Subspace Detector SAR (SDSAR) algorithm is described and detection performances between a classical SAR (CSAR) algorithm and the SDSAR one are compared when detecting a MMT in white Gaussian noise and in a simulated forest. [C3411]

"Ground Response Tracking for Improved Landmine Detection in Ground Penetrating Radar Data"

Recent advances in ground penetrating radar (GPR) fabrication and signal processing have made high fidelity detection of buried anti-tank landmines a practical possibility under field scenarios. However, detection of subsurface landmines at a low false alarm rate (FAR) requires the effective removal of the response from the air/ground interface (ground-bounce response). This in turn requires accurate and automatic tracking of the time of arrival of the air/ground interface in time-domain GPR data. Such tracking of the ground bounce response can be difficult to perform under certain conditions including the presence of surface-laid landmines, surface vegetation, snow drifts, and multiple subsurface structures like buried roadbeds. In this work, we will explore the application of a low-latency Kalman filter applied to ground bounce tracking in GPR data and resulting performance improvements for pre-screening algorithms under extreme weather conditions. [C3412]

"Accurate DEM Reconstruction from Permanent Scatterers and Multi-baseline Interferometry"

The application of the Permanent Scatterers (PS) Technique in multi-temporal data-sets, namely the identification and exploitation of sparse coherent targets, has shown that it is possible to estimate and remove interferometric phase components due to atmospheric effects and orbital fringes. So far, the application of the PS technique has been focused on the extraction of the motion field of the area of interest. However, it is also known that PS relative elevations can be estimated with sub-meter precision while smooth errors can be removed using a coarse resolution DEM or the data of the Shuttle Radar Topography Mission (SRTM). In this paper, we describe a new approach combining the PS Technique and standard interferometry to improve the quality of InSAR DEM's. ERS Tandem interferograms are exploited to increase the number of coherent pixels, while atmospheric effects are estimated and subtracted by means of the sparse PS grid. Prior information and PS elevation are used to reduce the probability of phase-unwrapping errors. Preliminary results are reported and the key-factors for its successful application (e.g. the number of Tandem acquisitions available, PS density) are discussed. [C3413]

"Evaluation of eCognition for Assisted Target Detection and Recognition in SAR Imagery"

Defence R&D Canada-Ottawa (DRDC Ottawa) has been assessing custom off-the-shelf (COTS) software products and developing custom tools that can assist image analysts (IAs) to complete their tasks more quickly and efficiently. In some cases, IAs are tasked with detecting targets of interest within large-area surveillance operations, and these detection tasks may be repeated with a regular flow of incoming imagery. SAR imagery is a data source of choice for large-scale detection operations due to its ability to image in all weather conditions without external illumination sources. An activity was undertaken to evaluate ecognition (a COTS product) for target detection in SAR imagery and as a means of facilitating workflow improvements in the course of target detection and surveillance activities. eCognition is segmentation-based classifier that uses fuzzy reasoning techniques, enabling users to represent fuzzy rules in a human reasoning-like form. It offers the promise of being a usable tool that fulfills the objective of providing improvements over the traditional practice of manual inspection for target detection and surveillance. This paper reports on the evaluation process and findings when using ecognition for ship detection and land vehicle detection in SAR imagery. [C3414]

"A Ka Band Imaging Radar: DRIVE on Board ONERA Motorglider"

Following previous studies, a concept of low-cost imaging Ka-Band radar is presented in this paper. This radar is integrated into under-wings pods that are fixed on a STEMME S10VT motorglider. This radar concept combines real aperture in the cross-track direction, by the antennas geometrical aperture, and synthetic aperture in the along-track direction, realized with the aircraft motion. Radar front-end uses FMCW (for Frequency Modulated Continuous Wave) technique which allows to reduce the power emission to a few Watts. In addition, the use of the millimeter band induces antennas size reduction, and makes possible the radar integration into pods. Thus, radar particularities are a low- size, a low-weight and a low-cost basis, making this radar suitable for future integration on board small vehicles, such as UAV (Unmanned Aerial Vehicle). The radar definition and specifications will be exposed, together with the first results obtained on April 2006. Two ways of operation will be exposed: An application as vertical sounder, using cylindrical horn antennas, and an application as SAR radar, using rectangular antennas. The two cases will be illustrated by samples of results. [C3415]

"A New Polarimetric CFAR Ship Detection System"

The objective of the proposed work is to develop optimal polarimetric Constant False Alarm Rate (CFAR) detector for ship detection. Polarimetric transformations and decompositions, clutter analysis, modeling, Principal Component Analysis (PCA), and multi-CFAR detection are the necessary components of optimal polarimetric CFAR ship detectors. The resulting CFAR detector outperforms the conventional polarimetric CFAR detector by providing higher probability of detection. Optimal polarimetric CFAR detection procedures are proposed in this report. Given the simulated polarimetric RADARSAT-2 data, different polarimetric transformations and decompositions are applied. The resulting images will be transmitted to an adaptive Principal Component Analysis (PCA) block. Through the adaptive PCA block, the image of the first principal component which has the highest SNR among all the images (including the original, transformed/decomposed images, and the images after the adaptive PCA) will be used for ship detection. Optimal multi-CFAR detection will be applied to this image and then the final decision will be made. [C3416]

"Target Classification by Means of Fully Polarimetric ISAR Images"

In ISAR systems, fully polarimetric capabilities have not been fully exploited for target classification or recognition. In this paper, a full system that reconstructs the polarimetric ISAR image and classifies the target is proposed and tested on simulated data. [C3417]

"The Gradient Structure Tensor as an Efficient Descriptor of Spatial Texture in Polarimetric SAR Data"

In this paper, the analysis of spatially nonstationary texture from polarimetric SAR data is studied. A previously introduced model named Anisotropic Gaussian Kernel (AGK) was shown to be a pertinent descriptor of local orientation and allowed a simple representation of the complex spatial structure in SAR images. Here, two methods for the estimation of the model parameters are proposed. The first one is an enhancement of the previously developed algorithm and the second one is a new approach based on the Gradient Structure Tensor (GST) operator. These two methods are employed to analyse texture in PolSAR intensity channels. [C3418]

"Copula-based Stochastic Kernels for Abrupt Change Detection"

This paper shows how to obtain a binary change map from similarity measures of the local statistics of images before and after a disaster. The decision process is achieved by the use of a zz-SVM in which a stochastic kernel has been defined. Stochastic kernel includes two similarity measures, based on the local statistics, to detect changes from the images: 1) A distance between marginal probability density functions (pdfs) and 2) the mutual information between the two observations. Distance between marginal pdfs is evaluated by using a series expansion of the Kullbak-Leibler distance. It is achieved by estimating cumulants up to order 4 from a sliding window of fixed size. Mutual information is estimated through a parametric model that is issued from the copulas theory. It is based on rank statistics and yields an analytic expression, that depends on the parameter of the copula only, to be evaluated to obtain the mutual information. Preliminary results are shown on a pair of Radarsat images acquire before and after a lava flow. A ground truth allows to show the accuracy of the stochastic kernels and the SVM decision. [C3419]

"Land-cover Classification using Multi-temporal/polarization C-band SAR Data"

This paper presents a fuzzy logic fusion methodology for land-cover classification with multi-temporal/polarization Radarsat-1 and ENVISAT ASAR data. For feature extraction from each multi-temporal/polarization data, a traditional feature extraction approach (i.e. extraction of average backscattering coefficient, temporal variability

and long-term coherence) and principal component analysis (PCA) were applied and compared. A data-driven fuzzy logic approach was applied to the classification of those features. In the fuzzy logic approach, fuzzy membership functions based on smoothed kernel density estimation and likelihood ratio functions were derived and various fuzzy combination operators were tested. A case study from an agricultural area has been carried out to illustrate the proposed methodology. [C3420]

"Simultaneous Perturbation Stochastic Approximation Algorithm for Automated Image Registration Optimization"

Automated intensity-based image registration approaches become popular and urgent when facing today's increasing data mining and frequent fusion demands. As a core part of an automated image registration system, many kinds of gradient-based optimizers were proposed in the past decade. In this paper, a local gradient-free optimizer, namely the simultaneous perturbation stochastic approximation (SPSA) algorithm, was firstly applied for the automated multi-source image registration using the mutual information as a similarity measure. Results of rigid experiments on the image pairs of ASTER-ASTER, ASTER-Map and SAR-SAR showed the SPSA optimizer has much more flexibility and efficiency than the traditional gradient ascent optimizer. It is more suitable as a local optimizer to the automated image registration system. The main shortcoming of this algorithm is too many control parameters needed during the execution process. [C3421]

"The Multiscale Change Profile: A Statistical Similarity Measure for Change Detection in Multitemporal SAR Images"

In this paper, we present a new similarity measure for automatic change detection in multitemporal SAR images. This measure is based on the evolution of the local statistics of the image between two dates. The local statistics are estimated using a cumulant-based series expansion which approximates the probability density functions in the neighborhood of each image pixel. The degree of evolution of the local statistics is measured using the Kullback-Leibler divergence. An analytical expression for this detector is given allowing a simple computation which depends only on the 4 first statistical moments of the pixels inside the analysis window. The concept of multiscale change profile (MCP) is also introduced and its optimized implementation is presented. MCP yields change information on a wide range of scales and better characterizes the appropriate scale to be used for the detection. Two simple examples of application show that the MCP allows the design of change indicators which provide better results than a monoscale analysis. [C3422]

"Random Feature Selection for Decision Tree Classification of Multi-temporal SAR Data"

The accuracy of supervised land cover classifications depends on variables like the chosen algorithm, adequate training data and the selection of features. It has been shown that classification results can be improved by classifier ensembles. In the present study decision trees have been generated with random selections of all available features and combined into such a multiple classifier. The influence of the number of selected features and the size of the multiple classifiers on classification accuracy is investigated using a set of 14 SAR images. Results of multiple classifiers are always better than those of a decision tree based on all available features. Maximum accuracies were achieved with multiple classifiers that use decision trees based on 70% of the available features. The visual inspection of produced maps underlines the high quality of the results. The area is classified into homogeneous fields with little noise, only. [C3423]

"Advantage of the Remote Sensing Data Utilization in Studying Inundation Risks in Terms of Land-Use"

A series of Landsat TM, ETM and radar data were used to establish land cover and flood risk maps as a function of land cover in Bac-Hung-Hai region in Northern Vietnam. Land cover is one key parameter which has an influence on the occurrence of inundation in that region. Both spectral and textural features were considered in order to improve land cover classification. The radar data was used to reduce the effects of cloud cover. The results obtained illustrate the important role that remote sensing can play in the assessment of flood risk. [C3424]

"The Application Image Coregistrator on Grid Technology"

This paper describes the co-registration image using the Grid technologies. Image co-registration is basilar for interferometry SAR remote sensing applications, but because of its very time-consuming algorithm and because of the necessity of elaborate interferometry image in real time, it can be greatly benefited by Grid computing. [C3425]

"The TerraSAR-X Active Calibration Instruments and Performance Analysis"

This paper describes the development and system concept for an active and highly integrated, digitally controlled SAR system calibrator. For precise and high-quality SAR data, precise ground targets are necessary for external calibration of the SAR data. Compared to passive targets, active radar targets like transponders offer more features. The recording of the transmitted radar signals from the satellite becomes possible and allows additional data analysis and data correction. A total of 18 active transponder and receiver systems and 16 receiver only systems will be fabricated for the TerraSAR-X calibration campaign in fall 2006. [C3426]

"Recent Advances in Polarimetry and Polarimetric Interferometry"

Radar polarimetry radar Interferometry and polarimetric SAR interferometry represent the current culmination in 'microwave remote sensing' technology, but we still need to progress very considerably in order to reach the limits of physical realizability. Whereas with radar polarimetry the textural fine-structure, target orientation, symmetries and material constituents can be recovered with considerable improvement above that of standard 'amplitude-only' radar; by implementing 'radar interferometry' the spatial (in depth) structure can be explored. With polarimetric interferometric synthetic aperture radar (POL-IN-SAR) imaging, it is possible to recover such co-registered textural and spatial information from POL-IN-SAR digital image data sets simultaneously, including the extraction of digital elevation maps (DEM) from either polarimetric (scattering matrix) or interferometric (dual antenna) SAR systems. Simultaneous polarimetric-plus-interferometric SAR imaging offers the additional benefit of obtaining co-registered textural-plus-spatial three-dimensional POL-IN-DEM information, which when applied to repeat-pass image-overlay interferometry provides differential background validation and environmental stress-change information with highly improved accuracy. Then, by either designing multiple dual polarization antenna POL-IN-SAR systems or by applying advanced POL-IN-SAR image compression techniques, will result in 'POL-arimetric TOMO-graphic' (multi-interferometric) SAR or POL-TOMO-SAR imaging. By advancing these EWB-D-POL-IN/TOMO-SAR imaging modes, we are slowly but steadily approaching the ultimate goal of eventually realizing airborne and spaceborne 'geo-environmental background validation, stress assessment, and stress-change monitoring and wide-area military surveillance of the terrestrial and planetary covers'. [C3427]

"Monte Carlo Evaluation of Multi-Look Effect on Entropy/Alpha /Anisotropy Parameters of Polarimetric Target Decomposition"

Entropy, alpha and anisotropy ($H/\alpha/A$) of the polarimetric target decomposition of Cloude and Pettier has been an effective and popular tool for polarimetric SAR image analysis and geophysical parameter estimation. However, multi-look processing can severely affect the values of these parameters. In this paper, a Monte Carlo method is used to evaluate the multi-look effect on these parameters for various media of grass, forest and urban. The effect of pixel correlation due to over sampling, and the mixed pixel effects will also be investigated. DLR/E-SAR and JPL/AIRSAR L-band data are used in this study. [C3428]

"Extended Multidimensional Speckle Noise Model and its Implications on the Estimation of Physical Information"

The presence of speckle noise in Synthetic Aperture Radar images prevents a correct interpretation, as well as, the information retrieval processes. It has been recently demonstrated that speckle noise may introduce biases into the retrieved physical information when multidimensional data is considered. In case of multidimensional SAR systems, for single-look data, it has been proved that speckle noise is due to the combination of multiplicative and additive noise sources. This paper details the extension of this noise model to multilook, multidimensional SAR data. [C3429]

"Study of Hurricanes and Typhoons from TRMM Precipitation Radar Observations: Self Organizing Map (SOM) Neural Network"

Precipitation radar (PR) on Tropical Rainfall Measuring Mission (TRMM) satellite provides high resolution vertical profile of reflectivity (VPR) of tropical storms. Three-dimensional downward-looking observations of tropical storms are very useful to study Hurricanes and Typhoons. The increased reflectivity measured in bright band (BB) region can lead to rainfall overestimate. It is also known that VPR of BB holds extensive information on the types of precipitation and their variability. Better knowledge of VPR of storms is important to understand cloud dynamics and microphysical processes, and to improve satellite retrieval algorithm. Because of a large number of VPR observation, it is of interesting to classify the VPR into characteristic profiles so that it can be useful in studying and comparing different vertical reflectivity profiles. In this study, Self Organizing Map (SOM) Neural Network is used as a method to study and classify VPR of Hurricanes and Typhoons. SOM is unsupervised neural network. It forms a non-linear mapping of the data to a two-dimensional map grid that can be used as an

exploratory data analysis tool for generating hypotheses on the relationships of VPR. Similarity relationships within the VPR data and its vertical structure can be visualized and interpreted. Preparation of vertical profile of reflectivity used as input vectors of SOM algorithm is one of the most vital steps. In total eleven Hurricanes and forty Typhoons are studied. VPR of Hurricanes and Typhoons are classified into characteristic profiles. The result of classification shows a distribution that indicates location of each characteristic profile within a storm when viewed from the PR. Percentages of contribution of each characteristic profile to Hurricanes and Typhoons can also be determined. By using SOM, VPR can be classified into various numbers of classes up to one hundred. In this study, VPR is classified into four classes. Two simple operations were performed. Firstly, SOM was applied to all VPR data regardless of rain type. Secondly, stratiform and convective portion of VPR was applied to SOM separately. For stratiform portion of Hurricanes and Typhoons, the bright band (BB) properties including the height of BB peak, BB thickness, reflectivity of BB peak and BB sharpness index of Hurricanes and Typhoons are investigated and compared to those of generic oceanic storm. Comparison of those BB properties of Hurricanes, Typhoons and generic oceanic storm reveals similarities and differences among them. [C3430]

"Development and Validation of Spaceborne Dualfrequency Precipitation Radar for GPM"

After the great success of the Tropical Rainfall Measuring Mission (TRMM), Global Precipitation Measurement (GPM) started as an international mission and follow-on mission of the TRMM project to obtain more accurate and frequent observations of precipitation. The accurate measurement of precipitation will be achieved by the DPR installed on the GPM core satellite. In order to estimate accurate precipitation rate value, calibration and validation of the DPR algorithms and products are essential. From the experiences of TRMM validations, it is important for the DPR algorithm validation to compare between precipitation rate through the calculation of DPR algorithm and that of the directly observed precipitation rate over the validation site. For this purpose, the most important and difficult issue is to construct the database of the physical parameters for the precipitation retrieval algorithms of DPR from the ground-based data using well-calibrated instruments. [C3431]

"The Role of C-band Dual Polarization Radars for GPM Ground Validation"

Dual polarization weather radars have brought in significant advancement to precipitation observation, as rainfall rate estimation, microphysical characterization, and hydrometeor classification. The improvements have been mostly demonstrated at S-band frequency where attenuation effects are usually negligible. In Europe C-band is largely adopted in operational and research radars because of larger differential phase measurements, reduced antenna size and an overall lower cost with respect to that of S-band systems. The major disadvantage is that the signal attenuation is not negligible. In the context of GPM Ground Validation, techniques to compensate the reflectivity measurements for propagation effects are thus necessary to obtain GV products from ground-based C-band radars. The attenuation correction methodology using differential phase shift as constraint has shown a good performance. One of the advantages of polarimetric radar measurements is their self-consistency. Starting from the initial guess of attenuation correction provided by the rain profiling algorithm, self-consistency is used in an iterative technique to improve the accuracy of attenuation correction at C-band. The obtained accuracy is evaluated in terms of bias and standard error using C-band profiles generated from S-band dual polarization observations. [C3432]

"Rain Retrieval Performance of a Dual-Frequency Radar Technique with Differential Attenuation Constraint"

Assessments on the performance of dual-frequency (13.6/35.5 GHz) precipitation radar (DPR) rain retrieval techniques are performed through simple vertical rain profiles synthesized with arbitrarily defined and disdrometer-measured raindrop size distribution (DSD) data. A DPR inversion technique (DPR-IT) with the estimates of differential attenuation (DA), which used to resolve the path-integrated attenuation (PIA) information instead of relying on surface reference or iterative methods, is considered mainly for the analysis. Preliminary simulation results show that the DPR-IT with DA constraint can work as an independent way to extract the DPR PIA information, hence, the DSD parameters, especially in the regions of moderate to strong rainfall rates. [C3433]

"A Time Series Approach for Soil Moisture Estimation"

Soil moisture is a key parameter in understanding the global water cycle and in predicting natural hazards. Polarimetric radar measurements have been used for estimating soil moisture of bare surfaces. In order to estimate soil moisture accurately, the surface roughness effect must be compensated properly. In addition, these algorithms will not produce accurate results for vegetated surfaces. It is difficult to retrieve soil moisture of a vegetated surface since the radar backscattering cross section is sensitive to the vegetation structure and environmental conditions such as the ground slope. Therefore, it is necessary to develop a method to estimate

the effect of the surface roughness and vegetation reliably. One way to remove the roughness effect and the vegetation contamination is to take advantage of the temporal variation of soil moisture. In order to understand the global hydrologic cycle, it is desirable to measure soil moisture with one- to two-days revisit. Using these frequent measurements, a time series approach can be implemented to improve the soil moisture retrieval accuracy. [C3434]

"Polarimetric Temporal Decorrelation Studies by Means of GBSAR Sensor Data"

In this paper, a study of the temporal evolution of the elements of 3 x 3 covariance matrix using an X-band polarimetric ground-based SAR sensor is proposed. Although the heterogeneity of the scenario allows to select different target typologies, the study is mainly focused on the analysis of azimuthally symmetric distributed targets. The fluctuations of the most representative elements of [C] as a function of time and the decorrelation among the polarimetric channels are investigated. A relation with atmospheric parameters like temperature, humidity and wind is considered in order to make out the weight these parameters can influence the polarimetric signature of the observed area. [C3435]

"The Elephant in Dual-Polarized Imaging Radar"

The elephant-in-the-room: It's so obvious, why didn't we see it before? In the context of "dual-polarized radar", especially Earth-observing synthetic aperture radar, the elephant is simply the relative phase between the two image outputs of a "dual-polarized" SAR. Capture the elephant-which for certain systems may be a minimal-cost transformation-to realize nearly a dozen quantitative image norms, most of which have not been exploited outside of the radar astronomy community. Even better, transmit circular polarization. [C3436]

"Early Results on Cloud Profiling Radar Post-launch Calibration and Operations"

The cloud profiling radar (CPR), the primary science instrument of the CloudSat Mission, is a 94-GHz nadir-looking radar that measures the power backscattered by clouds as a function of distance from the radar. This instrument will acquire a global time series of vertical cloud structure at 500-m vertical resolution and 1.4-km horizontal resolution. CPR will operate in a short-pulse mode and will yield measurements at a minimum detectable sensitivity of -28 dBZ. [C3437]

"Study of the Influence of Vessel Motions and Sea-Ship Interaction on Classification Algorithms Based on Single-Pass Polarimetric SAR Interferometry"

This paper analyzes the worsening effects the sea surface can induce on vessel classification algorithms working with SAR imagery. Two issues will be tackled, the complex motion history of ships and the polarimetric scattering mechanisms generated by the sea-hull interaction. Both can modify the information that allows to infer the geometry of ships dropping the classification capability. The current analysis will introduce a new classification approach based on polarimetric SAR interferometry that presents a low sensitivity respect the main distortions caused by the sea surface. Simulated SAR images obtained from GRECOSAR, a SAR simulator of complex targets, will show trustworthy vessel classification almost independent on the environmental conditions could be possible for incoming system configurations as Tandem TerraSAR-X. [C3438]

"Polarimetric Analysis of Radar Signature of a Manmade Structure"

First Page of the Article [C3439]

"Polarimetric Characteristics of Radar Echoes from the Sea Surface as a Function of Incidence Angle"

This paper presents some initial results of polarimetric radar measurements made over a range of look-down angles using the DSTO high resolution multi-band radar. Specifically, X-band polarimetric measurements of the sea were made from 95 m high cliffs along the Great Australian Bight, for look-down angles of 3deg, 4deg, 5deg, 10deg, 15deg, 20deg, 25deg and 30deg. The analysis is addressing scattering matrix element statistics, entropy-alpha space distributions and correlation with visible spectrum imagery. [C3440]

"Structural Parameter Estimation of Australian Flora with a Ground-based Polarimetric Radar Interferometer"

The application of polarimetric SAR interferometry technology is extended to ground based radar imaging (GB-POLInSAR), which has a limited field of view but provides wide band coverage. It also provides for easier deployment of broadband and multi-baseline techniques, from which we can estimate vegetation structure and

extinction propagation using model based techniques. This micro-scale multi-parameter combination with good temporal resolution is a unique feature of ground- based sensors. In this paper we present both polarimetric and interferometric coherence calibration results for such a GB-POLInSAR system we have developed at the University of Adelaide. We then show an initial study of height estimation of Australian native plants based on the coherence parameter retrieval models of the polarimetric SAR interferometry technique using the broadband GB-POLInSAR system. [C3441]

"PALSAR Characterization and Initial Calibration"

This paper describes the initial results of the PALSAR characterization using the data acquired in the commissioning phase for the five modes of FBS, FBD, DSN, SCANSAR and POL, and using the active radar calibrator deployed at the calibration site in Japan. This paper also describes the radiometric and geometric performances of the PALSAR images shortly. This paper will end up with the parameters which should be evaluated and determined within the calibration phase. [C3442]

"Improving Satellite Moderate Resolution Instrument Geolocation Accuracy in Rough Terrain"

When Earth-locating (geolocating) modern moderate resolution instrument data, such as from NASA's Moderate Resolution Imaging Spectroradiometer (MODIS) on the Earth Observing System (EOS) Terra and Aqua satellites, corrections for Earth terrain effects are applied to enable accurate retrieval of global geophysical parameters. The current approach to terrain correction calculates the pierce point of the center of each observation with a digital terrain model. With the recent Shuttle Radar Terrain Mapping Mission (SRTM) terrain model data, which has a higher spatial resolution and better accuracy than previous global terrain models, there is an opportunity to improve geolocation accuracy in rough terrain by using more advanced techniques to compute geolocations that are more representative of the centroid of each observation. The authors evaluate whether calculating geolocation using an observation weighting approach is significantly better than calculating the pierce point geolocation and if so under what conditions. The relative additional computational cost of an approximate technique is weighed against the possible increase in geolocation accuracy. [C3443]

"Mobile Aerosol Lidar for Earth Observation Atmospheric Correction"

A new atmospheric correction method of earth observation images based on the combination of satellite data and lidar data is proposed in this paper. A mobile scanning Mie lidar was developed to detect the aerosols' spatial and temporal distribution for the purpose above. To obtain more accurate data, future development plan of a multi-wavelength, multi-channel Raman lidar is discussed. Earth observation images processed by the radiative transfer model and this new method are presented. Also issues to approach the final goal of this new atmospheric correction method are discussed. [C3444]

"Extraction of Stream Channels in High-Resolution Digital Terrain Images Using Morphology"

Our paper proposes an approach for the extraction of stream channels from airborne laser swath mapping (ALSM) data. Recent advances in technology have led to high-resolution topographic data acquisition by means of ALSM yielding digital elevation model (DEM) datasets with horizontal resolutions of 1m and a vertical accuracy of 0.15 m. We apply morphological operations on an ALSM DEM to detect stream channels. The results are compared with an existing terrain analysis tool known as TauDEM. Tools like TauDEM use morphology over large-scale areas but they often fail in detecting stream networks over small-scale areas. The proposed method uses small-scale morphology to provide complementary results for streamline locations over a small catchment area. [C3445]

"Comparison of Surface Scattering Models for Gaussian and Exponential Surfaces"

In this paper, predictions from the small-slope approximation (SSA), the advanced integral equation model (AIEM), and the reduced third-order local curvature approximation (RLCA3) theories of rough surface scattering are compared with each other and with predictions obtained from numerical simulations for dielectric surfaces with Gaussian and exponential correlation functions. A discussion of the results obtained is provided, along with plans for continued investigations. [C3446]

"Exploiting Physical and Topographic Information within a Fuzzy Scheme to Map Flooded Area by SAR"

An inundation event occurred in Italy on November 1994 has been analysed in order to assess the capability to map the flooded areas by radar (SAR) images in support to civil protection interventions. ERS images collected before and after the inundation have shown the presence of different scattering mechanisms occurring in the

flooded areas and originating either an increase or a decrease of the backscattering coefficient, depending on the land covers type. This analysis has allowed us to develop a flood discrimination procedure based on a fuzzy approach able to integrate all the possible sources of available data (SAR images, land cover and a DEM) and prior information (cover dependent backscattering behaviour). A comparison with a ground survey providing the maximum flood extension has given encouraging results. [C3447]

"A First Experiment of 3D Imaging with a Ground based Parasitic SAR"

The present paper provides the first example of 3D imaging using the ground based parasitic SAR instrument developed in the past years at Politecnico di Milano. [C3448]

"A Fourth-Order Imaging Algorithm for Spaceborne Bistatic SAR"

Eldhuset's research, the fourth-order Extended Exact Transfer Function (EETF4), indicates that the range history of a high spatial resolution spaceborne SAR can be modeled by a fourth-order Taylor expansion in azimuth time. In this paper, this point of view is introduced in bistatic SAR, and the transfer functions in the 2-D frequency and the range-Doppler domains are derived. Using this method, an efficient bistatic focusing solution based on squinted mode chirp scaling (CS) algorithm which accommodates both tandem and TI case is developed. Quantitative analysis and simulations are also provided. [C3449]

"2D Inverse Scaling Bistatic Processing and the focused Image Quality Measurements"

This paper presents a bistatic focusing solution for the general case, when transmitter and receiver trajectories move along non parallel trajectories with different velocities. Processing in the general case turns out to be additionally truly azimuth time variant. This problem is solved by implementing a novel 2D inverse scaled FFT algorithm. In the second part of the paper the focused bistatic SAR image bistatic processing quality will be evaluated by measuring the geometric registration, amplitude and resolution, ISLR and PSLR of simulated point targets. [C3450]

"Reduction of the Reconstruction Bias in Synthetic Aperture Imaging Radiometry"

Synthetic Aperture Imaging Radiometers (SAIR) are powerful instruments for high-resolution observation of planetary surfaces at low microwave frequencies. This article is concerned with the reconstruction of radiometric brightness temperature maps from SAIR interferometric measurements. Even in the absence of modeling errors and radiometric noise, a systematic error, or bias, has been observed in the reconstructed maps. The origin of this bias is analyzed and an efficient solution is proposed for reducing it. Particular emphasis is laid on numerical simulations carried out for the SMOS space mission, a project led by the European Space Agency and devoted to the remote sensing of Soil Moisture and Ocean Salinity from a low orbit platform. [C3451]

"FPGA-based Implementation of a Polarimetric Radiometer with Digital Beamforming"

In [1] a general overview of the PAU system is provided. This work describes in more detail the implementation of the polarimetric and pseudo-correlation radiometer (PAU-RAD) that measures the four Stokes parameters. [C3452]

"Linear Deformation Rate Derivation from Multi-baseline Differential Interferogram Stacks"

Decorrelation caused by temporal changes influences phase unwrapping of differential interferogram in repeat-pass D-InSAR phase delay due to atmosphere disturbance degrades the accuracy of D-InSAR for small deformation monitoring. In this paper, we present a stacking D-InSAR approach using multi-baseline differential interferograms to estimate the linear deformation based on Rank Defect Free Network Adjustment Model (RDFNA) and to increase the deformation temporal sampling rate and estimate the linear deformation accurately. The Minimum Cost Flow (MCF) algorithm based on Delaunay triangulation network generated with sparse grids is adapted for phase unwrapping of individual interferogram. Scatterers with high coherence values over a given threshold in the interferogram stack are selected for the network generation. Therefore, with the multi-baseline differential interferogram stack, the linear deformation rate can be calculated with the unwrapped phase of each point accurately. [C3453]

"Error Evaluation of BAQ Algorithm for Internal Calibration Data of Spaceborne SAR"

BAQ is the efficient algorithm for SAR echoes data compression that has the Gauss distribution. Internal calibration is the important system resource, which is to calibrate the system gain change before and after the imaging and also provide more accurate reference function for the range compression. But the echoes are

different from calibration data. This paper discussed whether the error brought by BAQ compression algorithm could be accepted by this system. Both the theoretical simulation and the experimental results indicate that the internal calibration data only can be directly transmitted but not compressed, which has the important reference to engineering design. [C3454]

"Automatic Change Detections from SAR Images Using Fractal Dimension"

It is very difficult to detect changes from SAR images because of two major difficulties associated with SAR, which are the removal of speckle noise and the registration of information between images. Speckle is a chaotic phenomenon because that the scattering signals within a resolution cell are summed up coherently. Therefore, SAR signal can be modeled by a spatial chaotic system and characterized by its fractal dimension. Then, simplified procedures for SAR image change detection are proposed because that the process of image despeckling is unnecessary. The proposed approach is applied to multitemporal polarimetric SAR images for change detections. The experimental results of using a simple image difference (DI) technique, the principal component analysis (PCA), and the proposed (Fractal) approach are compared. The effects of misregistration for different approaches are also presented. Simulation results reveal that misregistration affects less and less as SNR is increased. When SNR is low, by using DI or PCA methods, the overall performance of change detection is degraded by spurious differences due to misregistration. On the contrary, Fractal method can tolerate misregistration effect at low SNR. In addition, when the difference between changed classes is small, it is fail to detect changes by using of either DI or PCA method. In contrast, the Fractal method can still effectively detect land cover changes. [C3455]

"Snow Cover Maps with Satellite Borne SAR: A New Approach in Harmony with Fractional Optical SCA Retrieval Algorithms"

The standard method for retrieving snow-covered area with C-band SAR is based on thresholding the ratio between a wet snow SAR image and a dry snow reference scene. A new approach is suggested here, where the snow cover fraction is retrieved by using a gradual transition between snow free and snow covered conditions. The paper discusses the method and applies it on a set of Radarsat data acquired in Norway in May 2003. A near simultaneous aerial optical image and data from field campaigns are used to verify the results. [C3456]

"Feasibility of Snow Avalanche Volume Retrieval by GB-SAR Imagery"

The feasibility to estimate the volume of snow displaced in an avalanche by means of the LISA (Linear SAR) ground-based synthetic aperture radar (GB-SAR) system has been investigated. During more than 100 days of the winter 2005- 2006 the system has acquired data in its topographic mode, being able to monitor near 50 natural avalanches and 4 artificially triggered. With an acquisition rate of one image every 12 minutes, the LISA instrument has shown its ability to monitor localized changes of the snow cover. The resolution in height of the topographic maps generated has been found to be inadequate to estimate the snow volume involved in the avalanches studied. [C3457]

"Remote Sensing Image Ground Segment Interoperability: PLEIADES-HR Case Study"

Pleiades-HR is a high-resolution optical Earth observation system developed by CNES, for civilian and military users. The launch of the first Pleiades satellite is scheduled in 2008, the second, 18 months later. The Pleiades-HR program is the French part of the French-Italian ORFEO program which also comprises COSMO-SkyMed, an Italian high-resolution radar system. The Pleiades-HR products will be distributed by SpotImage and will complete the existing SPOT product line. In such a multi-sensors and multi-users context, CNES has decided to design the new Pleiades-HR ground segment pointing the stress on systems interoperability in order to ease the data access from the end user point of view. After a synthetic presentation of the Pleiades HR ground segment and image products, this paper focuses on PLEIADES HR image product definition and cataloguing services, two major points for the image ground segment interoperability. Among all possible solutions, the image product and catalog services have been defined taking into account the PLEIADES-HR system characteristics, its performance requirements and the international standards (ISO-TC211, OGC, image standards, JPEG2000 ...) use and evolution capabilities. The results presented in the paper are also part of a European initiative of ground segment harmonisation studied in the frame of the HMA project with other European Space Agencies. [C3458]

"InSAR Co-registration Accuracy Assessment Based on Misregistration Value"

Based on estimated offset between the corresponding points in the master and the slave image by spectral diversity algorithm, a new indicator misregistration value is proposed to assess registration accuracy. After error analysis is carried out, the new indicator is compared with conventional indicators. Its advantage is the feasibility

to assess the registration accuracy in both directions. According to the three indicators, comparison results of several co-registration algorithms are obtained. Airborne X-band interferometric data are used to validate the new indicator. [C3459]

"Automated Content Extraction from SAR Data"

Segmentation algorithms are often used in many image processing applications like compression, restoration, content extraction, and classification. In particular as for content extraction works carried out in the past decade have demonstrated that multi-frequency fully polarimetric SAR observations are particularly interesting, thanks to physical properties of the backscattered signal at various frequencies and polarizations. To achieve a good classification, the main difficulty is that SAR images are often embedded in heavy speckle. Segmentation of multi/hyperspectral (optical) imagery is obtained by means of algorithms based on image models, which exploit the spatial dependencies of land-covers. Unfortunately, speckle noise hides such spatial dependencies in observed SAR data. With the aim of investigating on a content extraction algorithm capable of discriminating cover classes present in the observed SAR image, heterogeneity features are used here to emphasize spatial dependencies in the data. Thus, observed pixel values are mapped into features, that take "similar" values on "similar" textures. This allows for using the same procedure of the optical case. Obviously, homogeneity/heterogeneity feature and segmentation quality are fundamental for classification accuracy. Here, the problem is tackled through the joint use of information theoretic SAR features and of a segmentation algorithm based on Markov Random Fields (MRFs). [C3460]

"Performance Evaluation of Amplitude-Phase Algorithm for SAR Raw Data Compression"

This paper defines series of important performance evaluation parameters to evaluate amplitude-phase (AP) algorithm comparing with that of block adaptive quantization (BAQ) algorithm. The evaluation procedure is carried out in two domains, raw data domain and image domain. Numerical experiments based on ERS-2 data show that AP algorithm provides us with more compression ratio (CR) choices than BAQ and for certain CR, AP algorithm provides at least one choice whose performance is better than or equal to that of BAQ. These two algorithms neither affect spatial resolution nor generate geometric distortion. Both of them have only a little effect on radiometric resolution. [C3461]

"A Lidar Collaboratory Data Management System"

A data management system has been developed for the Connecticut State University (CSU) Lidar Collaboratory to facilitate user authentication, scheduling of remote lidar instrumentation control sessions, storage and retrieval of lidar datasets and generation of new data products. In addition to providing for efficient archival and retrieval of lidar data products, a major design goal of the data management system is to support collaborative, multidisciplinary, atmospheric sciences research projects. In this paper, we describe the framework of the CSU Lidar Collaboratory data management system and how the system interacts with the data acquisition and data analysis software. [C3462]

"A Theoretical Study of the Sensitivity of Spaceborne Bistatic Microwave Systems to Geophysical Parameters of Land Surfaces"

A research activity aiming to assess the potential of bistatic measurements of scattered radiation from the land surface is presented. The purpose is to identify the best configuration of a passive system measuring the signal originated by sources of opportunity, like GNSS or radars aboard a satellite. The preliminary result of the study consists of the validation of the electromagnetic model simulating bistatic scattering from bare soil, including the coherent component. A very preliminary sensitivity analysis to soil moisture is also presented. [C3463]

"The Associated Modeling and Precision Analysis of Spatial States and the Inter-Satellite Baseline of Formation Flying Satellites"

The inter-satellite baseline plays a vital role in the formation flying satellites missions. Based on the relation between the spatial states and the inter-satellite baseline, this paper erects a model to associate these two kinds of parameters. The error propagation relations are deduced in detail, which are described by the precision influence factors and error propagation matrices. Simulations are also carried out to show the baseline determination precision in some certain scenarios. [C3464]

"Phase Unwrapping with Phase-Singularity Spreading"

We propose a novel phase unwrapping method where we spread the singularity in phase map with fractional phase compensators. We find that the obtained digital elevation maps have higher quality than those obtained in

conventional network programming method. In addition, the calculation cost is very small. We present the basic idea and the processing procedure. [C3465]

"Formation Flying InSAR Configuration Error Simulation and Compensation"

Configuration error for airborne formation flying InSAR was studied. The aircraft interval changes are the most important error. Interval decreasing is taken as an example. Phase changes with baseline changes were derived in formula. The simulation result of plane interval changes is given out. A pentahedron on flat ground is set to show influence of the configuration error. Correct phase compensation is the key technology to get accurate interferogram. So azimuth slope eliminating was adopted. Two control points were arranged in observing area to compensate the phase error introduced by configuration error. This algorithm can improve the DEM precision for whole area. The pentahedron terrain is employed to verify compensation algorithm. The simulation terrain and compensation results prove that the algorithm is effective and efficient. [C3466]

"A Novel Height Reconstruction Approach Based on MLE Using Multi-frequency InSAR Data"

SAR interferometry allows height reconstruction of the earth surface. A method based on the use of multi-frequency interferograms and Maximum Likelihood Estimation (MLE) has recently been proposed. However without a priori knowledge of the terrain, the result of the reconstruction is unsatisfied in practical cases. In this paper, we present a novel method to reconstruct highly sloped and discontinuous terrain height profiles using multi-frequency interferograms. It is based on MLE using multi-frequency interferograms joint statistic property, combining with some conventional signal frequency phase unwrapping algorithm. The method can not only improve efficiency of the MLE, but also ensure reliability of the estimation. [C3467]

"Coherence Improvement of Cross-Interferometric Pair by a Block Azimuth Filtering"

ERS-ENVISAT cross-interferometry with a small height ambiguity is useful to measure the topography in the regions of low slope. Azimuth common-band filtering is a key pre-processing for the cross-interferometry. An adaptive block azimuth filtering was designed and applied to the ERS-ENVISAT tandem pair. As range bin increases, the Doppler centroid of the ERS increases while that of the ENVISAT decreases. It results in systematic increment of the Doppler centroid differences as range bin increases. The coherence of 0.7 in the near range reduced to 0.2 in the far ranges. The block azimuth filter estimates Doppler centroids of at each block, and adjusts band width of the filter. The coherence degradation caused by range-dependent Doppler centroid can be compensated by this method. The coherence is better than conventional azimuth filtering about 0.1 in far range. The resulting interferogram shows improved coherences between 0.8 to 0.4 in near and far range, respectively. However there is still gap of coherence in near and far ranges, it is resulted from inherent problem of less overlapped bandwidth at far range. Although the total improvement was not significant, it is valuable for selection of permanent scatterers in the far range. Test results are discussed in this paper. [C3468]

"An Unsupervised Classification for Fully Polarimetric SAR Data Using IHSL Transform and the FCM Agrithm"

In this paper, the IHSL transform and the fuzzy C-means (FCM) segmentation algorithm are combined together to perform the unsupervised classification for fully polarimetric SAR data. We apply the IHSL colour transform to H/alpha/SPAN space to obtain a new space (RGB colour space) which has a uniform distinguishability among inner parameters and contains the whole polarimetric information in H/alpha/SPAN. Then the fuzzy C-means algorithm is applied to this RGB space to finish the classification procedure. The main advantages of this method are that the parameters in the color space have similar interclass distinguishability, thus it can achieve a high performance in the pixel based segmentation algorithm, and since we can treat the parameters in the same way, the segmentation procedure can be simplified. The experiments show that it can provide an improved classification result compared with the method which uses the H/alpha/SPAN space directly during the segmentation procedure. [C3469]

"Two Novel Polarimetric Indices and Their Application on the Target Enhancement in POLSAR Images"

In this paper we introduce two new parameters for polarimetric SAR (POLSAR) images. For this purpose, the eigenvalues and corresponding eigenvectors of the coherence matrix is calculated. It can be assumed that there are different land cover features, and they are represented by different or slightly different coherence matrix so that eigenvalues and corresponding eigenvectors. However, the condition number and perturbation in the solution of the coherence matrix are calculated for each pixel in the POLSAR image. The results indicate that different scatterer properties so that the scattering mechanisms could be represented with these parameters.

[C3470]

"A New Method for DEM Generation using a Single POLSAR Flight Pass"

In this paper, we proposed a new method for DEM generation from a single POLSAR flight pass. As usual, orientation angles induced by azimuth slope can be estimated from POLSAR data. However, for DEM generation, Another condition is need to attain the orthogonal terrain slopes. Thus, shape from shading techniques, which is mostly used by the robot vision community and generate slopes in the range direction, could then be combined with polarimetry. After terrain slopes have been computed, these slopes data are then used to solve a Possion equation to estimate the elevation surface. [C3471]

"Building Extraction Using C Band Pol-SAR Image"

This paper introduces a method for building location information extraction using airborne C-band polarimetric SAR data. The method is based on the analysis of building feature. The method decomposes the scattering covariance matrix into three simple mechanism, i.e., odd-bounce; even-bounce; cross-bounce. Taking into account that the typical strong T-shaped echoes from quite large buildings are visible, a method is introduced to extract the location of the buildings. [C3472]

"S-Band, Polarimetric, Combined, Short Range Action Scatterometer-Radiometer for Platform and Vessel Application"

In this paper S-band (~3 GHz), polarimetric, combined, short pulse scatterometer-radiometer is described, for simultaneous and spatially coincident measurements of sea surface, snow, bear and vegetated soil microwave reflective, and emissive characteristics, and for backscattered radar signal frequency distribution statistical parameters estimation. The system may be successfully used for near sea surface wind and sea surface wave fields' parameters precise and unambiguous retrieval, as well as for land and sea surface signatures and targets detection and identification their origin. [C3473]

"On Position and Attitude Determination Requirements for future Bistatic SAR Experiments"

In future bistatic SAR experiments¹ the overlapping of transmitter and receiver antenna footprints is, due to the different trajectories and velocities of the involved platforms, an issue. In this paper we focus on the planned hybrid experiment with an aircraft and TerraSAR-X as carrier platforms. The effect of unknown rotations about the body-axes on the tie point of the antenna pointing vector in Earth's local tangent plane is described. Simulation results based on possible aircraft and satellite parameters are presented and discussed. Based on the suggested geometric modeling and results, positioning and attitude determination requirements can be easily derived for different constellations. [C3474]

"Optimization of bistatic Radar Configurations for Vegetation Monitoring"

Bistatic radars have been recently proposed as an alternative to conventional monostatic radars since they can provide additional information in many fields of remote sensing applications. However, up to now, no bistatic radar campaigns, nor laboratory experiments, having vegetation as the target have been set up. This paper presents theoretical simulations of the bistatic scattering coefficient of crop and forest canopies. The electromagnetic model developed at Tor Vergata has been used to analyse scattering as a function of the observation angle, both in azimuth and elevation, and it will be shown that biomass monitoring can be optimized at out-of-incidence scattering planes. [C3475]

"Modular SAR Simulator for Bi- and Multistatic Constellations"

Bi- and multistatic SAR missions are becoming increasingly important for the SAR data acquisition. Established methods for processing monostatic SAR signals and for mission planning have to be adapted to the bi- and multistatic case. To support this evolution, a suitable flexible and powerful simulation tool is essential, which is able to handle such complex scenarios and to provide corresponding simulation data. This paper presents a new simulator architecture. In particular, the modular approach to implement and to simulate this kind of bi- and multistatic SAR scenarios is discussed and an example is given. [C3476]

"A Solution for Bistatic Motion Compensation"

Bistatic synthetic aperture radar (SAR) missions have become attractive in the last years, because of their higher degree of freedom in choosing transmitter and (passive) receiver motion trajectories. In order to take advantage of this increased imaging flexibility, adequate processing algorithms have to be developed,

implemented and verified with experimental data. Currently some promising approaches have been published in this area. A further step in improving the focusing results within a bistatic SAR constellation where transmitter and receiver are mounted on different platforms essentially comprises the bistatic motion compensation (MC). We present a geometrical MC approach which requires high accurate position and velocity information of transmitter and receiver. [C3477]

"Evaluation and Optimisation of Configurations of a Hybrid Bistatic SAR Experiment Between TerraSAR-X and PAMIR"

The development of new technologies and algorithms in the field of bistatic SAR will lead to new instruments of remote sensing in various domains. One of the next important steps will be the realisation of challenging bistatic SAR experiments to prove, evaluate, and develop this new technique. In this context, we will conduct hybrid bistatic SAR experiments using the SAR satellite TerraSAR-X and the airborne SAR sensor PAMIR. This paper presents first considerations with respect to the optimisation of possible geometries between the spaceborne and the airborne SAR sensor. [C3478]

"Determination of Glacier Velocities on King George Island (Antarctica) by DInSAR"

The Antarctic Peninsula is a region highly sensitive to climate change. For ice dynamic modelling and climatic impact studies several parameters have to be known. Radar interferometry is a feasible method in such remote areas to derive velocity fields. For King George Island, the available ERS-1/2 tandem pairs with reasonable baselines have been processed. Due to temporal decorrelation only 2 out of 19 pairs showed almost everywhere high coherence and an additional 6 have partial moderate coherence. A SAR DEM was constructed by double differencing interferometry. Ascending and descending scenes were combined to derive a velocity field for the main part of the Island. External elevation data were additionally incorporated in the processing. Glacier velocities range between 0 m and about 120 m per year. Validation with DGPS measurements from several field campaigns shows good agreement with the interferometric derived velocities. Inaccuracies exist for the edges of the ice cap as here decorrelation effects hampered the generation of an InSAR DEM and no external data were available. [C3479]

"A Generalized Space-Time Formulation for Robust Persistent Scatterer Interferometry"

Differential synthetic aperture radar (SAR) interferometry allows measuring slow terrain movements. The extraction of this information is a complex task. Important advances were introduced by the persistent scatterer approach, with the ideas of minimizing the amplitude and phase dispersions in long series of SAR acquisitions. This approach exploits mainly the temporal properties of the signals. On the contrary, other approaches, more similar to classical differential interferometry, exploit first the spatial and then the temporal properties of the data. In this work, we present a generalized formulation of the persistent scatterer interferometry problem that contains the two approaches mentioned above as limiting cases. In the general case, the spatial and temporal properties of the data are exploited jointly, which helps recovering the correct solution even with a limited number of images. Tests performed on real ERS data show that the proposed approach is promising. [C3480]

"Combined Ground Penetrating Radar and Seismic System for Detecting Tunnels"

An experimental system to collect co-located ground penetrating radar (GPR) and seismic data was developed to investigate possibilities of using the sensors individually or in a cooperative manner to detect shallow tunnels. These sensors were chosen because they sense very different physical properties. The seismic sensor is sensitive to the differences between the mechanical properties of a tunnel and the soil while the GPR is sensitive to the dielectric properties. Raw and processed data from both sensors are presented. [C3481]

"Research on Bistatic SAR Imaging"

For reasons of stealth and other operational advantages, more attention has recently been focused on bistatic SAR. Bistatic SAR uses separated transmitter and receiver flying on different platforms, and has the ability of the exploitation of additional information contained in the bistatic reflectivity of targets. Besides of technical problems-like the synchronization of the oscillators-the processing of bistatic raw data imaging is not well studied theoretically all the same, which is a major area in bistatic SAR. This paper firstly describes the special case of equal velocity vectors and parallel flight paths of transmitter and receiver, and then makes detailed and mathematical study on the approximate bistatic-to-monostatic application (BTMA). Based on the BTMA, the bistatic imaging can be processed with a Standard SAR Processor. [C3482]

"An Adaptive Filtering Approach to Distributed Space-borne SAR Imaging"

An adaptive filtering approach to distributed space-borne SAR imaging is proposed in this paper. The signal model and principle of adaptive filtering imaging are presented at first. Then two categories of adaptive filters are evaluated. The performance analysis and comparison of those two filters indicates that the computation load is lower than with a Wiener filter and imaging quality is better than with a matched filter. Finally the numerical simulation results are presented to illustrate the results. [C3483]

"Simulations of L-Band Backscattering from a Quasi- Periodic Corn Canopy"

Retrieval of soil moisture under corn canopies has been investigated by many researchers and is still a problem that is not fully assessed. Corn is an organized canopy. This feature produces effects not observed from natural canopies. One such effect is the dependence of sensor response on the azimuthal direction. The aim of this study is to explore these distinguishing effects by Monte-Carlo simulations. [C3484]

"A Simple Model for Scattering Coefficients of Vegetation Canopies"

A new simple microwave backward and forward scattering model for vegetation canopies is developed in this study. This simple model has only ten input parameters for a natural earth surface, which is modeled as a two-layer structure comprising a vegetation layer and a ground layer. The computation results of this model are compared with the experimental measurements, which were obtained by a ground-based scatterometer and the NASA/JPL air-borne synthetic aperture radar (SAR) system. It is found that the scattering model agrees well with the experimental data, even though the model uses only ten input parameters. [C3485]

"Electromagnetic Scattering from Multilayer Rough Surfaces Separated by Arbitrary Dielectric Profiles"

Radar remote sensing of soil moisture content at low frequencies requires an accurate scattering model of realistic soils, which often involves multilayer rough surfaces and inhomogeneous dielectric profiles. In this paper, a hybrid analytical/numerical solution to two-dimensional scattering from multilayer rough surfaces separated by arbitrary dielectric profiles based on the extended boundary condition method (EBCM) and scattering matrix technique is presented. The reflection and transmission matrices of a rough interface are constructed using EBCM. The inhomogeneous dielectric profile is modeled as a stack of piecewise homogeneous dielectric thin layers. The scattering matrices of an inhomogeneous dielectric profile are computed by recursively cascading reflection and transmission matrices of individual dielectric interfaces from the bottom dielectric interface to the top interface. The interactions between the rough interfaces and the inhomogeneous dielectric profile are taken into account by applying the generalized scattering matrix technique, numerical simulations, the actual field-collected soil moisture data are used, in particular, the dielectric profiles during both dry and wet ground conditions are examined. The numerical simulations are performed to investigate both bistatic scattering coefficients and copolarized phase difference due to different subsurface roughness parameters and ground conditions. Simulation results show that the bistatic scattering coefficients at low frequencies are sensitive to subsurface roughness parameters and copolarized phase difference strongly depends on soil moisture contents. [C3486]

"Hydros Soil Moisture Retrieval Algorithms: Status and Relevance to Future Missions"

In 2002 the Hydrosphere State Mission (Hydros) was selected by NASA as the alternate mission for a flight opportunity under its Earth System Science Pathfinder program. The Hydros mission objective was to collect the first global scale measurements of the Earth's soil moisture and land surface freeze/thaw conditions, using a combined L band radiometer and radar system operating at 1.41 and 1.26 GHz, respectively. Although NASA cancelled the Hydros mission in December 2005 due to insufficient funding and its reversion back to alternate mission status, the development of accurate soil moisture retrieval algorithms and associated error analyses begun under the Hydros project are still relevant to SMOS and to other potential future soil moisture missions. [C3487]

"A New Semi-empirical Model for the Analysis of Surface Roughness Heterogeneity"

The use of a theoretical backscatter model to analyse medium to low spatial resolution microwave data is still very complicated, particularly because of the difficulty in defining a unique roughness parameter, capable of adequately representing heterogeneous terrain. In this paper, an approach is proposed for roughness analysis and the modelling of backscattering, under conditions of surface heterogeneity. The proposed backscattering model has been validated with IEM (integral equation model) simulations and radar data, for high radar incidence angles, and within its domain of roughness validity. [C3488]

"Assessing Vegetation Scattering Mechanisms of L-band AIRSAR Data on Sloping Forest Area"

In this paper an improvement of radiative transfer models that accounts for the depolarizing ground scattering and tilted scattering surface is presented to model vegetation scattering mechanisms. This study is implemented with the real L-band NASA (JPL) AIRSAR data in Jeju volcanic island. The vegetation scattering model in sloping surface is adequate to assess slight changes in microwave scattering mechanisms and to interpret the physical characteristics of eigen-parameters of the coherency matrix in sloping vegetated area. [C3489]

"Use of the SVM Classification with Polarimetric SAR Data for Land Use Cartography"

This study comes within the framework of the global cartography and inventory of the Polynesian landscape. An AIRSAR airborne acquired fully polarimetric data in L and P bands, in August 2000, over the main Polynesian Islands. This study focuses on Tubuai Island, where several ground surveys allow the validation of the different results. Different decompositions, such as H/A/alpha, or based on the Pauli formalism have shown their potential for land use discrimination. In order to take into account these different parameters into a supervised classification scheme, the SVM (Support Vector Machine) method is investigated. When dealing with only the coherent matrix elements, the results show that the SVM classification gives comparative results to those obtained with Wishart classification. Results are significantly improved when adding to the coherent matrix elements, other polarimetric parameters, as H/A/alpha or the co-polarized circular polarization correlation coefficient, ρ_{HRL} , for the Support Vector definition. Finally the best results are given when merging all the parameters for P and L bands, in addition to the only VV single channel acquired in C band. [C3490]

"Polarimetric SAR Detection of Man-Made Structures Using Normalized Circular-pol Correlation Coefficients"

Polarimetric synthetic aperture radar (SAR) backscatter from man-made structures is often quite different than scatter from predominantly natural areas. Backscatter from natural areas is often characterized by near zero values for linear-basis covariance matrix off-diagonal terms of the form $\langle \text{SHVS}^* \text{HH} \rangle$ and $\langle \text{SHVS}^* \text{VV} \rangle$. A new approach is proposed to detect man-made structures using circular-pol RR-LL correlation coefficients. This method uses a normalization term, which enhances the return from man-made structures and eliminates most of the unnecessary details of the backscatter from natural areas. [C3491]

"The Difference Scattering dRCS from a Dielectric Target above a Rough Surface"

The difference field RCS (d-RCS) has been defined to analyze the scattering from the target above a rough surface. The electric field integral equations (EFIEs) of the difference induced current on the rough surface, the induced electric current and magnetic current on the dielectric target under a TE wave incidence are derived. A small portion of the rough surface towards the target along the specular direction is taken to compute the scattering contribution from the rough surface towards the target, which improves the computation speed. A numerical iterative approach is developed to solve the EFIEs and bistatic d-RCS. The surface length for iterations is dependent on the scattering angle and discussed for comparison with Johnson's method. Using the Monte-Carlo method to generate the P-M (Pierson-Morkowitz) ocean-like rough surface, bistatic d-RCS of the dielectric target, e.g. a cylinder or a square column, above the rough surface is numerically simulated. The induced electric and magnetic currents on the dielectric target, and the difference induced current on the rough surface are numerically discussed. [C3492]

"A Numerical Model of Radar Scattering from Steep and Breaking Waves"

Ocean gravity waves can be rather steep and even breaking depending on wind speed. Analytical modeling of both the evolution of such strongly nonlinear waves and electromagnetic (EM) scattering from them is currently impossible. At the same time, numerical modeling of these processes poses a significant challenge in terms of the complexity of codes and computational time. In this study, we employ an efficient and fast numerical solver which is based on a uniform approach equally convenient when dealing with both hydrodynamic and EM parts of the problem. As a result, a sequence of large-scale wave profiles is produced that follows through all stages of wave breaking. The small-scale roughness is treated statistically by employing the Pierson-Moskowitz spectrum, and it is added on top of smooth gravity waves. Using the EM code, the scattering problem is solved assuming an impedance boundary condition. The same spline description of the surface profiles of gravity waves is used in both hydrodynamic and EM codes. Backscattering cross sections and corresponding Doppler spectra were the subjects of this study. The numerical calculations demonstrate spike events, with the backscattered signal at horizontal polarization exceeding the backscattering signal at vertical polarization. [C3493]

"The Application of Polarimetric Calibration using Polarimetric Scattering Characteristics of Urban"

Areas to ALOS PALSAR"

This paper discusses an ambiguity resolution of polarimetric calibration parameter. Since ALOS was successfully launched on January 24, 2006, the utilization of polarimetric data observed by PALSAR is expected for various remote sensing applications. Thus, polarimetric calibration becomes important issue. However, there is a possibility that calibration algorithm has a 180deg sign ambiguity with respect to cross-polarized components of a calibrated scattering matrix. The reason is that two polarimetric calibration parameter sets are derived. On the other hand, we found that a 180deg phase shift of cross-polarized component occurred due to the change of an angle between a direction parallel to a building wall and a radar line of sight in azimuth plane. Thus, we examined that this scattering property was applied for selecting a correct polarimetric calibration parameter set. The experimental result shows that urban structures can be used for polarimetric calibration. [C3494]

"Modeling Coastal Waters from Hyperspectral Imagery using Manifold Coordinates"

In [1] [2], we introduced a direct data driven method of modeling nonlinear structure in hyperspectral imagery based on Isometric Mapping [15]. More recently, we have further improved the scaling of the approach [2], making it a practical method for large-scale hyperspectral scenes. The new method extracts a set of data manifold coordinates that directly parameterize nonlinearities present in hyperspectral imagery, both on land and in the water column. In the water column, this is particularly important because of the nonlinear, attenuating properties of the medium. In this paper, we model hyperspectral imagery acquired by the NRL PHILLS [5] at the Indian River Lagoon, Florida in July 2004. In our previous efforts [3] using a small subset of data derived from the surf zone outside of the lagoon, dominant manifold coordinates were shown to parameterize bathymetry directly with a high degree of correlation to a radiative transfer look-up table (LUT) approach. In the present work, we construct a full scene manifold coordinate representation and use this as the basis of a LUT for samples with known depths as determined by the SHOALS LIDAR. Sequestered test data presented to the manifold based LUT yield a mean estimated depth which differs from the LOAR retrieved depth by less than 0.44 m for depths between 0-10 m with a standard deviation less than 1.2 m. [C3495]

"Calibration of Spaceborne Polarimetric SAR Data using Polarization Orientation"

For ALOS/PALSAR in orbit, removal of not only polarimetric system distortion but also the effect of Faraday rotation is important. The author investigated a new calibration method using polarization orientation induced in build-up areas. Its fundamental concept is simple and is that two polarization orientation angles from two polarization combinations should be identical after calibration. This method is applied to simulated data that is distorted from JAXA L-band Pi-SAR data. An advantage of this method is that strong backscatters from buildup areas can be used to decrease an influence of noise. [C3496]

"ALOS Calibration and Validation Activities in Sweden"

This paper describes the Swedish activities to support calibration and validation of the Japanese satellite ALOS. Data over three test sites from the instruments PALSAR and AVNIR-2 will be provided by JAXA for evaluation purposes. The main activity during 2006 is a PALSAR calibration experiment using four 5-m radar reflectors, which will be deployed at the test site in southern Sweden. The ALOS data will also be used for developing forest applications, e.g. detection of clear-cuts and storm damages. [C3497]

"On the use of Symmetric Target Tilt Angle for PALSAR Calibration"

PALSAR L-band SAR will be affected by Faraday rotation. In this study, PALSAR system is briefly described, and the Freeman calibration method is considered for PALSAR calibration. However, this method requires the deployment of a minimum of one corner reflector (CR) for the calibration of each scene, and this is not convenient in practice. In this paper, the use of human-made and natural symmetric targets is investigated for the calibration of SAR subject to Faraday rotation. The target scattering vector model (TSVM), which permits a unified decomposition of point and distributed target scattering, is used to derive a new calibration method that does not require the deployment of CRs. It is shown that the orientation (i.e. target tilt angle) and roll invariant maximum polarization parameters of symmetric target scattering can be used to measure and remove Faraday rotation and channel imbalance errors from PALSAR data. Antenna gain and cross-talk incidence angle variations are measured using data acquisitions over the Amazonian forests, under low Faraday rotation conditions. [C3498]

"Range Non-linearities Correction in FMCW SAR"

The limiting factor to the use of Frequency Modulated Continuous Wave (FMCW) technology with Synthetic Aperture Radar (SAR) techniques to produce lightweight, cost effective, low power consuming imaging sensors

with high resolution, is the well known presence of non-linearities in the transmitted signal. This results in contrast and range resolution degradation, especially when the system use is intended for long range applications, as it is the case for SAR. The paper presents a novel processing solution, which completely solves the non-linearity problem. It corrects the non-linearity effects for the whole range profile at once, differently from the algorithms described in literature so far, which work only for very short range intervals. The proposed method operates directly on the deramped data and it is very computationally efficient. [C3499]

"The BYU SAR: A Small, Student-Built SAR for UAV Operation"

Students at Brigham Young University have developed a new, low-cost synthetic aperture radar (SAR) system, the BYU muSAR. The simple design, based on a linear frequency modulated continuous wave signal (LFM-CW), reduces the size and power compared to a conventional pulsed SAR system. This enables the BYU muSAR to fly on a small UAV, further reducing the cost of operation and extending the use of SAR into new areas. Design parameters and specifications for the BYU muSAR are presented in this paper, together with results from experimental data collection and test flights. [C3500]

"Mapping and Projection Algorithm: A New Approach to SAR Imaging Simulation for Comprehensive Terrain Scene"

A novel fast algorithm of polarimetric image simulation for SAR observation over comprehensive terrain scene is developed based on the mapping and projection principles. It incorporates penetrable and impenetrable objects, volumetric and surface scatterers in the imaging space with the extinction, attenuation, shadowing and multiple scattering effects. Scattering of the vegetation canopy is modeled as a layer of random non-spherical particles by using the vector radiative transfer model. Scattering from the ground surface and building objects is calculated by using the IEM rough surface model. As an example, the polarimetric SAR images for a virtual terrain scene, composed by tree canopies, farmland, buildings, rough land surface, hills and rivers, are simulated. [C3501]

"Automatic Detection of Spots and Extraction of Frontiers in SAR Images by Means of the Wavelet Transform: Application to Ship and Coastline Detection"

After reviewing and discussing the difficulties of dealing with automatic interpretation methods in SAR imagery, the advantages of using a multiscale time-frequency framework will be established. Then, a specific technique for automatic spot detection, based on the Wavelet Transform (WT), will be presented and justified. The performance of the proposed algorithm will be tested, validated and compared with respect to other algorithms. The particular difficulties of automatic ship detection in near shore waters will be then briefly discussed and, aiming to increase ship detection rates in these regions, a novel automatic algorithm for the extraction of elongated structures such as the coastline will be presented and tested. [C3502]

"Inversion of Combined Radiative Transfer Models for Imaging Spectrometer and LIDAR Data"

The spectral information domain provided by imaging spectrometers contains information about the biochemical composition of a vegetation canopy such as foliage chlorophyll and water content. The spectral information content also enables indirect assessment to the biophysical parameters LAI and fractional cover. On the other hand, the information domain observed by LIDAR provides direct measurements of the vertical and horizontal canopy structure describing the canopy height and the vertical distribution of canopy elements. The leaf optical properties, which are directly related to the foliage biochemistry, scale to the canopy as function of canopy structure and spatial arrangement of canopy elements. Further, the spatial heterogeneity and canopy structure dominate the radiative transfer especially within forest stands. Consequently the LIDAR signal, e.g. recorded as full waveform, can improve the accuracy and robustness of forest canopy parameter retrieval by reducing uncertainties related to the canopy structure. On the other hand the accurate interpretation of the LIDAR signal depends on the spectral properties of canopy elements as well as the background. The two sensors and their different information domains are thus mutually dependent but also complement each other. A synergistic exploitation of the information domains observed by Imaging Spectrometry and LIDAR based on radiative transfer modeling will therefore provide a new approach to optimize the retrieval of forest foliage biochemical composition and the canopy structure. [C3503]

"Implementation of Differential Repeat-pass SAR Interferometry for the Search for Earthquake Precursory Land-cover Deformation in Taiwan"

Worldwide, medium- to short-term earthquake prediction is becoming ever more essential for safeguarding man due to an un-abating population increase, but hitherto there have been no verifiable methods of reliable earthquake prediction developed-except for a few isolated examples of earthquake prediction in China and in

Greece. This dilemma is a result of previous and still current approaches to earthquake prediction which are squarely based on the measurement of crustal movements, observable only after a tectonic stress-change discharge (earthquake) has occurred. The prediction models were derived from past histories of measurements, mainly carried out during the past 30-40 years, although initiated soon after the San Francisco Earthquake of 1906. During the past decade it was proved and shown that it is not possible to derive reliable models for earthquake predictions from crustal movement measurements alone, and that an entirely new approach must be taken and rigorously pursued over years and decades to come. In support of this conclusion, there have been reported throughout the history of man anecdotal historical up to scientifically verifiable earthquake precursor or "seismo-genic" signatures of various kind-biological, geological, geo-chemical and especially a rather large plethora of diverse electromagnetic ones on ground, in air and space, denoted as "seismo- electromagnetic" signatures. The existence of all of these signatures can no longer be denied even by the fiercest seismological expert opponents; and it is absolutely high noon that those signatures be more rigorously assessed in order to develop a strategy for designing and carrying out controlled "seismo-genic" and "seismo-electromagnetic" studies on how to set up world-wide a network of measurement sites for conducting a holistic set of measurements for providing an improved understanding on why and how such precursor signatures are generated, and how and where those may best be observed subject to the rather poor signal-to-noise ratio (SNR), requiring much improved digital instrumentation as time goes on due to the ever increasing man-made electromagnetic noise generation. A number of pilot studies had been initiated, had been supported for a few years, and then aborted because of the high operating costs involved, the poor SNR making signal detection tedious if not impossible with the current state of the art in instrumentation, and because earthquakes don't appear upon demand. For example such major studies as the USGS/NSF NEHER Program of the early 1990's after the Loma Prieta M 7 earthquake of 1987; in Japan the ERSFP after the Kobe Earthquake of 1995; in Greece the ongoing electro-potential methods of Varatsov; in China, and in various regions as well as independent states of the former Soviet Union. There exists a rather large number of fiercely competing groups in Russia coming up with their own diversified yet highly incomplete modeling approaches seeking support from the West for unfortunately all too low-cost scientific mercenary services. No clear picture has evolved and should not be expected; and a much wider internationally coordinated investigation is required, which may well last for several decades before a unified approach and with it a solution to this vital problem may be found-if ever. In this overview a systematic analysis of main historical records, a summary of pertinent "seismo-genic" as well as observed "seismo- electromagnetic" effects and modern ground-based to air- and space-borne metrological signature investigations are presented. Specifically, remote sensing techniques not yet conceived but in urgent need-such as the remote sensing of the groundwater table-for advancing our understanding of this highly interdisciplinary complicated geophysical problem are being identified, and input is sought from participants for possible active future involvement. [C3504]

"Meso-Scale Variability of Soils and Forest Canopy Properties is Connected to Geomorphologic Features in Eastern Amazonia"

In this study we investigated the relationships between landscape features such as terrain elevation and slope with two variables that drives forest productivity, soil texture and leaf area index (LAI). The study was carried out at the Tapajos region in Para State, eastern Amazonia. Twenty-four 0.25 ha plots were sampled along a ~150 km north-south transect in October 2002. Soil samples were collected (0-10 cm) in three random points in each plot for texture analysis. LAI was measured at 25 points regularly distributed in each plot. The geomorphologic attributes for each plot were extracted from the Shuttle Radar Topography Mission (SRTM) data linearly resample to 10 m spatial resolution. Terrain slope was linear and negatively related to the soil clay content ($r^2=0.73$). Soil sand content had an expected opposite pattern ($r^2=0.72$). The soil content of clay and sand along the elevation gradient can be strongly explained by a cubic polynomial curve ($r^2=0.82$ and 0.81 , respectively). LAI showed to be a logarithmic function of slope ($r^2=0.61$), excluding plots located in the Valley regions. Moreover, LAI showed a linear and positive relationship with soil clay content ($r^2=0.52$). Similarly to the relationships found between terrain elevation and soil texture, the 3rd order polynomial could explain 64% of the LAI variability over the Tapajos. Therefore, we concluded that topography is a major driver of the patterns of soil texture at the landscape scale and the combined effect of topography and soil can largely explain the patterns of LAI over the Tapajos. The combination of SRTM data and field-based information has the potential to increase the accuracy of ecosystem scale estimations of forest productivity in the Amazonia. [C3505]

"Synergistic use of AMSR-E and MODIS Data for Understanding Grassland Land Surface Phenologies"

In recent investigations into the response of native grasslands to global environmental changes, rainfall variability has been offered as a key factor for explaining ecosystem structure and function. In particular, changes in the temporal patterns of precipitation were shown to alter critical aspects of the carbon cycle. To understand the impact of rainfall variability in grasslands, an understanding of the dynamics of surface moisture is critical. Here

we characterize spatio-temporal patterns of two standard data products from AMSR-E: vegetation water content and surficial soil moisture. In addition, we explore the sensitivity of these products to an extreme precipitation event as modulated by land cover type. The sensitivities of vegetation water content and soil moisture retrievals were found to be dependent on the NDVI value, with an apparent loss of sensitivity at higher NDVI values. Despite the coarse spatial resolution of the data, the difference in between predawn and afternoon vegetation water content was found to be a potentially source of information about canopy water stress. [C3506]

"Monitoring of Tobacco Planted Acreage Based on Multiple Remote Sensing Sources"

Monitoring of tobacco planted acreage is a very important step for tobacco's management and monitoring. The paper presents a monitoring method by data fusion of multiple remote sensing sources. It extracts tobacco areas according to the NDVI value and classifies the fusion image with texture information, then classifies the SAR data to acquire tobacco plot in cloudy area. After classification post-processing and manual interpretation, the classification precise satisfies the demand. Applied results are in good agreement with the theoretical study, which shows its effectiveness and applicability. [C3507]

"Networking CSU-CHILL and CSU-Pawnee to Form a Bistatic Radar System"

This paper describes how the synchronization and networking capabilities of the transmit and receive chain used at the CSU-CHILL and CSU-Pawnee radars are used to form a bistatic radar system capable of observing clear air echoes from atmospheric boundary layer. An overview of the bistatic radar geometry and resolution volume are presented, along with a discussion of the methods used to achieve timing coherence. Some preliminary results from clear-air observations are included. [C3508]

"Waveform Design for First Generation CASA Testbed"

The first testbed of X-band radar systems deployed by the Center for Collaborative Adaptive Sensing of the Atmosphere (CASA), in central Oklahoma called IP-1 (Integrated Project 1) will have a low unambiguous velocity due to their short wavelength, and increasing the PRF will result in multiple trip overlays since storms can extend over a large distance. The range-velocity ambiguity is more severe for X-band radars compared to the conventional S-band. However, low cost radars limit the ability to support complex waveforms due to hardware requirements. In addition the radar observations at short ranges are contaminated by ground clutter. This paper describes the waveforms for the individual radar nodes based on operational requirements such as scan speeds, volume coverage pattern and system/hardware limitations to resolve range and velocity ambiguities along with clutter suppression. [C3509]

"C-Band SAR Based Estimation of Baltic Sea Ice Thickness Distributions"

These level ice charts are automatically derived from man-made ice thickness charts using novel SAR information [1]. The aim of the present study has been to include some navigationally meaningful information about the degree of ice deformation into these level ice thickness charts. To this end, we propose a procedure where the SAR image is first segmented, and then an ice thickness distribution is assigned to each segment. For this purpose ice thickness measurements based on a helicopter-borne electromagnetic induction sensor (EM) have been made in the Baltic Sea. The critical phase in the proposed approach is to establish a statistical relationships between the C-band SAR measurements and the EM-based ice thickness measurements. This analysis is fundamentally complicated by the location inaccuracies between SAR and EM data sets. [C3510]

"Low Back-scattering Bands Paralleling Pressure Ridges on First Year Sea-Ice"

Sea ice roughness characteristics are important parameters of climate and ocean circulation models. Pressure ridges are large features which size, orientation and density have a major impact on heat and momentum fluxes. Extraction of these information from satellite images is a necessary step since it could allow to introduce these parameter's variability into models. In this paper we explore the occurrence of linear structures of low back-scattering which had previously been observed alongside pressure ridges on satellite images recorded late at spring. Measurements described in this research paper were carried out offshore of Kuujuarapik on the East coast of the Hudson Bay. The ice sheet is composed of a first year ice ranging from 1m25 to 1m55 in thickness. Data were collected from mid-April to mid-May which covers the melt initiation period for this region of the bay. Measurement sites were chosen to sample a range of ridge orientations relative to the SAR incident beam. Selection criteria were set to get ridges that display homogeneity of the snow field along their axis. Data from 4 field works are presented. We show a correlation between low return bands and snow structure slopes that develop downwind of pressure ridges. Also, we discuss the impact of the snow wetness content on image resolution. [C3511]

"Assimilating Passive Microwave Brightness Temperature Data into a Land Surface Model to Improve the Snow Depth Predictability"

This paper introduces the application of the ensemble Kalman filter (EnKF) technique for the assimilation of passive microwave remote sensing observations into a landsurface model, to improve the snow depth (SD) predictability. A new landsurface model, currently developed at the Japan Meteorological Agency (JMA), which is based on the simple biosphere model (SiB), is used as a forward model to predict the change of the snow pack. The microwave emission model of layered snowpacks (MEMLS) is used as observation operator, to transfer the model prediction into the corresponding satellite brightness. The assimilation system was applied using data from the coordinated enhanced observation period (CEOP) Asia-Australia monsoon project (CAMP) Eastern Siberia Taiga region for the period from November 2002 to March 2003. The data sets includes JMA-GSM model output, which is used as forcing data, satellite brightness temperature observation from the advanced microwave scanning radiometer (AMSR-E) and in-situ snow depth (SD) observation and the current AMSR-E snow depth product for comparison. The assimilation results are in good agreement with the data from the snow depth observation sites in this region and improve the forecast of the land-surface model. Furthermore, comparison with the AMSR-E SD product showed, that the assimilation results are also in better agreement with the in-situ snow depth observation. [C3512]

"A Complex of Multi-Frequency at 3GHz, 5.6GHz, 20GHz and 37GHz, Polarimetric, Combined, Short Pulse, Short Range Action Radar- Radiometers for Soil and Snow Remote Sensing and Surveillance"

A complex of polarimetric (dual polarization), spatio- temporally combined active-passive devices of S (~3GHz), C (~5.6GHz), Ku (~0GHz), and Ka (~37GHz) band of frequencies is represented, for bare and vegetated soils, waved water surface and land snow cover microwave reflective and emissive characteristics multi-frequency, polarimetric, simultaneous and spatially coincident measurements. The complex is dedicated to solve problems applied to soil (bare and vegetated) and snow moistures retrieval, to near water surface wind and wave field parameters retrieval, by synergetic application of various kind microwave means of remote sensing, as well as applied to surface and sub-surface targets detection and identification tasks solution. The complex is set in ECOSERV Remote Observation Centre's control-test experimental site, in Armenia, which is equipped by facilities for microwave devices absolute calibration, by spatially distributed stations for in-situ measurements of soil and moistures and temperatures, and has a local meaning small weather station. This paper has an aim to attract attention of researchers who are interested in such kind measurements and to invite them to perform their own or joint measurements using available facilities. [C3513]

"Analysis of Aqua AMSR-E Derived Snow Water Equivalent over Himalayan Snow Covered Regions"

We have made an endeavor to investigate the snow water equivalent (SWE) variations in Himalayan mountain region which is the most difficult terrain to access during winter seasons. The area also covers the large glaciers such as Siachen and Gangotri. A time series multi scale of SWE L3 product derived from Aqua Advanced Microwave Scanning Radiometer (AMSR-E) data have been analysed for three consecutive winters during 2002 -2005 for Himalayan Snow cover region. A major emphasis is on the study of SWE trend in the two glacier areas viz. Siachen and Gangotri. It has been observed through AVISR- E 5-day product that snow cover area (SCA) over whole Himalayan region is very dynamic. AVISR-E derived 5-day SWE is analysed at the two test sites viz. Patsio (Lat 32deg 45 17.89" N and Lon 77deg, 15', 43.13"E) and Dhundi (Lat 32deg, 22, 05"N and Lon 77deg, 15 E) concurrently with the available in-situ data .The result indicates that in the peak winter days only we found reasonable co-relation. At the Patsio, minimum and maximum SWE observed are 26 mm and 108 mm respectively using in situ data. [C3514]

"Detecting Weather Radar Clutter by Information Fusion With Satellite Images and Numerical Weather Prediction Model Output"

A method for detecting clutter in weather radar images by information fusion is presented. Radar data, satellite images, and output from a numerical weather prediction model are combined and the radar echoes are classified using supervised classification. The presented method uses indirect information on precipitation in the atmosphere from Meteosat-8 multispectral images and near-surface temperature estimates from the DMIHIRLAM-S05 numerical weather prediction model. Alternatively, an operational now casting product called 'Precipitating Clouds' based on Meteosat-8 input is used. A scale-space ensemble method is used for classification and the clutter detection method is illustrated on a case of severe sea clutter contaminated radar data. Detection accuracies above 90 % are achieved and using an ensemble classification method the error rate is reduced by 40 %. [C3515]

"Time-dependent Second Order Scattering Theory for a Weather Radar with a Finite Beam Width"

Multiple scattering effects from spherical water particles of uniform diameter are studied for a W-band pulsed radar. The Gaussian transverse beam-profile and the rectangular pulse-duration are used for calculation. An second-order analytical solution is derived for a single layer structure, based on a time-dependent radiative transfer theory. When the range resolution is fixed, increase in footprint radius leads to increase in the second order reflectivity that is defined as the ratio of the second order return to the first order one. This undesirable feature becomes more serious as the range increases. Since the spaceborne millimeter-wavelength radar has a large footprint radius that is competitive to the mean free path, the multiple scattering effect must be taken into account for analysis. [C3516]

"Sensitivity of Dual-Frequency Rain DSD Retrieval to Particles in Melting Layer for Space-borne Radars"

Many dual-frequency DSD retrieval algorithms have been proposed for space-borne radars. A self-consistent backward iterative algorithm, based on non-Rayleigh scattering has been studied recently[1][2][3]. This algorithm is based on a certain DSD model of rain, for which the attenuation caused by the ice or mixed-phase particles should be extracted accurately. Any error in the attenuation correction at one of the two frequencies would affect the accuracy of the DSD retrievals for rain region. This paper examines how the DSD retrieval for rain is affected by the reflectivity correction for attenuation due to the ice or mixed-phase particles in bright band. First, a non-coalescence and non-break up (N-N) model, with an adjustable thickness and the DSD at the bottom of the melting layer is used to generate the reflectivity and specific attenuation profiles. The profiles for varying DSD (N_w from 1000 to 8000, D_0 from 1.0 mm to 1.75 mm) are used to derive the alpha and beta coefficients for k-Z relationships for different heights, for a certain thickness of the bright band. Then the k-Z relationships are incorporated in Hitschfeld-Bordan method to evaluate the two way attenuation at the two frequencies. Last, the reflectivities in rain region, considered of the attenuation correction error, are made of use of by the self-consistent backward iterative algorithm [2] to retrieve the DSD. The simulation shows that the accuracy of the attenuation correction for Ka-band, the higher frequency, is crucial for the dual-frequency iterative algorithm to correctly retrieve the DSD. While the attenuation correction error at Ku-band remain negligibly small, the error at Ka-band could be as large as 0.47 dB, and this error would have been too large for backward iterative method to correctly retrieve the DSD. The method presented in his paper can be used to evaluate any rain DSD retrieval algorithms proposed for GPM. [C3517]

"Multi-temporal High-resolution Polarimetric L-band SAR Observation of a Wine-producing Landscape"

In continuation of the BACCHUS project, aimed at establishing a reference high quality geographic information system for vineyards, an airborne SAR survey has been carried out in fall 2005 in the Frascati area, near Rome (Italy) to demonstrate the potential of airborne radar remote sensing in vineyard characterization. This contribution reports on the polarimetric L-band and dual polarization C-band SAR data acquisition campaign supported by ESA and carried out on two dates in October 2005 (the first during the grape harvest and the other after the vintage completion). [C3518]

"Self-organizing Neural Networks for Unsupervised Classification of Polarimetric SAR Data on Complex Landscapes"

This paper refers to a study on the pixel-by-pixel unsupervised classification of a polarimetric SAR image of a Central Italy landscape. The polarimetric data have been processed by self-organizing neural networks to test their performance in classifying a complex landscape. The discrimination accuracy attained by the self-organizing map method is compared both against that of H/A/alpha-Wishart unsupervised procedure and of a supervised scheme. [C3519]

"Oversampling and Whitening with the CASA Radar"

The CASA NSF ERC is using cutting edge radar technology to create a network of short range weather radar to observe the lower regions of the atmosphere that are currently out of sight. Range oversampling and whitening is one of the newest technologies available for increasing the accuracy of weather radar moment estimates. The CASA mission has incorporated range oversampling into the design of one the first prototype radars created for the mission. Due to several constraints, the MA-1 radar has several hardware design differences from the large state-of-the-art S-band weather radars that oversampling and whitening was developed and verified with. The oversampling and whitening process is validated with the suboptimal MA-1 radar configuration by producing

results that adhere to theoretical expectations. [C3520]

"Precipitation Spectral Moments Estimation and Clutter Mitigation using Parametric Time Domain Model"

In this study the problem of precipitation signal spectral moments estimation in case of clutter contamination is considered. It is proposed to use a parametric model to estimate spectral moments of precipitation echoes and clutter. To estimate these spectral moments the maximum likelihood estimator based on the properties of Gaussian joint distribution of complex time series is used. The main advantage of this approach is that it does not suppress any part of the signal and the properties of weather echoes and clutter are estimated simultaneously. The performance of the proposed method is evaluated based on simulations of radar signals and compared to the performance of GMAP (Gaussian model adaptive processing). The proposed procedure is also applied to measurements collected by CSU- CHILL radar collected during summer 2004. [C3521]

"Two-year Microwave Radiometric Observations of Low-level Boundary-layer Temperature Inversion Signatures"

Temperature inversion indicates that the atmospheric temperature decreases with increasing height. Its occurrence tends to inhibit vertical motion of the atmosphere. Under the occurrence of temperature inversion, air pollutants cannot be dissipated through vertical mixing of the atmosphere and are accumulated near the surface. When temperature inversion lasts for a long time, human health can be in jeopardy due to deterioration of air quality and secondary pollutants, which are formed through atmospheric photochemistry and more toxic than original ones. It is vital to investigate the dynamics of temperature inversion for understanding and resolving its resulting problems. In this paper, temperature inversion signatures over three major cities on Taiwan are analyzed. They are measured by ground-based microwave radiometers installed in Taipei, Taichung and Kaohsiung from 2002 to 2004 supported by the Environment Protection Agency (EPA) of Taiwan. Characteristics of temperature inversion at the three cities are extracted using different classification methods. The characteristics of temperature inversion in Taichung and Kaohsiung show a similar trend but are different from that in Taipei. The numbers of the occurrence of temperature inversion in Taichung and Kaohsiung were much larger than that in Taipei. The main types of temperature inversion in Taiwan are radiation and frontal inversions. Compared to frontal inversion, radiation inversion on average occurs at a lower altitude, lasts a longer period, has a deeper thickness, and reaches a higher temperature difference of inversion. Frontal inversion plays a significant role for the inversion event lasting over 12 hours. [C3522]

"Differential Reflectivity Calibration for NEXRAD"

There are now many S- and C-band weather radars around the world that are either dual polarized or soon will be. The most common polarization basis is horizontal and vertical. Dual polarization is accomplished via fast alternate transmission of horizontal and vertical polarization or simultaneous horizontal and vertical polarization transmission. In either case, such radars can measure copolar differential reflectivity (Z_{dr}) and copolar differential phase (Phidp). It has been shown that accurate estimation of these parameters can improve identification and quantification of precipitation. To minimize rainfall estimation error, measurement uncertainty of Z_{dr} should be less than 0.1 dB. Three methods for Z_{dr} calibration are presented and operational implementation is discussed. Concepts are illustrated with data from S-Pol, NCAR's polarimetric S-band radar. [C3523]

"Characterization of Rain Microphysics based on Disdrometer and Polarimetric Radar Observations"

Characterization of rain microphysics requires information on raindrop size distributions (DSDs). DSD measurements and retrievals, however, contain errors. In this paper, data from side-by-side disdrometer comparisons are presented to provide information that is not possible from single disdrometer measurements alone, allowing error effects to be quantified and a rain DSD model for radar retrieval to be improved. We also propose methods to mitigate sampling errors by filtering with sorting and averaging and by fitting to a Gamma DSD model with truncation and extrapolation. The Constrained-Gamma DSD model has thus been refined for the Southern Great Plains region of the United States. [C3524]

"Measurement of the Mesopause Dynamic Parameters of Lower Thermosphere using Accessible Radio Frequency Resources"

Use of an accessible radiofrequency resource as an emitted television-broadcasting signal in the spaced radar system of meteoric traces for measurement of dynamic parameters mesopause-lower thermosphere is offered in this work. Experimental results of registration of television signals reflected by meteoric traces on a Moscow-

Kharkiv line are submitted [C3525]

"The facility for Remote Sensing of the Near-Earth Space Environment"

The Department of Space Radio Physics that was established in 1964 at the Kharkiv V. N. Karazin National University conducts studies of the near-Earth space environment at its constituent Radiophysical Observatory that is continuously upgraded. The Radiophysical Observatory (49deg38'N, 36deg20'E) is a facility that includes the MF radar, the HF Doppler radar (at vertical and oblique incidence), the satellite radio beacon receivers, the magnetometers, and the ionosonde. The instrumentation allows to investigate the various interacting processes operating in the ionosphere within an altitude range of ~60-1000 km and the characteristics of radio-wave propagation within a frequency band of up to approximately 2 GHz, simultaneously with magnetometer measurements. The Radiophysical Observatory is included in the register of the most valuable scientific facilities in Ukraine [C3526]

"Modeling of rain fields at large scale"

This paper describes the modeling of rain fields at small (size of a rain cell) mid (100times100 km²) and very large scale (4000times4000 km²). The methodology lies on a cellular description of rain fields by HYCELL. Mid-scale fields are generated so that they account for local climatology and for spatial repartition of rain cells deduced from radar data. Very large scale fields are generated in two steps. First rainy areas are determined by thresholding a stationary Gaussian random field. In each point of the field, the probability of rain apparition is the one recommended by ITU and the covariance function is determined in order to reproduce the one observed by meteorological radar. Then rain intensity for rainy area is determined by applying mid-scale model to each mid-scale rainy area. Rain fields simulated are turned into attenuation fields and compared with ITU-R recommendations and radar observations [C3527]

"Research Airborne System for Remote Sensing in MM-Range of Radiowaves"

In this paper the research of airborne system for remote sensing in MM-range of radiowaves has been presented. The results of the research development are obtained and the example of experimental data obtained when using the system [C3528]

"Ionospheric Interference Suppression in HFSWR"

Over the past two decades, significant advances have been made in the use of high frequency surface wave radar (HFSWR) for remote sensing in an ocean environment. As one of the main outside interference, ionospheric interference may badly affect radar's performance. An effective method for ionospheric interference suppression in HFSWR based on time-sharing coherent side-lobe cancellation (CSLC) is presented. Experimental results acquired with the HF system OSMAR confirm that the method can achieve effective ionospheric interference suppression, but not decreasing the strength of the first-order sea echo [C3529]

"Design and Realization of Delay Mapping Receiver Based on GPS for Sea Surface Wind Measurement"

The delay mapping receiver (DMR) is for receiving and processing the reflected GPS signal to get the information of wind of sea surface by recording the reflected GPS signal and matching it to the theoretical model. The hardware structure, software design and difference from normal GPS receiver are introduced in this paper. The test results at near sea of Tianjin of China are provided, which prove the design of DMR is successful and the collected data are useful for the sea surface wind measurement [C3530]

"To the 60-year anniversary of Vladimir Vladimirovich Pustovoytenko"

{no data available} [C3531]

"Structured Covariance Estimation: Theory, Application, and Recent Results"

The maximum-likelihood approach to structured covariance estimation and spectrum estimation has wide applicability in time series analysis, spectroscopy, adaptive beamforming and detection, remote sensing, radio astronomy, and radar imaging. Standard structured covariance EM algorithm with full model matrices is computationally demanding. Computational requirements drastically reduced when model matrices are sparse. Sparse structure may be achieved through appropriately chosen data preprocessing. We are investigating application in problem of airborne radar imaging from multiple viewpoints, previously computationally unrealistic [C3532]

"Neuro-Fuzzy Model for Multi-Channel Underwater Imaging"

Multispectral imaging system usually consist 2-15 different color channels, hyperspectral system-100-200 channels. The image processing in each channel includes the complicated calculations and the final results have quite a large error. As is well known that there are large number of input parameters and some their uncertainty in the case of airborne and underwater LIDAR systems modeling. The using of statistical and determined models give the result having quite a large error of optical information processing and the given calculations take a lot of time to compute. The fundamentally different mathematical algorithms-the neural networks and the fuzzy logic is offered to use. It is realized with specially developed algorithms for multi-channel image processing. The new neuro-fuzzy model of foam coverage for four color channels has been developed to determine the interval of the minimal reflections and to obtain the images of non-foam covered areas [C3533]

"Radar Signal Classification Using Pca-Based Features"

Principal component analysis (PCA) has been used in many applications ranging from social science to space science, for the purpose of data compression and feature extraction. Usage of PCA for synthetic aperture radar (SAR) image classification, though widely reported by remote-sensing researchers, has not been exploited much by automatic target recognition (ATR) community. In the present paper, PCA has been used in SAR-ATR using the MSTAR data base, and comparison has been made with the conventional conditional Gaussian model based Bayesian classifier (M.D. DeVore and J.A. O'Sullivan, 2002). The results have been compared based on percentage of correct classification, receiver operating characteristics (ROC), and performance with limited amount of training data. By all standards of comparison, the PCA based classifier was observed to outperform the conditional Gaussian model based Bayesian classifier (CGBC) or at the worst it performs at par. And given the computational and algorithmic simplicity of PCA based classifier, the new algorithm was concluded to be a highly prospective candidate for real time ATR systems [C3534]

"Antennas for terahertz applications"

Interest in terahertz science has expanded rapidly in recent years due largely to the advent of new RF components and new fast-pulse optical time domain spectroscopic techniques. The two traditional development communities that border the terahertz gap-optical and microwave, are beginning to converge as we see more wide spread use of terahertz systems. One technology area where both these communities can benefit is in the design and realization of new forms of terahertz antennas and beam forming networks. Both frequency domain and optical time domain techniques make use of single mode, broad band terahertz antennas. However, most existing instruments utilize very simple structures that have been imported from the microwave community. The very special needs of newly proposed terahertz instruments, especially very wide band-width spectroscopy and high resolution imagers, require new antenna concepts and new ways of implementing already established antenna designs. More traditional applications for terahertz systems, in radio astronomy, remote sensing and radar, generally require large diameter, high surface accuracy antenna dishes that can benefit from active surface correction, new light weight materials and compact designs. This paper provides a brief overview of terahertz antenna issues from large scale reflectors to multipixel imaging systems. It is intended as an introduction to a field with both wide breadth and applications that cross many disciplines [C3535]

"Mobile Holographic Lidar"

Mobile holographic lidar for remote determination of quantitative characteristics of gas and aerosol air pollution with high accuracy and space resolution is proposed. Differences in reflectivity of liquid and solid particles give a possibility to form polarization holograms and observe liquid and solid aerosols separately. Quantitative analysis of composition and concentration of particles observed in their holographic images is characterized by high level of sensitivity. Determination of gas pollution composition and concentration is performed by the spectral analysis of scattered signals [C3536]

"Parametric Study of Stacked Patch Array Configurations as Alternative Feeds for Offset Reflectors"

A potential feed for the 12 m reflector antenna system was assessed for use in radiometer-scatterometer system to study soil moisture. The reflector system calls for seven feeds that can operate at 1.413 GHz and 1.26 GHz frequencies with one feed at the focus of the reflector and the other six forming a ring around the focus. Numerous configurations of patch arrays were studied and a hexagonal configuration consisting of seven elements with 0.76λ at 1.413 GHz spacing and tapered excitation on the outer ring was selected as the best design. Optimized hexagonal array has a similar pattern to the optimized corrugated horn at both frequencies and at all seven feed locations [C3537]

"Proposal for an ELF Radar of D-Region Ionospheric Anomalies Analyzed using a 3-D Geodesic FDTD Model of the Earth-Ionosphere Waveguide"

This paper proposes a novel extremely low frequency (ELF: 3-300 Hz) radar for locating and characterizing ionospheric anomalies within ~100 km of the Earth's surface. Employing a well-characterized controlled ELF source (as opposed to natural sources having a random occurrence and random properties), the proposed radar could provide continuous, inexpensive monitoring capabilities of the ionosphere within ~100 km of the Earth's surface. For this study the recently developed three-dimensional (3D) geodesic whole-Earth electromagnetic wave propagation model based upon the finite difference time domain (FDTD) solution of Maxwell's equations is used [C3538]

"Low-power Radar for Wireless Sensor Networks"

This paper presents the results of a short study on the feasibility of radars as the primary means of sensing in ad-hoc wireless sensor networks. Radar offers distinct advantages over others means of sensing, normally found in this kind of networks. The sensor networks being considered consist of battery powered nodes. Hence, power consumption is of prime importance. A simple detector front-end has been built to serve as a proof of concept and to verify performance metrics such as power consumption and detection range. The results clearly indicate radar as a suitable sensor for wireless sensor networks [C3539]

"An Interferometric CW-SF Radar for Remote Testing and Monitoring Large Structures"

The authors propose to use a high speed interferometric radar equipment for static and dynamic monitoring of large structures. The equipment is a CW-SF radar with very fast hopping capability in order to sample the movements at a rate high enough to enable structural analysis to be performed. Several experimental tests have been carried out on various structures, here are presented the Cadore highway bridge (near Belluno, Italy) and the Giotto's tower of S. Maria del Fiore (Cathedral of Firenze, Italy) [C3540]

"3rd European Radar Conference"

{no data available} [C3541]

"Amplitude-phase method allowing the determination of the complex dielectric permittivity of underlying surfaces using polarimetric radar remote sensing"

An amplitude-phase method is proposed allowing the determination of the complex dielectric permittivity of underlying surfaces based on the results of relative measurements of the signals in the orthogonal channels of a polarimetric radar receiver. The method assumes the determination of the voltage ratio and the phase difference in the orthogonal channels [C3542]

"Projection Approach for Estimating Radar Signal Multivariate Probability Density"

In the paper a new approach for estimating the radar signal multivariate probability density is suggested. It is based on the use of a projection of a random process to the set of random variables, with the probability density defined as a product of two-dimensional densities. The estimates of two-dimensional probability densities are obtained with the help of filtering the two-dimensional characteristic function. So we are suggesting a nonparametric estimate of the characteristic function. On the basis of these estimates nonparametric algorithms of signal detection are constructed. Examples for remote sensing of atmosphere are suggested [C3543]

"Airborne Weather Radar as Instrument for Remote Sensing of the Atmosphere"

This paper presents an overview and analysis of weather radars that are multifunctional avionics systems. Functional, methodical, and technological aspects of airborne weather radar as instrument to obtain quantitative information about the atmosphere are considered [C3544]

"A 94GHz real aperture 3D imaging radar"

The AVTIS radar developed in St Andrews is a ground-based, portable, 3D imaging radar designed for high resolution terrain mapping. The 94 GHz radar uses FMCW modulation and employs a mechanically scanned monostatic antenna configuration, achieving a maximum range of ~7 km with sub-metre range resolution. We discuss the significant factors which affect the imaging performance such as source phase noise and non-linearity, antenna pattern quality, and surface extraction algorithms. Field testing results gathered at a local quarry are presented to illustrate the effects of antenna pattern quality on the digital reconstruction of terrain

[C3545]

"Distributed Boundary Estimation using Sensor Networks"

We examine the problem of determining boundaries occurring in natural phenomena using sensor networks. Sensor nodes remotely collect data about various points on the boundary. From this data, we estimate the boundary along with the confidence intervals using a regression relationship among sensor locations and the distances to the boundary. The confidence intervals are guaranteed to be narrower than a specified maximum width. Our distributed boundary estimation strategy uses a hierarchical structure of clusters of sensor nodes and requires 20-50% less messages as compared to a centralized scheme. The computed intervals show desired coverage of the true boundary points. Further, motivated by the practical need to estimate the boundary with a minimum number of sensors, we develop an adaptive approach for turning sensors on and off. The number of ON sensors in this scheme is only about 15% more than what a practical Oracle needs, to evaluate the boundary and confidence intervals around it. Our algorithms are also evaluated using data from real sensors on a testbed [C3546]

"Unsupervised Change-Detection from Multi-Channel SAR Data"

Synthetic aperture radar (SAR) data presents a great potential for environmental monitoring applications and natural disaster management thanks to their insensitivity to atmospheric and Sun-illumination conditions. However, the automatic generation of change maps from multichannel SAR images acquired on the same geographic area at different times is still an open issue in the remote-sensing literature. In the present paper an automatic unsupervised contextual change-detection method is proposed for two-date multichannel SAR images, by integrating a SAR-specific extension of the Fisher transform with the expectation-maximization (EM) algorithm or with some of its variants (the Landgrebe-Jackson EM and the stochastic EM algorithms), applied according to a Markov random field model for the image data. The method is validated by experiments on SIR-C/XSAR data [C3547]

"Non-Clear Typhoon Eye Tracking by Artificial Ant Colony"

Generally, large volumes of complicate and precise computation are required during the tracking process of typhoon eye, especially non-clear ones, which is one of the most important aspects in the forecast and analysis of typhoon. Satellite digital photograph and corresponding interpretation technology make it possible to carry out such task by aid of modern digital and computer means of image processing. By means of constructing solution space and heuristic information, artificial ant colony (AAC) can be used to search for the best path in a constrained region, which provides an approach to obtain precise contour, and is proved to reach the best feasible boundary with minimum energy function value. Therefore, the contour of non-clear typhoon eye can be tracked intelligently, based on the satellite photograph. As an example, the computing methodology produced in this paper was applied in experimental cyclone forecasting by the Shanghai Meteorology Center. The proposed solutions was confirmed to have the potential for successful application to the problem of non-clear typhoon eye tracking, and the system is effective and the performance errors are acceptable for practical applications [C3548]

"Fusion of High-Resolution Satellite and Lidar Data for Individual Tree Recognition"

A major shift in the forest inventory and management paradigm toward the use of semi-automated analysis realized on an individual tree crown basis has been made possible by recent developments in high-resolution remote sensing. This paper discusses issues related to the fusion of high-resolution satellite imagery and LIDAR (light detection and ranging) data and their application in the classification of individual trees for precision forest management. The proposed methodological approach consists in the combination of spatial filtering object detection and reconstruction methods with a rule-based individual tree crown (ITC) system. Examples using QuickBird imagery combined with LIDAR data from an Alberta site (both boreal and mixed forest) demonstrate the advantages of the proposed fusion approach [C3549]

"EuRAD 2006 Sessions"

{no data available} [C3550]

"Proceedings of the 3rd European Radar Conference"

The following topics are dealt with: array processing; system signal processing; reflect arrays and active antennas; non-periodic and sparse array antennas; radar applications; multilateration, coding and beam forming; remote sensing; classification and imaging; ultra wideband radar; multifunctional and reconfigurable array; transceiver accuracy; ultra wideband technology [C3551]

"Space Qualification of W-band Devices for the CloudSat Cloud Profiling Radar"

The 94 GHz cloud profiling radar (CPR) instrument is on board the CloudSat spacecraft, launched in April, 2006. The radio frequency electronics subsystem (RFES) for this instrument consists of an up-converter, a receiver, and a transmitter calibrator assembly, which include W-band diodes (noise, Schottky and detector diodes) and MMIC amplifiers (LNA and MPA). W-band devices, in general, are not on the NASA parts selection list, and for most of them, CloudSat is their first use in a space application. Therefore, customized screening and qualification tests were developed for these devices, in order to insure high reliability to meet the 2 year CloudSat mission design life. High amplitude stability is also required for the noise source and transmitter power detector diodes, in order to provide accurate calibration of the overall cloud radar. The test approach and results are presented here [C3552]

"Processing Multichannel Radar Images by Modified Vector Sigma Filter FIR Edge Detection"

Some peculiarities of modified vector sigma filter are studied. In particular, its edge preservation ability is considered in case of processing multichannel remote sensing (RS) images. Such a problem is of high importance for many scene recognition and segmentation tasks. It is demonstrated through comparative quantitative and visual processing data that the proposed filter simultaneously provides efficient noise suppression and excellent edge preservation. Edge detection results that prove this fact are also depicted [C3553]

"MicroPhotonic remote sensor for perimeter security"

This paper addresses the issues inherent in electromechanical beam scanning which has found a new application in perimeter security. Through passive optics and MicroPhotonics, we introduce an architecture for a novel inertia-less long range laser scanner, based on the concept of an optical cavity featuring adaptive beam spacing. We also explore the feasibility of object detection based on intensity profiles. [C3554]

"Application of laser range scanner based terrain referenced navigation systems for aircraft guidance"

This paper discusses the various aspects of using airborne laser scanners (ALS) in terrain referenced navigation (TRN) systems. The paper addresses the system performance of these new ALS-based systems and compares their performance to traditional terrain referenced navigation systems based on radar altimeter and baro-altimeter sensors. The TRN system comparison also includes an inertial measurement unit (IMU) error sensitivity analysis and a discussion on the requirements imposed on the information content in the terrain elevation database by the remote sensor. The paper will use flight test data collected with Ohio University's DC-3 Flying Laboratory in Braxton, WV to evaluate the various methodologies and analyses [C3555]

"Dual-frequency SAR for the measurement of soil moisture at depth"

VHF/UHF dual-frequency and quad-polarized SAR (synthesized aperture radar) based on vector network analyzer is developed for measuring the soil moisture subcanopy and at depth. A discrete scattering model is used to simulate the scattering of vegetation. Rough surface layered media is as deep layered soil model. Semiempirical dielectric properties model of soil is used for soil moisture inversion. Simulation results are given. [C3556]

"A Ka-Band Low Power Doppler Radar System for Remote Detection of Cardiopulmonary Motion"

A low power Ka-band Doppler radar that can detect human heartbeat and respiration signals is demonstrated. This radar system achieves better than 80% detection accuracy at the distance of 2-m with 16-mW transmitted power. Indirect-conversion receiver architecture is chosen to reduce the DC offset and 1/f noise that can degrade signal-to-noise ratio and detection accuracy. In addition, the radar has also demonstrated the capability of detecting acoustic signals [C3557]

"Bistatic radar scattering from an ocean surface at L-band"

This paper presents a numerical analysis for bistatic scattering from the sea surface at L-band. The unifying scattering model small slope approximation (SSA) of the first order is applied to calculate normalized bistatic cross section (NBCS) of the ocean surface. The calculations were made by assuming the surface-height spectrum of Elfouhaily et al. The correlation function based on this spectrum is calculated. The negative region participation in surface scattering which is function of the incident angle, the wind speed and the exploring

wavelength is discussed. A comparison between SSA and geometric optics models shows that the last one is generally not accurate at L-band especially at large angles of incidences. Numerical results examine the wind dependency over a wide range of incident angles along the specular direction and in the forward scattering configuration. In addition, the NBCS behavior in fully bistatic configuration is predicted. Numerical results are obtained as a function of wind speed, incident/scattering angles and polarization states. [C3558]

"The legacy and future of civilian radar missions"

{no data available} [C3559]

"Computing the characteristic function for sums of sinusoidal random variables"

In this note we develop the methodology for computing the moments of the characteristic function for the superposition of sinusoidal transformed random variables. Thus we solve an important case of the Rayleigh problem, and point how to use this technique to completely solve it [C3560]

"Laser pulses from earth detected at Mars"

Over 500 pulses transmitted from a ground-based Nd:YAG laser were detected in Mars orbit, at with the MOLA instrument on-board the Mars Global Surveyor spacecraft on September 28, 2005, at distance of 80.1 Mkm. [C3561]

"A 1.57 μ m DIAL lidar system for range resolved measurements of atmospheric CO₂"

We describe a lidar system based on erbium doped fiber amplifiers, designed to make range resolved measurements of CO₂ within the lower atmosphere at very high precision at 1571 nm. [C3562]

"Seamless Registration of Multiple Range Images with Whole Block Adjustment"

Multiple range images registration is one of the most important problems in range image analysis. This paper proposes a new method to implement seamless registration of multiple range images under least squares, since all the range images constitute a circled network, which can be seen as the closed condition of the whole block adjustment. We experimented on real range images taken by laser scanners, and observed that our method worked successfully even for noise data, and it reduces significantly the level of the registration errors between all pairs in a set of range images. The proposed method has the distinct advantage of seamless and robustness [C3563]

"Behavior of DIAL remote sensed ethylene and ozone in presence of nitrogen oxides"

Correlation between ozone concentration and ethylene evolutions in the urban atmosphere in presence of nitrogen oxides is both demonstrated and is supported by a photochemical smog model. The results ascertain that ethylene has a role to play in the generation of tropospheric ozone. [C3564]

"Electronic steerable MEMS antennas"

Recent advances in the technology of radiofrequency (RF) circuits, such as RF-microelectromechanical systems (MEMS) make it possible to practically implement electronically reconfigurable antenna arrays paving the way to innovative communication systems including applications such as next generation mobile communications, radar applications, remote sensing and imaging. This paper reviews the basic implementations of such antenna systems, namely phased arrays and reflectarrays, as well as the algorithms allowing for beam shaping, beam steering, null placing etc., as well as the typical RF-MEMS circuitry for both amplitude and phase control. [C3565]

"Frequency-resolved coherent LIDAR using a femtosecond fiber laser"

We present a frequency comb-based, frequency-resolved coherent LIDAR (FReCL) that provides higher performance than that of conventional pulsed range/Doppler LIDARs, dramatically reduces local oscillator timing requirements, and compensates for path dispersion. [C3566]

"Differential absorption lidar using NH₃ -CO₂ laser"

We present the main features and calculated parameters of NH₃-CO₂DIAL. It is shown that our lidar can detect Freon-11 at a range up to 5 km with sensitivity 50 ppb. [C3567]

"A novel tiered sensor fusion approach for terrain characterization and safe landing assessment"

This paper presents a novel, tiered sensor fusion methodology for real-time terrain safety assessment. A combination of active and passive sensors, specifically, radar, lidar, and camera, operate in three tiers according to their inherent ranges of operation. Low-level terrain features (e.g. slope, roughness) and high-level terrain features (e.g. hills, craters) are integrated using principles of reasoning under uncertainty. Three methodologies are used to infer landing safety: fuzzy reasoning, probabilistic reasoning, and evidential reasoning. The safe landing predictions from the three fusion engines are consolidated in a subsequent decision fusion stage aimed at combining the strengths of each fusion methodology. Results from simulated spacecraft descents are presented and discussed [C3568]

"The UAVSAR phased array aperture"

The development of a microstrip patch antenna array for an L-band repeat-pass interferometric synthetic aperture radar (InSAR) is discussed in this paper. The instrument will be flown on an unmanned aerial vehicle (UAV) and will provide accurate topographic maps for Earth science by 2007. The antenna operates at a center frequency of 1.2575 GHz and with a bandwidth of 80 MHz, consistent with a number of radar instruments that JPL has previously flown. The antenna is designed to radiate orthogonal linear polarizations for fully-polarimetric measurements. Beam-pointing requirements for repeat-pass SAR interferometry necessitate electronic scanning in azimuth over a range of plusmn20degrees in order to compensate for aircraft yaw. Beam-steering is accomplished by transmit/receive (T/R) modules and a beamforming network implemented in a stripline circuit board. This paper focuses on the electromagnetic design of the antenna tiles and associated interconnects. An important aspect of the design of this antenna is that it has an amplitude taper of 10dB in the elevation direction. This is to reduce multipath reflections from the wing that would otherwise be detrimental to interferometric radar measurements. The amplitude taper is provided by coupling networks in the interconnect circuits as opposed to using attenuators in the T/R modules. Details are given of material choices and fabrication techniques that meet the demanding environmental conditions that the antenna must operate in. Predicted array performance is reported in terms of co-polarized and cross-polarized far-field antenna patterns, and also in terms of active reflection coefficient. Measured performance of a 4-element by 2-element antenna tile is presented [C3569]

"High power electronic scanning millimeter-wave radar system design"

Remote Sensing Solutions, Inc has received NASA funding to design a prototype millimeter-wave radar system that will lead to future generations of large aperture space-borne electronic scanning radars. A scanning millimeter-wave radar is critical tool for improving the remote sensing of the Earth and other bodies in our solar system. Low power solid-state scanning millimeter-wave radar systems cannot provide the necessary sensitivity to detect low reflectivity cloud particles, especially at longer ranges from space. Currently, adequate sensitivity can only be achieved using tube-based transmitters, which severely constrains the system design. Important design details and design trade-offs for a unique frequency-scanned antenna and wide-bandwidth radar system design are presented. The scanning radar design is compatible with the current series of space-qualified Klystron amplifier tubes used for the CloudSat Cloud Profiling Radar (CPR). New tube designs having a wider bandwidth will further improve the antenna efficiency for a given swath size. The prototype radar system design utilizes a 30 cm aperture, which is designed for compatibility with existing aircraft installations. This will allow for rapid demonstration of proof-of-concept. The design can be scaled to larger apertures to provide sufficient sensitivity from low and high earth orbit, and for future missions to other bodies in our solar system such as Titan where the Cassini mission has revealed the presence of volcanic and other clouds [C3570]

"GeoSTAR: developing a new payload for GOES satellites"

The geostationary synthetic thinned aperture radiometer (GeoSTAR) is a new concept for a microwave sounder, intended to be deployed on NOAA's next generation of geostationary weather satellites, the GOES-R series-due to first launch in 2012. This will fill a serious gap in our remote sensing capabilities of long standing-a key capability that NOAA is book keeping at the top of its list of "pre-planned product improvements" for GOES-R-i.e. the most urgently needed additional payload, which will be added as soon as funding has been allocated and programmatic issues resolved. A ground based prototype has been developed at the Jet Propulsion Laboratory, under NASA Instrument Incubator Program sponsorship, and is currently undergoing tests and performance characterization. GeoSTAR is expected to go forward as a space mission within the next decade [C3571]

"Wideband Optical TTD SAR Antenna"

Optical beam forming networks (OBFN) are an interesting alternative for the design of wideband antenna arrays.

They are potentially more power efficient and lighter than their microwave counterparts. These two characteristics make them especially appealing in space remote sensing applications. However, in a practical implementation of OBFN in a real SAR system, different architectural and technological tradeoffs need to be assessed. Taking as an example a free-space OBFN (D. Dolfi et al., 1991) and an existing SAR mission (M. Lisi et al., 1993), this paper studies the impact of different OBFN parameters like scalability, insertion loss and crosstalk in the performance of the antenna array system [C3572]

"Overcoming some of the issues in maintaining large urban area 3D models via a web browser"

This paper discusses recent work, in the VEPs Interreg project, that has been examining how to optimise operator based digital 3D modelling, of urban and rural environments, where the increasing availability of highly accurate LiDAR scanning offers appropriate remote sensed data. From this data bare earth digital terrain models (DTMs) can be processed semi-automatically, then draped with aerial imagery. Although both the resulting DTMs and geo-referenced aerial photography are of increasing detail and availability, buildings and similar structures are difficult to automatically extract at a level of detail that provides a credible sense of presence at street level. The LiDAR data itself is currently not captured often or extensively enough or at a sufficient level of detail that it could be relied on to keep VR analogues of real places up to date through an automated process alone, without additional modelling. Significant costs in modelling and updating urban settings to convey presence thus remain, be it through a combination of photogrammetry, CAD drawings and manual editing. It is argued that these costs are likely to limit large area 3D modelling to either broad brush overviews (as provided by Google Earth) or to credible presence models in those few locations where the high cost is justifiable, but in which, once the primary purpose of the model has been served, acceptance of the continuing cost of maintenance to reflect change is unlikely. Where updating of high presence models does happen this paper puts forward the view that currently, due to cost, it is likely to be piecemeal and take place over a long period of time. The paper describes one approach to reducing these costs by empowering heterogeneous groups of people to share the tasks of digitising and updating buildings that convey a credible sense of presence [C3573]

"Moving target indication with dual frequency millimeter wave SAR"

Ground moving target indication (GMTI) for synthetic aperture radar (SAR) provides information on non-static objects in a static ground scene. An efficient approach for GMTI is the use of multi-channel SAR systems for a space- and time-variant analysis of moving targets. This allows the indication, correction of position errors, and estimation of radial velocity components for moving targets in the SAR image. All three steps are possible because of the Doppler frequency shift in the radar signal caused by the radial target movement. Our work focuses on the millimeter wave (mmW) SAR system MEMPHIS with multi-channel amplitude-comparison monopulse data recording and the ability to use carrier frequencies of 35 and 94 GHz simultaneously, making it a dual frequency multi-channel SAR. Our discussions include mmW specific SAR GMTI considerations and an adaptive algorithm to collect information on moving targets with a mmW monopulse radar, and GMTI blind speed elimination and target velocity ambiguity resolving by dual frequency SAR. For an experiment with MEMPHIS, frequency spectra, processed SAR images with position corrected moving targets, and accurate target velocities and positions are presented to verify the developed algorithm. [C3574]

"Synergy Between Dual-Frequency Altimeters and Radiometers for Precipitation Studies"

Dual-frequency altimeter measurements can accurately detect rain events and can also be used to infer quantitative values. However, the accuracy of the rain rate estimate has been limited by the uncertainty in the height of the freezing level (FL) necessary to infer the surface rain rate from the measured signal attenuation. Altimetric satellites also carry microwave radiometers designed to correct for atmospheric water effects. Using a radiative transfer model and simplified rainy atmospheres, the microwave brightness temperatures can be inverted in terms of FL height. The surface rain rate is then computed from the altimeter attenuation and the radiometer FL. The rain climatology is computed for the three altimeters currently in operation using a mixed log-normal distribution. Comparison with the GPCP and SSM/I climatologies shows that the use of FL greatly improves the altimeter climatology which is of the same quality as SSM/I one for annual mean. The merging of the three altimeters is investigated. The resulting monthly mean rain rates are comparable to those derived from SSM/I [C3575]

"Proceedings. The 11th International Conference on Mathematical Methods in Electromagnetic Theory (IEEE Cat. No. 06EX1428)"

The following topics are dealt with: antennas; inverse problems; radar cross-sections and remote sensing; nanoelectromagnetics; asymptotic methods; computational techniques; propagation; time-domain methods; waveguide circuits; bandgap components; metamaterials; boundary value problems; nonclassical

electromagnetics; electromagnetic theory; scattering and diffraction; eigenvalue problems; nonclassical electrodynamics; gratings; frequency selective surfaces; and integral equation techniques [C3576]

"Extraction of the signature of a buried object using GPR"

This paper deals with the possibility of remotely detecting buried objects using impulse radiating GPR. Most GPR systems involve the B-scan or the C-scan of the ground requiring the usage of advanced imaging techniques. Identification of a buried target is done using only a single snapshot of the ground. An electromagnetic pulse is sent into the ground from a transmitting antenna. The target reflects the pulse and the reflection is received by a receiving antenna. A single temporal scan of the ground is utilized for identification of the target characteristics. The antenna responses are deconvolved out from the receiver response. The deconvolution is carried out by using the conjugate gradient method. Finally, the target response is identified by extracting the natural resonance frequencies by applying the matrix pencil method on the transient waveform. Successful identification of buried targets is achieved through this methodology. [C3577]

"L-Band Active and Passive Sensing of Soil Moisture through Forests"

Remote sensing of soil moisture under a mature forest canopy by active and passive techniques is discussed. Emphasis is placed on examining the sensitivity of the backscattering coefficient and the brightness temperature to soil moisture variations. The effects of the underlying surface roughness of the forest floor on these sensitivities are addressed. The backscattering coefficient from the forest is modeled using the distorted Born approximation. Using this method the backscatter response is decomposed into a direct or volume scattering component, an interaction component between the vegetation and the average surface, an interaction component between the vegetation and the surface fluctuations and finally direct backscatter from the surface attenuated by the vegetation. Peak's method is used to determine the brightness temperature. The models are validated using ground truth and remote sensing data taken during the Forest Ecosystem Dynamics (FED) experiment conducted near Rowland, Maine, USA in 1990. During this period, the AIRSAR synthetic aperture radar and the Push Broom Microwave Radiometer overflew the Rowland area collecting data. Once the model predictions are compared with the passive and active data, the results of a sensitivity analysis involving soil moisture and surface roughness will be presented [C3578]

"IWRAP: the Imaging Wind and Rain Airborne Profiler for remote sensing of the ocean and the atmospheric boundary layer within tropical cyclones"

IWRAP, the Imaging Wind and Rain Airborne Profiler, is the first high-resolution dual-band airborne Doppler radar designed to study the inner core of tropical cyclones (TCs). IWRAP is currently operated from a National Oceanic and Atmospheric Administration (NOAA) WP-3D aircraft during missions through TCs and severe ocean storms. The system is designed to provide high-resolution, dual-polarized, multi-beam C- and Ku-band reflectivity and Doppler velocity profiles of the atmospheric boundary layer within the inner core precipitation bands of TCs and to study the effects precipitation has on ocean wind scatterometry as it applies to TCs. This dual-wavelength system also provides for the use of differential attenuation techniques to derive the rainfall rate and to characterize the drops size distribution (DSD) within TCs. This prototype has demonstrated its capability to measure the wind field and the rainfall rate over the range of winds and rain rates usually present in this kind of scenario, and has served as a proof of concept for the design of similar instruments aboard other platforms such as unmanned aerial vehicles (UAV) flying at high altitudes, as well as for spaceborne applications. IWRAP implements a very unique measurement strategy, it profiles simultaneously at four separate incidence angles (approximately 30, 35, 40 and 50 degrees) while conically scanning at 60 RPM. A summary of the principles of operation and the system design of the instrument is given, and examples of IWRAP's unique imaging capabilities are presented and compared against high density sequences of GPS dropsondes and other radars aboard the aircraft. To our knowledge, the examples that will be presented include the highest-resolution measurements of the boundary layer winds in a hurricane ever obtained [C3579]

"Spacecraft hazard avoidance utilizing structured light"

At JPL, a <5 kg free-flying micro-inspector spacecraft is being designed for host-vehicle inspection. The spacecraft includes a hazard avoidance sensor to navigate relative to the vehicle being inspected. Structured light was selected for hazard avoidance because of its low mass and cost. Structured light is a method of remote sensing 3-dimensional structure of the proximity utilizing a laser, a grating, and a single regular APS camera. The laser beam is split into 400 different beams by a grating to form a regular spaced grid of laser beams that are projected into the field of view of an APS camera. The laser source and the APS camera are separated forming the base of a triangle. The distance to all beam intersections of the host are calculated based on triangulation [C3580]

"Multi-Sensor Microwave Soil Moisture Remote Sensing: NASA's Combined Radar/Radiometer (ComRAD) System"

This paper describes the development of a ground-based radar/radiometer system called ComRAD. The system under development is an outgrowth of a network analyzer-based L, C, and X band polarimetric radar system developed jointly by NASA/GSFC and the George Washington University. The system is mounted on a 19-m hydraulic boom truck and has provided reliable calibrated radar data in soil moisture field campaigns across the United States since the early 1990's. The truck instrument system is now being upgraded with the addition of a dual polarized 1.4 GHz total power radiometer. The new system includes a temperature monitoring and control system to keep the radiometer at a constant temperature. All front-end components have been placed on an aluminium plate whose temperature stability has been achieved by using Peltier cells. Periodic switching to the internal noise sources is used to reduce the influence of gain variations in the output voltage. A novel broadband stacked-patch dual-polarized feed resonates at both the 1.4 GHz radiometer and 1.25 GHz radar frequencies, enabling both the radar and the radiometer to share the same 1.22-m parabolic dish antenna. Having the radar and radiometer utilize the same antenna with the same 12deg field of view greatly simplifies the development of active/passive microwave retrieval algorithms. With these new capabilities, ComRAD will be an important tool in examining Earth science research topics such as the synergistic effects between active/passive microwave sensors for soil moisture estimation in the presence of vegetation [C3581]

"A New Approach to Improve Coherence in SAR/GMTI Processing of Distributed Micro-satellites Systems"

In order to improve the capability of clutter cancellation in bistatic SAR/GMTI processing, a new method to improve coherence between two sets of echoes from two receivers is developed based on the distributed micro-satellites system with the constellation of SAR-train. According to the idea of equivalent mono-static, the coherence improvement can be achieved by match filter to the spectra of equivalent squint angle, i.e. the bistatic bisector. In this way, the decorrelation component induced by the along-track baseline is removed. Because of Doppler equals to equivalent radial wave multiplied by equivalent squint angle spectra, this method can be realized in two steps, as the first step the compensation of equivalent radial wave number error is achieved through range spectra cut and shift of the narrow band echoes. As the second step, the Doppler spectra not overlapped should be removed, by which the bistatic bisector can be aligned. Simulation results show the decorrelation components introduced by the along-track baseline can be fully eliminated using this method [C3582]

"Using Boosting to Improve Oil Spill Detection in SAR Images"

Marine surveillance system which uses synthetic aperture radar (SAR) images to oil spill detection must minimize false alarms in order to improve its reliability. This paper presents an application that uses boosting method to minimize misclassification and yields better generalization. Different feature sets were applied to neural network classifiers and its performance compared do boosting methods. The experiments reached substantial improvement in the classification accuracy to discriminate oil spots from the look-alike ones [C3583]

"Comparing Different Localization Approaches of the Radon Transform for Road Centerline Extraction from Classified Satellite Imagery"

Using a local Radon transform helps improve the performance of the Radon transform-based linear feature detection. In this paper, three different approaches to localize the Radon transform are implemented and compared in the context of road centerline extraction from classified satellite imagery [C3584]

"Research and Application on Real-time Acquirement Technique of OpenFlight Digital Terrain Based On Grid"

Radar system simulation based on digital terrain is a new foreground of radar simulation. However, acquirement of enormous terrain data becomes a difficulty in radar simulation which influences the real time of simulation. The paper analyzes the limitation of structure of openflight digital terrain in radar simulation in detail. A new method for transforming terrain data to grid data is put forward. The method is applied to the design of a certain airborne radar simulation. It is shown that the method successfully solves the problem of digital terrain acquirement and improves the system performance [C3585]

"A New Approach for DEM Generation Based on Polarimetric SAR Interferometry"

In this paper, the polarimetric information is used to register the interferometric images and enhance the

interferometric phase. The similarity parameter is employed to register the images. This approach is more robust than the traditional method. The combination of the best phase among three polarimetric channels can be used to improve the phase quality and reduce the residues. Then a new phase filter based on the weighted median filter is proposed. This filter is used to reduce the residues sufficiently and make phase unwrapping easily. Finally, a multi-path method is introduced to unwrap the phase [C3586]

"Signal Processing Method for Distributed SAR Imaging Improvement"

A commonly known design requirement for synthetic aperture radar (SAR) systems is the minimum SAR antenna area constraint, and there are range-Doppler ambiguities. So in conventional SAR, there is a well known trade-off between unambiguous swathwidth and resolution. However, if spatial sampling is added, the maximum unambiguous illumination area will increase with the number of receivers; through this method multiple beams can be formed to reject range-Doppler ambiguities. As is well known, multistatic synthetic aperture radar operates with multiple receive antennas distributed among different platforms which can be used to increase the special sampling. And constellations of formation-flying microsatellites are currently under study in the Held of remote sensing. Basing on this multistatic modes, this paper is intended to study signal processing method of SAR Doppler ambiguities resolving to improve image quality [C3587]

"A perceptive uniform pseudo-color coding method of SAR images"

Synthetic aperture radar (SAR) can provide all-time and all-weather surveying of the earth, and SAR images often display in gray scale. Considering the fact that gray scale only has 60 to 90 just noticeable differences (JNDs), while color scale might give up to 500 JNDs, a new pseudo-color coding method based on CIE $L^*a^*b^*$ perceptive uniform color space is introduced for SAR image display. The method is a uniform color space in that equal difference of gray value is approximately equivalent to equal chromatism difference. The primary strongpoint of this method is that it does not generate distortion of SAR image. What's more, it can include all the information of a gray scale SAR image while improve the visual perception and cognitive ability of SAR image. Also, the Kullback-Leibler (KL) divergence is introduced to evaluate quality of this pseudo-coding method. Three SAR images of different terrain are tested with both CIE $L^*a^*b^*$ perceptive uniform pseudo-color coding method and the mostly commonly used rainbow pseudo-color coding method. Results indicate that the first is superior [C3588]

"Topography Adaptive Filtering of Phase Image Based On Residue Matrix"

At present, SAR interferometry (InSAR) is the foreland of radar remote sensing. This paper will suggest residual matrix used as the factor of filtering to interferometric phase image. Two kinds of filters for phase image are modified through utilizing residual matrix. The modified filters have different filter intensity in different areas of the phase image according to noise condition. Therefore they can realize an adaptive filtering effect and preserve topographical information and fringes in areas with steep slopes. The implementation of the filters is described in detail and the effectiveness is tested by using the interferometric phase data generated from ERS-1 repeat-pass [C3589]

"Novel Method for SAR Image Segmentation with Application to Bridge Detection"

A new method for SAR image segmentation is proposed in this paper. Region segmentation can be achieved by contour tracking, and we use the general Bayesian tracking framework to solve this problem. Due to the non-linearity of the tracking problem and the non-Gaussian noise of SAR image, Monte Carlo based particle filtering algorithm is adopted to obtain the Bayesian optimal solution. Based on the tracking framework, a particle filter based contour tracking method is proposed for region segmentation in SAR images. In this method, each particle is assigned to a linear segment with specific location and direction. The response of the local edge detector is used to calculate the particle weight while the global contextual knowledge, such as the smoothness of the region boundary, is guaranteed by the propagation of particles. The proposed method is employed for river boundary extraction on the SAR image. Furthermore, bridges over a river are detected [C3590]

"High Resolution Radar Imaging of the Sea Surface"

Applications are reviewed of high resolution radar sea surface imagery to remote sensing, wide area surveillance, target detection and tracking. The limitations imposed by sea surface motion on SAR imaging are discussed and illustrated, along with methods to exploit the motion such as along track interferometry. Ships on the sea are subject to roll, pitch and yaw motions, which defocus SAR imagery; analysis and signal processing to characterise and overcome the difficulties are described. Real aperture images of the sea are shown to contain detailed information on the propagation of surface waves, which may be used in algorithms to detect anomalies such as small surface vessel; these are also described and demonstrated [C3591]

"Novel Techniques for Error Minimization in SAR RF and Interferometric Signal Processing"

A lot of efforts have been put in so far in the satellite/air borne SAR interferometric RF signal processing to develop easier yet accurate methods of generating topographic maps and other earth deformations due natural hazards. However, there still remain short comings while taking into account certain important factors during various processing steps, which cause un-bearable errors. In this paper efforts have been made to encompass all areas in the conventional SAR interferometry where the processing errors are encountered. Methods and relationships have been developed including use of different RF wave polarizations to obtain accurate topographic maps and invert the errors. The relevant processing steps have been identified and recommendations have been made with the help of simulation results to bridge the gaps between the desired and the actual SAR signal processing. The necessary steps involved in wave transmission and processing the received data to the geometrically compensated digital models have been explained with the help of developed algorithms and resulting simulations [C3592]

"Computational Model of the Doppler Spectrum of Radar Returns from Rain"

This paper presents the computational model of Doppler spectrum that considers the influence of the shape of turbulence spectrum onto the spectrum of echo-signal from rain at different intensity of turbulence and rain rate. The inertia of raindrops is taken into account. The developed approach allows calculating Doppler spectrum at different conditions. Validation with real data is done [C3593]

"Surface Current Extraction by Onboard High Frequency SAR"

To meet the requirement of extracting sea surface current information by a single station, we present the new concept of high frequency SAR (HF-SAR), and consider the feasibility of extracting sea surface current by HF-SAR. Firstly the implementation aspects are described, then system model and velocity estimation algorithm are designed, and finally simulation model to extract surface current is implemented on a single resolution cell. Additive complex Gaussian noise is included in the model of SAR echo, and also an iterative approach is adopted to estimate the parameters of chirp signals. Simulation results show that by estimating the phase parameters from azimuth echoes, the velocity estimates of surface current are obtained, and the precision is enough to meet the requirements. It indicates that HF-SAR is theoretically feasible to be used in sea surface current extraction [C3594]

"Use of Neural Network for Turbulence and Precipitation Classification Procedure"

This paper describes a methodology of precipitation and turbulence classification based on radar echo signal features measured by polarimetric radar. A neural network classifier is used to distinguish between different precipitation and turbulence classes. The classification procedure takes a decision about the type of precipitation and turbulence intensity by simultaneous feature consideration. In this paper the turbulence classification using multi-parametric decision technique is described [C3595]

"Polarimetric Radar Pulse Echoes from Lunar Regolith Layer with Scatter Inhomogeneity and Rough Interfaces"

To explore the potential utilities of lower frequency (L band) radar pulse for lunar exploration, a theoretical model of stratified lunar regolith media and numerical simulation of polarimetric radar pulse echoes are developed. The lunar regolith layer consists of the low lossy regolith layer with randomly rough top and bottom interfaces, and a layer of random stone-scatterers (spatially oriented oblate spheroids are assumed) is embedded and overlays the underlying rock media. The time domain Mueller matrix solution is derived to take account for scattering mechanisms of the stratified scatter media. Temporal characteristics and structure of the polarimetric echo profile as functional dependence on model parameters such as the layer thickness and the content of $\text{FeO}+\text{TiO}_2$, are numerically simulated, and well display an image of regolith structures. It demonstrates a potential new way to explore moon surface in future. [C3596]

"InSAR Image Registration Using Modified Correlation Coefficient Algorithm"

In this paper, a modified correlation coefficient algorithm is proposed to accomplish image-registration for repeat-pass SAR interferometry. This algorithm utilizes a new definition of correlation coefficient to improve the calculation accuracy of offset between two images. Our simulation shows that Doppler centroid has a significant influence on the correlation coefficient and it should be removed before registration. SIR-C/X X- band experimental data has been processed to demonstrate the effect of the proposed algorithm. Also quantitative comparison between this paper's results and the results from the maximum-spectrum method is presented to

show the improvement. [C3597]

"Automatic Land-mine Detection System using Adaptive Sensing with Vector GPR"

Ground penetrating radar (GPR) is a promising sensor for landmine detection, but there are two major problems to overcome. One is the non-planer (e.g. rough and/or undulating) ground surface. It remains irremovable clutters on a sub-surface image output from GPR. Geography adaptive scanning is useful to image objects beneath non-planer ground surface. The other problem is the distance between the antennas of GPR. When imaging the small objects such as an anti-personnel landmine close to antennas, it increases the nonlinearity of the relationship between the time for propagation and the depth of a buried object. In this paper, we modify Kirchhoff migration so as to account for not only the variation of height and pose of the sensor head, but also the antennas alignment of the vector radar. The validity of this method is discussed through application to the signals acquired in experiments [C3598]

"Multi-mode Microwave Remote Sensing Antenna Subsystem on Satellites"

This paper presents briefly design, assembly and testing of the multi-mode microwave remote sensing antenna subsystem of China. It concentrates active and passive microwave remote sensors. A prime focus paraboloid reflector, with the diameter of 600 mm, is applied as the altimeter antenna. The scatterometer antennas consist of two prime-focus reflectors, which take conical scanning and form two pencil beams orthogonal in space and polarization. The radiometer antenna is an offset paraboloid reflector with multi-frequency, dual polarization and common aperture feed. Computer aided integrated design for multi discipline, advanced assembly and holographic measuring techniques, which are used to achieve high accuracy, are also introduced. [C3599]

"A New Approach for Ship Detection in SAR Imagery Based on Convolution between Different Polarization Channels"

A new approach is proposed for ship detection with SAR (Synthetic Aperture Radar) images based on the convolution between different polarimetric channels. The method takes advantages of different statistical behaviors among ships and surrounding ocean, interpreting the information through the convolution in order to provide a more reliable detection. The simulations show that the convolution is sensitive to the size and shape of ships not to sea state. The method can be used under high sea state and have no relation to the movement of ships. Moreover, the method is general which is not only suitable for dual polarization data but also for full polarization data. The detection performance over both simulated and real images confirms the robustness of the method. [C3600]

"Preconditioned Multilevel Fast Inhomogeneous Plane Wave Algorithm for Solving Electromagnetic Scattering Problems"

A mesh-neighbor preconditioner is implemented into the multilevel fast inhomogeneous plane wave algorithm (MLFIPWA), to solve three dimensional electromagnetic scattering problems more efficiently. The spectrum integration of the Green's function and grouping technique are used in FIPWA to translate the direct source and field interaction into aggregation, translation and disaggregation, to accelerate the matrix-vector multiplication. The computation complexity of this algorithm is $O(N^4/3)$. By applying a multilevel strategy, this complexity can be reduced to $O(N \log N)$. To further speed up the solution process, a mesh-neighbor preconditioner is applied into this fast algorithm. Numerical results show the accuracy and efficiency of this algorithm. [C3601]

"Laser Radar Cross-Section of Conducting Targets Using Horizontal Polarization"

This work presents a study to handle the behavior of radar cross section (RCS) of partially convex targets of large sizes up to five wavelengths in free space. The nature of incident wave is an important factor in the remote sensing and radar detection applications. To investigate the effects of incident wave nature on the RCS, scattering problems of plane and beam wave incidences are considered. Targets are taking large sizes to be bigger enough than the beam width with putting into consideration a horizontal incident wave polarization (E-wave incidence). The effects of the target configuration together with the beam width on the laser RCS compared to the case with the plane wave incidence are numerically analyzed. Therefore, we will be able to have some sort of control on radar detection using beam wave incidence. . [C3602]

"Analysis of Squint Angle in Point Target Assessment"

This paper analyzes the characteristics of impulse response function in squinted geometry. Based on this analysis the expression of side-lobe's slant angle is deduced explicitly. In the course of point target assessment, the proposed method picks the declining one-dimensional profiles by this angle. The simulation results show that

the method is highly effective and practical compared with the line-by-line searching method [C3603]

"Research on Echo Simulation of Space-borne Bistatic SAR"

In order to research imaging algorithm problems of space-borne bistatic SAR, it is necessary to simulate echo data of actual scene. On the basis of point target simulation, a method of simulating space-borne bistatic SAR raw echo data utilizing gray image data of airborne SAR is presented in this paper. First of all, gray data of airborne SAR image is added and averaged to compute different targets RCS. Then, raw data of actual scene is generated using the model of scene echo signal of space-borne bistatic SAR. Finally, imaging processing is fulfilled utilizing BP algorithm toward echo data. The imaging result verifies the correctness of this simulation method [C3604]

"Building Recognition and Reconstruction from Aerial Imagery and LIDAR Data"

Building information is extremely important for many applications such as urban planning, telecommunication, or environment monitoring etc. Previous attempts at automating the building detection process from images has met with limited success due to (1) spectral similarities between building rooftops and roads, (2) lack of spatial processing parameters for building geometry. A novel approach is presented in this paper based on aerial images and range images. By using the height information provided by range images, buildings could be easily distinguish from other objects (e.g. roads). A new perceptual grouping technique is introduced for the purpose of organizing the low-level features (arcs and line segments) which are extracted from aerial images. The final contours of the buildings are generated with the help of regularization algorithm. After reconstruction, a refinement is applied by an object-based perceptual grouping method. Finally, the approach is applied to two datasets and promising experimental results are shown [C3605]

"A Novel Fusion and Target Detection Method of Airborne SAR Images and Optical Images"

In this paper, the main problems of fusion techniques of airborne SAR and optical images are discussed. First, the regions of interest for target candidates in each mono-source data are independently segmented, and then the fusion is processed during the decision stage. A novel detection method of fusion images of targets which is based on "3S" technology is proposed. The experimental results demonstrate the advantage of this method [C3606]

"Experimental System and Experimental Results for Coast-ship Bi/multistatic Ground-wave Over-the-horizon Radar"

This paper deals with a novel bi/multistatic radar system, which is spoken of as the bi/multistatic ground-wave (GW) over-the-horizon (OTH) radar based on the technique of synthetic impulse and aperture radar (SIAR). This radar can also be named as multi-input single-output (MISO) radar which uses several antennas to transmit orthogonal waves in one sector or the whole space and uses an omnidirectional antenna to receive target echoes. The receiver is installed on a moving ship and the transmit beams are formed through space-time signal processing in the receiver, which is the same as "passive position" without emitting energy. In this paper, an introduction is given to the operating principle of this radar as well as the experimental system and the results obtained [C3607]

"A Kind of Dual-Channel GMTI Real-Time Processing Method Based on Frequency DPCA"

In this paper, current situation of GMTI technology would be discussed firstly. After that, a kind of dual-channel GMTI real-time processing method based on frequency DPCA would be presented. After analyzed the principle of clutter-suppression and the diagram of the algorithm, the processing result to both simulation data and real echo data from X-band dual-channel SAR system by the algorithm would be presented. The results proved this method is reasonable and reliable [C3608]

"A New Algorithm of Target Classification Based on Maximum and Minimum Polarizations"

The polarization signature of a given pixel in a radar image represents scattering mechanisms from various scattering elements. This paper presents an analysis of maximum and minimum polarizations of five kinds of polarization signatures: co-polarized, cross-polarized, completely polarized, completely unpolarized, and total available power signatures. We propose a new algorithm of target classification based on these maximum and minimum polarizations, then, conduct the experiment on the measured polarimetric SAR data. Experimental results show that this algorithm is robust to pixel-by-pixel target classification in radar images [C3609]

"High Performance MM-Wave Radar Techniques"

The Millimetre Wave and High-Field ESR Group at St Andrews has recently been developing a range of mm-wave radar technologies that have yielded the successful development of various advanced prototype systems exhibiting state-of-the-art performance, which are reviewed here. These include a long-range, high resolution FMCW imaging radar for volcano mapping, and a nanosecond pulsed, coherent, radar-like system developed for spectroscopy [C3610]

"Automatic SAR Image Registration by Using Element Triangle Invariants"

Due to the presence of speckle in synthetic aperture radar (SAR) image, the existing registration algorithms, which are successfully used in optical remote sensing image, are usually not applicable to it directly. An automatic SAR image registration algorithm is proposed in this paper. Firstly, the element triangles are constructed from the point targets detected from the SAR images; then they are matched by integrating triangle moment invariance proposed in this paper and region invariant moments; finally, the LMSE algorithm is used to estimate the affine transformation parameters, thus the SAR images can be registered automatically. The proposed algorithm is evaluated and compared with the existing methods by means of invariant moments (IM) and affine moment invariants (AMI). It is shown from Monte-Carlo simulations that the proposed algorithm is robust to detection error and partial correspondence of control points (CPs), and has higher ratio of correct matching than the methods using IM or AMI. Experimental results show that the proposed new algorithm is not only valid in the automatic registration of SAR images, but also can avoid the influence caused by speckle in feature detection and feature matching process [C3611]

"A case based reasoning data fusion scheme: application to offshore wind energy resource mapping"

A data fusion scheme is proposed for wind energy resource mapping at high spatial resolution. The resource assessment is based on wind speed and direction measurements. Remotely sensed data is a solution to get wind observations offshore. However, high spatial resolution data do not have a sufficient repetitiveness to establish reliable wind energy resource maps. The scheme proposed in this paper uses these measurements as typical situations which have to be merged with low spatial resolution data having a sufficient temporal repetitiveness. The fusion process builds a library of typical cases. To these typical cases are associated typical fields representing the information to be merged with the corresponding low spatial resolution data. In this paper, we give, firstly, the general fusion scheme. Then, we present the different tools needed by this process. We focus particularly on the definition of the typical situations. The retrieval of these situations is achieved by a classification process. Finally, some prospects are given [C3612]

"Assessment of Soil Parameter Estimation Errors for Fusion of Multichannel Radar Measurements"

The application of multichannel radar measurement techniques for estimation of bare soil parameters is based on different principles of radiowave and soil surface interaction depending on radiowave frequency, polarisation and incidence angle. The accuracy of soil parameter estimation depends on the number of radar measurements and the choice of radiowave parameters. Random and systematic errors present in radar data may also have the impact on estimation results. To improve the accuracy of soil parameters estimation by fusion of multichannel radar data we propose a new method for assessment of estimation errors. It is based on local linear approximation of the radiowave scattering model and takes into account impairment characteristics, measurement conditions and radar parameters. This new method is applied to an example to illustrate how the estimation accuracy of soil moisture and roughness parameters can be improved by optimising the radar operating frequencies [C3613]

"Assessment of Multi-Sensor Neural Image Fusion and Fused Data Mining for Land Cover Classification"

Recent studies suggest that the combination of imagery from earth observation satellites with complementary spectral, spatial, and temporal information may provide improved land cover classification performance. This paper assesses the benefits of new biologically-based image fusion and fused data mining methods for improving discrimination between spectrally-similar land cover classes using multi-spectral, multi-sensor, and multi-temporal imagery. For this investigation multi-season Landsat and Radarsat imagery of a forest region in central New York State was processed using opponent-band image fusion, multi-scale visual texture and contour enhancement, and the fuzzy ARTMAP neural classifier. These methods are shown to enable identification of sub-categories of land cover and provide improved classification accuracy compared to traditional statistical methods [C3614]

"Status Report on Predicted Current Measuring Capabilities of the Upcoming German Satellite TerraSAR-X"

The German satellite TerraSAR-X, scheduled for launch in late 2006, will permit high-resolution ocean current measurements by along-track interferometric synthetic aperture radar (along-track InSAR) in various experimental modes of operation, using different subsections of its X-band SAR antenna array with a total length of 4.8 m as individual receive antennas. Depending on antenna and receive chain settings, various InSAR time lags can be realized in combination with different noise levels, single-look resolutions, swath widths, and incidence angles. We give an overview of the possible InSAR modes and evaluate their suitability for current measurements on the basis of simulated data products. Our results indicate that interferometric stripmap data from TerraSAR-X will be clearly superior to the existing first spaceborne along-track InSAR data from the Shuttle Radar Topography Mission (SRTM); accurate current retrievals can be expected at effective spatial resolutions on the order of 500 m and usable swath widths of 15 or 30 km. Under certain conditions, also ScanSAR data with a maximum possible swath width of 100 km will be suitable. Finally, we consider fundamental relations between along-track baseline, instrument noise, and InSAR phase noise and discuss possible InSAR performance improvements of TerraSAR-X follow-on satellites [C3615]

"Ocean Surface Winds from Space-A Collaborative Education Effort"

Ocean surface winds play a significant role in the global ocean-atmosphere system. Surface winds drive the world's ocean currents, transport atmospheric heat and moisture, force nutrient rich upwelling areas, create surface waves and swell, and can reach destructive force in both extratropical and tropical cyclones. Although the oceans cover 70% of the Earth's surface, the network of ocean wind observations obtained from conventional buoys and ships is very sparse. The measurement of ocean surface winds using remote sensing technologies is the only means of obtaining wind information over large portions of the global ocean in a timely manner. The Ocean Surface Vector Winds Team (OSVWT) of the Satellite Oceanography and Climatology Division (SOCD) within the NOAA/NESDIS/Center for Satellite Applications and Research (STAR) has been producing satellite-derived ocean surface wind data since the mid 1990s. Wind products from several remotely sensed sources such as QuikSCAT and WindSat are available in near real time (NRT) on the Internet and are also distributed within NOAA. These wind products are used by operational forecasters, scientific researchers and the marine community. The researchers and forecasters from NOAA Ocean Prediction Center (OPC), the NESDIS STAR Ocean Winds Team and the University Corporation for Atmospheric Research (UCAR) have partnered to increase awareness of the various ocean surface wind vector products available and to develop the educational materials needed to expose these products and to educate teachers at various levels about the latest technology for measuring and interpreting remotely sensed ocean vector winds. To accomplish this it has been proposed to host an educator workshop OPC. This workshop would target educators that train professional and future mariners in meteorology, oceanography and storm avoidance. Teachers from state maritime colleges, federal academies, and professional training institutions would be among those invited--to participate. This workshop would be hosted by both researchers and forecasters and held within an operational forecast environment to promote hands-on experience. This paper will provide background information on current and new ocean surface wind remote sensing technologies, give examples of how products are used within the operational environment, and discuss the development of training material [C3616]

"Fusion of Multi-band SAR Images Based on Contourlet Transform"

Aim at the fusion of multi-band synthetic aperture radar (SAR) images, a new fused method using the contourlet transform is presented. Contourlet transform provides a flexible multiresolution, anisotropy and directional expansion for images. Compared with wavelets, it can afford more efficient presentation of image edges. This is employed for fusing the directional high-frequency coefficients. For the lowpass coefficients, an averaging fusion rule is used. For the directional high-frequency coefficients, the higher value of edge information measurement is used to select the better coefficients for fusion. The proposed method solves the problem of losing edge information for wavelet based fusion method. Finally, the example result of two bands SAR image fusion compared with wavelet fused method shows the vision effect and the statistical evaluation factors for fusion are both improved. [C3617]

"A Remote Aerial Robot for Topographic Survey"

In this paper a seminal system for the topographic survey with an unmanned aerial robot is presented. The proposed system has demonstrated the feasibility of acquiring initial 3D ground models using active laser range sensors on a low-flying helicopter platform. The robot system consists of a remote control helicopter with a laser sensor and a GPS (global positioning system) for collecting ground point data and a post-processing data sub-system for drawing a topographic map. This robot system has many potential applications, such as terrain

modeling, structure inspection or climate and weather measurement, etc. The experiment results verify the proposal robot system for topographic survey [C3618]

"Radar Remote Sensing Images Segmentation Using Fractal Dimension Field"

A new method for image segmentation that makes it possible to divide the image into clusters having different fractal dimension is proposed. Tree-like structure of the algorithm proposed is easy for program implementation and allows making the process of radar images analyzing almost unsupervised. Results of the method testing on real radar images are presented [C3619]

"A lightweight, ultra wideband polarimetric W-band radar with high resolution for environmental applications"

A lightweight, ultra wideband (UWB), polarimetric millimetre wave 94 GHz radar with high resolution is described for environmental and other short range applications. UWB and random signal W-band radar technologies are combined with polarimetric and super-resolution processing techniques to provide a compact remote sensing capability that is man-portable. An all-weather capability is provided for accurate and high resolution measurement of the physical size, relative distance, bearing, altitude, direction, velocity and classification of stationary and moving objects at ranges of less than 10 km. Attributed information relating to the sensed environment such as local surface features, water depth, terrain topology and object classification is derived from remote millimetre wave radar measurements including polarization [C3620]

"SAR Model Based Regularization Methods for Image Texture Classification"

Image texture classification and segmentation is a main topic in the analysis of many types of images. People usually use the least squares estimation (LSE) for analyzing SAR textures. But we find that the LSE is unstable in practical computation. Therefore, in this paper we present regularization methods for image texture classification and segmentation. Regularization is such a technique which can successfully suppress the instability due to noise or truncation error when computing. Several regularization techniques, including standard regularization (SR), penalized regularization (PR) and total variation based regularization (TVR), are exhibited to reduce instability in texture extraction. Experiment results demonstrate that the regularization methods are superior to LSE and seem to be promising in practical applications [C3621]

"Remote Sensing Target Recognition Based on Contourlet and Kernel Fisher Discriminant"

An efficient feature extraction method for remote sensing target recognition was proposed in this paper, which was based on contourlet and kernel Fisher discriminant (KFD). After the contourlet decomposition, the contourlet features are fused (the weight for fusion is chosen by cross validation), and then KFD was used for further feature extraction, finally k-nearest-neighbor (KNN) was used for classification. Experimental results show that the proposed feature extraction method reach a higher correct rate than KFD and the method which use KFD on the lowpass filtered images. Moreover, when dealing with large scale images our method achieves a lower computation complexity than KFD [C3622]

"Level Set Evolution Based Logic Fusion: A Novel Man-made Objects Segmentation from Radar Image"

Our purpose is to explore an application of level set evolution theory to seek the solution of objects (as bridge or dam) segmentation above river from radar imagery with unwelcome effects. We present a novel level set evolution formulation for improving accuracy of segmentation. Critically, a logic fusion term is constructed using logic operators defining in multi-source satellite imagery with high precision of registration by logical operations, such as union, intersection and negation, then incorporated into the general evolution equation. Under the logic framework, we combine diverse features both from radar and optical image into evolution equation so as to overcome disadvantages, such as missing information, image artifacts and weak boundary and help objects segmentation to radar image. Results of experiments on pairs of ERS and LANDSAT imagery and pairs of RADARSAT and SPOT imagery, demonstrate effectiveness and robust of our method to objects segmentation in complex cases [C3623]

"Separation of Micro-Doppler Signal Using an Extended Hough Transform"

In this paper, we present a separation method of micro-Doppler signal based on the Hough transform which is widely used in the image processing. Mechanical vibration or rotation of structures in a target may induce frequency modulation on returned signals and generate side-bands about the center frequency of the target's body, which is know as the micro-Doppler phenomenon. Then the body image will be contaminated due to the

interference from the rotating parts. Using an extended Hough transform, the spectrums of the rotating parts of the target can be eliminated from the spectrogram of the target. A computer simulation is given to illustrate the effectiveness of the proposed method [C3624]

"Detection of Roads in SAR Images using Particle Filter"

A novel method is presented to detect roads in synthetic aperture radar (SAR) images. A multi-segmented poly-line model is introduced to provide a more accurate description of the road as well as to ensure the road curve's smoothness in the model level. We then solve the road detection problem using the Bayesian tracking theory, where the particle filtering algorithm is adopted to provide a simple and consistent framework. The effectiveness and robustness of the proposed method is demonstrated by experimental results [C3625]

"2006 IEEE International Conference on Image Processing"

The following topics are dealt with: source/channel coding; distributed image and video coding; biomedical image segmentation; steganography and steganalysis; content summarization and clustering; fingerprint and iris analysis; image registration/alignment and mosaicking; stereoscopic and 3-D coding; visual tracking; deblurring and image restoration; face/facial expression detection and recognition; interpolation and inpainting; network-aware multimedia processing and communications; edge detection; transcoding; machine learning; image fusion; video networking and communications; watermarking; low-level indexing and retrieval of images; wavelets and filter banks; video streaming; video surveillance; soft computing in image processing; authentication and cryptography; forensics; radar imaging; block matching-based motion estimation; knowledge-based image processing for classification and recognition; biometrics; magnetic resonance imaging; image enhancement; image quality assessment; 3DTV: extraction, representation, compression and transmission; remote sensing [C3626]

"A Remote Imaging System Based on Reflected GPS Signals"

This paper describes a method for utilizing reflected Global Positioning System (GPS) signals to form an image of targets within a region of interest. The principle is based upon a type of bi-static synthetic aperture radar (SAR) in which a matched filter technique is employed to perform the image reconstruction. This method relies upon the fact that each component of the received signal resulting from a reflection from an individual target is subjected to a unique chirp. A major challenge to be tackled is the appalling signal to noise ratio associated with the received reflected GPS signals. Another difficulty is the masking of the reflected signals by power in the tails of the autocorrelation function of the direct signals which cannot be totally suppressed. Moreover, the reconstruction method results in an undesirable point spread function (PSF) which seriously smears the reconstructed image. We simulate the entire GPS signal generation and image reconstruction process as faithfully as possible within the limitations of the available computational effort. We are able to demonstrate that a spatial resolution of the order of the L1 wavelength (19 cm) is theoretically possible from realistic observation distances provided that sufficient coherent correlator integration time is allowed and that the direct signals can be sufficiently suppressed. For the rather simplified organization of targets within the simulation we are able to show that the image smeared by the PSF is able to be cleaned by means of a Wiener filter based deconvolution method. [C3627]

"Matching Radar and Satellite Images Employing the Hausdorff Distance for Ship Positioning and Trajectory Estimation"

The paper describes a technique to match satellite and radar images using the Hausdorff distance (HD). Minimization of the average of a truncated array of sorted Hausdorff distances is used to get estimates for the radar location, together with sensor bias errors and its platform speed vector. The technique is applied to maritime navigation, where geo-referenced satellite images (UTM) are matched to radar scan images. Good estimates are obtained for these variables, thus providing an alternative method to obtain a vehicle's location in GPS-denied environments or for indoor autonomous navigation [C3628]

"TarsierГ,B®, a unique Radar for Helping to keep Debris off Airport Runways"

The Tarsierreg millimetre wave FMCW radar is a unique system that has been developed by QinetiQ specifically for the detection of unwanted debris on airport runways. The speaker describes the stringent radar requirements, the evaluation of a prototype system and the subsequent full productisation. Examples are shown from the recent installation of four radar units at Vancouver International Airport [C3629]

"Measurement of Speed, Height and Direction of SeaWaves Using Optical Range Sensors"

The present paper proposes a sensing system for the speed, the height and the direction of sea waves. The measurement of the three quantities is achieved using three optical range sensors which are adequately located over the sea near the platform. For realizing this, the sensor outputs are modeled as outputs of a linear dynamic system and a Kalman filter and maximum likelihood method are applied. Not only a case of one sea wave but also a case of two overlapping sea waves with different directions are considered. The validity of the system is finally verified with simulations and experiments [C3630]

"Unifying the Experiment Design and Constrained Regularization Paradigms for Reconstructive Imaging with Remote Sensing Data"

In this paper, the problem of estimating from a finite set of measurements of the radar remotely sensed complex data signals, the power spatial spectrum pattern (SSP) of the wavefield sources distributed in the environment is cast in the framework of Bayesian minimum risk (MR) paradigm unified with the experiment design (ED) regularization technique. The fused MR-ED regularization of the ill-posed nonlinear inverse problem of the SSP reconstruction is performed via incorporating into the MR estimation strategy the projection-regularization ED constraints. The simulation examples are incorporated to illustrate the efficiency of the proposed unified MR-ED technique [C3631]

"Towards a Brillouin-LIDAR for remote sensing of the temperature profile in the ocean"

For remote sensing of temperature profiles in the ocean Brillouin scattering can be exploited as a temperature tracer. Such a lidar system is capable of delivering cost-effective on-line data from an extended region of the ocean compared to conventional in situ techniques. The acquired temperature profiles can give valuable input to climate studies and weather forecasts. In this contribution we present the current status of our experimental setup, consisting of a light source based on a multistage pulsed Yb:doped fiber amplifier and a receiver unit based on an excited state Faraday anomalous dispersion optical filter. Both components are advancements of laboratory experiments and possess the potential to be operated from an aircraft [C3632]

"Studying the Dynamics and Biological Significance of the Hudson River Using an Ocean Observatory"

The Lagrangian Transport and Transformation Experiment (LaTTE) was designed to quantify how physical, biological and chemical processes transform material in a buoyant river plume and to link these processes to wind forced changes in the plume structure. The three LaTTE field programs include a May 2004 pilot, a full scale effort in April 2005, and a final study planned for May 2006. In each field study, dye is released and tracked by two vessels for physical, biological and chemical sampling of the tagged water mass. The field study and data assimilation segments of LaTTE rely on a research-based coastal ocean observatory to provide a temporal and spatial context for these intensive process studies. The observatory includes a shelf-wide observational backbone (international satellites, nested HF Radars, and autonomous underwater gliders) that was locally enhanced with high-resolution relocatable moorings in the New York Bight apex for the process studies. During the experiments, a shore based operations center combined real-time datasets with forecasts from a high-resolution atmospheric model (WRF) and hindcasts from an ocean model (ROMS) to provide adaptive sampling guidance to the research vessels. Results from the April 2005 pilot and the May 2006 process study will be reviewed. During the strong outflows of April 2005, the ebb tide squirts flowing onto the shelf were observed to respond to a strong sea breeze, forming a recirculating eddy just south of the Harbor entrance. The eddy served as an incubator for biological productivity, resulting in high phytoplankton concentrations leading to depleted bottom dissolved oxygen in a location consistent with historical observations. Only a portion of the fresh river water entering the recirculation zone exited as the expected coastal current along the New Jersey shelf. Most of the freshwater was observed to flow cross-shelf along the southern flank of the Hudson Shelf Valley, consistent with historical remote sensing-- data. This newly observed transport pathway can have potentially significant impacts on material transport from the Hudson River plume onto the continental shelf. In 2006, wind driven circulation resulted in the plume advecting south along New Jersey and eventually detaching into two pieces. In 2006, wind driven ROMS forecasts were successful at predicting the transport of the river as validated by the drifters and glider data [C3633]

"On the use of the stochastic matched filter for ship wake detection in SAR images"

Detecting straight patterns like ship wakes on a SAR image is not easy because there is no a priori information on orientation and position, moreover, SAR images are speckle noised. This article describes a ship wake detection technique based on the discrete Radon transform and stochastic matched filtering (SMF) used in detection. The association of these two processing methods leads to a detection algorithm that only requires the knowledge of the second order statistics of the signal and the noise. Experimentation on real SAR images shows

the efficiency of the technique [C3634]

"SeaWinds Scatterometer Wind Vector Retrievals for Hurricane Claudette Using AMSR and NEXRAD To Perform Corrections for Precipitation Effects: Comparison of AMSR and NEXRAD retrievals of rain"

The estimation of sea surface winds near and within hurricanes, with the spatial coverage of a satellite radar (scatterometer), is an important objective for public safety. It is also a significant technical challenge when intense rain is present in the scatterometer Field-Of-View (FOV). The presence of rain affects the measured Ku-band normalized radar cross section (NRCS or SIGMA_0) in three ways: rain, cloud and vapor in the atmosphere attenuate the scatterometer signal; rain backscatter augments the signal that comes from the ocean surface; finally, rain hitting the ocean surface induces surface roughening ("splash") that also augments the wind-related signal from the ocean surface. Scatterometer wind retrievals assume that variations in the the measured SIGMA_0 are solely caused by variations in the wind-induced ocean surface roughening. Hence, any rain-related effects have to be accounted for before the scatterometer measurements in rain can be used to estimate the near-surface wind velocity. The MIDORI-II mission, during 2003, carried five earth-observing sensors including the SeaWinds scatterometer and the Advanced Microwave Scanning Radiometer (AMSR). The latter's six frequency brightness temperatures are collected to derive atmospheric water-related parameters and to measure the sea surface temperature. Since its coverage was closely coincident and collocated with the scatterometer, it provided the opportunity to obtain the precipitation measurements necessary to estimate the attenuation, volume backscatter and surface roughening by the raindrops within the scatterometer beam. Corrections to the scatterometer measurements of ocean surface winds can be pursued with either empirical or physical modeling. While both methods rely on the AMSR-based geophysical retrievals, they differ in how the information is used. The empirical method compares the observed sigmaO to the NCEP-model-wind-inferred SIGMA_0 to estimate the rain corrections (attenuation and backsca--tter that combines the rain backscatter and the "splash") as function of the AMSR-derived geophysical parameters. The physical method estimates the three rain effects separately using parametrized relationships between total liquid water, rain rate, surface roughening, volume attenuation and rain backscatter. As such, the physical method does not take into account the NCEP model winds and the produced corrections are more directly related to the AMSR-derived geophysical parameters. The AMSR was designed to measure atmospheric water-related parameters on a spatial scale comparable to the SeaWinds scatterometer (~25km). Optimal estimates of the volume backscatter and attenuation require a knowledge of the three dimensional distribution of reflectivity on a smaller scale comparable to that of the precipitation. Studies selected near the US coastline enable the much higher resolution NEXRAD reflectivity measurements to help evaluate, understand, and improve the AMSR estimates and to conduct research into the effects of different beam geometries and nonuniform beamfilling of precipitation within the field-of-view of the AMSR and the scatterometer [C3635]

"Satellite-aided Search and Rescue (SAR) System"

To carry out search and rescue of the peoples in distress on the distressed aircrafts/vessels, or on land, at sea or in a remote mountainous region, there are a number of different search and rescue systems and methods that are being used by the different national search and rescue organizations worldwide. In this paper the main terrestrial search and rescue (SAR) system that are in use are discussed in brief and a satellite-aided search and rescue (SAR) system COSPAS-SARSAT is discussed in detail highlighting its benefits over other SAR Systems [C3636]

"Decision Tree Based FPGA-Architecture for Texture Sea State Classification"

The target detection process in sea clutter background involves the use of different types of CFAR (constant false alarm rate) algorithms. These algorithms and their parameters should be configured to obtain the maximum detection probability and minimum false alarm probability at the current sea state (Beaufort scale). This paper present an FPGA-architecture for automatic classification based on texture recognition of sea states. The sea state texture classification allows select the appropriate CFAR algorithm and its parameters for the target detection process. The paper is centered in the hardware implementation for sea state texture classification, based on decision tree. The rules for decision tree are obtained from the analysis of the grey levels co-occurrence matrix features applied in an image of the sea state obtained in a radar scan. Results with simulated and real data are presented and discussed [C3637]

"UWB Radars for Chalenging Applications"

A number of challenging radar applications (such as antipersonnel mine detection and human being detection) has been discussed. In these applications UWB technology has a number of advantages of over the traditional

narrow-band approach, in particular very high positioning accuracy, rigidity to multi-path propagation and target classification abilities. On a number of examples recent advances of UWB technology in radar have been demonstrated and remaining challenges have been discussed [C3638]

"A New Unified Approach to Channel Imbalance and Cross-Talk Calibration of Polarimetric Data"

A new unified approach to channel imbalance and cross-talk calibration of polarimetric data is described. This approach is applied during the SAR image formation, employing the multilook SAR processing technique and the covariance matrix of observed data. This method makes no assumptions about the reciprocity of the distortion model and noise system, and about the presence of dominating target with azimuthal symmetry. The standard linear and nonreciprocal distortion model for the received signal is assumed for each polarimetric image obtained from three looks without overlapping. This leads to a set of equations that relate the observed covariance matrix and the distortion system parameters. The non-linear solution of the calibration parameters is solved by iterative approach based on numerical methods. Fully polarimetric SAR L-band data, acquired by CENSIPAM Airborne R99-SAR on the Tapajos Forest (Brazilian Amazon), was used to evaluate the method as well the polarization signature response of some trihedral corner reflectors deployed in the area. [C3639]

"Monitoring Urban Subsidence in the City of Tianjin (China) by Differential SAR Interferometry"

First Page of the Article [C3640]

"Moving Target Detection based on Sub-aperture Image"

First Page of the Article [C3641]

"Differential Interferometric Radar for Mountain Rock Slide Hazard Monitoring"

First Page of the Article [C3642]

"Extended Model of Raw Data Signals for Space-Time Adaptive Processing and Moving Target Indicators"

First Page of the Article [C3643]

"The Influence of Time and Frequency Synchronism to the ATI Interferometric Phase in the Distributed Satellite SAR System"

First Page of the Article [C3644]

"Characterization of Coastal Wetland Systems using Multiple Remote Sensing Data Types and Analytical Techniques"

First Page of the Article [C3645]

"Spaceborne Parasitic Multistatic SAR-GMTI by Along-Track Interferometry"

First Page of the Article [C3646]

"Statistical Behavior of Multi-Resolution SAR Clutter"

First Page of the Article [C3647]

"A Detailed Comparison between Radar and Optical Vessel Signatures"

First Page of the Article [C3648]

"One-Dimensional Model-based Approach for ISAR Imaging (2)"

First Page of the Article [C3649]

"ScanSAR Processor Based on Improved k-Algorithm and Workstation Cluster"

First Page of the Article [C3650]

"Performance Improvement of the Spaceborne Three-Channel SAR-GMTI System: A Novel Satellite Attitude Steering Technique"

First Page of the Article [\[C3651\]](#)

"Study on the Correction of Saturated SAR Data"

First Page of the Article [\[C3652\]](#)

"Partial Aperture Effect-Free Doppler Centroid Estimation Method for Airborne Side-looking SAR Based on Range-Doppler Domain Contrast Minimization"

First Page of the Article [\[C3653\]](#)

"Model Based Terrain Effect Analyses on ICESat GLAS Waveforms"

First Page of the Article [\[C3654\]](#)

"Design and Testing of a Java-based Digital SAR Signal Simulation System"

First Page of the Article [\[C3655\]](#)

"TD2D and TDEPAR Time Domain SAR Image Processors State of Art, Performance Evaluation and Comparisons"

First Page of the Article [\[C3656\]](#)

"Analysis of Urban Land Use Pattern Based on High Resolution Radar Imagery"

First Page of the Article [\[C3657\]](#)

"Robustness of a Tracking Algorithm for Roads Extraction in Peri-urban Areas"

First Page of the Article [\[C3658\]](#)

"Automatic Detection of Wind-Thrown Forest in VHF SAR Images"

First Page of the Article [\[C3659\]](#)

"Wetland Forest Observation and Its Biomass Estimation in Kushiro Wetland by using Multipolarization SAR Data"

First Page of the Article [\[C3660\]](#)

"Hypothesis Management for Building Reconstruction from High Resolution InSAR Imagery"

First Page of the Article [\[C3661\]](#)

"Building Recognition Fusing Multi-Aspect High-Resolution Interferometric SAR Data"

First Page of the Article [\[C3662\]](#)

"Fusion of Interferometric and Optical Data for 3D Reconstruction"

First Page of the Article [\[C3663\]](#)

"Radargrammetric Extraction of Building Features from High Resolution Multi-aspect SAR Data"

First Page of the Article [\[C3664\]](#)

"Airborne Synthetic Aperture Radar for Estimating Above-ground Woody Biomass in Tropical Savanna Woodland: A Case Study in Belize"

First Page of the Article [\[C3665\]](#)

"Development of Oceanic Wind Vector Model Function for AMSR Radiometer on ADEOS-II Satellite"

First Page of the Article [\[C3666\]](#)

"A Physics Based Multi-Resolution Technique for Extraction of Finite Duration Time Responses in ISAR"

First Page of the Article [\[C3667\]](#)

"SAR Image Compression Using Multiwavelet and Soft-thresholding"

First Page of the Article [\[C3668\]](#)

"SeaWinds Scatterometer Wind Vector Retrievals within Hurricanes using AMSR and NEXRAD to Perform Corrections for Precipitation Effects: Comparison of AMSR and NEXRAD Retrievals of Rain"

First Page of the Article [\[C3669\]](#)

"A Multivariate Approach to Iceberg and Ship Classification in HH/HV ASAR Data"

First Page of the Article [\[C3670\]](#)

"Modeling Height, Biomass, and Carbon in U.S. Forests from FIA, SRTM, and Ancillary National Scale Data Sets"

First Page of the Article [\[C3671\]](#)

"Isotropic and Anisotropic FEXP-Fractal Spectral Models for High Resolution Sea SAR Images"

First Page of the Article [\[C3672\]](#)

"Sub-aperture Behavior of SAR Signatures of Ships"

First Page of the Article [\[C3673\]](#)

"Optimized Implementation of Onboard Real-time Imaging for High-resolution Space-borne SAR"

First Page of the Article [\[C3674\]](#)

"Analysis of Time and Frequency Synchronization Errors in Spaceborne Parasitic InSAR System"

First Page of the Article [\[C3675\]](#)

"Determination of SAR System Parameters Constraints from a Soil Moisture Retrieval Scheme"

First Page of the Article [\[C3676\]](#)

"A Comparison of Contrast Metrics for Contrast-based Phase Calibration of Digital Beamforming Remote Sensing Systems"

First Page of the Article [\[C3677\]](#)

"A Reconfigurable, Scalable and Multifunctional Experimental AutoSAR and Its Applications"

First Page of the Article [\[C3678\]](#)

"Simulator of Interferometric Radar Altimeters: Concept and first Results"

First Page of the Article [\[C3679\]](#)

"Detecting Bistatically Reflected GPS Signals from Low Earth Orbit Over Land Surfaces"

First Page of the Article [\[C3680\]](#)

"Simulation of Multi-channel SAR Raw Data Based on Real Single Channel SAR Data"

First Page of the Article [\[C3681\]](#)

"Study on DEM Reconstruction for Spaceborne Parasitic InSAR"

First Page of the Article [\[C3682\]](#)

"An Energy Consumption Model for Off-The-Grid Radar Networks"

First Page of the Article [\[C3683\]](#)

"Some Techniques for Three-dimensional Doppler Weather Radar Data Processing"

First Page of the Article [\[C3684\]](#)

"A New Approach to Backscattering of Pulsed Beam Waves from Hydrometers"

First Page of the Article [\[C3685\]](#)

"Analysis on Speed Error for Airborne Formation Flying InSAR"

First Page of the Article [\[C3686\]](#)

"Supervised SAR Image MAP Segmentation Based on Region-based Hierarchical Model"

First Page of the Article [\[C3687\]](#)

"Measurement of Land Subsidence and Microwave Penetration of Drying Mudflat by using Radarsat-1 DInSAR and PolScat Laboratory Experiment"

First Page of the Article [\[C3688\]](#)

"Variation of Radar Backscattering Coefficient of Tidal Mudflat Observed by Radarsat-1 SAR and Polarimetric Scatterometer"

First Page of the Article [\[C3689\]](#)

"Backscattering Simulation of Birch Stands Using Coherence Model"

First Page of the Article [\[C3690\]](#)

"Contribution to Sea Scattering Estimation for Various Wind Direction"

First Page of the Article [\[C3691\]](#)

"A Novel Algorithm for Wide Beam SAR Motion Compensation Based on Frequency Division"

First Page of the Article [\[C3692\]](#)

"A Vessel Detection Method Using ASAR AP Data"

First Page of the Article [\[C3693\]](#)

"A Deramp Frequency Scaling Algorithm for Processing Space-Borne Spotlight SAR Data"

First Page of the Article [\[C3694\]](#)

"A New Weighting Method for Pulse Compression of Chirp Signal and Its Implementation in Real-time SAR Processor"

First Page of the Article [\[C3695\]](#)

"Detection, Location and Imaging of Fast Moving Targets Using Non-uniform Linear Antenna Array SAR"

First Page of the Article [C3696]

"Minimum-Latency Polar Format Algorithm"

First Page of the Article [C3697]

"An Efficient Mathematical Model for SAR Image Rectification"

First Page of the Article [C3698]

"Automatic Registration of Spaceborne SAR Images with the Enhanced FMI-SPOMF Technique"

First Page of the Article [C3699]

"Illicit Vessel Identification In Inland Waters using SAR Image"

First Page of the Article [C3700]

"Adaptive Despeckling SAR Images in the Undecimated Wavelet Domain Based on Scale Correlation"

First Page of the Article [C3701]

"Evaluation of Envisat-asar Data for Estimating Crop Area in Chengdu Plain"

First Page of the Article [C3702]

"ScanSAR Interferometry for Land Use Applications and Terrain Deformation"

First Page of the Article [C3703]

"A CGMRF-Like based Technique for Speckle Reduction in SAR Images"

First Page of the Article [C3704]

"Speckle Noise Removal of SAR Images Based on 2-Dimensional S-Transform"

First Page of the Article [C3705]

"DEMs and SAR Images"

First Page of the Article [C3706]

"Radargrammetry DEM from RADARSAT Imageries and Accuracy Validation"

First Page of the Article [C3707]

"Sea SAR Image Simulation using Isotropic and Anisotropic FEXP-Fractal Spectral Models"

First Page of the Article [C3708]

"Accuracy of Building Height Estimation from SAR Images"

First Page of the Article [C3709]

"Scene Analysis of SAR Images using Joint Time-Frequency Analysis"

First Page of the Article [C3710]

"Spotlight-Mode SAR Image Formation Utilizing the Chirp Z-Transform in Two Dimensions"

First Page of the Article [C3711]

"Ultra High Resolution Rain Retrieval from QuikSCAT Data"

First Page of the Article [\[C3712\]](#)

"A Comparison of Hurricane Eye Determination using Standard and Ultra-High Resolution QuikSCAT Winds"

First Page of the Article [\[C3713\]](#)

"Multifrequency Full Polarimetric SAR Classification with Multiple Sources of Statistical Evidence"

First Page of the Article [\[C3714\]](#)

"Variational Unsupervised Classification of Polarimetric Images"

First Page of the Article [\[C3715\]](#)

"Modelling of Scattering from Point Like Targets"

First Page of the Article [\[C3716\]](#)

"SAR Raw Data Generation Using Inverse SAR Image Formation Algorithms"

First Page of the Article [\[C3717\]](#)

"The Surface Effect of Rain on Microwave Backscatter from the Ocean"

First Page of the Article [\[C3718\]](#)

"Ground-based Radar Interferometry for Monitoring Unstable Slopes"

First Page of the Article [\[C3719\]](#)

"Oil Spill Detection with RADARSAT-1 in the Baltic Sea"

First Page of the Article [\[C3720\]](#)

"Change Detection using Multi-PASS and Multi- DATE Data at P and L bands"

First Page of the Article [\[C3721\]](#)

"Toward the use of Earth Observation Wind Data for Marine Search and Rescue Operations"

First Page of the Article [\[C3722\]](#)

"Use of Enhanced-resolution QuikScat/SeaWinds Data for Operational Ice Services and Climate Research: Sea Ice Edge, Type, Concentration and Drift"

First Page of the Article [\[C3723\]](#)

"The Effect of Rain on ERS Scatterometer Measurements"

First Page of the Article [\[C3724\]](#)

"ISAR and Aerial LIDAR Comparison to Observe and Quantify the Terrain and Environment of the Historical Native North Carolina Settlements"

First Page of the Article [\[C3725\]](#)

"Diurnal Melt Detection on Arctic Sea Ice Using Tandem QuikSCAT and SeaWinds Data"

First Page of the Article [\[C3726\]](#)

"Amplitude-Based Measurement Technique in Polarimetric Radar Remote Sensing for Determining

the Dielectric Permittivity of Earth Media"

A new method for measuring the complex dielectric permittivity of underlying surfaces is described. The method only uses amplitude measurements in two orthogonally polarized channels of a non-coherent polarimetric radar. [C3727]

"Data Acquisition Field Network in Support of Remote Sensing Investigations"

Integrated use of data collected during remote sensing experiments and data from in-situ measurements reveal more features of the land cover objects under study. This features incorporated into existing GIS databases leads to better understanding, representing, managing, and integrating many aspects of the Earth as a complex system. The in-situ gathered data such as, ground control points by GPS, current meteorological conditions, soil moisture, etc., provides additional information that is crucial in improving GIS effectiveness in decision support. To improve and facilitate the process of collection and storage of in-situ data a distributed mobile, wireless, field network was developed. The main components of the system are the autonomous, battery-powered micro controller devices wirelessly communicating with a central one. In this paper short description of the technical parameters and communication protocols between devices, hubs and the control center is outlined. From topological point of view two types of networks can be implemented -simple, used in small areas (usually less than 10 km²) and full, covering areas up to 50 km². Both networks has flexible structure, offered by a variable number of commands that could be easily adapted to meet the requirements of dissimilar measuring devices thus increasing the number of target applications -from land use to disaster monitoring. A prototype of the system successfully performed well on test polygons in North Bulgaria. [C3728]

"Analysis of Possibilities of Creating the Radioelectronic Complexes to be Made for Detection of Biological Objects Covered by Vegetation"

Materials about possibilities of object detection, correlated with its radiobrightness contrast to surroundings, are presented. The results of investigation of possibilities of biological object detection for objects, shaded by vegetation, are presented. The conclusion was made, that biological object (a man), shaded by vegetation, can be detected from a distance up to 15 km, if attenuation of electromagnetic waves, correlated with vegetation, is not more -25 dB. The experimental results of object detection are presented. [C3729]

"Results of Development of Radiometric Receivers mm and Submillimeter Range"

Results of development of space-based radiometric receivers in a frequency range 10 GHz ... 206 GHz is considered. Are resulted technical characteristics the developed radiometric systems intended for remote sensing of a surface of the Earth (including ocean) and atmosphere. Results of flight measurements also are submitted. [C3730]

"Experimental determination of soil characteristics from the parameters of scattered signals at X- and Ka-bands"

The results are described of bare soil remote sensing at X- and Ka-bands: the angular dependences of the normalized RCS for different test areas, dependence of the normalized RCS on soil moisture and surface roughness, polarization dependences of scattered signal on soil moisture and surface roughness. [C3731]

"Subsurface Investigations by MARSIS in Mars Express Mission"

The analysis of the surface return echoes in the subsurface data extraction in North Mars Polar region has shown the possibility to utilize simplified surface models, at least, for the purpose of the evaluation of the penetration depth capability. The surface simulation, obtained starting from MOLA data, has been utilized during the planning activity in order to select the MARSIS operative sequence in order to optimize the amount of scientific data taking into account the data rate available and the scientific target to be investigated during the next part of the mission. Moreover a simulator, still in progress, utilizing the surface characteristics will perform the analysis of the real data in order to make available the required information expected, by the mission, in terms of detection and identification of dielectric constant on the surface and subsurface. [C3732]

"Spatial (Aperture) Noise Generators"

Spatial noise generators with apertures of 200 mm, 270 mm, 1500 mm were developed in OKB MEL. Spatial noise generators with apertures of 200, 270 mm are Djuar vessels filled up by boiling liquid nitrogen, with metal cylinder, fixed in liquid nitrogen's zone. One of cylinder's founding is cooled by boiling nitrogen. It is covered by radio-absorption material. Another founding, covered by heat protection radio-transparent material, is radiating

aperture of spatial noise generator. Spatial noise generators with aperture of 1500 mm is a collimating system, which consists of the parabolic reflector (part of parabolic) and radiator, which consists of aperture noise generator and additional reflector (contra-reflector). Additional reflector also provides lighting of main mirror (parabolic reflector) and forming of plane parallel collimation beam. Methodology of noise temperature unevenness measurements in the section of the collimation beam is presented. [C3733]

"Space Monitoring of Atmosphere Pollution by Satellite Passive Radar System"

Nowadays the world community is paying great attention to the problem of atmosphere pollution. UN took several conventions including Kyoto protocol which restricts industrial waste outflow to atmosphere and water. As a result special importance is paid to the implementation of obligations taken by particular countries. The remote sensing system is the only means for solving this problem. In the present article passive radio specter method based on measuring the radiation levels of various substances at own resonance frequencies such as CH₄, CO, CO₂, SO₂, HCl, NO_x, ClO₂, as well as solid particles. [C3734]

"Polarimetric Analysis of Radar Signature of a Manmade Structure"

Identification of manmade structures from radar images has always been a difficult task, especially for single-polarization radar. Fully polarimetric radar, however, can provide detailed information on scattering mechanisms that could enable the target or the structure to be identified. Complexity remains stemming from overlaps of single bounce scattering, double bounce scattering and triple and higher order bounce scattering from various components of manmade structure that makes physical interpretation a challenge. In this paper, we will present an interesting example using polarimetric SAR data of the Great Belt Bridge, Denmark, to illustrate the capability of polarimetric SAR in analyzing radar signatures. Polarimetric target decomposition is used to differentiate the multiple bounce scattering contributions contained in the polarimetric SAR images. Two C-band Danish EMISAR data takes, the first obtained during the bridge's construction and the second after its completion, are used to extract the scattering characteristics of the bridge deck, bridge cables and supporting structures. [C3735]

"Determination of the Soil Parameters from Multichannel Remote Sensing Data"

Possibilities of soil parameter determination by dual-frequency multipolarization radar for terrain remote sensing are analyzed. It is shown that the sensitivity for soil moisture and roughness is rather weak at X- and Ka-bands. There is correlation between polarization ratios and soil erosion. [C3736]

"Methods for Lossy Compression of Images Corrupted by Multiplicative Noise"

Compression of images corrupted by multiplicative noise is characterized by some specific features. First, lossy image compression is preferable since lossless coding is ineffective. Second, in case of lossy compression, quality of a compressed noisy image evaluated with respect to noise-free one can become better than the corresponding quality of an original image. And there exists such compression ratio called optimal operation point for which the quality of lossy compressed image is the best. Below typical situations that can be observed in compression of remote sensing data, for example, radar images are considered. We evaluate the efficiency of two basic methods for lossy compression of images corrupted by pure multiplicative noise. A way to reach optimal operation point for providing the best quality of coded images is proposed. The corresponding automatic procedure is described. [C3737]

"Evaluation of the Efficiency of Object-Based Classification in the Identification of Geological Structures Case Study: Extraction of the Morphology of the Normal Faults"

First Page of the Article [C3738]

"Contextual approach for oil spill detection in SAR images using image fusion and markov random fields"

This paper presents a study for oil spill detection. The scheme incorporates contextual information using multi-conexity analysis. The image is modeled as a discrete Markov random field (MRF). Each pixel can be classified in two classes: {oil, not-oil}. To determine the class we optimized the a posteriori energy function by means of simulated annealing. The segmentation result contains different levels of information. In order to improve the detection, we propose a data fusion stage. To realize the data fusion we use a contextual algorithm. The result obtained is binary and shows in detail the oil spill in the analysis zone. [C3739]

"Simulation algorithm for noise waveform SAR with arbitrary motion trajectory of antenna phase"

center"

Methods for remote sensing of the environment with the help of Noise Waveform SAR systems with nonlinear antenna motion trajectory are widely applied at the present time. The elaboration of simulation models for the reflection and SAR imaging algorithms is necessary for successful design of such radar systems. The algorithm for numerical simulation of the reflected sequence of noise pulses obtained on the basis of the approximate model of local scattering sources for the case of SAR with an arbitrary antenna motion trajectory is presented in the paper. A universal SAR imaging algorithm with the range migration compensation is also presented; it can be used to obtain SAR images for both monostatic and bistatic cases while antenna trajectories of any type (linear, arc, etc) can be used for the survey. [C3740]

"Recent Developments of Radar Remote Sensing; Air- and Space-borne Multimodal SAR Remote Sensing in Forestry & Agriculture, Geology, Geophysics (Volcanology and Tectonology): Advances in POL-SAR, IN-SAR, POLinSAR and POL-DIFF-IN-SAR Sensing and Imaging with Applications to Environmental and Geodynamic Stress-change Monitoring"

In this overview, reasons are provided on why we do need to place multimodal, multi-band single and multiple pass POLinSAR monitoring platforms into air and space. The questions "on what POLinSAR monitoring can provide that POL-SAR and INSAR by themselves cannot accomplish" is assessed; whereupon facts and justifications on placing POL-IN-BISAR satellite clusters into space are presented. Reasons for this technology becoming a basic requirement for current, near-future and much more so for future all-day & night year around monitoring of the terrestrial covers are analyzed in view of the un-abating and uncontrollable terrestrial population explosion, which has, does and for ever will result in unavoidable conflicts deteriorating unfortunately at times into terrorism. The pertinent questions on how to reduce the exorbitant cost for initiating this "home-globe security protection" technology are therefore also broached, and the expected benefits are laid out. The pertinent National and International airborne and space borne multi-modal, multi-band SAR remote sensing and security conflict surveillance support agencies are herewith invited for co-sponsoring our proposal, which is timely and fleets of orbiting multi-band space-borne POLinSAR platforms are urgently required. [C3741]

"Image processing in the complex monitoring system radiometric channel"

In this paper two image processing methods for restoring radar image are compared. [C3742]

"HF-OTH Skywave Radar: A Method for Peak Power Evaluation"

This paper addresses the problem of peak power evaluation in HF OTH skywave radar. A wide number of factors affect the performance of such systems, specifically ionospheric propagation and absorption losses, as well as external radio noise interferences. A normalized version of the signal to noise ratio (SNRN) has been introduced in order to evaluate the power requirements over a wide range of environmental conditions. Finally, this paper attempts to provide a method for evaluating the peak power values required in OTH radar systems and also some useful project criteria. [C3743]

"Application of Polarization Coherence Tomography to GB-POLInSAR Data"

First Page of the Article [C3744]

"Identification of Individual Trees And Canopy Shapes using LiDAR Data for Fire Management"

First Page of the Article [C3745]

"Comparison of Small-footprint and Large-footprint Waveform Lidar for Terrestrial Surface Characterization"

First Page of the Article [C3746]

"Auto-Regressive Aperture Extrapolation for Multibaseline SAR Tomography"

First Page of the Article [C3747]

"Airborne Laser Mapping of Mangroves on the Biscayne Bay Coast, Miami, Florida"

First Page of the Article [C3748]

"A Large-Scale Ku-Band Backscatter Model of the East-Antarctic Megadune Fields"

First Page of the Article [\[C3749\]](#)

"Romulus: Along Track Formation of Radar Satellites for MTI (Moving Target Identification) and High SAR Performance"

First Page of the Article [\[C3750\]](#)

"Characterisation of Coherent Scatterers in Urban Areas by Means of Angular Diversity"

First Page of the Article [\[C3751\]](#)

"Capabilities of L-band SAR Data for arctic Glacier Motion Estimation"

First Page of the Article [\[C3752\]](#)

"Ionospheric Electron Concentration Effects on SAR and INSAR"

First Page of the Article [\[C3753\]](#)

"UHF RiverSonde Operation in a Tidal Marsh"

First Page of the Article [\[C3754\]](#)

"Microwave Radiometric Signal from the Sea Surface in the Presence of the Currents"

First Page of the Article [\[C3755\]](#)

"Comparison of Helicopter-borne Measurements of Sea-Ice Properties with ENVISAT ASAR APP Data for Amundsen Gulf"

First Page of the Article [\[C3756\]](#)

"A Wideband Radar for Mapping Near-Surface Layers in Snow"

First Page of the Article [\[C3757\]](#)

"Aerosol Layer Discrimination using Laser Radar and Genetic Algorithms"

First Page of the Article [\[C3758\]](#)

"A Multi-chromatic Approach to SAR Interferometry: Differential Analysis of Interferograms at Close Frequencies in the Spatial Domain and Frequency Domain"

First Page of the Article [\[C3759\]](#)

"Mapping of Wind-Thrown Forests Using the VHF-Band CARABAS-II SAR"

First Page of the Article [\[C3760\]](#)

"The Use of Environmental Data in Reliability Assessment of Oil Spill Detection by SAR Imagery"

First Page of the Article [\[C3761\]](#)

"Building Height Estimation using Fine Analysis of Altimetric Mixtures in Layover Areas on Polarimetric Interferometric X-band SAR Images"

First Page of the Article [\[C3762\]](#)

"High Resolution SAR Interferometry: Influence of Local Topography in the Context of Glacier Monitoring"

First Page of the Article [\[C3763\]](#)

"Preliminary Testing of a Water-Vapor Differential Absorption LIDAR (DIAL) Using a Widely Tunable Amplified Diode Laser Source"

First Page of the Article [C3764]

"An Imaging Bistatic Lidar System for Boundary Layer Monitoring"

First Page of the Article [C3765]

"Estimation of Built-up Area Characteristics from Polarimetric Interferometric Multiple Track L-Band SAR Data"

First Page of the Article [C3766]

"Complete Inversion of Agricultural Vegetation Parameters by Pol-InSAR: Multibaseline and .k-radar Approaches"

First Page of the Article [C3767]

"Polarimetric Characteristics of X-Band SAR Sea Clutter"

First Page of the Article [C3768]

"SAR Image Filtering based on the Stationary Contourlet Transform"

First Page of the Article [C3769]

"Network of RF Ground Sensors for Applications in Precision Agriculture"

First Page of the Article [C3770]

"Evaluation of Ground-based SAR System for Digital Beamforming Applications"

First Page of the Article [C3771]

"Advanced Spaceborne Rain Radar Instrument Concepts and Technology"

First Page of the Article [C3772]

"ARTINO: A New High Resolution 3D Imaging Radar System on an Autonomous Airborne Platform"

First Page of the Article [C3773]

"Hybrid-Polarity SAR Architecture"

First Page of the Article [C3774]

"Airborne Laser Scanning and Radar Interferometry for Digital Topographic Modelling in Coastal Environments"

First Page of the Article [C3775]

"Effect of Spatially Variant Apodization on SAR Image Classification"

First Page of the Article [C3776]

"TerraSAR-X Antenna Pattern Estimation by a Complex Treatment of Rain Forest Measurements"

First Page of the Article [C3777]

"InSAR Evaluation of Landslides in Support of Roadway Design and Realignment"

First Page of the Article [C3778]

"An Atmospheric Correction Method Based on Lidar Data"

First Page of the Article [C3779]

"Observation of the Soya Warm Current Combining HF Ocean Radar with Coastal Tide Gauges and Satellite Altimetry"

Three HF ocean radar stations were installed at the Soya/La Perouse Strait in the Sea of Okhotsk in order to monitor the Soya Warm Current. The frequency of the HF radar is 13.9 MHz, and the range and azimuth resolutions are 3 km and 5deg, respectively. The radar covers a range of approximately 70 km from the coast. It is shown that the HF radars clearly capture seasonal and short-term variations of the Soya Warm Current. The velocity of the Soya Warm Current reaches its maximum, approximately 1 m s⁻¹, in summer, and weakens in winter. The velocity core is located 20 to 30 km from the coast, and its width is approximately 50 km. The surface transport by the Soya Warm Current shows a significant correlation with the sea level difference along the strait, as derived from coastal tide gauge records. The cross-current sea level difference, which is estimated from the sea level anomalies observed by the Jason-1 altimeter and a coastal tide gauge, also exhibits variation in concert with the surface transport and along-current sea level difference. [C3780]

"High Resolution Sea Surface Current Maps Produced by Scanning with Ground Based Doppler Radar"

Pulsed coherent X-band radar has been operated from shore and from board a ship to scan the sea surface velocities by separating the influences from wind and underlying currents. Test sites lie at tidal inlets of the German Bight that is part of the North Sea. Under the use of Precise Differential Global Positioning Systems (PDGPS) geo-coded radar current maps were produced. [C3781]

"Coastal Current Observation in the Area of Abrupt Topographic Change with DBF Ocean Radar"

A DBF ocean radar can detect the surface current pattern every 15 minutes. The tidal current and the residual current were investigated through the continuous observation of the DBF (digital beam forming) radar in the middle-west area of Ariake Bay in autumn 2005. For the validation of the surface current data by the DBF ocean radar the ship-board ADCP measurements were also conducted at spring tide. As the result of the comparison of both surface current data, the correlation coefficient and the standard error of the current speed are 0.89 and 7.23cm/s, and those of the current direction are 0.92 and 35.89 degree. The harmonic analysis of the long-term data by the DBF ocean radar clarifies the spatial pattern of the principal tides and the residual currents. The residual currents in 15days flow south to southeastward caused mainly by the tidal residual currents due to the topographic asymmetry. [C3782]

"Observing Eddy Features in the Ocean Surface Wind Field by Assimilating HF Radar and Anemometer Measurements in a Wind Model"

Strong evidence for 10-40 km scale eddies in the surface wind field over Monterey Bay, California has been presented by Archer, Ludwig et al. using shore and buoy anemometers and satellite images. These cyclonic eddies are frequently present in the evening and early morning and are responsible for fog in the Santa Cruz area. We have previously demonstrated the ability of multifrequency HF radar (4.8 to 21.8 MHz) to map the ocean wind field. Observations over a year time span indicate standard errors of prediction of 1.7 m/s for wind speed and 25deg for direction with biases of 0.1 m/s and 0.3deg respectively. Here we report observation of a 10-20 km cyclonic eddy at the north end Monterey Bay. By combining HF radar wind vector estimates with shore based anemometer data in the WOCSS surface wind field model we are able to form a detailed (5 km resolution) image of an eddy over Monterey Bay and to follow its development and decay. This particular eddy contrasts with previous eddy observations in terms of season and meteorological setting. [C3783]

"An Empirical Approach for the Retrieval of Ocean Wave Parameters from Synthetic Aperture Radar Data"

Spaceborne Synthetic Aperture radar (SAR) is still the only instrument providing continuous two-dimensional (2-D) ocean wave measurements on a global basis. For more than a decade the European satellites ERS-1 and ERS-2 have acquired SAR data over the open ocean operating in wave mode. The ERS acquisitions are currently continued by the ENVISAT ASAR wave mode. It is well known that the derivation of ocean wave parameters from SAR data is not straightforward and different approaches have been proposed. In this study we present a new technique, which is based on an empirical SAR imaging model. The method has the calibrated SAR image as the only input. A data set of 6000 globally distributed ERS-2 wave mode image spectra and collocated ocean

wave spectra computed with the numerical model WAM are used to fit a linear model, which relates the SAR spectrum to integral wave parameters like, e.g., the significant wave height. This model is then used for ocean wave parameter retrieval. The radar cross section and the azimuthal cut-off wavelength estimated from the wave mode images are used as additional input variables. The method takes into account the coupling of the different parameters and is based on a least-square minimisation approach. The resulting coupled linear system of equations is solved using a singular value decomposition technique. Disjunct subsets of the collocated data set are used for fitting the model and retrieving ocean wave parameters. Scatterplots and global maps with the derived parameters are presented. It is shown that the standard deviation of the retrieved significant waveheight with respect to the WAM waveheight is in the order of 0.62 m. Other wave parameters, which are of practical relevance like mean wave periods are investigated as well. [C3784]

"Monitoring the Cryosphere using Radarsat-1 and SSM/I Data: an Overview of CRYSYS Related Accomplishments at INRS-ETE"

The cryosphere consists of ocean ice, glaciers, lake and river ice, snow cover, seasonally frozen ground and permafrost. During a decade (1995-2005), the CRYSYS project supported a network of researchers from universities and government laboratories involved in the monitoring of the Canadian cryosphere using remote sensing data and climatic models. Through this decade, INRS-ETE has been using remote sensing to develop tools for snow monitoring, seasonal frost mapping, and river ice characterization in Canada. This paper summarizes INRS-ETE main scientific accomplishments. [C3785]

"Use of Dual Polarization Radar Measurements to Understand the Azimuth Behavior of the Sea Surface Backscattered Signal"

We present an analysis of the azimuth anisotropy of the ocean radar backscatter from C-Band observations in VV and HH polarizations from the airborne radar STORM during the VALPARESO experiment. Comparisons with existing semi-empirical models show that none of them are in agreement with the anisotropy of the radar signal, and the trend with wind speed is too weak compared to the observations. This is attributed to a shortcoming in the description of the short surface waves anisotropy. By considering an additional mechanism for nonlinear wave interactions, we show that the short wave anisotropy is modified and can explain the anisotropy of the radar signal. [C3786]

"Spectral Behavior of the Ocean Surface Backscatter and the Atmospheric Boundary Layer at C- and Ku-band under High wind and Rain Conditions"

During the NOAA/NESDIS 2005 Hurricane Season (HS2005) and the 2006 Winter Experiment, the University of Massachusetts (UMass) installed two instruments on the NOAA N42RF WP-3D research aircraft: the Imaging Wind and Rain Airborne Profiler (IWRAP) and the Simultaneous Frequency Microwave Radiometer (SFMR). IWRAP is a dual-band (C- and Ku), dual-polarized pencil-beam airborne radar that profiles the volume backscatter and Doppler velocity from rain and that also measures the ocean backscatter response. It simultaneously profiles along four separate incidence angles while conically scanning at 60 RPM. SFMR is a C-band nadir viewing radiometer that measures the emission from the ocean surface and intervening atmosphere simultaneously at six frequencies. It is designed to obtain the surface wind speed and the column average rain rate. Both instruments have previously been flown during the 2002, 2003 and 2004 hurricane seasons. For the HS2005, the IWRAP system was modified to implement a raw data acquisition system. The importance of the raw data system arises when trying to profile the atmosphere all the way down to the surface with a non-nadir looking radar system. With this particular geometry, problems arise mainly from the fact that both rain and ocean provide a return echo coincident in time through the antenna's main lobe. This paper shows how this limitation has been removed and presents initial results demonstrating its new capabilities to derive the atmospheric boundary layer (ABL) wind field within the inner core of hurricanes to much lower altitudes than the ones the original system was capable of, and to analyze the spectral response of the ocean backscatter and the rain under different wind and rain conditions. [C3787]

"Development of 9.25MHz Ocean Radar for Measuring Ocean Waves"

The National Institute of Information and Communications Technology (NiCT) is developing a 9.25-MHz ocean radar for measuring sea surface currents and ocean waves offshore. This study clarifies the accuracy and validity of observing ocean waves with a 9.25-MHz ocean radar. The precision of the receiving signals of the 9.25-MHz ocean radar is evaluated by observing ocean waves with a wave gage mounted on a buoy. The results of observing ocean waves with a 9.25-MHz ocean radar are compared with the results of observing them with a wave gage. This comparison showed that the directional wave spectrum can be estimated from the receiving signals when the noise level is low during the day. [C3788]

"Research on Unification of Spatial Reference of Multi-source Data in 3S Integration"

Spatial reference unification is the foundation of "3S" integration project and is also complicated. This paper proposes and designs scheme for coordinate unification according to constitute of multi-source data and system requirements in digital tobacco "3S" monitoring project, then solves the two problem: WGS84 datum transformation with local datum and SAR image calibration with other spatial data in research area. The result proves that the scheme satisfies the precision requirement of this project which makes good preparation for the following monitoring work. [C3789]

"Bistatic Exploration using Spaceborne and Airborne SAR Sensors: A Close Collaboration Between FGAN, ZESS, and FOMAAS"

Following the goals of our cooperation treaty between FGAN and ZESS (University Siegen), we work closely together on the complex research field of bistatic exploration. Single tasks of the overall topic are for instance experimental missions, processing, image formation, position- and attitude estimation, synchronisation, simulation, parameter estimation, and visualization. This paper presents an overview about the common projects of FGAN, ZESS, and FOMAAS. [C3790]

"Evaluation of Convair-580 and Simulated Radarsat-2 Polarimetric SAR for Forest Change Detection"

Radarsat-2 is a significant advancement in technological capability over Radarsat-1 in terms of better spatial resolution and polarimetric parameters. To determine the effectiveness of C-band polarimetry of Radarsat-2 data for applications of forest typing, structure recognition and disturbance detection, C-band polarimetric data from Environment Canada's Convair-580 were acquired. We also obtained simulated Radarsat-2 data, a degraded version of the Convair-580 data. Polarimetric techniques, such as polarimetric filtering and decompositions, were performed on these data sets. The underlying backscatter phenomena were examined and the results were compared. Historical fire disturbance patterns were detected clearly with the Convair-580 data by using the Entropy- alpha decomposition technique. Moreover, the combination of the surface scattering and volume scattering decompositions showed results in obtaining clearcut information in forested areas. By using the simulated Radarsat-2 data, we gained an insight into what could be expected from real Radarsat-2 quad-pol products. Even though the simulated Radarsat-2 data had more noise than Convair-580 data, the fire scars in the same area were still detectable. [C3791]

"Data Fusion: Cumulative Effects of Discrete Fusion on Target Detection Probability"

This paper describes the culmination of a four-year research, application, and development program towards finding and quantifying a methodology for sensor and data fusion of remotely sensed targets. It builds on previous research reported in IGARSS'02 [1] and IGARSS'04 [2]. Here, we examine the effectiveness of the data fusion methodology, specifically, the impact of iterative data collection on the effective probability of detection of targets. Through statistical (Bayesian) combination of sensor iterations, low confidence sensors (those with moderate probability of detection and moderately low probability of false alarms) can provide high detection performance. This can be extended to multiple data source types. The goal is to make use of higher coverage data products which have only moderate detection performance in the detection and tracking of targets. This is made possible through a combination of discrete target data, along with the analysis of parameters from the respective remote sensing technologies. This process requires the existence of a reasonable maneuvering model or sufficient processing resources. [C3792]

"First ENVISAT and ERS-2 Parasitic Bistatic Fixed Receiver SAR Images Processed with the Subaperture Range-Doppler Algorithm"

Past and current SAR missions, such as SIR-C, ERS- 1/2, ENVISAT, SRTM, E-SAR, etc. had in common that the signal transmitter and the receiver were located at the same moving platform. New missions are being planned [1] based on the bistatic concept, where transmitter and receiver subsystems are located at different locations and thus may follow different trajectories. But before these missions become a reality, there are several experiments to be considered. One of them is the Parasitic Bistatic Fixed Receiver case, a novel and challenging configuration regarding hardware development and SAR processing techniques. This configuration will improve our experience in the bistatic field with cost effective measurements. In this paper, we will present the first images of the ongoing satellite bistatic campaign in our department. The images have been acquired with the specific hardware SABRINA (SAR bistatic fixed receiver for interferometric applications, fully developed at UPC) and processed with the Subaperture Range- Doppler Algorithm which will be explained in detail. We have been using ESA's ENVISAT and ERS-2 C-band SAR satellites as opportunity transmitters and we have located the

hardware prototype receiver at the roof of our department looking to the illuminated scene, a hill in front of the Campus. The mean bistatic angle is about 75deg, the capture window is only two seconds long and experiments have a period of 35 days due to the satellite revisiting time. [C3793]

"No Math: Bistatic SAR Processing Using Numerically Computed Transfer Functions"

Standard SAR processing algorithms use analytically derived transfer functions in the 2-D frequency and the range- Doppler domains. These rely on the assumption of hyperbolic range histories of monostatic SARs on straight flight paths. A moderate deviation from these conditions can often be handled satisfactorily by a range-variant velocity parameter. However, bistatic SARs with considerable separation between transmitter and receiver can no longer be approximated accurately enough by hyperbolic range histories. In [1] we have presented an alternative approach, NuSAR. We suggested using numerically computed transfer functions for bistatic SAR processing. We presented the idea and gave hints on how to compute the three transfer functions required for SAR processing. In this paper we present bistatic simulation results with the NuSAR algorithm. It is shown, that NuSAR works well even in extreme bistatic configurations, as long as we restricted ourselves to quasi-stationarity, i.e. where the velocity vectors of receiver and transmitter are similar enough that we may assume the point response function to be sufficiently azimuth-invariant within a single azimuth processing block. [C3794]

"Bistatic Space Borne / Airborne Experiment: Geometrical Modeling and Simulation"

In this paper, the geometrical setup of an airborne/spaceborne SAR experiment is described. This experiment is planned in cooperation of ZESS (University of Siegen) and FGAN (Forschungsgemeinschaft für angewandte Naturwissenschaften) [1]. While TerraSAR-X will be used as SAR illuminator, the reflected pulses will be received by FGAN's X-band system PAMIR. Due to the high difference between the velocities of the platforms, both systems must perform antenna steering to achieve an appropriate scene length in azimuth. [C3795]

"Digital Beamforming for HRWS-SAR Imaging: System Design, Performance and Optimization Strategies"

Multi-aperture synthetic aperture radar (SAR) systems in combination with an appropriate coherent processing of the individual aperture signals enable high resolution wide swath (HRWS) SAR imaging [1]-[8]. An innovative reconstruction algorithm for such a digital beamforming on receive was presented in [9]-[12] that allows for HRWS even in case of a non-uniformly sampled data array in azimuth. This paper will compare this algorithm to different azimuth processing strategies regarding their performance in dependency of the overall sampling. Further, optimization strategies are discussed to maximize the system's performance by pattern tapering on transmit and "Pre-Beamshaping on Receive" networks that allow for pattern tapering on receive and adaptively adjust the virtual sample positions. [C3796]

"The TerraSAR-X Orthorectification Service and Its Benefit for Land Use Applications"

The German Aerospace Center (DLR) currently develops the TerraSAR-X Payload Ground Segment. On request level 1b products will be distributed to the user. Two of the four basic products available are generated by the geocoding system. This system supports ellipsoid and terrain correction in order to provide orthorectified images. A new product called Enhanced Ellipsoid Corrected (EEC) will be offered that considers Digital Elevation Models (DEMs) of a moderately coarser resolution than the resolution of the TerraSAR-X modes. SRTM/X-band DEMs with approximately 25 m resolution will be the backbone for this operational and fully automated service. For high precision terrain correction first results of an experimental processor are presented using a high resolution DEM, tie- pointing and image adjustment. [C3797]

"Coastal Ocean Surface Current Retrievals from Sequences of TerraSAR-X Images"

Coastal surface currents have been computed for years from sequential infrared and more recently ocean color imagery using the Maximum Cross Correlation (MCC) technique. Preliminary results suggest that this MCC method may be applied to sequential Synthetic Aperture Radar (SAR) imagery yielding surface currents with a much higher spatial resolution which are independent of the presence of cloud cover which makes it impossible to use infrared or ocean color imagery. A requirement for the application of the MCC to SAR imagery is the presence of surface slicks, which are often related to ocean color patterns. Test applications are made to ENVISAT ASAR images. [C3798]

"Status of the TerraSAR-X Mission"

TerraSAR-X is a new German radar satellite scheduled to be launched in October 2006 with a lifetime of 5

years. It carries a high frequency X-band SAR sensor that can be operated in three different modes and polarizations. The Spotlight-, Stripmap- and ScanSAR-modes provide high resolution images for detailed analysis as well as wide swath data whenever a larger coverage is required. Imaging will be possible in single, dual and quad-polarization. TerraSAR-X will be an operational SAR-system for scientific and commercial applications. The Pre-launch AO was the first opportunity to apply for data for research purposes. Between June 13 and October 4 2005 172 Pis submitted 205 proposals representing more than 350 research groups. [C3799]

"TerraSAR-X Products and Product Performance Update"

TerraSAR-X is a German satellite to be launched towards end of the year 2006. The SAR instrument built by EADS/Astrium has a multipolarized active phased array antenna and is programmable in wide ranges. This allows to operate imaging modes such as e.g. stripmap, spotlight, ScanSAR and dual-polarization modes. By further dividing the antenna in halves with different position or different polarization, experimental modes for ground moving target detection (GMT) or Quad-Polarization are possible. As a consequence of the various sensor capabilities the tree of SAR products offered by the DLR Ground Segment contains many different variants of polarization, resolution and scene size. Even more product variants are caused by different processing parameters selectable by the user. Some product performance parameters, such as the radiometric accuracy as a function of geometric resolution or the image resolution as a function of incidence angle depend on both, sensor settings (PRF, pulse duration) and on processing parameters (bandwidth, weighting, multi-looking). The processing parameters for the products have been designed by DLR in a way so that valuable products with maximum information content are offered to the user. In order to generate the specified products, the TerraSAR Multi Mode SAR Processor TMSP has been designed by DLR. This processor will be operated at the DLR payload ground segment in Neustrelitz for commercial and scientific customers. The processor will also be operated at additional direct access partner stations of Infoterra GmbH, who will serve private and public customers. [C3800]

"The TanDEM-X Mission Concept"

TanDEM-X (TerraSAR-X add-on for Digital Elevation Measurement) is an innovative radar interferometry mission to generate a global, consistent and highly accurate digital elevation model (DEM) and to provide a configurable SAR interferometry platform for demonstrating new SAR techniques and applications. This paper summarizes the mission concept starting from the user requirements, the HELIX orbit and TanDEM-X operational modes to the expected height performance. Examples of new SAR techniques are presented.

[C3801]

"Use of Airborne LIDAR for the Assessment of Landscape Structure in the Pine Forests of Everglades National Park"

Remote sensing technologies have provided valuable data for landscape modeling, vegetation mapping and comprehensive studies of ecosystems. Airborne laser mapping or LIDAR (Light Detection and Ranging) can directly measure the three dimensional structure of plant canopies, as well as, provide accurate digital terrain models (DTM). While temperate and boreal pine forests have been studied using these methods, very limited work has been done in subtropical pine forests. In this study, airborne LIDAR was used to characterize the three dimensional structure of the forest on Long Pine Key at Everglades National Park. Analysis of the vertical distribution of airborne LIDAR data points has shown that distinctive patterns can be described which are characteristic of the vegetation communities and transition zones for pine forests, hammocks and marshes. This information is a valuable resource for forest managers by providing landscape structural data over large areas.

[C3802]

"A First Study on the use of TerraSAR-X for Meteorological Purposes"

In this paper we present the predicted performance of the TerraSAR-X for meteorological purposes. Principally, the study focuses on the possibility of measuring rain over ocean and forest. Regarding the acquisition geometry, we investigate the rain volume and voxel resolution, the signal-to-noise ratio and the signal-to-clutter ratio. The clutter interference has been evaluated for intra- and inter-pulse ground returns. Measurement of rain for nadir-looking geometry looks promising over forest and ocean under almost all conditions. However, for side-looking geometry, rain detection could be only possible at very high rain rates. [C3803]

"Bistatic Image Processing for a Hybrid SAR Experiment Between TerraSAR-X and PAMIR"

Future bi- and multistatic SAR systems could support the scientific community and the commercial market with an additional and powerful tool for imaging and exploration of interesting areas on earth. With the diversity of geometries between transmitter and receivers one can achieve for instance improvements in scene classification,

extractions of particular features, and cost reduction. New experiments are necessary to investigate the advantages as well as the problems of bi- and multistatic SAR systems. This paper describes the bistatic use of the spaceborne SAR system TerraSAR-X for future space- borne/airborne SAR exploration. TerraSAR-X will illuminate a particular scene while the receiver, the airborne SAR system PAMIR, will collect the reflected signals on board of an aircraft. [C3804]

"Retrieval of Surface-layer Refractivity using the CSU-CHILL Radar"

The surface-layer refractivity, i.e., the refractive index of air near the earth's surface, can be retrieved from radar using a technique developed by Frederic Fabry, et al. In warm weather, the equation for the index of refraction humidity dominates over temperature and pressure, which has a significant impact on the phase of propagating electromagnetic waves from a radar. Thus, the refractive index can be measured by observing the phase change between any two stationary ground targets along a radial from the radar at roughly the same ground level. This index, in turn, can be used to estimate the water vapor near the surface. With this data, the evolution of the near- surface boundary layer moisture field leading up to convective storm initiation and storm evolution can be detected to enhance quantitative precipitation forecasts. Stationary ground targets are those that return strong radar echoes and do not produce rapid phase changes under slowly varying humidity levels, unlike vegetation, for example, that adds a significant random component to the measured phase as it moves in the wind. The calibration stage, which determines the stationary targets and reference phase, is a critical step, currently requiring manual selection of scans, ideally under conditions of uniform humidity in the radar coverage space. This procedure was recently performed using the dual-polarized CSU-CHILL S-band radar to estimate the refractivity. Prior to this experiment, only single polarization had been used for this estimation. [C3805]

"Surface Displacement Monitoring on Reclaimed Land Using PSInSAR Technique"

Large portion of western coast of Korean peninsular has been reclaimed. Because the reclaimed land stands on weak foundation, the subsidence monitoring is required for civil protection. Newly developed PSInSAR technique is applied to monitor surface deformation on reclaimed land in Incheon Port. There was long lasting subsidence on test area up to 30 mm/year. APS and DEM error are also analyzed for the confirmation of the result. [C3806]

"Estimation of the Deformation Temporal Evolution Using Airborne Differential SAR Interferometry"

This paper presents airborne DInSAR results using a stack of 14 images, which were acquired by the Experimental SAR (E-SAR) system of the German Aerospace Center (DLR) during a time span of only three hours and fifteen minutes. An advanced differential technique is used to retrieve the error in the digital elevation model (DEM) and the temporal evolution of the deformation for every coherent pixel in the image. Furthermore, some modifications in the differential processing chain are included to deal with the existence of the so-called residual motion errors, which play a similar role as atmospheric artifacts in the spaceborne case. The detected deformation of a corner reflector and of some agricultural fields allows to validate the proposed techniques to measure deformation phenomena with an airborne platform. [C3807]

"Interferometric Triherence for Ground Movements Monitoring"

Minor movements-of the order of 10 cm-of earth surface often precede landslides. Interferometric techniques have a potential of detecting such movements before a landslide occurs. An interferometric quantity-called triherence-was adopted for mapping of points where the interferometric phase is stable over at least one triplet consisting of three consecutive SAR scenes in suitable interferometric conditions. The results from JERS and ASAR triplets of the two study sites suggest that the triherence measure enables to pick up some points in the landscape where the phase behaviour of SAR pixels is stable. Most of the stable points were identified in urban areas but many of them can also be found in natural areas. The initial hypothesis, that in case of sparse vegetation or sparse forest cover, some highly coherent scatterers might be found, seems to be pertinent even if it still needs to be thoroughly checked on the ground. [C3808]

"DEM Reconstruction Accuracy in Multi-Channel SAR Interferometry"

Interferometric SAR (InSAR) systems allow the estimation of the height profile of the Earth surface. Maximum Likelihood (ML) and Maximum A Posteriori (MAP) statistical techniques have shown to be effective for such problem if multiple interferograms, obtained with different baselines and/or with different frequencies, are used (multi-channel InSAR). In this paper, we evaluate the reconstruction performance of the considered ML and MAP statistical height estimation methods in terms of the Cramer-Rao Lower Bounds (CRLB) of the estimated height values. [C3809]

"Use of Disdrometer Data for X-Band Polarimetric Radar Simulation and Tropical Rain Characterization"

Natural variations in raindrop size distribution (DSD) were studied for simulated X band radar response from October 2004 to July 2005 (normal no-storm conditions) and during September 15th to 16th, 2004 when the tropical storm Jeanne passed over the island of Puerto Rico. Three types of estimators of rain rates were examined: A classical estimator $R(ZH)$ and two polarimetric radar estimators $R(KDP)$ and $R(ZH,ZDR)$. According to simulation results, the normalized errors (NEs) with respect data disdrometer of $R(ZH)$, $R(KDP)$ and $R(ZH,ZDR)$ for all DSD samples in October 2004 to July 2005 data are 40.85%, 14.73%, and 15.83% respectively, while for the tropical storm Jeanne they are 23.39%, 9.35% and 14.53%. The results show that the estimator $R(ZH)$ is the most sensitive to variations in DSD. Calibrated R-Z relations were developed for X-band for two conditions: storm/no-storm. Data from NASA TRMM satellite and rain gauges, the rain rate per hour was used for pinpointing areas of heaviest rain and for validation. [C3810]

"Improved Rain Attenuation Correction Algorithms for Radar Reflectivity and Differential Reflectivity with Adaptation to Drop Shape Model Variation"

One important goal of the Collaborated Adaptive Sensing of the Atmosphere (CASA) Engineering Research Center is to observe and monitor hazardous weather events in the low troposphere (below 1 km) by deploying networks of small, low- cost radars with small antennas. The first generation of CASA radar networks with dual-polarization capabilities is being deployed in Oklahoma. To achieve good sensitivity with small antenna size, high frequencies (X-Band) are selected. It is well known that signals transmitted at such high frequencies suffer attenuation due to rain along the propagation path. This article describes improved rain attenuation correction algorithms which correct radar reflectivity (Z_h) and differential reflectivity (Z_{dr}) through measured differential propagation phase ($Phdp$). [C3811]

"Advances on DInSAR with ERS and ENVISAT Data using the Coherent Pixels Technique (CPT)"

In this paper, improvements on the Coherent Pixels Technique (CPT) for deformation phenomena monitoring are presented. Advances are made in the different steps of the algorithm (from data selection to their processing) improving quality of the results and computational time. Deformation results of different studied areas are presented revealing the power of DInSAR techniques for risk management and for the understanding of much geological process. [C3812]

"Testing and Validation of the CASA DCAS System"

We present a system emulator that provides a versatile environment for testing and validating a distributed system for sensing of the lower atmosphere during its development lifecycle. The emulator, along with its comprehensive RAPIDS toolbox, provide the necessary infrastructure to experiment with different parameters of the system to ensure that the system specifications are being met, while also providing the scope of experimenting with newer configurations and futuristic designs. Extensive monitoring of the system possible through RAPIDS, allows to expose bugs and performance bottlenecks. The remote experimentation feature of the system allows several users to drive/monitor the system without requiring physical access to the emulator. [C3813]

"A Radar Sensing Algorithm by Gabor Theory"

In this paper, an alternative target density function (TDF) is proposed for narrowband radar model. This is achieved by estimating a new target density function by Gabor theory. It is shown how Gabor transform can be used to obtaining wideband target density function by transmitting a waveform which is a kernel for this transform. The windowing characteristics of this theory is plausible to reaching an accurate result. The presented wideband target density function is developed in a various manner different from the conventional methods. [C3814]

"Consideration of the Correlation between Beta-angle and Lineament Patterns by Using Polarimetric SAR Images"

This paper describes the relationship between a polarimetric parameter, the beta-angle, and the lineament features based on the eigenvalues and eigenvectors of the coherency matrix of the polarimetric SAR (POLSAR) data. First, coherency matrix was calculated from the Pauli vector of the POLSAR image set. Then, eigenvalues and corresponding eigenvectors of the coherency matrix were calculated. Subsequently, beta-angle, derived from the eigenvalue and the corresponding eigenvectors. However, the beta-angle has the potential to represent the orientation of the scatterer about the radar line of sight. In addition, alpha-angle has been obtained using the

same eigenvector above. We validate them using fully polarimetric L-band SAR data. The relationship between these two angles is also discussed, and a two-dimensional feature space is constructed (beta-alpha space). We then show initial results of applying the beta-alpha space to the Japanese airborne polarimetric and interferometric SAR (Pi-SAR) to extract features of lineaments as one of the geological features of the land surface. The results demonstrate that the effectiveness of the proposed extraction algorithm. [C3815]

"Segura River Aquifer (SE Spain) Obtained by Means of Advanced DInSAR"

The hydrological quality of an aquifer system is evaluated by means of two parameters: its capabilities to transmit water (transmissivity, T) and to store water (storage coefficient, S). In this work, a method based on temporal data of the surface subsidence is employed to calculate storage coefficients (S) and transmissivities (T) of the Vega Media of the Segura river aquifer-system. Subsidence data are obtained by means of differential SAR interferometry. The retrieved values of S for all available wells vary from 3.2 times 10^{-5} to 1.9 times 10^{-3} m/m. For the only well where water flow is available, a T value of 0.302 m²/day is estimated. First results show a reasonable agreement between data calculated with this technique and other acquired by means of in situ measurements. [C3816]

"A Simulation for Synthetic Aperture Radar with Digital Beam-Forming in Elevation"

In conventional SAR system high azimuth resolution and wide swath width are parameters that can not be improved simultaneously. A High-Resolution Wide-Swath (HRWS) Synthetic Aperture Radar (SAR) system was design to reconcile those two contradictory requirements. In the paper presented is a simulation of the HRWS SAR system including some of possible system failures and nonidealities of system components. The goal of the simulation is the evaluation of the influence of distortions and failures and prediction of the systems performance in elevation. [C3817]

"Road Extraction from High-Resolution SAR Image on Urban Area"

Because of active and side-look imaging and speckles in the SAR image, the road edge is blur and it is difficult to determinate the road edge. Therefore, extraction of the road from high-resolution SAR image can't use the methods that were used to the optical image. In this paper, we research how to extract the information of zonal road and how to get the vector road from the high-resolution SAR image. Usually, urban road is regular. In remote sensing image, the road has many characters, such as functional character, spectral character, geometric character and texture character so on. These characters consist of the knowledge of road extraction. After accurately expressing the character knowledge with mathematical equations, we can extract the road information more accurately. Therefore, we must construct road model after analyzing the road characters in the high-resolution SAR image. Based on the above analysis, we may accurately extract road from SAR image. By our experiment, the result proves that our method is a good idea. [C3818]

"Sea Ice Type and Open Water Discrimination for Operational Ice Monitoring with RADARSAT-2"

Envisat ASAR alternating polarization (AP) modes are evaluated to determine the potential utility of multi-polarization data for operational sea ice monitoring in preparation for RADARSAT-2. [C3819]

"InSAR Monitoring of Post-Landslide Activity"

In this study we used differential InSAR techniques to monitor current post slide activity at several landslides along transportation and energy corridors. The landslide materials vary from rock debris, glacial till to permafrost alluvium. Our results show that motion is triggered by spring melt and heavy rainfall events. In the northern Mackenzie Valley pipeline corridor seasonal landslide activity is related to permafrost melt during warm summer months. [C3820]

"InSAR Derived Deformation Patterns Related to the Aigion Earthquake (Greece)"

The detectability of the deformation pattern produced by the June 15, 1995 Aigion earthquake with DInSAR techniques is ensured by its magnitude ($M_w=6.3$), shallow depth and dip-slip mechanism. In this paper, stacking procedures are applied to a series of ERS interferograms in order to filter out from the differential phase field the atmospheric signal, and an a posteriori test is used to check the statistical properties of the atmospheric signal both in time and space. Based on the DInSAR-derived deformation pattern, a new fault model is proposed that takes into account the crustal layering of the western part of the Gulf of Corinth. [C3821]

"TerraSAR-X for Oceanography"

TerraSAR-X is a German X-band radar satellite to be launched in 2006. The system will provide synthetic aperture radar (SAR) data with high spatial resolution for both commercial and scientific use. The spacecraft will be equipped with a phased array X-band SAR, which can operate in different polarisations and has furthermore beam steering capabilities. In addition the system has a split antenna mode, which is able to provide along track interferometric information. The instrument is designed for multiple imaging modes like Stripmap, Spotlight and ScanSAR. Due to its polarimetric and interferometric capabilities as well as the high spatial resolution of up to 1 m, the TerraSAR-X sensor is a very interesting tool for oceanography. The presentation will give an overview of several applications, which are of both scientific and commercial interest like current and ocean wave measurements, monitoring of morphodynamical processes or high resolution wind field retrieval. The potential as well as limitations of the instrument are summarized and compared with existing sensors. Necessary steps to translate existing C-band SAR inversion algorithms for wind and wave measurements to X-band are discussed. A strategy is outlined to achieve this by a combination of theoretical investigations and the use of existing experimental data acquired by both airborne and groundbased X-band radar. [C3822]

"Studies of Ocean Surface Profile Retrieval from Simulated LGA Radar Data"

Retrieval of one dimensional ocean surface profile information is studied through the use of S and X band radar backscattering data at low grazing incidence. The required backscatter data is obtained through the use of numerical electromagnetic scattering codes. The simulations compute backscatter at multiple frequencies in each time step, so that range-resolved radar cross sections are obtained after an FFT operation. Profile retrievals are obtained through a simple "tilted Bragg" assumption, which allows local incidence angles on the surface to be directly determined from RCS data. These local incidence angles are then translated into surface slopes, and further integrated to construct the estimated profile. Initial results from this process are reported in this paper; further studies are in progress to quantify the overall accuracy achieved as a function of various surface and sensor parameters. [C3823]

"A New Set of the Parameters for the Terrain Surface Classification in Polarimetric SAR Image Based on Deorientation of Polarimetric Scattering Vector"

Deorientation theory of polarimetric scattering targets is developed, which transforms the scattering vector of spatially oriented targets into a certain status with minimization of cross polarization. A new set of the parameters u, v, w, Ψ is defined to describe and classify different terrain surfaces. Based on the vector radiative transfer (VRT) model of non-spherical particles above a rough surface, numerical simulations illustrate the parameters u, v, w, Ψ and the entropy H . These parameters are applied to the unsupervised classification in polarimetric images. The terrain surfaces of polarimetric SIR-C and airborne SAR images are classified and orientation-analyzed. [C3824]

"Bistatic Radar Cross Section Measurements of Ocean Scattered GPS Signals from Low Earth Orbit"

Signals from the Global Positioning System are constantly being scattered off the entire Earth's surface. These signals can be detected from airplanes, surface platforms and in Low Earth orbit and are known to contain information on the oceans. Recently, a new opportunity to study GPS reflections in space has been realized with the launch in October 2003 of the United Kingdom's Disaster Monitoring Constellation (UK-DMC) satellite. The UK-DMC carries a dedicated GPS reflections receiver and a custom designed downward facing antenna. Using this GPS experiment it is possible to process surface scattered signals and estimate the ocean wind and waves. This paper will present a method for calculating a bistatic radar cross section (BRCS) for ocean scattered GPS signals. This method will then be applied over a range of signals detected by the UK-DMC experiment. For purposes of comparison, numerous data collections have been collocated with National Data Buoy Center (NDBC) buoys. These buoys provide an independent measurement of the ocean wind, waves and often a wave frequency spectrum from which the surface mean square slopes, an indication of ocean roughness, can be determined. BRCS values have been estimated over a range of ocean conditions (from less than 2 m/s winds to greater than 14 m/s winds) and vary generally as expected when compared to buoy measurements of the ocean wind and waves. An empirical relationship between the estimated BRCS and the ocean wind speeds and surface roughness will be presented for a limited set of data gathered by the UK-DMC experiment. [C3825]

"A Multiple-Band Algorithm for Separating Land Surface Emissivity and Temperature from ASTER Imagery"

We intend to propose a multiple-band algorithm which can simultaneously retrieve land surface temperature and emissivity from ASTER data. We build four radiance transfer equations for ASTER band 11, 12, 13, 14, which involve six unknown parameters (average atmosphere temperature, land surface temperature and four bands

emissivity). We also analyze the emissivity characteristics of common objects about 160 kinds provided by JPL spectral database between thermal band 11, 12, 13, 14 and find that there is approximate linear relationship between them. For common 80 kinds of errors, the average emissivities error of band 11 and 14 are all under 0.01, the max emissivity error is under 0.0097 for band 11 and 14. So we can obtain six equations and six unknown parameters. In order to improve the accuracy, we can make some classification before retrieving land surface temperature. We can use three methods to resolve the equations. The first is that we make classification for image and get different equation, then resolve the equation. The second is Least-squares. The third is that, we can simulate database according to the characteristics of objects and utilize the neural network to resolve equations. The analysis indicates that the neural network can improve the practical and accuracy of algorithm.

[C3826]

"An Overview of Hampton University's 48-Inch Lidar System"

In 2004 Hampton University was the benefactor, via governmental surplus, of a world-class lidar system that is built around a 48-inch diameter-receiving telescope. LIDAR, is an acronym for light detection and ranging, which is the optical analog of microwave radar. The telescope for the LIDAR system has been positioned in HU's Observatory so that data can be taken at the zenith, viewing the sky through the movable dome roof. The proposed research develops a new capable LIDAR at HU for investigating novel laser remote sensing techniques and devices to strengthen our remote sensing program. This paper outlines HU's 48-inch lidar system, and the expected measurements it makes. Once the 48-inch LIDAR system is fully operational at HU it is to be a part of the Cloud-Aerosol LIDAR and Infrared Pathfinder Satellite Observation (CALIPSO) Quid Pro Quo Validation program. The program is important in validating the calibration and algorithms for the CALIPSO data. Data was taken while CALIPSO overpasses, and comparisons made. [C3827]

"Estimation of Friction Velocity Using Tower Based Marine Radars"

The friction velocity is estimated from image sequences of a marine Radar, which operates at grazing incidence with X-band at horizontal polarization in transmit and receive. Therefore, radar image sequences are analyzed in space and time. The direction of the friction velocity is extracted from streak like features visible in the image resulting from the temporal integrated radar image sequence. The orientation of these streaks are determined by derivation of local gradients of the radar images. The magnitude of the friction velocity is derived from the measured normalized radar cross section by a geophysical model function (GMF), which is parameterized by training of a Neural Network. For further improvement of the GMF the radar retrieved signal to noise ratio, which is strongly related to the significant wave height, is taken into account. The methodology is validated at FINO-I, a research platform in the North Sea, where various meteorological and oceanographical parameters are measured on an operational basis. The radar retrieved friction velocities are compared to in-situ wind directions as well as to the friction velocities estimated from in situ measurements using the TOGA COARE formulation. The comparison resulted in a standard deviation of 13deg for wind direction and 0.41 ms⁻¹ for the magnitude of the friction velocity. In contrast to traditional measurements the retrieval of friction velocity from marine radars is free of platform induced effects, e.g., turbulence, and can be used from moving platforms. [C3828]

"Oil Spill Surveillance and Tracking with Combined use of SAR and Modis Imagery: A Case Study"

The use of satellite remote sensing for oil spills detection has been attempted, traditionally, with synthetic aperture radar (SAR) sensors. These sensors are the most suitable instruments to the detection of slicks, since they damp strongly short waves measured by SAR and oil spills appear as a dark patch on the SAR image. However, SAR systems do not offer the required temporal acquisition rate of the same area, to guarantee the possibility to monitoring large oil spill movement on the sea. We propose the use of the Modis (Moderate Resolution Imaging Spectroradiometer) images acquired in sun glint conditions to reveal smoothed regions such as those affected by oil pollution. In this work we present a case study, in the Mediterranean Sea near the French coast, in which we have applied this methodology to a large oil spill detected on a SAR image of the 8th July 2002. Using two Modis acquisitions in the same day, one by Modis/TERRA 20 minutes later the ERS2-SAR acquisition and the other by Modis/AQUA 80 minutes later the first Modis acquisition, we show that it is possible to surveil the oil spill in its movement towards north-west. Wind speeds and directions at 10 m above the sea surface were retrieved using the semi-empirical backscatter model CMOD4 on the SAR image, and utilized to track the movement of oil spill. Surface wind vectors predicted by the meteorological ECMWF model were exploited as guess input to SAR wind inversion procedure. The comparison between Modis images and the predicted position of the oil spill show an adequate agreement. [C3829]

"A Marine-Radar Wind Sensor"

A method, called WiRAR, is developed to measure the wind vector using a marine X-band radar as sensor.

WiRAR extracts local wind directions from wind induced streaks, which are visible in radar images at scales above 50 m. It is shown that the streaks are very well aligned with the mean surface wind directions. Wind speeds are derived with WiRAR from the normalized radar cross section (NRCS), by parametrization of its dependency on the wind vector, which was performed by training of a Neural Network. The dependency of the NRCS on sea state and atmospheric parameters, such as air-sea temperatures and humidity, were studied with respect to further improvement of WiRAR. Therefore, sea state parameters are extracted from radar-image sequences by derivation of the Signal-to-Noise Ratio (SNR) and wave phase speed at the spectral peak cp. The SNR is directly related to the significant wave height H_s . Recently, the research platform FINO-I has been set-up in the German Bight. This platform provides various environmental data, such as wind measurements at different heights of up to 100 m for studying the atmospheric boundary layer, as well as air-sea temperatures, humidity, and other meteorological and oceanographical parameters. WiRAR is applied to radar-image sequences acquired by a marine X-band radar aboard FINO-I. The derived wind vectors are compared to wind measurements at the platform. The comparison of wind directions resulted in a correlation coefficient of 0.99 with a standard deviation of 12.8deg and for wind speeds with a correlation coefficient of 0.99 with a standard deviation of 0.41 ms⁻¹, respectively. In contrast to traditional offshore wind sensors, the retrieval of the wind vector from the backscatter of the ocean surface makes the system independent of the sensors motion and installation height and reduces the effects due to platform induced blockage and turbulence effects. [C3830]

"Effects of Wind on Internal Waves Synthetic Aperture Radar Images"

A theory of internal wave synthetic aperture radar (SAR) imaging has been improved by applying Korteweg-de Vries (KdV) equation, Bragg back scatter model, and replacing surface wave action equation with high frequency ocean wave spectrum balance equation. An analytical expression for an ocean internal wave SAR image will be obtained. Based on the new theory, the effects of wind on internal waves SAR images are studied with theoretical and scale analysis. The results indicate that the effects of wind are comparable with the hydrodynamic parameters, and the signature of internal waves can be imaged on the SAR only when oceanic state is low. The results agree well with some observations. [C3831]

"Mapping of Snow Water Equivalent and Snow Coverage from Combined EO and in situ Data for Climatic Studies and Hydrological Forecasting Models"

Information on physical snow cover characteristics, such as snow water equivalent (SWE) and the areal coverage fraction of snow covered area (SCA), can be obtained from space-borne remote sensing data. The feasible instruments include optical spectrometers and microwave radars (SCA mapping), and microwave radiometers (SWE mapping). As data assimilation techniques are applied, the EO data-derived information can improve the performance of river discharge forecasting models and the knowledge on snow climatology. The results discussed here indicate that the assimilation of EO data-based SCA estimates to hydrological modeling significantly improves the accuracy of operational river discharge forecasts. The results also indicate that the employment of space-borne microwave radiometer data using the data assimilation technique improves the SWE or snow depth mapping accuracy when compared with the use of values interpolated from synoptic observations. [C3832]

"Using Shuttle Radar Topography Mission Elevation Data to Map Mangrove Forest Height in the Caribbean"

In this paper we describe a methodology to map mangrove forests in 3D in the Caribbean region. We used shuttle radar topography mission (SRTM) elevation, lidar and field data to estimate mangrove mean tree height at the landscape scale. This paper emphasizes two regions which are undergoing ecosystem restoration activities: The Everglades National Park, USA and Cienaga Grande de Santa Marta, Colombia. In these regions we used, respectively, airborne and spaceborne (ICESat (ice, cloud, and land elevation satellite)) lidar data to calibrate SRTM data and estimate mean tree height. Our results show the method is accurate if mangrove forest canopy vertical structure is well characterized. [C3833]

"Aquarius Mission Technical Overview"

Aquarius is an L-band microwave instrument being developed to map the surface salinity field of the oceans from space. It is part of the Aquarius/SAC-D mission, a partnership between the USA (NASA) and Argentina (CONAE) with launch scheduled for early in 2009. The primary science objective of this mission is to monitor the seasonal and interannual variation of the large scale features of the surface salinity field in the open ocean with a spatial resolution of 150 km and a retrieval accuracy of 0.2 psu globally on a monthly basis. [C3834]

"The Aquarius Scatterometer: An Active System for Measuring Surface Roughness for Sea-

"Surface Brightness Temperature Correction"

The Aquarius scatterometer is a total-power L-band radar system for estimating ocean surface roughness. Its measurements will enable the removal of wind effects from the Aquarius radiometer ocean-surface brightness temperature measurements being used to retrieve ocean salinity. The Aquarius scatterometer is a relatively simple, low-spatial resolution power-detecting radar, without ranging capability. But to meet its science requirement, it must be very stable, with repeatability on the order of 0.1 dB over several days, and calibrated accuracy to this level over several months. Data from this instrument over land as well as ocean areas will be available for a variety of geophysical applications. [C3835]

"Comparison of PolSAR Speckle Filtering Techniques"

The objective of this paper is to compare the most widely used and the most recent speckle polarimetric synthetic aperture radar (PolSAR) filters. Two new conceptual approaches in PolSAR filtering are evaluated on simulated PolSAR images. The criteria of comparison includes indicator of speckle reduction capability, edge sharpness and preservation of scattering properties. Results indicate better performances with the partial differential equation (PDE) -based filters. [C3836]

"Spatially Variant Restoration for Polarimetric Synthetic Aperture Radar Imagery"

A. spatially variant speckle filter is proposed for multi-look polarimetric synthetic aperture radar (POLSAR) imagery. The central idea is that the filtering is applied only to homogeneous areas based on the scattering properties, while for detected edges, lines and point-like textural features, the original complex covariance matrix of these features is restored in order to preserve the actual features. The capabilities of the proposed filter were examined using nine-look NASA/JPL POLSAR C-band data. Based on the obtained results, the proposed filter showed a promising performance in speckle removal and radiometric preservation. Moreover, the point-like textural features as well as structural features (i.e. edges and lines) were well-retained in the filtered outputs. [C3837]

"Polar Decomposition and Polarimetric SAR Analysis: A Quaternion Approach"

We assess here the use of polar decomposition in SAR polarimetry, based on the quaternion formalism. Quaternions are helpful to obtain compact and original expressions of polar decomposition parameters, with straightforward extensions in bi-static polarimetry. Once the formalism of quaternions has been presented, both coherent and incoherent polarimetry approaches are discussed in this joint framework of polar decomposition and quaternions. Preliminary tests and comparisons with Cloude-Pottier parameters are conducted on ONERA/Ramses SAR data takes. [C3838]

"Classification of Polarimetric SAR Data Using Spectral Graph Partitioning"

A new approach for classification of Polarimetric Synthetic Aperture Radar (POLSAR) data is proposed using segmentation that is formulated as a graph partitioning problem. This work is motivated by the fact that human experts are very good at visual interpretation and segmentation of POLSAR data, which is often challenging for automated analysis techniques. Spectral graph partitioning, a framework that has recently emerged in computer vision for solving grouping problems with perceptually plausible results, is used with modifications necessary to accommodate POLSAR data. Using the similarity of edge- aligned patch histograms and spatial proximity, classification performance that is superior to the Wishart classifier is achieved. This approach also provides a way to combine region-based and contour-based segmentation techniques, as it can accommodate different representations of polarimetric data as well as other data sources (e.g., optical imagery). [C3839]

"Scattering and Propagation of Polarimetric Radar Signals in Storms and Clouds"

The introduction of differential reflectivity (Z_{dr}) and propagation differential phase ($Phidp$) was originally intended for improving radar estimates of rainfall rate. These parameters together with the effective reflectivity factor (Z_h) proved to be very useful for other applications as well. They have been shown to produce significant improvements over conventional single polarization radars in discriminating liquid and ice phase hydrometeors and, with the aid of several other polarimetric parameters (linear depolarization ratio and co-polar correlation coefficient), for classifying different hydrometeor types. Radar techniques developed for these purposes are being used in research applications and will soon become operational tools. The classification of ice phase hydrometeors and the quantitative estimation of their bulk parameters (e.g., median size, ice mass content, etc.) are necessary for better understanding storms and clouds. As methodologies are developed for extracting more information about hydrometeors using polarimetric radars, it becomes increasingly important to model the hydrometeors more accurately. Their shape, size, fall behavior, and composition must be represented with

sufficient detail, capturing the dominant features that influence the measured radar parameters. This paper reviews developments in hydrometeor modeling for dual-polarization radar remote sensing applications. The use of these modeling results in various applications such as rainfall rate estimation and hydrometeor classification are illustrated with the aid of experimental measurements. The first application of the "self-consistency" principle is discussed using dual-frequency polarimetric radar parameters (S-band Z_h and Z_{dr} with X-band Z_h and specific attenuation A_h). [C3840]

"Relation Between Coherence, Forest Biomass, and L-band σ_0 "

Relation between coherence, forest biomass, and L-band σ_0 were examined by using the L-band data taken by Japanese Polarimetric and Interferometric Airborne SAR (PiSAR). Several PiSAR observations were performed over a well-managed national forest, in which four kinds of conifers were dominantly planted. A coherence map over the forest area was made from two flight data, whose observation interval was about 30 minutes. The coherence in this site are ranging from 0.5 to 0.8. High coherence values of 0.7 ~ 0.8 were appeared at the young stands. On the other hands, some stands with high biomass also show high coherence value. Since the coherence values are weakly correlated with σ_{0HH} and σ_{0HV} at the stands with high biomass, the high coherence value and the high σ_0 value are considered to be the same origin. The regression curve between the coherence and a stem volume derived in this analysis shows higher coherence value than the other two JERS-1 (L-band) 44-day pair data and one ERS 1/2 C-band 1-day pair data. This may be due to the shorter repeat-cycle of the PiSAR pair data and difference of the scattering elements. [C3841]

"Yamase-derived Gap Winds Off the Western Hokkaido Coasts and Their Effects on Sea Surface Temperature Fields"

Suttu, which is located in the western Hokkaido, is known to be the 4th strongest windy place in Japan, where topographical gaps efficiently develop strong winds. These gap winds over the ocean and their effects on sea surface temperature (SST) fields are investigated by scatterometer- and synthetic aperture radar (SAR)-observed wind fields and the Advanced Very High Resolution Radiometer (AVHRR)-derived SST data. The SAR wind field observed by a wide-swath ScanSAR mode reveals a series of wind jet/wake patterns, which correspond to upstream land topography. The strong jets extend offshore over 100 km. It is found by several SAR-derived wind fields that these gap winds develop under the condition of upstream easterly winds. The easterly winds are common in spring and summer, which are known as the Yamase phenomena in northern Japan. Low/high SST patterns, which correspond to the jet/wake, are frequently observed off the western Hokkaido coasts in summertime. We create a composite image of the SST spatial anomalies for windy days, based on in situ wind measurements in Suttu. The composite image shows well-defined local SST cooling/warming stripes along general wind jet/wake regions. These are probably induced by the difference of the diurnal warming amplitude. [C3842]

"Wetland Characterization using Polarimetric RADARSAT-2 Capability"

Wetlands play a key role in regional and global environments and are critically linked to many major issues such as climate change, water quality, the hydrological and carbon cycles, and wildlife habitat and biodiversity. Mapping wetlands and monitoring their change in a systematic and repeatable manner for the Canadian Wetland Inventory (CWI), led by the Canadian Wildlife Service of Environment Canada (EC), are important in order to manage and protect significant wetland areas in Canada. The use of RADARSAT-1 Synthetic Aperture Radar (SAR) data has been shown to be important for wetland water extent characterization. However, the limited capability of RADARSAT-1's single-polarization C-band SAR in vegetation type discrimination makes the use of clear-sky- dependent visible near-infrared (VNIR) satellite data necessary for wetland mapping. In this paper, the unique polarimetric capability of RADARSAT-2 is investigated for wetland classification. The roll invariant incoherent target decomposition, the TSVM-ICTD [11], is used for optimum characterization of wetland target scattering. It is shown that like RADARSAT-1 HH polarization, the magnitude of the complex symmetric scattering is not effective for vegetation type discrimination. The phase of the symmetric scattering type has to be used for a more complete characterization of wetland vegetation species. This new phase scattering parameter introduced in [11] has been shown to be very promising for wetland classification using Convair-580 polarimetric SAR data. [C3843]

"Design and implementation of PALSAR Ground Data System at ERSDAC"

The Phased Array type L-band Synthetic Aperture Radar (PALSAR) is one of the imaging sensors onboard the Advanced Land Observing Satellite (ALOS) launched on January 24, 2006. The antenna of PALSAR is beam steerable to realize a variety of off-nadir angles. There are multi-polarimetric (dual and quad) observation modes and single polarimetric modes. It has also ScanSAR modes to observe a wide swath (250 km-350 km). PALSAR

Ground Data System (GDS) has been developed at ERSDAC since 1999. In the system, raw data provided from JAXA are processed to SAR images as final products which are archived and distributed to the worldwide users. The SAR data processor of PALSAR GDS is designed to achieve optimal data quality as well as maximum performance to meet the requirements from various users. [C3844]

"Dual-polarization Developments at CNR: Past and Present Research"

This paper reviews the research activities carried out by the radar meteorology group that was established at the Institute of Atmospheric Physics of the National Research Council of Italy. The group started in the late 1970s, and, after the publication of a keystone paper on the use of linear polarization by Seliga and Bringi (1976), its primary focus has been on polarimetric radar techniques and their meteorological applications. The research efforts, realized through close cooperation first with Pennsylvania State University and later with Colorado State University, have produced positive results that have contributed to a spread in the knowledge of dual-polarization techniques and in learning important information about microphysical processes in clouds and precipitation. This paper highlights some of these research achievements. [C3845]

"Development of a C-band Polarimetric and Pulse Compression Radar in Okinawa, Japan"

National Institute of Information and Communication Technology (NICT, formally CRI) has developed a new C-band (5340 MHz) multi-parameter Doppler radar system with a bistatic Doppler radar network to establish the next-generation technology of rain observation for meteorological and hydrological applications such as weather forecasts and run-off analysis in predicting floods. This new radar is named COBRA (CRI Okinawa Bistatic polarimetric RADar). The weather targets of this system are typhoons, Baiu-frontal rainfall, meso-scale precipitation in subtropical zones, and clear air turbulence. Two transmitter (klystron) units are used for the polarization observation. The transmission polarization for each pulse is selected from six possible polarizations. Additionally, NICT has developed equipment for weather radar that modulates the transmitting signal and demodulates the received signal (i.e., a pulse compression function). This equipment has been added to the existing COBRA system, forming a new system referred to as COBRA+. The COBRA+ system uses two traveling-wave tube amplifier (TWTA) transmitter units. [C3846]

"Chill Radar Dual Polarization"

The CHILL radar was originally designed as dual polarization radar. It was put into operation in late 1971. The original concept was a dual frequency X-band and S-band system. In 1972, the idea of using it as polarization radar was suggested by Drs. Tom Seliga and Viswanathan Bringi. After several years, the X-band radar was discarded and the system became a dual polarization radar instead. This discussion outlines the changes that were preformed on the system to make it a good polarization system. The radar was dual polarization capable from the beginning with a switch which changed the polarization of the transmit signal. A short list of the changes that were made in the radar and there success and problems are presented. The changes started with an electrical operated switch (original design) which took a second to switch but no special processing; a modified processor and the same switch changing to a 4 second cycle; a ferrite switch with 2 microseconds switching time and changing the processor to one with more channels; two channel separate transmitter and receiver; new antenna; and finally a second new antenna. Most of these upgrades also involved signal processing updates. [C3847]

"The Development of the Chilbolton Radar 1977 to 1988"

The development of the Chilbolton Radar as a fast switched linear dual-polarization radar is given for the period 1977 to 1988. Reasons are given for the direction of the development, the solution of technical problems in the context of the technology of the time and the significance of international collaboration that gave impetus to the work. [C3848]

"The Application of AMSR-E Soil Moisture for Improved Global Agricultural Assessment and Forecasting"

Soil moisture is estimated by the U. S. Department of Agriculture (USDA) Production Estimates and Crop Assessment Division (PECAD) by utilizing a modified two-layer Palmer water balance model derived from temperature and precipitation observations. It is envisaged that these soil moisture estimates can be improved by integrating passive microwave data which has greater temporal frequency and covers larger spatial domains than available in the past. By integrating direct observations from the EOS Advanced Microwave Scanning Radiometer (AMSR-E) into the current PECAD soil moisture model, more accurate soil moisture and correspondingly crop yield estimates may be possible. This paper presents a methodology for soil moisture data assimilation using a simple bias correction and 1D Ensemble Kalman Filter data assimilation algorithm. An

outline of the technical approach is presented. [C3849]

"Ground-based Radar Interferometry for Terrain Mapping"

First Page of the Article [C3850]

"Suppression of Surface Clutter Interference with TRMM Precipitation Radar Observation"

First Page of the Article [C3851]

"Joint Statistical Distribution of Multi-Baseline SAR Interferograms"

First Page of the Article [C3852]

"Interferometric Model Order Selection: Validation of ITC Methods with Airborne Three-antenna SAR Data"

First Page of the Article [C3853]

"Global Precipitation Map using Satelliteborne Microwave Radiometers by the GSMap Project: Production and Validation"

First Page of the Article [C3854]

"Comparison of MODIS Atmospheric Water Vapor Retrieval, Meteorological Models Tropospheric Delay Estimation with the Results Derived from GPS"

First Page of the Article [C3855]

"Bright Band Reference Technique to Adjust the Observation of Spaceborne Radar"

First Page of the Article [C3856]

"Comparison of Instantaneous Rain Rate of Stratiform Rainfall from TRMM/TMI with PR"

First Page of the Article [C3857]

"Speckle Filtering of PolSAR and PolInSAR Images using Trace-based Partial Differential Equations"

First Page of the Article [C3858]

"Significance of LiDAR Return Signal Intensities in Coastal Zone Mapping Applications"

First Page of the Article [C3859]

"Dynamic Filtering and Mining Triggers in Mesoscale Meteorology Forecasting"

First Page of the Article [C3860]

"Exploring Small Footprint Lidar Intensity Data in a Forested Environment"

First Page of the Article [C3861]

"The Influence of Lidar Acquisition Settings on Canopy Penetration and Laser Pulse Return Characteristics"

First Page of the Article [C3862]

"Real-Time Processing Algorithm for Wide Swath Radar Interferometry of Ocean Surface"

First Page of the Article [C3863]

"Confirmation of the Surface Displacements by Using ENVISAT Repeat-pass Interferometry in East

Coast of Taiwan"

First Page of the Article [C3864]

"Simulation of Nadir Looking P-BAND Radar Return for Biomass Retrieval Applications"

First Page of the Article [C3865]

"Multi-variate Bayesian Classification of Soil Drainage using Feature-level Fusion of Topographic and Hydrologic Data"

First Page of the Article [C3866]

"Comparison of Forest Canopy Structures in SRTM to LIDAR Data"

First Page of the Article [C3867]

"Measuring Urban Parcel Lawn Greenness by Using an Object-oriented Classification Approach"

First Page of the Article [C3868]

"Evaluating the Potential of SAR-R99B L and X Bands Data for Amazon Deforestation Increment Mapping"

First Page of the Article [C3869]

"Using ERS-1 and ASAR Imagery for Mapping Forest in French Guiana"

First Page of the Article [C3870]

"Hierarchical Land-Use Classification Using Optical Imagery and LiDAR Data"

First Page of the Article [C3871]

"A SAR Image Classification Method Based on Dempster-Shafer Theory and Markov Context with Parametric and Kernel Method Estimation"

First Page of the Article [C3872]

"Influence of Snow and Plant Covers on the Seasonal Radar Remote Sensing Signal Variations"

First Page of the Article [C3873]

"Comparison of Antarctic Ice Sheet Elevation Between ICESat GLAS and InSAR DEM"

First Page of the Article [C3874]

"Research of the Effect Produced by Transients on the Correlation Properties of the Signals with Pseudorandom Phase Shift Keying in the Systems of the Radar Remote Sensing of the Earth"

First Page of the Article [C3875]

"Optimal Polarimetric Radar Rain Rate Estimator for Semi-arid Regions"

First Page of the Article [C3876]

"Polarimetric Covariance Matrix Least Squares Estimation for Weather Radar Applications"

First Page of the Article [C3877]

"High Wind Vector Retrieved from SSM/I"

First Page of the Article [C3878]

"Modelling Systematic Residuals in Absolute ZTD Estimation from GPS"

First Page of the Article [C3879]

"An Improved High Resolution Wind Ambiguity Removal Procedure for SeaWinds"

First Page of the Article [C3880]

"Attenuation Statistics for X-band Radar Design"

First Page of the Article [C3881]

"Statistical Modeling for Spatiotemporal Radar Observations and Its Applications to Nowcasting"

First Page of the Article [C3882]

"TRMM-derived Range-adjustment of Ground-based Radars in two Mediterranean Countries"

First Page of the Article [C3883]

"Accuracy and Limitations of Airborne LiDAR Surveys in Coastal Environments"

First Page of the Article [C3884]

"Monitoring Snow Cover Characteristics with Multifrequency Active and Passive Microwave Sensors"

The importance of microwave sensors in monitoring snow parameters is well recognized. However, several problems are still open regarding the reliability of remote sensing for operational use. In 2002-2005 a series of ERS SAR and ENVISAT ASAR images were collected on the Italian Alps to monitor the temporal evolution of snow cover. In the same time a long sequence of multi-frequency radiometric data was collected with ground based sensors. The measurements confirmed the potential of microwave active and passive sensors in monitoring the extent of wet snow cover and in estimating the liquid water content of wet snow and the snow water equivalent of refrozen snow. [C3885]

"Hurricane Winds Measured with Synthetic Aperture Radars"

Since 1999 several synthetic aperture radar (SAR) images of hurricanes have been acquired by the Canadian satellite RADARSAT-1 as well as the European satellite ENVISAT. Several of these SAR images have captured hurricanes of category 4 and 5. These SAR images provide a unique opportunity to investigate the utility of SAR data for estimation of hurricane winds as well as for the improvement of hurricane forecasting. Using the SAR wind retrieval algorithm WiSAR, we have obtained good accuracies (root mean square error of 18' circ and 1.5 ms-1) for low to moderate wind speed conditions. The algorithm enables one to retrieve wind fields with a resolution of up to 300 m over a swath width of up to 500 km. WiSAR is an algorithm, which has shown to give good results under low and moderate wind conditions. The algorithm extracts wind directions from wind induced streaks imaged by the SAR at scales above 200 m. Wind speeds are extracted from the SAR measured normalized radar cross section (NRCS) utilizing the C-band model CMOD5, which describes the dependency of the NRCS on wind. It will be shown that the algorithm enables to measure wind directions as well as wind speeds of over 50 m s-1. The SAR-retrieved wind fields are compared to results of a high resolution numerical hurricane model. [C3886]

"L-band Polarimetric Interferometry in Boreal Forest Parameter Estimation, a Case Study"

In this study we concentrate on the application and validation of forest height estimation by polarimetric SAR interferometry for boreal forest. The study material was collected during the FinnSAR campaign, carried out in Finland in fall 2003. The main instruments of the campaign were E-SAR airborne radar (L- and X-band) and HUTSCAT helicopter-borne profiling scatterometer (X- and C-band). The validated forest height estimation algorithm is based on random volume over ground (RVoG) model inversion by using POLinSAR data. We compare POLinSAR-derived forest height with results from profiling HUTSCAT scatterometer measurements and with ground measurements and discuss the results. Our results show that the forest height values, estimated by means of two different instruments, are in good agreement. [C3887]

"Tropical Cyclone Parameters Derived from Synthetic Aperture Radar (SAR) Images"

Ocean waves play an important role in the dynamics of extreme events like hurricanes or typhoons by

conditioning the air/sea fluxes of momentum, heat and moisture. In this study a data set of ENVISAT ASAR Scan SAR images (400 times 400 km coverage) are used to observe the structure of tropical cyclones and typhoons at the sea surface. The following features of hurricanes were determined: wavelength and direction of boundary layer rolls for information of mixed boundary layer depth, radius of maximum wind speed, sea state in terms of wavelength, and direction. These image parameters are related to parametric models of hurricanes and validated by aircraft measurements from the National Hurricane Center (NHC). The work aims at the improvement of prediction of the cyclone track, intensity and sea state at these high wind speed conditions. The paper focuses on two illustrative case studies from August 2005, e.g., images of Hurricane Katrina acquired over the Gulf of Mexico and of Typhoon Talim acquired over the NW Pacific. [C3888]

"Progress in Determination of Wind Vectors from SAR Images"

During the past decade, the ability to determine detailed information of ocean surface wind from Synthetic Aperture Radar (SAR) has been generally accepted. It is expected that SAR will provide all-day and all-weather wind parameters with high spatial resolution and high accuracy, which would provide valuable data to marine weather forecasters and SAR model designers. However, the methodology for retrieving wind fields from SAR is far from complete. Present procedures require that a prior wind direction must be available in order to get wind speed information from SAR images. Errors in wind direction can result in significant biases in the SAR-retrieved wind speed. The prior wind direction can be acquired from measurements of other instruments (scatterometer, buoys etc.), from meteorological model outputs, or from wind-induced slicks if evident in the SAR images. The latter method may be limited by the image; many SAR images don't have any obvious wind-induced slicks. He et al. [2005] developed a new gradient method model (GM), which can retrieve wind directions from SAR images without trying to infer slicks. However, thus far, this method can only be used in relatively uniform wind field situations. In this paper, two modifications to the GM method have been developed by introducing an optimal analysis method. Wind speed and direction (with ambiguity) can be retrieved directly. In this method, sigma0 from two overlapped sub-blocks of the SAR image are used to retrieve wind parameters, which would violate the original GM method, because it cannot be used in highly varied winds, such as hurricanes. The chief advantage of this method is that wind speed can be retrieved without additional reference wind directional information. The wind direction ambiguity can be removed by background geophysical information of the SAR image or by in-situ measurements. Two cases are considered to illustrate this new method. One is a simulated image with relatively uniform wind field, and the other is a Radarsat-1 image which captures the eye of hurricane Isabel before it made landfall in North Carolina in 2003 as a category 2 storm. In both cases, the retrieved wind result is shown to compare well with Quikscat measurements and in-situ data. However, error exists for highly-varied wind field, especially for the retrieved wind direction. Future investigation will focus on this limitation, and also conduct further comparisons. [C3889]

"Severe Weather Applications over the Oceans using ERS SAR Wavemode Data"

Due to the relatively small amount of in situ data available for the open oceans, particularly during extreme events, under such conditions remote sensing techniques take an important role in the retrieval of geophysical information. Up to now the only remote sensing system capable of providing information on two dimensional sea state on a global and continuous scale and under all weather conditions is the Synthetic Aperture Radar (SAR). In the scope of the project Wave Atlas, ESA provided a two years wave-mode dataset of ERS-2 SAR raw data, mainly collected during 1999 and 2000, which was reprocessed to single-look- complex imagerettes at DLR using the BSAR processor. In this study the data were used for a statistical evaluation resulting in global ocean maps of different basic image parameters and oceanic parameters like wind speed, significant wave height, mean period and their respective regional and temporal variability during the seasons of the year using the empirical algorithms CWIND1.0 and CWAVE1.0. Global statistics are given for the time frame of 1998 to 2000 and examples of severe storms are analysed in detail. In future, the reprocessing of wavemode data is planned to be extended to the full lifetime of ERS-1 and ERS-2, which is at least 1991-2006. As wave mode data are also available from the ENVISAT mission, there is the possibility for future expansion. [C3890]

"The Results of Spatio-Temporally Combined, Microwave Active-Passive Measurements of Snow, Bear and Vegetated Soil at 37GHz"

In this paper preliminary results of simultaneous and spatially coincident, polarimetric measurements of snow, bear and vegetated soil microwave reflective (radar backscattering coefficient) and proper radio thermal emission (brightness temperature) characteristics at 37GHz are presented. [C3891]

"Polarimetric Passive Microwave Signatures and RFI Suppression During the Soil Moisture Experiment/ Polarimetry Land Experiment in 2005"

The Soil Moisture Experiments in 2005 (SMEX05) and Polarimetry Land experiments (POLEX) were conducted jointly by the US Naval Research Laboratory, the USDA ARS Hydrology and Remote Sensing Laboratory and other cooperators in Ames, Iowa between 13 June and 3 July 2005. Leveraging upon proven methodology and existing facilities and experience from the preceding SMEX02 experiment, SMEX05/POLEX was designed to address algorithm development and validation issues related to current and future soil moisture sensor systems, including enhancement of the Aqua AMSR-E and WindSat soil moisture validation. It also encompasses three unique elements in its scientific objectives: (1) Exploration of unique polarimetric information from satellite sensors such as WindSat and CMIS for soil moisture with supporting NRL aircraft instrumentation. (2) Exploration of diurnal effects associated with soil, vegetation and atmosphere at the 6 am/6 pm observing times of WindSat, CMIS, Hydros, and SMOS. (3) Statistics and mitigation of RFI for CMIS risk reduction. In this paper, we present an overview of the experiment and some preliminary data analysis. [C3892]

"Forest Parameter Estimation Using JERS-1 Repeat-pass Interferometry: Stem Volume Retrieval in Siberia and Sweden"

This paper presents results from estimation of stem volume in boreal forest using backscatter and interferometric coherence from the L-band SAR on the Japanese Earth Resources Satellite (JERS-1). Five test areas in Siberia and one in Sweden have been included in the study. Data from 14 JERS-1 44-day pairs from Siberia and 12 pairs covering the Swedish test area have been evaluated. The best multitemporal combinations of the measurements give relative RMSE values ranging from 33% to 48%. When considering one of the two observables only, the lowest retrieval errors are obtained under frozen conditions when inverting the coherence and under unfrozen conditions when inverting the backscatter. [C3893]

"SAR Interferometric Approaches for the Analysis of Structural Forest Parameters: State of the Art and Perspectives for Brazilian Studies"

This paper presents three practical examples of airborne InSAR data application to improve the knowledge of forest structures. Two experiments were done in the Amazon tropical forest to study the spatial distribution of VLTs in the primary forest using LM filtering and a series of Markov processes and others, to map and model the estimation of biomass variations in primary and secondary forests. The third experiment refers to the relation of SAR data and the volumetric configuration of Eucalyptus sp. stands. The advances on the analysis of PolInSAR data are very helpful to increase, in the near future, the regional inventorying of land cover changes in the Brazilian territory. [C3894]

"Digital Height Modeling (DHM) of Tropical Forests using Multi-frequency InSAR Methodology"

The objective of this study was to verify how digital elevation models (DEM) built by P-band repeat pass synthetic aperture radar (SAR) interferometry (InSAR) and X band InSAR can be used for estimating a digital height model (DHM) of forested environments and assess its quality. P band signal penetrates towards the forest floor which potentially generates a ground level DEM. X band radar reflects on the top of the vegetation cover, so X band InSAR produces a digital surface model (DSM). The DSM-DEM difference is a map of the vegetation cover height, the DHM. The estimated DHM can be used for forest volume estimation over large areas and used for improving SAR image interpretation either in P or X band. In September 2000, the National Institute for Space Research of Brazil (INPE) and the Brazilian Army Cartographic Service Division (DSG) conducted a mission over the Tapajo acutes National Forest, Para acute State, Brazil when X and P band InSAR data was obtained. Extensive ground data collection, forest inventory, land cover identification and differential GPS altitude measurements was done over the area to permit proper results assessment. It was concluded that the estimated DHM has a good relationship with the vegetation cover height, ($r^2 \sim 0.96$) estimated from forest parameters measured on the ground survey. [C3895]

"Forest Height Estimation in Tropical Rain Forest using Pol-InSAR Techniques"

Tropical rain forest environments are highly complex and heterogeneous in terms of species composition and structure and is often difficult to access. Radar remote sensing is for large tropical regions the only available information source for monitoring. Pol-InSAR is a novel developed radar remote sensing technique sensible to the vertical structure of forest that allows the estimation and mapping of forest height. In this paper we demonstrate forest height inversion at two frequencies-L band and P band-by means of Pol-InSAR using INDREX-II data and addresses the problem of temporal decorrelation. [C3896]

"Relation between the Attenuation Coefficients and Interferometric Phase Center Heights Behaviors from P-band to L-band"

The objective of this paper is to examine the link between the attenuation coefficients and the interferometric phase center heights, for several frequencies from P-band to L-band, and to study in what extent it depends on the canopy architecture and description. This study relies on the use of a coherent and full polarimetric scattering model, which simulates the backscattered fields by a forested area. In a first part, we study the frequential behavior of the interferometric phase center heights and in the second part, we focus on the attenuation coefficients. The behaviors of these two quantities are compared and in a third part, we propose to empirically derive a relation between these two quantities and the mean forest height. Finally, we investigate if a change of the incidence angle has an impact on the determination of this relation. [C3897]

"An Approach for Multisensor Harmonization in Snow Cover Area Mapping"

In this study, we have developed an approach for fusion of optical and SAR data for snow cover fraction (SCF) retrieval that avoids the typical blending effects when combining independently retrieved geophysical data from different sensors. Instead of undertaking the sensor fusion at the geophysical parameter level, the fusion is done at the electromagnetic signal level. A state model, based on hidden Markov model theory, has been developed for the simultaneous signal from the optical and the SAR sensors. The model goes through a given set of states through the snowmelt season where transition probability distribution functions of time have been determined for each state transition. A coupling between corresponding models for optical and SAR observations has been developed in order to make a more reliable model of the sensor co-variation. [C3898]

"Tropical-Forest Density Profiles from Multibaseline Interferometric SAR"

Vertical profiles of forest density potentially are robust indicators of forest biomass, fire susceptibility and ecosystem function. Tropical forests, which are among the most dense and complicated targets for remote sensing, contain about 45% of the world's biomass. Remote sensing of tropical forest structure is therefore an important component to global biomass and carbon monitoring. As in radio astronomy, which uses multibaseline radio interferometry to measure the structure of celestial objects, so multibaseline interferometric SAR (InSAR) can be used to estimate the vertical structure of forests. Vegetation density profiles, along with radar backscattering characteristics and attenuation, determine the radar brightness profile "seen" by InSAR. This paper will describe an experiment at La Selva Biological Station in Costa Rica (~3m rainfall/year) in which we flew 18 effective fixed baselines over tropical forests at C-band (0.056 m wavelength) and L-band (0.25 m). Preliminary inversions for radar brightness profiles will be compared to extensive lidar profiles measured in the same area. They will also be compared to field-measured profiles. [C3899]

"Snow Water Equivalence Retrieval Using X and Ku band Dual-Polarization Radar"

In this study, we evaluated the feasibility of using the dual frequency (X-band 9.6 GHz and Ku-band 17 GHz) and dual polarization (W and VH) radar to estimate snow water equivalence through numerical simulations. [C3900]

"Development of Techniques to Retrieve Snow Covered Area (SCA) in Boreal Forests from Spaceborne Microwave Observations"

The feasibility of SAR data for the operational mapping of the fraction of Snow Covered Area (SCA) is investigated by applying Radarsat observations together with the modeling of error propagation. Additionally, the performance of SAR retrievals is compared with optical satellite data-based (MODIS) SCA estimates. The results indicate performance characteristics comparable with those of optical data retrievals even when wide swath Radarsat ScanSAR Wide A data are applied. The developed Radarsat data processing system is also implemented for the operative use to aid hydrological forecasting at the Finnish Environment Institute (SYKE). [C3901]

"Retrospective Change Detection based upon a Multi-season, Sparse Temporal Sequence of JERS-1 SAR Data"

First Page of the Article [C3902]

"Estimation of Soil Moisture from Multiincidence ASAR-ENVISAT Radar Data"

First Page of the Article [C3903]

"AMSR-E Accomplishments and Ongoing Activities"

First Page of the Article [C3904]

"Monitoring Urban Changes in Rome, Italy by Multi-Temporal ERS-SAR Images"

First Page of the Article [\[C3905\]](#)

"High Resolution Change Estimation of Soil Moisture by Combination of TMI Brightness Temperature and PR Surface Cross Section"

First Page of the Article [\[C3906\]](#)

"Spatial Characterization of Soil Moisture Using SAR Data"

First Page of the Article [\[C3907\]](#)

"Soil and Vegetation Moisture Variability Analyzed Through Combination of SAR and Optical Images and Theoretical Models"

First Page of the Article [\[C3908\]](#)

"Impact of Filtering Soil Roughness Low Frequencies on the Radar Backscattering Coefficient Simulated by the IEM Model"

First Page of the Article [\[C3909\]](#)

"SAR Estimation of River Surface Currents: A Sub-Aperture Analysis Approach"

First Page of the Article [\[C3910\]](#)

"Wave Measurements using a Dual-beam Interferometer Near Gulf Stream Boundary"

First Page of the Article [\[C3911\]](#)

"Observations of an ARSR System in Canton, MI with the L-band Interference Suppressing Radiometer"

First Page of the Article [\[C3912\]](#)

"Integration of MERIS and ASAR Data for LAI Estimation of Wheat Fields"

The objective of this work is to assess the accuracy of LAI maps retrieved from ENVISAT MERIS data over wheat fields. The method consists of comparing, at catchment scale, the LAI maps retrieved from MERIS data to those retrieved from ASAR AP data. The latter were preliminary validated, at field scale, by means of in situ data. The experimental site is an agricultural area, mainly devoted to wheat cultivation, located in the Basilicata region, close to Matera city (Italy). On this area ENVISAT MERIS, ASAR AP and ground data were intensively acquired during the 2004 growing season. Results indicate that errors affecting wheat LAI estimations derived from optical and radar data are comparable. [\[C3913\]](#)

"Use of Tandem-X in a Squinted Split Antenna Mode Configuration to Retrieve 2-D Current and Ocean Wave Information"

First Page of the Article [\[C3914\]](#)

"High Resolution Soil Moisture Mapping Using AIRSAR Observations During SMEX02"

First Page of the Article [\[C3915\]](#)

"Clutter Suppression Techniques for River Surface Current Measurements"

First Page of the Article [\[C3916\]](#)

"Mitigation of Terrestrial Radar Interference in L-Band Spaceborne Microwave Radiometers"

First Page of the Article [\[C3917\]](#)

"Decision Fusion of Hyperspectral and SAR Data for Trafficability Assessment"

First Page of the Article [C3918]

"Potential scientific applications of seawinds and its follow-on"

{no data available} [C3919]

"Modeling of atmospheric effects on InSAR by incorporating terrain elevation information"

{no data available} [C3920]

"Phase shifting error of active coded transponder in SAR external radiometric calibration"

{no data available} [C3921]

"Rainfall representativeness at TRMM & GPM PR resolution"

{no data available} [C3922]

"Characteristics of the melting layer in the mediterranean region from dual polarization radar measurements at vertical incidence"

{no data available} [C3923]

"Improving classification accuracy in through-wall radar imaging using hybrid prony~s and singular value decomposition method"

{no data available} [C3924]

"International charter 'space and major disasters' status report"

{no data available} [C3925]

"Rapid EO disaster mapping service: added value, feedback and perspectives after 4 years of charter actions"

{no data available} [C3926]

"The relation between the order parameter of K-distribution in high-resolution polarimetric SAR data and forest biomass"

{no data available} [C3927]

"Through-wall radar image reconstruction based on time-domain transient signals in the presence of noise"

{no data available} [C3928]

"INDREX II-indonesian airborne radar experiment campaign over tropical forest in L- and P-band: first results"

{no data available} [C3929]

"Estimation of the ocean current velocities from radar altimetry and applications to the North Pacific Ocean"

{no data available} [C3930]

"Measurement of scattering properties of vegetation at Ka-band by 35GHz polarimetric scatterometer"

{no data available} [C3931]

"Intensity-driven-adaptive-neighborhood technique for POLSAR parameters estimation"

{no data available} [C3932]

"A comparison of the different models used for interferograms flattening"

{no data available} [C3933]

"Polarimetric calibration of space SAR data subject to faraday rotation -a three-target approach"

{no data available} [C3934]

"Estimating scattering mechanism at oyster farm site by polarimetry SAR"

{no data available} [C3935]

"VHF scattering model from multilayer mixed species forests on top of a multilayer rough ground"

{no data available} [C3936]

"FDTD and single scattering formulation for simulation of foliage camouflaged hard targets"

{no data available} [C3937]

"Estimation of forest height and forested area with polarimetric SAR interferometry"

{no data available} [C3938]

"Statistical method for data compression and enhancement of multifrequency polarimetric SAR imagery"

{no data available} [C3939]

"Initial point selection and validation in PS-InSAR using integrated amplitude calibration"

{no data available} [C3940]

"Delineation of dry and melt snow zones in antarctica using microwave remote sensing data"

{no data available} [C3941]

"Proposal of bilinear surface compensation of distortion in least-squares phase unwrapping"

{no data available} [C3942]

"An extension to the wide swath ocean altimeter concept"

{no data available} [C3943]

"Retrieval of snow water equivalent with envisat ASAR in a norwegian hydropower catchment"

{no data available} [C3944]

"Two dimensional phase unwrapping of interferometric SAR data by means of wavelet technique"

{no data available} [C3945]

"Theoretical evaluation of phase center of artificial metal structure in NASA(IPL) topsar data"

{no data available} [C3946]

"Measurement of river surface currents using SAR techniques"

{no data available} [C3947]

"Digital elevation model enhancement from multiple interferograms"

{no data available} [C3948]

"Multi-incidence angle DEM generation and analysis using ENVISAT/ASAR data"

{no data available} [C3949]

"Change detection of enhanced, no-changed and reduced scattering in multi-temporal ERS-2 SAR images using the two-thresholds EM and MRF algorithms"

{no data available} [C3950]

"Unsupervised change detection in urban area using multitemporal ERS-1/2 InSAR data"

{no data available} [C3951]

"Fusion Of High Resolution Radar And Low Resolution Multi-spectral Optical Imagery"

{no data available} [C3952]

"Application of image matching technology based on SAR image to integrated navigation system"

{no data available} [C3953]

"Investigation of SAR wind field retrieval with respect to hurricane winds"

{no data available} [C3954]

"Implementation of ground-based SAR demonstrator system for digital beam forming"

{no data available} [C3955]

"Ocean surface wind vector retrievals using active and passive microwave sensing on ADEOS-II"

{no data available} [C3956]

"Ocean surface winds and wind waves off the northeastern Japanese coast by combined use of high-resolution active microwave sensors"

{no data available} [C3957]

"Coprocesing of radar coherence and spectral optical data"

{no data available} [C3958]

"Results from an airborne SAR GMTI experiment supporting TerraSAR-X traffic processor development"

{no data available} [C3959]

"A new method of parallel SAR image classification"

{no data available} [C3960]

"SPECAN filtering for dual-channel stripmap-SAR GMTI"

{no data available} [C3961]

"SAR ground moving target imaging based on keystone transform without interpolation"

{no data available} [C3962]

"Study on co-registration method based on correlation coefficient for InSAR signal processing"

{no data available} [C3963]

"Ocean features separation from multifrequency polarimetric SAR imagery"

{no data available} [C3964]

"Automatic detection of water bodies from spaceborne SAR images"

{no data available} [C3965]

"Classification of ASAR images based on texture"

{no data available} [C3966]

"Natural objects monitoring using polarimetric interferometric ground-based SAR (GB-SAR) system"

{no data available} [C3967]

"Using a ground based interferometric synthetic aperture radar (GBinSAR) sensor to monitor a landslide in Japan"

{no data available} [C3968]

"Disastrous environment after earthquake observed by airborne SAR (Pi-SAR)"

{no data available} [C3969]

"Polarimetric analysis of the disastorus environment by using Pi-SAR"

{no data available} [C3970]

"Use of radar profilers in multi-sensor ground validation for TRMM and GPM"

{no data available} [C3971]

"Development and cal/val plan of spaceborne dual-frequency precipitation radar for GPM"

{no data available} [C3972]

"Step frequency synthetic radar techniques for free-space and sub-surface imaging"

{no data available} [C3973]

"Image reconstruction by a ground-based SAR system"

{no data available} [C3974]

"A four-component decomposition of POLSAR image"

{no data available} [C3975]

"Analysis of ambiguity for synthetic aperture radar satellite with mechanical distortion in phased array antenna"

{no data available} [C3976]

"SAR system technology development for korean peninsula"

{no data available} [C3977]

"Forward looking radar imaging method using multiple receiver antennas and digital beam forming technique"

{no data available} [C3978]

"2-D Fourier domain SAR raw signal simulation accounting for sensor trajectory deviations"

{no data available} [C3979]

"Versatile SAR sensors for south east asian applications"

{no data available} [C3980]

"Spaceborne small SAR technology demonstration"

{no data available} [C3981]

"An airborne SAR development demonstration in Korea"

{no data available} [C3982]

"An experimental automobile-based SAR/InSAR"

{no data available} [C3983]

"Polarimetric calibration for low frequency UWBSAR system"

{no data available} [C3984]

"Bistatic GPR by using an optical electric field sensor"

In order to apply to land mine detection effectively, bistatic GPR using an optical electric field sensor as a receiver has been developed. The optical electric field sensor is very small and uses optical fiber instead of metallic coaxial cable. With the combination of these advantages and the bistatic radar system, it can be possible for an operator to measure quite flexible and safely. The sensor has been tested in stepped frequency radar system with frequency which consists of a vector network analyzer, a fixed double ridged horn antenna as transmitter and computer controlled receiver-positioner for 2D scanning. For considering effectiveness in real field, we applied impulse radar system, which consist of a digital oscilloscope and an impulse generator to produce the impulse with 250 psec pulse width and the diffraction stacking has been adopted for 3D image reconstruction. Detection of a PMN2 mine model was carried out by the impulse radar system at a sand pit with two modes of data acquisition: the stepped data acquisition and the continuous data acquisition. The PMN2 were detected clearly with sufficiently high resolution in TM mode measurement in both modes, the target contrast was almost the same while the scanning time decreased down to 1/18, 9 min/m² in case of continuous data acquisition mode which satisfies the requirement for practical use. [C3985]

"Evaluation of an array type directional borehole radar system"

An array type directional borehole radar system employing passive sensors, optical electric field sensors was developed. The system uses a dipole antenna for transmission and four optical electric field sensors for reception. Four sensors are evenly arranged in the circumferential direction to constitute an antenna array. Although an optical electric field sensor itself does not have directivity, azimuth angle of a target can be known from phase differences among the four sensors. Difficulty of this approach lies in the fact that, due to the size of a borehole, the spacing between sensors is limited to a few centimeters that is significantly smaller than the wavelength. As a result, phase difference to be extracted is small and easily subject to noise. In addition, mutual coupling between the antenna elements may causes distortion of target signal. In this paper, we discuss feasibility of target azimuth detection. A laboratory experiment was carried out to examine capability of extracting a small phase difference and to evaluate the mutual coupling between antenna elements. [C3986]

"Road extraction from high-resolution SAR imagery using Hough transform"

This paper presents a technique for the extraction of roads in a high resolution synthetic aperture radar (SAR) image using Hough transform. Roads in a high resolution SAR image can be modeled as a homogeneous dark area bounded by two parallel boundaries. Dark areas, which represent the candidate positions for roads, are extracted from the image using a Gaussian probability iteration segmentation, and the roads are accurately detected by Hough transform. For this purpose, we designed an average Hough transform, which is more reasonable than general Hough transform for the extraction of lines. We search the peak values in Hough space and try to reduce its overall computational cost by introducing a global CFAR detector. In this process, to detect roads more accurately, post-processing, including noisy dark regions removal and false roads removal, is

performed. We applied our method to MSTAR clutter images of Redstone that have a resolution of about 1 ft Ч 1 ft. The experimental results show that our method can accurately detect roads. [C3987]

"Synthesis of generalized vertical-plane weather radar imagery along aircraft flight paths"

A method for synthesizing weather pictures in vertical planes along aircraft flight paths is presented. The weather data are derived from a number of Doppler radars covering different parts of the flight path. The flight path consists of straight segments with arbitrary offset and orientation with respect to individual radar locations. The intersection of radar scanning cones with the vertical plane segments are described as families of radial lines or hyperbolas depending on whether the flight path passes over a given radar or is offset from it. Radar data may be stretched or interpolated between radials to achieve continuity and smoothness of display. Schemes are incorporated for optimally using redundant data from multiple radars. Both scalar and vector weather data may be displayed. Such display is of great value for flight planning. [C3988]

"Effective 3D GPR survey and its application to the exploration of old remains"

Since the buried cultural relics are three-dimensional (3D) objects in nature, 3D survey is more preferable in archeological exploration. 3D ground penetrating radar (GPR) survey based on very dense data in principle, however, might need much higher cost and longer time of exploration than other geophysical methods. We developed a small-scale continuous data acquisition system which consists of two sets of GPR antennas and the precise positioning device tracking the moving-path of GPR antenna automatically and continuously. Besides this hardware system, we adopted a concept of data acquisition at arbitrary locations not along the pre-established profile lines, since the high cost of field work may be partly attributed to establishing many profile lines. Using the developed system, we performed 3D GPR survey to investigate the possible historical remains of Baekje Kingdom at Buyeo city, South Korea, prior to the excavation. Owing to the newly devised system, we could obtain 3D GPR data of this survey area having a real extent over about 17,000 m² within only six-hours field work. Although the GPR data were obtained at random locations not along the pre-established profile lines, we could obtain high-resolution 3D images showing many distinctive anomalies, which could be interpreted as old agricultural lands, waterways, and artificial structures or remains. This case history led us to the conclusion that 3D GPR method is very useful not only to examine a small anomalous area but also to investigate the wider region of the archeological interests. [C3989]

"Adaptive wire bow-tie antenna for ground penetrating radar"

In this paper the basic design of an adaptive GPR antenna is introduced. The antenna is able to adapt its input impedance to a variation in the antenna elevation and soil type to keep reflections at the antenna's terminal minimum. As a result, the energy radiated by the antenna into the ground for different antenna elevations and soil types would be maximized. The antenna is based on a wire bow-tie structure with variable flare angle for adjusting the antenna's input impedance. The flare angle variation is realized by short-circuiting the gaps which separate the wires from the antenna feed point. Electronic switching devices such as PIN diodes could be used to allow fast and convenient control of the antenna's flare angle. [C3990]

"Drill head mounted obstacle avoidance radar"

Horizontal drilling in soft soil provides an efficient and cost effective solution for the installation of utilities. However, with the increased congestion of underground utilities, the probability of damaging mislocated or unknown utilities increases, reducing the financial benefits of this technology and increasing the possibility catastrophic damage such as striking gas lines. It is hence important to develop instrumentation that is capable of locating obstacles lying along the bore paths. This paper discusses the development of a obstacle avoidance system based on ground penetrating radar technology. The system is a stepped frequency continuous wave (SFCW) radar that has been designed to fit within a standard 2.75 inch diameter drill head. The only above-ground components are the human machine interface (HMI) and power supply. Communication and power are transmitted underground via a wireline technique. An advanced demonstration model has been built and tested. The paper provides an overview of the requirements of an obstacle avoidance radar system. This is followed by a brief discussion of radar and antenna development required to implement the system. Finally results of indoor and outdoor field trials will be provided. [C3991]

"Subsurface water-filled fracture detection by borehole radar: a case history"

Borehole radar is a special mode of ground penetrating radar. It has several distinguished features from surface radar. For examples, by means of borehole access to deep regions below the surface, the radar sonde can be located relatively close to the anomalies or targets to be measured, this results in more precise targets response than surface measurement. The experimental site is located on the top of a granite hill west of Beijing, China.

There are a group of boreholes intersected by many fractures. The measured single-hole reflection data are processed and interpreted. The radial detecting range is more than 30 meters at this site. The subsurface fracture distribution can be imaged very clearly. Many fractures can be "seen", and their distance from borehole and their dip angle can be determined. The azimuth determinations for these fractures are possible in some situations. It is concluded that the borehole radar is an effective tool for subsurface imaging. [C3992]

"POLARSAR speckle filtering with structural feature and scattering property preservation"

In this paper two speckle filters for multi-look polarimetric synthetic aperture radar (POLARSAR) imagery are proposed, which preserve structural features, i.e. edges and line, as well as scattering properties. The filtering operations are performed spatially variant for the edges/lines along their orientation and for the homogeneous areas based on the scattering properties. The capabilities of both filters are demonstrated for the NASA/JPL nine-look POLARSAR C-band data, whereby comparisons with the Boxcar, Lee refined and Annealing filters are provided. In summary, both proposed filters show a good performance in speckle removal, structural feature retention and radiometric preservation. [C3993]

"Estimation of a buried pipe location by borehole radar"

A new parametric inversion technique to estimate a buried pipe location was developed for borehole radar cross-hole measurements. This technique evaluates the shapes of the approximated and measured arrival time curves instead of the first arrival time itself or wavefield in conventional inversion or tomographic techniques. In this study, we propose an algorithm of the technique and demonstrate its performance for synthetic and measured datasets. [C3994]

"One-dimensional model-based approach for ISAR imaging"

In this paper, we extend the estimation of scattering centre parameters to the case of ISAR imaging. The representation of a target by a set of individual scattering centres has shown promising results for applications where high resolution is needed (high-resolution imaging, classification, NCTR). In practice, methods extract time-delay and amplitude parameters associated with strong scattering sources from complex-valued reflectivity samples in the frequency domain. The principle has been successfully applied with samples from one or several segments. We show that a one-dimensional model can be used to create a two-dimensional ISAR image. After presenting the principle of ISAR matrix data collection and processing, we propose two methods for building the ISAR model matrix. We show that the technique processing the Doppler information first is more suitable for building ISAR-Model. As an example, we consider the case of a corrupted data matrix, which can be restored by coherently processing sparse sub-bands. Samples from a simulated Mig25 are used to illustrate the technique. [C3995]

"Oil slick detection and characterization by satellite and airborne sensors: experimental results with SAR, hyperspectral and lidar data"

Efficient observation means are required for regional-scale detection of oil slicks at sea, as well as for local-scale quantitative mapping in order to support operational fight and recovering operations, including reliable choice and guidance of maritime and airborne fighting means. An efficient oil slick detection algorithm based on a multiscale approach is proposed for operational regional-scale detection from satellite SAR images. The potential of combining airborne passive hyperspectral imagery and active fluorescence laser technology is proposed for local-scale quantitative characterization. The ways towards the use of both satellites and airborne remote sensors for use in operational emergency scenarios are discussed. [C3996]

"A new classification method based on Cloude Pottier eigenvalue/eigenvector decomposition"

In this paper, a new polarimetric scattering parameter, the averaged intensity (I), is introduced to present the backscatter intensity of fully polarimetric SAR data. According to the particular analysis on the properties of I , α angle and entropy H , the mapping rule of I - α - H feature space onto the intensity-hue-saturation (I - H - S) color space is proposed. We use the IHS transform instead of segmentation algorithm to finish the classification. The important advantages of this method are that the information contained in the I - α - H feature space is preserved without any loss in the resulting image, and the execution time is saved since IHS transform is faster than most complicated segmentations. The result shows that I has the additional information which is not contained in α and H , and the classification result is more readable than that of $H/\alpha/A$. [C3997]

"Statistical agreement between observed microwave satellite radiances and NWP hydrometeors including hexagonal plates and rosettes"

Accurate global observation of precipitation for all latitudes and seasons, and for all land, sea, and ice surfaces remains an elusive goal. One major obstacle to progress is lack of reliable global ground truth on horizontal and vertical scales consistent with those observed by satellite. For example, radar and scatter-dependent radiometric techniques respond to precipitation aloft, not on the ground, and can be unduly sensitive to large hydrometeors. On the other hand, rain gauges are excessively sensitive to local rainfall inhomogeneities and wind, and well-instrumented sites are rare. This paper quantitatively compares satellite observations with mesoscale numerical weather predictions of microwave brightness temperatures at those millimeter wavelengths most sensitive to hydrometeor structures and to the physics of precipitation. Only such models with high horizontal and vertical resolution allow comparisons of different sensors in detail. A Mesoscale Model, MM5, and a forward radiance program, TBSCAT, have been used to simulate radiances that would be observed from the Advanced Microwave Sounding Unit (AMSU-A and AMSU-B) aboard the NOAA-16 satellite for twenty-four globally representative storm systems, including 28,200 AMSU-A and 255,640 AMSU-B footprints, spanning a year. Good agreement has been obtained between histograms of coincident MM5-simulated and observed AMSU-A and AMSU-B radiances by adjusting ice parameter values in TBSCAT. Ice parameter values are consistent with the scattering for ice habits observed aloft, as computed using a Discrete Dipole Approximation program, DDSCAT6.1. These results suggest the potential use of MM5 as a rich new statistical form of ground-truth that will permit development of better precipitation estimators and improved understanding of precipitation itself, particularly in the more problematic areas of the globe. [C3998]

"Topography accommodation during motion compensation in interferometric repeat-pass SAR images"

This paper presents a new motion compensation algorithm to process airborne interferometric repeat-pass SAR data. It accommodates topography variations during SAR data processing, using an external digital elevation model. The proposed approach avoids phase artifacts, azimuth coregistration errors and impulse response degradation, which usually appear due to the assumption of a constant reference height during motion compensation. It accurately modifies phase history of all targets before azimuth compression, resulting in an enhanced image quality. Airborne L-band repeat-pass interferometric data of the German Aerospace Center (DLR) experimental airborne SAR (E-SAR) are used to validate the algorithm. [C3999]

"Signal processing algorithms for FMCW moving target indicator synthetic aperture radar"

The combination of frequency modulated continuous wave (FMCW) technology and synthetic aperture radar (SAR) leads to lightweight, cost-effective imaging sensors of high resolution. In FMCW SAR applications the conventional stop-and-go approximation used in pulse radar algorithms cannot be considered valid anymore, so the motion within the sweep needs to be taken into account. Analytical development of an FMCW SAR algorithm starting from the deramped signal and without using the stop-and-go approximation is presented in this paper; it is then validated processing simulated and real data. Furthermore, the effects of a moving target as they appear in an FMCW SAR image are described and the results can be used to assist moving target indicator (MTI) capabilities. [C4000]

"Snow covered area estimation using satellite radar wide swath images"

The feasibility of HUT snow covered area (SCA) method for operational snow melt monitoring, using large area satellite images has been determined. Previously the feasibility of the method has been proven for snow melt monitoring using spatially limited ERS-2 data. However, the spatial coverage of the data is an essential factor determining the operative usability of the method. Thus the adaptation of the method for Radarsat ScanSAR Wide (SCW) and Envisat ASAR wide swath medium resolution (WSM) data has been carried out, and the feasibility of the method using these data products has been studied. The analysis of the method was conducted by comparing the SCA estimates acquired from WSM and SCW data to reference data derived by optical remote sensing means. The analysis showed that the HUT SCA method is suitable for operational use with large area satellite radar images. [C4001]

"Ultra wideband radar assembly kit"

Ultra wideband sounding has been found to be suitable for a large number of applications in various areas. This results in a variety of different requirements concerning the measurement electronics. The article describes a conception of a measurement system, which provides for high flexibility in adapting performance to the actual need. [C4002]

"Synthetic aperture sonar 3-D imaging of targets in air using multiple, non-parallel shot lines"

Subsurface borehole radar imaging is an attractive technology in a number of applications. In order to test

algorithm development beyond pure simulation, acoustics radar (sonar) offers valuable insights into the practical performance of an algorithm. A sonar system operating at 40 kHz in air has been developed to allow the capture of acoustic image data in a laboratory environment. A deconvolution filter is generated for range compression, via a calibration technique, in which the system response is measured by pointing the transmitting transducer directly at the receiving transducer. The focused image is obtained by time domain synthetic aperture focusing/migration techniques. The practical drilling of boreholes results in non-parallel holes which can, however, be logged in three dimensions. A 3D reconstructed algorithm has been developed and implemented to reconstruct the image of the scene by multiplying the magnitude images acquired from multiple, non-parallel shot lines. The paper is structured as follows: firstly the inverse synthetic aperture sonar (ISAS) imaging experiment is described, followed by the signal processing techniques. Thereafter, the 3D imaging technique using focused magnitude images from non-parallel shot lines and the reconstruction grid spacing are described. [C4003]

"CryoSat prelaunch status and performance"

The CryoSat Earth Explorer Opportunity Mission will be the first mission to accurately determine the marine and land ice mass fluxes at a global scale. Its space segment is currently in its final test phase and will be shipped to its launch site Plesetsk in Russia by end of July. This paper gives a brief overview on the measured prelaunch performance of the CryoSat payload. [C4004]

"Polarization discrimination ratio approach to retrieve bare soil moisture at X-band"

An observation has been carried out at different incidence angle by X-band scatterometer for like polarizations (i.e., Horizontal-Horizontal and Vertical-Vertical) to retrieve the soil moisture of bare field. To retrieve the soil moisture with minimizing the surface roughness effect on the soil moisture a polarimetric discrimination ratio (PDR) ($PDR = (\sigma^\circ_{VV} - \sigma^\circ_{HH}) / (\sigma^\circ_{VV} + \sigma^\circ_{HH})$ where σ° is scattering coefficient for VV and HH-polarization) approach is proposed. Generally in microwave applications, polarization is sensitive to the size, shape and orientation of target elements, whereas frequency functions primarily as a size filter with important consequences regarding attenuation. In the polarization, the horizontal polarization gives a measure of the horizontal dimension of the emitting elements, while the vertical polarization essentially gives a measure of the vertical dimension. The power observed to the system is a complicated function of each particle size, shape and density, therefore we have normalized the value of HH- and VV-pol to the range $-1 \leq PDR \leq 1$ to partially minimize the effect of orientation and shape on dielectric properties of the scattering elements and results mainly the effect of dielectric (i.e., moisture content) on σ° . The angular dependence of PDR on moisture is observed and it was found that the suitable incidence angle to observe the soil moisture at X-band with PDR is 35° . An empirical relation has been developed between PDR and soil moisture to retrieve the moisture content at X-band. The results are validated with another set of data. The retrieved values of soil moisture are in good agreement (standard error-1.02) with observed values of soil moisture. The significance of the results has been tested by F-ratio test and quite significant results were obtained. This type of results are helpful to use the microwave techniques to assess the soil moisture by the air-borne or space borne sensor and propose the suitable angle of incidence to observe the soil moisture with minimum effect of surface roughness at X-band. [C4005]

"Salient features of radar nodes of the first generation NetRad System"

The recently established National Science Foundation Engineering Research Center for Collaborative Adaptive Sensing of the Atmosphere (CASA) will be deploying the first generation of an automated network of four low-power, short-range, X-band, polarimetric, Doppler radars, known as NetRad, in central Oklahoma in late 2005. This network is developed with the goal of tracking tornadoes with high spatial and temporal resolution as well as mapping severe weather events in the lowest 2 km of the troposphere. Each radar node has been developed to accomplish this system goal through the coordinated interaction with other radars in the network via a real-time, closed-loop software control system. This paper will describe the characteristics of the individual radar nodes in the system, with emphasis on those aspects of the design that lend themselves toward operation as a coordinated network. Calibration results and performance characteristics of the single node radar of the first generation system will also be presented. [C4006]

"Speckle filtering influence on unsupervised terrain classification based on polarimetric scattering mechanisms"

Two scattering model-based decompositions (the first one, developed by Freeman and Burden (1998), where pixels are divided into three scattering categories: surface, volume, and double bounce, and the second, developed by Cloude and Pottier (1997), where scattering mechanisms, characterized by entropy H , and α -angle, are used for classification) were investigated in terms of speckle filtering influence on classification parameters. Freeman and Burden decomposition gives us less problems with relation to speckle filtering.

Whereas in Cloude and Pottier decomposition, speckle filtering and averaging are very critical moments. Polarimetric radar images of Moscow region acquired in 1994/10/09 by SIR-C/X SLC L-band data are used for illustration. Results from unfiltered and Lee-filtered (Lee et al., 1999) Burden and Freeman decomposition images and entropy images are compared. A great influence of speckle filtering on Cloude and Pottier classification parameters was demonstrated. [C4007]

"Data acquisition for 3D city models from LIDAR extracting buildings and roads"

This paper deals with the automatic extraction of buildings and roads for 3D city models using LIDAR. The results presented in this paper show both the potential and the limitations of LIDAR data with respect to these tasks. [C4008]

"Improvement of road extraction in high resolution SAR data by a context-based approach"

This paper deals with the problem of road extraction in high resolution SAR data. The presented method is an improvement of previous works. The process is an almost automatic algorithm based on a Hough transform and a road tracking algorithm. The main limitations of the process are due to the road context. First investigations to exploit contextual information in the process are presented. [C4009]

"Unsupervised oil slick detection by SAR imagery using kernel expansion"

Spaceborne synthetic aperture radar is well adapted to detect ocean pollution independently from daily or weather condition. In fact, oil slicks have specific impact on ocean wave spectra. Initial wave spectra may be characterized by three kinds of waves, big, medium and small, which correspond physically to gravity and gravity-capillary waves. The increase of viscosity due to the presence of oil damps gravity-capillary waves. This induces a damping of the backscattering to the sensor, but also a damping of the energy of the wave spectra. Thus, local segmentation of wave spectra may be achieved by the segmentation of a multiscale decomposition of the original SAR image. In this work, an unsupervised oil slick detection is proposed by using kernel-based novelty detection into the wavelet decomposition of a SAR image. It performs accurate detection with no consideration to signal stationarity nor to the presence of strong backscatters (such as ships). The algorithm has been applied on ENVISAT ASAR images. It yields accurate segmentation results, even for small slicks, with a very limited number of false alarms. [C4010]

"Derivation of near surface soil moisture patterns from ENVISAT ASAR data"

Water and energy fluxes at the interface between the land surface and atmosphere are strongly depending on the surface soil moisture content which is highly variable in space and time. It has been shown in numerous studies that microwave remote sensing can provide spatially distributed patterns of surface soil moisture. New sensor generations as ENVISAT ASAR or RADARSAT allow for image acquisitions in different imaging modes and geometries. Imaging modes with large area coverage capabilities as the wide swath mode of ENVISAT ASAR are of special interest for practical applications in this context. The paper presents a semiempirical soil moisture inversion scheme for ENVISAT ASAR data. Different land cover types as well as mixed image pixels are taken into account in the soil moisture retrieval process. The inversion results are validated against in situ measurements and a sensitivity analysis of the model is conducted. [C4011]

"Incorporating a vegetation index into a soil moisture retrieval model \$results from Convair-580 SAR data"

A flexible method of introducing a SAR vegetation index into the Dubois model for soil moisture retrieval using polarimetric SAR data is introduced. Based on the vegetation sensitivity at each pixel, the vegetation index is incorporated on a pixel by pixel basis using the water cloud model. An approach for minimizing the need for ground measurements, by remotely estimating the parameters required for the vegetation index, is suggested. The proposed model is applied to CV-580 airborne SAR data and the vegetation correction was found to reduce the rms error in the model. [C4012]

"A simple method for spatial disaggregation of radiometer derived soil moisture using higher resolution radar observations"

The SMEX02 experiments held in June-July 2002, at Iowa demonstrated the potential of the L band radiometer (PALS) in estimation of near surface soil moisture under dense vegetation canopy conditions. The L band radar was also shown to be sensitive to near surface soil moisture. However, the spatial resolution of a typical satellite L band radiometer is of the order of tens of kilometers, which is not sufficient to serve the full range of science needs for land surface hydrology and weather modeling applications. Disaggregation schemes for deriving sub

pixel estimates of soil moisture from radiometer data using higher resolution radar observations may provide the means for making available global soil moisture observations at much finer scale. This paper presents a simple approach for disaggregation of coarser resolution radiometer estimates of soil moisture using higher resolution radar backscatter and vegetation water content measurements. The algorithm has been applied to coincident PALS radiometer and Aisars datasets of 400 m and 30 m spatial resolutions respectively acquired during the SMEX02 campaign. PALS radiometer estimates of soil moisture at a 400 m resolution have been disaggregated to 100 m resolution. [C4013]

"Signal processing method for detection of subsurface objects by ultra-wideband SAR"

The problem of subsurface target detection has been studied. Modifications of a damped exponential model has been applied for reducing the clutter due to a rough boundary. Utilizing numerical simulations, a sensitivity analysis is performed to investigate the features of detection of low-contrast targets. The dependence of the received signal on the properties of an inhomogeneous medium, rough surface and the locations of the objects has been studied. The calculations have been performed for randomly buried objects. It has been found that it is possible to significantly improve the ratio between the scattered signal from subsurface objects and the scattering from a rough boundary. [C4014]

"Landmine imaging by a hand-held GPR and metal detector sensor (ALIS)"

We are developing a new landmine detection system, namely advanced landmine imaging system (ALIS), which is equipped with metal detector (MD) and ground penetrating radar (GPR). Despite it is a hand-held system, we can record the MD and GPR signals together with the sensor position information acquired by CCD camera. Therefore, MD image and GPR image can be obtained after signal processing. Since ALIS is a hand-held system, the sensor position is random when it is operated in the field. So interpolation processing is needed to provide a gridded data set for both MD and GPR. A good MD image can be achieved after interpolation. Also, interpolation can prepare the gridded data set for migration. 3D Kirchhoff migration is used to enhance the signal-clutter ratio for effective image reconstruction. The ALIS was tested in Afghanistan in December 2004 and showed a good performance. In particular, the GPR could obtain a good image of anti-personnel (AP) mine buried at more than 20 cm depth. Also images from both sensors could be combined to distinguish a mine from a metal fragment. [C4015]

"The MOSS VHF/UHF spaceborne SAR system testbed"

Summary form only given. This paper details our recent development of a system prototype for a spaceborne sensor that addresses the current NASA science priority of measuring soil moisture "under a substantial vegetation canopy and reaching a useful depth within the uppermost soil layer". The mission is named MOSS, for the Microwave Observatory of Subcanopy and Subsurface. It will enable measurement and derivation of data products not obtained from any other current, planned, or proposed instrument, with a solution that offers high science value through a low-mass and, in the long-term, low-cost approach. The proposed system is a spaceborne synthetic aperture radar (SAR) operating at the two low frequencies of 435 MHz (UHF, P-band) and 137 MHz (VHF) to enable sensing through vegetation and down into soil. The future mission scenario is achieved from a Sun synchronous orbit of 1313 km altitude, with a swath width of 430 km, incidence angle ranges of 17-30 degrees, resolution of 1 km, and a 7-day exact repeat consistent with the temporal scale of variations of the subcanopy and subsurface soil moisture. We describe a tower-based test-bed that we have developed to validate the spaceborne measurement concept. The processing software, including polarimetric calibration aspects, is detailed, and example science products are presented. The procedures and algorithms to estimate subsurface moisture are presented in detail, and the use an iterative estimation procedure is explained. The results are validated by comparing against detailed ground truth. [C4016]

"Land-surface parameters estimation from ERS Wind Scatterometer: a case study in China"

The ERS-1/2 Wind Scatterometer (WSC) operates at a frequency of 5.3 GHz (C-Band) with vertically like-polarised antennas both in transmission and reception (W-polarization). It continuously provides global measurement of radar cross-section from August 1991 to December 2000. WSC has a resolution cell of about 50 km but provides a high repetition rate (less than four days) and makes measurements at multiple incidence angles. The method presented in this paper combines a theoretical model and an empirical algorithm developed by previous authors to estimate land-surface parameters. The method is implemented using 15 days WSC data in China, a good agreement is observed between retrieved fractional vegetation and NDVI, and the temporal-spatial distribution of soil moisture is reasonable, too. [C4017]

"Soil moisture maps from ENVISAT ASAR images in both flat and mountainous areas"

In this paper the actual capabilities of ENVISAT/ASAR images in providing soil moisture maps have been tested. Several SAR images were collected on two test areas in Italy: a flat agricultural region in the Alessandria area and a mountain zone on the Cordevole watershed (Arabba). An inversion algorithm based on artificial neural networks (ANN) to retrieve soil moisture from backscattering data was tested and successfully compared to ground measurements. [C4018]

"Soil moisture retrieval from ASAR measurements over natural surfaces with a large roughness variability"

In this work, the accuracy of soil moisture retrieved from ASAR data over bare or sparsely vegetated surfaces is investigated by means of a simulation study. The soil moisture retrieval method is based on an optimization algorithm that appropriately inverts theoretical direct models by assimilating a priori information on surface parameters. In order to account for a large variability of roughness conditions, two complementary models have been used, namely the integral equation method model and the geometrical optics model. The performance of the inversion method has been assessed on simulated noisy ASAR data, as a function of different a priori information quality level. [C4019]

"Airborne measurements of rain and the ocean surface backscatter response at C- and Ku-band"

During the 2002, 2003, and 2004 Hurricane seasons, and the 2005 Ocean Winds and Rain Winter Experiment, the University of Massachusetts (UMass) installed two instruments on the NOAA N42RF WP-3D research aircraft: the Imaging Wind and Rain Airborne Profiler (IWRAP) and the Simultaneous Frequency Microwave Radiometer (SFMR). IWRAP is a dual-band (C- and Ku), dual-polarized pencil-beam airborne radar that profiles the volume backscatter and Doppler velocity from rain and that also measures the ocean backscatter response. It simultaneously profiles along four separate incidence angles while conically scanning at 60 RPM. SFMR is a C-band nadir viewing radiometer that measures the emission from the ocean surface and intervening atmosphere simultaneously at six frequencies. It is designed to obtain the surface wind speed and the column average rain rate. Both instruments have previously been flown during hurricane seasons 2002, 2003 and 2004. Spectral techniques can be used to differentiate the contributions of the volume backscatter from rain from the ocean surface backscatter. Initial results from the Winter 2005 datasets are presented. Attenuation from rain is also particularly important at high microwave frequencies such as Ku-band. Thanks to IWRAP's profiling capabilities, Ku-band attenuation models and dropsizes distribution (DSD) parameters of the observed precipitation from dual-wavelength techniques within tropical cyclones are presented. [C4020]

"RADARSAT-1 background mission monitoring of the Arctic"

RADARSAT-1 baseline data acquisition planning has been performed for the past nine years under the Canadian Space Agency's Background Mission. Background Mission is about building uniform, global archives in support of RADARSAT-1 Program objectives of time- and site-specific data collections. Most of these objectives were met in the first five years of the nominal mission duration. An extended phase of Background Mission is under way, the most important element of which is a continuous four-season coverage of the Arctic Basin. This paper reports on the progress of this coverage campaign, which started in mid-2003, and has since been implemented uninterruptedly for summer, fall, winter and spring snapshots of the northern polar cap and a large area around it. It is expected that the systematic, sustained RADARSAT Background Mission coverage of the Arctic would result into valuable temporal records of a part of the world that is particularly sensitive to global climate change. [C4021]

"RADARSAT-2 Program update"

RADARSAT-2 will be the next Canadian commercial Earth observation SAR satellite. The construction of the spacecraft and the development of the ground segment are progressing well. This paper presents an overview of the mission, some featured innovations, imaging capabilities and data distribution aspects. [C4022]

"Constant false alarm rate in fire detection for MODIS data"

{no data available} [C4023]

"RADARSAT-1 image quality excellence in the extended mission"

RADARSAT-1, the first Canadian SAR remote sensing satellite, continues to provide calibrated data to worldwide users since the start of its routine operation on April 1, 1996, more than 9 years after its launch on November 4, 1995. Both single beams and ScanSAR imagery are still monitored routinely for radiometric calibration performance based on images of the Amazon Rainforest, and for image quality performance using imagery of

the RADARSAT-1 precision transponders. This paper briefly describes image quality results and recalibration work. [C4024]

"Applications potential of RADARSAT-2-update"

In this paper, we briefly preview and demonstrate how the technical improvements included in RADARSAT-2 will impact the system's potential utility for 32 applications in the fields of agriculture, cartography, disaster management, forestry, geology, hydrology, oceans, and sea and land ice. [C4025]

"Application of multiresolution and multispectral polarimetric techniques for reliable vessel monitoring and control"

Carrying out an effective monitoring and control of fishing activities is indispensable to guarantee a sustainable exploitation of sea resources. Nowadays, it is widely assumed that spaceborne synthetic aperture radar (SAR) constitutes a valuable and effective tool for this purpose. Nevertheless, automatic interpretation of SAR images is often puzzling. Hence this paper proposes a new framework for the understanding and handling of SAR data based on the wavelet transform. Specifically, a novel algorithm for ship detection is proposed, justified and tested. On the other hand, this paper aims at bringing some insight at ship detection capabilities of light polarimetric systems. [C4026]

"Countdown for RADARSAT-2 system operations"

RADARSAT-1 has been operating for over nine years as the world's first commercial space-borne synthetic aperture radar (SAR) remote sensing system. RADARSAT-2 provides for a continuation of the RADARSAT-1 services, enhanced performance, new features, and a more commercial approach to both the development and operation of the system. This paper describes some key aspects of the development from an operations perspective along with the system integration and preparation for operations. Following a system operations overview, constraints, driving requirements, and mission characteristics determining the operations concept are described. Operations lessons learned from RADARSAT-1 system development and operation and factored into the RADARSAT-2 approach are summarized. Organizational and technical challenges and solutions for development and system operations are explored using RADARSAT-2 examples. A key challenge is to perform the system integration for RADARSAT-2 without interference to continuing RADARSAT-1 operations. The paper describes the phases, major activities and milestones of the system integration, and key features of the operations preparation for the system components. [C4027]

"Test evolution: RADARSAT-1 to RADARSAT-2"

Test methodology for large spacecraft like RADARSAT-1 and RADARSAT-2 has been modified over the last decade resulting in changes to test environments. These changes in the required test environment have necessitated improvements in the test configuration modelling, instrumentation, and data acquisition systems. This paper will identify the significant changes and how the RADARSAT-2 assembly integration and test program has implemented these improvements. [C4028]

"Application of ERS SAR to the study of korean tidal flats"

{no data available} [C4029]

"Interference of short range radar with radio astronomy base stations"

{no data available} [C4030]

"Verification of timber age mapping with shuttle radar topography mission and national elevation datasets in the U.S."

{no data available} [C4031]

"Research of deformation of the fine phase structure of ultra wideband radar signals when passing through the system of identical selective filters"

{no data available} [C4032]

"Radiometric correction and calibration for low frequency UWB SAR system"

{no data available} [C4033]

"Spot image / SARCOM: distribution of envisat images and direct receiving stations for various land applications"

{no data available} [C4034]

"Land motion monitoring in Japan using PSInSAR technique"

{no data available} [C4035]

"Verification of X-band SRTM DEM data quality in New Zealand"

{no data available} [C4036]

"Extraction of maintenance information on irrigation ponds using polarimetric SARdata"

{no data available} [C4037]

"Comparison of polarimetric SAR techniques for the measurement of directional ocean wave spectra"

Several methods have been investigated which use fully polarimetric synthetic aperture radar (POLSAR) data to measure directional ocean wave slope spectra. Independent techniques have been developed to measure wave slopes in the orthogonal SAR (azimuth/range) directions. In this paper, wave spectra measured using two polarimetric methods are investigated. Spectra developed using: a) intensity-based polarimetric SAR methods and b) a more recent orientation/alpha angle algorithm are compared. NASA/JPL/AIRSAR L-band data from two-sites in California coastal waters have been used. [C4038]

"The inherent error in passive microwave rainfall estimation as inferred from the TRMM data"

Analyses of data collected by the Tropical Rainfall Measuring Mission (TRMM) microwave imager (TMI) and precipitation radar (PR) show that the radiometric responses to rainfall profiles are sensitive to spatial inhomogeneities within the sensor field of view (FOV). The uncertainty, the so-called beam-filling error, is associated with the variability in horizontal and vertical rainfall structures within a sensor FOV coupled to the non-linear relationship between brightness temperature (T_b) and rain rate (R). This study classifies the beam-filling error as an inherent error because the sensor itself has the non-unique radiometric signatures associated with the rainfall inhomogeneity. The specific forward models hardly overcome the error inherent in the sensor. It is also shown that lower resolution retrievals are less sensitive to the inherent error than the retrievals at higher resolutions due to the less non-linearity in the T_b - R relationship at lower resolutions. [C4039]

"Application of overcomplete ICA to SAR image compression"

In this paper the application of a transform coding technique, based on overcomplete independent component analysis (ICA), for the compression of single look intensity synthetic aperture radar (SAR) images is explored. The method has the advantage of representing the image through almost statistically independent coefficients, with an assigned distribution, so that a scalar entropy constrained quantizer, optimized for the coefficients statistics, can be used. Numerical results on ERS-1 data are presented. [C4040]

"Global Precipitation Measurement update"

Global Precipitation Measurement (GPM) is an international cooperative program whose objectives are to (a) increase understanding of rainfall processes, and (b) make frequent rainfall measurements on a global basis. The National Aeronautics and Space Administration and the Japanese Aviation Exploration Agency have entered into a cooperative effort for the formulation and development of GPM. This effort represents a continuation of the partnership that developed the highly successful Tropical Rainfall Measuring Mission (TRMM). Several activities discussed within this paper reflect the maturity of the project formulation activities that have been completed and forms a basis for the anticipated receipt of approval to begin project implementation during the forthcoming year. [C4041]

"Sampling simulation for estimating the sampling error of space-time average rain rate for TRMM and GPM mission"

Sampling errors of space-time average rain rate in 1-30 day integration times and 0.1° - 5.0° space domains, for simulated GPM (Global Precipitation Measurement) eight-satellite group, were estimated using 3-year radar-AMeDAS composites data around Japan. Moreover, we formulated sampling error RMS (%) as a function of space scale A (degree), time scale T (day), and true average rain rate R (mm/h). [C4042]

"Surface deformation in Mokpo area observed with synthetic aperture radar interferometry"

Mokpo city is a coastal city located at the south western coast of the Korean Peninsula. Large regions within Mokpo are subjected to significant subsidence because about 70% of the city area is a reclaimed land from the sea. In this study, we aimed to estimate the subsidence rate over Mokpo city by using twenty-six JERS-1 SAR dataset from September 1992 to October 1998. Several tens of differential interferograms were processed from JERS-1 dataset and STRM 3-arc DEM. The results indicate continuous subsidence in Dongmyung-dong, Hadang-dong and Wonsan-dong in city, and the subsidence velocity reach over 4 cm/yr in the most highly sinking area. For facilitating the analysis of time-varying surface change, we also carried out an interferometric SAR time series analysis using permanent scatterer and consequently determined space-time maps of surface deformation at each acquisition time of JERS-1 SAR. [C4043]

"Atmospheric fronts off the east coast of Taiwan studied by ERS synthetic aperture radar imagery"

Synthetic aperture radar (SAR) images acquired by the European Remote Sensing satellites ERS-1 and ERS-2 over the east coast of Taiwan around 10:30 local time often show frontal features that are located typically 50 km off the coast. We show that they are not sea surface manifestations of a land breeze front, but of a quasi-stationary atmospheric front that persists over the whole day or even over the next day(s). Evidence for this interpretation is obtained mainly from the comparison of the SAR images with sequences of cloud images acquired by the Japanese Geostationary Meteorological Satellite GMS-4. [C4044]

"Model based SAR data compression"

In this paper a wavelet based method for SAR data denoising and compression is presented. An unsupervised stochastic model based approach to image denoising is presented. SAR image is modeled in wavelet domain Gauss Markov random field and noise is considered as Gaussian with unknown variance. The parameters are estimated from incomplete data using mixtures of wavelet coefficients, and expectation maximization algorithm. The expectation maximization algorithm is used to efficiently compute a maximum a posteriori estimate. Observed wavelet coefficient is estimated using inter and intra scale of wavelet coefficients to estimate image and noise model parameters. Presented wavelet based method efficiently removes noise from SAR images. The second step is to design an entropy coder that efficiently codes despeckled image. The texture parameters obtained at the despeckling stage are used in the compression process. The image coder is tested on X-SAR data with and achieves comparable compression results with the wavelet based state-of-the art coders for SAR data compression. [C4045]

"Change detection for the urban area based on multiple sensor information fusion"

In this paper, change detection for urban area based on multiple sensor information fusion is studied. The images acquired at different times are used to identify the differences during the process of city construction and reconstruction. The proposed method in this paper consists of three steps: image pre-processing and registration, information fusion for multiple sensor images and image change detection. Wavelet packet transform is used in the fusion stage. More detailed features can be extracted by high frequency components as well as low frequency components decomposition. The experiments are carried on optical and SAR images taken at different periods. The results show that the method based on multi-source information fusion can effectively detect changed regions. [C4046]

"The potential of TRMM/PR data to monitor snow in Tibetan Plateau"

This paper presents a study to demonstrate the potential of a spaceborne Ku-band APR (active phase-array radar)-Tropical Rainfall Measuring Mission (TRMM) precipitation radar (PR) to monitor snow cover in Tibetan Plateau. A method based on the difference of backscattering from snow covered ground with zenithal/non-zenithal incidence angles was carried out and validated by a second-order RT model. In the end, we use the TRMM/PR data from 2003-01 to 2004-04 to do the snow monitor of several areas in Tibetan Plateau. [C4047]

"New eigenvalue-based parameters for natural media characterization"

The aim of this paper is to present two novel polarimetric parameters, the eigenvalue relative difference (ERD) and the single bounce eigenvalue relative difference (SERD), to characterize natural media. These parameters

are derived from the eigen-decomposition of the coherency matrix considering the reflection symmetry hypothesis. An analysis of these parameters is performed on multi-frequency polarimetric SAR data acquired on bare soils and forested areas. [C4048]

"Polarimetric characteristics of radar echoes from near shore wave fields at low grazing angles"

This paper presents the results of polarimetric measurements of the near shore wave fields made in the low grazing angle regime. The variations in the distribution of the polarimetric entropy, anisotropy and mean scattering alpha of the radar echoes are examined in the H-A- α space to characterise the dominant scattering mechanisms for two situations; one where the incident wave field is almost monochromatic and the other where a broader spectrum of waves is present. [C4049]

"Evaluation of the ESPRIT approach in polarimetric interferometric SAR"

This paper presents a first evaluation of the ESPRIT approach in polarimetric interferometric SAR. This evaluation is carried out by using 3D images obtained by SAR tomographic like an alternative to the acquisition of ground-truth data, which is an extremely complex task in the case of volume areas. All parameters over a volumetric area are directly visible in a tomographic image and can, therefore, be employed to validate the ESPRIT approach by comparing parameters generated by ESPRIT and the SAR tomography approach. This allows to identify the principal deficiencies of the ESPRIT method, which occur over high vegetation areas, where there is a misinterpretation of the ESPRIT results. Whereas, the ESPRIT approach is useful for building characterisation, identifying a good applicability area. Airborne L-band repeat-pass interferometric data of the German Aerospace Center (DLR) experimental airborne SAR are used to perform this evaluation. [C4050]

"Investigating polarimetric SAR data for cryospheric monitoring in a Canadian environment"

Since the early 90's, INKS has been developed tools for snow monitoring, river ice characterization and seasonal frost mapping in Canada. The focus to date has been on the use of monopolarized or multipolarized SAR data. With the forthcoming of RADARSAT-2, we have undergone a series of studies to assess the potential information gain from polarimetric SAR data. Airborne polarimetric SAR data from the Canadian CV-580 have been acquired over three different Canadian sites in winter: 1) a boreal forest 2) an agricultural watershed and 3) the Saint-Francois River. This paper presents the preliminary results obtained from the polarimetric data set over the Saint-Francois River in February 2003. [C4051]

"Synthetic aperture radar (SAR)-based mapping of wildfire burn severity and recovery"

New radar based techniques for efficient identification of forest damage caused by wildfire and subsequent recovery are applied to data acquired over the 2002 Rodeo-Chediski, Arizona and 1988 Yellowstone National Park wildfire complexes. Fully polarimetric C-, L- and P-band airborne synthetic aperture radar data were acquired in approximately east-west and north-south swaths over the northern half of the Rodeo-Chediski wildfire scar on August 1, 2002, 25 days after the last active fire was contained. The AIRSAR instrument also acquired fully polarimetric data in C-, L- and P-band over Yellowstone on October 11, 1994, approximately 6 years after the event. We combine single frequency polarimetric parameters in composite images for optimal identification of fire-induced damage to the forests. For the Rodeo-Chediski fire, we demonstrate that polarimetric parameters-such as average scattering mechanism-readily identify bare surfaces, pine trees with intact needles, trees with exposed branches, and trees with residual burned trunks. In particular, a single-pass of polarimetric SAR provides identification of the perimeters and within-burn variability. This work shows that fully polarimetric SAR is sensitive to scattering changes wrought by wildfire in two types of predominantly coniferous forests. By extension, this technique should help quantify different degrees of burn severity in ecosystems where the canopy is altered. We anticipate that these results will provide a new method of responding to wildfires, perhaps even at the tactical fire-fighting level. [C4052]

"Global current measurements in rivers by spaceborne along-track InSAR"

The global monitoring of volume transports of large rivers is a challenging technological problem with a number of important applications. It is highly desirable to use satellite-based remote sensing techniques for consistent worldwide measurements on a regular basis. While water level measurements in rivers with spaceborne altimeters have already been demonstrated a few years ago, instruments for routine current measurements from space have not been available until now. This will change with the advent of along-track interferometric synthetic aperture radars (along-track InSARs) on upcoming satellites such as the German TerraSAR-X, which is scheduled for launch in 2006. In this paper we evaluate the potential of such instruments for current measurements in rivers. We consider fundamental theoretical issues as well as existing InSAR data from the Shuttle Radar Topography Mission (SRTM) and numerical simulation results. We find that currents in the Elbe

river estuary (Germany) can be derived from SRTM data quite well. A similar data quality is predicted for TerraSAR-X. We discuss the potential of TerraSAR-X for routine current measurements in rivers and propose the development of a comprehensive data synthesis system which combines water level and current data from satellites and other sources in such a way that a maximum amount of information on rivers is obtained. [C4053]

"Polarimetric SAR image classification employing subaperture polarimetric analysis"

Polarimetric SAR image classification remains an important research area. Various methods continue to be developed for specific applications. High-resolution polarimetric SAR systems and advances in computational and data storage capabilities have revived interest in novel polarimetric analysis techniques. Accordingly, subaperture analysis of polarimetric SAR data has received renewed attention. A central assumption of SAR image formation is that individual radar scatterers are stationary; they have no structure and provide a constant reflectivity during the imaging process. However, with increased resolution, and hence fewer scatterers per pixel, the nonstationary response from any given scatterer is more likely to influence total radar backscatter of a pixel. We present a method to assess the polarimetric variability across the full aperture. [C4054]

"Polarimetric SAR stereo using Pi-SAR square loop path"

This paper shows first results of polarimetric SAR stereo applied to urban areas. SAR stereo is known as a useful technique for three-dimensional mapping. Until now many approaches and results have been reported, based on single polarization measurements. But stereogrammetry has not been used with polarimetric information. In this paper, we use polarimetric SAR measurements acquired during a square loop flight. It is shown that typical objects, like a TV tower can be reconstructed and its polarimetric properties analysed using this method. [C4055]

"Analysis of land topography using Radar Altimeter 2"

In this work a simulator based on Envisat Radar Altimeter-2 has been developed in order to analyze characteristics of reflected waveforms over land surfaces. Using this simulator new approaches have been developed to classify surface characteristics and to make measurements on some land surface types. [C4056]

"Ground deformation monitoring of the Santorini volcano using satellite radar interferometry"

The island complex of Santorini is located at the central part of the Hellenic Volcanic Arc in the Southern Aegean Sea. This volcano complex basically consists of five islands, Thera, Therassia, Palea Kammeni, Nea Kammeni and Aspronisi forming a caldera of 83 km² with 390 m depth. The last significant volcanic activity took place between 1925 and 1950. However, the volcano is at a rest state during the last 50 years. The present work refers to the ground deformation monitoring of the area using ERS1, ERS2 and Envisat radar scenes from 1993 to 2004. A total number of four ERS1&2 SLC radar images covering the period 1993 to 1999, and two ENVISAT ASAR images for the period 2003-2004 were used. The method applied was the two-passes interferometry with a contribution of a high resolution Digital Elevation Model. The interferometric results show that although the volcano is at a rest phase, in the two volcanic centers of Palea and Nea Kammeni ground deformation (subsidence) of 62 mm along the line of sight of the satellite was detected. [C4057]

"Building damage detection from post-earthquake aerial imagery using building grey-value and gradient orientation analyses"

The collapsed buildings due to 1999 Kocaeli earthquake were detected from post-event panchromatic aerial imagery based on grey-value and the gradient orientation of the buildings. The building boundaries were available and stored in a GIS as vector polygons. The building polygons were utilized to perform the assessments in a building specific manner. The approach was implemented in a selected area of Golcuk, which is one of the urban areas most strongly hit by the earthquake. First, the buildings were selected one-by-one from the integrated vector (building boundaries) and raster (aerial photo) data set. The building damage detection process was then divided into two branches. In the first branch, the detection was performed using the building grey-value information. To do that, a greyvalue threshold (T1) was determined for discriminating the collapsed buildings from the un-collapsed ones. In the second branch, a group of operations including the gradient calculation and the determination of gradient orientation were performed. By utilizing the orientation information, an optimum threshold level (T2) was determined for the standard deviation of the angle distribution of the building pixels. When assessing the condition of a building, the results of the two branches were combined and a final decision was made in an integrated manner. Of the 284 buildings analyzed, 254 were labeled correctly as collapsed or un-collapsed providing an overall accuracy of 89.44%. The results reveal that the collapsed buildings due to the earthquake can be successfully detected from post-event aerial images. [C4058]

"Radiometric measurements of the Canadian boreal forest using RADARSAT-1 beam patterns"

This paper describes exploratory work in evaluating the use of the Canadian boreal forest in potential support to radiometric calibration of the RADARSAT-1 Synthetic Aperture Radar (SAR) sensor. The primary site for SAR calibration performance and monitoring, in the Amazon rain forest, requires the use of the spacecraft's On-Board Recorder (OBR) to store the images until they can be downloaded to a Canadian data reception facility. In mid 2002, aging considerations for the OBR led to the survey of natural sites within data reception mask of Canadian ground stations. Several boreal forest and mixed Tundra-Taiga sites were tested for their ability to support radiometric analyses in case of an OBR failure. A boreal forest-type area, near Hearst, in the province of Ontario, was chosen for a more comprehensive study. Radiometric measurements covering the entire incidence angle range of RADARSAT-1 were performed using an elevation pattern measurement method adapted from the existing methodology used for Amazon image analyses. Radiometric measurements over the chosen area are reported, examining temporal and seasonal variations. Antenna gain pattern shape determination is also attempted, based on seasonal backscattering profiles of the region. The differences between extracted pattern shapes and their corresponding calibrated patterns then provide indications on the mean term, across swath backscattering behavior of the boreal forest, confirming its potential suitability for radiometric calibration monitoring. [C4059]

"Model of diurnal/seasonal variations of ELF natural radio signal based on OTD data"

Knowledge of expected parameters of natural extremely low frequency (ELF) radio signal arriving from the global lightning activity to observatory is necessary when one looks for the signals originating from other sources, in particular, for the electromagnetic precursors of a future earthquake shock. The radio waves of seismic and cosmic origin might be expected in the bands of ultra-low (ULF, 0.01-3 Hz) and ELF (3 Hz-3 kHz), i.e., at frequencies where natural electromagnetic radiation exists in the Earth-ionosphere cavity. Radiation from the magnetosphere or from underground electric activity provides additional signals to be discriminated from the ordinary lightning induced pattern. We construct the model variations of natural ELF radio signal on the daily and monthly scales. The maps of global distribution of lightning flashes are used as initial data. These were recorded by the OTD satellite (optical transient detector) and by LIS (lightning image sensor). The model developed provides expected variations of the ELF power on the diurnal and seasonal scales thus describing typical behavior of Schumann resonance background. [C4060]

"On the potential of current measurements by spaceborne along-track InSAR for river runoff monitoring"

The global monitoring of volume transports of large rivers is a challenging technological problem with a number of important applications. It is highly desirable to use satellite-based remote sensing techniques for consistent worldwide measurements on a regular basis. While water level measurements in rivers with spaceborne altimeters have already been demonstrated a few years ago, instruments for routine current measurements from space have not been available until now. This will change with the advent of along-track interferometric synthetic aperture radars (along-track InSARs) on upcoming satellites such as the German TerraSAR-X, which is scheduled for launch in 2006. In this paper we evaluate the potential of such instruments for current measurements in rivers. We consider fundamental theoretical issues as well as existing InSAR data from the Shuttle Radar Topography Mission (SRTM) and numerical simulation results. We find that currents in the Elbe river estuary (Germany) can be derived from SRTM data quite well. A similar data quality is predicted for TerraSAR-X. We discuss the potential of TerraSAR-X for routine current measurements in rivers and propose the development of a comprehensive data synthesis system which combines water level and current data from satellites and other sources in such a way that a maximum amount of information on river is obtained. [C4061]

"Seismotectonic investigation on the Bam earthquake prone area (Iran) based on ASAR interferometry"

In this study the Satellite Radar Interferometry (InSAR) was applied to investigate the crustal deformation caused by the Bam Earthquake ($M_w=6.5$) that occurred in Iran on December 26, 2003. It was a multiple seismic event that destroyed the historical City of Bam and provoked great damages in the urban centers of the region. The Bam area in the south-eastern part of Iran is an active seismic zone and the Bam Fault System is comprised by three specific segments (north, east and SE of Bam). The three-pass interferometric technique was applied using ENVISAT ASAR scenes. According to the interferometric processing results subsidence has occurred in the area NE of Bam City, while dextral strike-slip displacement has taken place in the southern area of Bam. The last deformation could be attribute to a parallel hidden segment of the Bam Fault that is reaching the surface according to the shear displacement during the earthquake. [C4062]

"Maintaining RADARSAT-1 image quality performance in extended mission"

This paper discusses the synthetic aperture radar (SAR) calibration and image quality monitoring of RADARSAT-1 in its extended mission, as evolved from the earlier phases of the calibration plan, after its launch in 1995 and the start its routine operation in 1996. Since the early qualification period of the mission, both single beams and ScanSAR operating modes are monitored routinely, based on Amazon Rainforest images for radiometric calibration performance, and on images of Precision Transponders for image quality performance. After an initial calibration phase, radiometric monitoring showed changes in the characteristics of several previously calibrated elevation antenna patterns and compensation for these changes were, and are still made in the image processor. In addition, a major upgrade of the ScanSAR processor completed at the Canadian Data Processing Facility (CDPF) in 2002 provided significant improvements in image quality and radiometry. Through the five-year nominal mission which ended in 2001 and the four years of the current extended mission, radiometrically and geometrically calibrated imagery products were continuously provided to worldwide users. In late October 2000 however, concerns began to rise of the possibility of failure of the Horizon Scanner 1 (HS1), which would result in operating the spacecraft in a degraded attitude control mode, compared to the current primary operation. Experiments were conducted to better understand the impact on image quality when operating in backup attitude control mode. In mid 2002, aging considerations for the On-Board Recorder also led to survey natural sites within Canadian data reception masks for their potential to support radiometric analyses, as an alternative to the Amazon Rainforest, where images are recorded. [C4063]

"Space in the service of society: a Canadian case study"

Canada places great emphasis on using space science and technology for the benefit of its citizens. Canada's first satellite, Alouette-1, was launched to study the ionosphere in order to advance our understanding of a range of phenomena associated with solar storms-from disturbances in radio communications in Canada's North to the majestic Northern Lights. The Canadian space program has recognized that adapting space-based technologies and processes for applications on Earth is the best way to surmount uniquely Canadian challenges, such as the vast distances and variety of landscapes and climatic conditions that define Canada. In the sixties, while looking for a way to connect communities scattered over our vast expanse, Canada came up with a proposal for its own national communications satellite system. Another project, Canada's Radarsat-1 satellite, provides surveillance of the country's huge expanse of land and sea. In addition, it has captured 15% of the global commercial market for Earth observation data. Canadian researchers have collaborated with NASA to build the robotic arm onboard the Space Shuttle. This led to an invitation for Canadian astronauts to participate in NASA's Human Spaceflight program. To date, there have been 11 flights by Canadians. [C4064]

"The Liverpool Bay coastal observatory"

The pilot coastal observatory in the eastern Irish Sea integrates (near) real-time measurements with coupled models in a pre-operational coastal prediction system. The aim is to develop the underpinning science for marine management, focusing on the impacts of storms, eutrophication and the relative importance of events viz-a-viz the mean. Real time current measurements are obtained from a seabed mounted acoustic Doppler current profiler; deployment started in August 2002, via acoustic modems and the Orbcomm satellite e-mail system, and from a shore based HF radar via telephone landlines. There are also real time measurements from a surface buoy and a directional wave buoy and from an instrumented ferry, all via Orbcomm. The measurements are integrated with a suite of nested 3-dimensional hydrodynamic and ecological models run daily, focusing on the Observatory area by covering the ocean/shelf of northwest Europe (at 12 km resolution), the Irish Sea (at 1.8 km) and Liverpool Bay (at 200-300m resolution). All measurements and model outputs are displayed on the Web-site (<http://coastobs.pol.ac.uk>). [C4065]

"Remote sensing, LIDAR, automated data capture and the VEPS project"

There has been research into the 3D modelling of urban settings and landscapes since the early 1980s, initially, primarily for visual impact assessment, and more recently, for wider simulation and analysis. This paper discusses recent project work that has been examining how to minimise operator based digital 3D modelling of urban and rural environments, where remotely sensed data is available. The increasing availability of highly accurate LIDAR data offers these opportunities, but currently is not captured so often nor is yet a sufficiently extensive coverage that it can be relied on to keep VR analogues of real places up to date. This places increasing importance on developing an 'urban data fusion' of different types including: LIDAR; digital elevation models derived from radar altimetry and similar data (SAR interferometry); real-time video photogrammetry; and thus on standards. 3D models of proposed changes then need to comply with these standards as they emerge. [C4066]

"Field intercomparison of Channel Master ADCP with RiverSonde radar for measuring river discharge"

The RiverSonde radar makes non-contact measurement of a horizontal swath of surface velocity across a river section. This radar, which has worked successfully at several rivers in the western USA, has shown encouraging correlation with simultaneous measurements of average currents at one level recorded by an acoustic travel-time system. This work reports a field study intercomparing data sets from a 600 kHz Channel Master ADCP with the RiverSonde radar. The primary goal was to begin to explore the robustness of the radar data as a reliable index of discharge. This site is at Three Mile Slough in northern California, USA. The larger intent of the work is to examine variability in space and time of the radar's surface currents compared with subsurface flows across the river section. Here we examine data from a couple of periods with strong winds. [C4067]

"Gulf of Maine Ocean Observing System (GoMOOS): current measurement approaches in a prototype integrated ocean observing system"

The Gulf of Maine Ocean Observing System (GoMOOS) was established in the summer of 2001 as a real-time pilot integrated observing system that includes a comprehensive array of moored physical and optical sensors, shore based long-range HF radar systems, circulation and wave modeling, satellite observations, and Web delivery of data and data products. The system is automated and operational. The GoMOOS moored buoy array presently consists of 10 solar-powered, automated buoy systems that telemeter data hourly via cellular/iridium phone and GOES satellite transmitters. The operational protocol is that 20 buoys and instrument suites are rotated through the 10 locations on a six-month cycle. Current measurements are made at 2 m depth using Aanderaa RCM9 in situ Doppler current meters, and subsurface currents are made with downward-looking RIM Doppler profilers. In addition, near-surface currents in the Gulf of Maine are being measured using a 5-megahertz long-range HF radar system manufactured by CODAR Ocean Systems Inc. Comparisons of the three current measurement systems are presented, and the operational logistics of current monitoring using these technologies in the challenging Gulf of Maine environment is discussed. [C4068]

"Sea surface slicks characterization in SAR images"

The authors present a new method to characterise and discriminate oil slicks and some look-alikes in ERS-2 SAR images according only to the observed sea roughness, to reduce oil spill detection and monitoring systems cost. It exploits sea wave spectrum images from the multiscale analysis based on a modified morphological pyramid. Many backscatter characteristics extracted at each level, depended on object and background features are normalized to make its spectral scales be identical. Twenty objects (spot and border) backscatter features have been measured. Eleven sea surface slicks types have been analysed, namely oil, atmospheric instability, wind front, unstable air-mass, current front, falling land wind, large gravity waves, low wind area, natural slicks, swell visible and wind sheltered area. The results presented as smoothed basic profiles and textural spectra allow to tackle oil slicks supervised classification in new images. Oil slicks and current front are discriminated. But, some ambiguities of slicks discrimination in SAR images remain persistent. [C4069]

"RAST 2005. Proceedings of 2nd International Conference on Recent Advances in Space Technologies (IEEE Cat. No. 05EX1011)"

{no data available} [C4070]

"Oil slick detection by SAR imagery using Support Vector Machines"

Spaceborne Synthetic Aperture Radar (SAR) is well adapted to detect ocean pollution independently from daily or weather condition. In fact, oil slicks have specific impact on ocean wave spectra. Initial wave spectra may be characterized by three kinds of waves, big, medium and small, which correspond physically to gravity and gravity-capillary waves. The increase of viscosity is due to the presence of oil damps gravity-capillary waves. This induces a damping of the backscattering to the sensor, but also a damping of the energy of the wave spectra. Thus, local segmentation of wave spectra may help oil slick detection. It can be achieved by the segmentation of a multiscale decomposition of the original SAR image. In this work, a supervised oil slick detection is proposed by using Support Vector Machines into the wavelet decomposition of a SAR image. It performs accurate detection with no consideration to signal stationarity nor to the presence of strong backscatters (such as ship). Moreover, when using normalized SAR images, the kernel expansion may be generalized from one image to an other to make a near unsupervised detection scheme. The algorithm has been applied on Envisat ASAR images. First experiments yield accurate segmentation results with a very limited number of false alarms. [C4071]

"Fast Fourier techniques for SAS imagery"

Fast block-processing Fourier techniques were originally developed for satellite-borne synthetic aperture radars (SAR) employing a colocated single transmitter/single receiver geometry. In contrast, almost all synthetic aperture sonars (SAS) now have a single transmitter/multiple receiver geometry and so some preprocessing is required to coerce the data into a single receiver format. If this is not done carefully, much of the inherent efficiencies of the Fourier-based block-processing is lost. Additionally there is the preprocessing required to achieve motion compensation as well as the phase center approximations required to correct for the underlying bistatic nature of the collected data. [C4072]

"Operational quantitative mapping of oil pollutions at sea by joint use of an hyperspectral imager and a fluorescence lidar system on-board a fixed-wing aircraft"

Efficient observation means are required for supporting operational fight against oil pollutions at sea and recovery operations, including reliable choice and guidance of maritime and airborne fighting means. Among the suite of sensors available, the potential of airborne passive hyperspectral imagery and active fluorescence laser systems have been studied in the past. The potential of combining these two kinds of sensors for quantitative mapping of oil slicks at sea and for supporting the recovering operations is proposed for evaluation in that pilot project. Location, extents, volume of the oil spilled and its spatial distribution are the main useful parameters to be estimated. Ways towards the design of an operational system including both passive and active airborne optical sensors are presented. [C4073]

"First assessment of C-band polarization ratio from ENVISAT ASAR imagery"

{no data available} [C4074]

"Observations and modeling of the ocean radar backscatter at C-band in HH- and VV-polarizations"

{no data available} [C4075]

"Coastal wind jets flowing into the kanmon strait by SAR observations"

{no data available} [C4076]

"Effect of radar frequency on waterline mapping from airborne SAR image in the intertidal zone"

{no data available} [C4077]

"Satellite remote sensing of the oceanic environment in China"

{no data available} [C4078]

"An automatic detection of oil spills in sar images by using image segmentation approach"

{no data available} [C4079]

"Sea state analysis for coastal waters using dual polarization ENVISAT ASAR data"

{no data available} [C4080]

"An empirical SAR imaging model for ocean wave measurements"

{no data available} [C4081]

"Ocean wave spectrum from sar image using 2D-ARMA model"

{no data available} [C4082]

"Oceanpal® a GPS-reflection coastal instrument to monitor tide and sea-state"

The Global Navigation Satellite Systems (GNSS, such as the GPS and GLONASS constellations) and their augmentation systems (WAAS, EGNOS) constitute premium sources of opportunity for passive remote sensing. By 2010, after the deployment of the European Galileo constellation, more than 50 GNSS satellites will be

emitting self-calibrating, dual-frequency, rain-immune, L-band spread spectrum signals with long-term availability and stability. The use of GNSS reflections (GNSS-R) for sea-surface monitoring is a bistatic radar technique only requiring a receiving system. The concept was initially proposed by M. Martin-Neira in 1993 and has, since then, been successfully implemented in coastal receivers, in aircraft and recently, in space. The potential applications include sea-surface altimetry, sea-state, surface roughness, surface currents and salinity, both for scientific and operational oceanography. In this paper, we present Oceanpal®, a GNSS-R sensor developed by Starlab for operational coastal monitoring. It is an inexpensive, all-weather, dry and passive concept which can be deployed on multiple platforms, static (coasts, harbors, off-shore), and slowly moving (boats, floating platforms, buoys). In its present form, Oceanpal® can deliver two kinds of Level-2 products: the sea-surface height and the significant wave height. [C4083]

"Space-based radar: overview, history and recent developments"

{no data available} [C4084]

"HF radar wave measurements in the presence of ship echoes-problems and solutions"

HF radar is an important tool to remotely measure oceanographic parameters like currents and waves from shore over large areas up to 6500 km². Maps of these parameters can be obtained 3 times per hour. In areas of high ship traffic, there are ship echoes within the radar backscatter signal, which can appear in the frequency bands of the Doppler spectrum which are used to extract current- and wave information. While the current speed is derived from the first-order Bragg peaks, wave height and direction is calculated from the second-order bands around the first-order peaks. The second-order bands require 15 to 20 times the bandwidth of the first-order peaks and their amplitude is about 20 dB lower. Due to these facts, ship echoes can cause problems especially to wave algorithms. This paper discusses the special signatures of ship echoes and shows possibilities to identify and to track ships. [C4085]

"Shallow angle LIDAR for wave measurement"

The Exeter University Marine Dynamics Group has developed a shallow angle LIDAR for wave measurement purposes. This paper introduces the system and illustrates some metrology issues specific to this method. The LIDAR system uses a 532 nm (green) Q switched, high repetition rate, nanosecond pulsed laser. The system is designed to be scanned along a line or over an area. A 100 point square plot requires typically 0.5 seconds to complete. Whereas fixed-wing airborne LIDAR is continuously moving, the system described here is mounted in a fixed position and it is therefore possible to record sea surface shape and wave evolution over time. A plot comprises a set of surface elevation measurements determined by a combination of time of flight and high precision angle measurement. Unlike airborne LIDAR systems, the system is fitted to a shore or vessel mounted platform (with motion compensation in the case of vessel mounting) and the incident beam typically makes an angle with the sea surface of less than 10 degrees. The signal returns from airborne LIDARs, at approximately normal incidence, are strong compared to the very weak returns from the shallow angle system described in this paper. This fact has previously inhibited the development of such shallow angle systems. Some features of this system which make it viable are: a minimum field of view optical system, a very short pulse length high repetition rate laser system, an ultra high resolution beam scanner and what is effectively a one-dimensional image processing style coherent hybrid detection system operating with GHz data rates. The use of 532nm wavelength allows the scattering of light from calcareous plankton particles as well as other suspended particles and foam or aeration. The different nature of the light scattering from suspended particles or from foam or highly aerated water also allows the qualitative identification of breaking or foaming waves. The paper presents recordings of the real-time evolution of spatially resolved wave profile data obtained using this system. The shallow angle LIDAR system is shown to offer significant advantages over existing methods for wave measurement such as wavebuoys, wavestaffs, acoustic Doppler and radar, both in terms of the precision of the data returned and in the flexibility of deployment. Examples are presented of both near-shore and offshore applications. This system is one of the very few techniques capable of returning spatially resolved 'wave videos'. Another important feature of the new system for near-shore applications is that it avoids the vulnerability to damage of systems mounted in the surf and swash zones. The system can be installed at any state of the tide with no requirement to undertake installation work below the high water mark. The system is shown to be an ideal choice for most types of wave measurement applications and is eminently suited to the most extreme sea conditions. It is shown to be a portable remote sensing system capable of rapid temporary deployment, at sites of interest, during any sea conditions. [C4086]

"System concepts and technologies for high orbit SAR"

This paper discusses large aperture, high orbit radar concepts for measuring sub-centimeter-level surface

displacements from space. These measurements will enable applications such as earthquake simulation, modeling and forecasting. We explain the need for large aperture, high orbit arrays and discuss the technologies required to achieve these missions. [C4087]

"Influence of a nonlinear RAR modulation on the SAR imaging of ocean waves"

{no data available} [C4088]

"Status of a UAVSAR designed for repeat pass interferometry for deformation measurements"

NASA's Jet Propulsion Laboratory is currently implementing a reconfigurable polarimetric L-band synthetic aperture radar (SAR), specifically designed to acquire airborne repeat track interferometric (RTI) SAR data, also known as differential interferometric measurements. Differential interferometry can provide key deformation measurements, important for the scientific studies of earthquakes and volcanoes. Using precision real-time GPS and a sensor controlled flight management system, the system will be able to fly predefined paths with great precision. The expected performance of the flight control system will constrain the flight path to be within a 10 m diameter tube about the desired flight track. The radar will be designed to operate on a UAV (unpiloted aerial vehicle) but will initially be demonstrated on a minimally piloted vehicle (MPV), such as the Proteus built by scaled composites or on a NASA Gulfstream III. The radar design is a fully polarimetric with an 80 MHz bandwidth (2 m range resolution) and 16 km range swath. The antenna is an electronically steered along track to assure that the actual antenna pointing can be controlled independent of the wind direction and speed. Other features supported by the antenna include an elevation monopulse option and a pulse-to-pulse restearing capability that will enable some novel modes of operation. The system will nominally operate at 45,000 ft (13800 m). The program began out as an Instrument Incubator Project (IIP) funded by NASA Earth Science and Technology Office (ESTO). [C4089]

"Status and trends for space-borne phased array radar"

The first European SAR based on an active phased array was launched in March 2002 on board Envisat and is operational. Several SAR instruments with active array antennas are currently under development in Europe and new instrument concepts are under discussion for the next generation. How will new technologies, currently under development in the commercial and military sectors, influence radar design based on existing architectures and new concepts? This paper discusses the current technology status and identifies future trends. [C4090]

"Long-term UHF RiverSonde river velocity observations at Castle Rock, Washington and Threemile Slough, California"

Long-term, non-contact river velocity measurements have been made using a UHF RiverSonde system for several months at each of two locations having quite different flow characteristics. Observations were made on the Cowlitz River at Castle Rock, Washington from October 2003 to June 2004, where the unidirectional flow of the river ranged from about 1.0 to 3.5 m/s. The radar velocity was highly correlated with the stage height which was continually measured by the U. S. Geological Survey. The profile of the along-channel velocity across the water channel also compared favorably with in-situ measurements performed by the Survey. The RiverSonde was moved to Threemile Slough, in central California, in September 2004 and has been operating there for several months. At Threemile Slough, which connects the Sacramento and San Joaquin Rivers, the flow is dominated by tidal effects and reverses direction four times per day, with a maximum speed of about 0.8 m/s in each direction. Water level and water velocity are continually measured by the Survey at the Threemile Slough site, with velocity recorded every 15 minutes from measurements made by an ultrasonic velocity meter (UVM). Over a period of several months, the radar and UVM velocity measurements have been highly correlated, with a coefficient of determination R^2 of 0.976. [C4091]

"Deep ground penetrating radar (GPR) WIPD-D models of buried sub-surface radiators"

The proliferation of strategic subsurface sanctuaries has increased the need for enhanced remote sensing techniques providing for the accurate detection and identification of deeply buried objects. A new ground penetrating radar (GPR) concept is proposed in this paper to use subsurface radiators, delivered as earth penetrating non-explosive, electronic "e-bombs", as the source of strong radiated transmissions for GPR experiments using ground contact or airborne receivers. Three-dimensional imaging techniques for deeply buried targets are being developed based on two-dimensional synthetic aperture radar (SAR) data collection techniques. Experiments over deep mine shafts have been performed to validate the 2D SAR processing algorithms. WIPD-D models have been used to verify the significant enhancement in the received signal-to-noise ratio obtained by burying the transmitter under the surface of the earth. Simple ray-tracing techniques have also

been used to confirm the enhancements. [C4092]

"Applications of MIMO techniques to sensing of cardiopulmonary activity"

Remote monitoring of cardiopulmonary activity based on Doppler shifts in radio signals shows promise in medical and security applications, however the problems of motion artifacts and presence of multiple subjects limit the usefulness of this technique. By applying MIMO signal processing, it is possible to overcome limitations of current systems and isolate signals from multiple sources. [C4093]

"Multiplicative multifractal modeling of sea clutter"

Sea clutter refers to the radar returns from a patch of ocean surface. Accurate modeling of sea clutter and robust detection of low observable targets within sea clutter are important problems in remote sensing and radar signal processing applications. In this paper, we introduce a multiplicative multifractal process for modeling the sea clutter. Through analysis of 392 amplitude time series of 14 sea clutter datasets measured under various sea and weather conditions, we show that the data are consistent with multifractals over certain time scale range, and that the generalized dimension spectrum D_q accurately detects low observable targets within sea clutter. The method is computationally very fast and practically easily implemented. These attributes strongly suggest that the method may be developed into an automated target detector within sea clutter. [C4094]

"GPRS based power quality monitoring system"

A cost effective scheme was proposed to realize real-time power quality monitoring for remote distribution system. The key point is to realize the communication between monitoring substations and monitoring centre. The communication can be carried out based on general packet radio service (GPRS). And it has the merit of always on-line, flexible structure and low cost. The design scheme was applied to power quality monitoring systems and satisfactory results were achieved. The scheme can work where the monitoring substations were located in remote wild farms or on mountains. The communication method can also be used in applications where the data flow is not so heavy and there is difficult in wire communication. [C4095]

"Hyper-temporal radarsat SAR data of a forested terrain"

First Page of the Article [C4096]

"A wavelet-based change-detection technique for multitemporal SAR images"

First Page of the Article [C4097]

"Evaluation of multi-temporal and multi-polarization ASAR for Boreal Forests in Hinton"

First Page of the Article [C4098]

"Assessment of current field plots and lidar 'virtual' plots as guides to classification procedures for multitemporal analysis of historic and current landsat data for determining forest age classes"

First Page of the Article [C4099]

"Problems of surface change detection based on SS-InBSAR"

SS-BSAR comprises of a space borne transmitter moving relative to an observed surface and a stationary receiver on the ground. Interferometric SS-BSAR (SS-InBSAR) contains two spatially separated receiving antennas and appropriate channels. SS-InBSAR can be used for a number of remote sensing applications and in particular for surface change detection. The SS-InBSAR CD compares two consecutive InBSAR images to detect changes in the earth's surface. This is done by calculating the decorrelation between the two images. This can lead to decorrelation between images in SS-InBSAR CD even when there is no deformation of the acquired surface. This paper reports methods and results of the decorrelation investigation for SS-InBSAR. [C4100]

"Geometrical considerations for terrain mapping in SBR applications"

Knowledge aided signal processing calls for the use of existing information such as digitized image maps to further suppress clutter in a typical radar detection operation. In the context of space based radar (SBR) applications, given the SBR parameters and the look angles the first problem is to translate these parameters

into a data point on a map. This is realized by converting these parameters into conventional latitude and longitude and then using the corresponding image intensity to estimate the clutter covariance matrix. Using this approach, it is possible to pre-compute the desired weight vector for a location of interest on earth that the SBR is assigned to visit. As a result, using the measured data together with the weight vector, it is possible to test for target detection hypothesis accurately at the time of visit by the SBR. [C4101]

"Development of signal processing algorithms for high resolution airborne millimeter wave FMCW SAR"

For airborne Earth observation applications, there is a special interest in lightweight, cost effective, imaging sensors of high resolution. The combination of frequency modulated continuous wave (FMCW) technology and synthetic aperture radar (SAR) techniques can lead to such a sensor. In this paper, a developed algorithm for SAR imaging that takes into account the special characteristics of FMCW signals is presented. Constrains for the validity of the stop and go approximation are shown. A demonstrator system has been built at Delft University of Technology and some results from the last airborne campaign are presented. [C4102]

"Whitening spatial correlation filtering for hyperspectral anomaly detection"

Matched and adaptive subspace detectors apply to a wide range of problems in radar, sonar, and data communication, where the signal is constrained to lie in a multidimensional linear subspace. These detectors generalize known results in matched and adaptive detection theory. In this paper we propose an original approach to anomaly detection based on whitening and spatial correlation filtering (WSCF). The performance is investigated in terms of the detection probability, and the false alarm ratio. A comparison permits us to show how this new method can outperform the well-known Reed and Xiaoli Yu (RX) algorithm. [C4103]

"SeaWinds radiometer (SRad) brightness temperature calibration and validation"

NASA's SeaWinds scatterometer, on Japan's ADEOS-II satellite, is a special purpose radar remote sensor used to measure ocean surface wind vector (speed and direction). The paper presents a novel use of this instrument as a SeaWinds radiometer (SRad) to measure the ocean microwave emissions (brightness temperature). The derivation of the SRad radiometric transfer function is presented, which is used to calculate the apparent brightness temperature collected simultaneously with the radar scattering measurement. Results are presented for the on-orbit calibration and validation of the SRad brightness temperature algorithm performed using simultaneous measurements from the advanced microwave scanning radiometer (AMSR) also on the ADEOS-II. [C4104]

"Advances in non-linear apodization for irregularly shaped and sparse two dimensional apertures"

Presented in this paper are selected new methods and applications of non-linear apodization for irregularly-shaped and sparse coherent apertures and arrays. The benefits include improved impulse response performance, i.e. reduced peak sidelobes and integrated sidelobe power, along with improved mainlobe resolution, compared to classic windowing techniques. Non-linear apodization (NLA) techniques can also serve as powerful engines for effective superresolution and bandwidth extrapolation of coherent data for filling sparse apertures. The sparse aperture filling property of superresolution algorithms for radar data forms the basis for a new concept which is introduced here: synthetic multiple aperture radar technology (SMART). Increased swath and/or reduced antenna size are some of the benefits postulated for SMART applied to synthetic aperture radar (SAR) systems. The benefits of these new methods and applications for nonlinear apodization are then demonstrated for two specific applications: 1) side lobe control for Y-type synthetic aperture radiometers, such as the European soil moisture and ocean salinity (SMOS) system [12] and JPL's proposed GeoSTAR [13] concept; and, 2) filling of sparse synthetic aperture radar data by exploiting the bandwidth extrapolation properties of non-linear apodization based superresolution techniques. The methods that have been developed and demonstrated here have potential application to a wide range of passive and e microwave remote sensing and radar systems. [C4105]

"Automatic classification of hydrometeors based on polarimetric weather radar measurements"

With the development of modern electron and computer techniques, the ability of weather radar detecting precipitation echo has been greatly improved. However, the improvement of the of echo detecting precision doesn't mean the improvement of quantitative precipitation estimates due to different distribution and type of precipitation particles as well as other hardware factors. In this paper, the author propose to construct the membership function of fuzzy logic method based on the characteristic of scattering and orientation of different kinds of hydrometeors. The authors also present details of the algorithm for classification of hydrometeors and a methodology for sensitivity analysis to the various polarimetric variables used for classification. [C4106]

"Mathematical simulation of remote detection of human breathing and heartbeat by multifrequency radar on the background of local objects reflections"

The mathematical description of signal processing basic stages in multifrequency radar intended for detection of human breathing and heartbeat is given. Cross-correlation functions of different kinds of the multifrequency probing signals, modelling optimum processing of impulses are compared in view of resolution, levels of lateral lobes and presence of diffractive maxima. The model of multifrequency radar signal taking into account breath and palpitation of the person is offered. For remote allocation of person's breath and heartbeat realizations with selection on range cells the spectral analysis in each range element is used. Such a selection besides definition of range up to the living human allows excluding reflections from motionless and inactive local objects, available in other range cells. [C4107]

"A hybrid genetic algorithm-based edge detection method for SAR image"

In this paper, a new edge detection method for SAR image using a hybrid genetic algorithm (HGA) is proposed depending on a full study about the characteristics of SAR images. According to this method, firstly some new types of edges are defined, and then the edge detection is reduced to an optimization problem. Not only original image data, but also some local information of edge, such as the continuity, thickness and regional difference of edges are included to define a cost function. Therefore, by the global searching capability of genetic algorithm, more continuous and accurate edges can be detected than other traditional methods. Moreover, a local optimization operator is employed to speed up the convergence of algorithm. So the method presents a remarkably rapider speed than classical genetic algorithm, as well as better edges. The simulations results also demonstrate its efficiency. [C4108]

"Change detection analysis in wetlands using JERS-1 radar data:tonle Sap Great Lake, Cambodia"

{no data available} [C4109]

"Remote sensing techniques"

Remote sensing of ocean currents is becoming an operational tool in many countries. Wyatt reviews phased-array HF radar systems, with examples of wave, wind and current measurements from operational systems, and she provides an assessment of their accuracy. Observations from HF radar on board an oil platform in the Gulf of Mexico, as described by Barrick et al., show tremendous strides forward when working in this difficult environment, where only one system may be feasible and the structure of the rig distorts the antenna pattern. In contrast, Kohut et al. describe results from a "triple nested HF radar array" that combines lower frequency long-range systems with high-resolution radars and several other techniques to map the plume of the Hudson River in New York Bight. Advances in theory continue to be made, which may lead to future improvements in practical current and wave radars. Wang and colleagues describe new ideas on nonlinear polarisation vector translation. Dugan and Piotrowski argue that aircraft remote sensing is advantageous for rivers and estuaries where currents may change rapidly in time and space. Using images of light scattered by near surface sediment, mean flow vectors have been derived and compared with ADCP data. Terray and colleagues report on their assessment of the feasibility of studying horizontal dispersion and vertical mixing on metre to kilometre space scales using measurements of dye dispersion from an airborne lidar. [C4110]

"Wave, current and wind monitoring using HF radar"

Measurements of waves, winds and currents with the HF radar are presented to demonstrate their operational monitoring capabilities. These include measurements made during a 15 month deployment of the Pisces radar in the Celtic Sea to assess the feasibility of including radar as part of the UK wave monitoring Network, WAVENET, and measurements with the WERA radar on the Norwegian coast as part of the EuroROSE project. The accuracy of the measurements is discussed. [C4111]

"Antennae variety for remote sensing of surroundings"

This paper is an overview of different types of antennae applications for observation of surroundings including remote sensing of Earth surface, atmosphere, ground penetration, and aircraft collision avoidance. The overview covers all frequency bands from millimeter waves up to very long waves. Some recently obtained results on Doppler-polarimetric methods of atmosphere research as well as on new airborne collision avoidance system creation are included. Specificity of antennae of different applications is discussed. This paper mainly reflects the works, which were done with author participation, and does not aspire to saturation coverage of the entire infinite field of antennae application. [C4112]

"Fiber lasers for lidar"

Advances in fiber laser technology can be used to further the capabilities of lidar remote sensing systems. The paper provides an overview of lidar requirements, where current fiber technology can play a role, and advances needed for future systems. [C4113]

"New expressed nonlinear polarization vector translation and its application in HF Radar"

The nonlinear polarization-vector translation algorithm proposed by A.J. Poelman is expressed by ellipticity ratio and orientation angle on a right-handed circular/left-handed circular polarization vector basis. It is inconvenient in the processing of signals expressed by the polarization parameters of amplitude-ratio and relative phase on a horizontal/vertical polarization vector basis. A new expressed NPVT algorithm is given to solve this problem in this paper, and the relation between the two NPVT algorithms is described mathematically. A good performance is obtained by the application of the new algorithm in suppressing of sky-wave radio interference in an HF surface wave radar compared with some other polarization filters. [C4114]

"Airborne fluorescence imaging of the ocean mixed layer"

We report preliminary results from a pilot experiment to image the dispersion of fluorescent dye in the ocean surface layer using an airborne LIDAR. In-situ observations of currents, stratification, and dye concentration were also made from a ship. We give an overview of the experiment, and propose an inversion method for estimating dye concentration from observations of fluorescence and backscatter. [C4115]

"Advance warning of loop current from single-site SeaSonde on Genesis oil platform in the Gulf of Mexico"

A single SeaSonde HF radar operates on Chevron's Genesis deep-water floating platform in the Gulf of Mexico. The radar's purpose is to provide advance warning of strong loops or eddies that approach the rig. A single radar like this, however, only produces a map of the surface current component toward or away from the radar, called a radial map. A pair of radars with overlapping coverage is required for a 2D total vector map. Despite this limitation, and overcoming the strong antenna pattern distortions caused by the all-steel rig, useful information was obtained to a distance of 90 km. To verify the accuracy and utility, comparisons were done with an ADCP 72 km away. Low-pass filtering was used to remove short-term inertial oscillations, revealing close agreement with the 40-m deep ADCP measurement of the persistent geostrophic loops. Both saw the strong loop features. [C4116]

"Observed response of the Hudson River plume to wind forcing using a nested HF radar array"

One objective of the Lagrangian Transport and Transformation Experiment (LaTTE) is to determine the relative advantages of studying the Hudson River plume within the spatial and temporal context provided by an operational research observatory. Towards this end, a shelf-wide observational backbone was locally enhanced with high-resolution relocatable systems in the New York Bight apex. The permanent backbone includes local acquisition of international satellite ocean color imagery, a network of long-range High Frequency radars, and a cross-shelf Endurance line occupied by an autonomous underwater glider. The high resolution systems, including higher resolution HF Radar, glider and mooring networks, were moved to the New York Bight Apex to support the specific interdisciplinary process study. During the LaTTE field effort, datasets from the nested observation network, including a triple nested HF Radar array, were assembled in real-time at a shore-based acquisition center, and high-resolution atmospheric forecasts were performed. Surface current observations will be reviewed, with specific emphasis placed on the observed response of the Hudson River plume to local winds. The observatory results provide a spatial and temporal context for viewing the LaTTE dye release, chemical and biological results. [C4117]

"Asian dust signatures at Barrow: observed and simulated. Incursions and impact of Asian dust over Northern Alaska"

Atmospheric aerosols affect the Earth's radiation budget both directly, through interactions with solar and terrestrial radiation, and indirectly, as cloud condensation and ice nuclei. Against the typically clean polar atmospheres, small increases in aerosol concentrations can perturb radiative fluxes significantly. During spring 2002, dust storms from the deserts of China and Mongolia were tracked over the Arctic, establishing that such remote regions are not immune to the dispersion of Asian dust. Increased aerosol optical depths and lidar measurements at Barrow, AK, in conjunction with trajectory analyses and dust transport provide corroborating evidence for transport of dust to the Arctic. The primary impact of the dust layer can be determined by

examining its radiative properties relative to the underlying snow and intervening pristine background environment. Through a sequence of ground-based visibility measurements of the aerosols coupled with lidar measurements of the layer height, a realistic dust cloud was ported into Moderate Resolution Transmittance (MODTRAN™) code. A suite of MODTRAN calculations, constructed around this cloud description, provided spectrally integrated forcing terms at the surface, along with estimates of the local heating/cooling at altitude, with and without the dust cloud. This then led to a closure experiment where MODTRAN predictions of surface forcing are in remarkably good agreement with measurements for a set of solar-zenith angles and aerosol optical depths. [C4118]

"Global aerosol distribution from the GLAS polar orbiting lidar instrument"

The Geoscience Laser Altimeter System (GLAS) launched in 2003 has provided the first global aerosol profiling from space. GLAS is a two wavelength nadir viewing instrument. The measurement requirement to profile all radiatively significant aerosol layers has been exceeded. Data processing algorithms have provided aerosol scattering cross section profiles, boundary detection and height for all aerosol layers, aerosol optical depth and extinction cross section for data from 2003. The data products are openly available to the global science community. [C4119]

"532/1064 nm ACA lidar measurements of Asian dust at Suwon, Korea during 2002–2004"

Asian dust in the middle and lower troposphere has been measured continuously by ACA lidar at Suwon station (37.2°N-127.6°E) during 2002-2004. The lidar system consists of 532/1064 nm laser transmitter and multi-receiving channels. The output optical parameters of the lidar are 532/1064 nm backscatters, 532 nm depolarization ratio, and 1064/532 nm color ratio. During three years of intensive observations of the Asian dust, more than 25 episodes were successfully monitored. The significant dust in March 2002 to May 2004 showed the dust layers are located in the altitude range of 0.4-6 km with the depolarization ratios, 10-30%, the backscattering ratio, 1-5, and the aerosol color ratio, 0.3-0.9 respectively. The backward trajectory applied to those episodes showed that the dust mainly came from Mongolia and Takaramakan deserts. [C4120]

"Seasonal soil moisture variation analysis using RADARSAT-1 satellite image in a semi-arid coastal watershed"

{no data available} [C4121]

"Forty Years of Aerosol Remote Sensing"

{no data available} [C4122]

"AEROCAN: the Canadian Sunphotometer Network"

Growing out of the 2-site BOREAS sunphotometer network of 1994, the current AEROCAN network comprises 12 stations with at least one site in each of Canada's major geographic regions. The network, a joint collaboration between the Universite de Sherbrooke and Meteorological Services of Canada, is a member of the much larger AERONET system of CIMEL sunphotometers. The overall AEROCAN objective is to provide a sampling density of columnar aerosol properties which are as representative as possible of national, regional and local variations across Canada. Most of the sites are rural, but several of the sites have been "twined" with an urban sunphotometer. A number of the AEROCAN sites are in the most northern regions of Canada, >55 degrees north latitude (Churchill, Kuujuarapik, and Resolute Bay) with a new CIMEL and starphotometer to be located in Eureka (80°N). Cimel sunphotometers have also been deployed for very short durations in support of regional air quality and trans-boundary flow studies. Over the last several years the AEROCAN network has generated about 1000 days of observations/year. The network goal is to increase the number of possible observation days by minimizing problems that limit data collection and transmission. The AEROCAN network is now being used to support satellite and airborne remote sensing projects, investigate cross border pollution issues, supplement LIDAR observations of aerosols and provide inputs to large scale aerosol transport models. While working within the AERONET protocols our group is experimenting with new methods to collect data on aerosol parameters including increasing optical depth observations to once every 4-5 minutes and near real-time assimilation of this information into air quality forecast models. The network will expand in the coming year with several new sites planned. [C4123]

"Spaceborne lidar aerosol retrieval approaches based on improved aerosol model constraints"

Aerosol retrievals at 532 nm for the current GLAS and upcoming CALIPSO satellite lidar missions employ/will employ a table look-up approach to select climatologically based Samodel values for these retrievals when

alternate, less uncertain methods for either defining S_a (the aerosol extinction-to-backscatter ratio, or aerosol lidar ratio) or providing the needed auxiliary information are unavailable. Reagan et al. (2004, 2005) addressed a revised table look-up approach that incorporated two notable revisions for improved S_a selection, which, as a consequence, enable more bounded aerosol retrievals. One is a refined, more bounded set of S_a values, both for 532 nm and 1064 nm, representative of a definitive set of aerosol types/models determined from an extensive analysis of the AERONET database. The other is an accompanying set of key spectral ratio parameters (i.e., dual wavelength, 532 nm to 1064 nm, ratios of backscatter, extinction and S_a) also derived from the AERONET data which offer additional ways to bound the lidar aerosol retrievals. Thus, aerosol retrievals can be obtained subject to the constraints that the lidar data yield retrievals with spectral ratio parameters consistent with a given aerosol model (or models), to confirm the model choice and better bound the retrievals. This paper presents the simulation results made by assuming different models in support of the two-wavelength lidar constrained ratio aerosol model-fit (CRAM) retrieval approach. In addition, a performance function and multiple scattering corrections based on LITE signals are also investigated. [C4124]

"Monitoring aerosol distribution from ground based elastic scattering lidar: a review"

The original lidars were incoherent elastic backscatter systems, and one of the original applications for such systems was profiling the vertical distribution of aerosol. In the beginning there was significant limitation in both the practicality of the lidar hardware and in using data for aerosol retrievals of significant parameters such as the aerosol extinction and backscatter cross section. The paper reviews the use of lidars for remote sensing of atmospheric aerosols. [C4125]

"Multiwavelength lidar measurements at the City College of New York in support of the NOAA-NEAQS and NASA-INTEx-NA experiments"

Satellite measurements do not provide the vertical information needed to assess aerosol transport mechanisms. To supply this information, multiwavelength lidar measurements are needed to study the vertical structure of aerosol events. In support of NASA-INTEx and NOAA-NEAQS transport experiments; we present lidar retrievals, which identify multiple stratified particulate plumes occurring over New York City on 2004 July 21 in support of MODIS imagery. In particular, multiwavelength measurements at CCNY are used to determine the Engström coefficient of the plumes that unambiguously identifies them as fine mode particulates and not cloud particles. A description of our lidar system capabilities and processing algorithms used to process simultaneous backscatter lidar measurements with Aeronet CIMEL Optical Depth (OD) data is presented and back trajectory analysis is used to confirm the source of the plumes to be from Alaskan wild fires. Finally, surface measurements from in situ particle counters are presented and show no enhanced PM_{2.5} loading. This result is supported by lidar measurements, which confirm that nearly all of the aerosol plumes are located above the normal aerosol boundary layer showing that satellite measurements are often incomplete and is not useful to assess surface air quality. In particular, we show that high PM_{2.5} events are triggered from more local sources such as the Ohio Basin and climatological conditions which drive the pollution to the surface. [C4126]

"Impact of oscillator noise in bistatic and multistatic SAR"

{no data available} [C4127]

"On the requirements of SAR processing for airborne differential interferometry"

{no data available} [C4128]

"Singular value decomposition applied to 4D SAR imaging"

{no data available} [C4129]

"Scatterer characterisation using polarimetric SAR tomography"

{no data available} [C4130]

"Topography independent InSAR coherence estimation in a multiresolution scheme"

{no data available} [C4131]

"A raw data simulator for cross-track InSAR based on land clutter model"

{no data available} [C4132]

"DEM, tide and velocity over Sulzberger ice shelf, West Antarctica"

{no data available} [C4133]

"Disaster area extraction algorithm development using repeat-pass SAR interferometry"

{no data available} [C4134]

"C-band interferometric SAR measurements of water level change in the wetlands: examples from florida and louisiana"

{no data available} [C4135]

"Multistatic sar satellite formations: potentials and challenges"

{no data available} [C4136]

"First trials of fourier and adaptive tomo-doppler sar imaging"

{no data available} [C4137]

"Analysis of forest-slab height inversion from multibaseline SAR data"

{no data available} [C4138]

"L-band doppler radar echoes of the sea surface in coastal zone"

{no data available} [C4139]

"Microwave remote sensing of falling snow"

{no data available} [C4140]

"Moving targets detection and velocity estimation via multi-channel along-track interferometry"

{no data available} [C4141]

"Remote sensing the sea surface using a multichannel ATI SAR: imaging sea spikes"

{no data available} [C4142]

"Interferometric digital elevation model reconstruction-experiences from SRTM and multi channel approaches for future missions"

{no data available} [C4143]

"Land-cover classification-based persistent scatterers identification for peri-urban applications"

{no data available} [C4144]

"Processing the hydros SAR data"

{no data available} [C4145]

"Comparison of satellite imagery DEMs produced using photogrammetry and radargrammetry techniques"

{no data available} [C4146]

"An autonomous, non-cooperative, wide-area traffic monitoring system using space-based radar (TRAMRAD)"

{no data available} [C4147]

"Building reconstruction from LIDAR data and aerial imagery"

{no data available} [C4148]

"Crustal deformation monitoring using repeat-pass interferometry in the vicinity of Hua-Tung Longitudinal Valley, Taiwan"

{no data available} [C4149]

"Clutter effects on ground moving targets' interferometric phase"

{no data available} [C4150]

"A-priori information driven detection of moving objects for traffic monitoring by SAR"

{no data available} [C4151]

"Radar antenna architectures and sampling strategies for space based moving target recognition"

{no data available} [C4152]

"SAR/GMTI using $\Sigma\Delta$ -beams based on signal subspace processing"

{no data available} [C4153]

"Multi-temporal, multi-resolution data fusion for Antarctica DEM determination using InSAR and altimetry"

{no data available} [C4154]

"Estimating soil moisture for vegetated terrain: a discussion of possible approaches relevant to the HYDROS mission"

{no data available} [C4155]

"Estimation of soil moisture with the combined L-band radar and radiometer measurements"

{no data available} [C4156]

"Overview of hydros radar soil moisture algorithm"

{no data available} [C4157]

"A soil moisture retrieval technique based on the semi-empirical scattering model for HH-, HV-, and VV-polarized radar observations"

{no data available} [C4158]

"Validation of a feature fusion scheme for urban DSM retrieval from high resolution SAR interferogram"

{no data available} [C4159]

"Improved observational updating for efficient fusion of incomplete image data"

{no data available} [C4160]

"Joint feature and pixel-based change detection in high resolution SAR data"

{no data available} [C4161]

"Polarimetric analysis of fine resolution X-band SAR sea clutter data"

{no data available} [C4162]

"Multifrequency SAR remote sensing of ocean internal waves"

{no data available} [C4163]

"Image georeferencing using LIDAR data"

{no data available} [C4164]

"Radargrammetry for DEM generation using minimal control points"

{no data available} [C4165]

"Rain-rate estimate algorithm evaluation and rainfall characterization in tropical environments using 2DVD, rain gauges and TRMM data"

{no data available} [C4166]

"Development of laser waveform digitization for airborne LIDAR topographic mapping instrumentation"

{no data available} [C4167]

"Project polar epsilon: joint space-based wide area surveillance and support capability"

{no data available} [C4168]

"Possibilities and plans for utilization of RADARSAT-2 data"

{no data available} [C4169]

"Ship detection experiments using RADARSAT/SAR images"

{no data available} [C4170]

"Estimates of bare soil surface parameters from multi-polarization and multi-angle SAR data"

{no data available} [C4171]

"High resolution PolInSAR with the ground-based SAR (GB-SAR) system: measurement and modelling"

{no data available} [C4172]

"Improving the total rotation vector estimation via a bistatic isar system"

{no data available} [C4173]

"Polarimetric interferometry and time-frequency analysis applied to a urban area at X-band"

{no data available} [C4174]

"Azimuth-invariant, bistatic airborne SAR processing strategies based on monostatic algorithms"

{no data available} [C4175]

"Bistatic SAR processing using an Omega-K type algorithm"

{no data available} [C4176]

"The development of a ground based polarimetric SAR interferometer (GB-POLInSAR)"

{no data available} [C4177]

"Advances in polinsar retrieval algorithms of agricultural crops"

{no data available} [C4178]

"Resolution effects on polarimetric high resolution X band data"

{no data available} [C4179]

"Polarimetric interferometry over urban areas: information extraction using coherent scatterers"

{no data available} [C4180]

"AIRSAR automated web-based data processing and distribution system"

{no data available} [C4181]

"A joint analysis of radiometric and scatterometric simulations to tune an electromagnetic forward model within a common theoretical framework"

{no data available} [C4182]

"Compartmentalization of coastal sea surface wind by statistical approach using high-resolution SAR-derived winds"

{no data available} [C4183]

"Predictions of SAR polarimetry and InSAR coherence for a model wheat canopy"

{no data available} [C4184]

"Study on velocity measurement of AT-INSAR in the cluster micro-satellite system"

{no data available} [C4185]

"Methods to evaluate the accuracy of high frequency radar by in-situ measurements"

{no data available} [C4186]

"Speckle cross-correlation in multilook sar images of dynamic sea surface processed with partially overlapped sub-reference signals"

{no data available} [C4187]

"Optimal SAR parameters for ship detection"

{no data available} [C4188]

"Estimation of the skewness coefficient using Jason-1 altimeter data"

{no data available} [C4189]

"Model development and analysis of radar backscatter in Ross Island, Antarctica"

{no data available} [C4190]

"Bi-static scattering width control of multiple coated PEC cylinder"

{no data available} [C4191]

"Numerical simulation of the doppler spectrum of a flying target above dynamic oceanic surface by using the FEM-DDM method"

{no data available} [C4192]

"Unsupervised classification of a central italy landscape by polarimetric L-band SAR data"

{no data available} [C4193]

"SAR imaging of a forested area based on a coherent 3-D model of wave scattering: application to remote sensing of a hidden target in VHF band"

{no data available} [C4194]

"Simulation of SAR image of ship"

{no data available} [C4195]

"FDTD modelling of a borehole radar wave propagation: a 3-D simulation study in conductive media"

{no data available} [C4196]

"Analysis of non-gaussian speckle statistics in high-resolution SAR images"

{no data available} [C4197]

"Comparison between small slope approximation and two scale model in bistatic configuration"

{no data available} [C4198]

"Segmentation of ALSM point data and the prediction of subcanopy sunlight distribution"

Sunlight flux in forest canopies is an important source of energy for the productivity of forests and is therefore an important input to biophysical process models. High-resolution three-dimensional estimates of sunlight flux are derived from directional foliage density measured from airborne laser swath mapping data. Forest edges are shown to exhibit measurable differences in flux. A method for determining appropriate in situ sampling intervals is also presented. [C4199]

"The application research on subsidence monitoring of coal mining area with D-InSAR"

{no data available} [C4200]

"Large scale InSAR deformation time series: Phoenix and Houston case studies"

{no data available} [C4201]

"Extracted grounding line of the Antarctic ice sheet from ERS-1/2 interferometric SAR data"

{no data available} [C4202]

"Detection of compression structures from SAR ERS imagery: example of the Central Japan seismic area"

{no data available} [C4203]

"On the assessment of co-seismic InSAR images of different time span associated to Athens (Greece) 1999 earthquake"

{no data available} [C4204]

"Temporal and spatial pattern of the 1997 Manyi Earthquake using differential InSAR"

{no data available} [C4205]

"Accuracy comparison of DEMs derived from multisource SAR images"

{no data available} [C4206]

"ERS tandem DInSAR: the change of ground surface in 24 hours"

{no data available} [C4207]

"Measuring mining induced subsidence with InSAR"

{no data available} [C4208]

"Exploration of the lower atmosphere with millimeter-wave radar"

{no data available} [C4209]

"An improved attenuation correction algorithm using dual-polarization radar observations of precipitation"

{no data available} [C4210]

"Performance of dual-polarization radar measurement in hybrid mode for precipitation"

{no data available} [C4211]

"Field campaign of observing precipitation in the 2004 rainy season of Okinawa, Japan"

{no data available} [C4212]

"Adaptive clutter suppression for multistatic observations with equatorial atmosphere radar"

{no data available} [C4213]

"Glacier velocity measurements using differential interferometric SAR in Antarctic Grove Mountain"

{no data available} [C4214]

"Detecting ice motion with repeat-pass ENVISAT ASAR interferometry over Nunataks region in Grove Mountain, East Antarctic-the preliminary result"

{no data available} [C4215]

"An improved autoregressive model for analysis of decadal elevation change time series over Antarctica"

{no data available} [C4216]

"Analysis of the influence of NESZ variations on cross-polarized signatures of sea ice"

{no data available} [C4217]

"Picosecond mid-infrared LIDAR system"

With a picosecond mid-infrared LIDAR system based on a pulsed difference-frequency generation laser system concentrations of methane are measured in the plume of an aircraft engine. [C4218]

"Dual-frequency dual-polarized sixteen-element stacked patch microstrip array antenna for soil moisture and sea surface salinity missions"

A dual-polarized dual-band active/passive (radar/radiometer) microstrip array for remote-sensing applications is described. The measurement results meet the requirements for center-frequencies and frequency-bands, low-sidelobes (90%) and low cross-polarization ([C4219]

"Standoff sensing of natural gas leaks: evolution of the remote methane leak detector (RMLD)"

Development of a handheld standoff laser-based sensor developed specifically for inspection of municipal natural gas pipelines is described. The remote methane leak detector is fundamentally a Differential Absorption LIDAR system using wavelength modulation spectroscopy. [C4220]

"A compact 100-km FMCW fiber laser radar"

Frequency-modulated continuous wave (FMCW) measurements of Rayleigh back-scattering and Fresnel

reflection from 95-km fiber have been demonstrated with a compact piezo-electrically-tuned sub-kilohertz-linewidth fiber laser. This is, to our knowledge, the longest distance measurement with FMCW. [C4221]

"The forward scattering surface interaction region"

This paper presents measured data from a low grazing, rough sea forward scattering measurement which shows that, while the forward scattering is generally restricted to the first few Fresnel zones for crosswind waves, measurable scattering frequently occurs many zones out for downwind waves. [C4222]

"An architecture for sentient GPRS-enabled MicroBots"

Ambient intelligence is a user-centered concept which combines several computing disciplines with the purpose of enhancing/facilitating the user's daily activities. We deem that autonomous or semiautonomous (remotely controlled) sentient MicroBots may also be first-class citizens within ambient intelligence. Those MicroBots would interact with their surrounding environment assisted by their built-in sensors, effectors and communication facilities, on behalf of the users they serve. In essence, they would also profit as users do from Ambient Intelligence to achieve their programmed goals. In this paper, we contribute with a solution to enable the realtime remote control of GPRS-accessible semiautonomous sentient MicroBots. Moreover, we discuss the extensions necessary to convert those MicroBots into care assistants for disabled and elderly people. [C4223]

"Indirect method of RCS estimate of conducting target in random medium"

This paper discusses an indirect estimate of the RCS of a conducting cylinder with a partially convex cross-section under the condition that the backscattering enhancement occurs in a random medium. Once we evaluate the spatial coherence length (SCL) of incident waves around the cylinder in random medium, we may approximately estimate the RCS from the RCS in free space with beam wave incidence in which the spot size equals the SCL. This method is restricted only to the case where the SCL is larger than the target size [C4224]

"Numerical study of wide-band low-grazing HF clutter from ocean-like surfaces"

Backscattering of a vertically polarized, ultra-wide band HF pulse (3-30 MHz) from one-dimensional Pierson-Moskowitz impedance surfaces is studied using method of moments (MoM)-based numerical simulations. With the field source located near the surface, low-gazing regime is realized for the most of the illuminated region. The direct numerical solution is compared to approximate calculations based on the small perturbation method (SPM). Once the Norton surface wave effects are included in the SPM scattering coefficient, average clutter levels as well as waveform shapes generally show good agreement. As the sea state increases, backscatter returns from farther ranges exhibit larger discrepancies. In such a situation, using the "effective surface impedance" (that accounts for surface roughness) brings SPM-based average clutter levels in agreement with their MoM counterparts: however, the differences in waveform shapes persist. Future studies will use the simulation capability described in this paper to investigate the ability of a short-pulse, ultrawideband HF radar to image ocean waves, measure surface currents and surface current shear, and detect targets. [C4225]

"A wide-band dual-polarized VHF microstrip antenna for global sensing of sea ice thickness"

A VHF microstrip patch antenna was developed to achieve a bandwidth of 45 MHz (300%) from 127 MHz to 172 MHz with dual-linear-polarization capability. This microstrip antenna uses foam substrates and dual stacked patches with capacitive probe feeds to achieve wide bandwidth. Four such capacitive feeds were used to achieve dual polarization with less than -20 dB of cross-polarization level. Twenty-four shorting pins were used on the lower patch to achieve acceptable isolation between the four feed probes. This antenna has a measured gain of 8.5 dB at 137 MHz and 10 dB at 162 MHz. By using the method of moments technique, multipath scattering patterns were calculated when the antenna is mounted on the outside of a Twin Otter aircraft. [C4226]

"SAR image segmentation based on immune algorithm"

The immune algorithm-IA is proposed with analogies to the concept and the theory of immunity in biotic science. It inherits the CA's advantages and avoids the deterioration-phenomenon. The IA needs the feature or knowledge of problem-space as the vaccine. Spatial matrix describes the probabilities that one area is the neighbor of other areas. Different areas in SAR images have different textural features and have big contrast. Therefore the spatial matrix of a SAR image has the character that the probability of the areas of same kind is the largest and the probability of the areas of different kinds is the smallest. Using this feature as the vaccine this paper employs IA to find the best segmentation-threshold. Simulation results show that this method is effective for SAR image segmentation. [C4227]

"Gust front detection in weather radar images by entropy matched functional template"

We describe a new gust front detection method using functional template correction (FTC) and entropy. The new method provides better boundaries than does a previously developed method by our group (V. DeBrunner and E. Matusiak, 2003). Our proposed method described in this paper requires only one template for detection, thereby reducing the computational complexity and so yielding an algorithm that is more suitable for real time detection than that previously developed one. [C4228]

"Application of SRTM-DEM based two-pass SAR interferometry for detecting seismic deformation on high-altitude rugged terrain -- a case study in Kokoxili Ms8.1 Earthquake, 2001"

{no data available} [C4229]

"Classification of SAR imagery based on the multiscale stochastic process"

This paper presents efficient non-parameter and multiscale approach to segmentation of natural clutter in synthetic aperture radar (SAR) imagery. The method we propose not only exploit the coherent nature of SAR sensor, and take of advantage of the characteristic statistical difference in imagery of different terrain types, but also do not require distribution of pixels due to using bootstrap method. Firstly, we employ multiscale autoregressive (MAR) model for describing random processes that evolve in scale. Secondly, the confidence internals of the parameters in MAR model for each category of terrain of interest are calculated using bootstrap technical. Then, for each pixel, we generate a set of parameter estimation that characterizes the local evolution in scale. The pixel is classified by relation between the parameters estimation and the confidence internal of each type. Finally, test images are classified to demonstrate the method. [C4230]

"An adaptive multiscale approach to unsupervised change detection in multitemporal SAR images"

A novel adaptive multiscale approach to unsupervised change detection in multitemporal synthetic aperture radar (SAR) images is proposed. This approach is based on a multiresolution decomposition of the log-ratio image (obtained by a comparison of a pair of co-registered images acquired at different times on the same area) in a set of scale-dependent images characterized by a different trade-off between speckle reduction and preservation of geometrical details. For each pixel to be analyzed, a sub-set of reliable scales is identified according to an automatic local analysis of the statistic of the data. The final change-detection map is obtained according to an adaptive scale-driven fusion algorithm, which properly exploits the results of the analysis at different scales for producing an accurate and reliable change-detection map in both homogeneous and border areas. Experimental results confirm the effectiveness of the proposed technique. [C4231]

"How to reconstruct the original shape of a radar signal?"

The shape of the radar signal can provide us with the additional information about the reflecting surface. However, to decrease the noise, radars use filtering, and filtering changes the shapes of the radar signal. It is therefore necessary to reconstruct the original shape of the radar signal. [C4232]

"A diode pumped, Nd:YAG, Q-switched unstable resonator developed for multi-billion shot, spaced based remote sensing applications"

This highly efficient Nd:YAG laser was designed as a prototype NASA-funded transmitter for space-based LIDAR missions. This design completed a 4.8 billion shot lifetest at 242 Hz with 10-15 mJ per pulse and 10 ns pulsewidth. [C4233]

"Segmentation of coherence maps for flood damage assessment"

Multitemporal coherence map has been successfully used for various types of surface characterized by the same level of interferometric correlation. This paper examines the possible benefits of this source of information to detect the damages caused by the flooding of rivers and lakes. As test case the Yangtze river flooding of summer 1998 was chosen. The interferometric coherence map was obtained using ERS tandem mission images during the flood and a pair dating December 1995. The low level of water surface coherence allows to segment the flooded areas in an easy way with respect to the method which exploits the backscatter intensity. The approach proposed is based on fuzzy connectivity concepts of the flooded areas with reference to the original river bed. [C4234]

"Eye safe solid state lasers for remote sensing and coherent laser radar"

This study demonstrates a second generation version of a three-level injection seeded Er:glass laser that works as a transform limited coherent laser radar. This laser is designed to maximize the average power that can be extracted from a bulk glass host. It uses pulsed pump diode lasers and a conduction cooled, co-planar folded zig-zag slab (CPFS) gain medium in an injection seeded, long Q switched pulsed configuration. This laser can operate at 60 mJ per pulse at 10 Hz in a standing wave configuration. For eye-safe operation it should not exceed 10 mJ per pulse. The resonator used in this work is developed specifically for generating long pulse, single frequency Q-switched outputs in low gain laser media. This work describes the latest results of this prototype laser and its properties for coherent single frequency sensing. A design for a third generation of this laser are also be discussed. [C4235]

"Advances in multipass SAR image registration"

{no data available} [C4236]

"A comparison of change detection statistics in POLSAR images"

{no data available} [C4237]

"SAR interferogram filtering with 2D Vondrak filter"

{no data available} [C4238]

"Phase unwrapping based on network flow algorithm and divide and conquer strategy"

{no data available} [C4239]

"A framework for the analysis of speckle noise effects in multidimensional SAR imagery"

{no data available} [C4240]

"Data classification based on PolInSAR coherence shapes"

{no data available} [C4241]

"New blind source separation technique for removing vegetation bias in polarimetric SAR interferometer measurements"

{no data available} [C4242]

"A unified model for decomposition of coherent and partially coherent target scattering using polarimetric SARs"

{no data available} [C4243]

"Applying polarimetric SAR interferometric data for forest classification"

{no data available} [C4244]

"Wind field and ocean wave measurements in extreme weather situations"

{no data available} [C4245]

"Refined estimation of time-varying baseline errors in airborne SAR interferometry"

{no data available} [C4246]

"The distribution of internal waves in the East China Sea and the Yellow Sea studied by multi-sensor satellite images"

{no data available} [C4247]

"Uniqueness of the ERS scatterometer for nowcasting and typhoon forecasting"

{no data available} [C4248]

"Spaceborne radar interferometry for coastal DEM construction"

{no data available} [C4249]

"InSAR PS adaptive detection and its application in Beijing area"

{no data available} [C4250]

"Quality assessment of SAR data available for SAR interferometry"

{no data available} [C4251]

"Introduction on an experimental airborne InSAR system"

{no data available} [C4252]

"InSAR unwrapping using pre-existent topographic information-Application to the DEM derivation on the test site of Marseille/Gardanne (France)"

{no data available} [C4253]

"Segmentation and extraction of linear features for detecting discrepancies between LIDAR data strips"

{no data available} [C4254]

"Update of road network in GIS by fusing multi-sensor imagery"

{no data available} [C4255]

"Ka-band, short pulse, polarimetric, combined Doppler radar-radiometer system"

{no data available} [C4256]

"A hierarchical procedure for segmentation and classification of airborne LIDAR images"

{no data available} [C4257]

"Development of a precipitation algorithm optimized for the heavy rainfall using TRMM/TMI data"

{no data available} [C4258]

"Attenuation statistics for X band radar design"

{no data available} [C4259]

"Melting layer observation by the broad band radar(BBR)"

{no data available} [C4260]

"Ice water content (IWC) retrieval from cirrus clouds using millimeter-wave radar and in-situ ice crystal airborne data"

{no data available} [C4261]

"DSD characterization and computations of expected reflectivity using data from a two-dimensional video disdrometer deployed in a tropical environment"

{no data available} [C4262]

"TerraSAR-X: calibration concept of a multiple mode high resolution SAR"

{no data available} [C4263]

"The system engineering and calibration segment of the TerraSAR-X ground segment"

{no data available} [C4264]

"Polarization orientation effects in urban areas on SAR data"

{no data available} [C4265]

"Status of the TerraSAR-X Mission"

{no data available} [C4266]

"TerraSAR-X: science exploration of polarimetric and interferometric SAR"

{no data available} [C4267]

"The TerraSAR-X ground calibration system and pattern estimation software"

{no data available} [C4268]

"A complex of polarimetric, combined, short pulse radar-radiometers of S-, Ku, and Ka -band of frequencies for platform and vessel application"

{no data available} [C4269]

"Use of TerraSAR-X for oceanography"

{no data available} [C4270]

"TanDEM-X: mission concept and performance analysis"

{no data available} [C4271]

"From VCL to Glory: the risk management approach to changing an existing spacecraft configuration"

The Glory satellite program is underway at the Orbital Sciences campus in northern Virginia under contract with NASA GSFC. The Glory satellite bus was previously known as the vegetation canopy LIDAR (VCL), a satellite designed to measure the Earth's vegetation coverage, depth, and topography. The Glory program is using this existing NASA asset from the VCL program, which was terminated while the bus was in integration and test (I&T) due to instrument problems. The bus is being revamped for the Glory Science mission, which includes atmospheric aerosol measurements and total solar irradiance monitoring. There are many changes being made to the VCL bus to configure it for the Glory program objectives. The risk management and safety approach to Glory requires extra effort to not only analyze the current work, but all work done in the past under the VCL program. This includes extensive audits of the VCL program hardware and software to ensure safety and compliance with the Glory mission and safety requirements. Risk management is an integral part of any program in order to achieve mission success. In this program, it has special application not only for current program work, but past work as it pertains to the current requirements. To date the Glory team has expended considerable effort in a full component and documentation audit for the VCL program, uncovering situations requiring unique handling for a safe and reliable program. This paper describes the process of risk management in application to the current program that relies on work performed on a previous program. This includes mitigation approaches to newly raised issues and past issues that may have gone unresolved at the close of the VCL program. Using this approach of risk management and lessons learned, the story is told of how an existing bus may be reused while considering the balance of risk and cost and maximizing use of existing hardware. [C4272]

"Utilization of fully polarimetric SAR data for improved measurement of directional ocean wave spectra"

New methods have been investigated which use fully-polarimetric synthetic aperture radar (SAR) image data to measure ocean wave slope spectra. Independent techniques have been developed to measure wave slopes in the orthogonal SAR (azimuth/range) directions. These measurements must still contend with motion-induced nonlinearities in the SAR processing. The methods are, however, physically based, robust, and utilize a parametrically simpler modulation transfer function. NASA/JPL/AiRSAR L-band data from California coastal waters has been used. Wave spectra measured using the new methods are compared with spectra developed

using both conventional SAR intensity-based methods and NDBC buoys. [C4273]

"Sea surface radar-radiometer joint image's natural origin signatures radio contrast and spatial size's distributions properties for various meteorology and seas"

The results of field experimental (airborne) researches of distribution features of sea surface background, natural origin radar-radio thermal joint signatures (anomalous formations) are presented. Statistical characteristics of spatial sizes and radar contrasts distributions are estimated, for sea surface radar-radiometer joint image natural origin signatures. [C4274]

"Study about the radiation properties of an antenna for ground-penetrating radar"

The ground penetrating radar (GPR) system is an effective tool for nondestructively sensing subsurface environment. One of the most critical hardware components for the performance of the GPR system is the antenna. The system demands an antenna with fewer multiple reflections of the input signal from different parts of the antenna. There are only a few types of antennas that are widely used in GPR systems, such as resistively loaded cylindrical monopoles, resistively or resistor-loaded bow-tie antennas, TEM horns and their modification, and spiral antennas. In the paper, a GPR antenna with discrete exponential resistive loading is present, and it can terminate the ringing. The near-zone radiation pattern and waveform of the antenna are analyzed through the finite-difference time domain (FDTD) method. At last, the comparison of the simulation and measured results were shown when the transmitter and receiver antennas on the above of the dry sand. [C4275]

"Rainfall rate from meteorological radar data for microwave applications in Malaysia"

This paper present the rainfall rate obtained from the analysis of a meteorological radar data in Malaysia. Rainfall rate is an important parameter for a microwave link because it enables the attenuation due to rain to be determined. An important parameter in rain attenuation studies is the rain rate for 0.01% of the time or R0.01. Design and system engineers use this value to construct communications system such that the link is available for 99.99% of the time. This result is obtained by utilizing the radar data from the Malaysian Meteorological Department. Knowing the rainfall rate, rain attenuation can be calculated. This information is useful for microwave link applications. [C4276]

"C-band, narrow pulse, polarimetric Doppler-scatterometer for platform application"

In this paper C-band (5.6 GHz), polarimetric (dual polarization), narrow pulse (30 ns) Doppler scatterometer is described. The scatterometer was developed for a short distance (6.5 m) remote sensing application and for simultaneous and coincident measurements of water surface microwave reflective and backscattered signal's spectrum characteristics. In spite of the system was developed for a platform application, it may have successful vessel and airborne application for both land and sea surface remote sensing. [C4277]

"QuikSCAT Radiometer (QRad) rain rates for wind vector quality control"

The Sea Winds scatterometer onboard the QuikSCAT satellite measures the ocean normalized radar cross section to infer the surface wind vector. In addition, SeaWinds simultaneously measures the polarized microwave brightness temperature of the ocean/atmosphere, and this passive microwave measurement capability is known as the QuikSCAT Radiometer (QRad). QRad brightness temperatures are used to infer instantaneous rain rates over oceans using a statistical retrieval algorithm that has been developed using collocated QRad brightness temperatures with TRMM Microwave Imager (TMI) rain rate measurements. In this paper, QRad retrieved rain rate examples are presented and comparisons are made with independent near simultaneous rain observations including the TRMM 3B42RT data product. This near-real-time global precipitation data product combines all passive microwave with geostationary visible/infrared precipitation estimates in global 3-hour universal time windows. Results demonstrate that QRad rain measurements agree well with these independent microwave rain observations, which demonstrates the utility of using QRad rain retrievals as a "stand alone rain quality flag". [C4278]

"Satellite calibration and validation utilizing the Airborne Polarimetric Microwave Imaging Radiometer (APMIR)"

The Airborne Polarimetric Microwave Imaging Radiometer (APMIR) was designed and built by the Naval Research Laboratory, Washington, D.C., as a tool for calibration and validation of the Coriolis WindSat and Defense Meteorological Satellite Program SSMIS satellite radiometer sensors. The satellite sensor data aids in short-term weather modeling and general climatic information via measurements of ocean winds, water vapor, soil moisture, rain rates, and ice/snow characteristics. The APMIR sensor was designed to assist in the

fulfillment of the airborne portion of the calibration/validation effort. By underflying a satellite, the airborne sensor data is coincident in space and time with the satellite, allowing an accurate comparison of the viewed scene. Extensive testing of the APMIR system included tip curves, pool views, and radiative transfer model comparisons. The encompassing test methods achieve a high degree of confidence in the APMIR system. APMIR underflew the SSMIS satellite during a March/April 2004 field campaign. Based on the high confidence of the APMIR sensor, and the excellent data comparison of the SSMIS satellite, the APMIR instrument demonstrates itself as a precision tool for calibration and validation activities. The results of the underflights during the March/April 2004 field campaign for the SSMIS satellite are presented. [C4279]

"A measuring complex of polarimetric, combined radar-radiometers of S-, and Ku-band of frequencies for vessel and airborne application"

A complex of polarimetric (dual polarization), combined active-passive devices of S (3 GHz), and Ku-band (20 GHz) of frequencies for sea surface microwave reflective and emissive characteristics simultaneous and coincident measurements is presented. The complex is dedicated to solve the problem applied to near sea surface wind and surface wave fields' parameters precise and unambiguous retrieval, as well as for sea surface signatures detection and identification. Developed systems are set on a mobile bogie moving on the height of 6.5 m along a stationary platform of 26 m of length. The measuring platform allows carry out polarimetric (vv, vh, hh, hv), multifrequency, simultaneous and coincident measurements of pool water surface microwave reflective and emissive parameters at the same or at various angles of incidence from the while of 0-60°. This paper has an aim to attract attention of researchers interested in measurements by such kind sensors and to invite them to perform their own or joint measurements using available microwave devices and in-situ and calibration facilities. [C4280]

"Joint processing of the signals backscattered from and emitted by the sea surface"

In this presentation, the results of theoretical and experimental researches related to a joint processing of the sea surface radar and proper radio thermal signals are presented. [C4281]

"Analysis of rain cell size distribution from meteorological radar data for rain attenuation studies"

The ability of radar to scan a wide area around the radar site and not just a particular path made it a very attractive for many types of investigations. Radar can be used to measure the rainfall rate indirectly. This is achieved by knowing the radar reflectivity and then converting them into rainfall rate. The S-band frequency of the meteorological radar ensures that propagation effects such as attenuation are negligible. Radar provides valuable information that is relevant in modelling rain-induced propagation effects. Radar also provides spatially and temporally continuous measurements that are immediately available at one location. Rain cell size distribution is obtained from radar data. 'Virtual' microwave links of 20-km path lengths were constructed in the scanning area of the radar. However, rain cell size distribution from radar data is limited to 1-km integration size. This is due to the fact that the radar uses a range bin size of 1 km. The radar data is obtained from the Kluang Radar Station of the Meteorological Department of Malaysia. This paper present an analysis of rain cell size distribution obtained from the meteorological radar data. Rain cell size is an important parameter in the study of attenuation of radio propagation through rain. This parameter is used for attenuation predictions, link budget estimation, microwave system planning, slant path rain attenuation modeling and remote sensing of the Earth's surface, and have important applications in attenuation mitigation techniques such as space diversity. Analysis was done to find the rain cell size distribution. [C4282]

"The using multifrequency airborne radar complex MARS for subsurface remote sensing"

This paper presents some results of using airborne radar multifrequency complex MARS for subsurface remote sensing. Experimental data and theoretical basis are given. [C4283]

"Information extraction from sensor nodes using air-borne radar and back-scatter modulation"

Radar imaging is a powerful tool in remote sensing due to its ability to image vast areas with high resolution. However, the ability to sense a particular parameter depends on the extent to which the parameter affects the reflected microwave radiation. In this respect, multi-functional sensor nodes offer an immense potential to sense environmental parameters which cannot be directly sensed by radar imaging techniques. With this motivation, we develop techniques to collect information at an air-borne radar from a large group of sensor nodes. Back-scatter modulation is used on the sensors. The techniques utilize synthetic aperture radar (SAR) processing to resolve responses from multiple sensors and to simultaneously obtain a geographic map of the sensor locations. Sensor and clutter returns are separated by utilizing the ability of the sensors to modulate the radar return. The sensor modulation is structured such that sensor and clutter returns can be separated in the spatial frequency domain

[C4284]

"Dual-channel radiometers for Earth and atmosphere monitoring (DREAM) on micro satellite STSAT-2"

The dual-channel radiometers for Earth and atmosphere monitoring (DREAM) is the main payload for the science and technology satellite-2 (STSAT-2) mission. This instrument is the first spaceborne microwave radiometer in Korea. It is a two-frequency, total power microwave radiometer with linear polarization. It operates at 23.8 GHz and 37 GHz for remote sensing of the Earth. In this paper, we present its system configuration and system design. [C4285]

"A high accuracy calibration and receive instrument for TerraSAR-X ground calibration"

TerraSAR-X is a new Earth observing satellite which is launched in spring 2006. It carries a high resolution X-band SAR sensor. For high image data quality, accurate ground calibration targets are necessary. This paper describes a novel system concept for an active and highly integrated, digitally controlled SAR system calibrator. A total of 16 active transponder and receiver systems and 17 receiver only systems will be fabricated for a calibration campaign. The calibration units serve for absolute radiometric calibration of the SAR image data. Additionally, they are equipped with an extra receiver path for 2D satellite antenna pattern recognition. The calibrator is monitored by a dedicated digital control unit. For antenna pattern estimation, an algorithm is presented. [C4286]

"Design of delay mapping receiver for GPS remote sensing"

Backgrounds and advantages of sea surface wind remote sensing technique based on GPS and the ocean scattered signal measure technique are introduced. Five main techniques are discussed as improving the signal noise ratio, dual front-end receiver design, calculating the specular point code delay, working modes configuration and the embedded firmware function. Inshore flight tests were done in Tianjin with the receiver mounted on an airplane. Results show that the delay mapping receiver (DMR) can receive direct and ocean scattered GPS signal simultaneously which achieves the performance specifications [C4287]

"Difference RCS of electromagnetic scattering from the target above a randomly rough surface"

The difference field RCS (d-RCS) has been defined to analyze the scattering from the target above a rough surface, which takes account of the scattering from the target and multiple interactions of the target and underlying rough surface. The d-RCS removes the effect of the finite illuminated surface length, under the tapered wave incidence. In this paper, our newly fast iterative approach is briefly reported. The electric field integral equations (EFIE) of the difference induced current on the rough surface and the induced current on the target are derived. An iterative approach is developed to solving the two EFIEs and scattering from both the target and underlying surface. How to choose the illuminated length of the rough surface for numerical iterations is discussed. Using the Monte Carlo method to realize the ocean-like rough surface, bistatic scatterings from the target, e.g. a cylinder or a square column, above a P-M (Pierson-Morkowitz spectrum) rough oceanic surface are numerically simulated for TE tapered wave incidence. [C4288]

"Antennas for Space: Some Recent European Developments and Trends"

This paper reviews some of the requirements and proposed solutions for present and future space missions. Mobile telecommunications at L and S bands require very large apertures and digital beam formers to generate multiple beams. New approaches are proposed for unfurlable reflectors and their feed systems. For navigation, the Galileosat dual-band array at L-band must provide isoflux on the Earth with a very accurate knowledge of antenna phase centre. Broadcasting at Ku-band remains a key application where flexibility in coverage pattern and channel allocation is a strong driver. New reconfigurable antennas are proposed to allow coverage and traffic flexibility. Two-way broadband multimedia broadband communications at Ka-band require affordable multiple beam antennas with wide beam scanning and low sidelobes. Both reflector and array solutions are being studied to replace the multiple reflectors with one feed per beam which are currently flown. Reconfigurable antennas with fade compensation are another challenging innovation. Low cost ground terminals are needed for all these applications with particularly challenging requirements for mobile users (aircraft, ships, trains, cars, laptop users...). A breakthrough is still needed to make arrays affordable for the users. Future remote sensing missions will involve multi-band passive and active sensors from various orbits. At the low frequency end, P-band synthetic aperture radars (SAR) will require very large deployable apertures for which membrane solutions are being considered. SAR at higher frequency will require more resolution and lower costs: reflector based SAR with multiple feeds and reflect-arrays are potential solutions under study. At millimetre-wave frequencies and

higher, atmospheric sounding from low Earth orbit, and possibly from geostationary orbit, require innovative designs and solutions. Large scanning reflector systems as well as aperture synthesis schemes are being studied. Science radio-astronomy-- missions also have very challenging requirements at these high frequencies, including extremely low levels for stray-light or sidelobes and detectors operating at close to 0degK temperatures. The challenges and technologies outlined above will be discussed in the paper [C4289]

"A cross-entropy based parameter for ship detection from a polarimetric SAR image"

A cross-entropy based parameter is proposed to measure the difference between a river area and others. This parameter can be employed for ship detection from a polarimetric SAR image. After deciding the boundaries of the river area, ships are detected only in the river area instead of the whole site. Therefore, most of the false alarms are eliminated. Finally, the performance of this new approach is validated by the X-band full polarimetric SAR data in Niigata area of Japan [C4290]

"Calibration/validation of the SeaWinds radiometer rain rate algorithm"

The SeaWinds scatterometer, which has been flown on both the QuikSCAT and ADEOS-II satellites was designed to remotely sense ocean surface wind vectors. Because ocean wind retrievals are occasionally contaminated by rain in the tropics and because there is no independent rain measurement on QuikSCAT, a SeaWinds rain-estimation method was developed and implemented. This technique utilizes the SeaWinds receiver noise to measure ocean radiometric brightness temperature (Tb) and then applies a statistical regression algorithm to estimate the integrated rain rate. This rain algorithm was originally "trained" with QuikSCAT SeaWinds Tband near-simultaneous rain rate measurements from the Tropical Rainfall Measuring Mission (TRMM) Microwave Imager (TMI). In this study, the SeaWinds instrument on ADEOS-II and the Advanced Microwave Scanning Radiometer (AMSR), also onboard ADEOS-II, were used to refine the algorithm. This provided truly simultaneous and collocated measurements from the same platform and over the same swath, which was ideal for improving the SeaWinds rain algorithm. The improved algorithm can now be applied on QuikSCAT using the SeaWinds radiometric measurement. [C4291]

"Corrections to scatterometer wind vectors from the effects of rain, using high resolution NEXRAD radar collocations"

Rain in the atmosphere and impacts on the ocean surface lead to erroneous observations of the Ku-band normalized radar cross section (NRCS) for the ocean surface, which is collected by orbiting Scatterometers. Rain can cause large errors in satellite-based estimates of the sea surface wind speed and direction derived from the affected data, depending on the surface wind speed and the rainrate. Rain within the radar beam results in attenuation and additive volume backscatter to the satellite. In order to correct each NRCS using a physically based electromagnetic model, the 3-D rain reflectivity must be measured throughout the satellite's Ku-band beam with high resolution, and be nearly simultaneous with the satellite. Using satellite observations within the range of the NWS NEXRAD radars, these S-band data provide 2 km horizontal resolution and comparable vertical resolution, within 4 minutes of the satellite overpass. The correction technique also includes removal of the augmented surface roughness due to rain impacts. The surface wind vectors are then recalculated using the corrected NRCS, with the same wind-retrieval algorithm as that is used to produce the SeaWinds data product. Case studies will be presented that show the improved wind vector estimates over a significant area in several coastal regions, (the U.S. East Coast and the Gulf of Mexico), when comparing the corrected winds with the NCEP winds and buoy measurements. [C4292]

"Integrated Marine Mammal Monitoring and Protection System (IMAPS)"

The IMAPS mission is to establish a global solution for protecting the marine environment through the development and implementation of a modular assessment and protection system. The limitations of current technologies are based on them being individually inadequate to fully achieve the mitigation objectives. All the sources of information related to the detection and classification of marine mammals such as active sonar, passive sonar, radar, visual and distribution databases need to be fused to provide a robust protection system. In order to successfully standardize, transport, interface and fuse the information being supplied and requested by the diverse sensor modalities, two essential tool of the IMAPS global system are being developed: the Integrated Tracker and the Integration Architecture. The Integrated Tracker employs a data fusion algorithm that combines sensor information to refine estimates of target position, velocity, identity to provide integrated tracking and classification. A data fusion architecture has been chosen and a Bayesian approach for fusion and classification is developed. A data fusion and transport approach has been taken to develop a set of IMAPS prototypes that consist of simulated active sonar, passive sonar, radar and visual modalities communicating in real-time via the Integration Architecture, and to supply the sensor data, and other information necessary for the

fusion, to the Integrated Tracker. The main functionality of the Integration Architecture is to provide information transport and common services in the form of a 'plug and play' capability, implemented with a software framework developed upon the Test & Training ENabling Architecture (TENA). The TENA software framework provides for the implementation of common software interfaces to disparate sensor modalities, thereby enabling the integration of different data sources using a common data representation and transport medium. Sensor outputs such as target detections and environmental information are being transformed in object-orientated data representations that are easily interpreted, manipulated, and interfaced. In addition to the Global IMAPS initiative, the active sonar modality was designed, built, and tested during the MAST 04 experiment producing detections of whales and preliminary synthesis of whale tracks. [C4293]

"A methodology for the efficient storage and processing of coastal point data"

The seamless integration between terrestrial and sub-aqueous surfaces has long stymied the geospatial industry. The collection of high-resolution, accurate elevation data in the nearshore zone proved difficult for many organizations. However, the advent of shallow water based LiDAR collection systems, technological improvements in shallow water hydrographic multibeam systems and the ability to collect bathymetry from hyperspectral remotely sensed imagery is changing the face of the coastal mapping community. Through the functionality of ArcGIS Terrains, users of these multisource, multiscale data will be able to seamlessly integrate coastal point data into an efficient storage mechanism. Terrains have the capability to generate small to large scale Triangulated Irregular Networks (TINs) on-the-fly. This paper discusses and demonstrates the functionality of this new technology in the context of a coastal mapping project. Topographic LiDAR, multibeam bathymetry, and SHOALS bathymetry LiDAR is incorporated into a geospatial database. Supplementary data, such as breaklines, erosion control devices are added to further assist in accurate model generation at multiple scales. Subsequent modeling at varying resolutions is performed through spatial analysis techniques which further demonstrate the utility of ArcGIS Terrains for shoreline mapping. In a 3D context, visualization techniques are explored using ArcScene and ArcGlobe. This technology has the potential to assist clients in the arena of military applications, pipeline/cable landfall applications, coastal zone management and flood risk modeling. The three main areas that make it difficult for geospatial analysts to work with coastal data are: a) the sheer volume of data associated with LiDAR and SoNAR data, b) the variability of resolution requirements (i.e. regional mapping requires decimated data, large scale mapping requires high-resolution), and c) storage and management of varying data sources encompassing the same geography. The paper addresses these areas of concern by explaining the underlying concepts and methodologies that ArcGIS Terrains employ to import, manage, and present these data at varying scales. [C4294]

"Bathymetry of shallow coastal regions derived from space-borne hyperspectral sensor"

Hyperion is a hyperspectral sensor on board NASA's EO-1 satellite. Its spatial resolution is about 30 meters with a swath of 7 Km. Though Hyperion was not designed for ocean studies, its unique spectral configuration (430 nm-2400 nm with a 10 nm step) makes it especially attractive to study the effectiveness of such kind of sensor for observing complex coastal waters. In this study, Hyperion data over two sites of the Florida coasts were acquired, with one focused on the clear Key West waters, and the other focused on the relatively turbid Tampa Bay waters. From both data sets, water properties and bottom bathymetry were simultaneously derived from atmosphere-corrected Hyperion data using a spectral matching technique. More importantly, in the top-to-bottom processing of Hyperion data, there was no use of any a priori or ground truth information. For the Key West site, derived bathymetry and water properties were validated with NAVOCEANO CHARTS (active bathymetric LIDAR system) and field measurements, respectively. It is found that the retrieved depths (in a range of 1-20 m) match LIDAR depths very well (15% average error), indicating significant potential of using hyperspectral satellite sensor for efficient and repetitive observation of shallow coastal regions. [C4295]

"The application of GPS to high frequency oceanic detecting radar"

High frequency oceanic detecting radar is a powerful tool to monitor environment of ocean. It can detect the parameters of wind, wave and current. While the radar is fabricated, it must be calibrated by responder first. And the position of responder can be obtained by GPS. In the paper a novel application of GPS to high frequency oceanic detecting radar is discussed. The data format of the GPS receiver is commonly NEMA0183 communication standard. In the paper this standard is analyzed and the characteristic is found. There are large amount of data in the format, including latitude, longitude, altitude, velocity, date, time, course and satellite status. It makes a heavy burden while communicating between GPS and responder. So we must reduce the output data of GPS receiver. Among twelve items of the data format, only the degree of latitude, the hemisphere of latitude, the degree of longitude and the hemisphere of longitude are useful. By extracting these four items and wiping off the others, the data are reduced efficient. Then the reduced data are transmitted to the station of radar by data radio. So the position of the responder can be obtained. In addition, for the update rate of data is

1 time/second, it is to say the data transmitted in one second are the same, the transmitting rate can be set as N second. N is configured as we need. The block diagram of the system is given in the paper. The functions of each part can be achieved by FPGA chips and VHDL. The simulation proved that the transmitted data have been reduced greatly by the system we proposed here. It is only ten percent of the original data. [C4296]

"Evaluation of marine surface winds observed by active and passive microwave sensors on ADEOS-II"

Marine surface winds observed by two microwave sensors, SeaWinds and Advanced Microwave Scanning Radiometer (AMSR), on the Advanced Earth Observing Satellite-II (ADEOS-II) are evaluated by comparison with off-shore moored buoy observations. The wind speed and direction observed by SeaWinds are in good agreement with buoy data with root-mean-squared (rms) differences of approximately 1 m s⁻¹ and 20°, respectively. No systematic biases depending on wind speed or cross-track wind vector cell location are discernible. The effects of oceanographic and atmospheric environments on the scatterometry are negligible. Though the wind speed observed by AMSR also exhibited reasonable agreement with the buoy data in general with rms difference of 1.3 m s⁻¹ it is systematically lower than the buoy data for wind speeds lower than 5 m s⁻¹. Similar results are obtained in an intercomparison of wind speeds globally observed by SeaWinds and AMSR on the same orbits. Global wind speed histograms of the SeaWinds data and European Centre for Medium-range Weather Forecasts (ECMWF) analyses agree precisely with each other, while that of the AMSR wind shows slight deviation from them. [C4297]

"NOAA Ocean Surface Topography Mission Jason-2 project overview"

The Ocean Surface Topography Mission (OSTM) is a joint effort among four organizations: NOAA (National Oceanic and Atmospheric Administration), EUMETSAT (European Organisation for the Exploitation of Meteorological Satellites), CNES (Centre Nationale D'Etudes Spatiales), and JPL (Jet Propulsion Laboratory), to measure sea surface height by using a radar altimeter mounted on a low-earth orbiting satellite. The collection of high accuracy radar altimetry measurements is essential for global ocean circulation and sea surface studies. Current research satellites, TOPEX/Poseidon and Jason-1, have been instrumental in providing NOAA's operational need for sea surface height measurements necessary for ocean modeling, forecasting El Nino/La Nina events, and hurricane intensity prediction. In future, the Jason-2 satellite will replace current research satellites and NOAA has been entrusted with operational responsibilities for the Jason-2 satellite. The Jason-2 satellite is scheduled for launch in mid 2008. The goal of the OSTM/Jason-2 is to maintain continuity of the OSTM/Jason-1 and TOPEX/Poseidon satellite missions. This paper presents the Jason-2 Project Overview and effort performed by NOAA to support the operational Jason-2 satellite mission. For the Jason-2 routine operational phase, NOAA will provide complete ground system support including command and data acquisition, satellite control and monitoring, science data processing, data/products archiving and data/product distribution. NOAA will be providing these services by collaboratively participating with its partners in managing the satellite, and sharing the science data and products. [C4298]

"Hurricane wind retrievals using the SeaWinds scatterometer on QuikSCAT"

Meteorologists require reliable real-time measurements of tropical cyclone (TC) conditions to issue hurricane forecasts and advisories. The models they utilize assimilate many sources of data including airborne and spaceborne surface wind estimates. One instrument that has the potential for operational use is the SeaWinds Scatterometer on QuikSCAT. Unfortunately, the adverse effects of rain on the scatterometer signal make these measurements unreliable. Intense rain volumes can drown out radar echo with a combination of attenuation and high backscatter, while the standard resolution of wind measurements tends to wash out high wind retrievals. Furthermore, traditional geophysical model functions (GMF), which relate wind speed and direction with radar backscatter (sigma-0), have not been tuned for the high wind conditions of storms because sampling of these events is poor. Thus, scatterometers tend to underestimate TC winds. By utilizing a combined active/passive retrieval algorithm developed specifically for TCs, we are able to simultaneously retrieve wind speed and rain rates using the SeaWinds Scatterometer. Unreliable wind measurements are flagged based on rain estimates. To certify that wind retrievals are ready for operational use, wind speeds are compared with H*Wind wind fields developed by the Hurricane Research Division of NOAA. [C4299]

"Repeat-track SAS interferometry: feasibility study"

Repeat track interferometry is a commonly used technology in radar. It permits to obtain topography and elevation variation of ground. This technology is not used with sonar system, even though this configuration could provide interesting applications for underwater environment knowledge. This paper presents a study on repeat-track interferometry feasibility with sonar system, and especially for synthetic aperture sonar (SAS). We

shortly expose the SAS and interferometry principle in the first part. Then we present the multi-track interferometry and discuss on limitation. In a third part, experimental results based on data acquired with the experimental low frequency SAS (LFSAS) of GESMA (France), are detailed and we expose methods to circumvent problems induced by repeat-track interferometry. Finally we discuss on future strategies to improve the encouraging results we obtained. [C4300]

"Seamless access to surface current vectors from the IOOS HF radar backbone"

A demonstration prototype has been developed using the Open source Project for a Network Data Access Protocol (OPeNDAP) to illustrate the potential that distributed data access can provide to the HF radar backbone within the Integrated Ocean Observing System (IOOS). An individual HF radar site produces maps of radial surface velocity. Since two or more radar sites are needed to provide vector currents, most operators of these systems deploy radars at multiple sites and produce current vector maps in the region of overlapping coverage of their sites. The underlying premise of the prototype is that each HF radar site within the backbone is considered a unique and separate data source. In our approach the radials from each HF radar site are accessed directly to compute the surface current vectors in response to a user's request. This allows radials from different operators to be combined, with the potential to compute surface current vectors for regions outside the vector coverage region of either operator. Since each HF radar site is recognized as a separate data source, new HF radar sites can be readily incorporated to extend the backbone's spatial coverage. Additionally, by directly accessing the radials the prototype demonstrates the capability to specify the latitude/longitude grid that surface current vectors are computed for, which can be different from that of existing operators. The prototype can be configured with a default latitude/longitude grid representation on which vectors are calculated, or extended using the functional interface capabilities available within the OPeNDAP constraint syntax to allow requesting applications to specify a latitude/longitude grid, or list of grid cell locations. The demonstration prototype consists of two specialized OPeNDAP servers: a Radial Server that is installed at the HF radar sites to read and serve the CODAR radial files stored at the remote locations and the Combining Server, which is the primary application within the prototype. It operates to identify the HF radar sites within the backbone that have radials that can be combined to calculate the surface current vectors given the user's requested spatial and temporal extent. It communicates with the remote Radial servers, using the OPeNDAP protocol, to request only those radials necessary within the requested spatial and temporal extent. It then combines the radials from two or more HF radar sites to calculate the surface current vectors and the associated uncertainties at specific grid cell locations and returns these data to the requesting client. [C4301]

"A wavelet based method for the extraction of sea wave orientation"

In this paper, a method for determining sea wave orientation from image data is presented. Instead of focusing on images that cover vast distances such as those obtained from satellite synthetic aperture radar (SAR), this research is concerned with images acquired on a local level such as those obtained from a ship based, mast mounted camera. The developed method is based on the two-dimensional wavelet transform and its ability to isolate (or preserve) directional features contained in the root image. Another important property associated with wavelets is the notion of scale or resolution. The dominant wave features of the image are extracted through the use of a multi-scale wavelet analysis. These features are then used to determine the overall wave orientation for the image. Results are shown for images taken from both traditional visual cameras and forward-looking infrared (FLIR) based cameras. [C4302]

"Microwave and HF multi-frequency radars for dual-use coastal remote sensing applications"

We discuss the synergistic application of microwave radars and HF radars to remote sensing of ocean waves and currents in the coastal zone. A new marine radar family (coherent and non-coherent) operating at 10-m scales can map nearshore bathymetry, and measure ocean currents and wave spectra at distances out to a few kilometers. The HF radar family operates using multiple frequencies on a pulse-to-pulse basis at 1-km scales, making use of either beam-forming or direction-of-arrival methods to map radial current fields. Both radar families are designed around a digital transceiver PCI card family supporting antenna arrays of one to 32 elements. Some results are presented for both radar systems. [C4303]

"Some Practical Ways to Determine Coastal Current's Vertical Structure"

Remote sensing technology has made it possible to rapidly observe wide areas of the ocean surface. To determine subsurface conditions from these observations requires the application of hydrodynamic principles. For coastal currents, the viscous dynamics can be applied to efficiently project surface data downward to obtain the current's vertical structure in real time. This method has been developed for use with remotely sensed surface current data obtained from HF radars, and now is being extended to use remote sensing images. In this case,

the surface currents are determined together with subsurface currents from the dynamic and conservation equations, as opposed to tracking or correlating image patterns in time. Alternatively, the surface data can be assimilated into a numerical coastal ocean model that solves for depth-dependent currents. But, presently, efficient assimilative computation appears to be feasible only with depth-integrated ocean models. In this case, a method can be developed to obtain current structure from the depth-integrated solution via the use of surface and bottom boundary stresses and associated shear equations. This method of determination can be practical as it requires only the depth-integrated solution and surface and bottom boundary conditions at the location of interest as input, in contrast to conventional modeling approach of determining currents over the whole model domain. Demonstration of the use of the various methods noted here will be given by means of numerical examples and comparisons with some field experimental data [C4304]

"Bio-physical Interactions in Ocean Margin Ecosystems (BIOME): understanding coastal dynamics in the Southern Mid-Atlantic Bight"

Coastal regions within the Mid-Atlantic Bight (MAB) are significantly influenced by regional freshwater fluxes emanating from several large bay systems, most notably the Hudson-Raritan river systems, the Delaware and Chesapeake Bays. The outflows from these bays have high sediment loads and high levels of nutrients, particulate and dissolved organic matter (POM and DOM) associated with them which strongly influence the adjacent coastal margin ecosystems. Our research and observational effort includes the development and deployment of an observing system aimed at characterizing and monitoring the influence of the Chesapeake Bay on the adjacent coastal ocean margin ecosystem. A primary focus of this effort is to develop and apply state-of-the-art technologies and methodologies to support research, observation, monitoring, and management applications in the coastal ocean. We have developed a program that addresses coastal spatial and temporal scales. Our observing system consists of four components including 1) High Frequency (HF) Radar: 3 long-range HF Radar systems for mapping coastal ocean surface currents along Delmarva and 2 standard-range systems for the Chesapeake Bay mouth region, 2) a Coastal Ocean Bio-optical buoy (COBY), which will be deployed southeast of the Maryland-Virginia border at about 40m water depth, and will be instrumented with an above-water spectroradiometer (19 channel UV-VIS-NIR, 10nm BW, sea- and sky-viewing radiometers plus solar reference) on a robotic arm to measure water-leaving radiances, meteorological package, in-water mooring instruments with ADCP, CTD, nitrate sensor, ac-9, ac-s, and fluorometers for chlorophyll, colored dissolved organic matter (CDOM) and phycoerythrin detection; 3) seasonal cruises in the Mid-Atlantic Bight collecting optical, biological, and chemical data; and 4) the Ocean-Atmosphere Sensor Integration System (OASIS), which is comprised of a fleet (6-12) of solar-powered surface autonomous vehicles deployed offshore to measure surface ocean currents, meteorological measurements, surface ocean salinity and temperature, air-sea CO₂ fluxes, water-leaving radiances, chlorophyll and CDOM fluorescence, HAB detection, etc. The HF radars, COBY and OASIS are being deployed this summer, with plans for a fully deployed observing system by the end of 2005 or early 2006. [C4305]

"Oceanic rain identification using multifractal analysis of QuikSCAT Sigma-0"

The presence of rain over oceans interferes with the measurement of sea surface wind speed and direction from the Sea Winds scatterometer, and as a result, in rain regions wind measurements contain biases. In past research at the Central Florida Remote Sensing Lab, it has been observed that rain has multifractal behavior. In this paper we present an algorithm to detect the presence of rain so that rain regions are flagged. The forward and aft views of the high resolution horizontal polarization backscatter are used for the extraction of textural information with the help of multifractals. A negated multifractal exponent is computed to discriminate between wind and rain. Pixels with exponent value above a threshold are classified as rain pixels and those that do not meet the threshold are further examined with the help of correlation of the multifractal exponent within a predefined neighborhood of individual pixels. It was observed that the rain has less correlation within a neighborhood compared to wind. This property is utilized for reactivation of the pixels that fall below a certain threshold of correlation. An adaptive multifractal exponent and threshold is used, as we deal with a wide range of latitudes. Validation results are presented through comparison with the Tropical Rainfall Measurement Mission Microwave Imager (TMI) 2A12 rain retrieval product for one day. The results show that the algorithm is effective in identifying rain pixels. Some algorithm deficiencies in high wind speed regions are also discussed. Comparisons with other proposed approaches are also presented. [C4306]

"Ocean surface feature extraction and targets detection from SAR images using neural network"

In this paper, a novel system is presented for the targets detection from synthetic aperture radar (SAR) images of ocean. The proposed system consists of two neural networks. The first network cluster the extracted target fractal feature vectors in smaller sub-portions of the image, and the second GA RBF network integrates the information from the first network to determine the presence or absence of a target in the entire image [C4307]

"A Novel Active and Passive Microwave Remote Sensing Technique for Measuring Ocean Surface Wind Vector"

This paper describes a novel technique of ocean surface vector wind measurement using active and passive microwave sensing from a satellite. For over a decade, satellite microwave scatterometers have remotely sensed ocean wind vector (speed and direction) by measuring ocean radar backscatter (σ_0) at several different azimuth angles (looking forward and aft). Also, ocean wind speeds have been measured by conical scanning passive microwave radiometers looking either forward or aft. This paper combines these two techniques to obtain wind speed and direction from a conical scanning instrument that scans either forward or aft, which is extremely desirable from an instrument design and satellite accommodations standpoint. An overview of the active/passive wind vector algorithm is discussed, and wind vector retrievals are presented using microwave measurements from Japan's ADEOS-II satellite. These results are compared with wind vectors from the Sea Winds scatterometer [C4308]

"Simulation study for aerosol distribution retrieval from bistatic, imaging lidar data"

A bistatic imaging lidar system is being developed on the basis of a novel telescope concept. The schematic of bistatic lidar measurement and the retrieval algorithm of the bistatic imaging lidar data are described, with the results of simulation studies. [C4309]

"Doppler radar sensing of multiple subjects in single and multiple antenna systems"

Doppler radar life sensing has shown promise in medical and security applications, however the problems of motion artifacts and presence of multiple subjects limit the usefulness of this technique. By leveraging recent advances in signal processing and wireless communications technologies, the Doppler radar technique has the potential to overcome these limitations. We explore the single and multiple antenna systems and SIMO/MIMO signal processing to isolate desired radar return signals from multiple subjects. It has been experimentally demonstrated that up to two subjects can be separated in a single antenna systems. Simulations have also shown that in case two subjects have identical cardiovascular behavior, it is possible to distinguish them using MIMO techniques. [C4310]

"Remote laser-induced fluorescence imaging for assessment of cultural heritage"

In this paper, we propose to perform remote laser-induced fluorescence imaging for assessment of cultural heritage. The experiments are performed using the lidar system consist of frequency-tripled Nd:YAG laser at 355 nm with a spot size of ~4 cm diameter and the signal is collected using a coaxial 40-cm-diameter Newtonian telescope. The fluorescence light is focused into an optical fibre and guided a time-gated optical multichannel analyser system, where the fluorescence spectrum is recorded. Then the laser directed to the next point and thus a fluorescence image can be produced [C4311]

"Remote sensing and statistical analysis of Asian dust measured by 532/1064 nm Lidar during 2002-2005"

Asian dust over Suwon (127.1E, 37.04N) Korea during 2002-2005 have been measured by 532/1064 nm lidar and optical characteristics of them, backscattering coefficients at 532 and 1064 nm, depolarization ratio at 532 nm, and color ratio of IR/UV are statistically analyzed. [C4312]

"3D imaging system based on FMCW millimeter wave radar"

3D radar imaging systems are highly requested for use in guidance system for aircraft landing and shipping navigation. These systems usually work in difficult weather conditions such as fog, snow, dust. Use of 3-mm wavelength FMCW radar allows getting images at distances up to 1000m with high spatial resolution. [C4313]

"Cognitive radar networks"

In my previous publication, I described, for the first time, the novel idea of cognitive radar, its attributes and potential applications. This article expands on one of the applications described therein-namely, cognitive radar networks. After briefly describing the constitution of this new radar system, we focus on the specific application of homeland security, for which a cognitive radar network is rather well suited. [C4314]

"Unified Bayesian-experiment design regularization technique for high-resolution reconstruction of the remote sensing imagery"

In this paper, the problem of estimating from a finite set of measurements of the radar remotely sensed complex data signals, the power spatial spectrum pattern (SSP) of the wavefield sources distributed in the environment is cast in the framework of Bayesian minimum risk (MR) paradigm unified with the experiment design (ED) regularization technique. The fused MR-ED regularization of the ill-posed nonlinear inverse problem of the SSP reconstruction is performed via incorporating into the MR estimation strategy the projection-regularization ED constraints. The simulation examples are incorporated to illustrate the efficiency of the proposed unified MR-ED technique [C4315]

"Rayleigh-Mie lidar for accurate temperature profiling of the troposphere"

A Rayleigh-Mie scattering lidar system has been developed for temperature profiling of the troposphere using a new multi-cavity Fabry-Perot filter at 355 nm wavelength. The temperature error less than 1 K was obtained at 3.0 km altitude with a compact system. [C4316]

"1st IEEE International Workshop on Computational Advances in Multi-Sensor Adaptive Processing (IEEE Cat. No.05EX1140C)"

{no data available} [C4317]

"Exploiting fundamental properties of SAR data for compression of tactical SAR imagery"

This paper introduces a technique that exploits the statistical properties of complex synthetic aperture radar (SAR) data to effectively compress tactical SAR imagery. The technique combines Fourier transforms and analysis/synthesis algorithms into a hybrid compression architecture that exploits the temporal correlation of the complex radar returns. In addition the technique incorporates the fact that the viewable SAR image is based on the magnitude of the complex imagery. This enables a vocoding technique that can preserve the frequency information and discard the phase information with little perceptual degradation in the image content. Finally the holographic property of SAR is also exploited. The performance of the new algorithm is compared with the JPEG compression standard. The results show that compression ratios of over 100:1 are achievable and far surpass the compression capabilities of the conventional JPEG algorithm [C4318]

"Mueller matrix modeling of atmospheric scattering medium through polarized laser beam"

The atmospheric scattering and absorption in turbid medium is characterized through Mueller matrix modeling of backscattered polarized laser radiation. The scattering medium is homogeneous and contains one kind of randomly distributed asymmetric particles. We used polarized He-Ne laser of specific wavelength focused on scattering medium. Different polarization components of backscattered light are obtained by varying the polarization state of incident laser light and the analyzer configuration. The calculation of the 16 element of the output Mueller matrix experimentally confirmed that theoretically only seven elements of backscattered light are independent and remaining nine can be calculated through symmetry relation. Matrix calculus concept for backscattered light fully characterized the material. Our results for turbid atmospheric system predict the absorption and scattering parameters closed to the parameters in literature. This study will be useful in remote sensing, aerospace technology, radar and lidar applications, weather predictions and upper and lower atmospheric observations [C4319]

"The story of Glory: Earth and solar science on one unique satellite"

The Glory satellite program is underway at the orbital sciences campus in northern Virginia. This program is under contract with NASA Goddard Space Flight Center (GSFC). The Glory satellite bus was previously used for the vegetation canopy LIDAR (VCL) program, a mission designed to measure the Earth's vegetation coverage, depth, and topography by using short laser pulses from a LIDAR (light detection and ranging) system. The Glory program is refurbishing the VCL bus that was in the middle of integration and test when the VCL program was shut down. Many changes are being made to the VCL bus to configure it to serve the Glory science mission objectives. The Glory science mission includes polar atmospheric aerosol measurements with cloud observation and total solar irradiance monitoring. The low Earth orbit satellite (LEO) is scheduled for launch in late 2007 with the intention of broadening the search for the causes of global warming. The mission is intended to measure the composition of greenhouse gases, which little is known about currently, as well as solar effects on the environment using the following instruments: an aerosol polarimetry sensor (APS), cloud cameras and a total irradiance monitor (TIM). The APS instrument is a multispectral polarimetric sensor designed for collection of visible, near-infrared, and shortwave infrared polarized radiometric data scattered from aerosols and clouds. The APS is a continuous scanning, nadir-viewing sensor that makes along-track, multiangle observations of Earth and atmospheric spectral radiance. The cloud cameras are dual-band, imagers that employ a nonscanning,

staring detector array that is akin to a star tracker, but Earth-viewing. The cloud cameras provide continuous cross-track coverage over a narrow swath centered on the APS along-track footprint using an optical imaging system. The TIM is an active cavity solar irradiance radiometer that consists of four identical radiometer cavities to provide redundancy and help- detect changes in instrument response caused by exposure to solar radiation and other orbital effects. It takes data continuously throughout the orbit and does periodic calibrations on the disc of the sun and of the redundant cavities to monitor the effects of aging. Using a combination of heritage data and knowledge from the Orb View 3 and 4 programs as well as VCL, the Glory program is dedicated to a successful mission. This paper describes the design differences at system and subsystem levels between VCL and Glory focusing on the science missions, as well as the heritage program influences that are employed.

[C4320]

"An airborne pod-mounted dual beam interferometer"

Dual beam interferometer (DBI) has been developed by the University of Massachusetts (UMass) to study ocean surface waves and currents in coastal regions. This airborne radar operates at C-band (5.3 GHz) with a bandwidth of 25 MHz and VV polarization. DBI consists of two pairs of microstrip patch array antennas, one squinted 20deg forward of broadside and the other 20deg aft. Each pair of antennas is separated in the along-track direction a distance of 1.23 meters forming an interferometer. Over several years, DBI was flown on a National Oceanic and Atmospheric Administration's WP-3D research aircraft in a number of successful missions collecting the data both over land and ocean. These deployments and subsequent data analysis were carried out in collaboration with Naval Research Laboratory (NRL). This paper describes the hardware integration and use of the system to generate surface current vector maps [C4321]

"Space based radar technology challenges"

Space based radars are gaining significant acceptance for world-wide, all-weather, on-demand surveillance and earth resources monitoring. The main impediment has been affordability, followed closely by the limitations by satellite communications for providing near real time target detection data to the users. Recent advances in active electronic scanned arrays and on-board signal processing are enabling SBR development for both surface and fixed target imaging and moving target detection. The real challenge is for future surveillance of airborne targets. This paper outlines some critical SBR design architectures, and a roadmap for developing the enabling technologies to meet future surveillance needs [C4322]

"Remote element tracing of trans-uranium plumes using an interactive UV laser DIAL coupled with a phoswich detector"

In this work, an interactive remote sensing system is suggested. It consists of two main parts; a phoswich detector to trace hard X-ray emission of these elements and a DIAL coupled with a 2ndharmonic Nd:YAG pumped higher harmonic Ti:Sa laser. It serves as a tunable UV coherent source for rapid determination of the unknown radioactive elements within the plume as well as the corresponding concentration and the exact location. [C4323]

"Remote LIBS and Raman imaging for assessment of cultural heritage"

In this paper, we propose to perform remote laser-induced breakdown spectroscopy (LIBS) and Raman imaging of historical monuments to assess the state of a building. The lidar system is equipped with a Nd:YAG pumped optical parametrical oscillator (OPO) system, allowing laser radiation in the wavelength range 220 nm-4 μ m. The laser radiation can be sent through a roof-top dome which can steer the radiation onto the point of interest [C4324]

"An intelligent tropical cyclone eye fix system using motion field analysis"

Tropical cyclones (TCs) are weather systems with vast destructive power. Accurate location of their circulation centers, or "eyes", is thus important to forecasters. However, the eye fix process is often done manually in practice. While multiple factors are considered in the process, with subjective elements in these methods, forecasters could disagree. This paper describes a TC eye fix system that uses a novel motion field structure analysis method. It can handle TCs without well-defined structure that are partially out of the image. The system also adapts user inputs and past results to improve its accuracy. Implemented on a commodity desktop computer, the system can process about 5 images per minute, giving an average error of about 0.16 degrees in latitude/longitude on Mercator projected map for TCs that are completely inside the radar image. This is well within the relative error of about 0.3-0.4 degrees given by different TC warning centers. This TC eye fix system is useful in giving an objective TC center location in contrast to traditional manual analysis [C4325]

"Integrated dual spectral system of Earth surface monitoring"

Design principles of the integrated dual spectral (millimeter and infra-red ranges) system for Earth surface monitoring are presented. Technical characteristics of the system proposed have been also estimated according to the presented relations [C4326]

"The distribution of interferometric phase differentials and a self-initialising PolInSAR classifier"

This paper describes an unsupervised classifier for polarimetric interferometric SAR (PolInSAR) data. Expectation maximisation is used to estimate class parameters that maximise the probability of a dataset for a given number of classes. Polarimetric information, in the form of coherency matrices, and interferometric information, in the form of complex coherences, is taken into account. Phase differentials between complex coherences in different polarisation bases are used to make the classifier sensitive to the vertical structure of the scene under observation, and a distribution of such phase differentials is developed. The classifier is self initialising in that it does not rely on decompositions or thresholds. Classification results based on real data are presented and discussed [C4327]

"Characterisation of buildings using polarimetric interferometric multiple track L-band SAR data"

In this paper a multiple view POL-InSAR approach for the analysis of urban areas is introduced: as a first step, a polarimetric classification scheme is applied that allows the identification of three basic scattering mechanisms: volume diffusion, double bounce and surface reflections. A relation between the interferometric phases of the Pauli polarization basis and the polarimetric scattering mechanisms is established. A method to estimate the phase corresponding to the surface is introduced. These phases are used to extract the height of buildings. Finally, the data is geocoded in order to synchronize images acquired from different positions. The proposed methods are applied to fully polarimetric and repeat pass interferometric data at L-band acquired by the DLR's experimental E-SAR system on August 1st, 2000 over the city of Dresden in Germany. The flight tracks form a rectangle [C4328]

"Dry snow extent monitoring using multi-frequency and multi-temporal polarimetric indicators"

A new method to discriminate dry snow in alpine regions is presented. Due to the wide variety of Alpine environments, the scene under study is first segmented into surface and forested area classes from L and C-band summer polarimetric SAR data. Dry snow is then discriminated over each class using adapted methods. A new polarimetric multi-temporal optimization procedure, named PCVE, is proposed to increase the slight polarimetric contrast due to the presence of snow over surfaces. Snow covered forests are discriminated using performing polarimetric indicators resulting from a decomposition of incoherent matrix representations. The effectiveness of this method is demonstrated over a French alpine test site using SIR-C L and C-band polarimetric SAR data [C4329]

"New eigenvalue-based parameters for natural media characterization"

The aim of this paper is to present two novel polarimetric parameters, the eigenvalue relative difference (ERD) and the single bounce eigenvalue relative difference (SERD), to characterize natural media. These parameters are derived from the eigen-decomposition of the coherency matrix considering the reflection symmetry hypothesis. An analysis of these parameters is performed on multi-frequency polarimetric SAR data acquired on bare soils and forested areas [C4330]

"Evaluating PolInSAR parameter estimation using tomographic imaging results"

This paper concentrates on the forest height and ground topography estimation by means of polarimetric SAR interferometry and tomography. In polarimetric SAR interferometry, one of the most important methods described in literature is the line-fitting approach in the complex unitary circle (S.R. Cloude and K.P. Papathanassiou, 2003). Although it has shown their principal potential, an open issue is still the precise validation of the estimated parameters, as ground-truth collection is an extremely complex task in the case of forest parameters. SAR tomography is an alternative technique, which generates a fully three-dimensional representation of the imaged scene through coherent combination of a greater number of tracks (A. Reigber and A. Moreira, 2000) (S. Guillaso and A. Reigber, 2005). Forest ground and canopy are directly visible in a tomographic image; a tomographic image can therefore be used as an ideal validation base for PolInSAR forest parameter estimation. This paper compares high-resolution polarimetric SAR tomograms with PolInSAR forest height estimations, both derived from the same data set. This allows to identify areas of good applicability, as well as principal deficiencies of the different PolInSAR approaches [C4331]

"The using multifrequency airborne radar complex MARS for subsurface remote sensing"

In this paper presents some results of using airborne radar multifrequency complex MARS for subsurface remote sensing. Experimental data and the theoretical basis are given [C4332]

"A high accuracy calibration and receive instrument for TerraSAR-X ground calibration"

TerraSAR-X is a new Earth observing satellite which is scheduled for launched in spring 2006. It carries a high resolution X-band SAR sensor. For high image data quality, accurate ground calibration targets are necessary. This paper describes a novel system concept for an active and highly integrated, digitally controlled SAR system calibrator. A total of 16 active transponder and receiver systems and 17 receiver only systems will be fabricated for a calibration campaign. The calibration units serve for absolute radiometric calibration of the SAR image data. Additionally, they are equipped with an extra receiver path for two dimensional satellite antenna pattern recognition. The calibrator is monitored by a dedicated digital control unit. For antenna pattern estimation, an algorithm is presented [C4333]

"Radar system concept for simultaneous BSM of complicated and non-stable targets measurements"

The algorithms of the signal processing and the functional scheme of the polarization radar with simultaneous back scattering matrices measurements are given in this paper. The radar is destined for low atmosphere remote sensing [C4334]

"High precision waterlevel gauge with an FMCW radar under limited bandwidth"

Limitation of bandwidth, which is requested by the regulation for license-free radio systems, is a serious drawback for the ranging accuracy of a radar system. Nonetheless, a license-free radar application is favorable to users because of the easiness of adoption. In Japan, for example, available bandwidth is regulated within 76 MHz, which implies the range resolution cannot be less than 197 cm. Under such bandwidth limitation, an excellent S/N is required for an accurate ranging. We have developed a radar waterlevel gauge, which meets the bandwidth regulation and achieves a few centimeters in accuracy [C4335]

"EuRAD 2005 Sessions"

{no data available} [C4336]

"Applications of polarimetric interferometric ground-based SAR (GB-SAR) system to environment monitoring and disaster prevention"

Polarimetric and interferometric ground-based synthetic aperture radar (Pol-GB-SAR, In-GB-SAR) system has been developed. In this paper, two measurements of outdoor test sites in polarimetric and interferometric configurations are introduced and results are presented. In the developed In-GB-SAR system, the technique of differential interferometry is used to detect small changes at different times and under different conditions. Experimental results demonstrate that the system is very efficient and can detect small changes of the scale of 2 cm at the range distance of 5 m. Polarimetric analysis was done using the Pol-GB-SAR system with a coniferous tree as a target. The system has superior ability in polarimetric applications. Applying polarimetric and interferometric analysis which were developed for spaceborne and satellite radar remote sensing datasets, we can find detailed scattering mechanisms and detect deformations. The GB-SAR has a wide range of applications like environmental monitoring, resources management as well as monitoring of different natural phenomena [C4337]

"A risk-based object-oriented approach to sensor management"

Sensor systems play a critical role in providing situational awareness and threat assessment. Management of adaptive multifunction radars and sensor suites in today's combat systems is mostly based on an operator-defined set of priorities. Such a set can be very complex and requires a thorough understanding of the sensor capabilities and performance and of the operational needs. Changing such a set in strongly varying scenarios is prone to creation of sub-optimal system performance. In this paper a novel approach to assigning priorities to individual objects in the environment of a naval vessel is presented. This priority assignment is accomplished by means of dynamic evaluation of the risk imposed by each object with respect to the completion of the mission. More in particular a three-stage sensor management system is proposed that first uses the uncertainty related to each object's attributes, such as the state vector, classification and identification to determine the allocation of surveillance, track or recognition tasks. The sensor manager then selects the most appropriate sensor for the

task and finally distributes the available time budget based on priorities in case of multiple tasks. The risk is estimated by a dynamic Bayesian network modeling relevant operational knowledge. The nodes in this DBN represent the different object states in time and the events leading to them. A computer simulation was developed to prove the viability of this concept. [C4338]

"Spectral Signature Calculations for Remote Sensing"

Remote sensing radar has shown to be an important tool to observe severe and hazardous weather and to provide operational forecasters prompt information of such rapidly evolving phenomena. Although the history of tornado measurements is long, there have been only a few successes in obtaining spectral signatures. This is largely because neither the technology to process spectra nor the technology to record voluminous amounts of time series data were available, except for a few customized systems. However, present day radar technology and computer resources are now advanced enough to study tornado spectral signature in a systematic manner. The research WSR-88D (weather surveillance radar) locally operated by the National Severe Storm Laboratory (NSSL) in Norman has the unique capability of collecting massive volumes of Level I time series data over many hours which provides a rich environment for evaluating our new post-processing algorithms. In this work, an approach of identifying tornado vortices in Doppler spectra is proposed and investigated through the use of neural networks [C4339]

"A novel approach for the automatic detection of punctual isolated targets in a noisy background in SAR imagery"

Several distinctive capabilities of satellite-based synthetic aperture radar (SAR) systems make them a powerful tool for Earth observation purposes. In fact, SAR systems can provide an efficient, quick and cost effective coverage of any area independently from weather effects and from the day-night cycle. Nevertheless, the automatic interpretation of SAR images usually constitutes a complicated task due to the presence of speckle and to the reduced dimensions of the target compared to the sensor resolution. This papers aims at presenting a novel algorithm for the detection of punctual isolated targets in a noisy background based on the wavelet theory. It will be shown that this can be useful for example for ship detection purposes [C4340]

"Influence of acquisition conditions on forest classification using L-band Pol-inSAR data"

This paper introduces an approach to forest mapping and classification using complementary polarimetric and interferometric information. Strictly polarimetric and polarimetric interferometric data are first analyzed and classified separately. Pertinent polarimetric indicators permit to classify the observed scene into three canonical scattering types, whereas the segmentation of an optimized interferometric coherency set leads to the discrimination of decorrelating volumetric media used ton infer a forest map. The classification of forest constituents is achieved by means of a supervised Pol-inSAR classifier. The influence of temporal and spatial baselines is investigated and it is shown that temporal decorrelation may be a severe limitation for forest classification at L band [C4341]

"Quantitative assessment of physical information retrieved via multidimensional radar systems"

The advent of multidimensional synthetic aperture radar (SAR) systems in the last decade has made possible the quantitative retrieval of physical parameters to characterize the Earth's surface. As a result, nowadays, radar technology has an important and leading role in remote sensing. Despite the clear advantages respect to other remote sensing techniques, the presence of speckle noise in SAR systems represents still an important drawback, which is even more critical for multidimensional systems. This paper is devoted to present a novel multidimensional speckle noise model which, as demonstrated, allows the characterization of multidimensional data and permits to identify and quantify the effects of speckle in the process to estimate physical information. Special attention is devoted to polarimetric systems [C4342]

"Vehicle control classification and identification through ISAR imaging"

The great advantages arisen in millimeter-wave frequencies have made possible the development of high range resolution radars. The capability of using high bandwidths (Gigahertz) increases the range resolution allowing the obtaining of target's radar signatures. Through these signatures some patterns of the targets can be extracted like its size, velocity or maybe some specific features which facilitates its recognition, classification and even identification. The increase in azimuth dimension obtained, like it is explained in this paper, thanks to Doppler processing, allows to get better estimations of the targets characteristics [C4343]

"Effect of the data pre-processing on GPR mine detector performance"

The performance of GPR as an anti-personal mine (APM) detector heavily depends on the quality of the acquired data. A scheme of the quantitative evaluation of the quality of the raw GPR data in terms of stability of certain parameters and the set of the procedures, which compensate the instabilities found are presented. We demonstrate the performance of the data pre-processing chain (DPPC), which includes spectral filtering of A-scans, control of the mutual alignment of B-scans, and time and voltage axis's instabilities compensation in the whole C-scan. The performance of the DPPC is judged both in terms of the stabilization of certain statistical parameters of the data, and by its effect on the receiver operation characteristics (ROC) curve [C4344]

"Spot image / SARCOM: satellite imagery to reinforce maritime surveillance"

{no data available} [C4345]

"Investigation of physical characteristics of intertidal zone using NASA/JPL fully polarimetric AIRSAR data"

{no data available} [C4346]

"New methods for landslide identification and mapping using SAR polarimetry obtained during the PacRim 2000 mission in Taiwan"

{no data available} [C4347]

"Comparative analysis of the performance of metric-analog cameras, amateur-digital cameras, and LIDAR"

{no data available} [C4348]

"Forest detection in varying terrain using full-polarisation SAR data"

{no data available} [C4349]

"Sensitivity of radar backscatter to mangrove forest structure and AIRSAR imaging parameters"

{no data available} [C4350]

"The role of LiDAR data in understanding the relation between forest structure and SAR imagery"

{no data available} [C4351]

"Generalized minimum-error thresholding for unsupervised change detection from SAR amplitude imagery"

{no data available} [C4352]

"The contribution of PACRIM II to forest assessment in Queensland, Australia"

{no data available} [C4353]

"The interferometric data calibration for the AIRSAR PacRim II mission"

{no data available} [C4354]

"Comparison of methods for extracting and utilizing radar target characteristic parameters"

{no data available} [C4355]

"Development and observation of the broad-band radar for meteorological application"

{no data available} [C4356]

"AMPER: network on applied multiparameter environmental remote sensing: an EU sponsored research and training network"

{no data available} [C4357]

"On the polarization entropy"

{no data available} [C4358]

"Backscattering enhancement for Marshall-Palmer distributed rains for a W-band nadir-pointing radar with a finite beam width"

{no data available} [C4359]

"Application of cross-polar optimal polarizations for precipitation sensing"

{no data available} [C4360]

"Principles and design considerations for short-range energy balanced radar networks"

{no data available} [C4361]

"High resolution dual-polarization radar observation of tornados: implications for radar development and tornado detection"

{no data available} [C4362]

"Polarimetric doppler measurements for weather radar applications"

{no data available} [C4363]

"The study of filter algorithm for Lidar intension image"

{no data available} [C4364]

"Sea surface wind and cold tongue over the winter South China Sea"

{no data available} [C4365]

"Data segmentation for geometric feature extraction from lidar point clouds"

{no data available} [C4366]

"Automatic plane extraction from LIDAR data based on octree splitting and merging segmentation"

{no data available} [C4367]

"A new fast wind vector retrieval algorithm for seawinds scatterometer"

{no data available} [C4368]

"An experiment for high resolution airborne SAR imaging based on phase gradient autofocus"

{no data available} [C4369]

"Auto-combination of sub-band for spotlight SAR imaging"

{no data available} [C4370]

"Corrections to scatterometer wind vectors from the effects of rain, using high resolution NEXRAD radar collocations"

{no data available} [C4371]

"Evaluation of microwave scatterometers and radiometers as satellite anemometers"

{no data available} [C4372]

"Estimation of bare surface soil moisture with L-band multi-polarization radar measurements"

{no data available} [C4373]

"Examination of the semi-empirical polarimetric scattering model using field-measured data and existing theoretical models"

{no data available} [C4374]

"Monitoring of mining induced surface deformation using L-band SAR interferometry"

{no data available} [C4375]

"Measure groundwater pumping induced subsidence with D-InSAR"

{no data available} [C4376]

"A comparisons of model based and image based surface parameters estimation from polarimetric SAR"

{no data available} [C4377]

"Computation of bistatic RCS with NEC2 in a context of passive ISAR system"

{no data available} [C4378]

"Different approximations to the computation of reflected and refracted angles thanks to snell-descartes laws and fresnel coefficients"

{no data available} [C4379]

"PolSARpro v2.0: the polarimetric SAR data processing and educational toolbox"

{no data available} [C4380]

"Complex object's ISAR image simulation"

{no data available} [C4381]

"Automatic detection of targets using fractal dimension"

{no data available} [C4382]

"Detection methods of submerged mobile using SAR images"

{no data available} [C4383]

"The application of cloud texture and motion derived from geostationary satellite images in rain estimation-a study on mid-latitude depressions"

{no data available} [C4384]

"A novel prescreening method for UWB SAR target detection using adaptive nonlinear filters"

{no data available} [C4385]

"A high-resolution imaging algorithm based on scattered waveform estimation for UWB pulse radar systems"

{no data available} [C4386]

"DInSAR for mine subsidence monitoring using multi-source satellite SAR images"

{no data available} [C4387]

"Architecture of a flexible on-board real-time SAR-processor"

{no data available} [C4388]

"A new GPR calibration method for high accuracy thickness and permittivity measurement of multi-layered pavement"

{no data available} [C4389]

"A real-time back projection imaging algorithm for impulse surface penetrating radar"

{no data available} [C4390]

"Assimilating TOPEX/Poseidon data into an adjoint numerical tidal model in the East China Sea"

Eleven tidal constituents: O1, K1, P1, Q1, M2, S2, N2, K2, M4, MS4 and M6 are extracted from 10-year TOPEX/Poseidon altimetry data along track points in the East China Sea. Then the eight major tidal constituents (O1, K1, P1, Q1, M2, S2, N2 and K2) are assimilated into a two-dimension non-linear tidal model with the adjoint method. In this paper, two different experiments are applied for different kinds of assimilating data and the results show that, assimilating the altimetry data and the in situ data simultaneously is better than assimilating the altimetry data alone. And the bias between calculations and observations are provided. The deviations of M2 are 3.5 cm in amplitude and 2.9 deg in phase-lag. Those of O1 are 1.3 cm and 5.8 deg accordingly. The co-tidal charts of the eight constituents are also drawn. The general patterns are in good agreement with those literatures cited. [C4391]

"IGARSS 2005. IEEE International Geoscience and Remote Sensing Symposium"

{no data available} [C4392]

"Assimilation of ASAR data for wheat yield prediction: Matera case study"

The objective of this work is to investigate the synergistic use of leaf area index (LAI) retrieved by ENVISAT ASAR data and crop growth models, such as CERES-Wheat, to improve the accuracy of wheat yield predictions. The estimate reliability of CERES-Wheat strongly depends on the accuracy of its numerous inputs, which are not always available or accurate. As a consequence, the model would largely benefit from using updated information on the wheat status, provided by remote sensing at field scale. This work shows that the assimilation of ENVISAT ASAR AP data into the model lead to significant improvements in the wheat dry biomass and the grain yield model predictions. [C4393]

"Freeze-thaw processes radar remote sensing modeling and image processing"

In this paper, a theoretical model for radar backscatter in the permafrost area was developed and validated with the use of backscatter values derived from the radar images taken with the ERS-2 and JERS-1 in C and L bands, respectively. The employed backscatter model incorporates a spectroscopic dielectric model, which account for the unfrozen water dielectric properties at the temperatures below 0° C, and the measured temperature profiles and moisture values, regarding the active layer. The period from August 1997 to January 1998 was covered to include freeze/thaw processes in the active layer. The radar imaging of tundra in the Franklin Bluffs area, Alaska was used for analysis. A justification for that was the existence of a permafrost observatory in this area, which provides for measured soil temperature and moisture through year cycles. Reasonable correlation between modeled and observed backscatter seasonal trends has been found. This proves possibility for the theoretical model suggested to be used as a foundation for developing physically based algorithms, which are applicable to radar remote sensing technique in terms of freeze/thaw processes studies and radar images classification. [C4394]

"SAR in agriculture: sensitivity of backscattering to grapes"

{no data available} [C4395]

"Multitemporal evaluation with ASAR of boreal forests"

{no data available} [C4396]

"The utilization of equatorial atmosphere radar (EAR) and global precipitation climatology project (GPCP) in indicating of rainfall intensity over Kototabang, West Sumatera, Indonesia"

{no data available} [C4397]

"Application of spatial information technology for emergency response in traffic accident"

{no data available} [C4398]

"InSAR and mathematical modelling for measuring surface deformation due to geothermal water extraction in New Zealand"

{no data available} [C4399]

"Sea surface effects on phase coherence in emulated bistatic radar systems"

{no data available} [C4400]

"A space-time minimum cost flow phase unwrapping algorithm for the generation of DInSAR deformation time-series"

{no data available} [C4401]

"Determination of baseline and orientation of platforms for airborne bistatic radars"

{no data available} [C4402]

"Comparison on mitigating techniques to enhance bistatic STAP"

{no data available} [C4403]

"Application of the coherent pixels technique to the generation of deformation maps with ERS and ENVISAT data"

{no data available} [C4404]

"Application of principal component analysis in radar polarimetry"

{no data available} [C4405]

"On the status of bistatic polarimetry theory"

{no data available} [C4406]

"Coherent processing of long series of SAR images"

{no data available} [C4407]

"On the statistical aspects of radar polarimetry"

{no data available} [C4408]

"Optimization based underground cylindrical objects position and electromagnetic parameters joint reversion"

{no data available} [C4409]

"Oil spill detection using GLCM and MRF"

{no data available} [C4410]

"Comparison of ship detection algorithms in spaceborne SAR imagery"

{no data available} [C4411]

"Operational use of ship detection to combat illegal fishing in the Southern Indian Ocean"

{no data available} [C4412]

"Feasibility of satellite Ku-band scatterometer data for retrieval of seasonal snow characteristics in Finland"

{no data available} [C4413]

"An attempt to sense ocean winds and waves empirically using bi-static GNSS reflections in low Earth orbit"

{no data available} [C4414]

"Comparison of doppler centroid estimators in bistatic airborne SAR"

{no data available} [C4415]

"From EO data to snow covered area (SCA) end products using automated processing system"

{no data available} [C4416]

"Multi-sensor monitoring of snow parameters in Nordic mountainous areas"

{no data available} [C4417]

"High resolution SAR imaging of moving ships"

{no data available} [C4418]

"The analysis of time synchronization error in bistatic SAR system"

{no data available} [C4419]

"Tomographic inverse scattering approach for radar imaging with multistatic acquisition"

{no data available} [C4420]

"A new jamming method on parasitic spaceborne SAR system"

{no data available} [C4421]

"Study of along track interferometric technology for the bistatic SAR"

{no data available} [C4422]

"Narrowband multistatic ISAR imagery system"

{no data available} [C4423]

"Using multifrequency HF radar to estimate ocean wind fields"

{no data available} [C4424]

"Sea monitoring for detecting dangerous seas and tsunamis using space based GNSS bi-static radar technology"

{no data available} [C4425]

"Control sidelobes in UWB SAR images"

{no data available} [C4426]

"Multi-target ISAR imaging method"

{no data available} [C4427]



"The optimum selection of common master image for series of differential SAR processing to estimate long and slow ground deformation"

{no data available} [C4428]

"Land subsidence monitoring in city area by time series interferometric SAR data"

{no data available} [C4429]

"A "Real-like" polarimetric weather radar data generation using physical and statistical models"

Realistic model of rain radar returns is of interest to improve the performances of rainfall estimation applications and to develop new approximations in case of lack of measured data-bases. In this paper, we propose a method to generate a "Real-like" polarimetric rain radar data based on a dual approach referring to both a physical and a statistical models of rain target. Combining informations from these two models accords us an opportunity to obtain more realistic results than a single model based approach. Theoretical foundation of the actual work was exposed all along the paper. An example of data generation, for a fixed physical configuration, was given so as to illustrate comparison between ideal and realistic rain radar data. [C4430]

"Observing coal mining subsidence from JERS-1 permanent scatterer analysis"

{no data available} [C4431]

"A new estimation method for DEM error by miscoregistration"

{no data available} [C4432]

"Polarization discrimination for improving foliage-camouflaged target detection"

{no data available} [C4433]

"A new anti-jamming method for parasitic spaceborne SAR system"

{no data available} [C4434]

"Comparison of FMCW and pulse type groundpenetrating radar(GPR) for water leakage detection"

{no data available} [C4435]

"GPR signal simulations in the course of freeze/thaw process for a permafrost area"

{no data available} [C4436]

"DEM generation from radarsat stereo images in high relief areas"

{no data available} [C4437]

"3D positioning assessment for stereo configuration conditions of airborne SAR images in mountainous area"

{no data available} [C4438]

"Refined extended chirp scaling algorithm for spaceborne ScanSAR imaging"

{no data available} [C4439]

"A new method of SAR image segmentation"

{no data available} [C4440]

"A new method of SAR image target recognition based on SVM"

{no data available} [C4441]

"Segmentation and aspect estimation in SAR image of target chip"

{no data available} [C4442]

"Implementation of the SAR data processing module based on component"

{no data available} [C4443]

"Ship detection in SAR images using multi-polarimetric information"

{no data available} [C4444]

"Nonlinear diffusion equation for speckle reducing and resolution enhancement"

{no data available} [C4445]

"Inversion of the low frequency UWB SAR"

{no data available} [C4446]

"A real time autofocus algorithm for high resolution airborne SAR"

{no data available} [C4447]

"Wind measurements at FINO-I using marine radar-image sequences"

{no data available} [C4448]

"Man-made targets pose estimation using time-frequency distribution in UWB SAR"

{no data available} [C4449]

"Automatic mosaicing for airborne SAR imaging based on subaperture processing"

{no data available} [C4450]

"Range alignment for ISAR using genetic algorithms"

{no data available} [C4451]

"Study on SAR image simulation based on SRTM DEM and landcover data"

{no data available} [C4452]

"General radar analysis and computation environment"

{no data available} [C4453]

"Implementation of a co/decoding method in SAR processing based on time domain correlation: experimental validation"

{no data available} [C4454]

"The global satellite mapping of precipitation (GSMaP) project"

{no data available} [C4455]

"Computer simulation of wind measurements by increment's cumulant approach"

{no data available} [C4456]

"A methodology to study bright band structure on a global scale from TRMM precipitation radar"

{no data available} [C4457]

"Introduction of a melting layer model to a rain retrieval algorithm for microwave radiometers"

{no data available} [C4458]

"Low altitude flying for high resolution imaging satellite: comparison of low circular and elliptical orbits"

{no data available} [C4459]

"Improved physically-based AMSR-E oceanic rainfall algorithm"

{no data available} [C4460]

"Signal processing architecture for a single radar node in a networked radar environment (NETRAD)"

{no data available} [C4461]

"Radiometric calibration of the advanced wind scatterometers carried on-board the METOP satellites"

{no data available} [C4462]

"Seawinds radiometer (SRad) on ADEOS-II brightness temperature calibration/validation"

{no data available} [C4463]

"Spaceborne dual-wavelength radar techniques for retrieval of hydrometeor profiles"

{no data available} [C4464]

"VHF SAR image formation implemented on a GPU"

{no data available} [C4465]

"A framework for investigating space-borne polarimetric interferometry using the ALOS-PALSAR sensor"

{no data available} [C4466]

"Correction method for saturated SAR data to improve radiometric accuracy"

{no data available} [C4467]

"Improved beat frequency estimation in the MLBF Doppler ambiguity resolver"

{no data available} [C4468]

"Calibration of ALOS/PALSAR polarimetric data affected by faraday rotation"

{no data available} [C4469]

"A GPM dual frequency DSD retrieval method based on linear model for DSD vertical profile"

{no data available} [C4470]

"An assessment on the performance of GPM dual-frequency precipitation radar rain profiling methods through numerical simulation"

{no data available} [C4471]

"Research plans for developing a L-band wind retrieval model function by using ALOS/PALSAR"

{no data available} [C4472]

"Uncertainties in the rain retrieval algorithm for the GPM dual-frequency precipitation radar"

{no data available} [C4473]

"Lake shoreline detection and tracing in SAR images using wavelet transform and ACM method"

{no data available} [C4474]

"A new interferogram generation method"

{no data available} [C4475]

"Detection of the flood boundary in SAR image using texture"

{no data available} [C4476]

"Mapping of wind-thrown forests in Southern Sweden using space- and airborne SAR"

{no data available} [C4477]

"Monitoring flood using multi-temporal ENVISAT ASAR data"

{no data available} [C4478]

"Deformation field over Western Taiwan Island using satellite InSAR"

{no data available} [C4479]

"Geo-referencing airborne interferometric SAR data"

{no data available} [C4480]

"Application of scatter-cluster InSAR in China country"

{no data available} [C4481]

"An accurate co-registration method of spaceborne repeat-pass InSAR based on matrix transformation"

{no data available} [C4482]

"An interferogram filtering method using wavelet transform"

{no data available} [C4483]

"Analysis of the unbiased complex coherence estimation using varying ERS interferometric data"

{no data available} [C4484]

"Fine registration of SPOT5 and Envisat/ASAR images and ortho-image production: a fully automatic approach"

{no data available} [C4485]

"Registering of synthetic aperture radar and optical data"

{no data available} [C4486]

"Image fusion using fuzzy-nonparametric interpolation approach"

{no data available} [C4487]

"Stem volume retrieval with spaceborne L-band repeat-pass coherence: multi-temporal combination for boreal forest"

{no data available} [C4488]

"Detecting forest trails occluded by dense canopies using ALSM data"

{no data available} [C4489]

"Phase unwrapping for DEM generation as an inverse problem"

{no data available} [C4490]

СПИСОК ЛИТЕРАТУРЫ

- C3411.** Durand R. Man Made Target Detection in a Forest with a Subspace Detector SAR Processor. / Durand R., Thirion L., Ginolhac G., Forster P. // 2006. IGARSS 2006. IEEE International Conference on Geoscience and Remote Sensing Symposium. - Denver, CO, July 31 2006-Aug. 4 2006. - P. 149-152. ↑
- C3412.** Torrione P. Ground Response Tracking for Improved Landmine Detection in Ground Penetrating Radar Data. / Torrione P., Collins L. // 2006. IGARSS 2006. IEEE International Conference on Geoscience and Remote Sensing Symposium. - Denver, CO, July 31 2006-Aug. 4 2006. - P. 153-156. ↑
- C3413.** Parizzi A. Accurate DEM Reconstruction from Permanent Scatterers and Multi-baseline Interferometry. / Parizzi A., Perissin D., Prati C., Rocca F., Ferretti A. // 2006. IGARSS 2006. IEEE International Conference on Geoscience and Remote Sensing Symposium. - Denver, CO, July 31 2006-Aug. 4 2006. - P. 157-160. ↑
- C3414.** Robson M. Evaluation of eCognition for Assisted Target Detection and Recognition in SAR Imagery. / Robson M., Vachon P.W., Seeker J. // 2006. IGARSS 2006. IEEE International Conference on Geoscience and Remote Sensing Symposium. - Denver, CO, July 31 2006-Aug. 4 2006. - P. 145-148. ↑
- C3415.** Nouvel J.F. A Ka Band Imaging Radar: DRIVE on Board ONERA Motorglider. / Nouvel J.F., Jeuland H., Bonin G., Roques S., Du Plessis O., Peyret J. // 2006. IGARSS 2006. IEEE International Conference on Geoscience and Remote Sensing Symposium. - Denver, CO, July 31 2006-Aug. 4 2006. - P. 134-136. ↑
- C3416.** Ting Liu. A New Polarimetric CFAR Ship Detection System. / Ting Liu, Lampropoulos G. // 2006. IGARSS 2006. IEEE International Conference on Geoscience and Remote Sensing Symposium. - Denver, CO, July 31 2006-Aug. 4 2006. - P. 137-140. ↑
- C3417.** Martorella M. Target Classification by Means of Fully Polarimetric ISAR Images. / Martorella M., Berizzi F., Soletti R., Cantini L., Corucci A., Haywood B., Palmer J. // 2006. IGARSS 2006. IEEE International Conference on Geoscience and Remote Sensing Symposium. - Denver, CO, July 31 2006-Aug. 4 2006. - P. 141-144. ↑
- C3418.** D'Hondt O. The Gradient Structure Tensor as an Efficient Descriptor of Spatial Texture in Polarimetric SAR Data. / D'Hondt O., Ferro-Famil L., Pottier E. // 2006. IGARSS 2006. IEEE International Conference on Geoscience and Remote Sensing Symposium. - Denver, CO, July 31 2006-Aug. 4 2006. - P. 164-167. ↑
- C3419.** Mercier G. Copula-based Stochastic Kernels for Abrupt Change Detection. / Mercier G., Derronde S., Pieczynski W., Nicolas J.-M., Joannic-Chardin A., Inglada J. // 2006. IGARSS 2006. IEEE International Conference on Geoscience and Remote Sensing Symposium. - Denver, CO, July 31 2006-Aug. 4 2006. - P. 204-207. ↑
- C3420.** No-Wook Park. Land-cover Classification using Multi-temporal/polarization C-band SAR Data. / No-Wook Park, Kwang-Hoon Chi. // 2006. IGARSS 2006. IEEE International Conference on Geoscience and Remote Sensing Symposium. - Denver, CO, July 31 2006-Aug. 4 2006. - P. 188-191. ↑
- C3421.** Qi Li. Simultaneous Perturbation Stochastic Approximation Algorithm for Automated Image Registration Optimization. / Qi Li, Sato I., Murakami Y. // 2006. IGARSS 2006. IEEE International Conference on Geoscience and Remote Sensing Symposium. - Denver, CO, July 31 2006-Aug. 4 2006. - P. 184-187. ↑
- C3422.** Inglada J. The Multiscale Change Profile: A Statistical Similarity Measure for Change Detection in Multitemporal SAR Images. / Inglada J., Mercier G. // 2006. IGARSS 2006. IEEE International Conference on

Geoscience and Remote Sensing Symposium. - Denver, CO, July 31 2006-Aug. 4 2006. - P. 212-215. ↑

C3423. Waske B. Random Feature Selection for Decision Tree Classification of Multi-temporal SAR Data. / Waske B., Schiefer S., Braun M. // 2006. IGARSS 2006. IEEE International Conference on Geoscience and Remote Sensing Symposium. - Denver, CO, July 31 2006-Aug. 4 2006. - P. 168-171. ↑

C3424. Due Viet Bui. Advantage of the Remote Sensing Data Utilization in Studying Inundation Risks in Terms of Land-Use. / Due Viet Bui, Goita K. // 2006. IGARSS 2006. IEEE International Conference on Geoscience and Remote Sensing Symposium. - Denver, CO, July 31 2006-Aug. 4 2006. - P. 279-282. ↑

C3425. Grasso E. The Application Image Coregistrator on Grid Technology. / Grasso E., Stigliano S., Lore V.A. // 2006. IGARSS 2006. IEEE International Conference on Geoscience and Remote Sensing Symposium. - Denver, CO, July 31 2006-Aug. 4 2006. - P. 241-244. ↑

C3426. Lenz R. The TerraSAR-X Active Calibration Instruments and Performance Analysis. / Lenz R., Wiesbeck W. // 2006. IGARSS 2006. IEEE International Conference on Geoscience and Remote Sensing Symposium. - Denver, CO, July 31 2006-Aug. 4 2006. - P. 97-100. ↑

C3427. Boerner W.-M. Recent Advances in Polarimetry and Polarimetric Interferometry. 2006. IGARSS 2006. IEEE International Conference on Geoscience and Remote Sensing Symposium. - Denver, CO, July 31 2006-Aug. 4 2006. - P. 49-51. ↑

C3428. Jong-Sen Lee. Monte Carlo Evaluation of Multi-Look Effect on Entropy/Alpha /Anisotropy Parameters of Polarimetric Target Decomposition. / Jong-Sen Lee, Ainsworth T.L., Grimes M.R., Lopez-Martinez C. // 2006. IGARSS 2006. IEEE International Conference on Geoscience and Remote Sensing Symposium. - Denver, CO, July 31 2006-Aug. 4 2006. - P. 52-55. ↑

C3429. Lopez-Martinez C. Extended Multidimensional Speckle Noise Model and its Implications on the Estimation of Physical Information. / Lopez-Martinez C., Pottier E. // 2006. IGARSS 2006. IEEE International Conference on Geoscience and Remote Sensing Symposium. - Denver, CO, July 31 2006-Aug. 4 2006. - P. 56-59. ↑

C3430. Direk K. Study of Hurricanes and Typhoons from TRMM Precipitation Radar Observations: Self Organizing Map (SOM) Neural Network. / Direk K., Chandrasekar V. // 2006. IGARSS 2006. IEEE International Conference on Geoscience and Remote Sensing Symposium. - Denver, CO, July 31 2006-Aug. 4 2006. - P. 45-48. ↑

C3431. Shimizu S. Development and Validation of Spaceborne Dualfrequency Precipitation Radar for GPM. / Shimizu S., Oki R., Kachi M., Kojima M., Iguchi T., Nakamura K. // 2006. IGARSS 2006. IEEE International Conference on Geoscience and Remote Sensing Symposium. - Denver, CO, July 31 2006-Aug. 4 2006. - P. 29-31. ↑

C3432. Gorgucci E. The Role of C-band Dual Polarization Radars for GPM Ground Validation. / Gorgucci E., Baldini L., Chandrasekar V. // 2006. IGARSS 2006. IEEE International Conference on Geoscience and Remote Sensing Symposium. - Denver, CO, July 31 2006-Aug. 4 2006. - P. 32-35. ↑

C3433. Adhikari N.B. Rain Retrieval Performance of a Dual-Frequency Radar Technique with Differential Attenuation Constraint. / Adhikari N.B., Iguchi T., Seto S., Takahashi N. // 2006. IGARSS 2006. IEEE International Conference on Geoscience and Remote Sensing Symposium. - Denver, CO, July 31 2006-Aug. 4 2006. - P. 36-40. ↑

C3434. Yunjin Kim. A Time Series Approach for Soil Moisture Estimation. / Yunjin Kim, van Zyl J. // 2006. IGARSS 2006. IEEE International Conference on Geoscience and Remote Sensing Symposium. - Denver, CO, July 31 2006-Aug. 4 2006. - P. 60-62. ↑

C3435. Pipia L. Polarimetric Temporal Decorrelation Studies by Means of GBSAR Sensor Data. / Pipia L., Fabregas X., Lopez-Martinez C., Aguasca A., Mallorqui J.J. // 2006. IGARSS 2006. IEEE International Conference on Geoscience and Remote Sensing Symposium. - Denver, CO, July 31 2006-Aug. 4 2006. - P. 79-82. ↑

C3436. Raney R.K. The Elephant in Dual-Polarized Imaging Radar. 2006. IGARSS 2006. IEEE International Conference on Geoscience and Remote Sensing Symposium. - Denver, CO, July 31 2006-Aug. 4 2006. - P. 83-

84. ↑

C3437. Im E. Early Results on Cloud Profiling Radar Post-launch Calibration and Operations. / Im E., Durden S.L., Tanelli S., Kyung Pak. // 2006. IGARSS 2006. IEEE International Conference on Geoscience and Remote Sensing Symposium. - Denver, CO, July 31 2006-Aug. 4 2006. - P. 93-96. ↑

C3438. Margarit G. Study of the Influence of Vessel Motions and Sea-Ship Interaction on Classification Algorithms Based on Single-Pass Polarimetric SAR Interferometry. / Margarit G., Mallorqui J.J., Fabregas X. // 2006. IGARSS 2006. IEEE International Conference on Geoscience and Remote Sensing Symposium. - Denver, CO, July 31 2006-Aug. 4 2006. - P. 75-78. ↑

C3439. Lee J.-S. Polarimetric Analysis of Radar Signature of a Manmade Structure. / Lee J.-S., Ainsworth T., Krogagor E., Boerner W.-M. // 2006. IGARSS 2006. IEEE International Conference on Geoscience and Remote Sensing Symposium. - Denver, CO, USA, July 31 2006-Aug. 4 2006. - P. 63-66. ↑

C3440. Morris J.T. Polarimetric Characteristics of Radar Echoes from the Sea Surface as a Function of Incidence Angle. / Morris J.T., Anderson S.J. // 2006. IGARSS 2006. IEEE International Conference on Geoscience and Remote Sensing Symposium. - Denver, CO, July 31 2006-Aug. 4 2006. - P. 67-70. ↑

C3441. Zheng-Shu Zhou. Structural Parameter Estimation of Australian Flora with a Ground-based Polarimetric Radar Interferometer. / Zheng-Shu Zhou, Cloude S.R. // 2006. IGARSS 2006. IEEE International Conference on Geoscience and Remote Sensing Symposium. - Denver, CO, July 31 2006-Aug. 4 2006. - P. 71-74. ↑

C3442. Shimada M. PALSAR Characterization and Initial Calibration. / Shimada M., Watanabe M., Moriyama T., Tadono T. // 2006. IGARSS 2006. IEEE International Conference on Geoscience and Remote Sensing Symposium. - Denver, CO, July 31 2006-Aug. 4 2006. - P. 332-335. ↑

C3443. Wolfe R.E. Improving Satellite Moderate Resolution Instrument Geolocation Accuracy in Rough Terrain. / Wolfe R.E., Nishihama M., Kuyper J.R. // 2006. IGARSS 2006. IEEE International Conference on Geoscience and Remote Sensing Symposium. - Denver, CO, July 31 2006-Aug. 4 2006. - P. 1123-1125. ↑

C3444. Wei Gong. Mobile Aerosol Lidar for Earth Observation Atmospheric Correction. / Wei Gong, Zhongmin Zhu, Pingxiang Li, Qianqing Qin, Zhongyu Hao, Mengyu Liu, Yingying Ma. // 2006. IGARSS 2006. IEEE International Conference on Geoscience and Remote Sensing Symposium. - Denver, CO, July 31 2006-Aug. 4 2006. - P. 1126-1129. ↑

C3445. Hyun-chong Cho. Extraction of Stream Channels in High-Resolution Digital Terrain Images Using Morphology. / Hyun-chong Cho, Srinivasan S., Sedighi A., Slatton K.C. // 2006. IGARSS 2006. IEEE International Conference on Geoscience and Remote Sensing Symposium. - Denver, CO, July 31 2006-Aug. 4 2006. - P. 1078-1081. ↑

C3446. Darawankul A. Comparison of Surface Scattering Models for Gaussian and Exponential Surfaces. / Darawankul A., Johnson J.T., Chen K.S. // 2006. IGARSS 2006. IEEE International Conference on Geoscience and Remote Sensing Symposium. - Denver, CO, July 31 2006-Aug. 4 2006. - P. 1036-1039. ↑

C3447. Macina F. Exploiting Physical and Topographic Information within a Fuzzy Scheme to Map Flooded Area by SAR. / Macina F., Bignami C., Chini M., Pierdicca N. // 2006. IGARSS 2006. IEEE International Conference on Geoscience and Remote Sensing Symposium. - Denver, CO, July 31 2006-Aug. 4 2006. - P. 1052-1055. ↑

C3448. Colesanti C. A First Experiment of 3D Imaging with a Ground based Parasitic SAR. / Colesanti C., Perissin D. // 2006. IGARSS 2006. IEEE International Conference on Geoscience and Remote Sensing Symposium. - Denver, CO, July 31 2006-Aug. 4 2006. - P. 1192-1195. ↑

C3449. Hua Zhong. A Fourth-Order Imaging Algorithm for Spaceborne Bistatic SAR. / Hua Zhong, Xingzhao Liu. // 2006. IGARSS 2006. IEEE International Conference on Geoscience and Remote Sensing Symposium. - Denver, CO, July 31 2006-Aug. 4 2006. - P. 1196-1199. ↑

C3450. Natroshvili K. 2D Inverse Scaling Bistatic Processing and the focused Image Quality Measurements. / Natroshvili K., Loffeld O., Nies H., Ender J.H.G. // 2006. IGARSS 2006. IEEE International Conference on Geoscience and Remote Sensing Symposium. - Denver, CO, July 31 2006-Aug. 4 2006. - P. 1188-1191. ↑

- C3451.** Anterrieu E. Reduction of the Reconstruction Bias in Synthetic Aperture Imaging Radiometry. 2006. IGARSS 2006. IEEE International Conference on Geoscience and Remote Sensing Symposium. - Denver, CO, July 31 2006-Aug. 4 2006. - P. 1164-1167. ↑
- C3452.** Bosch-Lluis X. FPGA-based Implementation of a Polarimetric Radiometer with Digital Beamforming. / Bosch-Lluis X., Camps A., Marchan-Hernandez J.F., Ramos-Perez I., Prehn R., Izquierdo B., Banque X., Yeste J. // 2006. IGARSS 2006. IEEE International Conference on Geoscience and Remote Sensing Symposium. - Denver, CO, July 31 2006-Aug. 4 2006. - P. 1176-1179. ↑
- C3453.** Ge D.Q. Linear Deformation Rate Derivation from Multi-baseline Differential Interferogram Stacks. / Ge D.Q., Guo X.F., Zhang L., Liu S.W., Fan J.H. // 2006. IGARSS 2006. IEEE International Conference on Geoscience and Remote Sensing Symposium. - Denver, CO, July 31 2006-Aug. 4 2006. - P. 763-766. ↑
- C3454.** Xiao-Bing Ma. Error Evaluation of BAQ Algorithm for Internal Calibration Data of Spaceborne SAR. / Xiao-Bing Ma, Zhen-Yong Guo, Wei-Dong Yu, Ping Zhang. // 2006. IGARSS 2006. IEEE International Conference on Geoscience and Remote Sensing Symposium. - Denver, CO, July 31 2006-Aug. 4 2006. - P. 794-797. ↑
- C3455.** Tzeng Y.C. Automatic Change Detections from SAR Images Using Fractal Dimension. / Tzeng Y.C., Chiu S.H., Chen K.S. // 2006. IGARSS 2006. IEEE International Conference on Geoscience and Remote Sensing Symposium. - Denver, CO, July 31 2006-Aug. 4 2006. - P. 759-762. ↑
- C3456.** Pettinato S. Snow Cover Maps with Satellite Borne SAR: A New Approach in Harmony with Fractional Optical SCA Retrieval Algorithms. / Pettinato S., Malnes E., Haarpaintner J. // 2006. IGARSS 2006. IEEE International Conference on Geoscience and Remote Sensing Symposium. - Denver, CO, July 31 2006-Aug. 4 2006. - P. 735-738. ↑
- C3457.** Martinez-Vazquez A. Feasibility of Snow Avalanche Volume Retrieval by GB-SAR Imagery. / Martinez-Vazquez A., Fortuny-Guasch J. // 2006. IGARSS 2006. IEEE International Conference on Geoscience and Remote Sensing Symposium. - Denver, CO, July 31 2006-Aug. 4 2006. - P. 743-746. ↑
- C3458.** Baillarin S. Remote Sensing Image Ground Segment Interoperability: PLEIADES-HR Case Study. / Baillarin S., Gasperi J., Dabin C., Panem C., Chausserie-Lapree B., Gleyzes J.-P., Kubik P., Latry C., Floissac P., Hillairet E. // 2006. IGARSS 2006. IEEE International Conference on Geoscience and Remote Sensing Symposium. - Denver, CO, July 31 2006-Aug. 4 2006. - P. 928-931. ↑
- C3459.** Bai Lu. InSAR Co-registration Accuracy Assessment Based on Misregistration Value. / Bai Lu, Wang Yanping, Wei Lideng, Hong Wen, Peng Hailiang. // 2006. IGARSS 2006. IEEE International Conference on Geoscience and Remote Sensing Symposium. - Denver, CO, July 31 2006-Aug. 4 2006. - P. 964-967. ↑
- C3460.** Aiazzi B. Automated Content Extraction from SAR Data. / Aiazzi B., Baronti S., Alparone L., Cuzzo G., D'Elia C., Schirizzi G. // 2006. IGARSS 2006. IEEE International Conference on Geoscience and Remote Sensing Symposium. - Denver, CO, July 31 2006-Aug. 4 2006. - P. 821-824. ↑
- C3461.** Hai-ming Qi. Performance Evaluation of Amplitude-Phase Algorithm for SAR Raw Data Compression. / Hai-ming Qi, Wei-dong Yu, Xin-zhe Yuan, Zhen-yong Guo, Xu-wen Tian. // 2006. IGARSS 2006. IEEE International Conference on Geoscience and Remote Sensing Symposium. - Denver, CO, July 31 2006-Aug. 4 2006. - P. 809-812. ↑
- C3462.** Sharma N.C.P. A Lidar Collaboratory Data Management System. / Sharma N.C.P., Parikh J.A. // 2006. IGARSS 2006. IEEE International Conference on Geoscience and Remote Sensing Symposium. - Denver, CO, July 31 2006-Aug. 4 2006. - P. 817-820. ↑
- C3463.** Ticconi F. A Theoretical Study of the Sensitivity of Spaceborne Bistatic Microwave Systems to Geophysical Parameters of Land Surfaces. / Ticconi F., Pierdicca N., Pulvirenti L., Brogioni M. // 2006. IGARSS 2006. IEEE International Conference on Geoscience and Remote Sensing Symposium. - Denver, CO, July 31 2006-Aug. 4 2006. - P. 1200-1203. ↑
- C3464.** Jing Yao. The Associated Modeling and Precision Analysis of Spatial States and the Inter-Satellite Baseline of Formation Flying Satellites. / Jing Yao, Dong-yun Yi, De-feng Gu. // 2006. IGARSS 2006. IEEE International Conference on Geoscience and Remote Sensing Symposium. - Denver, CO, July 31 2006-Aug. 4 2006. - P. 1255-1258. ↑

- C3465.** Hirose A. Phase Unwrapping with Phase-Singularity Spreading. / Hirose A., Yamaki R. // 2006. IGARSS 2006. IEEE International Conference on Geoscience and Remote Sensing Symposium. - Denver, CO, July 31 2006-Aug. 4 2006. - P. 1259-1261. ↑
- C3466.** Tang Zhi. Formation Flying InSAR Configuration Error Simulation and Compensation. / Tang Zhi, Li Jingwen, Zhou Yinqing, Liu Ligu. // 2006. IGARSS 2006. IEEE International Conference on Geoscience and Remote Sensing Symposium. - Denver, CO, July 31 2006-Aug. 4 2006. - P. 1251-1254. ↑
- C3467.** Bin Zou. A Novel Height Reconstruction Approach Based on MLE Using Multi-frequency InSAR Data. / Bin Zou, Wei Wang, Deming Sun, Lamei Zhang. // 2006. IGARSS 2006. IEEE International Conference on Geoscience and Remote Sensing Symposium. - Denver, CO, July 31 2006-Aug. 4 2006. - P. 1244-1247. ↑
- C3468.** Sang-Hoon Hong. Coherence Improvement of Cross-Interferometric Pair by a Block Azimuth Filtering. / Sang-Hoon Hong, Joong-Sun Won. // 2006. IGARSS 2006. IEEE International Conference on Geoscience and Remote Sensing Symposium. - Denver, CO, July 31 2006-Aug. 4 2006. - P. 1248-1250. ↑
- C3469.** Cao Fang. An Unsupervised Classification for Fully Polarimetric SAR Data Using IHSL Transform and the FCM Agrithm. / Cao Fang, Hong Wen, Wu Yirong. // 2006. IGARSS 2006. IEEE International Conference on Geoscience and Remote Sensing Symposium. - Denver, CO, July 31 2006-Aug. 4 2006. - P. 1273-1276. ↑
- C3470.** Muhtar Qong. Two Novel Polarimetric Indices and Their Application on the Target Enhancement in POLSAR Images. / Muhtar Qong, Iwashita A. // 2006. IGARSS 2006. IEEE International Conference on Geoscience and Remote Sensing Symposium. - Denver, CO, July 31 2006-Aug. 4 2006. - P. 1277-1280. ↑
- C3471.** Chen Xi. A New Method for DEM Generation using a Single POLSAR Flight Pass. / Chen Xi, Zhang Hong, Wang Chao. // 2006. IGARSS 2006. IEEE International Conference on Geoscience and Remote Sensing Symposium. - Denver, CO, July 31 2006-Aug. 4 2006. - P. 1270-1272. ↑
- C3472.** Bin Zou. Building Extraction Using C Band Pol-SAR Image. / Bin Zou, Deming Sun, Lamei Zhang, Wei Wang. // 2006. IGARSS 2006. IEEE International Conference on Geoscience and Remote Sensing Symposium. - Denver, CO, July 31 2006-Aug. 4 2006. - P. 1262-1265. ↑
- C3473.** Arakelyan A.K. S-Band, Polarimetric, Combined, Short Range Action Scatterometer-Radiometer for Platform and Vessel Application. / Arakelyan A.K., Hambaryan A.K., Karyan V.V., Hovhannisyan G.G., Pogosyan N.G., Manukyan M.R., Arakelyan A.A., Hambaryan V.K., Grigoryan M.L., Hakobyan I.K., Darbinyan S. // 2006. IGARSS 2006. IEEE International Conference on Geoscience and Remote Sensing Symposium. - Denver, CO, July 31 2006-Aug. 4 2006. - P. 1266-1269. ↑
- C3474.** Knedlik S. On Position and Attitude Determination Requirements for future Bistatic SAR Experiments. / Knedlik S., Loffeld O., Gebhardt U. // 2006. IGARSS 2006. IEEE International Conference on Geoscience and Remote Sensing Symposium. - Denver, CO, July 31 2006-Aug. 4 2006. - P. 1216-1219. ↑
- C3475.** Vecchia A.D. Optimization of bistatic Radar Configurations for Vegetation Monitoring. / Vecchia A.D., Ferrazzoli P., Guerriero L., Cacucci I., Marzano M., Pierdicca N., Ticconi F. // 2006. IGARSS 2006. IEEE International Conference on Geoscience and Remote Sensing Symposium. - Denver, CO, July 31 2006-Aug. 4 2006. - P. 1220-1223. ↑
- C3476.** Kalkuhl M. Modular SAR Simulator for Bi- and Multistatic Constellations. / Kalkuhl M., Droste P., Wiechert W., Nies H., Loffeld O. // 2006. IGARSS 2006. IEEE International Conference on Geoscience and Remote Sensing Symposium. - Denver, CO, July 31 2006-Aug. 4 2006. - P. 1212-1215. ↑
- C3477.** Nies H. A Solution for Bistatic Motion Compensation. / Nies H., Loffeld O., Natroshvili K., Ortiz A.M. // 2006. IGARSS 2006. IEEE International Conference on Geoscience and Remote Sensing Symposium. - Denver, CO, July 31 2006-Aug. 4 2006. - P. 1204-1207. ↑
- C3478.** Klare J. Evaluation and Optimisation of Configurations of a Hybrid Bistatic SAR Experiment Between TerraSAR-X and PAMIR. / Klare J., Walterscheid I., Brenner A.R., Ender J.H.G. // 2006. IGARSS 2006. IEEE International Conference on Geoscience and Remote Sensing Symposium. - Denver, CO, July 31 2006-Aug. 4 2006. - P. 1208-1211. ↑
- C3479.** Moll A. Determination of Glacier Velocities on King George Island (Antarctica) by DInSAR. / Moll A., Braun M. // 2006. IGARSS 2006. IEEE International Conference on Geoscience and Remote Sensing

Symposium. - Denver, CO, July 31 2006-Aug. 4 2006. - P. 1236-1239. ↑

C3480. Costantini M. A Generalized Space-Time Formulation for Robust Persistent Scatterer Interferometry. / Costantini M., Guglielmi M., Malvarosa F., Minati F. // 2006. IGARSS 2006. IEEE International Conference on Geoscience and Remote Sensing Symposium. - Denver, CO, July 31 2006-Aug. 4 2006. - P. 1240-1243. ↑

C3481. Scott W.R. Combined Ground Penetrating Radar and Seismic System for Detecting Tunnels. / Scott W.R., Counts T., Larson G.D., Gurbuz A.C., McClellan J.H. // 2006. IGARSS 2006. IEEE International Conference on Geoscience and Remote Sensing Symposium. - Denver, CO, July 31 2006-Aug. 4 2006. - P. 1232-1235. ↑

C3482. Zhu Zhenbo. Research on Bistatic SAR Imaging. / Zhu Zhenbo, Tang Ziyue, Jiang Xingzhou. // 2006. IGARSS 2006. IEEE International Conference on Geoscience and Remote Sensing Symposium. - Denver, CO, July 31 2006-Aug. 4 2006. - P. 1224-1227. ↑

C3483. Xin-Zhe Yuan. An Adaptive Filtering Approach to Distributed Space-borne SAR Imaging. / Xin-Zhe Yuan, Hai-Min Qi, Zhen-Yong Guo, Ping Zhang. // 2006. IGARSS 2006. IEEE International Conference on Geoscience and Remote Sensing Symposium. - Denver, CO, July 31 2006-Aug. 4 2006. - P. 1228-1231. ↑

C3484. Utku C. Simulations of L-Band Backscattering from a Quasi- Periodic Corn Canopy. / Utku C., Lang R.H. // 2006. IGARSS 2006. IEEE International Conference on Geoscience and Remote Sensing Symposium. - Denver, CO, July 31 2006-Aug. 4 2006. - P. 458-460. ↑

C3485. Jin-Young Hong. A Simple Model for Scattering Coefficients of Vegetation Canopies. / Jin-Young Hong, Yisok Oh. // 2006. IGARSS 2006. IEEE International Conference on Geoscience and Remote Sensing Symposium. - Denver, CO, July 31 2006-Aug. 4 2006. - P. 461-464. ↑

C3486. Chih-hao Kuo. Electromagnetic Scattering from Multilayer Rough Surfaces Separated by Arbitrary Dielectric Profiles. / Chih-hao Kuo, Moghaddam M. // 2006. IGARSS 2006. IEEE International Conference on Geoscience and Remote Sensing Symposium. - Denver, CO, July 31 2006-Aug. 4 2006. - P. 454-457. ↑

C3487. O'Neill P. Hydros Soil Moisture Retrieval Algorithms: Status and Relevance to Future Missions. / O'Neill P., Owe M., Gouweleeuw B., Njoku E., Shi J.C., Wood E. // 2006. IGARSS 2006. IEEE International Conference on Geoscience and Remote Sensing Symposium. - Denver, CO, July 31 2006-Aug. 4 2006. - P. 436-439. ↑

C3488. Zribi M. A New Semi-empirical Model for the Analysis of Surface Roughness Heterogeneity. / Zribi M., Baghdadi N., Guerin C. // 2006. IGARSS 2006. IEEE International Conference on Geoscience and Remote Sensing Symposium. - Denver, CO, July 31 2006-Aug. 4 2006. - P. 451-453. ↑

C3489. Sang-Eun Park. Assessing Vegetation Scattering Mechanisms of L-band AIRSAR Data on Sloping Forest Area. / Sang-Eun Park, Moon W.M. // 2006. IGARSS 2006. IEEE International Conference on Geoscience and Remote Sensing Symposium. - Denver, CO, July 31 2006-Aug. 4 2006. - P. 489-492. ↑

C3490. Lardeux C. Use of the SVM Classification with Polarimetric SAR Data for Land Use Cartography. / Lardeux C., Frison P.-L., Rudant J.-P., Souyris J.-C., Tison C., Stoll B. // 2006. IGARSS 2006. IEEE International Conference on Geoscience and Remote Sensing Symposium. - Denver, CO, July 31 2006-Aug. 4 2006. - P. 493-496. ↑

C3491. Schuler D.L. Polarimetric SAR Detection of Man-Made Structures Using Normalized Circular-pol Correlation Coefficients. / Schuler D.L., Lee J.S., Ainsworth T.L. // 2006. IGARSS 2006. IEEE International Conference on Geoscience and Remote Sensing Symposium. - Denver, CO, July 31 2006-Aug. 4 2006. - P. 485-488. ↑

C3492. Ya-Qiu Jin. The Difference Scattering dRCS from a Dielectric Target above a Rough Surface. / Ya-Qiu Jin, Hongxia Ye. // 2006. IGARSS 2006. IEEE International Conference on Geoscience and Remote Sensing Symposium. - Denver, CO, July 31 2006-Aug. 4 2006. - P. 465-468. ↑

C3493. Voronovich A.G. A Numerical Model of Radar Scattering from Steep and Breaking Waves. / Voronovich A.G., Zavorotny V.U.A. // 2006. IGARSS 2006. IEEE International Conference on Geoscience and Remote Sensing Symposium. - Denver, CO, July 31 2006-Aug. 4 2006. - P. 469-472. ↑

C3494. Moriyama T. The Application of Polarimetric Calibration using Polarimetric Scattering Characteristics of

Urban Areas to ALOS PALSAR. / Moriyama T., Shimada M., Watanabe M., Tadono T. // 2006. IGARSS 2006. IEEE International Conference on Geoscience and Remote Sensing Symposium. - Denver, CO, July 31 2006-Aug. 4 2006. - P. 348-351. ↑

C3495. Bachmann C.M. Modeling Coastal Waters from Hyperspectral Imagery using Manifold Coordinates. / Bachmann C.M., Ainsworth T.L., Gillis D.B., Maness S.J., Montes M.J., Donato T.F., Bowles J.H., Korwan D.R., Fusina R.A., Lamela G.M., Rhea W.J. // 2006. IGARSS 2006. IEEE International Conference on Geoscience and Remote Sensing Symposium. - Denver, CO, July 31 2006-Aug. 4 2006. - P. 356-359. ↑

C3496. Kimura H. Calibration of Spaceborne Polarimetric SAR Data using Polarization Orientation. 2006. IGARSS 2006. IEEE International Conference on Geoscience and Remote Sensing Symposium. - Denver, CO, July 31 2006-Aug. 4 2006. - P. 344-347. ↑

C3497. Ulander L.M.H. ALOS Calibration and Validation Activities in Sweden. / Ulander L.M.H., Eriksson L., Smith Jonforsen G., Fransson J.E.S., Olsson H. // 2006. IGARSS 2006. IEEE International Conference on Geoscience and Remote Sensing Symposium. - Denver, CO, July 31 2006-Aug. 4 2006. - P. 336-339. ↑

C3498. Touzi R. On the use of Symmetric Target Tilt Angle for PALSAR Calibration. / Touzi R., Shimada M., Papathanassiou K., Corr D. // 2006. IGARSS 2006. IEEE International Conference on Geoscience and Remote Sensing Symposium. - Denver, CO, July 31 2006-Aug. 4 2006. - P. 340-343. ↑

C3499. Meta A. Range Non-linearities Correction in FMCW SAR. / Meta A., Hoogeboom P., Ligthart L.P. // 2006. IGARSS 2006. IEEE International Conference on Geoscience and Remote Sensing Symposium. - Denver, CO, July 31 2006-Aug. 4 2006. - P. 403-406. ↑

C3500. Zaugg E.C. The BYU SAR: A Small, Student-Built SAR for UAV Operation. / Zaugg E.C., Hudson D.L., Long D.G. // 2006. IGARSS 2006. IEEE International Conference on Geoscience and Remote Sensing Symposium. - Denver, CO, July 31 2006-Aug. 4 2006. - P. 411-414. ↑

C3501. Feng Xu. Mapping and Projection Algorithm: A New Approach to SAR Imaging Simulation for Comprehensive Terrain Scene. / Feng Xu, Ya-Qiu Jin. // 2006. IGARSS 2006. IEEE International Conference on Geoscience and Remote Sensing Symposium. - Denver, CO, July 31 2006-Aug. 4 2006. - P. 399-402. ↑

C3502. Tello M. Automatic Detection of Spots and Extraction of Frontiers in SAR Images by Means of the Wavelet Transform: Application to Ship and Coastline Detection. / Tello M., Lopez-Martinez C., Mallorqui J.J., Bonastre R. // 2006. IGARSS 2006. IEEE International Conference on Geoscience and Remote Sensing Symposium. - Denver, CO, July 31 2006-Aug. 4 2006. - P. 383-386. ↑

C3503. Koetz B. Inversion of Combined Radiative Transfer Models for Imaging Spectrometer and LIDAR Data. / Koetz B., Sun G., Morsdorf F., Ranson K.J., Kneubuhler M., Itten K., Allgower B. // 2006. IGARSS 2006. IEEE International Conference on Geoscience and Remote Sensing Symposium. - Denver, CO, July 31 2006-Aug. 4 2006. - P. 395-398. ↑

C3504. Boerner W.-M. Implementation of Differential Repeat-pass SAR Interferometry for the Search for Earthquake Precursory Land-cover Deformation in Taiwan. 2006. IGARSS 2006. IEEE International Conference on Geoscience and Remote Sensing Symposium. - Denver, CO, July 31 2006-Aug. 4 2006. - P. 497-500. ↑

C3505. Shimabukuro Y.E. Meso-Scale Variability of Soils and Forest Canopy Properties is Connected to Geomorphologic Features in Eastern Amazonia. / Shimabukuro Y.E., Aragao L.E.O., Williams M. // 2006. IGARSS 2006. IEEE International Conference on Geoscience and Remote Sensing Symposium. - Denver, CO, July 31 2006-Aug. 4 2006. - P. 675-678. ↑

C3506. Doubkova M. Synergistic use of AMSR-E and MODIS Data for Understanding Grassland Land Surface Phenologies. / Doubkova M., Henebry G.M. // 2006. IGARSS 2006. IEEE International Conference on Geoscience and Remote Sensing Symposium. - Denver, CO, July 31 2006-Aug. 4 2006. - P. 683-685. ↑

C3507. Mei Xin. Monitoring of Tobacco Planted Acreage Based on Multiple Remote Sensing Sources. / Mei Xin, Cui Weihong, Zhang Xuexia, Zhao Na, Niu Zhenguo. // 2006. IGARSS 2006. IEEE International Conference on Geoscience and Remote Sensing Symposium. - Denver, CO, July 31 2006-Aug. 4 2006. - P. 668-670. ↑

C3508. George J. Networking CSU-CHILL and CSU-Pawnee to Form a Bistatic Radar System. / George J., Brunkow D., Chandrasekar V. // 2006. IGARSS 2006. IEEE International Conference on Geoscience and

Remote Sensing Symposium. - Denver, CO, July 31 2006-Aug. 4 2006. - P. 656-659. ↑

C3509. Bharadwaj N. Waveform Design for First Generation CASA Testbed. / Bharadwaj N., Chandrasekar V. // 2006. IGARSS 2006. IEEE International Conference on Geoscience and Remote Sensing Symposium. - Denver, CO, July 31 2006-Aug. 4 2006. - P. 660-663. ↑

C3510. Simila M. C-Band SAR Based Estimation of Baltic Sea Ice Thickness Distributions. / Simila M., Karvonen J., Haas C., Hallikainen M. // 2006. IGARSS 2006. IEEE International Conference on Geoscience and Remote Sensing Symposium. - Denver, CO, July 31 2006-Aug. 4 2006. - P. 710-713. ↑

C3511. Hudier E. Low Back-scattering Bands Paralleling Pressure Ridges on First Year Sea-Ice. 2006. IGARSS 2006. IEEE International Conference on Geoscience and Remote Sensing Symposium. - Denver, CO, July 31 2006-Aug. 4 2006. - P. 731-734. ↑

C3512. Graf T. Assimilating Passive Microwave Brightness Temperature Data into a Land Surface Model to Improve the Snow Depth Predictability. / Graf T., Koike T., Xin Li, Hirai M., Tsutsui H. // 2006. IGARSS 2006. IEEE International Conference on Geoscience and Remote Sensing Symposium. - Denver, CO, July 31 2006-Aug. 4 2006. - P. 706-709. ↑

C3513. Hambaryan A. A Complex of Multi-Frequency at 3GHz, 5.6GHz, 20GHz and 37GHz, Polarimetric, Combined, Short Pulse, Short Range Action Radar- Radiometers for Soil and Snow Remote Sensing and Surveillance. / Hambaryan A., Arakelyan A.K., Manukyan M.R., Karyan V.V., Hovhannisyan G.G., Darbinyan S. // 2006. IGARSS 2006. IEEE International Conference on Geoscience and Remote Sensing Symposium. - Denver, CO, July 31 2006-Aug. 4 2006. - P. 698-701. ↑

C3514. Kumar V. Analysis of Aqua AMSR-E Derived Snow Water Equivalent over Himalayan Snow Covered Regions. / Kumar V., Rao Y.S., Venkataraman G., Sarwade R.N., Snehmani. // 2006. IGARSS 2006. IEEE International Conference on Geoscience and Remote Sensing Symposium. - Denver, CO, July 31 2006-Aug. 4 2006. - P. 702-705. ↑

C3515. Bovith T. Detecting Weather Radar Clutter by Information Fusion With Satellite Images and Numerical Weather Prediction Model Output. / Bovith T., Nielsen A.A., Hansen L.K., Overgaard S., Gill R.S. // 2006. IGARSS 2006. IEEE International Conference on Geoscience and Remote Sensing Symposium. - Denver, CO, July 31 2006-Aug. 4 2006. - P. 511-514. ↑

C3516. Kobayashi S. Time-dependent Second Order Scattering Theory for a Weather Radar with a Finite Beam Width. / Kobayashi S., Tanelli S., Im E., Ito S., Oguchi T. // 2006. IGARSS 2006. IEEE International Conference on Geoscience and Remote Sensing Symposium. - Denver, CO, July 31 2006-Aug. 4 2006. - P. 515-518. ↑

C3517. Wanyu Li. Sensitivity of Dual-Frequency Rain DSD Retrieval to Particles in Melting Layer for Spaceborne Radars. / Wanyu Li, Chandrasekar V., Thurai M. // 2006. IGARSS 2006. IEEE International Conference on Geoscience and Remote Sensing Symposium. - Denver, CO, July 31 2006-Aug. 4 2006. - P. 507-510. ↑

C3518. Burini A. Multi-temporal High-resolution Polarimetric L-band SAR Observation of a Wine-producing Landscape. / Burini A., Del Frate F., Minchella A., Schiavon G., Solimini D., Bianchi R., Fusco L., Horn R. // 2006. IGARSS 2006. IEEE International Conference on Geoscience and Remote Sensing Symposium. - Denver, CO, July 31 2006-Aug. 4 2006. - P. 501-503. ↑

C3519. Putignano C. Self-organizing Neural Networks for Unsupervised Classification of Polarimetric SAR Data on Complex Landscapes. / Putignano C., Schiavon G., Solimini D., Trisasongko B. // 2006. IGARSS 2006. IEEE International Conference on Geoscience and Remote Sensing Symposium. - Denver, CO, July 31 2006-Aug. 4 2006. - P. 504-506. ↑

C3520. Hefner E. Oversampling and Whitening with the CASA Radar. / Hefner E., Chandrasekar V. // 2006. IGARSS 2006. IEEE International Conference on Geoscience and Remote Sensing Symposium. - Denver, CO, July 31 2006-Aug. 4 2006. - P. 648-651. ↑

C3521. Nguyen C.M. Precipitation Spectral Moments Estimation and Clutter Mitigation using Parametric Time Domain Model. / Nguyen C.M., Moiseev D.N., Chandrasekar V. // 2006. IGARSS 2006. IEEE International Conference on Geoscience and Remote Sensing Symposium. - Denver, CO, July 31 2006-Aug. 4 2006. - P. 652-655. ↑

- C3522.** Yuei-An Liou. Two-year Microwave Radiometric Observations of Low-level Boundary-layer Temperature Inversion Signatures. / Yuei-An Liou, Shiang-Kun Yan. // 2006. IGARSS 2006. IEEE International Conference on Geoscience and Remote Sensing Symposium. - Denver, CO, July 31 2006-Aug. 4 2006. - P. 644-647. ↑
- C3523.** Hubbert J.C. Differential Reflectivity Calibration for NEXRAD. / Hubbert J.C., Pratte F. // 2006. IGARSS 2006. IEEE International Conference on Geoscience and Remote Sensing Symposium. - Denver, CO, July 31 2006-Aug. 4 2006. - P. 519-522. ↑
- C3524.** Qing Cao. Characterization of Rain Microphysics based on Disdrometer and Polarimetric Radar Observations. / Qing Cao, Guifu Zhang, Schuur T., Ryzhkov A., Brandes E., Ikeda K. // 2006. IGARSS 2006. IEEE International Conference on Geoscience and Remote Sensing Symposium. - Denver, CO, July 31 2006-Aug. 4 2006. - P. 523-528. ↑
- C3525.** A.N. Oleynikov. Measurement of the Mesopause Dynamic Parameters of Lower Thermosphere using Accessible Radio Frequency Resources. / A. N. Oleynikov, D. M. Sosnovchik. // 2006. CriMiCO '06. 16th International Crimean Conference Microwave and Telecommunication Technology. - Sevastopol, Crimea, Sept. 2006. - Vol. 2. - P. 969-970. ↑
- C3526.** K.P. Garmash. The facility for Remote Sensing of the Near-Earth Space Environment. / K. P. Garmash, L. S. Kostrov, V. T. Rozumenko, A. M. Tsybal, O. F. Tyrnov. // 2006. CriMiCO '06. 16th International Crimean Conference Microwave and Telecommunication Technology. - Sevastopol, Crimea, Sept. 2006. - Vol. 2. - P. 954-955. ↑
- C3527.** Jeannin N. Modeling of rain fields at large scale. / Jeannin N., Feral L., Sauvageot H., Castanet L., Lemorton J. // 2006 International Workshop on Satellite and Space Communications. - Madrid, 14-15 Sept. 2006. - P. 233-236. ↑
- C3528.** A.A. Khrustalev. Research Airborne System for Remote Sensing in MM-Range of Radiowaves. / A. A. Khrustalev, S. N. Egorov. // 2006. CriMiCO '06. 16th International Crimean Conference Microwave and Telecommunication Technology. - Sevastopol, Crimea, Sept. 2006. - Vol. 2. - P. 1001-1002. ↑
- C3529.** Huang Liang. Ionospheric Interference Suppression in HFSWR. / Huang Liang, Wen Biyang, Yao Min. // 2006 1ST IEEE Conference on Industrial Electronics and Applications. - Singapore, 24-26 May 2006. - P. 1-4. ↑
- C3530.** Yang D.K. Design and Realization of Delay Mapping Receiver Based on GPS for Sea Surface Wind Measurement. / Yang D.K., Zhang Q.S., Zhang Y.Q., Hu R.L. // 2006 1ST IEEE Conference on Industrial Electronics and Applications. - Singapore, 24-26 May 2006. - P. 1-4. ↑
- C3531.** {no data available}. To the 60-year anniversary of Vladimir Vladimirovich Pustovoytenko. 2006. CriMiCO '06. 16th International Crimean Conference Microwave and Telecommunication Technology. - Sevastopol, Sept. 2006. - Vol. 1. - P. K. ↑
- C3532.** Fuhrmann D.R. Structured Covariance Estimation: Theory, Application, and Recent Results. 2006. Fourth IEEE Workshop on Sensor Array and Multichannel Processing. - Waltham, MA, 12-14 July 2006. - P. 0-62. ↑
- C3533.** Contarino V.M. Neuro-Fuzzy Model for Multi-Channel Underwater Imaging. / Contarino V.M., Molchanov P.A., Petrosyuk I.M., Podobna Y.Y., Asmolova O.V. // 2006. Fourth IEEE Workshop on Sensor Array and Multichannel Processing. - Waltham, MA, 12-14 July 2006. - P. 651-654. ↑
- C3534.** Mishra A.K. Radar Signal Classification Using Pca-Based Features. / Mishra A.K., Mulgrew B. // 2006. ICASSP 2006 Proceedings. 2006 IEEE International Conference on Acoustics, Speech and Signal Processing. - Toulouse, 14-19 May 2006. - Vol. 3. - P. III. ↑
- C3535.** Siegel P.H. Antennas for terahertz applications. / Siegel P.H., de Maagt P., Zaghloul A.I. // IEEE Antennas and Propagation Society International Symposium 2006. - Albuquerque, NM, 9-14 July 2006. - P. 2383-2386. ↑
- C3536.** Titar V.P. Mobile Holographic Lidar. / Titar V.P., Shpachenko O.V., Yartsev V.I. // 8-th International Conference on Laser and Fiber-Optical Networks Modeling. - Kharkiv, June 29 2006-July 1 2006. - P. 187-190. ↑



- C3537.** Kona K.S. Parametric Study of Stacked Patch Array Configurations as Alternative Feeds for Offset Reflectors. / Kona K.S., Bahadori K., Rahmat-Samii Y. // IEEE Antennas and Propagation Society International Symposium 2006. - Albuquerque, NM, 9-14 July 2006. - P. 4331-4334.
- C3538.** Simpson J.J. Proposal for an ELF Radar of D-Region Ionospheric Anomalies Analyzed using a 3-D Geodesic FDTD Model of the Earth-Ionosphere Waveguide. / Simpson J.J., Taflove A. // IEEE Antennas and Propagation Society International Symposium 2006. - Albuquerque, NM, 9-14 July 2006. - P. 3491-3494.
- C3539.** Ditzel M. Low-power Radar for Wireless Sensor Networks. / Ditzel M., Elferink F.H. // 2006. EuRAD 2006. 3rd European Radar Conference. - Manchester, 13-15 Sept. 2006. - P. 139-141.
- C3540.** Fratini M. An Interferometric CW-SF Radar for Remote Testing and Monitoring Large Structures. / Fratini M., Pieraccini M., Parrini F., Bernardini G., Atzeni C. // 2006. EuRAD 2006. 3rd European Radar Conference. - Manchester, 13-15 Sept. 2006. - P. 135-138.
- C3541.** {no data available}. 3rd European Radar Conference. 2006. EuRAD 2006. 3rd European Radar Conference. - Manchester, UK, Sept. 2006. - P. 1-15.
- C3542.** Kolyadov D.V. Amplitude-phase method allowing the determination of the complex dielectric permittivity of underlying surfaces using polarimetric radar remote sensing. / Kolyadov D.V., Ligthart L.P., Kozlov A.I. // 2006. EuRAD 2006. 3rd European Radar Conference. - Manchester, 13-15 Sept. 2006. - P. 142-145.
- C3543.** Sinitsyn R.B. Projection Approach for Estimating Radar Signal Multivariate Probability Density. 2006. EuRAD 2006. 3rd European Radar Conference. - Manchester, 13-15 Sept. 2006. - P. 178-181.
- C3544.** Yanovsky F.J. Airborne Weather Radar as Instrument for Remote Sensing of the Atmosphere. 2006. EuRAD 2006. 3rd European Radar Conference. - Manchester, 13-15 Sept. 2006. - P. 162-165.
- C3545.** Macfarlane D.G. A 94GHz real aperture 3D imaging radar. / Macfarlane D.G., Robertson D.A. // 2006. EuRAD 2006. 3rd European Radar Conference. - Manchester, 13-15 Sept. 2006. - P. 154-157.
- C3546.** Subhasri Duttgupta. Distributed Boundary Estimation using Sensor Networks. / Subhasri Duttgupta, Krithi Ramamritham, Parmesh Ramanathan. // 2006 IEEE International Conference on Mobile Adhoc and Sensor Systems (MASS). - Vancouver, BC, Oct. 2006. - P. 316-325.
- C3547.** Moser G. Unsupervised Change-Detection from Multi-Channel SAR Data. / Moser G., Serpico S.B. // 2006. NORSIG 2006. Proceedings of the 7th Nordic Signal Processing Symposium. - Reykjavik, 7-9 June 2006. - P. 246-249.
- C3548.** Zhang Q.P. Non-Clear Typhoon Eye Tracking by Artificial Ant Colony. / Zhang Q.P., Lai H., Wei H., Zong X.F. // 2006 International Conference on Machine Learning and Cybernetics. - Dalian, China, 13-16 Aug. 2006. - P. 4063-4068.
- C3549.** Marek B. Zaremba. Fusion of High-Resolution Satellite and Lidar Data for Individual Tree Recognition. / Marek B. Zaremba, Francois A. Gougeon. // 2006. CCECE '06. Canadian Conference on Electrical and Computer Engineering. - Ottawa, Ont., May 2006. - P. 1112-1115.
- C3550.** {no data available}. EuRAD 2006 Sessions. 2006. EuRAD 2006. 3rd European Radar Conference. - Manchester, UK, Sept. 2006. - P. nil12.
- C3551.** {no data available}. Proceedings of the 3rd European Radar Conference. 2006. EuRAD 2006. 3rd European Radar Conference. - Manchester, 13-15 Sept. 2006. - P. nil2.
- C3552.** LaBelle R. Space Qualification of W-band Devices for the CloudSat Cloud Profiling Radar. 2006. 36th European Microwave Conference. - Manchester, 10-15 Sept. 2006. - P. 1469-1472.
- C3553.** Lukin V.V. Processing Multichannel Radar Images by Modified Vector Sigma Filter FIR Edge Detection. / Lukin V.V., Tsymbal O.V., Vozel B., Chehdi K. // 2006. ICASSP 2006 Proceedings. 2006 IEEE International Conference on Acoustics, Speech and Signal Processing. - Toulouse, 14-19 May 2006. - Vol. 2. - P. II.

- C3554.** Sahba K. MicroPhotonic remote sensor for perimeter security. / Sahba K., Alameh K.E., Smith C. // 2006. DELTA 2006. Third IEEE International Workshop on Electronic Design, Test and Applications. 17-19 Jan. 2006. - P. 6 ↑
- C3555.** Maarten Uijt de Haag. Application of laser range scanner based terrain referenced navigation systems for aircraft guidance. / Maarten Uijt de Haag, Vadlamani A., Campbell J.L., Dickman J. // 2006. DELTA 2006. Third IEEE International Workshop on Electronic Design, Test and Applications. - Kuala Lumpur, 17-19 Jan. 2006. - P. 6 P.-274. ↑
- C3556.** Xiaojuan Zhang. Dual-frequency SAR for the measurement of soil moisture at depth. / Xiaojuan Zhang, Wenji Zhang, Xiaorong Lu, Gaojian Kang, Guangyou Fang. // 2006. APMC 2006. Asia-Pacific Microwave Conference. - Yokohama, 12-15 Dec. 2006. - P. 556-559. ↑
- C3557.** Yanming Xiao. A Ka-Band Low Power Doppler Radar System for Remote Detection of Cardiopulmonary Motion. / Yanming Xiao, Jenshan Lin, Boric-Lubecke O., Lubecke V.M. // 2005. IEEE-EMBS 2005. 27th Annual International Conference of the Engineering in Medicine and Biology Society. - Shanghai, 17-18 Jan. 2006. - P. 7151-7154. ↑
- C3558.** Awada A. Bistatic radar scattering from an ocean surface at L-band. / Awada A., Khenchaf A., Coatanhay A. // 2006 IEEE Conference on Radar. 24-27 April 2006. - P. 8 ↑
- C3559.** Elachi C. The legacy and future of civilian radar missions. 2006 IEEE Conference on Radar. 24-27 April 2006. - P. 0_16-0_19. ↑
- C3560.** Gray J.E. Computing the characteristic function for sums of sinusoidal random variables. / Gray J.E., Addison S.R. // 2006. SSST '06. Proceeding of the Thirty-Eighth Southeastern Symposium on System Theory. - Cookeville, TN, 5-7 March 2006. - P. 338-343. ↑
- C3561.** Abshire J.B. Laser pulses from earth detected at Mars. / Abshire J.B., Xiaoli Sun, Neumann G., McGarry J., Zagwodzki T., Jester P., Riris H., Zuber M., Smith D. // 2006 and 2006 Quantum Electronics and Laser Science Conference. CLEO/QELS 2006. Conference on Lasers and Electro-Optics. - Long Beach, CA, 21-26 May 2006. - P. 1-2. ↑
- C3562.** Riris H. A 1.57 μ m DIAL lidar system for range resolved measurements of atmospheric CO₂. / Riris H., Burris J., Krainak M., Sun X., Abshire J. // 2006 and 2006 Quantum Electronics and Laser Science Conference. CLEO/QELS 2006. Conference on Lasers and Electro-Optics. - Long Beach, CA, 21-26 May 2006. - P. 1-2. ↑
- C3563.** Ruifang Zhai. Seamless Registration of Multiple Range Images with Whole Block Adjustment. / Ruifang Zhai, Jianqing Zhang, Shunyi Zheng. // 2006. IMSCCS '06. First International Multi-Symposiums on Computer and Computational Sciences. - Hanzhou, Zhejiang, 20-24 June 2006. - Vol. 1. - P. 753-758. ↑
- C3564.** Gasmi T. Behavior of DIAL remote sensed ethylene and ozone in presence of nitrogen oxides. 2006 and 2006 Quantum Electronics and Laser Science Conference. CLEO/QELS 2006. Conference on Lasers and Electro-Optics. - Long Beach, CA, 21-26 May 2006. - P. 1-2. ↑
- C3565.** Sorrentino R. Electronic steerable MEMS antennas. / Sorrentino R., Gatti R.V., Marcaccioli L., Mencagli B. // 2006. EuCAP 2006. First European Conference on Antennas and Propagation. - Nice, 6-10 Nov. 2006. - P. 1-8. ↑
- C3566.** Swann W.C. Frequency-resolved coherent LIDAR using a femtosecond fiber laser. / Swann W.C., Newbury N.R. // 2006 and 2006 Quantum Electronics and Laser Science Conference. CLEO/QELS 2006. Conference on Lasers and Electro-Optics. - Long Beach, CA, 21-26 May 2006. - P. 1-2. ↑
- C3567.** Vasil'ev B.I. Differential absorption lidar using NH₃ -CO₂ laser. / Vasil'ev B.I., Mannoun O.M. // 2006 and 2006 Quantum Electronics and Laser Science Conference. CLEO/QELS 2006. Conference on Lasers and Electro-Optics. - Long Beach, CA, 21-26 May 2006. - P. 1-2. ↑
- C3568.** Serrano N. A novel tiered sensor fusion approach for terrain characterization and safe landing assessment. / Serrano N., Bajracharya M., Howard A., Seraji H. // 2006 IEEE Aerospace Conference. - Big Sky, MT, 2006. - P. 10 ↑
- C3569.** Chamberlain N. The UAVSAR phased array aperture. / Chamberlain N., Zawadzki M., Sadowy G.,

Oakes E., Brown K., Hodges R. // 2006 IEEE Aerospace Conference. - Big Sky, MT, 2006. - P. 13 ↑

C3570. Sekelsky S.M. High power electronic scanning millimeter-wave radar system design. / Sekelsky S.M., Carswell J. // 2006 IEEE Aerospace Conference. - Big Sky, MT, 2006. - P. 6 ↑

C3571. Lambrigtsen B. GeoSTAR: developing a new payload for GOES satellites. 2006 IEEE Aerospace Conference. - Big Sky, MT, 2006. - P. 10 ↑

C3572. Dalmases F. Wideband Optical TTD SAR Antenna. / Dalmases F., Blanch S., Romeu J., Jofre L., Vidal B., Marti J., McKenzie I., Vez E., Santamaria J. // 2006. MELECON 2006. IEEE Mediterranean Electrotechnical Conference. - Malaga, 16-19 May 2006. - P. 336-339. ↑

C3573. Counsell J. Overcoming some of the issues in maintaining large urban area 3D models via a web browser. / Counsell J., Smith S., Richman A. // 2006. IV 2006. Tenth International Conference on Information Visualization. - London, England, 5-7 July 2006. - P. 331-336. ↑

C3574. Ruegg M. Moving target indication with dual frequency millimeter wave SAR. / Ruegg M., Hagelen M., Meier E., Nuesch D. // 2006 IEEE Conference on Radar. - Verona, NY, USA, 2006. - P. 8 ↑

C3575. Tournadre J. Synergy Between Dual-Frequency Altimeters and Radiometers for Precipitation Studies. / Tournadre J., Piolle J.-F. // 2006 IEEE MicroRad. - SanJuan, 2006. - P. 282-287. ↑

C3576. {no data available}. Proceedings. The 11th International Conference on Mathematical Methods in Electromagnetic Theory (IEEE Cat. No. 06EX1428). 2006 International Conference on Mathematical Methods in Electromagnetic Theory. - Kharkiv, 2006. - P. 1. ↑

C3577. Ghosh D. Extraction of the signature of a buried object using GPR. / Ghosh D., Sarkar T.K. // 2006 IEEE Conference on Radar. 24-27 April 2006. - P. 6 ↑

C3578. Lang R.H. L-Band Active and Passive Sensing of Soil Moisture through Forests. / Lang R.H., Chauhan N., Utku C., Le Vine D.M. // 2006 IEEE MicroRad. - SanJuan, 2006. - P. 193-196. ↑

C3579. Fernandez D.E. IWRAP: the Imaging Wind and Rain Airborne Profiler for remote sensing of the ocean and the atmospheric boundary layer within tropical cyclones. / Fernandez D.E., Chang P.S., Carswell J.R., Contreras R.F., Frasier S.J. // 2006 IEEE Aerospace Conference. - Big Sky, MT, 2006. - P. 7 ↑

C3580. Liebe C.C. Spacecraft hazard avoidance utilizing structured light. / Liebe C.C., Padgett C., Chapsky J., Wilson D., Brown K., Jerebets S., Goldberg H., Schroeder J. // 2006 IEEE Aerospace Conference. - Big Sky, MT, 2006. - P. 10 ↑

C3581. O'Neill P.E. Multi-Sensor Microwave Soil Moisture Remote Sensing: NASA's Combined Radar/Radiometer (ComRAD) System. / O'Neill P.E., Lang R.H., Kurum M., Utku C., Carver K.R. // 2006 IEEE MicroRad. - SanJuan, 2006. - P. 50-54. ↑

C3582. Zhenhua Zhang. A New Approach to Improve Coherence in SAR/GMTI Processing of Distributed Micro-satellites Systems. / Zhenhua Zhang, Tong Wang, Jinshan Ding, Zheng Bao. // 2006. CIE '06. International Conference on Radar. - Shanghai, 16-19 Oct. 2006. - P. 1-4. ↑

C3583. Ramalho G.L.B. Using Boosting to Improve Oil Spill Detection in SAR Images. / Ramalho G.L.B., Medeiros F.N.S. // 2006. ICPR 2006. 18th International Conference on Pattern Recognition. - Hong Kong, 2006. - Vol. 2. - P. 1066-1069. ↑

C3584. Qiaoping Zhang. Comparing Different Localization Approaches of the Radon Transform for Road Centerline Extraction from Classified Satellite Imagery. / Qiaoping Zhang, Couloigner I. // 2006. ICPR 2006. 18th International Conference on Pattern Recognition. - Hong Kong, 2006. - Vol. 2. - P. 138-141. ↑

C3585. Fang Wei. Research and Application on Real-time Acquirement Technique of OpenFlight Digital Terrain Based On Grid. / Fang Wei, He You, Jiang BenQing. // 2006. CIE '06. International Conference on Radar. - Shanghai, 16-19 Oct. 2006. - P. 1-4. ↑

C3586. Xiong Tao. A New Approach for DEM Generation Based on Polarimetric SAR Interferometry. / Xiong Tao, Yang Jian, Peng Yingning. // 2006. CIE '06. International Conference on Radar. - Shanghai, 16-19 Oct.

2006. - P. 1-4. ↑

C3587. Zuo Yanjun. Signal Processing Method for Distributed SAR Imaging Improvement. / Zuo Yanjun, Yang Ruliang. // 2006. CIE '06. International Conference on Radar. - Shanghai, 16-19 Oct. 2006. - P. 1-4. ↑

C3588. Xiaodong Zhou. A perceptive uniform pseudo-color coding method of SAR images. / Xiaodong Zhou, Chunhua Zhang. // 2006. CIE '06. International Conference on Radar. - Shanghai, 16-19 Oct. 2006. - P. 1-4. ↑

C3589. Yang L. Topography Adaptive Filtering of Phase Image Based On Residue Matrix. / Yang L., Feng Q., Wang Z. // 2006 8th International Conference on Signal Processing. 16-20 2006. - Vol. 2. - {no data available}. ↑

C3590. Yilun Chen. Novel Method for SAR Image Segmentation with Application to Bridge Detection. / Yilun Chen, Jiong Chen, Jian Yang. // 2006 8th International Conference on Signal Processing. 16-20 Nov. 2006. - Vol. 2. - {no data available}. ↑

C3591. Ward Keith. High Resolution Radar Imaging of the Sea Surface. / Ward Keith, Tough Robert. // 2006. The Institution of Engineering and Technology Seminar on High Resolution Imaging and Target Classification. - London, 21-21 Nov. 2006. - P. 39-52. ↑

C3592. Bawar Zahid Hasan. Novel Techniques for Error Minimization in SAR RF and Interferometric Signal Processing. / Bawar Zahid Hasan, Teng Long, Zeng Tao. // 2006. RFM 2006. International RF and Microwave Conference. - Putra Jaya, 12-14 Sept. 2006. - P. 169-173. ↑

C3593. Khraisat Y.S.H. Computational Model of the Doppler Spectrum of Radar Returns from Rain. 2006 International Conference on Mathematical Methods in Electromagnetic Theory. - Kharkiv, 2006. - P. 167-169. ↑

C3594. Wenhua Xue. Surface Current Extraction by Onboard High Frequency SAR. / Wenhua Xue, Mingmin Zhang, Jinsong Tang, Shuzong Han. // TENCON 2006. 2006 IEEE Region 10 Conference. - Hong Kong, 14-17 Nov. 2006. - P. 1-4. ↑

C3595. Ostrovsky Y.P. Use of Neural Network for Turbulence and Precipitation Classification Procedure. / Ostrovsky Y.P., Yanovsky F.J. // 2006 International Conference on Mathematical Methods in Electromagnetic Theory. - Kharkiv, 2006. - P. 161-163. ↑

C3596. Ya-Qiu Jin. Polarimetric Radar Pulse Echoes from Lunar Regolith Layer with Scatter Inhomogeneity and Rough Interfaces. / Ya-Qiu Jin, Feng Xu, Wenzhe Fa. // 2006. ISAPE '06. 7th International Symposium on Antennas, Propagation & EM Theory. - Guilin, 26-29 Oct. 2006. - P. 1-4. ↑

C3597. Xiaojin Shi. InSAR Image Registration Using Modified Correlation Coefficient Algorithm. / Xiaojin Shi, Yunhua Zhang, Jingshan Jiang. // 2006. ISAPE '06. 7th International Symposium on Antennas, Propagation & EM Theory. - Guilin, 26-29 Oct. 2006. - P. 1-4. ↑

C3598. Fukuda T. Automatic Land-mine Detection System using Adaptive Sensing with Vector GPR. / Fukuda T., Hasegawa Y., Kawai Y., Sato S., Zakariya Z., Matsuno T. // IECON 2006-32nd Annual Conference on IEEE Industrial Electronics. - Paris, 6-10 Nov. 2006. - P. 4498-4503. ↑

C3599. Ye Yunshang. Multi-mode Microwave Remote Sensing Antenna Subsystem on Satellites. / Ye Yunshang, Li Yang, Li Quanming. // 2006. ISAPE '06. 7th International Symposium on Antennas, Propagation & EM Theory. - Guilin, 26-29 Oct. 2006. - P. 1-4. ↑

C3600. Li Haiyan. A New Approach for Ship Detection in SAR Imagery Based on Convolution between Different Polarization Channels. / Li Haiyan, He Yijun, Wang Wenguang. // 2006. ISAPE '06. 7th International Symposium on Antennas, Propagation & EM Theory. - Guilin, 26-29 Oct. 2006. - P. 1-4. ↑

C3601. Yongpin Chen. Preconditioned Multilevel Fast Inhomogeneous Plane Wave Algorithm for Solving Electromagnetic Scattering Problems. / Yongpin Chen, Jun Hu, Zaiping Nie, Min Meng. // 2006. ISAPE '06. 7th International Symposium on Antennas, Propagation & EM Theory. - Guilin, 26-29 Oct. 2006. - P. 1-3. ↑

C3602. El-Ocla H. Laser Radar Cross-Section of Conducting Targets Using Horizontal Polarization. 2006. ISAPE '06. 7th International Symposium on Antennas, Propagation & EM Theory. - Guilin, 26-29 Oct. 2006. - P. 1-4. ↑

- C3603.** Zhang Fan. Analysis of Squint Angle in Point Target Assessment. / Zhang Fan, Hong Wen. // 2006. CIE '06. International Conference on Radar. - Shanghai, 16-19 Oct. 2006. - P. 1-4. ↑
- C3604.** Shun-sheng Zhang. Research on Echo Simulation of Space-borne Bistatic SAR. / Shun-sheng Zhang, Teng Long, Tao Zeng, Juan Chen. // 2006. CIE '06. International Conference on Radar. - Shanghai, 16-19 Oct. 2006. - P. 1-4. ↑
- C3605.** Minghong Xie. Building Recognition and Reconstruction from Aerial Imagery and LIDAR Data. / Minghong Xie, Kun Fu, Yirong Wu. // 2006. CIE '06. International Conference on Radar. - Shanghai, 16-19 Oct. 2006. - P. 1-4. ↑
- C3606.** Mingxin Nie. A Novel Fusion and Target Detection Method of Airborne SAR Images and Optical Images. / Mingxin Nie, Ling Lu, Wei Xu. // 2006. CIE '06. International Conference on Radar. - Shanghai, 16-19 Oct. 2006. - P. 1-4. ↑
- C3607.** Chen Baixiao. Experimental System and Experimental Results for Coast-ship Bi/multistatic Ground-wave Over-the-horizon Radar. / Chen Baixiao, Chen Duofang, Zhang Shouhong, Zhang Hao, Liu Maocang. // 2006. CIE '06. International Conference on Radar. - Shanghai, 16-19 Oct. 2006. - P. 1-5. ↑
- C3608.** Longmei Xi. A Kind of Dual-Channel GMTI Real-Time Processing Method Based on Frequency DPCA. / Longmei Xi, Changyao Zhang. // 2006. CIE '06. International Conference on Radar. - Shanghai, 16-19 Oct. 2006. - P. 1-4. ↑
- C3609.** Wang Yang. A New Algorithm of Target Classification Based on Maximum and Minimum Polarizations. / Wang Yang, Lu Jiaguo, Zhang Changyao. // 2006. CIE '06. International Conference on Radar. - Shanghai, 16-19 Oct. 2006. - P. 1-4. ↑
- C3610.** Robertson Duncan A. High Performance MM-Wave Radar Techniques. / Robertson Duncan A., Macfarlane David G., Cruickshank Paul A.S., Bolton David R., Hunter Robert I., Smith Graham M. // 2006. The Institution of Engineering and Technology Seminar on MM-Wave Products and Technologies. - London, 16-16 Nov. 2006. - P. 19-26. ↑
- C3611.** Xin Kang. Automatic SAR Image Registration by Using Element Triangle Invariants. / Xin Kang, Chongzhao Han, Yi Yang. // 2006 9th International Conference on Information Fusion. - Florence, 10-13 July 2006. - P. 1-7. ↑
- C3612.** Ticha M.B.B. A case based reasoning data fusion scheme: application to offshore wind energy resource mapping. / Ticha M.B.B., Ranchin T. // 2006 9th International Conference on Information Fusion. - Florence, 10-13 July 2006. - P. 1-5. ↑
- C3613.** Kurekin A. Assessment of Soil Parameter Estimation Errors for Fusion of Multichannel Radar Measurements. / Kurekin A., Marshall D., Radford D., Lever K., Kulemin G. // 2006 9th International Conference on Information Fusion. - Florence, 10-13 July 2006. - P. 1-8. ↑
- C3614.** Pugh M. Assessment of Multi-Sensor Neural Image Fusion and Fused Data Mining for Land Cover Classification. / Pugh M., Waxman A., Fay D. // 2006 9th International Conference on Information Fusion. - Florence, 10-13 July 2006. - P. 1-8. ↑
- C3615.** Romeiser R. Status Report on Predicted Current Measuring Capabilities of the Upcoming German Satellite TerraSAR-X. / Romeiser R., Runge H. // OCEANS 2006. - Boston, MA, 18-21 Sept. 2006. - P. 1-6. ↑
- C3616.** Ahn J.M.V. Ocean Surface Winds from Space-A Collaborative Education Effort. / Ahn J.M.V., Jelenak Z., Sienkiewicz J.M., Brennan M.J. // OCEANS 2006. - Boston, MA, 18-21 Sept. 2006. - P. 1-6. ↑
- C3617.** Yong-an Zheng. Fusion of Multi-band SAR Images Based on Contourlet Transform. / Yong-an Zheng, Changsheng Zhu, Jianshe Song, Xunhui Zhao. // 2006 IEEE International Conference on Information Acquisition. - Shandong, 20-23 Aug. 2006. - P. 420-424. ↑
- C3618.** Xiaoguang Zhao. A Remote Aerial Robot for Topographic Survey. / Xiaoguang Zhao, Jing Liu, Min Tan. // 2006 IEEE/RSJ International Conference on Intelligent Robots and Systems. - Beijing, 9-15 Oct. 2006. - P. 3143-3148. ↑

- C3619.** Ivanov V.K. Radar Remote Sensing Images Segmentation Using Fractal Dimension Field. / Ivanov V.K., Paschenko R.E., Stadnyk O.M., Yatsevich S.Ye. // 2006. EuRAD 2006. 3rd European Radar Conference. - Manchester, 13-15 Sept. 2006. - P. 217-220. ↑
- C3620.** Holliday R. A lightweight, ultra wideband polarimetric W-band radar with high resolution for environmental applications. / Holliday R., Rhys-Roberts M., Wynn D.A. // 2006. EuRAD 2006. 3rd European Radar Conference. - Manchester, 13-15 Sept. 2006. - P. 194-197. ↑
- C3621.** Su Limin. SAR Model Based Regularization Methods for Image Texture Classification. / Su Limin, Wang Yaowei, Wang Yanfei. // 2006. CCC 2006. Chinese Control Conference. - Harbin, 7-11 Aug. 2006. - P. 1857-1861. ↑
- C3622.** Rui Hu. Remote Sensing Target Recognition Based on Contourlet and Kernel Fisher Discriminant. / Rui Hu, Licheng Jiao, Weida Zhou, Yi Gao. // 2006 International Conference on Computational Intelligence and Security. - Guangzhou, 3-6 Nov. 2006. - Vol. 2. - P. 1716-1721. ↑
- C3623.** Yun Yang. Level Set Evolution Based Logic Fusion: A Novel Man-made Objects Segmentation from Radar Image. / Yun Yang, Hongchao Ma. // 2006 International Conference on Computational Intelligence and Security. - Guangzhou, 3-6 Nov. 2006. - Vol. 2. - P. 1700-1705. ↑
- C3624.** Zhang Qun. Separation of Micro-Doppler Signal Using an Extended Hough Transform. / Zhang Qun, Guan Hua, Guo Ying, Bai Youqing. // 2006 International Conference on Communications, Circuits and Systems Proceedings. - Guilin, June 2006. - Vol. 1. - P. 361-365. ↑
- C3625.** Yilun Chen. Detection of Roads in SAR Images using Particle Filter. / Yilun Chen, Qiong Yang, Yuantao Gu, Jian Yang. // 2006 IEEE International Conference on Image Processing. - Atlanta, GA, 8-11 Oct. 2006. - P. 2337-2340. ↑
- C3626.** {no data available}. 2006 IEEE International Conference on Image Processing. 2006 IEEE International Conference on Image Processing. - Atlanta, GA, 8-11 Oct. 2006. - P. i. ↑
- C3627.** Usman M. A Remote Imaging System Based on Reflected GPS Signals. / Usman M., Armitage D.W. // 2006 International Conference on Advances in Space Technologies. - Islamabad, 2-3 Sept. 2006. - P. 173-178. ↑
- C3628.** Bustos J.P. Matching Radar and Satellite Images Employing the Hausdorff Distance for Ship Positioning and Trajectory Estimation. / Bustos J.P., Donoso F., Guesalaga A., Torres M. // 2006 IEEE International Conference on Image Processing. - Atlanta, GA, 8-11 Oct. 2006. - P. 2797-2800. ↑
- C3629.** Beasley Patrick. Tarsier™, a unique Radar for Helping to keep Debris off Airport Runways. 2006. The Institution of Engineering and Technology Seminar on The Future of Civil Radar. - London, 15-15 June 2006. - P. 11-28. ↑
- C3630.** Oka K. Measurement of Speed, Height and Direction of SeaWaves Using Optical Range Sensors. / Oka K., Kouno S., Tanaka S. // 2006. International Joint Conference SICE-ICASE. - Busan, 18-21 Oct. 2006. - P. 1980-1985. ↑
- C3631.** Shkvarko Y.V. Unifying the Experiment Design and Constrained Regularization Paradigms for Reconstructive Imaging with Remote Sensing Data. / Shkvarko Y.V., Leyva-Montiel J.L., Villalon-Turrubiates I.E. // 2006 IEEE International Conference on Image Processing. - Atlanta, GA, 8-11 Oct. 2006. - P. 3241-3244. ↑
- C3632.** Schorstein K. Towards a Brillouin-LIDAR for remote sensing of the temperature profile in the ocean. / Schorstein K., Popescu A., Scheich G., Walther T., Fry E.S. // OCEANS 2006. - Boston, MA, 18-21 Sept. 2006. - P. 1-6. ↑
- C3633.** Schofield O. Studying the Dynamics and Biological Significance of the Hudson River Using an Ocean Observatory. / Schofield O., Glenn S., Kahl A., Kohut J., Oliver M., Chant R. // OCEANS 2006. - Boston, MA, 18-21 Sept. 2006. - P. 1-5. ↑
- C3634.** Chaillan F. On the use of the stochastic matched filter for ship wake detection in SAR images. / Chaillan F., Courmontagne P. // OCEANS 2006. - Boston, MA, 18-21 Sept. 2006. - P. 1-6. ↑
- C3635.** Weissman D.E. SeaWinds Scatterometer Wind Vector Retrievals for Hurricane Claudette Using AMSR

and NEXRAD To Perform Corrections for Precipitation Effects: Comparison of AMSR and NEXRAD retrievals of rain. OCEANS 2006. - Boston, MA, 18-21 Sept. 2006. - P. 1-9. ↑

C3636. Ahmed M. Satellite-aided Search and Rescue (SAR) System. 2006 International Conference on Advances in Space Technologies. - Islamabad, 2-3 Sept. 2006. - P. 43-48. ↑

C3637. Santos Lopez-Estrada. Decision Tree Based FPGA-Architecture for Texture Sea State Classification. / Santos Lopez-Estrada, Rene Cumplido. // 2006. ReConFig 2006. IEEE International Conference on Reconfigurable Computing and FPGA's. - San Luis Potosi, Sept. 2006. - P. 1-7. ↑

C3638. A.G. Yarovoy. UWB Radars for Challenging Applications. / A. G. Yarovoy, L. P. Ligthart. // The Third International Conference Ultrawideband and Ultrashort Impulse Signals. - Sevastopol, Sept. 2006. - P. 50-55. ↑

C3639. Mura J.C. A New Unified Approach to Channel Imbalance and Cross-Talk Calibration of Polarimetric Data. / Mura J.C., Correia A.H., Freitas C.C. // 2006. IGARSS 2006. IEEE International Conference on Geoscience and Remote Sensing Symposium. - Denver, CO, July 31 2006-Aug. 4 2006. - P. 1281-1283. ↑

C3640. Fan J. Monitoring Urban Subsidence in the City of Tianjin (China) by Differential SAR Interferometry. / Fan J., Guo X., Ge D., Liu S., Liu G., Guo H. // 2006. IGARSS 2006. IEEE International Conference on Geoscience and Remote Sensing Symposium. - Denver, CO, USA, July 31 2006-Aug. 4 2006. - P. 3321-3324. ↑

C3641. Zhang W. Moving Target Detection based on Sub-aperture Image. / Zhang W., Peng Y., Li W. // 2006. IGARSS 2006. IEEE International Conference on Geoscience and Remote Sensing Symposium. - Denver, CO, USA, July 31 2006-Aug. 4 2006. - P. 3325-3328. ↑

C3642. Norland R. Differential Interferometric Radar for Mountain Rock Slide Hazard Monitoring. 2006. IGARSS 2006. IEEE International Conference on Geoscience and Remote Sensing Symposium. - Denver, CO, USA, July 31 2006-Aug. 4 2006. - P. 3293-3296. ↑

C3643. Lidicky L. Extended Model of Raw Data Signals for Space-Time Adaptive Processing and Moving Target Indicators. / Lidicky L., Hooeboom P. // 2006. IGARSS 2006. IEEE International Conference on Geoscience and Remote Sensing Symposium. - Denver, CO, USA, July 31 2006-Aug. 4 2006. - P. 3301-3304. ↑

C3644. Bin Z. The Influence of Time and Frequency Synchronism to the ATI Interferometric Phase in the Distributed Satellite SAR System. / Bin Z., Xiaoling Z., Shunji H. // 2006. IGARSS 2006. IEEE International Conference on Geoscience and Remote Sensing Symposium. - Denver, CO, USA, July 31 2006-Aug. 4 2006. - P. 3352-3356. ↑

C3645. Civco D. Characterization of Coastal Wetland Systems using Multiple Remote Sensing Data Types and Analytical Techniques. / Civco D., Hurd J., Prisloe S., Gilmore M. // 2006. IGARSS 2006. IEEE International Conference on Geoscience and Remote Sensing Symposium. - Denver, CO, USA, July 31 2006-Aug. 4 2006. - P. 3442-3446. ↑

C3646. Yang F. Spaceborne Parasitic Multistatic SAR-GMTI by Along-Track Interferometry. / Yang F., Wang M., Liang D. // 2006. IGARSS 2006. IEEE International Conference on Geoscience and Remote Sensing Symposium. - Denver, CO, USA, July 31 2006-Aug. 4 2006. - P. 3342-3344. ↑

C3647. Yousefi A. Statistical Behavior of Multi-Resolution SAR Clutter. / Yousefi A., Liu T., Lampropoulos G. // 2006. IGARSS 2006. IEEE International Conference on Geoscience and Remote Sensing Symposium. - Denver, CO, USA, July 31 2006-Aug. 4 2006. - P. 3345-3348. ↑

C3648. Greidanus H. A Detailed Comparison between Radar and Optical Vessel Signatures. / Greidanus H., Kourti N. // 2006. IGARSS 2006. IEEE International Conference on Geoscience and Remote Sensing Symposium. - Denver, CO, USA, July 31 2006-Aug. 4 2006. - P. 3267-3270. ↑

C3649. Borrión H. One-Dimensional Model-based Approach for ISAR Imaging (2). / Borrión H., Griffiths H., Tait P., Money D., Baker C. // 2006. IGARSS 2006. IEEE International Conference on Geoscience and Remote Sensing Symposium. - Denver, CO, USA, July 31 2006-Aug. 4 2006. - P. 3196-3199. ↑

C3650. Hu Y. ScanSAR Processor Based on Improved k-Algorithm and Workstation Cluster. / Hu Y., Wu Y. // 2006. IGARSS 2006. IEEE International Conference on Geoscience and Remote Sensing Symposium. - Denver,

CO, USA, July 31 2006-Aug. 4 2006. - P. 3200-3203. ↑

C3651. Yu Z. Performance Improvement of the Spaceborne Three-Channel SAR-GMTI System: A Novel Satellite Attitude Steering Technique. / Yu Z., Zhou Y., Chen J., Li C., Pengbo W., Min H. // 2006. IGARSS 2006. IEEE International Conference on Geoscience and Remote Sensing Symposium. - Denver, CO, USA, July 31 2006-Aug. 4 2006. - P. 3184-3187. ↑

C3652. Mei Z. Study on the Correction of Saturated SAR Data. / Mei Z., Yunkai D., Zhimin Z. // 2006. IGARSS 2006. IEEE International Conference on Geoscience and Remote Sensing Symposium. - Denver, CO, USA, July 31 2006-Aug. 4 2006. - P. 3192-3195. ↑

C3653. Yu M. Partial Aperture Effect-Free Doppler Centroid Estimation Method for Airborne Side-looking SAR Based on Range-Doppler Domain Contrast Minimization. / Yu M., Xu J., Peng Y.-N., Xiutan T., Xu B. // 2006. IGARSS 2006. IEEE International Conference on Geoscience and Remote Sensing Symposium. - Denver, CO, USA, July 31 2006-Aug. 4 2006. - P. 3212-3215. ↑

C3654. Pang Y. Model Based Terrain Effect Analyses on ICESat GLAS Waveforms. / Pang Y., Li Z., Lefsky M., Sun G., Yu X. // 2006. IGARSS 2006. IEEE International Conference on Geoscience and Remote Sensing Symposium. - Denver, CO, USA, July 31 2006-Aug. 4 2006. - P. 3232-3235. ↑

C3655. Allan J. Design and Testing of a Java-based Digital SAR Signal Simulation System. / Allan J., Collins M. // 2006. IGARSS 2006. IEEE International Conference on Geoscience and Remote Sensing Symposium. - Denver, CO, USA, July 31 2006-Aug. 4 2006. - P. 3204-3207. ↑

C3656. Milillo G. TD2D and TDEPAR Time Domain SAR Image Processors State of Art, Performance Evaluation and Comparisons. / Milillo G., Serra M., Lore V., Stigliano S., Valentino A. // 2006. IGARSS 2006. IEEE International Conference on Geoscience and Remote Sensing Symposium. - Denver, CO, USA, July 31 2006-Aug. 4 2006. - P. 3208-3211. ↑

C3657. Esch T. Analysis of Urban Land Use Pattern Based on High Resolution Radar Imagery. / Esch T., Roth A., Dech S. // 2006. IGARSS 2006. IEEE International Conference on Geoscience and Remote Sensing Symposium. - Denver, CO, USA, July 31 2006-Aug. 4 2006. - P. 3615-3618. ↑

C3658. Spigai M. Robustness of a Tracking Algorithm for Roads Extraction in Peri-urban Areas. / Spigai M., Fraieu J., Amberg V. // 2006. IGARSS 2006. IEEE International Conference on Geoscience and Remote Sensing Symposium. - Denver, CO, USA, July 31 2006-Aug. 4 2006. - P. 3623-3626. ↑

C3659. Folkesson K. Automatic Detection of Wind-Thrown Forest in VHF SAR Images. / Folkesson K., Hallberg B., Smith-Jonforsen G., Ulander L., Fransson J., Magnusson M. // 2006. IGARSS 2006. IEEE International Conference on Geoscience and Remote Sensing Symposium. - Denver, CO, USA, July 31 2006-Aug. 4 2006. - P. 3599-3602. ↑

C3660. Nakamura K. Wetland Forest Observation and Its Biomass Estimation in Kushiro Wetland by using Multipolarization SAR Data. / Nakamura K., Shinsho H., Wakabayashi H., Uratsuka S., Satake M., Umehara T., Nadai A., Matsuoka T. // 2006. IGARSS 2006. IEEE International Conference on Geoscience and Remote Sensing Symposium. - Denver, CO, USA, July 31 2006-Aug. 4 2006. - P. 3603-3606. ↑

C3661. Cellier F. Hypothesis Management for Building Reconstruction from High Resolution InSAR Imagery. / Cellier F., Oriot H., Nicolas J.-M. // 2006. IGARSS 2006. IEEE International Conference on Geoscience and Remote Sensing Symposium. - Denver, CO, USA, July 31 2006-Aug. 4 2006. - P. 3639-3642. ↑

C3662. Thiele A. Building Recognition Fusing Multi-Aspect High-Resolution Interferometric SAR Data. / Thiele A., Cadario E., Schulz K., Thoennessen U., Soergel U. // 2006. IGARSS 2006. IEEE International Conference on Geoscience and Remote Sensing Symposium. - Denver, CO, USA, July 31 2006-Aug. 4 2006. - P. 3643-3646. ↑

C3663. Tupin F. Fusion of Interferometric and Optical Data for 3D Reconstruction. 2006. IGARSS 2006. IEEE International Conference on Geoscience and Remote Sensing Symposium. - Denver, CO, USA, July 31 2006-Aug. 4 2006. - P. 3627-3630. ↑

C3664. Soergel U. Radargrammetric Extraction of Building Features from High Resolution Multi-aspect SAR Data. / Soergel U., Michaelsen E., Thiele A., Thoennessen U. // 2006. IGARSS 2006. IEEE International

Conference on Geoscience and Remote Sensing Symposium. - Denver, CO, USA, July 31 2006-Aug. 4 2006. - P. 3635-3638. ↑

C3665. Viergever K. Airborne Synthetic Aperture Radar for Estimating Above-ground Woody Biomass in Tropical Savanna Woodland: A Case Study in Belize. / Viergever K., Woodhouse I., Stuart N. // 2006. IGARSS 2006. IEEE International Conference on Geoscience and Remote Sensing Symposium. - Denver, CO, USA, July 31 2006-Aug. 4 2006. - P. 3595-3598. ↑

C3666. Soisuvarn S. Development of Oceanic Wind Vector Model Function for AMSR Radiometer on ADEOS-II Satellite. / Soisuvarn S., Jones W., Jelenak Z. // 2006. IGARSS 2006. IEEE International Conference on Geoscience and Remote Sensing Symposium. - Denver, CO, USA, July 31 2006-Aug. 4 2006. - P. 3567-3570. ↑

C3667. Lanett N. A Physics Based Multi-Resolution Technique for Extraction of Finite Duration Time Responses in ISAR. / Lanett N., Tjuatja S., Gunnala S., Kollipara A. // 2006. IGARSS 2006. IEEE International Conference on Geoscience and Remote Sensing Symposium. - Denver, CO, USA, July 31 2006-Aug. 4 2006. - P. 3571-3574. ↑

C3668. Wang A. SAR Image Compression Using Multiwavelet and Soft-thresholding. / Wang A., Zhang Y., Gu Y. // 2006. IGARSS 2006. IEEE International Conference on Geoscience and Remote Sensing Symposium. - Denver, CO, USA, July 31 2006-Aug. 4 2006. - P. 3553-3558. ↑

C3669. Weissman D. SeaWinds Scatterometer Wind Vector Retrievals within Hurricanes using AMSR and NEXRAD to Perform Corrections for Precipitation Effects: Comparison of AMSR and NEXRAD Retrievals of Rain. / Weissman D., Hristova-Veleva S., Callahan P. // 2006. IGARSS 2006. IEEE International Conference on Geoscience and Remote Sensing Symposium. - Denver, CO, USA, July 31 2006-Aug. 4 2006. - P. 3557-3562. ↑

C3670. Howell C. A Multivariate Approach to Iceberg and Ship Classification in HH/HV ASAR Data. / Howell C., Mills J., Power D., Youden J., Dodge K., Randell C., Churchill S., Flett D. // 2006. IGARSS 2006. IEEE International Conference on Geoscience and Remote Sensing Symposium. - Denver, CO, USA, July 31 2006-Aug. 4 2006. - P. 3583-3586. ↑

C3671. Kelldorfer J. Modeling Height, Biomass, and Carbon in U.S. Forests from FIA, SRTM, and Ancillary National Scale Data Sets. / Kelldorfer J., Walker W., LaPoint E., Hoppus M., Westfall J. // 2006. IGARSS 2006. IEEE International Conference on Geoscience and Remote Sensing Symposium. - Denver, CO, USA, July 31 2006-Aug. 4 2006. - P. 3591-3594. ↑

C3672. Bertacca M. Isotropic and Anisotropic FEXP-Fractal Spectral Models for High Resolution Sea SAR Images. / Bertacca M., Berizzi F., Dalle Mese E. // 2006. IGARSS 2006. IEEE International Conference on Geoscience and Remote Sensing Symposium. - Denver, CO, USA, July 31 2006-Aug. 4 2006. - P. 3575-3578. ↑

C3673. Greidanus H. Sub-aperture Behavior of SAR Signatures of Ships. 2006. IGARSS 2006. IEEE International Conference on Geoscience and Remote Sensing Symposium. - Denver, CO, USA, July 31 2006-Aug. 4 2006. - P. 3579-3582. ↑

C3674. Min H. Optimized Implementation of Onboard Real-time Imaging for High-resolution Space-borne SAR. / Min H., Zhou Y., Chen J., Li C., Yu Z., Pengbo W. // 2006. IGARSS 2006. IEEE International Conference on Geoscience and Remote Sensing Symposium. - Denver, CO, USA, July 31 2006-Aug. 4 2006. - P. 3180-3183. ↑

C3675. Yongsheng Z. Analysis of Time and Frequency Synchronization Errors in Spaceborne Parasitic InSAR System. / Yongsheng Z., Diannong L., Zhen D. // 2006. IGARSS 2006. IEEE International Conference on Geoscience and Remote Sensing Symposium. - Denver, CO, USA, July 31 2006-Aug. 4 2006. - P. 3047-3050. ↑

C3676. Grings F. Determination of SAR System Parameters Constraints from a Soil Moisture Retrieval Scheme. / Grings F., Tiffenberg J., Karszenbaum H., Perna P., Jacobo-Berles J. // 2006. IGARSS 2006. IEEE International Conference on Geoscience and Remote Sensing Symposium. - Denver, CO, USA, July 31 2006-Aug. 4 2006. - P. 3051-3054. ↑

C3677. Lopez-Dekker P. A Comparison of Contrast Metrics for Contrast-based Phase Calibration of Digital

Beamforming Remote Sensing Systems. / Lopez-Dekker P., Farquharson G., Frasier S. // 2006. IGARSS 2006. IEEE International Conference on Geoscience and Remote Sensing Symposium. - Denver, CO, USA, July 31 2006-Aug. 4 2006. - P. 3036-3039. ↑

C3678. Wang Y. A Reconfigurable, Scalable and Multifunctional Experimental AutoSAR and Its Applications. / Wang Y., Zhou L.-F., Liang X.-D., Li D.-J. // 2006. IGARSS 2006. IEEE International Conference on Geoscience and Remote Sensing Symposium. - Denver, CO, USA, July 31 2006-Aug. 4 2006. - P. 3044-3046. ↑

C3679. Thibaut P. Simulator of Interferometric Radar Altimeters: Concept and first Results. / Thibaut P., Germain O., Collard F., Picard B., Buck C. // 2006. IGARSS 2006. IEEE International Conference on Geoscience and Remote Sensing Symposium. - Denver, CO, USA, July 31 2006-Aug. 4 2006. - P. 3066-3069. ↑

C3680. Gleason S. Detecting Bistatically Reflected GPS Signals from Low Earth Orbit Over Land Surfaces. 2006. IGARSS 2006. IEEE International Conference on Geoscience and Remote Sensing Symposium. - Denver, CO, USA, July 31 2006-Aug. 4 2006. - P. 3086-3089. ↑

C3681. Zhang H. Simulation of Multi-channel SAR Raw Data Based on Real Single Channel SAR Data. / Zhang H., Yang R. // 2006. IGARSS 2006. IEEE International Conference on Geoscience and Remote Sensing Symposium. - Denver, CO, USA, July 31 2006-Aug. 4 2006. - P. 3055-3058. ↑

C3682. Sun Z. Study on DEM Reconstruction for Spaceborne Parasitic InSAR. / Sun Z., Liang D., Dong Z. // 2006. IGARSS 2006. IEEE International Conference on Geoscience and Remote Sensing Symposium. - Denver, CO, USA, July 31 2006-Aug. 4 2006. - P. 3063-3065. ↑

C3683. Donovan B. An Energy Consumption Model for Off-The-Grid Radar Networks. / Donovan B., Kurose J., McLaughlin D. // 2006. IGARSS 2006. IEEE International Conference on Geoscience and Remote Sensing Symposium. - Denver, CO, USA, July 31 2006-Aug. 4 2006. - P. 3031-3035. ↑

C3684. Zhang P. Some Techniques for Three-dimensional Doppler Weather Radar Data Processing. / Zhang P., Shu H., Liu Y., Li Y. // 2006. IGARSS 2006. IEEE International Conference on Geoscience and Remote Sensing Symposium. - Denver, CO, USA, July 31 2006-Aug. 4 2006. - P. 2884-2887. ↑

C3685. Ito S. A New Approach to Backscattering of Pulsed Beam Waves from Hydrometers. / Ito S., Kobayashi S., Oguchi T. // 2006. IGARSS 2006. IEEE International Conference on Geoscience and Remote Sensing Symposium. - Denver, CO, USA, July 31 2006-Aug. 4 2006. - P. 2935-2938. ↑

C3686. Zhi T. Analysis on Speed Error for Airborne Formation Flying InSAR. / Zhi T., Jingwen L., Baofa W. // 2006. IGARSS 2006. IEEE International Conference on Geoscience and Remote Sensing Symposium. - Denver, CO, USA, July 31 2006-Aug. 4 2006. - P. 2806-2807. ↑

C3687. Yong Y. Supervised SAR Image MAP Segmentation Based on Region-based Hierarchical Model. / Yong Y., Hong S., Chu H. // 2006. IGARSS 2006. IEEE International Conference on Geoscience and Remote Sensing Symposium. - Denver, CO, USA, July 31 2006-Aug. 4 2006. - P. 2818-2821. ↑

C3688. Lee H. Measurement of Land Subsidence and Microwave Penetration of Drying Mudflat by using Radarsat-1 DInSAR and PolScat Laboratory Experiment. / Lee H., Chae H., Cho S.-J. // 2006. IGARSS 2006. IEEE International Conference on Geoscience and Remote Sensing Symposium. - Denver, CO, USA, July 31 2006-Aug. 4 2006. - P. 2973-2976. ↑

C3689. Chae H. Variation of Radar Backscattering Coefficient of Tidal Mudflat Observed by Radarsat-1 SAR and Polarimetric Scatterometer. / Chae H., Lee H., Cho S.-J., Park N.-W. // 2006. IGARSS 2006. IEEE International Conference on Geoscience and Remote Sensing Symposium. - Denver, CO, USA, July 31 2006-Aug. 4 2006. - P. 3003-3006. ↑

C3690. Liu D. Backscattering Simulation of Birch Stands Using Coherence Model. / Liu D., Sun G., Guo Z. // 2006. IGARSS 2006. IEEE International Conference on Geoscience and Remote Sensing Symposium. - Denver, CO, USA, July 31 2006-Aug. 4 2006. - P. 2942-2944. ↑

C3691. Awada A. Contribution to Sea Scattering Estimation for Various Wind Direction. / Awada A., Khenchaf A., Coatanhay A. // 2006. IGARSS 2006. IEEE International Conference on Geoscience and Remote Sensing Symposium. - Denver, CO, USA, July 31 2006-Aug. 4 2006. - P. 2953-2956. ↑

- C3692.** Zheng X. A Novel Algorithm for Wide Beam SAR Motion Compensation Based on Frequency Division. / Zheng X., Yu W., Li Z. // 2006. IGARSS 2006. IEEE International Conference on Geoscience and Remote Sensing Symposium. - Denver, CO, USA, July 31 2006-Aug. 4 2006. - P. 3160-3163. ↑
- C3693.** Tian S. A Vessel Detection Method Using ASAR AP Data. / Tian S., Wang C., Zhang H. // 2006. IGARSS 2006. IEEE International Conference on Geoscience and Remote Sensing Symposium. - Denver, CO, USA, July 31 2006-Aug. 4 2006. - P. 3164-3166. ↑
- C3694.** Pengbo W. A Deramp Frequency Scaling Algorithm for Processing Space-Borne Spotlight SAR Data. / Pengbo W., Zhou Y., Chen J., Li C., Yu Z., Min H. // 2006. IGARSS 2006. IEEE International Conference on Geoscience and Remote Sensing Symposium. - Denver, CO, USA, July 31 2006-Aug. 4 2006. - P. 3148-3151. ↑
- C3695.** Xiao-Gang L. A New Weighting Method for Pulse Compression of Chirp Signal and Its Implementation in Real-time SAR Processor. / Xiao-Gang L., Chen-Xi C., Ru-Liang Y. // 2006. IGARSS 2006. IEEE International Conference on Geoscience and Remote Sensing Symposium. - Denver, CO, USA, July 31 2006-Aug. 4 2006. - P. 3156-3159. ↑
- C3696.** Li G. Detection, Location and Imaging of Fast Moving Targets Using Non-uniform Linear Antenna Array SAR. / Li G., Xu J., Peng Y.-N., Xia X.-G. // 2006. IGARSS 2006. IEEE International Conference on Geoscience and Remote Sensing Symposium. - Denver, CO, USA, July 31 2006-Aug. 4 2006. - P. 3173-3176. ↑
- C3697.** Yocky D. Minimum-Latency Polar Format Algorithm. / Yocky D., Wahl D. // 2006. IGARSS 2006. IEEE International Conference on Geoscience and Remote Sensing Symposium. - Denver, CO, USA, July 31 2006-Aug. 4 2006. - P. 3177-3179. ↑
- C3698.** Zhang W. An Efficient Mathematical Model for SAR Image Rectification. / Zhang W., Zhang H., Wang C. // 2006. IGARSS 2006. IEEE International Conference on Geoscience and Remote Sensing Symposium. - Denver, CO, USA, July 31 2006-Aug. 4 2006. - P. 3167-3169. ↑
- C3699.** Chen F. Automatic Registration of Spaceborne SAR Images with the Enhanced FMI-SPOMF Technique. / Chen F., Wang C., Zhang H. // 2006. IGARSS 2006. IEEE International Conference on Geoscience and Remote Sensing Symposium. - Denver, CO, USA, July 31 2006-Aug. 4 2006. - P. 3170-3172. ↑
- C3700.** Zhang F. Illicit Vessel Identification In Inland Waters using SAR Image. / Zhang F., Wu B., Zhang L., Huang H., Tian Y. // 2006. IGARSS 2006. IEEE International Conference on Geoscience and Remote Sensing Symposium. - Denver, CO, USA, July 31 2006-Aug. 4 2006. - P. 3144-3147. ↑
- C3701.** Chen G. Adaptive Despeckling SAR Images in the Undecimated Wavelet Domain Based on Scale Correlation. / Chen G., Liu X. // 2006. IGARSS 2006. IEEE International Conference on Geoscience and Remote Sensing Symposium. - Denver, CO, USA, July 31 2006-Aug. 4 2006. - P. 3111-3114. ↑
- C3702.** Xu W. Evaluation of Envisat-asar Data for Estimating Crop Area in Chengdu Plain. / Xu W., Huang J., Tian Y., Zhang Y., He B. // 2006. IGARSS 2006. IEEE International Conference on Geoscience and Remote Sensing Symposium. - Denver, CO, USA, July 31 2006-Aug. 4 2006. - P. 3115-3118. ↑
- C3703.** Wiesmann A. ScanSAR Interferometry for Land Use Applications and Terrain Deformation. / Wiesmann A., Werner C., Santoro M., Wegmuller U., Strozzi T. // 2006. IGARSS 2006. IEEE International Conference on Geoscience and Remote Sensing Symposium. - Denver, CO, USA, July 31 2006-Aug. 4 2006. - P. 3103-3106. ↑
- C3704.** Li H. A CGMRF-Like based Technique for Speckle Reduction in SAR Images. / Li H., Hong W., Wu Y. // 2006. IGARSS 2006. IEEE International Conference on Geoscience and Remote Sensing Symposium. - Denver, CO, USA, July 31 2006-Aug. 4 2006. - P. 3107-3110. ↑
- C3705.** He B. Speckle Noise Removal of SAR Images Based on 2-Dimensional S-Transform. / He B., Tong L., Han X., Xu W., Chen X. // 2006. IGARSS 2006. IEEE International Conference on Geoscience and Remote Sensing Symposium. - Denver, CO, USA, July 31 2006-Aug. 4 2006. - P. 3134-3135. ↑
- C3706.** Teng H.-T. DEMs and SAR Images. / Teng H.-T., Tay L.-T. // 2006. IGARSS 2006. IEEE International Conference on Geoscience and Remote Sensing Symposium. - Denver, CO, USA, July 31 2006-Aug. 4 2006. - P. 3137-3139. ↑

- C3707.** Hu D.-Y. Radargrammetry DEM from RADARSAT Imageries and Accuracy Validation. / Hu D.-Y., Li J., Chen Y.-H., Deng L., Ramli K. // 2006. IGARSS 2006. IEEE International Conference on Geoscience and Remote Sensing Symposium. - Denver, CO, USA, July 31 2006-Aug. 4 2006. - P. 3119-3122. ↑
- C3708.** Bertacca M. Sea SAR Image Simulation using Isotropic and Anisotropic FEXP-Fractal Spectral Models. / Bertacca M., Berizzi F., Dalle Mese E. // 2006. IGARSS 2006. IEEE International Conference on Geoscience and Remote Sensing Symposium. - Denver, CO, USA, July 31 2006-Aug. 4 2006. - P. 3130-3133. ↑
- C3709.** Franceschetti G. Accuracy of Building Height Estimation from SAR Images. / Franceschetti G., Guida R., Iodice A., Riccio D., Ruello G. // 2006. IGARSS 2006. IEEE International Conference on Geoscience and Remote Sensing Symposium. - Denver, CO, USA, July 31 2006-Aug. 4 2006. - P. 3647-3650. ↑
- C3710.** Kersten P. Scene Analysis of SAR Images using Joint Time-Frequency Analysis. / Kersten P., Jansen R., Luc K., Ainsworth T. // 2006. IGARSS 2006. IEEE International Conference on Geoscience and Remote Sensing Symposium. - Denver, CO, USA, July 31 2006-Aug. 4 2006. - P. 4176-4179. ↑
- C3711.** Yocky D. Spotlight-Mode SAR Image Formation Utilizing the Chirp Z-Transform in Two Dimensions. / Yocky D., Wahl D., Jakowatz Jr. C. // 2006. IGARSS 2006. IEEE International Conference on Geoscience and Remote Sensing Symposium. - Denver, CO, USA, July 31 2006-Aug. 4 2006. - P. 4180-4182. ↑
- C3712.** Long D. Ultra High Resolution Rain Retrieval from QuikSCAT Data. 2006. IGARSS 2006. IEEE International Conference on Geoscience and Remote Sensing Symposium. - Denver, CO, USA, July 31 2006-Aug. 4 2006. - P. 4130-4133. ↑
- C3713.** Halterman R. A Comparison of Hurricane Eye Determination using Standard and Ultra-High Resolution QuikSCAT Winds. / Halterman R., Long D. // 2006. IGARSS 2006. IEEE International Conference on Geoscience and Remote Sensing Symposium. - Denver, CO, USA, July 31 2006-Aug. 4 2006. - P. 4134-4137. ↑
- C3714.** Frery A. Multifrequency Full Polarimetric SAR Classification with Multiple Sources of Statistical Evidence. / Frery A., Correia A., Freitas C. // 2006. IGARSS 2006. IEEE International Conference on Geoscience and Remote Sensing Symposium. - Denver, CO, USA, July 31 2006-Aug. 4 2006. - P. 4195-4197. ↑
- C3715.** Ben Ayed I. Variational Unsupervised Classification of Polarimetric Images. / Ben Ayed I., Mitiche A., Belhadj Z. // 2006. IGARSS 2006. IEEE International Conference on Geoscience and Remote Sensing Symposium. - Denver, CO, USA, July 31 2006-Aug. 4 2006. - P. 4198-4200. ↑
- C3716.** Arnesen T. Modelling of Scattering from Point Like Targets. / Arnesen T., Weydahl D., Eldhuset K. // 2006. IGARSS 2006. IEEE International Conference on Geoscience and Remote Sensing Symposium. - Denver, CO, USA, July 31 2006-Aug. 4 2006. - P. 4187-4190. ↑
- C3717.** Khwaja A. SAR Raw Data Generation Using Inverse SAR Image Formation Algorithms. / Khwaja A., Ferro-Famil L., Pottier E. // 2006. IGARSS 2006. IEEE International Conference on Geoscience and Remote Sensing Symposium. - Denver, CO, USA, July 31 2006-Aug. 4 2006. - P. 4191-4194. ↑
- C3718.** Contreras R. The Surface Effect of Rain on Microwave Backscatter from the Ocean. / Contreras R., Plant W. // 2006. IGARSS 2006. IEEE International Conference on Geoscience and Remote Sensing Symposium. - Denver, CO, USA, July 31 2006-Aug. 4 2006. - P. 4122-4125. ↑
- C3719.** Noferini L. Ground-based Radar Interferometry for Monitoring Unstable Slopes. / Noferini L., Pieraccini M., Luzi G., Mecatti D., Macaluso G., Atzeni C. // 2006. IGARSS 2006. IEEE International Conference on Geoscience and Remote Sensing Symposium. - Denver, CO, USA, July 31 2006-Aug. 4 2006. - P. 4088-4091. ↑
- C3720.** Karvonen J. Oil Spill Detection with RADARSAT-1 in the Baltic Sea. / Karvonen J., Heiler I., Simila M., Tahvonen K. // 2006. IGARSS 2006. IEEE International Conference on Geoscience and Remote Sensing Symposium. - Denver, CO, USA, July 31 2006-Aug. 4 2006. - P. 4092-4095. ↑
- C3721.** Dupuis X. Change Detection using Multi-PASS and Multi- DATE Data at P and L bands. / Dupuis X., Dreuillet P., Ulander L., Gustavsson A. // 2006. IGARSS 2006. IEEE International Conference on Geoscience and Remote Sensing Symposium. - Denver, CO, USA, July 31 2006-Aug. 4 2006. - P. 4044-4047. ↑
- C3722.** Choisnard J. Toward the use of Earth Observation Wind Data for Marine Search and Rescue

Operations. / Choisnard J., Power D., Randell C., Davidson F., Ratsimandresy A., Stone B. // 2006. IGARSS 2006. IEEE International Conference on Geoscience and Remote Sensing Symposium. - Denver, CO, USA, July 31 2006-Aug. 4 2006. - P. 4084-4087. ↑

C3723. Haarpaintner J. Use of Enhanced-resolution QuikScat/SeaWinds Data for Operational Ice Services and Climate Research: Sea Ice Edge, Type, Concentration and Drift. / Haarpaintner J., Porcires M. // 2006. IGARSS 2006. IEEE International Conference on Geoscience and Remote Sensing Symposium. - Denver, CO, USA, July 31 2006-Aug. 4 2006. - P. 4115-4118. ↑

C3724. Nie C. The Effect of Rain on ERS Scatterometer Measurements. / Nie C., Long D. // 2006. IGARSS 2006. IEEE International Conference on Geoscience and Remote Sensing Symposium. - Denver, CO, USA, July 31 2006-Aug. 4 2006. - P. 4119-4121. ↑

C3725. Matthis II M. ISAR and Aerial LIDAR Comparison to Observe and Quantify the Terrain and Environment of the Historical Native North Carolina Settlements. / Matthis II M., LeCompte M., Garland A., Hayden L. // 2006. IGARSS 2006. IEEE International Conference on Geoscience and Remote Sensing Symposium. - Denver, CO, USA, July 31 2006-Aug. 4 2006. - P. 4096-4099. ↑

C3726. Hicks B. Diurnal Melt Detection on Arctic Sea Ice Using Tandem QuikSCAT and SeaWinds Data. / Hicks B., Long D. // 2006. IGARSS 2006. IEEE International Conference on Geoscience and Remote Sensing Symposium. - Denver, CO, USA, July 31 2006-Aug. 4 2006. - P. 4112-4114. ↑

C3727. Kolyadov D.V. Amplitude-Based Measurement Technique in Polarimetric Radar Remote Sensing for Determining the Dielectric Permittivity of Earth Media. / Kolyadov D.V., Ligthart L.P., Kozlov A.I. // 2006. MIKON 2006. International Conference on Microwaves, Radar & Wireless Communications. - Krakow, 22-24 May 2006. - P. 495-498. ↑

C3728. Georgiev G. Data Acquisition Field Network in Support of Remote Sensing Investigations. / Georgiev G., Petkov D., Nikolov H. // 2006. MIKON 2006. International Conference on Microwaves, Radar & Wireless Communications. - Krakow, 22-24 May 2006. - P. 298-301. ↑

C3729. Bragin I.V. Analysis of Possibilities of Creating the Radioelectronic Complexes to be Made for Detection of Biological Objects Covered by Vegetation. / Bragin I.V., Sgibnev V.P., Chebotarev A.S., Kamenkov M.B., Elizavetova E.L., Shevaldykina T.B., Zheltikov I.A., Gil A.M., Khidasheli D. // 2006. MIKON 2006. International Conference on Microwaves, Radar & Wireless Communications. - Krakow, 22-24 May 2006. - P. 1196-1199. ↑

C3730. Bragin I.V. Results of Development of Radiometric Receivers mm and Submillimeter Range. / Bragin I.V., Sgibnev V.P., Kamenkov M.B., Bragin S.I., Shevaldykina T.B., Morozov A.A., Chebotarev A.S., Savin B.N., Maslova N.S., Elizavetova E.L., Khidasheli D. // 2006. MIKON 2006. International Conference on Microwaves, Radar & Wireless Communications. - Krakow, 22-24 May 2006. - P. 901-904. ↑

C3731. Kulemin G. Experimental determination of soil characteristics from the parameters of scattered signals at X- and Ka-bands. / Kulemin G., Goroshko E., Tarnavsky E. // 2006. IRS 2006. International Radar Symposium. - Krakow, 24-26 May 2006. - P. 1-4. ↑

C3732. Picardi G. Subsurface Investigations by MARSIS in Mars Express Mission. / Picardi G., Biccara D., Cartacci M., Cicchetti A., Iorio M., Seu R., Masdea A., Plaut J., Jordan R.L., Huff R., Safaenili A., Orosei R., Bombaci O., Calabrese D., Zampolini E., Melacci P.T. // 2006. IRS 2006. International Radar Symposium. - Krakow, 24-26 May 2006. - P. 1-15. ↑

C3733. Bragin I.V. Spatial (Aperture) Noise Generators. / Bragin I.V., Sgibnev V.P., Kamenkov M.B., Istuakov I.V., Zheltikov I.A., Savin B.N., Shevaldykina T.B., Elizavetova E.L., Maslova N.S., Kontorin E.O., Kochergin E.N. // 2006. MIKON 2006. International Conference on Microwaves, Radar & Wireless Communications. - Krakow, 22-24 May 2006. - P. 275-278. ↑

C3734. Bragin I.V. Space Monitoring of Atmosphere Pollution by Satellite Passive Radar System. / Bragin I.V., Sgibnev V.P., Bragin S.I., Shevaldykina T.B., Kamenkov M.B., Khidasheli D., Polischuk G.M., Bragina O.N., Glebov V.P., Chen W., Lu L., Dolecki J. // 2006. MIKON 2006. International Conference on Microwaves, Radar & Wireless Communications. - Krakow, 22-24 May 2006. - P. 58-61. ↑

C3735. Krogager Ernst. Polarimetric Analysis of Radar Signature of a Manmade Structure. / Krogager Ernst,

Lee Jong-Sen, Boerner Wolfgang-Martin, Ainsworth Thomas L. // 2006. IRS 2006. International Radar Symposium. - Krakow, Poland, 24-26 May 2006. - P. 1-4. ↑

C3736. Kulemin G. Determination of the Soil Parameters from Multichannel Remote Sensing Data. 2006. TCSET 2006. International Conference Modern Problems of Radio Engineering, Telecommunications, and Computer Science. - Lviv-Slavsko, Feb. 28 2006-March 4 2006. - P. 313-316. ↑

C3737. Ponomarenko N. Methods for Lossy Compression of Images Corrupted by Multiplicative Noise. / Ponomarenko N., Lukin V., Zriakhov M., Pogrebnyak O. // 2006. TCSET 2006. International Conference Modern Problems of Radio Engineering, Telecommunications, and Computer Science. - Lviv-Slavsko, Feb. 28 2006-March 4 2006. - P. 278-281. ↑

C3738. Marpu P. Evaluation of the Efficiency of Object-Based Classification in the Identification of Geological Structures Case Study: Extraction of the Morphology of the Normal Faults. / Marpu P., Gloaguen R., Niemeier I. // 2006. IGARSS 2006. IEEE International Conference on Geoscience and Remote Sensing Symposium. - Denver, CO, USA, July 31 2006-Aug. 4 2006. - P. 4213-4216. ↑

C3739. Lopez L. Contextual approach for oil spill detection in SAR images using image fusion and markov random fields. / Lopez L., Moctezuma M., Parmiggiani F. // 2006. MWSCAS 06. 49th IEEE International Midwest Symposium on Circuits and Systems. - San Juan, 6-9 Aug. 2006. - Vol. 2. - P. 137-139. ↑

C3740. Suprun D. Yu. Simulation algorithm for noise waveform SAR with arbitrary motion trajectory of antenna phase center. / Suprun D. Yu., Mogyla A. A. // 2006. IRS 2006. International Radar Symposium. - Krakow, Poland, 24-26 May 2006. - P. 1-4. ↑

C3741. Boerner W.-M. Recent Developments of Radar Remote Sensing; Air- and Space-borne Multimodal SAR Remote Sensing in Forestry & Agriculture, Geology, Geophysics (Volcanology and Tectonology): Advances in POL-SAR, IN-SAR, POLInSAR and POL-DIFF-IN-SAR Sensing and Imaging with Applications to Environmental and Geodynamic Stress-change Monitoring. / Boerner W.-M., Morisaki J.J. // 2006. IRS 2006. International Radar Symposium. - Krakow, 24-26 May 2006. - P. 1-4. ↑

C3742. Prudyus I. Image processing in the complex monitoring system radiometric channel. / Prudyus I., Denysov O., Lazko L. // 2006. TCSET 2006. International Conference Modern Problems of Radio Engineering, Telecommunications, and Computer Science. - Lviv-Slavsko, Feb. 28 2006-March 4 2006. - P. 271-272. ↑

C3743. Capria A. HF-OTH Skywave Radar: A Method for Peak Power Evaluation. / Capria A., Berizzi F., Soleti R., Mese E.D. // 2006. IRS 2006. International Radar Symposium. - Krakow, 24-26 May 2006. - P. 1-4. ↑

C3744. Zhou Z.-S. Application of Polarization Coherence Tomography to GB-POLInSAR Data. / Zhou Z.-S., Cloude S. // 2006. IGARSS 2006. IEEE International Conference on Geoscience and Remote Sensing Symposium. - Denver, CO, USA, July 31 2006-Aug. 4 2006. - P. 4040-4043. ↑

C3745. Loos R. Identification of Individual Trees And Canopy Shapes using LiDAR Data for Fire Management. / Loos R., Niemann O. // 2006. IGARSS 2006. IEEE International Conference on Geoscience and Remote Sensing Symposium. - Denver, CO, USA, July 31 2006-Aug. 4 2006. - P. 3755-3757. ↑

C3746. Neuenschwander A. Comparison of Small-footprint and Large-footprint Waveform Lidar for Terrestrial Surface Characterization. / Neuenschwander A., Gutierrez R., Schutz B., Urban T. // 2006. IGARSS 2006. IEEE International Conference on Geoscience and Remote Sensing Symposium. - Denver, CO, USA, July 31 2006-Aug. 4 2006. - P. 3758-3761. ↑

C3747. Chen H. Auto-Regressive Aperture Extrapolation for Multibaseline SAR Tomography. / Chen H., Kasilingam D. // 2006. IGARSS 2006. IEEE International Conference on Geoscience and Remote Sensing Symposium. - Denver, CO, USA, July 31 2006-Aug. 4 2006. - P. 3743-3745. ↑

C3748. Zhang K. Airborne Laser Mapping of Mangroves on the Biscayne Bay Coast, Miami, Florida. / Zhang K., Houle P., Ross M., Ruiz P., Simard M. // 2006. IGARSS 2006. IEEE International Conference on Geoscience and Remote Sensing Symposium. - Denver, CO, USA, July 31 2006-Aug. 4 2006. - P. 3750-3754. ↑

C3749. Lambert B. A Large-Scale Ku-Band Backscatter Model of the East-Antarctic Megadune Fields. / Lambert B., Long D. // 2006. IGARSS 2006. IEEE International Conference on Geoscience and Remote Sensing Symposium. - Denver, CO, USA, July 31 2006-Aug. 4 2006. - P. 3832-3834. ↑

- C3750.** Aguttes J. Romulus: Along Track Formation of Radar Satellites for MTI (Moving Target Identification) and High SAR Performance. / Aguttes J., Attia S., Amiot T., Vaizan B., Desjonqueres J.-D., Chretien J., Tison C., Ovarlez J.-P. // 2006. IGARSS 2006. IEEE International Conference on Geoscience and Remote Sensing Symposium. - Denver, CO, USA, July 31 2006-Aug. 4 2006. - P. 3838-3841. ↑
- C3751.** Schneider R. Characterisation of Coherent Scatterers in Urban Areas by Means of Angular Diversity. / Schneider R., Papathanassiou K., Hajnsek I., Moreira A. // 2006. IGARSS 2006. IEEE International Conference on Geoscience and Remote Sensing Symposium. - Denver, CO, USA, July 31 2006-Aug. 4 2006. - P. 3782-3785. ↑
- C3752.** Strozzi T. Capabilities of L-band SAR Data for arctic Glacier Motion Estimation. / Strozzi T., Wiesmann A., Sharov A., Kouraev A., Wegmuller U., Werner C. // 2006. IGARSS 2006. IEEE International Conference on Geoscience and Remote Sensing Symposium. - Denver, CO, USA, July 31 2006-Aug. 4 2006. - P. 3816-3819. ↑
- C3753.** Wegmuller U. Ionospheric Electron Concentration Effects on SAR and INSAR. / Wegmuller U., Werner C., Strozzi T., Wiesmann A. // 2006. IGARSS 2006. IEEE International Conference on Geoscience and Remote Sensing Symposium. - Denver, CO, USA, July 31 2006-Aug. 4 2006. - P. 3731-3734. ↑
- C3754.** Teague C. UHF RiverSonde Operation in a Tidal Marsh. / Teague C., Barrick D., Lilleboe P., Styles R. // 2006. IGARSS 2006. IEEE International Conference on Geoscience and Remote Sensing Symposium. - Denver, CO, USA, July 31 2006-Aug. 4 2006. - P. 3665-3667. ↑
- C3755.** Irisov V. Microwave Radiometric Signal from the Sea Surface in the Presence of the Currents. 2006. IGARSS 2006. IEEE International Conference on Geoscience and Remote Sensing Symposium. - Denver, CO, USA, July 31 2006-Aug. 4 2006. - P. 3668-3671. ↑
- C3756.** Peterson I. Comparison of Helicopter-borne Measurements of Sea-Ice Properties with ENVISAT ASAR APP Data for Amundsen Gulf. / Peterson I., Prinsenberg S., Holladay J. // 2006. IGARSS 2006. IEEE International Conference on Geoscience and Remote Sensing Symposium. - Denver, CO, USA, July 31 2006-Aug. 4 2006. - P. 3651-3654. ↑
- C3757.** Rink T. A Wideband Radar for Mapping Near-Surface Layers in Snow. / Rink T., Kanagaratnam P., Braaten D., Akins T., Gogineni S. // 2006. IGARSS 2006. IEEE International Conference on Geoscience and Remote Sensing Symposium. - Denver, CO, USA, July 31 2006-Aug. 4 2006. - P. 3655-3657. ↑
- C3758.** Parikh J. Aerosol Layer Discrimination using Laser Radar and Genetic Algorithms. / Parikh J., Sharma N. // 2006. IGARSS 2006. IEEE International Conference on Geoscience and Remote Sensing Symposium. - Denver, CO, USA, July 31 2006-Aug. 4 2006. - P. 3700-3703. ↑
- C3759.** Veneziani N. A Multi-chromatic Approach to SAR Interferometry: Differential Analysis of Interferograms at Close Frequencies in the Spatial Domain and Frequency Domain. / Veneziani N., Giacomazzo V. // 2006. IGARSS 2006. IEEE International Conference on Geoscience and Remote Sensing Symposium. - Denver, CO, USA, July 31 2006-Aug. 4 2006. - P. 3723-3726. ↑
- C3760.** Ulander L. Mapping of Wind-Thrown Forests Using the VHF-Band CARABAS-II SAR. / Ulander L., Gustavsson A., Fransson J., Magnusson M., Smith-Jonforsen G., Folkesson K., Hallberg B., Eriksson L. // 2006. IGARSS 2006. IEEE International Conference on Geoscience and Remote Sensing Symposium. - Denver, CO, USA, July 31 2006-Aug. 4 2006. - P. 3684-3687. ↑
- C3761.** Tahvonen K. The Use of Environmental Data in Reliability Assessment of Oil Spill Detection by SAR Imagery. / Tahvonen K., Pyhalahti T. // 2006. IGARSS 2006. IEEE International Conference on Geoscience and Remote Sensing Symposium. - Denver, CO, USA, July 31 2006-Aug. 4 2006. - P. 3688-3691. ↑
- C3762.** Cellier F. Building Height Estimation using Fine Analysis of Altimetric Mixtures in Layover Areas on Polarimetric Interferometric X-band SAR Images. / Cellier F., Colin E. // 2006. IGARSS 2006. IEEE International Conference on Geoscience and Remote Sensing Symposium. - Denver, CO, USA, July 31 2006-Aug. 4 2006. - P. 4004-4007. ↑
- C3763.** Vasile G. High Resolution SAR Interferometry: Influence of Local Topography in the Context of Glacier Monitoring. / Vasile G., Petillot I., Julea A., Trouve E., Bolon P., Bombrun L., Gay M., Landes T., Grussenmeyer P., Nicolas J.-M. // 2006. IGARSS 2006. IEEE International Conference on Geoscience and Remote Sensing Symposium. - Denver, CO, USA, July 31 2006-Aug. 4 2006. - P. 3688-3691. ↑

Symposium. - Denver, CO, USA, July 31 2006-Aug. 4 2006. - P. 4008-4011. ↑

C3764. Obland M. Preliminary Testing of a Water-Vapor Differential Absorption LIDAR (DIAL) Using a Widely Tunable Amplified Diode Laser Source. / Obland M., Repasky K., Shaw J., Carlsten J. // 2006. IGARSS 2006. IEEE International Conference on Geoscience and Remote Sensing Symposium. - Denver, CO, USA, July 31 2006-Aug. 4 2006. - P. 3949-3952. ↑

C3765. Sharma N. An Imaging Bistatic Lidar System for Boundary Layer Monitoring. / Sharma N., Barnes J., Kaplan T. // 2006. IGARSS 2006. IEEE International Conference on Geoscience and Remote Sensing Symposium. - Denver, CO, USA, July 31 2006-Aug. 4 2006. - P. 3953-3955. ↑

C3766. Sauer S. Estimation of Built-up Area Characteristics from Polarimetric Interferometric Multiple Track L-Band SAR Data. / Sauer S., Ferro-Famil L., Reigber A., Pottier E. // 2006. IGARSS 2006. IEEE International Conference on Geoscience and Remote Sensing Symposium. - Denver, CO, USA, July 31 2006-Aug. 4 2006. - P. 4032-4035. ↑

C3767. Lopez-Sanchez J. Complete Inversion of Agricultural Vegetation Parameters by Pol-InSAR: Multibaseline and .k-radar Approaches. / Lopez-Sanchez J., Ballester-Berman J. // 2006. IGARSS 2006. IEEE International Conference on Geoscience and Remote Sensing Symposium. - Denver, CO, USA, July 31 2006-Aug. 4 2006. - P. 4036-4039. ↑

C3768. Stacy N. Polarimetric Characteristics of X-Band SAR Sea Clutter. / Stacy N., Preiss M., Crisp D. // 2006. IGARSS 2006. IEEE International Conference on Geoscience and Remote Sensing Symposium. - Denver, CO, USA, July 31 2006-Aug. 4 2006. - P. 4017-4020. ↑

C3769. Foucher S. SAR Image Filtering based on the Stationary Contourlet Transform. / Foucher S., Farage G., Benie G. // 2006. IGARSS 2006. IEEE International Conference on Geoscience and Remote Sensing Symposium. - Denver, CO, USA, July 31 2006-Aug. 4 2006. - P. 4021-4024. ↑

C3770. Liao D. Network of RF Ground Sensors for Applications in Precision Agriculture. / Liao D., Sarabandi K. // 2006. IGARSS 2006. IEEE International Conference on Geoscience and Remote Sensing Symposium. - Denver, CO, USA, July 31 2006-Aug. 4 2006. - P. 3943-3946. ↑

C3771. Kim J. Evaluation of Ground-based SAR System for Digital Beamforming Applications. / Kim J., Wiesbeck W. // 2006. IGARSS 2006. IEEE International Conference on Geoscience and Remote Sensing Symposium. - Denver, CO, USA, July 31 2006-Aug. 4 2006. - P. 3849-3852. ↑

C3772. Im E. Advanced Spaceborne Rain Radar Instrument Concepts and Technology. / Im E., Durden S. // 2006. IGARSS 2006. IEEE International Conference on Geoscience and Remote Sensing Symposium. - Denver, CO, USA, July 31 2006-Aug. 4 2006. - P. 3853-3856. ↑

C3773. Klare J. ARTINO: A New High Resolution 3D Imaging Radar System on an Autonomous Airborne Platform. / Klare J., Weiss M., Peters O., Brenner A., Ender J. // 2006. IGARSS 2006. IEEE International Conference on Geoscience and Remote Sensing Symposium. - Denver, CO, USA, July 31 2006-Aug. 4 2006. - P. 3842-3845. ↑

C3774. Raney R. Hybrid-Polarity SAR Architecture. 2006. IGARSS 2006. IEEE International Conference on Geoscience and Remote Sensing Symposium. - Denver, CO, USA, July 31 2006-Aug. 4 2006. - P. 3846-3848. ↑

C3775. Ge L. Airborne Laser Scanning and Radar Interferometry for Digital Topographic Modelling in Coastal Environments. / Ge L., Chang H.-C., Mitchell A., Milne T. // 2006. IGARSS 2006. IEEE International Conference on Geoscience and Remote Sensing Symposium. - Denver, CO, USA, July 31 2006-Aug. 4 2006. - P. 3869-3871. ↑

C3776. Colone F. Effect of Spatially Variant Apodization on SAR Image Classification. / Colone F., Viscito M., Pastina D., Lombardo P. // 2006. IGARSS 2006. IEEE International Conference on Geoscience and Remote Sensing Symposium. - Denver, CO, USA, July 31 2006-Aug. 4 2006. - P. 3903-3906. ↑

C3777. Alvarez-Perez J. TerraSAR-X Antenna Pattern Estimation by a Complex Treatment of Rain Forest Measurements. / Alvarez-Perez J., Schwerdt M., Bachmann M. // 2006. IGARSS 2006. IEEE International Conference on Geoscience and Remote Sensing Symposium. - Denver, CO, USA, July 31 2006-Aug. 4 2006. - P. 3907-3910. ↑

P. 3857-3860.

C3778. Power D. InSAR Evaluation of Landslides in Support of Roadway Design and Realignment. / Power D., Youden J., English J., Russell K., Churchill S., Anderson S., Surdahl R., Blair A., Lofgren D., Anderson D. // 2006. IGARSS 2006. IEEE International Conference on Geoscience and Remote Sensing Symposium. - Denver, CO, USA, July 31 2006-Aug. 4 2006. - P. 3865-3868. ↑

C3779. Zhu Z. An Atmospheric Correction Method Based on Lidar Data. / Zhu Z., Gong W., Qin Q., Li P., Ma Y., Liu M., Hao Z. // 2006. IGARSS 2006. IEEE International Conference on Geoscience and Remote Sensing Symposium. - Denver, CO, USA, July 31 2006-Aug. 4 2006. - P. 2798-2801. ↑

C3780. Ebuchi N. Observation of the Soya Warm Current Combining HF Ocean Radar with Coastal Tide Gauges and Satellite Altimetry. / Ebuchi N., Fukamachi Y., Ohshima K.I., Shirasawa K., Wakatsuchi M. // 2006. IGARSS 2006. IEEE International Conference on Geoscience and Remote Sensing Symposium. - Denver, CO, July 31 2006-Aug. 4 2006. - P. 1860-1863. ↑

C3781. Ziemer F. High Resolution Sea Surface Current Maps Produced by Scanning with Ground Based Doppler Radar. / Ziemer F., Marius C. // 2006. IGARSS 2006. IEEE International Conference on Geoscience and Remote Sensing Symposium. - Denver, CO, July 31 2006-Aug. 4 2006. - P. 1864-1866. ↑

C3782. Sakai S. Coastal Current Observation in the Area of Abrupt Topographic Change with DBF Ocean Radar. / Sakai S., Tsubono T., Matsuyama M., Tada A., Mizunuma M. // 2006. IGARSS 2006. IEEE International Conference on Geoscience and Remote Sensing Symposium. - Denver, CO, July 31 2006-Aug. 4 2006. - P. 1852-1855. ↑

C3783. Vesecky J.F. Observing Eddy Features in the Ocean Surface Wind Field by Assimilating HF Radar and Anemometer Measurements in a Wind Model. / Vesecky J.F., Drake J., Laws K., Ludwig F.L., Teague C.C., Paduan J.D., Sinton D. // 2006. IGARSS 2006. IEEE International Conference on Geoscience and Remote Sensing Symposium. - Denver, CO, July 31 2006-Aug. 4 2006. - P. 1856-1859. ↑

C3784. Schulz-Stellenfleth J. An Empirical Approach for the Retrieval of Ocean Wave Parameters from Synthetic Aperture Radar Data. / Schulz-Stellenfleth J., Konig T., Lehner S. // 2006. IGARSS 2006. IEEE International Conference on Geoscience and Remote Sensing Symposium. - Denver, CO, July 31 2006-Aug. 4 2006. - P. 1875-1878. ↑

C3785. Bernier M. Monitoring the Cryosphere using Radarsat-1 and SSM/I Data: an Overview of CRYSYS Related Accomplishments at INRS-ETE. / Bernier M., Gauthier Y. // 2006. IGARSS 2006. IEEE International Conference on Geoscience and Remote Sensing Symposium. - Denver, CO, July 31 2006-Aug. 4 2006. - P. 1879-1882. ↑

C3786. Mouche A. Use of Dual Polarization Radar Measurements to Understand the Azimuth Behavior of the Sea Surface Backscattered Signal. / Mouche A., Hauser D., Caudal G., Kudryavstev V., Chapron B. // 2006. IGARSS 2006. IEEE International Conference on Geoscience and Remote Sensing Symposium. - Denver, CO, July 31 2006-Aug. 4 2006. - P. 1867-1870. ↑

C3787. Fernandez D.E. Spectral Behavior of the Ocean Surface Backscatter and the Atmospheric Boundary Layer at C- and Ku-band under High wind and Rain Conditions. / Fernandez D.E., Chang P., Carswell J., Contreras R., Chu T. // 2006. IGARSS 2006. IEEE International Conference on Geoscience and Remote Sensing Symposium. - Denver, CO, July 31 2006-Aug. 4 2006. - P. 1871-1874. ↑

C3788. Kojima S. Development of 9.25MHz Ocean Radar for Measuring Ocean Waves. 2006. IGARSS 2006. IEEE International Conference on Geoscience and Remote Sensing Symposium. - Denver, CO, July 31 2006-Aug. 4 2006. - P. 1848-1851. ↑

C3789. Mei Xin. Research on Unification of Spatial Reference of Multi-source Data in 3S Integration. / Mei Xin, Cui Weihong, Wu Mengquan. // 2006. IGARSS 2006. IEEE International Conference on Geoscience and Remote Sensing Symposium. - Denver, CO, July 31 2006-Aug. 4 2006. - P. 1824-1827. ↑

C3790. Ender J.H.G. Bistatic Exploration using Spaceborne and Airborne SAR Sensors: A Close Collaboration Between FGAN, ZESS, and FOMAAS. / Ender J.H.G., Klare J., Walterscheid I., Brenner A.R., Weiss M., Kirchner C., Wilden H., Loffeld O., Kolb A., Wiechert W., Kalkuhl M., Knedlik S., Gebhardt U., Nies H., Natroshvili K., Ige S., Ortiz A.M., Amankwah A. // 2006. IGARSS 2006. IEEE International Conference on

Geoscience and Remote Sensing Symposium. - Denver, CO, July 31 2006-Aug. 4 2006. - P. 1828-1831. ↑

C3791. Goodenough D.G. Evaluation of Convair-580 and Simulated Radarsat-2 Polarimetric SAR for Forest Change Detection. / Goodenough D.G., Hao Chen, Dyk A. // 2006. IGARSS 2006. IEEE International Conference on Geoscience and Remote Sensing Symposium. - Denver, CO, July 31 2006-Aug. 4 2006. - P. 1788-1791. ↑

C3792. Churchill S. Data Fusion: Cumulative Effects of Discrete Fusion on Target Detection Probability. / Churchill S., Randell C., Gill E. // 2006. IGARSS 2006. IEEE International Conference on Geoscience and Remote Sensing Symposium. - Denver, CO, July 31 2006-Aug. 4 2006. - P. 1800-1803. ↑

C3793. Sanz-Marcos J. First ENVISAT and ERS-2 Parasitic Bistatic Fixed Receiver SAR Images Processed with the Subaperture Range-Doppler Algorithm. / Sanz-Marcos J., Mallorqui J.J., Aguasca A., Prats P. // 2006. IGARSS 2006. IEEE International Conference on Geoscience and Remote Sensing Symposium. - Denver, CO, July 31 2006-Aug. 4 2006. - P. 1840-1843. ↑

C3794. Bamler R. No Math: Bistatic SAR Processing Using Numerically Computed Transfer Functions. / Bamler R., Meyer F., Liebhart W. // 2006. IGARSS 2006. IEEE International Conference on Geoscience and Remote Sensing Symposium. - Denver, CO, July 31 2006-Aug. 4 2006. - P. 1844-1847. ↑

C3795. Gebhardt U. Bistatic Space Borne / Airborne Experiment: Geometrical Modeling and Simulation. / Gebhardt U., Loffeld O., Nies H., Natroshvili K., Knedlik S. // 2006. IGARSS 2006. IEEE International Conference on Geoscience and Remote Sensing Symposium. - Denver, CO, July 31 2006-Aug. 4 2006. - P. 1832-1835. ↑

C3796. Gebert N. Digital Beamforming for HRWS-SAR Imaging: System Design, Performance and Optimization Strategies. / Gebert N., Krieger G., Moreira A. // 2006. IGARSS 2006. IEEE International Conference on Geoscience and Remote Sensing Symposium. - Denver, CO, July 31 2006-Aug. 4 2006. - P. 1836-1839. ↑

C3797. Huber M. The TerraSAR-X Orthorectification Service and Its Benefit for Land Use Applications. / Huber M., Wessel B., Roth A. // 2006. IGARSS 2006. IEEE International Conference on Geoscience and Remote Sensing Symposium. - Denver, CO, July 31 2006-Aug. 4 2006. - P. 1922-1925. ↑

C3798. Emery W.J. Coastal Ocean Surface Current Retrievals from Sequences of TerraSAR-X Images. / Emery W.J., Gade M., Romeiser R. // 2006. IGARSS 2006. IEEE International Conference on Geoscience and Remote Sensing Symposium. - Denver, CO, July 31 2006-Aug. 4 2006. - P. 1926-1929. ↑

C3799. Roth A. Status of the TerraSAR-X Mission. 2006. IGARSS 2006. IEEE International Conference on Geoscience and Remote Sensing Symposium. - Denver, CO, July 31 2006-Aug. 4 2006. - P. 1918-1920. ↑

C3800. Breit H. TerraSAR-X Products and Product Performance Update. / Breit H., Eineder M., Fritz T., Schattler B., Huber M., Mittermayer J. // 2006. IGARSS 2006. IEEE International Conference on Geoscience and Remote Sensing Symposium. - Denver, CO, July 31 2006-Aug. 4 2006. - P. 1921. ↑

C3801. Zink M. The TanDEM-X Mission Concept. / Zink M., Fiedler H., Hajnsek I., Krieger G., Moreira A., Werner M. // 2006. IGARSS 2006. IEEE International Conference on Geoscience and Remote Sensing Symposium. - Denver, CO, July 31 2006-Aug. 4 2006. - P. 1938-1941. ↑

C3802. Houle P.A. Use of Airborne LIDAR for the Assessment of Landscape Structure in the Pine Forests of Everglades National Park. / Houle P.A., Keqi Zhang, Ross M.S., Simard M. // 2006. IGARSS 2006. IEEE International Conference on Geoscience and Remote Sensing Symposium. - Denver, CO, July 31 2006-Aug. 4 2006. - P. 1960-1963. ↑

C3803. Marquez Martinez J. A First Study on the use of TerraSAR-X for Meteorological Purposes. / Marquez Martinez J., Alvarez Perez J.-L. // 2006. IGARSS 2006. IEEE International Conference on Geoscience and Remote Sensing Symposium. - Denver, CO, July 31 2006-Aug. 4 2006. - P. 1930-1933. ↑

C3804. Walterscheid I. Bistatic Image Processing for a Hybrid SAR Experiment Between TerraSAR-X and PAMIR. / Walterscheid I., Ender J.H.G., Loffeld O. // 2006. IGARSS 2006. IEEE International Conference on Geoscience and Remote Sensing Symposium. - Denver, CO, July 31 2006-Aug. 4 2006. - P. 1934-1937. ↑

- C3805.** Fritz J. Retrieval of Surface-layer Refractivity using the CSU-CHILL Radar. / Fritz J., Chandrasekar V., Kennedy P., Roberts R. // 2006. IGARSS 2006. IEEE International Conference on Geoscience and Remote Sensing Symposium. - Denver, CO, July 31 2006-Aug. 4 2006. - P. 1914-1917. ↑
- C3806.** Jun-su Kim. Surface Displacement Monitoring on Reclaimed Land Using PSInSAR Technique. / Jun-su Kim, Sang-Eun Park, Moon W.M. // 2006. IGARSS 2006. IEEE International Conference on Geoscience and Remote Sensing Symposium. - Denver, CO, July 31 2006-Aug. 4 2006. - P. 1890-1893. ↑
- C3807.** Prats P. Estimation of the Deformation Temporal Evolution Using Airborne Differential SAR Interferometry. / Prats P., Reigber A., Mallorqui J.J., Blanco P., Moreira A. // 2006. IGARSS 2006. IEEE International Conference on Geoscience and Remote Sensing Symposium. - Denver, CO, July 31 2006-Aug. 4 2006. - P. 1894-1897. ↑
- C3808.** Rauste Y. Interferometric Triherence for Ground Movements Monitoring. / Rauste Y., Louhisuo M., Henry J.-B., Kuzuoka S., Morohoshi T., Hame T. // 2006. IGARSS 2006. IEEE International Conference on Geoscience and Remote Sensing Symposium. - Denver, CO, July 31 2006-Aug. 4 2006. - P. 1883-1885. ↑
- C3809.** Ferraiuolo G. DEM Reconstruction Accuracy in Multi-Channel SAR Interferometry. / Ferraiuolo G., Meglio F., Pascasio V., Schirizzi G. // 2006. IGARSS 2006. IEEE International Conference on Geoscience and Remote Sensing Symposium. - Denver, CO, July 31 2006-Aug. 4 2006. - P. 1886-1889. ↑
- C3810.** Baquero M. Use of Disdrometer Data for X-Band Polarimetric Radar Simulation and Tropical Rain Characterization. / Baquero M., Cruz-Pol S., Brangi V.N., Chandrasekar V. // 2006. IGARSS 2006. IEEE International Conference on Geoscience and Remote Sensing Symposium. - Denver, CO, July 31 2006-Aug. 4 2006. - P. 1906-1909. ↑
- C3811.** Yuxiang Liu. Improved Rain Attenuation Correction Algorithms for Radar Reflectivity and Differential Reflectivity with Adaptation to Drop Shape Model Variation. / Yuxiang Liu, Brangi V.N. // 2006. IGARSS 2006. IEEE International Conference on Geoscience and Remote Sensing Symposium. - Denver, CO, July 31 2006-Aug. 4 2006. - P. 1910-1913. ↑
- C3812.** Blanco P. Advances on DInSAR with ERS and ENVISAT Data using the Coherent Pixels Technique (CPT). / Blanco P., Mallorqui J.J., Duque S., Navarrete D. // 2006. IGARSS 2006. IEEE International Conference on Geoscience and Remote Sensing Symposium. - Denver, CO, July 31 2006-Aug. 4 2006. - P. 1898-1901. ↑
- C3813.** Bekkerman A. Testing and Validation of the CASA DCAS System. / Bekkerman A., Lakamraju V., Koren I., Krishna C.M. // 2006. IGARSS 2006. IEEE International Conference on Geoscience and Remote Sensing Symposium. - Denver, CO, July 31 2006-Aug. 4 2006. - P. 1902-1905. ↑
- C3814.** Demirkol A. A Radar Sensing Algorithm by Gabor Theory. / Demirkol A., Acar L., Woodley R.S. // 2006. IGARSS 2006. IEEE International Conference on Geoscience and Remote Sensing Symposium. - Denver, CO, July 31 2006-Aug. 4 2006. - P. 1768-1771. ↑
- C3815.** Iwashita A. Consideration of the Correlation between Beta-angle and Lineament Patterns by Using Polarimetric SAR Images. / Iwashita A., Qong M. // 2006. IGARSS 2006. IEEE International Conference on Geoscience and Remote Sensing Symposium. - Denver, CO, July 31 2006-Aug. 4 2006. - P. 1533-1536. ↑
- C3816.** Tomas R. Segura River Aquifer (SE Spain) Obtained by Means of Advanced DInSAR. / Tomas R., Lopez-Sanchez J.M., Delgado J., Mallorqui J.J. // 2006. IGARSS 2006. IEEE International Conference on Geoscience and Remote Sensing Symposium. - Denver, CO, July 31 2006-Aug. 4 2006. - P. 1553-1556. ↑
- C3817.** Ossowska A. A Simulation for Synthetic Aperture Radar with Digital Beam-Forming in Elevation. / Ossowska A., Junghyo Kim, Wiesbeck W. // 2006. IGARSS 2006. IEEE International Conference on Geoscience and Remote Sensing Symposium. - Denver, CO, July 31 2006-Aug. 4 2006. - P. 1407-1410. ↑
- C3818.** Chuanzhao Han. Road Extraction from High-Resolution SAR Image on Urban Area. / Chuanzhao Han, Zhixin Zhou, Zhu Junjie, Ding Chibiao. // 2006. IGARSS 2006. IEEE International Conference on Geoscience and Remote Sensing Symposium. - Denver, CO, July 31 2006-Aug. 4 2006. - P. 1454-1457. ↑
- C3819.** Arkett M. Sea Ice Type and Open Water Discrimination for Operational Ice Monitoring with RADARSAT-2. / Arkett M., Flett D., De Abreu R., Gillespie C. // 2006. IGARSS 2006. IEEE International Conference on Geoscience and Remote Sensing Symposium. - Denver, CO, July 31 2006-Aug. 4 2006. - P. 1458-1461. ↑

1631-1634. ↑

C3820. Singhroy V. InSAR Monitoring of Post-Landslide Activity. / Singhroy V., Couture R., Molch K., Poncos V. // 2006. IGARSS 2006. IEEE International Conference on Geoscience and Remote Sensing Symposium. - Denver, CO, July 31 2006-Aug. 4 2006. - P. 1635-1638. ↑

C3821. Nitti D.O. InSAR Derived Deformation Patterns Related to the Aigion Earthquake (Greece). / Nitti D.O., Bovenga F., Nutricato R., Refice A., Chiaradia M.T. // 2006. IGARSS 2006. IEEE International Conference on Geoscience and Remote Sensing Symposium. - Denver, CO, July 31 2006-Aug. 4 2006. - P. 1564-1567. ↑

C3822. Lehner S. TerraSAR-X for Oceanography. / Lehner S., Schulz-Stellenfleth J. // 2006. IGARSS 2006. IEEE International Conference on Geoscience and Remote Sensing Symposium. - Denver, CO, July 31 2006-Aug. 4 2006. - P. 1342-1345. ↑

C3823. Guangdong Pan. Studies of Ocean Surface Profile Retrieval from Simulated LGA Radar Data. / Guangdong Pan, Burkholder R.J., Johnson J.T., Toporkov J.V., Sletten M.A. // 2006. IGARSS 2006. IEEE International Conference on Geoscience and Remote Sensing Symposium. - Denver, CO, July 31 2006-Aug. 4 2006. - P. 1335-1337. ↑

C3824. Ya-Qiu Jin. A New Set of the Parameters for the Terrain Surface Classification in Polarimetric SAR Image Based on Deorientation of Polarimetric Scattering Vector. / Ya-Qiu Jin, Feng Xu. // 2006. IGARSS 2006. IEEE International Conference on Geoscience and Remote Sensing Symposium. - Denver, CO, July 31 2006-Aug. 4 2006. - P. 1403-1406. ↑

C3825. Gleason S. Bistatic Radar Cross Section Measurements of Ocean Scattered GPS Signals from Low Earth Orbit. / Gleason S., Zavorotny V. // 2006. IGARSS 2006. IEEE International Conference on Geoscience and Remote Sensing Symposium. - Denver, CO, July 31 2006-Aug. 4 2006. - P. 1308-1311. ↑

C3826. Kebiao Mao. A Multiple-Band Algorithm for Separating Land Surface Emissivity and Temperature from ASTER Imagery. / Kebiao Mao, Jiancheng Shi, Zhaoliang Li, Zhihao Qin, Xiufeng Wang, Lingmei Jiang. // 2006. IGARSS 2006. IEEE International Conference on Geoscience and Remote Sensing Symposium. - Denver, CO, July 31 2006-Aug. 4 2006. - P. 1358-1361. ↑

C3827. Paul S.D. An Overview of Hampton University's 48-Inch Lidar System. / Paul S.D., McCormick M.P. // 2006. IGARSS 2006. IEEE International Conference on Geoscience and Remote Sensing Symposium. - Denver, CO, July 31 2006-Aug. 4 2006. - P. 1390-1393. ↑

C3828. Horstmann J. Estimation of Friction Velocity Using Tower Based Marine Radars. / Horstmann J., Dankert H. // 2006. IGARSS 2006. IEEE International Conference on Geoscience and Remote Sensing Symposium. - Denver, CO, July 31 2006-Aug. 4 2006. - P. 1323-1326. ↑

C3829. Adamo M. Oil Spill Surveillance and Tracking with Combined use of SAR and Modis Imagery: A Case Study. / Adamo M., De Carolis G., De Pasquale V., Pasquariello G. // 2006. IGARSS 2006. IEEE International Conference on Geoscience and Remote Sensing Symposium. - Denver, CO, July 31 2006-Aug. 4 2006. - P. 1327-1330. ↑

C3830. Dankert H. A Marine-Radar Wind Sensor. / Dankert H., Horstmann J. // 2006. IGARSS 2006. IEEE International Conference on Geoscience and Remote Sensing Symposium. - Denver, CO, July 31 2006-Aug. 4 2006. - P. 1296-1299. ↑

C3831. Haiyan Li. Effects of Wind on Internal Waves Synthetic Aperture Radar Images. / Haiyan Li, Yijun He, Tao Du, Hui Shen. // 2006. IGARSS 2006. IEEE International Conference on Geoscience and Remote Sensing Symposium. - Denver, CO, July 31 2006-Aug. 4 2006. - P. 1319-1322. ↑

C3832. Pulliainen J. Mapping of Snow Water Equivalent and Snow Coverage from Combined EO and in situ Data for Climatic Studies and Hydrological Forecasting Models. / Pulliainen J., Karna J.-P., Hallikainen M., Luojus K., Metsamäki S., Huttunen M., Anttila S. // 2006. IGARSS 2006. IEEE International Conference on Geoscience and Remote Sensing Symposium. - Denver, CO, July 31 2006-Aug. 4 2006. - P. 1709-1712. ↑

C3833. Simard M. Using Shuttle Radar Topography Mission Elevation Data to Map Mangrove Forest Height in the Caribbean. / Simard M., Keqi Zhang, Ross M.S., Rivera Monroy V.H., Castaeda Moya E., Twilley R. // 2006. IGARSS 2006. IEEE International Conference on Geoscience and Remote Sensing Symposium. - Denver, CO, ↑

July 31 2006-Aug. 4 2006. - P. 1713-1716. ↑

C3834. Le Vine D.M. Aquarius Mission Technical Overview. / Le Vine D.M., Lagerloef G.S.E., Yueh S., Pellerano F., Dinnat E., Wentz F. // 2006. IGARSS 2006. IEEE International Conference on Geoscience and Remote Sensing Symposium. - Denver, CO, July 31 2006-Aug. 4 2006. - P. 1678-1680. ↑

C3835. Freedman A. The Aquarius Scatterometer: An Active System for Measuring Surface Roughness for Sea-Surface Brightness Temperature Correction. / Freedman A., McWatters D., Spencer M. // 2006. IGARSS 2006. IEEE International Conference on Geoscience and Remote Sensing Symposium. - Denver, CO, July 31 2006-Aug. 4 2006. - P. 1685-1688. ↑

C3836. Farage G. Comparison of PolSAR Speckle Filtering Techniques. / Farage G., Foucher S., Benie G.B. // 2006. IGARSS 2006. IEEE International Conference on Geoscience and Remote Sensing Symposium. - Denver, CO, July 31 2006-Aug. 4 2006. - P. 1760-1763. ↑

C3837. Ken Yoong Lee. Spatially Variant Restoration for Polarimetric Synthetic Aperture Radar Imagery. / Ken Yoong Lee, Bretschneider T. // 2006. IGARSS 2006. IEEE International Conference on Geoscience and Remote Sensing Symposium. - Denver, CO, July 31 2006-Aug. 4 2006. - P. 1764-1767. ↑

C3838. Jean-Claude S. Polar Decomposition and Polarimetric SAR Analysis: A Quaternion Approach. / Jean-Claude S., Celine T. // 2006. IGARSS 2006. IEEE International Conference on Geoscience and Remote Sensing Symposium. - Denver, CO, July 31 2006-Aug. 4 2006. - P. 1752-1755. ↑

C3839. Ersahin K. Classification of Polarimetric SAR Data Using Spectral Graph Partitioning. / Ersahin K., Cumming I.G., Yedlin M.J. // 2006. IGARSS 2006. IEEE International Conference on Geoscience and Remote Sensing Symposium. - Denver, CO, July 31 2006-Aug. 4 2006. - P. 1756-1759. ↑

C3840. Aydin K. Scattering and Propagation of Polarimetric Radar Signals in Storms and Clouds. 2006. IGARSS 2006. IEEE International Conference on Geoscience and Remote Sensing Symposium. - Denver, CO, July 31 2006-Aug. 4 2006. - P. 1674. ↑

C3841. Watanabe M. Relation Between Coherence, Forest Biomass, and L-band σ . / Watanabe M., Shimada M. // 2006. IGARSS 2006. IEEE International Conference on Geoscience and Remote Sensing Symposium. - Denver, CO, July 31 2006-Aug. 4 2006. - P. 1651-1654. ↑

C3842. Isoguchi O. Yamase-derived Gap Winds Off the Western Hokkaido Coasts and Their Effects on Sea Surface Temperature Fields. / Isoguchi O., Toyozumi T., Sakaida F., Kawamura H. // 2006. IGARSS 2006. IEEE International Conference on Geoscience and Remote Sensing Symposium. - Denver, CO, July 31 2006-Aug. 4 2006. - P. 1655-1658. ↑

C3843. Touzi R. Wetland Characterization using Polarimetric RADARSAT-2 Capability. 2006. IGARSS 2006. IEEE International Conference on Geoscience and Remote Sensing Symposium. - Denver, CO, July 31 2006-Aug. 4 2006. - P. 1639-1642. ↑

C3844. Takeda M. Design and implementation of PALSAR Ground Data System at ERSDAC. / Takeda M., Otsubox A., Otsubo A., Ota H., Mouri K., Kumai M., Watanabe H., Tsu H. // 2006. IGARSS 2006. IEEE International Conference on Geoscience and Remote Sensing Symposium. - Denver, CO, July 31 2006-Aug. 4 2006. - P. 1647-1650. ↑

C3845. Gorgucci E. Dual-polarization Developments at CNR: Past and Present Research. / Gorgucci E., Baldini L., Scarchilli G. // 2006. IGARSS 2006. IEEE International Conference on Geoscience and Remote Sensing Symposium. - Denver, CO, July 31 2006-Aug. 4 2006. - P. 1666-1669. ↑

C3846. Nakagawa K. Development of a C-band Polarimetric and Pulse Compression Radar in Okinawa, Japan. / Nakagawa K., Hanado H., Takahashi N., Satoh S., Fukutani K., Iguchi T. // 2006. IGARSS 2006. IEEE International Conference on Geoscience and Remote Sensing Symposium. - Denver, CO, July 31 2006-Aug. 4 2006. - P. 1670-1673. ↑

C3847. Mueller E.A. Chill Radar Dual Polarization. / Mueller E.A., Brunkow D.A. // 2006. IGARSS 2006. IEEE International Conference on Geoscience and Remote Sensing Symposium. - Denver, CO, July 31 2006-Aug. 4 2006. - P. 1659-1661. ↑

- C3848.** Cherry S.M. The Development of the Chilbolton Radar 1977 to 1988. 2006. IGARSS 2006. IEEE International Conference on Geoscience and Remote Sensing Symposium. - Denver, CO, July 31 2006-Aug. 4 2006. - P. 1662-1665. ↑
- C3849.** Bolten J. The Application of AMSR-E Soil Moisture for Improved Global Agricultural Assessment and Forecasting. / Bolten J., Crow W., Zhan X., Jackson T., Reynolds C., Doom B. // 2006. IGARSS 2006. IEEE International Conference on Geoscience and Remote Sensing Symposium. - Denver, CO, July 31 2006-Aug. 4 2006. - P. 2032-2035. ↑
- C3850.** Noferini L. Ground-based Radar Interferometry for Terrain Mapping. / Noferini L., Pieraccini M., Luzi G., Mecatti D., Macaluso G., Atzeni C. // 2006. IGARSS 2006. IEEE International Conference on Geoscience and Remote Sensing Symposium. - Denver, CO, USA, July 31 2006-Aug. 4 2006. - P. 2569-2572. ↑
- C3851.** Tagawa T. Suppression of Surface Clutter Interference with TRMM Precipitation Radar Observation. / Tagawa T., Okamoto K., Hanado H., Kozu T. // 2006. IGARSS 2006. IEEE International Conference on Geoscience and Remote Sensing Symposium. - Denver, CO, USA, July 31 2006-Aug. 4 2006. - P. 2573-2576. ↑
- C3852.** Meglio F. Joint Statistical Distribution of Multi-Baseline SAR Interferograms. / Meglio F., Pascazio V., Schirinzi G. // 2006. IGARSS 2006. IEEE International Conference on Geoscience and Remote Sensing Symposium. - Denver, CO, USA, July 31 2006-Aug. 4 2006. - P. 2549-2552. ↑
- C3853.** Lombardini F. Interferometric Model Order Selection: Validation of ITC Methods with Airborne Three-antenna SAR Data. / Lombardini F., Rossing L., Ender J., Cai F. // 2006. IGARSS 2006. IEEE International Conference on Geoscience and Remote Sensing Symposium. - Denver, CO, USA, July 31 2006-Aug. 4 2006. - P. 2565-2568. ↑
- C3854.** Kubota T. Global Precipitation Map using Satelliteborne Microwave Radiometers by the GSMaP Project: Production and Validation. / Kubota T., Hashizume H., Takahashi N., Shige S., Okamoto K., Ushio T., Aonashi K., Kachi M. // 2006. IGARSS 2006. IEEE International Conference on Geoscience and Remote Sensing Symposium. - Denver, CO, USA, July 31 2006-Aug. 4 2006. - P. 2584-2587. ↑
- C3855.** Liu S. Comparison of MODIS Atmospheric Water Vapor Retrieval, Meteorological Models Tropospheric Delay Estimation with the Results Derived from GPS. / Liu S., Zhang C., Guo X., Chu Y., Ge D., Fan J. // 2006. IGARSS 2006. IEEE International Conference on Geoscience and Remote Sensing Symposium. - Denver, CO, USA, July 31 2006-Aug. 4 2006. - P. 2615-2618. ↑
- C3856.** Zafar B. Bright Band Reference Technique to Adjust the Observation of Spaceborne Radar. / Zafar B., Chandrasekar V. // 2006. IGARSS 2006. IEEE International Conference on Geoscience and Remote Sensing Symposium. - Denver, CO, USA, July 31 2006-Aug. 4 2006. - P. 2577-2579. ↑
- C3857.** Takahashi N. Comparison of Instantaneous Rain Rate of Stratiform Rainfall from TRMM/TMI with PR. 2006. IGARSS 2006. IEEE International Conference on Geoscience and Remote Sensing Symposium. - Denver, CO, USA, July 31 2006-Aug. 4 2006. - P. 2580-2583. ↑
- C3858.** Foucher S. Speckle Filtering of PolSAR and PolInSAR Images using Trace-based Partial Differential Equations. / Foucher S., Farage G., Benie G. // 2006. IGARSS 2006. IEEE International Conference on Geoscience and Remote Sensing Symposium. - Denver, CO, USA, July 31 2006-Aug. 4 2006. - P. 2545-2548. ↑
- C3859.** Long B. Significance of LiDAR Return Signal Intensities in Coastal Zone Mapping Applications. / Long B., Xharde R., Boucher M., Forbes D. // 2006. IGARSS 2006. IEEE International Conference on Geoscience and Remote Sensing Symposium. - Denver, CO, USA, July 31 2006-Aug. 4 2006. - P. 2424-2427. ↑
- C3860.** Vijayakumar N. Dynamic Filtering and Mining Triggers in Mesoscale Meteorology Forecasting. / Vijayakumar N., Plale B., Ramachandran R., Li X. // 2006. IGARSS 2006. IEEE International Conference on Geoscience and Remote Sensing Symposium. - Denver, CO, USA, July 31 2006-Aug. 4 2006. - P. 2449-2452. ↑
- C3861.** Langford J. Exploring Small Footprint Lidar Intensity Data in a Forested Environment. / Langford J., Niemann O., Frazer G., Wulder M., Nelson T. // 2006. IGARSS 2006. IEEE International Conference on Geoscience and Remote Sensing Symposium. - Denver, CO, USA, July 31 2006-Aug. 4 2006. - P. 2416-2419. ↑

- C3862.** Hopkinson C. The Influence of Lidar Acquisition Settings on Canopy Penetration and Laser Pulse Return Characteristics. 2006. IGARSS 2006. IEEE International Conference on Geoscience and Remote Sensing Symposium. - Denver, CO, USA, July 31 2006-Aug. 4 2006. - P. 2420-2423. ↑
- C3863.** Simard M. Real-Time Processing Algorithm for Wide Swath Radar Interferometry of Ocean Surface. / Simard M., Rodriguez E. // 2006. IGARSS 2006. IEEE International Conference on Geoscience and Remote Sensing Symposium. - Denver, CO, USA, July 31 2006-Aug. 4 2006. - P. 2538-2541. ↑
- C3864.** Iwashita A. Confirmation of the Surface Displacements by Using ENVISAT Repeat-pass Interferometry in East Coast of Taiwan. / Iwashita A., Baba H., Hara M., Lin Y.-F., Sheu H.-C. // 2006. IGARSS 2006. IEEE International Conference on Geoscience and Remote Sensing Symposium. - Denver, CO, USA, July 31 2006-Aug. 4 2006. - P. 2542-2544. ↑
- C3865.** Dechambre M. Simulation of Nadir Looking P-BAND Radar Return for Biomass Retrieval Applications. 2006. IGARSS 2006. IEEE International Conference on Geoscience and Remote Sensing Symposium. - Denver, CO, USA, July 31 2006-Aug. 4 2006. - P. 2473-2476. ↑
- C3866.** Krekeler C. Multi-variate Bayesian Classification of Soil Drainage using Feature-level Fusion of Topographic and Hydrologic Data. / Krekeler C., Slatton K., Cohen M. // 2006. IGARSS 2006. IEEE International Conference on Geoscience and Remote Sensing Symposium. - Denver, CO, USA, July 31 2006-Aug. 4 2006. - P. 2522-2525. ↑
- C3867.** Kenyi L. Comparison of Forest Canopy Structures in SRTM to LIDAR Data. / Kenyi L., Dubayah R., Hofton M., Hyde P., Blair J. // 2006. IGARSS 2006. IEEE International Conference on Geoscience and Remote Sensing Symposium. - Denver, CO, USA, July 31 2006-Aug. 4 2006. - P. 2670-2672. ↑
- C3868.** Zhou W. Measuring Urban Parcel Lawn Greenness by Using an Object-oriented Classification Approach. / Zhou W., Troy A., Grove M. // 2006. IGARSS 2006. IEEE International Conference on Geoscience and Remote Sensing Symposium. - Denver, CO, USA, July 31 2006-Aug. 4 2006. - P. 2693-2696. ↑
- C3869.** Zaloti Jr. O. Evaluating the Potential of SAR-R99B L and X Bands Data for Amazon Deforestation Increment Mapping. / Zaloti Jr. O., Goncalves F., Freitas C., Joao S., Sant'Anna S., dos Santos J. // 2006. IGARSS 2006. IEEE International Conference on Geoscience and Remote Sensing Symposium. - Denver, CO, USA, July 31 2006-Aug. 4 2006. - P. 2662-2665. ↑
- C3870.** Henry J.-B. Using ERS-1 and ASAR Imagery for Mapping Forest in French Guiana. / Henry J.-B., Hame T., Rauste Y., Sirro L., Ahola H., De Grandi G., Stach N. // 2006. IGARSS 2006. IEEE International Conference on Geoscience and Remote Sensing Symposium. - Denver, CO, USA, July 31 2006-Aug. 4 2006. - P. 2666-2669. ↑
- C3871.** Yoon C.-R. Hierarchical Land-Use Classification Using Optical Imagery and LiDAR Data. / Yoon C.-R., Kim K.-O., Shin J.-S., Lee H.-R., Hwang C.-J. // 2006. IGARSS 2006. IEEE International Conference on Geoscience and Remote Sensing Symposium. - Denver, CO, USA, July 31 2006-Aug. 4 2006. - P. 2746-2749. ↑
- C3872.** Chu H. A SAR Image Classification Method Based on Dempster-Shafer Theory and Markov Context with Parametric and Kernel Method Estimation. / Chu H., Gui-Song X., Hong S. // 2006. IGARSS 2006. IEEE International Conference on Geoscience and Remote Sensing Symposium. - Denver, CO, USA, July 31 2006-Aug. 4 2006. - P. 2742-2745. ↑
- C3873.** Mironov V. Influence of Snow and Plant Covers on the Seasonal Radar Remote Sensing Signal Variations. / Mironov V., Komarov S., Baikalova T., Skoroglyadov V. // 2006. IGARSS 2006. IEEE International Conference on Geoscience and Remote Sensing Symposium. - Denver, CO, USA, July 31 2006-Aug. 4 2006. - P. 2705-2707. ↑
- C3874.** Yamanokuchi T. Comparison of Antarctic Ice Sheet Elevation Between ICESat GLAS and InSAR DEM. / Yamanokuchi T., Doi K., Shibuya K. // 2006. IGARSS 2006. IEEE International Conference on Geoscience and Remote Sensing Symposium. - Denver, CO, USA, July 31 2006-Aug. 4 2006. - P. 2712-2715. ↑
- C3875.** Zolotarev I. Research of the Effect Produced by Transients on the Correlation Properties of the Signals with Pseudorandom Phase Shift Keying in the Systems of the Radar Remote Sensing of the Earth. / Zolotarev I., Miller Y., Pozharsky T. // 2006. IGARSS 2006. IEEE International Conference on Geoscience and Remote

Sensing Symposium. - Denver, CO, USA, July 31 2006-Aug. 4 2006. - P. 2792-2794. ↑

C3876. Elmzoughi A. Optimal Polarimetric Radar Rain Rate Estimator for Semi-arid Regions. / Elmzoughi A., Abdelfattah R., Belhadj Z., Santalla del Rio V. // 2006. IGARSS 2006. IEEE International Conference on Geoscience and Remote Sensing Symposium. - Denver, CO, USA, July 31 2006-Aug. 4 2006. - P. 2627-2630. ↑

C3877. Santalla del Rio V. Polarimetric Covariance Matrix Least Squares Estimation for Weather Radar Applications. 2006. IGARSS 2006. IEEE International Conference on Geoscience and Remote Sensing Symposium. - Denver, CO, USA, July 31 2006-Aug. 4 2006. - P. 2631-2634. ↑

C3878. He Y. High Wind Vector Retrieved from SSM/I. / He Y., Meng L., Shen H. // 2006. IGARSS 2006. IEEE International Conference on Geoscience and Remote Sensing Symposium. - Denver, CO, USA, July 31 2006-Aug. 4 2006. - P. 2619-2622. ↑

C3879. Jin S. Modelling Systematic Residuals in Absolute ZTD Estimation from GPS. / Jin S., Park J.-U., Park P.-H., Cho J.-H. // 2006. IGARSS 2006. IEEE International Conference on Geoscience and Remote Sensing Symposium. - Denver, CO, USA, July 31 2006-Aug. 4 2006. - P. 2623-2626. ↑

C3880. Williams B. An Improved High Resolution Wind Ambiguity Removal Procedure for SeaWinds. / Williams B., Long D. // 2006. IGARSS 2006. IEEE International Conference on Geoscience and Remote Sensing Symposium. - Denver, CO, USA, July 31 2006-Aug. 4 2006. - P. 2643-2646. ↑

C3881. Willie D. Attenuation Statistics for X-band Radar Design. / Willie D., Li W., Wang Y., Chadrakeker V. // 2006. IGARSS 2006. IEEE International Conference on Geoscience and Remote Sensing Symposium. - Denver, CO, USA, July 31 2006-Aug. 4 2006. - P. 2647-2650. ↑

C3882. Xu G. Statistical Modeling for Spatiotemporal Radar Observations and Its Applications to Nowcasting. / Xu G., Chandrasekar V. // 2006. IGARSS 2006. IEEE International Conference on Geoscience and Remote Sensing Symposium. - Denver, CO, USA, July 31 2006-Aug. 4 2006. - P. 2635-2638. ↑

C3883. Gabella M. TRMM-derived Range-adjustment of Ground-based Radars in two Mediterranean Countries. / Gabella M., Corinati L., Perona G., Morin E. // 2006. IGARSS 2006. IEEE International Conference on Geoscience and Remote Sensing Symposium. - Denver, CO, USA, July 31 2006-Aug. 4 2006. - P. 2639-2642. ↑

C3884. Xharde R. Accuracy and Limitations of Airborne LiDAR Surveys in Coastal Environments. / Xharde R., Long B., Forbes D. // 2006. IGARSS 2006. IEEE International Conference on Geoscience and Remote Sensing Symposium. - Denver, CO, USA, July 31 2006-Aug. 4 2006. - P. 2412-2415. ↑

C3885. Brogioni M. Monitoring Snow Cover Characteristics with Multifrequency Active and Passive Microwave Sensors. / Brogioni M., Macelloni G., Paloscia S., Pampaloni P., Pettinato S., Santi E. // 2006. IGARSS 2006. IEEE International Conference on Geoscience and Remote Sensing Symposium. - Denver, CO, July 31 2006-Aug. 4 2006. - P. 2167-2170. ↑

C3886. Horstmann J. Hurricane Winds Measured with Synthetic Aperture Radars. / Horstmann J., Koch W., Thompson D.R., Graber H.C. // 2006. IGARSS 2006. IEEE International Conference on Geoscience and Remote Sensing Symposium. - Denver, CO, July 31 2006-Aug. 4 2006. - P. 2224-2227. ↑

C3887. Praks J. L-band Polarimetric Interferometry in Boreal Forest Parameter Estimation, a Case Study. / Praks J., Hallikainen M., Kugler F., Papathanassiou K., Hajsek I. // 2006. IGARSS 2006. IEEE International Conference on Geoscience and Remote Sensing Symposium. - Denver, CO, July 31 2006-Aug. 4 2006. - P. 2216-2219. ↑

C3888. Reppucci A. Tropical Cyclone Parameters Derived from Synthetic Aperture Radar (SAR) Images. / Reppucci A., Lehner S., Schulz-Stellenfleth J. // 2006. IGARSS 2006. IEEE International Conference on Geoscience and Remote Sensing Symposium. - Denver, CO, July 31 2006-Aug. 4 2006. - P. 2220-2223. ↑

C3889. Hui Shen. Progress in Determination of Wind Vectors from SAR Images. / Hui Shen, Perrie W., Yijun He. // 2006. IGARSS 2006. IEEE International Conference on Geoscience and Remote Sensing Symposium. - Denver, CO, July 31 2006-Aug. 4 2006. - P. 2228-2231. ↑

C3890. Lehner S. Severe Weather Applications over the Oceans using ERS SAR Wavemode Data. / Lehner

S., Konig T., Schulz-Stellenfleth J., Reppucci A. // 2006. IGARSS 2006. IEEE International Conference on Geoscience and Remote Sensing Symposium. - Denver, CO, July 31 2006-Aug. 4 2006. - P. 2232-2235. ↑

C3891. Arakelyan A.A. The Results of Spatio-Temporally Combined, Microwave Active-Passive Measurements of Snow, Bear and Vegetated Soil at 37GHz. / Arakelyan A.A., Manukyan M.R., Hambaryan A.K., Arakelyan A.K. // 2006. IGARSS 2006. IEEE International Conference on Geoscience and Remote Sensing Symposium. - Denver, CO, July 31 2006-Aug. 4 2006. - P. 2044-2047. ↑

C3892. Li L. Polarimetric Passive Microwave Signatures and RFI Suppression During the Soil Moisture Experiment/ Polarimetry Land Experiment in 2005. / Li L., Jackson T., Gaiser P., Bindlish R., Bobak J., Kunkee D., Cosh M. // 2006. IGARSS 2006. IEEE International Conference on Geoscience and Remote Sensing Symposium. - Denver, CO, July 31 2006-Aug. 4 2006. - P. 2036-2039. ↑

C3893. Eriksson L.E.B. Forest Parameter Estimation Using JERS-1 Repeat-pass Interferometry: Stem Volume Retrieval in Siberia and Sweden. / Eriksson L.E.B., Askne J., Santoro M., Wiesmann A. // 2006. IGARSS 2006. IEEE International Conference on Geoscience and Remote Sensing Symposium. - Denver, CO, July 31 2006-Aug. 4 2006. - P. 2212-2215. ↑

C3894. dos Santos J.R. SAR Interferometric Approaches for the Analysis of Structural Forest Parameters: State of the Art and Perspectives for Brazilian Studies. / dos Santos J.R., Neeff T., Dutra L.V., Gama F.F., Mura J.C., Freitas C.C. // 2006. IGARSS 2006. IEEE International Conference on Geoscience and Remote Sensing Symposium. - Denver, CO, July 31 2006-Aug. 4 2006. - P. 2201-2204. ↑

C3895. Dutra L.V. Digital Height Modeling (DHM) of Tropical Forests using Multi-frequency InSAR Methodology. / Dutra L.V., dos Santos J.R., Freitas C.C., Mura J.C., Neeff T., Elmiro M.A.T., Moura P. // 2006. IGARSS 2006. IEEE International Conference on Geoscience and Remote Sensing Symposium. - Denver, CO, July 31 2006-Aug. 4 2006. - P. 2190-2192. ↑

C3896. Florian K. Forest Height Estimation in Tropical Rain Forest using Pol-InSAR Techniques. / Florian K., Kostas P.P., Irena H., Dirk H. // 2006. IGARSS 2006. IEEE International Conference on Geoscience and Remote Sensing Symposium. - Denver, CO, July 31 2006-Aug. 4 2006. - P. 2193-2196. ↑

C3897. Thirion L. Relation between the Attenuation Coefficients and Interferometric Phase Center Heights Behaviors from P-band to L-band. / Thirion L., Colin E. // 2006. IGARSS 2006. IEEE International Conference on Geoscience and Remote Sensing Symposium. - Denver, CO, July 31 2006-Aug. 4 2006. - P. 2197-2200. ↑

C3898. Solberg R. An Approach for Multisensor Harmonization in Snow Cover Area Mapping. / Solberg R., Koren H., Malnes E., Haarpaintner J., Lauknes I. // 2006. IGARSS 2006. IEEE International Conference on Geoscience and Remote Sensing Symposium. - Denver, CO, July 31 2006-Aug. 4 2006. - P. 2171-2175. ↑

C3899. Treuhaft R.N. Tropical-Forest Density Profiles from Multibaseline Interferometric SAR. / Treuhaft R.N., Chapman B.D., dos Santos J.R., Dutra L.V., Goncalves F.G., da Costa Freitas C., Mura J.C., de Graca P.M.A., Drake J.B. // 2006. IGARSS 2006. IEEE International Conference on Geoscience and Remote Sensing Symposium. - Denver, CO, July 31 2006-Aug. 4 2006. - P. 2205-2207. ↑

C3900. Jiancheng Shi. Snow Water Equivalence Retrieval Using X and Ku band Dual-Polarization Radar. 2006. IGARSS 2006. IEEE International Conference on Geoscience and Remote Sensing Symposium. - Denver, CO, July 31 2006-Aug. 4 2006. - P. 2183-2185. ↑

C3901. Luoju K. Development of Techniques to Retrieve Snow Covered Area (SCA) in Boreal Forests from Space-borne Microwave Observations. / Luoju K., Karna J.-P., Hallikainen M., Pulliainen J. // 2006. IGARSS 2006. IEEE International Conference on Geoscience and Remote Sensing Symposium. - Denver, CO, July 31 2006-Aug. 4 2006. - P. 2180-2182. ↑

C3902. McNeill S. Retrospective Change Detection based upon a Multi-season, Sparse Temporal Sequence of JERS-1 SAR Data. / McNeill S., Belliss S., Pairman D., North H. // 2006. IGARSS 2006. IEEE International Conference on Geoscience and Remote Sensing Symposium. - Denver, CO, USA, July 31 2006-Aug. 4 2006. - P. 2353-2356. ↑

C3903. Zribi M. Estimation of Soil Moisture from Multiincidence ASAR-ENVISAT Radar Data. / Zribi M., Baghdadi N., Holah N. // 2006. IGARSS 2006. IEEE International Conference on Geoscience and Remote Sensing Symposium. - Denver, CO, USA, July 31 2006-Aug. 4 2006. - P. 2350-2352. ↑

- C3904.** Lobl E. AMSR-E Accomplishments and Ongoing Activities. / Lobl E., Spencer R. // 2006. IGARSS 2006. IEEE International Conference on Geoscience and Remote Sensing Symposium. - Denver, CO, USA, July 31 2006-Aug. 4 2006. - P. 2383-2385. ↑
- C3905.** Bonci E. Monitoring Urban Changes in Rome, Italy by Multi-Temporal ERS-SAR Images. / Bonci E., Del Frate F., Solimini D. // 2006. IGARSS 2006. IEEE International Conference on Geoscience and Remote Sensing Symposium. - Denver, CO, USA, July 31 2006-Aug. 4 2006. - P. 2357-2360. ↑
- C3906.** Narayan U. High Resolution Change Estimation of Soil Moisture by Combination of TMI Brightness Temperature and PR Surface Cross Section. / Narayan U., Lakshmi V. // 2006. IGARSS 2006. IEEE International Conference on Geoscience and Remote Sensing Symposium. - Denver, CO, USA, July 31 2006-Aug. 4 2006. - P. 2336-2337. ↑
- C3907.** Merzouki A. Spatial Characterization of Soil Moisture Using SAR Data. / Merzouki A., Teillet P., Bannari A., King D. // 2006. IGARSS 2006. IEEE International Conference on Geoscience and Remote Sensing Symposium. - Denver, CO, USA, July 31 2006-Aug. 4 2006. - P. 2332-2335. ↑
- C3908.** Notarnicola C. Soil and Vegetation Moisture Variability Analyzed Through Combination of SAR and Optical Images and Theoretical Models. / Notarnicola C., Posa F. // 2006. IGARSS 2006. IEEE International Conference on Geoscience and Remote Sensing Symposium. - Denver, CO, USA, July 31 2006-Aug. 4 2006. - P. 2346-2349. ↑
- C3909.** Chanzy A. Impact of Filtering Soil Roughness Low Frequencies on the Radar Backscattering Coefficient Simulated by the IEM Model. / Chanzy A., Molineaux B. // 2006. IGARSS 2006. IEEE International Conference on Geoscience and Remote Sensing Symposium. - Denver, CO, USA, July 31 2006-Aug. 4 2006. - P. 2338-2341. ↑
- C3910.** Ainsworth T. SAR Estimation of River Surface Currents: A Sub-Aperture Analysis Approach. / Ainsworth T., Sletten M., Jansen R., Lee J.-S. // 2006. IGARSS 2006. IEEE International Conference on Geoscience and Remote Sensing Symposium. - Denver, CO, USA, July 31 2006-Aug. 4 2006. - P. 2397-2399. ↑
- C3911.** Hwang P. Wave Measurements using a Dual-beam Interferometer Near Gulf Stream Boundary. / Hwang P., Toporkov J., Sletten M., Lamb D., Perkovic D. // 2006. IGARSS 2006. IEEE International Conference on Geoscience and Remote Sensing Symposium. - Denver, CO, USA, July 31 2006-Aug. 4 2006. - P. 2404-2407. ↑
- C3912.** Niamsuwan N. Observations of an ARSR System in Canton, MI with the L-band Interference Suppressing Radiometer. / Niamsuwan N., Guner B., Johnson J. // 2006. IGARSS 2006. IEEE International Conference on Geoscience and Remote Sensing Symposium. - Denver, CO, USA, July 31 2006-Aug. 4 2006. - P. 2285-2288. ↑
- C3913.** Satalino G. Integration of MERIS and ASAR Data for LAI Estimation of Wheat Fields. / Satalino G., Dente L., Mattia F. // 2006. IGARSS 2006. IEEE International Conference on Geoscience and Remote Sensing Symposium. - Denver, CO, July 31 2006-Aug. 4 2006. - P. 2255-2258. ↑
- C3914.** Schulz-Stellenfleth J. Use of Tandem-X in a Squinted Split Antenna Mode Configuration to Retrieve 2-D Current and Ocean Wave Information. / Schulz-Stellenfleth J., Hajnsek I., Lehner S. // 2006. IGARSS 2006. IEEE International Conference on Geoscience and Remote Sensing Symposium. - Denver, CO, USA, July 31 2006-Aug. 4 2006. - P. 2408-2411. ↑
- C3915.** Bindlish R. High Resolution Soil Moisture Mapping Using AIRSAR Observations During SMEX02. / Bindlish R., Jackson T., Van der Velde R. // 2006. IGARSS 2006. IEEE International Conference on Geoscience and Remote Sensing Symposium. - Denver, CO, USA, July 31 2006-Aug. 4 2006. - P. 2324-2327. ↑
- C3916.** Runge H. Clutter Suppression Techniques for River Surface Current Measurements. / Runge H., Suchandt S., Horn R., Eiglsperger T. // 2006. IGARSS 2006. IEEE International Conference on Geoscience and Remote Sensing Symposium. - Denver, CO, USA, July 31 2006-Aug. 4 2006. - P. 2400-2403. ↑
- C3917.** Piepmeier J. Mitigation of Terrestrial Radar Interference in L-Band Spaceborne Microwave Radiometers. / Piepmeier J., Pellerano F. // 2006. IGARSS 2006. IEEE International Conference on Geoscience and Remote Sensing Symposium. - Denver, CO, USA, July 31 2006-Aug. 4 2006. - P. 2292-2296. ↑

- C3918.** Chouinard P. Decision Fusion of Hyperspectral and SAR Data for Trafficability Assessment. / Chouinard P., Kerekes J. // 2006. IGARSS 2006. IEEE International Conference on Geoscience and Remote Sensing Symposium. - Denver, CO, USA, July 31 2006-Aug. 4 2006. - P. 2313-2316. ↑
- C3919.** Liu W.T. Potential scientific applications of seawinds and its follow-on. / Liu W.T., Xiaosu Xie. // 2005. IGARSS '05. Proceedings. 2005 IEEE International Geoscience and Remote Sensing Symposium. 25-29 July 2005. - Vol. 6. - P. 4208-4210. ↑
- C3920.** Zhiwei Li. Modeling of atmospheric effects on InSAR by incorporating terrain elevation information. / Zhiwei Li, Xiaoli Ding, Cheng Huang, Wadge G., Dawei Zheng, Weibao Zou. // 2005. IGARSS '05. Proceedings. 2005 IEEE International Geoscience and Remote Sensing Symposium. 25-29 July 2005. - Vol. 6. - P. 4240-4243. ↑
- C3921.** Wang Yiding. Phase shifting error of active coded transponder in SAR external radiometric calibration. / Wang Yiding, Tu Guofang. // 2005. IGARSS '05. Proceedings. 2005 IEEE International Geoscience and Remote Sensing Symposium. 25-29 July 2005. - Vol. 6. - P. 4150-4153. ↑
- C3922.** Calheiros R.V. Rainfall representativeness at TRMM & GPM PR resolution. / Calheiros R.V., Machado R. // 2005. IGARSS '05. Proceedings. 2005 IEEE International Geoscience and Remote Sensing Symposium. 25-29 July 2005. - Vol. 6. - P. 4130-4133. ↑
- C3923.** Baldini L. Characteristics of the melting layer in the mediterranean region from dual polarization radar measurements at vertical incidence. / Baldini L., Gorgucci E. // 2005. IGARSS '05. Proceedings. 2005 IEEE International Geoscience and Remote Sensing Symposium. 25-29 July 2005. - Vol. 6. - P. 4138-4141. ↑
- C3924.** Ho A.T.S. Improving classification accuracy in through-wall radar imaging using hybrid prony's and singular value decomposition method. / Ho A.T.S., Tham W.H., Low K.S. // 2005. IGARSS '05. Proceedings. 2005 IEEE International Geoscience and Remote Sensing Symposium. 25-29 July 2005. - Vol. 6. - P. 4267-4270. ↑
- C3925.** Mahmood A. International charter 'space and major disasters' status report. / Mahmood A., Cubero-Castan E., Bequignon J., Lauritson L., Soma P., Platzeck G. // 2005. IGARSS '05. Proceedings. 2005 IEEE International Geoscience and Remote Sensing Symposium. 25-29 July 2005. - Vol. 6. - P. 4362-4365. ↑
- C3926.** Allenbach B. Rapid EO disaster mapping service: added value, feedback and perspectives after 4 years of charter actions. / Allenbach B., Andreoli R., Battiston S., Bestault C., Clandillon S., Fella K., Henry J.-B., Meyer C., Scius H., Tholey N., Yesou H., de Fraipont P. // 2005. IGARSS '05. Proceedings. 2005 IEEE International Geoscience and Remote Sensing Symposium. 25-29 July 2005. - Vol. 6. - P. 4373-4378. ↑
- C3927.** Haipeng Wang. The relation between the order parameter of K-distribution in high-resolution polarimetric SAR data and forest biomass. / Haipeng Wang, Ouchi K. // 2005. IGARSS '05. Proceedings. 2005 IEEE International Geoscience and Remote Sensing Symposium. 25-29 July 2005. - Vol. 6. - P. 4339-4342. ↑
- C3928.** Ho A.T.S. Through-wall radar image reconstruction based on time-domain transient signals in the presence of noise. / Ho A.T.S., Tham W.H., Low K.S. // 2005. IGARSS '05. Proceedings. 2005 IEEE International Geoscience and Remote Sensing Symposium. 25-29 July 2005. - Vol. 6. - P. 4271-4274. ↑
- C3929.** Hajnsek I. INDREX II-indonesian airborne radar experiment campaign over tropical forest in L- and P-band: first results. / Hajnsek I., Kugler F., Papathanassiou K., Horn R., Scheiber R., Moreira A., Hoekman D., Davidson M. // 2005. IGARSS '05. Proceedings. 2005 IEEE International Geoscience and Remote Sensing Symposium. 25-29 July 2005. - Vol. 6. - P. 4335-4338. ↑
- C3930.** Seung-Bum Kim. Estimation of the ocean current velocities from radar altimetry and applications to the North Pacific Ocean. 2005. IGARSS '05. Proceedings. 2005 IEEE International Geoscience and Remote Sensing Symposium. 25-29 July 2005. - Vol. 8. - P. 5416-5419. ↑
- C3931.** Tagawa T. Measurement of scattering properties of vegetation at Ka-band by 35GHz polarimetric scatterometer. / Tagawa T., Okamoto K., Ushio T. // 2005. IGARSS '05. Proceedings. 2005 IEEE International Geoscience and Remote Sensing Symposium. 25-29 July 2005. - Vol. 8. - P. 5501-5504. ↑
- C3932.** Vasile G. Intensity-driven-adaptive-neighborhood technique for POLSAR parameters estimation. / Vasile G., Trouve E., Ciuc M., Bolon P., Buzuloiu V. // 2005. IGARSS '05. Proceedings. 2005 IEEE International

Geoscience and Remote Sensing Symposium. 25-29 July 2005. - Vol. 8. - P. 5509-5512. ↑

C3933. Yanjie Zhang. A comparison of the different models used for interferograms flattening. 2005. IGARSS '05. Proceedings. 2005 IEEE International Geoscience and Remote Sensing Symposium. 25-29 July 2005. - Vol. 8. - P. 5494-5496. ↑

C3934. Fujita M. Polarimetric calibration of space SAR data subject to faraday rotation -a three-target approach. 2005. IGARSS '05. Proceedings. 2005 IEEE International Geoscience and Remote Sensing Symposium. 25-29 July 2005. - Vol. 8. - P. 5497-5500. ↑

C3935. Seung-Kuk Lee. Estimating scattering mechanism at oyster farm site by polarimetry SAR. / Seung-Kuk Lee, Sang-Wan Kim. // 2005. IGARSS '05. Proceedings. 2005 IEEE International Geoscience and Remote Sensing Symposium. 25-29 July 2005. - Vol. 8. - P. 5513-5516. ↑

C3936. Moghaddam M. VHF scattering model from multilayer mixed species forests on top of a multilayer rough ground. / Moghaddam M., Tabatabaenejad A. // 2005. IGARSS '05. Proceedings. 2005 IEEE International Geoscience and Remote Sensing Symposium. 25-29 July 2005. - Vol. 8. - P. 5526. ↑

C3937. Dehmollaian M. FDTD and single scattering formulation for simulation of foliage camouflaged hard targets. / Dehmollaian M., Mosallaei H., Sarabandi K. // 2005. IGARSS '05. Proceedings. 2005 IEEE International Geoscience and Remote Sensing Symposium. 25-29 July 2005. - Vol. 8. - P. 5527-5529. ↑

C3938. Qong M. Estimation of forest height and forested area with polarimetric SAR interferometry. / Qong M., Iwashita A. // 2005. IGARSS '05. Proceedings. 2005 IEEE International Geoscience and Remote Sensing Symposium. 25-29 July 2005. - Vol. 8. - P. 5520-5522. ↑

C3939. Chitroub S. Statistical method for data compression and enhancement of multifrequency polarimetric SAR imagery. / Chitroub S., AlSultan S. // 2005. IGARSS '05. Proceedings. 2005 IEEE International Geoscience and Remote Sensing Symposium. 25-29 July 2005. - Vol. 8. - P. 5523-5525. ↑

C3940. Ketelaar G. Initial point selection and validation in PS-InSAR using integrated amplitude calibration. / Ketelaar G., van Leijen F., Marinkovic P., Hanssen R. // 2005. IGARSS '05. Proceedings. 2005 IEEE International Geoscience and Remote Sensing Symposium. 25-29 July 2005. - Vol. 8. - P. 5490-5493. ↑

C3941. Hongxing Liu. Delineation of dry and melt snow zones in antarctica using microwave remote sensing data. / Hongxing Liu, Lei Wang, Jezek K.C. // 2005. IGARSS '05. Proceedings. 2005 IEEE International Geoscience and Remote Sensing Symposium. 25-29 July 2005. - Vol. 8. - P. 5452-5455. ↑

C3942. Oishi T. Proposal of bilinear surface compensation of distortion in least-squares phase unwrapping. / Oishi T., Suksmono A.B., Hirose A. // 2005. IGARSS '05. Proceedings. 2005 IEEE International Geoscience and Remote Sensing Symposium. 25-29 July 2005. - Vol. 8. - P. 5463-5466. ↑

C3943. Buck C. An extension to the wide swath ocean altimeter concept. 2005. IGARSS '05. Proceedings. 2005 IEEE International Geoscience and Remote Sensing Symposium. 25-29 July 2005. - Vol. 8. - P. 5436-5439. ↑

C3944. Larsen Y. Retrieval of snow water equivalent with envisat ASAR in a norwegian hydropower catchment. / Larsen Y., Malnes E., Engen G. // 2005. IGARSS '05. Proceedings. 2005 IEEE International Geoscience and Remote Sensing Symposium. 25-29 July 2005. - Vol. 8. - P. 5444-5447. ↑

C3945. Rahnmooonfar M. Two dimensional phase unwrapping of interferometric SAR data by means of wavelet technique. / Rahnmooonfar M., Rahmati M., Tavakoli A., Saradjian M.R. // 2005. IGARSS '05. Proceedings. 2005 IEEE International Geoscience and Remote Sensing Symposium. 25-29 July 2005. - Vol. 8. - P. 5467-5470. ↑
















C3946. Jun-su Kim. Theoretical evaluation of phase center of artificial metal structure in NASA(IPL) topsar data. / Jun-su Kim, Sang-Eun Park, Duk-jin Kim, Wooil M. Moon. // 2005. IGARSS '05. Proceedings. 2005 IEEE International Geoscience and Remote Sensing Symposium. 25-29 July 2005. - Vol. 8. - P. 5479-5481. ↑

C3947. Suchandt S. Measurement of river surface currents using SAR techniques. / Suchandt S., Runge H., Eineder M., Scheiber R. // 2005. IGARSS '05. Proceedings. 2005 IEEE International Geoscience and Remote Sensing Symposium. 25-29 July 2005. - Vol. 8. - P. 5486-5489. ↑

- C3948.** Ferraiuolo G. Digital elevation model enhancement from multiple interferograms. / Ferraiuolo G., Pascasio V., Schirizzi G. // 2005. IGARSS '05. Proceedings. 2005 IEEE International Geoscience and Remote Sensing Symposium. 25-29 July 2005. - Vol. 8. - P. 5471-5474. ↑
- C3949.** Xinwu Li. Multi-incidence angle DEM generation and analysis using ENVISAT/ASAR data. / Xinwu Li, Huadong Guo, Zhen Li, Changlin Wang, Lei Wang. // 2005. IGARSS '05. Proceedings. 2005 IEEE International Geoscience and Remote Sensing Symposium. 25-29 July 2005. - Vol. 8. - P. 5475-5478. ↑
- C3950.** Ya-Qiu Jin. Change detection of enhanced, no-changed and reduced scattering in multi-temporal ERS-2 SAR images using the two-thresholds EM and MRF algorithms. 2005. IGARSS '05. Proceedings. 2005 IEEE International Geoscience and Remote Sensing Symposium. 25-29 July 2005. - Vol. 6. - P. 3994-3997. ↑
- C3951.** Liming Jiang. Unsupervised change detection in urban area using multitemporal ERS-1/2 InSAR data. / Liming Jiang, Mingsheng Liao, Lijun Lu, Hui Lin. // 2005. IGARSS '05. Proceedings. 2005 IEEE International Geoscience and Remote Sensing Symposium. 25-29 July 2005. - Vol. 6. - P. 4002-4005. ↑
- C3952.** Mercer J.B. Fusion Of High Resolution Radar And Low Resolution Multi-spectral Optical Imagery. / Mercer J.B., Edwards D., Maduck J., Gang Hong, Yun Zhang. // 2005. IGARSS '05. Proceedings. 2005 IEEE International Geoscience and Remote Sensing Symposium. 25-29 July 2005. - Vol. 6. - P. 3931-3934. ↑
- C3953.** Feizhou Zhang. Application of image matching technology based on SAR image to integrated navigation system. / Feizhou Zhang, Ting Zhang, Xiuwan Chen. // 2005. IGARSS '05. Proceedings. 2005 IEEE International Geoscience and Remote Sensing Symposium. 25-29 July 2005. - Vol. 6. - P. 3952-3955. ↑
- C3954.** Horstmann J. Investigation of SAR wind field retrieval with respect to hurricane winds. / Horstmann J., Graber H.C., Koch W., Iris S. // 2005. IGARSS '05. Proceedings. 2005 IEEE International Geoscience and Remote Sensing Symposium. 25-29 July 2005. - Vol. 6. - P. 4018-4021. ↑
- C3955.** Jung Hyo Kim. Implementation of ground-based SAR demonstrator system for digital beam forming. / Jung Hyo Kim, Younis M., Wiesbeck W. // 2005. IGARSS '05. Proceedings. 2005 IEEE International Geoscience and Remote Sensing Symposium. 25-29 July 2005. - Vol. 6. - P. 4037-4040. ↑
- C3956.** Soisuvann S. Ocean surface wind vector retrievals using active and passive microwave sensing on ADEOS-II. / Soisuvann S., Jones W.L., Kasparis T. // 2005. IGARSS '05. Proceedings. 2005 IEEE International Geoscience and Remote Sensing Symposium. 25-29 July 2005. - Vol. 6. - P. 4006-4009. ↑
- C3957.** Shimada T. Ocean surface winds and wind waves off the northeastern Japanese coast by combined use of high-resolution active microwave sensors. / Shimada T., Kawamura H. // 2005. IGARSS '05. Proceedings. 2005 IEEE International Geoscience and Remote Sensing Symposium. 25-29 July 2005. - Vol. 6. - P. 4010-4013. ↑
- C3958.** Mironov V.L. Coprocessing of radar coherence and spectral optical data. / Mironov V.L., Chimitdorzhiev T.N., Dagurov P.N., Dmitriev A.V. // 2005. IGARSS '05. Proceedings. 2005 IEEE International Geoscience and Remote Sensing Symposium. 25-29 July 2005. - Vol. 6. - P. 3913-3915. ↑
- C3959.** Suchandt S. Results from an airborne SAR GMTI experiment supporting TerraSAR-X traffic processor development. / Suchandt S., Palubinskas G., Scheiber R., Meyer F., Runge H., Reinartz P., Horn R. // 2005. IGARSS '05. Proceedings. 2005 IEEE International Geoscience and Remote Sensing Symposium. 25-29 July 2005. - Vol. 4. - P. 2949-2952. ↑
- C3960.** Xiaorong Xue. A new method of parallel SAR image classification. / Xiaorong Xue, Qiming Zeng, Shuyi Zhang. // 2005. IGARSS '05. Proceedings. 2005 IEEE International Geoscience and Remote Sensing Symposium. 25-29 July 2005. - Vol. 6. - P. 3761-3764. ↑
- C3961.** Sikaneta I. SPECAN filtering for dual-channel stripmap-SAR GMTI. 2005. IGARSS '05. Proceedings. 2005 IEEE International Geoscience and Remote Sensing Symposium. 25-29 July 2005. - Vol. 4. - P. 2942-2945. ↑
- C3962.** Daiyin Zhu. SAR ground moving target imaging based on keystone transform without interpolation. / Daiyin Zhu, Zhaoda Zhu, Ling Wang. // 2005. IGARSS '05. Proceedings. 2005 IEEE International Geoscience and Remote Sensing Symposium. 25-29 July 2005. - Vol. 4. - P. 2946-2948. ↑

- C3963.** Zhi Tang. Study on co-registration method based on correlation coefficient for InSAR signal processing. / Zhi Tang, Yinqing Zhou, Jingwen Li. // 2005. IGARSS '05. Proceedings. 2005 IEEE International Geoscience and Remote Sensing Symposium. 25-29 July 2005. - Vol. 6. - P. 3867-3870. ↑
- C3964.** Jingsong Yang. Ocean features separation from multifrequency polarimetric SAR imagery. / Jingsong Yang, Qingmei Xiao, Weigen Huang, Bin Fu, Peng Chen, Lu Yao. // 2005. IGARSS '05. Proceedings. 2005 IEEE International Geoscience and Remote Sensing Symposium. 25-29 July 2005. - Vol. 6. - P. 3892-3894. ↑
- C3965.** Ahtonen P. Automatic detection of water bodies from spaceborne SAR images. / Ahtonen P., Hallikainen M. // 2005. IGARSS '05. Proceedings. 2005 IEEE International Geoscience and Remote Sensing Symposium. 25-29 July 2005. - Vol. 6. - P. 3845-3848. ↑
- C3966.** Han Chunming. Classification of ASAR images based on texture. / Han Chunming, Guo Huadong, Shao Yun, Liao Jingjuan. // 2005. IGARSS '05. Proceedings. 2005 IEEE International Geoscience and Remote Sensing Symposium. 25-29 July 2005. - Vol. 6. - P. 3849-3851. ↑
- C3967.** Hamasaki T. Natural objects monitoring using polarimetric interferometric ground-based SAR (GB-SAR) system. / Hamasaki T., Sato M., Ferro-Famil L., Pottier E. // 2005. IGARSS '05. Proceedings. 2005 IEEE International Geoscience and Remote Sensing Symposium. 25-29 July 2005. - Vol. 6. - P. 4092-4095. ↑
- C3968.** Leva D. Using a ground based interferometric synthetic aperture radar (GBinSAR) sensor to monitor a landslide in Japan. / Leva D., Rivolta C., Rossetti I.B., Kuzuoka S., Mizuno T. // 2005. IGARSS '05. Proceedings. 2005 IEEE International Geoscience and Remote Sensing Symposium. 25-29 July 2005. - Vol. 6. - P. 4096-4099. ↑
- C3969.** Uratsuka S. Disastrous environment after earthquake observed by airborne SAR (Pi-SAR). / Uratsuka S., Moriyama T., Umehara T., Nadai A., Matsuoka T., Nakamura K., Masuko H. // 2005. IGARSS '05. Proceedings. 2005 IEEE International Geoscience and Remote Sensing Symposium. 25-29 July 2005. - Vol. 6. - P. 4081-4083. ↑
- C3970.** Moriyama T. Polarimetric analysis of the disastrous environment by using Pi-SAR. / Moriyama T., Uratsuka S., Umehara T., Nadai A., Matsuoka T., Nakamura K., Masuko H. // 2005. IGARSS '05. Proceedings. 2005 IEEE International Geoscience and Remote Sensing Symposium. 25-29 July 2005. - Vol. 6. - P. 4084-4087. ↑
- C3971.** Gage K.S. Use of radar profilers in multi-sensor ground validation for TRMM and GPM. / Gage K.S., Williams C.R. // 2005. IGARSS '05. Proceedings. 2005 IEEE International Geoscience and Remote Sensing Symposium. 25-29 July 2005. - Vol. 6. - P. 4116-4119. ↑
- C3972.** Shimizu S. Development and cal/val plan of spaceborne dual-frequency precipitation radar for GPM. / Shimizu S., Hanado H., Kojima M., Iguchi T., Nakamura K. // 2005. IGARSS '05. Proceedings. 2005 IEEE International Geoscience and Remote Sensing Symposium. 25-29 July 2005. - Vol. 6. - P. 4124-4126. ↑
- C3973.** Pieraccini M. Step frequency synthetic radar techniques for free-space and sub-surface imaging. 2005. IGARSS '05. Proceedings. 2005 IEEE International Geoscience and Remote Sensing Symposium. 25-29 July 2005. - Vol. 6. - P. 4100-4103. ↑
- C3974.** Herrmann R. Image reconstruction by a ground-based SAR system. / Herrmann R., Sato M. // 2005. IGARSS '05. Proceedings. 2005 IEEE International Geoscience and Remote Sensing Symposium. 25-29 July 2005. - Vol. 6. - P. 4104-4107. ↑
- C3975.** Yamaguchi Y. A four-component decomposition of POLSAR image. / Yamaguchi Y., Ishido M., Yamada H., Moriyama T. // 2005. IGARSS '05. Proceedings. 2005 IEEE International Geoscience and Remote Sensing Symposium. 25-29 July 2005. - Vol. 6. - P. 4073-4076. ↑
- C3976.** Jie Chen. Analysis of ambiguity for synthetic aperture radar satellite with mechanical distortion in phased array antenna. / Jie Chen, Zhu Wen, Yinqing Zhou. // 2005. IGARSS '05. Proceedings. 2005 IEEE International Geoscience and Remote Sensing Symposium. 25-29 July 2005. - Vol. 6. - P. 4049-4052. ↑
- C3977.** Woo-Kyung Lee. SAR system technology development for korean peninsula. / Woo-Kyung Lee, Young-Kil Kwag. // 2005. IGARSS '05. Proceedings. 2005 IEEE International Geoscience and Remote Sensing Symposium. 25-29 July 2005. - Vol. 6. - P. 4053-4056. ↑

- C3978.** Suwa K. Forward looking radar imaging method using multiple receiver antennas and digital beam forming technique. / Suwa K., Iwamoto M. // 2005. IGARSS '05. Proceedings. 2005 IEEE International Geoscience and Remote Sensing Symposium. 25-29 July 2005. - Vol. 6. - P. 4041-4044. ↑
- C3979.** Franceschetti G. 2-D Fourier domain SAR raw signal simulation accounting for sensor trajectory deviations. / Franceschetti G., Iodice A., Perna S., Riccio D. // 2005. IGARSS '05. Proceedings. 2005 IEEE International Geoscience and Remote Sensing Symposium. 25-29 July 2005. - Vol. 6. - P. 4045-4048. ↑
- C3980.** Zahn R. Versatile SAR sensors for south east asian applications. 2005. IGARSS '05. Proceedings. 2005 IEEE International Geoscience and Remote Sensing Symposium. 25-29 July 2005. - Vol. 6. - P. 4065-4068. ↑
- C3981.** Kwag Y.K. Spaceborne small SAR technology demonstration. 2005. IGARSS '05. Proceedings. 2005 IEEE International Geoscience and Remote Sensing Symposium. 25-29 July 2005. - Vol. 6. - P. 4069-4072. ↑
- C3982.** Suk-Ho Lee. An airborne SAR development demonstration in Korea. / Suk-Ho Lee, Bo-Yeon Koh, Yong-Chul Hwang. // 2005. IGARSS '05. Proceedings. 2005 IEEE International Geoscience and Remote Sensing Symposium. 25-29 July 2005. - Vol. 6. - P. 4057-4060. ↑
- C3983.** Young-Kyun Kong. An experimental automobile-based SAR/InSAR. / Young-Kyun Kong, Byoung-Lae Cho, Young-Soo Kim. // 2005. IGARSS '05. Proceedings. 2005 IEEE International Geoscience and Remote Sensing Symposium. 25-29 July 2005. - Vol. 6. - P. 4061-4064. ↑
- C3984.** Zou Kun. Polarimetric calibration for low frequency UWBSAR system. / Zou Kun, Liang Diannong. // 2005. IGARSS '05. Proceedings. 2005 IEEE International Geoscience and Remote Sensing Symposium. 25-29 July 2005. - Vol. 8. - P. 5534-5537. ↑
- C3985.** Seong-Jun Cho. Bistatic GPR by using an optical electric field sensor. / Seong-Jun Cho, Tanaka R., Sato M. // 2005. IGARSS '05. Proceedings. 2005 IEEE International Geoscience and Remote Sensing Symposium. 25-29 July 2005. - Vol. 1. - P. 4 ↑
- C3986.** Takayama T. Evaluation of an array type directional borehole radar system. / Takayama T., Sato M. // 2005. IGARSS '05. Proceedings. 2005 IEEE International Geoscience and Remote Sensing Symposium. 25-29 July 2005. - Vol. 1. - P. 4 ↑
- C3987.** Jia Cheng-Li. Road extraction from high-resolution SAR imagery using Hough transform. / Jia Cheng-Li, Ji Ke-Feng, Jiang Yong-Mei, Kuang Gang-Yao. // 2005. IGARSS '05. Proceedings. 2005 IEEE International Geoscience and Remote Sensing Symposium. 25-29 July 2005. - Vol. 1. - P. 4 ↑
- C3988.** Mahapatra P.R. Synthesis of generalized vertical-plane weather radar imagery along aircraft flight paths. / Mahapatra P.R., Makkapati V.V. // 2005. IGARSS '05. Proceedings. 2005 IEEE International Geoscience and Remote Sensing Symposium. 25-29 July 2005. - Vol. 1. - P. 4 ↑
- C3989.** Jung-Ho Kim. Effective 3D GPR survey and its application to the exploration of old remains. / Jung-Ho Kim, Myeong-Jong Yi, Jeong-Sul Son, Seong-Jun Cho, Sam-Gyu Park. // 2005. IGARSS '05. Proceedings. 2005 IEEE International Geoscience and Remote Sensing Symposium. 25-29 July 2005. - Vol. 1. - P. 4 ↑
- C3990.** Lestari A.A. Adaptive wire bow-tie antenna for ground penetrating radar. / Lestari A.A., Yarovoy A.G., Ligthart L.P. // 2005. IGARSS '05. Proceedings. 2005 IEEE International Geoscience and Remote Sensing Symposium. 25-29 July 2005. - Vol. 1. - P. 4 ↑
- C3991.** Inggs M. Drill head mounted obstacle avoidance radar. / Inggs M., Langman A., Kothari K., du Toit L.J., Hanson D. // 2005. IGARSS '05. Proceedings. 2005 IEEE International Geoscience and Remote Sensing Symposium. 25-29 July 2005. - Vol. 1. - P. 4 ↑
- C3992.** Sixin Liu. Subsurface water-filled fracture detection by borehole radar: a case history. / Sixin Liu, Zhaofa Zeng, Sato M. // 2005. IGARSS '05. Proceedings. 2005 IEEE International Geoscience and Remote Sensing Symposium. 25-29 July 2005. - Vol. 1. - P. 4 ↑
- C3993.** Yoong K. POLSAR speckle filtering with structural feature and scattering property preservation. / Yoong K., Bretschneider T. // 2005. IGARSS '05. Proceedings. 2005 IEEE International Geoscience and Remote Sensing Symposium. 25-29 July 2005. - Vol. 1. - P. 4 ↑

- C3994.** Takahashi K. Estimation of a buried pipe location by borehole radar. / Takahashi K., Sato M. // 2005. IGARSS '05. Proceedings. 2005 IEEE International Geoscience and Remote Sensing Symposium. 25-29 July 2005. - Vol. 1. - P. 4 
- C3995.** Borrión H. One-dimensional model-based approach for ISAR imaging. / Borrión H., Griffiths H.D., Tait P., Money D., Baker C.J. // 2005. IGARSS '05. Proceedings. 2005 IEEE International Geoscience and Remote Sensing Symposium. 25-29 July 2005. - Vol. 1. - P. 4 
- C3996.** Lennon M. Oil slick detection and characterization by satellite and airborne sensors: experimental results with SAR, hyperspectral and lidar data. / Lennon M., Thomas N., Mariette V., Babichenko S., Mercier G. // 2005. IGARSS '05. Proceedings. 2005 IEEE International Geoscience and Remote Sensing Symposium. 25-29 July 2005. - Vol. 1. - P. 4 
- C3997.** Cao Fang. A new classification method based on Cloude Pottier eigenvalue/eigenvector decomposition. / Cao Fang, Hong Wen. // 2005. IGARSS '05. Proceedings. 2005 IEEE International Geoscience and Remote Sensing Symposium. 25-29 July 2005. - Vol. 1. - P. 4 
- C3998.** Surussavadee C. Statistical agreement between observed microwave satellite radiances and NWP hydrometeors including hexagonal plates and rosettes. / Surussavadee C., Staelin D.H. // 2005. IGARSS '05. Proceedings. 2005 IEEE International Geoscience and Remote Sensing Symposium. 25-29 July 2005. - Vol. 1. - P. 4 
- C3999.** Prats P. Topography accommodation during motion compensation in interferometric repeat-pass SAR images. / Prats P., Reigber A., Mallorqui J.J. // 2005. IGARSS '05. Proceedings. 2005 IEEE International Geoscience and Remote Sensing Symposium. 25-29 July 2005. - Vol. 1. - P. 4 
- C4000.** Meta A. Signal processing algorithms for FMCW moving target indicator synthetic aperture radar. / Meta A., Hoozeboom P. // 2005. IGARSS '05. Proceedings. 2005 IEEE International Geoscience and Remote Sensing Symposium. 25-29 July 2005. - Vol. 1. - P. 4 
- C4001.** Luoju K. Snow covered area estimation using satellite radar wide swath images. / Luoju K., Pulliainen J., Metsamäki S., Hallikainen M. // 2005. IGARSS '05. Proceedings. 2005 IEEE International Geoscience and Remote Sensing Symposium. 25-29 July 2005. - Vol. 1. - P. 4 
- C4002.** Sachs J. Ultra wideband radar assembly kit. / Sachs J., Kmec M., Zetik R., Peyerl P., Rauschenbach P. // 2005. IGARSS '05. Proceedings. 2005 IEEE International Geoscience and Remote Sensing Symposium. 25-29 July 2005. - Vol. 1. - P. 4 
- C4003.** Mukhopadhyay P.K. Synthetic aperture sonar 3-D imaging of targets in air using multiple, non-parallel shot lines. / Mukhopadhyay P.K., Wilkinson A.J., Inggis M.R. // 2005. IGARSS '05. Proceedings. 2005 IEEE International Geoscience and Remote Sensing Symposium. 25-29 July 2005. - Vol. 1. - P. 4 
- C4004.** Rostan F. CryoSat prelaunch status and performance. / Rostan F., Mallow U., Riegger S. // 2005. IGARSS '05. Proceedings. 2005 IEEE International Geoscience and Remote Sensing Symposium. 25-29 July 2005. - Vol. 1. - P. 4 
- C4005.** Singh D. Polarization discrimination ratio approach to retrieve bare soil moisture at X-band. 2005. IGARSS '05. Proceedings. 2005 IEEE International Geoscience and Remote Sensing Symposium. 25-29 July 2005. - Vol. 1. - P. 4 
- C4006.** Junyent F. Salient features of radar nodes of the first generation NetRad System. / Junyent F., Chandrasekar V., McLaughlin D.J., Frasier S., Insanici E., Ahmed R., Bharadwaj N., Knapp E., Krnan L., Tessier R. // 2005. IGARSS '05. Proceedings. 2005 IEEE International Geoscience and Remote Sensing Symposium. 25-29 July 2005. - Vol. 1. - P. 4 
- C4007.** Rodionova N.V. Speckle filtering influence on unsupervised terrain classification based on polarimetric scattering mechanisms. 2005. IGARSS '05. Proceedings. 2005 IEEE International Geoscience and Remote Sensing Symposium. 25-29 July 2005. - Vol. 1. - P. 4 
- C4008.** Rottensteiner F. Data acquisition for 3D city models from LIDAR extracting buildings and roads. / Rottensteiner F., Trinder J., Clode S. // 2005. IGARSS '05. Proceedings. 2005 IEEE International Geoscience and Remote Sensing Symposium. 25-29 July 2005. - Vol. 1. - P. 4 

- C4009.** Amberg V. Improvement of road extraction in high resolution SAR data by a context-based approach. / Amberg V., Coulon M., Marthon P., Spigai M. // 2005. IGARSS '05. Proceedings. 2005 IEEE International Geoscience and Remote Sensing Symposium. 25-29 July 2005. - Vol. 1. - P. 4 ↑
- C4010.** Mercier G. Unsupervised oil slick detection by SAR imagery using kernel expansion. / Mercier G., Girard-Ardhuin F. // 2005. IGARSS '05. Proceedings. 2005 IEEE International Geoscience and Remote Sensing Symposium. 25-29 July 2005. - Vol. 1. - P. 4 ↑
- C4011.** Low A. Derivation of near surface soil moisture patterns from ENVISAT ASAR data. / Low A., Ludwig R., Mauser W. // 2005. IGARSS '05. Proceedings. 2005 IEEE International Geoscience and Remote Sensing Symposium. 25-29 July 2005. - Vol. 1. - P. 4 ↑
- C4012.** Sikdar M. Incorporating a vegetation index into a soil moisture retrieval model \$results from Convair-580 SAR data. / Sikdar M., Macintosh S., Cumming I., Brisco B. // 2005. IGARSS '05. Proceedings. 2005 IEEE International Geoscience and Remote Sensing Symposium. 25-29 July 2005. - Vol. 1. - P. 4 ↑
- C4013.** Narayan U. A simple method for spatial disaggregation of radiometer derived soil moisture using higher resolution radar observations. / Narayan U., Lakshmi V. // 2005. IGARSS '05. Proceedings. 2005 IEEE International Geoscience and Remote Sensing Symposium. 25-29 July 2005. - Vol. 1. - P. 5 ↑
- C4014.** Timchenko A.I. Signal processing method for detection of subsurface objects by ultra-wideband SAR. / Timchenko A.I., Zurk L. // 2005. IGARSS '05. Proceedings. 2005 IEEE International Geoscience and Remote Sensing Symposium. 25-29 July 2005. - Vol. 1. - P. 3 ↑
- C4015.** Xuan Feng. Landmine imaging by a hand-held GPR and metal detector sensor (ALIS). / Xuan Feng, Sato M. // 2005. IGARSS '05. Proceedings. 2005 IEEE International Geoscience and Remote Sensing Symposium. 25-29 July 2005. - Vol. 1. - P. 4 ↑
- C4016.** Pierce L. The MOSS VHF/UHF spaceborne SAR system testbed. / Pierce L., Moghaddam M. // 2005. IGARSS '05. Proceedings. 2005 IEEE International Geoscience and Remote Sensing Symposium. 25-29 July 2005. - Vol. 1. - P. 1 ↑
- C4017.** Chen Q. Land-surface parameters estimation from ERS Wind Scatterometer: a case study in China. / Chen Q., Zhen Li, Lei Wang. // 2005. IGARSS '05. Proceedings. 2005 IEEE International Geoscience and Remote Sensing Symposium. 25-29 July 2005. - Vol. 1. - P. 3 ↑
- C4018.** Santi E. Soil moisture maps from ENVISAT ASAR images in both flat and mountainous areas. / Santi E., Paloscia S., Pettinato S., Poggi P. // 2005. IGARSS '05. Proceedings. 2005 IEEE International Geoscience and Remote Sensing Symposium. 25-29 July 2005. - Vol. 1. - P. 4 ↑
- C4019.** Satalino G. Soil moisture retrieval from ASAR measurements over natural surfaces with a large roughness variability. / Satalino G., Mattia F., Pasquariello G., Dente L. // 2005. IGARSS '05. Proceedings. 2005 IEEE International Geoscience and Remote Sensing Symposium. 25-29 July 2005. - Vol. 1. - P. 4 ↑
- C4020.** Fernandez D.E. Airborne measurements of rain and the ocean surface backscatter response at C- and Ku-band. / Fernandez D.E., Chang P.S., Carswell J.R., Contreras R.F., Frasier S.J. // 2005. IGARSS '05. Proceedings. 2005 IEEE International Geoscience and Remote Sensing Symposium. 25-29 July 2005. - Vol. 1. - P. 4 ↑
- C4021.** Mahmood A. RADARSAT-1 background mission monitoring of the Arctic. 2005. IGARSS '05. Proceedings. 2005 IEEE International Geoscience and Remote Sensing Symposium. 25-29 July 2005. - Vol. 1. - P. 4 ↑
- C4022.** Brule L. RADARSAT-2 Program update. / Brule L., Delisle D., Baeggli H., Graham J. // 2005. IGARSS '05. Proceedings. 2005 IEEE International Geoscience and Remote Sensing Symposium. 25-29 July 2005. - Vol. 1. - P. 3 ↑
- C4023.** Di Bisceglie M. Constant false alarm rate in fire detection for MODIS data. / Di Bisceglie M., Episcopo R., Galdi C., Ullo S.L. // 2005. IGARSS '05. Proceedings. 2005 IEEE International Geoscience and Remote Sensing Symposium. 25-29 July 2005. - Vol. 8. - P. 5717-5720. ↑
- C4024.** Srivastava S.K. RADARSAT-1 image quality excellence in the extended mission. / Srivastava S.K.,

Cote S., Le Dantec P., Hawkins R.K. // 2005. IGARSS '05. Proceedings. 2005 IEEE International Geoscience and Remote Sensing Symposium. 25-29 July 2005. - Vol. 1. - P. 4 ↑

C4025. van der Sanden J.J. Applications potential of RADARSAT-2-update. / van der Sanden J.J., Thomas S.J., Lukowski T.I., Charbonneau F.J., DeAbreu R., Hawkins R.K., Livingstone C.E., McNairn H., Scheuchl B., Singhroy V., Toutin T., Touzi R., Vachon P.W. // 2005. IGARSS '05. Proceedings. 2005 IEEE International Geoscience and Remote Sensing Symposium. 25-29 July 2005. - Vol. 1. - P. 4 ↑

C4026. Tello M. Application of multiresolution and multispectral polarimetric techniques for reliable vessel monitoring and control. / Tello M., Mallorqui J.J., Lopez-Martinez C. // 2005. IGARSS '05. Proceedings. 2005 IEEE International Geoscience and Remote Sensing Symposium. 25-29 July 2005. - Vol. 1. - P. 4 ↑

C4027. Hillman A. Countdown for RADARSAT-2 system operations. / Hillman A., Comi D., Branson W., Rolland P. // 2005. IGARSS '05. Proceedings. 2005 IEEE International Geoscience and Remote Sensing Symposium. 25-29 July 2005. - Vol. 1. - P. 4 ↑

C4028. Graham J.A. Test evolution: RADARSAT-1 to RADARSAT-2. / Graham J.A., Bannon P., Biggs J., Collins G., Ahmed S., Dumoulin J.-G. // 2005. IGARSS '05. Proceedings. 2005 IEEE International Geoscience and Remote Sensing Symposium. 25-29 July 2005. - Vol. 1. - P. 4 ↑

C4029. Joong-Sun Won. Application of ERS SAR to the study of korean tidal flats. / Joong-Sun Won, Sang-Hoon Hong, Myung-Ki Kim. // 2005. IGARSS '05. Proceedings. 2005 IEEE International Geoscience and Remote Sensing Symposium. 25-29 July 2005. - Vol. 8. - P. 5683-5686. ↑

C4030. Wiesbeck W. Interference of short range radar with radio astronomy base stations. / Wiesbeck W., Sorgel W., Baldauf M.A., Younis M. // 2005. IGARSS '05. Proceedings. 2005 IEEE International Geoscience and Remote Sensing Symposium. 25-29 July 2005. - Vol. 8. - P. 5574-5577. ↑

C4031. Joon Heo. Verification of timber age mapping with shuttle radar topography mission and national elevation datasets in the U.S. 2005. IGARSS '05. Proceedings. 2005 IEEE International Geoscience and Remote Sensing Symposium. 25-29 July 2005. - Vol. 8. - P. 5592-5593. ↑

C4032. Zolotaryov I.D. Research of deformation of the fine phase structure of ultra wideband radar signals when passing through the system of identical selective filters. / Zolotaryov I.D., Miller Ya.E., Pozharsky T.O. // 2005. IGARSS '05. Proceedings. 2005 IEEE International Geoscience and Remote Sensing Symposium. 25-29 July 2005. - Vol. 8. - P. 5538-5542. ↑

C4033. Zou Kun. Radiometric correction and calibration for low frequency UWB SAR system. / Zou Kun, Liang Diannong. // 2005. IGARSS '05. Proceedings. 2005 IEEE International Geoscience and Remote Sensing Symposium. 25-29 July 2005. - Vol. 8. - P. 5543-5546. ↑

C4034. Baillarin-Ribbes F. Spot image / SARCOM: distribution of envisat images and direct receiving stations for various land applications. / Baillarin-Ribbes F., Chikhi M., Campenon P. // 2005. IGARSS '05. Proceedings. 2005 IEEE International Geoscience and Remote Sensing Symposium. 25-29 July 2005. - Vol. 8. - P. 5667-5669. ↑

C4035. Kuzuoka S. Land motion monitoring in Japan using PSInSAR technique. / Kuzuoka S., Mizuno T. // 2005. IGARSS '05. Proceedings. 2005 IEEE International Geoscience and Remote Sensing Symposium. 25-29 July 2005. - Vol. 8. - P. 5681-5682. ↑

C4036. McNeill S.J. Verification of X-band SRTM DEM data quality in New Zealand. / McNeill S.J., Belliss S.E., North H.C., Pairman D., Barringer J. // 2005. IGARSS '05. Proceedings. 2005 IEEE International Geoscience and Remote Sensing Symposium. 25-29 July 2005. - Vol. 8. - P. 5594-5597. ↑

C4037. Ito Y. Extraction of maintenance information on irrigation ponds using polarimetric SARdata. / Ito Y., Yamamoto M., Nissho M.F., Mizobuchi H. // 2005. IGARSS '05. Proceedings. 2005 IEEE International Geoscience and Remote Sensing Symposium. 25-29 July 2005. - Vol. 8. - P. 5663-5666. ↑

C4038. Schuler D.L. Comparison of polarimetric SAR techniques for the measurement of directional ocean wave spectra. / Schuler D.L., Lee J.S., Pottier E., De Grandi G. // 2005. IGARSS '05. Proceedings. 2005 IEEE International Geoscience and Remote Sensing Symposium. 25-29 July 2005. - Vol. 1. - P. 4 ↑

- C4039.** Dong-Bin Shin. The inherent error in passive microwave rainfall estimation as inferred from the TRMM data. / Dong-Bin Shin, Chiu L.S. // 2005. IGARSS '05. Proceedings. 2005 IEEE International Geoscience and Remote Sensing Symposium. 25-29 July 2005. - Vol. 1. - P. 4 ↑
- C4040.** Budillon A. Application of overcomplete ICA to SAR image compression. / Budillon A., Cuozzo G., D'Elia C., Schirinz G. // 2005. IGARSS '05. Proceedings. 2005 IEEE International Geoscience and Remote Sensing Symposium. 25-29 July 2005. - Vol. 1. - P. 4 ↑
- C4041.** Flaming G.M. Global Precipitation Measurement update. 2005. IGARSS '05. Proceedings. 2005 IEEE International Geoscience and Remote Sensing Symposium. 25-29 July 2005. - Vol. 1. - P. 4 ↑
- C4042.** Iida Y. Sampling simulation for estimating the sampling error of space-time average rain rate for TRMM and GPM mission. / Iida Y., Okamoto K., Ushio T., Oki R. // 2005. IGARSS '05. Proceedings. 2005 IEEE International Geoscience and Remote Sensing Symposium. 25-29 July 2005. - Vol. 1. - P. 4 ↑
- C4043.** Sang-Wan Kim. Surface deformation in Mokpo area observed with synthetic aperture radar interferometry. / Sang-Wan Kim, Chang-Oh Kim, Joong-Sun Won, Dong-Cheon Lee, Jeong-Woo Kim. // 2005. IGARSS '05. Proceedings. 2005 IEEE International Geoscience and Remote Sensing Symposium. 25-29 July 2005. - Vol. 1. - P. 3 ↑
- C4044.** Alpers W. Atmospheric fronts off the east coast of Taiwan studied by ERS synthetic aperture radar imagery. / Alpers W., Jen-Ping Chen, I-I Lin. // 2005. IGARSS '05. Proceedings. 2005 IEEE International Geoscience and Remote Sensing Symposium. 25-29 July 2005. - Vol. 1. - P. 4 ↑
- C4045.** Gleich D. Model based SAR data compression. / Gleich D., Datcu M., Cucej Z. // 2005. IGARSS '05. Proceedings. 2005 IEEE International Geoscience and Remote Sensing Symposium. 25-29 July 2005. - Vol. 1. - P. 4 ↑
- C4046.** Junping Zhang. Change detection for the urban area based on multiple sensor information fusion. / Junping Zhang, Xiaofei Wang, Tao Chen, Ye Zhang. // 2005. IGARSS '05. Proceedings. 2005 IEEE International Geoscience and Remote Sensing Symposium. 25-29 July 2005. - Vol. 1. - P. 4 ↑
- C4047.** Shengli Wu. The potential of TRMM/PR data to monitor snow in Tibetan Plateau. / Shengli Wu, Kebiao Mao, Jinyang Du, Lina Xu, Jianming Wang. // 2005. IGARSS '05. Proceedings. 2005 IEEE International Geoscience and Remote Sensing Symposium. 25-29 July 2005. - Vol. 1. - P. 4 ↑
- C4048.** Allain S. New eigenvalue-based parameters for natural media characterization. / Allain S., Lopez-Martinez C., Ferro-Famil L., Pottier E. // 2005. IGARSS '05. Proceedings. 2005 IEEE International Geoscience and Remote Sensing Symposium. 25-29 July 2005. - Vol. 1. - P. 4 ↑
- C4049.** Morris J.T. Polarimetric characteristics of radar echoes from near shore wave fields at low grazing angles. / Morris J.T., Anderson S.J. // 2005. IGARSS '05. Proceedings. 2005 IEEE International Geoscience and Remote Sensing Symposium. 25-29 July 2005. - Vol. 1. - P. 4 ↑
- C4050.** Guillaso S. Evaluation of the ESPRIT approach in polarimetric interferometric SAR. / Guillaso S., Reigber A., Ferro-Famil L. // 2005. IGARSS '05. Proceedings. 2005 IEEE International Geoscience and Remote Sensing Symposium. 25-29 July 2005. - Vol. 1. - P. 4 ↑
- C4051.** Bernier M. Investigating polarimetric SAR data for cryospheric monitoring in a Canadian environment. / Bernier M., Gauthier Y., Mermoz S., Gherboudj I., El Battay A., Khaldoune J. // 2005. IGARSS '05. Proceedings. 2005 IEEE International Geoscience and Remote Sensing Symposium. 25-29 July 2005. - Vol. 1. - P. 4 ↑
- C4052.** Czuchlewski K.R. Synthetic aperture radar (SAR)-based mapping of wildfire burn severity and recovery. / Czuchlewski K.R., Weissel J.K. // 2005. IGARSS '05. Proceedings. 2005 IEEE International Geoscience and Remote Sensing Symposium. 25-29 July 2005. - Vol. 1. - P. 4 ↑
- C4053.** Romeiser R. Global current measurements in rivers by spaceborne along-track InSAR. / Romeiser R., Sprenger J., Stammer D., Runge H., Suchandt S. // 2005. IGARSS '05. Proceedings. 2005 IEEE International Geoscience and Remote Sensing Symposium. 25-29 July 2005. - Vol. 1. - P. 4 ↑
- C4054.** Ainsworth T.L. Polarimetric SAR image classification employing subaperture polarimetric analysis. / Ainsworth T.L., Lee J.S. // 2005. IGARSS '05. Proceedings. 2005 IEEE International Geoscience and Remote Sensing Symposium. 25-29 July 2005. - Vol. 1. - P. 4 ↑

Sensing Symposium. 25-29 July 2005. - Vol. 1. - P. 3 ↑

C4055. Hamasaki T. Polarimetric SAR stereo using Pi-SAR square loop path. / Hamasaki T., Sato M., Ferro-Famil L., Pottier E. // 2005. IGARSS '05. Proceedings. 2005 IEEE International Geoscience and Remote Sensing Symposium. 25-29 July 2005. - Vol. 1. - P. 4 ↑

C4056. Osmanoglu B. Analysis of land topography using Radar Altimeter 2. / Osmanoglu B., Kartal M. // 2005. RAST 2005. Proceedings of 2nd International Conference on Recent Advances in Space Technologies. 9-11 June 2005. - P. 648-652. ↑

C4057. Lagios E. Ground deformation monitoring of the Santorini volcano using satellite radar interferometry. / Lagios E., Parcharidis I., Fomelis M., Sakkas V. // 2005. RAST 2005. Proceedings of 2nd International Conference on Recent Advances in Space Technologies. 9-11 June 2005. - P. 667-672. ↑

C4058. Sumer E. Building damage detection from post-earthquake aerial imagery using building grey-value and gradient orientation analyses. / Sumer E., Turker M. // 2005. RAST 2005. Proceedings of 2nd International Conference on Recent Advances in Space Technologies. 9-11 June 2005. - P. 577-582. ↑

C4059. Cote S. Radiometric measurements of the Canadian boreal forest using RADARSAT-1 beam patterns. / Cote S., Lukowski T.I., Le Dantec P., Srivastava S.K., Hawkins R.K. // 2005. RAST 2005. Proceedings of 2nd International Conference on Recent Advances in Space Technologies. 9-11 June 2005. - P. 593-598. ↑

C4060. Nickolaenko A.P. Model of diurnal/seasonal variations of ELF natural radio signal based on OTD data. 2005. IEEE 6th International Symposium on Electromagnetic Compatibility and Electromagnetic Ecology. 21-24 June 2005. - P. 247-250. ↑

C4061. Romeiser R. On the potential of current measurements by spaceborne along-track InSAR for river runoff monitoring. Oceans 2005-Europe. 20-23 June 2005. - Vol. 2. - P. 787-792. ↑

C4062. Parcharidis I. Seismotectonic investigation on the Bam earthquake prone area (Iran) based on ASAR interferometry. / Parcharidis I., Zare M., Fomelis M., Lagios E. // 2005. RAST 2005. Proceedings of 2nd International Conference on Recent Advances in Space Technologies. 9-11 June 2005. - P. 673-677. ↑

C4063. Cote S. Maintaining RADARSAT-1 image quality performance in extended mission. / Cote S., Srivastava S.K., Le Dantec P., Hawkins R.K. // 2005. RAST 2005. Proceedings of 2nd International Conference on Recent Advances in Space Technologies. 9-11 June 2005. - P. 678-683. ↑

C4064. Garneau M. Space in the service of society: a Canadian case study. 2005. RAST 2005. Proceedings of 2nd International Conference on Recent Advances in Space Technologies. 9-11 June 2005. - P. 1-6. ↑

C4065. Howarth M.J. The Liverpool Bay coastal observatory. / Howarth M.J., Proctor R., Smithson M.J., Player R., Knight P.J. // 2005. Proceedings of the IEEE/OES Eighth Working Conference on Current Measurement Technology. 28-29 June 2005. - P. 132-136. ↑

C4066. Richman A. Remote sensing, LIDAR, automated data capture and the VEPS project. / Richman A., Hamilton A., Arayici Y., Counsell J. // 2005. Proceedings. Ninth International Conference on Information Visualisation. 6-8 July 2005. - P. 151-156. ↑

C4067. Spain P. Field intercomparison of Channel Master ADCP with RiverSonde radar for measuring river discharge. / Spain P., Marsden R., Barrick D., Teague C., Ruhl C. // 2005. Proceedings of the IEEE/OES Eighth Working Conference on Current Measurement Technology. 28-29 June 2005. - P. 111-116. ↑

C4068. Pettigrew N.R. Gulf of Maine Ocean Observing System (GoMOOS): current measurement approaches in a prototype integrated ocean observing system. / Pettigrew N.R., Wallinga J.P., Neville F.P., Schlenker K.R. // 2005. Proceedings of the IEEE/OES Eighth Working Conference on Current Measurement Technology. 28-29 June 2005. - P. 127-131. ↑

C4069. Kanaa T.F.N. Sea surface slicks characterization in SAR images. / Kanaa T.F.N., Mercier G., Tonye E. // Oceans 2005-Europe. 20-23 June 2005. - Vol. 1. - P. 686-691. ↑

C4070. {no data available}. RAST 2005. Proceedings of 2nd International Conference on Recent Advances in Space Technologies (IEEE Cat. No. 05EX1011). 2005. RAST 2005. Proceedings of 2nd International Conference

on Recent Advances in Space Technologies. 9-11 June 2005. - {no data available}. ↑

C4071. Mercier G. Oil slick detection by SAR imagery using Support Vector Machines. / Mercier G., Girard-Ardhuin F. // Oceans 2005-Europe. 20-23 June 2005. - Vol. 1. - P. 90-95. ↑

C4072. Gough P.T. Fast Fourier techniques for SAS imagery. / Gough P.T., Hayes M.P. // Oceans 2005-Europe. 20-23 June 2005. - Vol. 1. - P. 563-568. ↑

C4073. Lennon M. Operational quantitative mapping of oil pollutions at sea by joint use of an hyperspectral imager and a fluorescence lidar system on-board a fixed-wing aircraft. / Lennon M., Thomas N., Mariette V., Babichenko S., Mercier G. // Oceans 2005-Europe. 20-23 June 2005. - Vol. 2. - P. 848-853. ↑

C4074. Horstmann J. First assessment of C-band polarization ratio from ENVISAT ASAR imagery. / Horstmann J., Monaldo F., Thompson D.R., Elfouhaily T.M. // 2005. IGARSS '05. Proceedings. 2005 IEEE International Geoscience and Remote Sensing Symposium. 25-29 July 2005. - Vol. 2. - P. 1002-1005. ↑

C4075. Alexis M. Observations and modeling of the ocean radar backscatter at C-band in HH- and VV-polarizations. / Alexis M., Daniele H., Vladimir K. // 2005. IGARSS '05. Proceedings. 2005 IEEE International Geoscience and Remote Sensing Symposium. 25-29 July 2005. - Vol. 2. - P. 1006-1009. ↑

C4076. Isoguchi O. Coastal wind jets flowing into the kanmon strait by SAR observations. / Isoguchi O., Kawamura H. // 2005. IGARSS '05. Proceedings. 2005 IEEE International Geoscience and Remote Sensing Symposium. 25-29 July 2005. - Vol. 2. - P. 995-998. ↑

C4077. Duk-jin Kim. Effect of radar frequency on waterline mapping from airborne SAR image in the intertidal zone. / Duk-jin Kim, Sang-Eun Park, Wooil M. Moon, Hyo-Sung Lee. // 2005. IGARSS '05. Proceedings. 2005 IEEE International Geoscience and Remote Sensing Symposium. 25-29 July 2005. - Vol. 2. - P. 999-1001. ↑

C4078. Jianxiang Chen. Satellite remote sensing of the oceanic environment in China. / Jianxiang Chen, Weigen Huang, Jingsong Yang. // 2005. IGARSS '05. Proceedings. 2005 IEEE International Geoscience and Remote Sensing Symposium. 25-29 July 2005. - Vol. 2. - P. 1018-1020. ↑

C4079. Chang L. An automatic detection of oil spills in sar images by using image segmentation approach. / Chang L., Cheng C.M., Tang Z.S. // 2005. IGARSS '05. Proceedings. 2005 IEEE International Geoscience and Remote Sensing Symposium. 25-29 July 2005. - Vol. 2. - P. 1021-1024. ↑

C4080. Nieto Borge J.C. Sea state analysis for coastal waters using dual polarization ENVISAT ASAR data. / Nieto Borge J.C., Schneiderhan T., Schulz-Stellenfleth J., Konig T., Lehner S. // 2005. IGARSS '05. Proceedings. 2005 IEEE International Geoscience and Remote Sensing Symposium. 25-29 July 2005. - Vol. 2. - P. 1010-1013. ↑

C4081. Schulz-Stellenflet J. An empirical SAR imaging model for ocean wave measurements. / Schulz-Stellenflet J., Niedermeier A., Nieto Borge J.C. // 2005. IGARSS '05. Proceedings. 2005 IEEE International Geoscience and Remote Sensing Symposium. 25-29 July 2005. - Vol. 2. - P. 1014-1017. ↑

C4082. Qing Dong. Ocean wave spectrum from sar image using 2D-ARMA model. / Qing Dong, Huadong Guo, Zhen Li, Jinghui Liu. // 2005. IGARSS '05. Proceedings. 2005 IEEE International Geoscience and Remote Sensing Symposium. 25-29 July 2005. - Vol. 2. - P. 991-994. ↑

C4083. Dunne S. Oceanpal® a GPS-reflection coastal instrument to monitor tide and sea-state. / Dunne S., Soulat F., Caparrini M., Germain O., Farres E., Barroso X., Ruffini G. // Oceans 2005-Europe. 20-23 June 2005. - Vol. 2. - P. 1351-1356. ↑

C4084. Pierro R.S. Space-based radar: overview, history and recent developments. 2005. IEEE Conference Long Island Systems, Applications and Technology. 6 May, 2005. - P. 30-35. ↑

C4085. Gurgel K.-W. HF radar wave measurements in the presence of ship echoes-problems and solutions. / Gurgel K.-W., Schlick T. // Oceans 2005-Europe. 20-23 June 2005. - Vol. 2. - P. 937-941. ↑

C4086. Horwood J.M.K. Shallow angle LIDAR for wave measurement. / Horwood J.M.K., Thurley R.W.F., Belmont M.R., Baker J. // Oceans 2005-Europe. 20-23 June 2005. - Vol. 2. - P. 1151-1154. ↑

- C4087.** Moussessian A. System concepts and technologies for high orbit SAR. / Moussessian A., Chen C., Edelstein W., Madsen S., Rosen P. // 2005 IEEE MTT-S International Microwave Symposium Digest. 12-17 June 2005. - P. 4 ↑
- C4088.** Fouques S. Influence of a nonlinear RAR modulation on the SAR imaging of ocean waves. / Fouques S., Johnsen H., Krogstad H.E. // 2005. IGARSS '05. Proceedings. 2005 IEEE International Geoscience and Remote Sensing Symposium. 25-29 July 2005. - Vol. 2. - P. 987-990. ↑
- C4089.** Hensley S. Status of a UAVSAR designed for repeat pass interferometry for deformation measurements. / Hensley S., Wheeler K., Sadowy G., Miller T., Shaffer S., Muellerschoen R., Jones C., Zebker H., Madsen S., Rosen P. // 2005 IEEE MTT-S International Microwave Symposium Digest. 12-17 June 2005. - P. 4 ↑
- C4090.** Ludwig M. Status and trends for space-borne phased array radar. / Ludwig M., Buck C.H., Coromina F., Suess M. // 2005 IEEE MTT-S International Microwave Symposium Digest. 12-17 June 2005. - P. 4 ↑
- C4091.** Teague C.C. Long-term UHF RiverSonde river velocity observations at Castle Rock, Washington and Threemile Slough, California. / Teague C.C., Barrick D.E., Lilleboe P.M., Cheng R.T., Ruhl C.A. // 2005. Proceedings of the IEEE/OES Eighth Working Conference on Current Measurement Technology. 28-29 June 2005. - P. 85-89. ↑
- C4092.** Norgard J.D. Deep ground penetrating radar (GPR) WIPD-D models of buried sub-surface radiators. / Norgard J.D., Wicks M.C., Musselman R.L. // 2005. IEEE/ACES International Conference on Wireless Communications and Applied Computational Electromagnetics. 3-7 April 2005. - P. 114-119. ↑
- C4093.** Smardzija D. Applications of MIMO techniques to sensing of cardiopulmonary activity. / Smardzija D., Boric-Lubecke O., Host-Madsen A., Lubecke V.M., Sizer T. II, Droitcour A.D., Kovacs G.T.A. // 2005. IEEE/ACES International Conference on Wireless Communications and Applied Computational Electromagnetics. 3-7 April 2005. - P. 618-621. ↑
- C4094.** Yi Zheng. Multiplicative multifractal modeling of sea clutter. / Yi Zheng, Jianbo Gao, Kung Yao. // 2005 IEEE International Radar Conference. 9-12 May 2005. - P. 962-966. ↑
- C4095.** Hongliang Zhou. GPRS based power quality monitoring system. 2005. Proceedings. 2005 IEEE Networking, Sensing and Control. 19-22 March 2005. - P. 496-501. ↑
- C4096.** Sharma R. Hyper-temporal radarsat SAR data of a forested terrain. / Sharma R., Leckie D., Hill D., Crooks B., Bhogal A.S., Arbour P., D'eon S. // 2005 International Workshop on the Analysis of Multi-Temporal Remote Sensing Images. 16-18 May 2005. - P. 71-75. ↑
- C4097.** Bovolo F. A wavelet-based change-detection technique for multitemporal SAR images. / Bovolo F., Bruzzone L. // 2005 International Workshop on the Analysis of Multi-Temporal Remote Sensing Images. 16-18 May 2005. - P. 85-89. ↑
- C4098.** Goodenough D.G. Evaluation of multi-temporal and multi-polarization ASAR for Boreal Forests in Hinton. / Goodenough D.G., Hao Chen, Dyk A., Tian Han. // 2005 International Workshop on the Analysis of Multi-Temporal Remote Sensing Images. 16-18 May 2005. - P. 6-9. ↑
- C4099.** Cooke W.H. Assessment of current field plots and lidar 'virtual' plots as guides to classification procedures for multitemporal analysis of historic and current landsat data for determining forest age classes. / Cooke W.H., Prabhu C., Wallis R., Morris J., Smith B., Gilreath J. // 2005 International Workshop on the Analysis of Multi-Temporal Remote Sensing Images. 16-18 May 2005. - P. 67-70. ↑
- C4100.** Antoniou M. Problems of surface change detection based on SS-InBSAR. / Antoniou M., Cherniakov M., Tao Zeng. // 2005 IEEE International Radar Conference. 9-12 May 2005. - P. 791-795. ↑
- C4101.** Ke Yong Li. Geometrical considerations for terrain mapping in SBR applications. / Ke Yong Li, Mangiat S., Pillai S.R., Himed B. // 2005 IEEE International Radar Conference. 9-12 May 2005. - P. 143-148. ↑
- C4102.** Meta A. Development of signal processing algorithms for high resolution airborne millimeter wave FMCW SAR. / Meta A., Hoogeboom P. // 2005 IEEE International Radar Conference. 9-12 May 2005. - P. 326-331. ↑

- C4103.** Gaucel J.-M. Whitening spatial correlation filtering for hyperspectral anomaly detection. / Gaucel J.-M., Guillaume M., Bourennane S. // 2005. Proceedings. (ICASSP '05). IEEE International Conference on Acoustics, Speech, and Signal Processing. 18-23 March 2005. - Vol. 5. - P. v/333. ↑
- C4104.** Rastogi M. SeaWinds radiometer (SRad) brightness temperature calibration and validation. / Rastogi M., Jones W.L., Adams I. // 2005. Proceedings. IEEE SoutheastCon. 8-10 April 2005. - P. 287-295. ↑
- C4105.** Stankwitz H.C. Advances in non-linear apodization for irregularly shaped and sparse two dimensional apertures. / Stankwitz H.C., Taylor S.P. // 2005 IEEE International Radar Conference. 9-12 May 2005. - P. 635-640. ↑
- C4106.** JunWu Cao. Automatic classification of hydrometeors based on polarimetric weather radar measurements. / JunWu Cao, LiPing Liu. // 2005 IEEE International Radar Conference. 9-12 May 2005. - P. 737-741. ↑
- C4107.** Bugaev A.S. Mathematical simulation of remote detection of human breathing and heartbeat by multifrequency radar on the background of local objects reflections. / Bugaev A.S., Chapursky V.V., Ivashov S.I. // 2005 IEEE International Radar Conference. 9-12 May 2005. - P. 359-364. ↑
- C4108.** Wang Min. A hybrid genetic algorithm-based edge detection method for SAR image. / Wang Min, Yuan Shuyuan. // 2005 IEEE International Radar Conference. 9-12 May 2005. - P. 503-506. ↑
- C4109.** Milne A.K. Change detection analysis in wetlands using JERS-1 radar data: tonle Sap Great Lake, Cambodia. / Milne A.K., Tapley I.J. // 2005 International Workshop on the Analysis of Multi-Temporal Remote Sensing Images. 16-18 May 2005. - P. 146-150. ↑
- C4110.** {no data available}. Remote sensing techniques. 2005. Proceedings of the IEEE/OES Eighth Working Conference on Current Measurement Technology. 28-29 June 2005. - P. 51. ↑
- C4111.** Wyatt L.R. Wave, current and wind monitoring using HF radar. / Wyatt L.R., Green J.J., Middleditch A. // 2005. Proceedings of the IEEE/OES Eighth Working Conference on Current Measurement Technology. 28-29 June 2005. - P. 53-57. ↑
- C4112.** Yanovsky F.J. Antennae variety for remote sensing of surroundings. 2005. 5th International Conference on Antenna Theory and Techniques. 24-27 May 2005. - P. 105-109. ↑
- C4113.** Koroshetz J.E. Fiber lasers for lidar. 2005. Technical Digest. OFC/NFOEC Optical Fiber Communication Conference. 6-11 March 2005. - Vol. 5. - P. 3 P. Vol. 6. ↑
- C4114.** Wang J.T. New expressed nonlinear polarization vector translation and its application in HF Radar. / Wang J.T., Zhang G.Y., Hou H.Q. // 2005. Proceedings of the IEEE/OES Eighth Working Conference on Current Measurement Technology. 28-29 June 2005. - P. 66-70. ↑
- C4115.** Terray E.A. Airborne fluorescence imaging of the ocean mixed layer. / Terray E.A., Ledwell J.R., Sundermeyer M.A., Donoghue T., Bohra S., Cunningham A.G., LaRoque P.E., Lillycrop W.J., Wiggins C.E. // 2005. Proceedings of the IEEE/OES Eighth Working Conference on Current Measurement Technology. 28-29 June 2005. - P. 76-81. ↑
- C4116.** Barrick D. Advance warning of loop current from single-site SeaSonde on Genesis oil platform in the Gulf of Mexico. / Barrick D., Long R., Whelan C., Cooper C., Abadin J. // 2005. Proceedings of the IEEE/OES Eighth Working Conference on Current Measurement Technology. 28-29 June 2005. - P. 58-62. ↑
- C4117.** Kohut J.T. Observed response of the Hudson River plume to wind forcing using a nested HF radar array. / Kohut J.T., Roarty H.J., Glenn S.M., Schofield O., Chant R.J., Creed E. // 2005. Proceedings of the IEEE/OES Eighth Working Conference on Current Measurement Technology. 28-29 June 2005. - P. 63-65. ↑
- C4118.** Stone R. Asian dust signatures at Barrow: observed and simulated. Incursions and impact of Asian dust over Northern Alaska. / Stone R., Anderson G., Andrews E., Dutton E., Harris J., Shettle E., Berk A. // 2005. IEEE Workshop on Remote Sensing of Atmospheric Aerosols. 5-6 April 2005. - P. 74-79. ↑
- C4119.** Spinhirne J.D. Global aerosol distribution from the GLAS polar orbiting lidar instrument. / Spinhirne J.D., Palm S.P., Hlavka D.L., Hart W.D., Welton E.J. // 2005. IEEE Workshop on Remote Sensing of

Atmospheric Aerosols. 5-6 April 2005. - P. 2-8. ↑

C4120. Choo Hie Lee. 532/1064 nm ACA lidar measurements of Asian dust at Suwon, Korea during 2002-2004. / Choo Hie Lee, Chan Bong Park, Jin Hwan Kim. // 2005. IEEE Workshop on Remote Sensing of Atmospheric Aerosols. 5-6 April 2005. - P. 9-13. ↑

C4121. Drunpob A. Seasonal soil moisture variation analysis using RADARSAT-1 satellite image in a semi-arid coastal watershed. / Drunpob A., Chang N.B., Beaman M., Wyatt C., Slater C. // 2005 International Workshop on the Analysis of Multi-Temporal Remote Sensing Images. 16-18 May 2005. - P. 186-190. ↑

C4122. Reagan J.A. Forty Years of Aerosol Remote Sensing. 2005. IEEE Workshop on Remote Sensing of Atmospheric Aerosols. 5-6 April 2005. - P. 1. ↑

C4123. Freemantle J. AEROCAN: the Canadian Sunphotometer Network. / Freemantle J., O'Neill N., Royer A., McArthur B., Abboud I. // 2005. IEEE Workshop on Remote Sensing of Atmospheric Aerosols. 5-6 April 2005. - P. 32-35. ↑

C4124. Wang X. Spaceborne lidar aerosol retrieval approaches based on improved aerosol model constraints. / Wang X., Reagan J., Catrall C., Thome K. // 2005. IEEE Workshop on Remote Sensing of Atmospheric Aerosols. 5-6 April 2005. - P. 36-42. ↑

C4125. Spinhirne J.D. Monitoring aerosol distribution from ground based elastic scattering lidar: a review. / Spinhirne J.D., Welton E.J., Campbell J.R., Berkoff T. // 2005. IEEE Workshop on Remote Sensing of Atmospheric Aerosols. 5-6 April 2005. - P. 14-15. ↑

C4126. Hassebo Y. Multiwavelength lidar measurements at the City College of New York in support of the NOAA-NEAQS and NASA-INTEX-NA experiments. / Hassebo Y., Yu Zhao, Gross B., Moshary F., Ahmed S. // 2005. IEEE Workshop on Remote Sensing of Atmospheric Aerosols. 5-6 April 2005. - P. 16-23. ↑

C4127. Krieger G. Impact of oscillator noise in bistatic and multistatic SAR. / Krieger G., Cassola M.R., Younis M., Metzger R. // 2005. IGARSS '05. Proceedings. 2005 IEEE International Geoscience and Remote Sensing Symposium. 25-29 July 2005. - Vol. 2. - P. 1043-1046. ↑

C4128. de Macedo K.A.C. On the requirements of SAR processing for airborne differential interferometry. / de Macedo K.A.C., Andres C., Scheiber R. // 2005. IGARSS '05. Proceedings. 2005 IEEE International Geoscience and Remote Sensing Symposium. 25-29 July 2005. - Vol. 4. - P. 2693-2696. ↑

C4129. Serafino F. Singular value decomposition applied to 4D SAR imaging. / Serafino F., Soldovieri F., Lombardini F., Fornaro G. // 2005. IGARSS '05. Proceedings. 2005 IEEE International Geoscience and Remote Sensing Symposium. 25-29 July 2005. - Vol. 4. - P. 2701-2704. ↑

C4130. Guillaso S. Scatterer characterisation using polarimetric SAR tomography. / Guillaso S., Reigber A. // 2005. IGARSS '05. Proceedings. 2005 IEEE International Geoscience and Remote Sensing Symposium. 25-29 July 2005. - Vol. 4. - P. 2685-2688. ↑

C4131. Lopez-Martinez C. Topography independent InSAR coherence estimation in a multiresolution scheme. / Lopez-Martinez C., Pottier E. // 2005. IGARSS '05. Proceedings. 2005 IEEE International Geoscience and Remote Sensing Symposium. 25-29 July 2005. - Vol. 4. - P. 2689-2692. ↑

C4132. Bin Zou. A raw data simulator for cross-track InSAR based on land clutter model. / Bin Zou, Xing Bao, Lin Hao. // 2005. IGARSS '05. Proceedings. 2005 IEEE International Geoscience and Remote Sensing Symposium. 25-29 July 2005. - Vol. 4. - P. 2711-2714. ↑

C4133. Sangho Baek. DEM, tide and velocity over Sulzberger ice shelf, West Antarctica. / Sangho Baek, Shum C.K., Hyongki Lee, Yuchan Yi, Kwoun O., Zhong Lu, Braun A. // 2005. IGARSS '05. Proceedings. 2005 IEEE International Geoscience and Remote Sensing Symposium. 25-29 July 2005. - Vol. 4. - P. 2726-2728. ↑

C4134. Iwashita A. Disaster area extraction algorithm development using repeat-pass SAR interferometry. / Iwashita A., Qong M. // 2005. IGARSS '05. Proceedings. 2005 IEEE International Geoscience and Remote Sensing Symposium. 25-29 July 2005. - Vol. 4. - P. 2705-2707. ↑

C4135. Sang-Wan Kim. C-band interferometric SAR measurements of water level change in the wetlands:

examples from florida and louisiana. / Sang-Wan Kim, Wdowinski S., Amelung F., Dixon T.H. // 2005. IGARSS '05. Proceedings. 2005 IEEE International Geoscience and Remote Sensing Symposium. 25-29 July 2005. - Vol. 4. - P. 2708-2710. ↑

C4136. Krieger G. Multistatic sar satellite formations: potentials and challenges. / Krieger G., Moreira A. // 2005. IGARSS '05. Proceedings. 2005 IEEE International Geoscience and Remote Sensing Symposium. 25-29 July 2005. - Vol. 4. - P. 2680-2684. ↑

C4137. Lombardini F. First trials of fourier and adaptive tomo-doppler sar imaging. / Lombardini F., Fornaro G. // 2005. IGARSS '05. Proceedings. 2005 IEEE International Geoscience and Remote Sensing Symposium. 25-29 July 2005. - Vol. 4. - P. 2656-2659. ↑

C4138. Liseno A. Analysis of forest-slab height inversion from multibaseline SAR data. / Liseno A., Papathanassiou K.P., Moreira A., Pierri R. // 2005. IGARSS '05. Proceedings. 2005 IEEE International Geoscience and Remote Sensing Symposium. 25-29 July 2005. - Vol. 4. - P. 2660-2663. ↑

C4139. Forget P. L-band doppler radar echoes of the sea surface in coastal zone. / Forget P., Saillard M., Currier P., Broche P., Barbin Y. // 2005. IGARSS '05. Proceedings. 2005 IEEE International Geoscience and Remote Sensing Symposium. 25-29 July 2005. - Vol. 4. - P. 2590-2593. ↑

C4140. Min-Jeong Kim. Microwave remote sensing of falling snow. / Min-Jeong Kim, Wang J.R., Meneghini R., Johnson B., Tanelli S., Roman-Nieves J.I., Sekelsky S.M., Skofronick-Jackson G. // 2005. IGARSS '05. Proceedings. 2005 IEEE International Geoscience and Remote Sensing Symposium. 25-29 July 2005. - Vol. 4. - P. 2645-2648. ↑

C4141. Budillon A. Moving targets detection and velocity estimation via multi-channel along-track interferometry. / Budillon A., Pascazio V., Schirizzi G. // 2005. IGARSS '05. Proceedings. 2005 IEEE International Geoscience and Remote Sensing Symposium. 25-29 July 2005. - Vol. 4. - P. 2672-2675. ↑

C4142. Barber B.C. Remote sensing the sea surface using a multichannel ATI SAR: imaging sea spikes. 2005. IGARSS '05. Proceedings. 2005 IEEE International Geoscience and Remote Sensing Symposium. 25-29 July 2005. - Vol. 4. - P. 2676-2679. ↑

C4143. Eineder M. Interferometric digital elevation model reconstruction-experiences from SRTM and multi channel approaches for future missions. / Eineder M., Krieger G. // 2005. IGARSS '05. Proceedings. 2005 IEEE International Geoscience and Remote Sensing Symposium. 25-29 July 2005. - Vol. 4. - P. 2664-2667. ↑

C4144. Refice A. Land-cover classification-based persistent scatterers identification for peri-urban applications. / Refice A., Bovenga F., Nutricato R., Chiaradia M.T., Wasowski J. // 2005. IGARSS '05. Proceedings. 2005 IEEE International Geoscience and Remote Sensing Symposium. 25-29 July 2005. - Vol. 4. - P. 2668-2671. ↑

C4145. Girard R. Processing the hydros SAR data. / Girard R., Seguin G., Lapointe M. // 2005. IGARSS '05. Proceedings. 2005 IEEE International Geoscience and Remote Sensing Symposium. 25-29 July 2005. - Vol. 4. - P. 2748-2751. ↑

C4146. Ricchetti E. Comparison of satellite imagery DEMs produced using photogrammetry and radargrammetry techniques. 2005. IGARSS '05. Proceedings. 2005 IEEE International Geoscience and Remote Sensing Symposium. 25-29 July 2005. - Vol. 4. - P. 2903-2906. ↑

C4147. Hounam D. An autonomous, non-cooperative, wide-area traffic monitoring system using space-based radar (TRAMRAD). / Hounam D., Baumgartner S., Bethke K.H., Gabele M., Kempfner E., Klement D., Krieger G., Rode G., Wagel K. // 2005. IGARSS '05. Proceedings. 2005 IEEE International Geoscience and Remote Sensing Symposium. 25-29 July 2005. - Vol. 4. - P. 2917-2920. ↑

C4148. Liang-Chien Chen. Building reconstruction from LIDAR data and aerial imagery. / Liang-Chien Chen, Tee-Ann Teo, Rau J.-Y., Jin-King Liu, Wei-Chen Hsu. // 2005. IGARSS '05. Proceedings. 2005 IEEE International Geoscience and Remote Sensing Symposium. 25-29 July 2005. - Vol. 4. - P. 2846-2849. ↑

C4149. Iwashita A. Crustal deformation monitoring using repeat-pass interferometry in the vicinity of Hua-Tung Longitudinal Valley, Taiwan. / Iwashita A., Baba H., Hara M., Yu-Feng Lin, Hwa-Chu Sheu. // 2005. IGARSS '05. Proceedings. 2005 IEEE International Geoscience and Remote Sensing Symposium. 25-29 July 2005. - Vol. 4. - P. 2896-2898. ↑

- C4150.** Chiu S. Clutter effects on ground moving targets' interferometric phase. / Chiu S., Gierull C.H., Durak A. // 2005. IGARSS '05. Proceedings. 2005 IEEE International Geoscience and Remote Sensing Symposium. 25-29 July 2005. - Vol. 4. - P. 2928-2931. ↑
- C4151.** Meyer F. A-priori information driven detection of moving objects for traffic monitoring by SAR. / Meyer F., Hinz S., Laika A., Bamler R. // 2005. IGARSS '05. Proceedings. 2005 IEEE International Geoscience and Remote Sensing Symposium. 25-29 July 2005. - Vol. 4. - P. 2932-2936. ↑
- C4152.** Ender J.H.G. Radar antenna architectures and sampling strategies for space based moving target recognition. / Ender J.H.G., Cerutti-Maori D., Burger W. // 2005. IGARSS '05. Proceedings. 2005 IEEE International Geoscience and Remote Sensing Symposium. 25-29 July 2005. - Vol. 4. - P. 2921-2924. ↑
- C4153.** Mingwei Shen. SAR/GMTI using $\Sigma\Delta$ -beams based on signal subspace processing. / Mingwei Shen, Daiyin Zhu, Zhaoda Zhu. // 2005. IGARSS '05. Proceedings. 2005 IEEE International Geoscience and Remote Sensing Symposium. 25-29 July 2005. - Vol. 4. - P. 2925-2927. ↑
- C4154.** Sang Hoon Lee. Multi-temporal, multi-resolution data fusion for Antarctica DEM determination using InSAR and altimetry. / Sang Hoon Lee, Sangho Baek, Shum C.K. // 2005. IGARSS '05. Proceedings. 2005 IEEE International Geoscience and Remote Sensing Symposium. 25-29 July 2005. - Vol. 4. - P. 2827-2829. ↑
- C4155.** van Zyl J.J. Estimating soil moisture for vegetated terrain: a discussion of possible approaches relevant to the HYDROS mission. / van Zyl J.J., Yunjin Kim. // 2005. IGARSS '05. Proceedings. 2005 IEEE International Geoscience and Remote Sensing Symposium. 25-29 July 2005. - Vol. 4. - P. 2763-2766. ↑
- C4156.** Jiancheng Shi. Estimation of soil moisture with the combined L-band radar and radiometer measurements. / Jiancheng Shi, Kim Y., Van Zyl J.J., Njoku E., Jackson T., Chen K.S., O'Neill P. // 2005. IGARSS '05. Proceedings. 2005 IEEE International Geoscience and Remote Sensing Symposium. 25-29 July 2005. - Vol. 4. - P. 2767-2770. ↑
- C4157.** Yunjin Kim. Overview of hydros radar soil moisture algorithm. / Yunjin Kim, van Zyl J. // 2005. IGARSS '05. Proceedings. 2005 IEEE International Geoscience and Remote Sensing Symposium. 25-29 July 2005. - Vol. 4. - P. 2756-2758. ↑
- C4158.** Yisok Oh. A soil moisture retrieval technique based on the semi-empirical scattering model for HH-, HV-, and VV-polarized radar observations. 2005. IGARSS '05. Proceedings. 2005 IEEE International Geoscience and Remote Sensing Symposium. 25-29 July 2005. - Vol. 4. - P. 2759-2762. ↑
- C4159.** Tison C. Validation of a feature fusion scheme for urban DSM retrieval from high resolution SAR interferogram. / Tison C., Tupin F., Nicolas J.-M., Maitre H. // 2005. IGARSS '05. Proceedings. 2005 IEEE International Geoscience and Remote Sensing Symposium. 25-29 July 2005. - Vol. 4. - P. 2795-2798. ↑
- C4160.** Hojin Jhee. Improved observational updating for efficient fusion of incomplete image data. / Hojin Jhee, Sweung Cheung, Slatton K.C. // 2005. IGARSS '05. Proceedings. 2005 IEEE International Geoscience and Remote Sensing Symposium. 25-29 July 2005. - Vol. 4. - P. 2807-2810. ↑
- C4161.** Lisini G. Joint feature and pixel-based change detection in high resolution SAR data. / Lisini G., Dell'Acqua F., Gamba P. // 2005. IGARSS '05. Proceedings. 2005 IEEE International Geoscience and Remote Sensing Symposium. 25-29 July 2005. - Vol. 4. - P. 2779-2782. ↑
- C4162.** Stacy N.J.S. Polarimetric analysis of fine resolution X-band SAR sea clutter data. / Stacy N.J.S., Crisp D., Goh A., Badger D., Preiss M. // 2005. IGARSS '05. Proceedings. 2005 IEEE International Geoscience and Remote Sensing Symposium. 25-29 July 2005. - Vol. 4. - P. 2787-2790. ↑
- C4163.** Jingsong Yang. Multifrequency SAR remote sensing of ocean internal waves. / Jingsong Yang, Qingmei Xiao, Weigen Huang, Bin Fu, Peng Chen, Lu Yao. // 2005. IGARSS '05. Proceedings. 2005 IEEE International Geoscience and Remote Sensing Symposium. 25-29 July 2005. - Vol. 4. - P. 2588-2589. ↑
- C4164.** Habib A.F. Image georeferencing using LIDAR data. / Habib A.F., Ghanma M.S., Mitishita E.A., Kim E.M., Kim C.J. // 2005. IGARSS '05. Proceedings. 2005 IEEE International Geoscience and Remote Sensing Symposium. 25-29 July 2005. - Vol. 2. - P. 1158-1161. ↑
- C4165.** Hong-Gyoo Sohn. Radargrammetry for DEM generation using minimal control points. / Hong-Gyoo

Sohn, Yeong-Sun Song, Gi-Hong Kim. // 2005. IGARSS '05. Proceedings. 2005 IEEE International Geoscience and Remote Sensing Symposium. 25-29 July 2005. - Vol. 2. - P. 1162-1164. ↑

C4166. Baquero M. Rain-rate estimate algorithm evaluation and rainfall characterization in tropical environments using 2DVD, rain gauges and TRMM data. / Baquero M., Cruz-Pol S., Brangi V.N., Chandrasekar V. // 2005. IGARSS '05. Proceedings. 2005 IEEE International Geoscience and Remote Sensing Symposium. 25-29 July 2005. - Vol. 2. - P. 1146-1149. ↑

C4167. Gutierrez R. Development of laser waveform digitization for airborne LIDAR topographic mapping instrumentation. / Gutierrez R., Neuenschwander A., Crawford M.M. // 2005. IGARSS '05. Proceedings. 2005 IEEE International Geoscience and Remote Sensing Symposium. 25-29 July 2005. - Vol. 2. - P. 1154-1157. ↑

C4168. Butler M.P.J. Project polar epsilon: joint space-based wide area surveillance and support capability. 2005. IGARSS '05. Proceedings. 2005 IEEE International Geoscience and Remote Sensing Symposium. 25-29 July 2005. - Vol. 2. - P. 1194-1197. ↑

C4169. Arnesen T.N. Possibilities and plans for utilization of RADARSAT-2 data. / Arnesen T.N., Olsen R.B., Eldhuset K. // 2005. IGARSS '05. Proceedings. 2005 IEEE International Geoscience and Remote Sensing Symposium. 25-29 July 2005. - Vol. 2. - P. 1198-1201. ↑

C4170. Chan-Su Yang. Ship detection experiments using RADARSAT/SAR images. / Chan-Su Yang, Chang-Gu Kang. // 2005. IGARSS '05. Proceedings. 2005 IEEE International Geoscience and Remote Sensing Symposium. 25-29 July 2005. - Vol. 2. - P. 1177-1180. ↑

C4171. Sahebi M.R. Estimates of bare soil surface parameters from multi-polarization and multi-angle SAR data. / Sahebi M.R., McNairn H., Gauthier E. // 2005. IGARSS '05. Proceedings. 2005 IEEE International Geoscience and Remote Sensing Symposium. 25-29 July 2005. - Vol. 2. - P. 1188-1193. ↑

C4172. Morrison K. High resolution PolInSAR with the ground-based SAR (GB-SAR) system: measurement and modelling. / Morrison K., Williams M.L. // 2005. IGARSS '05. Proceedings. 2005 IEEE International Geoscience and Remote Sensing Symposium. 25-29 July 2005. - Vol. 2. - P. 1105-1108. ↑

C4173. Martorella M. Improving the total rotation vector estimation via a bistatic isar system. / Martorella M., Palmero J., Berizzi F., Dalle Mese E. // 2005. IGARSS '05. Proceedings. 2005 IEEE International Geoscience and Remote Sensing Symposium. 25-29 July 2005. - Vol. 2. - P. 1068-1071. ↑

C4174. Colin E. Polarimetric interferometry and time-frequency analysis applied to a urban area at X-band. / Colin E., Titin-schneider C., Tabbara W., Reigber A. // 2005. IGARSS '05. Proceedings. 2005 IEEE International Geoscience and Remote Sensing Symposium. 25-29 July 2005. - Vol. 2. - P. 1077-1080. ↑

C4175. Rodriguez-Cassola M. Azimuth-invariant, bistatic airborne SAR processing strategies based on monostatic algorithms. / Rodriguez-Cassola M., Krieger G., Wendler M. // 2005. IGARSS '05. Proceedings. 2005 IEEE International Geoscience and Remote Sensing Symposium. 25-29 July 2005. - Vol. 2. - P. 1047-1050. ↑

C4176. Walterscheid I. Bistatic SAR processing using an Omega-K type algorithm. / Walterscheid I., Ender J.H.G., Brenner A.R., Loffeld O. // 2005. IGARSS '05. Proceedings. 2005 IEEE International Geoscience and Remote Sensing Symposium. 25-29 July 2005. - Vol. 2. - P. 1064-1067. ↑

C4177. Zheng-Shu Zhou. The development of a ground based polarimetric SAR interferometer (GB-POLInSAR). / Zheng-Shu Zhou, Cloude S.R. // 2005. IGARSS '05. Proceedings. 2005 IEEE International Geoscience and Remote Sensing Symposium. 25-29 July 2005. - Vol. 2. - P. 1097-1100. ↑

C4178. Juan M. Lopez-Sanchez. Advances in polinsar retrieval algorithms of agricultural crops. / Juan M. Lopez-Sanchez, Ungria E., Ballester-Berman J.D., Fortuny-Guasch J. // 2005. IGARSS '05. Proceedings. 2005 IEEE International Geoscience and Remote Sensing Symposium. 25-29 July 2005. - Vol. 2. - P. 1101-1104. ↑

C4179. Garestier F. Resolution effects on polarimetric high resolution X band data. / Garestier F., Dubois-Fernandez P., Paillou P., Dupuis X. // 2005. IGARSS '05. Proceedings. 2005 IEEE International Geoscience and Remote Sensing Symposium. 25-29 July 2005. - Vol. 2. - P. 1085-1088. ↑

C4180. Schneider R.Z. Polarimetric interferometry over urban areas: information extraction using coherent scatterers. / Schneider R.Z., Papathanassiou K., Hajnsek I., Moreira A. // 2005. IGARSS '05. Proceedings. 2005

IEEE International Geoscience and Remote Sensing Symposium. 25-29 July 2005. - Vol. 2. - P. 1089-1092. ↑

C4181. Anhua Chu. AIRSAR automated web-based data processing and distribution system. / Anhua Chu, van Zyl J., Yunjin Kim, Yunling Lou, Imel D., Tung W., Chapman B., Durden S. // 2005. IGARSS '05. Proceedings. 2005 IEEE International Geoscience and Remote Sensing Symposium. 25-29 July 2005. - Vol. 2. - P. 1218-1220. ↑

C4182. Marcantoni D. A joint analysis of radiometric and scatterometric simulations to tune an electromagnetic forward model within a common theoretical framework. / Marcantoni D., Pierdicca N., Pulvirenti L., Zecchetto S. // 2005. IGARSS '05. Proceedings. 2005 IEEE International Geoscience and Remote Sensing Symposium. 25-29 July 2005. - Vol. 4. - P. 2523-2526. ↑

C4183. Shimada T. Compartmentalization of coastal sea surface wind by statistical approach using high-resolution SAR-derived winds. / Shimada T., Kawamura H. // 2005. IGARSS '05. Proceedings. 2005 IEEE International Geoscience and Remote Sensing Symposium. 25-29 July 2005. - Vol. 4. - P. 2535-2538. ↑

C4184. Williams M.L. Predictions of SAR polarimetry and InSAR coherence for a model wheat canopy. / Williams M.L., Cloude S.R. // 2005. IGARSS '05. Proceedings. 2005 IEEE International Geoscience and Remote Sensing Symposium. 25-29 July 2005. - Vol. 2. - P. 1383-1386. ↑

C4185. Bao Houbing. Study on velocity measurement of AT-INSAR in the cluster micro-satellite system. / Bao Houbing, Zhang Xiaoling. // 2005. IGARSS '05. Proceedings. 2005 IEEE International Geoscience and Remote Sensing Symposium. 25-29 July 2005. - Vol. 2. - P. 1496-1499. ↑

C4186. Hui Shen. Methods to evaluate the accuracy of high frequency radar by in-situ measurements. / Hui Shen, Yi-Jun He, Yuan-Fu Sun, Zhong-Feng Qiu. // 2005. IGARSS '05. Proceedings. 2005 IEEE International Geoscience and Remote Sensing Symposium. 25-29 July 2005. - Vol. 4. - P. 2560-2563. ↑

C4187. Haipeng Wang. Speckle cross-correlation in multilook sar images of dynamic sea surface processed with partially overlapped sub-reference signals. / Haipeng Wang, Ouchi K. // 2005. IGARSS '05. Proceedings. 2005 IEEE International Geoscience and Remote Sensing Symposium. 25-29 July 2005. - Vol. 4. - P. 2580-2583. ↑

C4188. Weigen Huang. Optimal SAR parameters for ship detection. / Weigen Huang, Lu Yao, Jingsong Yang, Bin Fu, Qingmei Xiao, Peng Chen. // 2005. IGARSS '05. Proceedings. 2005 IEEE International Geoscience and Remote Sensing Symposium. 25-29 July 2005. - Vol. 4. - P. 2554-2555. ↑

C4189. Thibaut P. Estimation of the skewness coefficient using Jason-1 altimeter data. / Thibaut P., Amarouche L., Ferreira F., Zanife O.Z., Vincent P. // 2005. IGARSS '05. Proceedings. 2005 IEEE International Geoscience and Remote Sensing Symposium. 25-29 July 2005. - Vol. 4. - P. 2556-2559. ↑

C4190. Albert M.D. Model development and analysis of radar backscatter in Ross Island, Antarctica. / Albert M.D., Syahali S., Ewe H.T., Chuah H.T. // 2005. IGARSS '05. Proceedings. 2005 IEEE International Geoscience and Remote Sensing Symposium. 25-29 July 2005. - Vol. 2. - P. 1361-1364. ↑

C4191. Tezel N.S. Bi-static scattering width control of multiple coated PEC cylinder. / Tezel N.S., Parker S. // 2005. IGARSS '05. Proceedings. 2005 IEEE International Geoscience and Remote Sensing Symposium. 25-29 July 2005. - Vol. 2. - P. 1330-1332. ↑

C4192. Ya-Qiu Jin. Numerical simulation of the doppler spectrum of a flying target above dynamic oceanic surface by using the FEM-DDM method. / Ya-Qiu Jin, Peng Liu. // 2005. IGARSS '05. Proceedings. 2005 IEEE International Geoscience and Remote Sensing Symposium. 25-29 July 2005. - Vol. 2. - P. 1333-1336. ↑

C4193. Putignano C. Unsupervised classification of a central Italy landscape by polarimetric L-band SAR data. / Putignano C., Schiavon G., Solimini D., Trisasongko B. // 2005. IGARSS '05. Proceedings. 2005 IEEE International Geoscience and Remote Sensing Symposium. 25-29 July 2005. - Vol. 2. - P. 1291-1294. ↑

C4194. Nguyen H. SAR imaging of a forested area based on a coherent 3-D model of wave scattering: application to remote sensing of a hidden target in VHF band. / Nguyen H., Roussel H., Tabbara W. // 2005. IGARSS '05. Proceedings. 2005 IEEE International Geoscience and Remote Sensing Symposium. 25-29 July 2005. - Vol. 2. - P. 1326-1329. ↑

- C4195.** Ji Kefeng. Simulation of SAR image of ship. / Ji Kefeng, Kuang Gangyao, Su Yi, Yu Wenxian. // 2005. IGARSS '05. Proceedings. 2005 IEEE International Geoscience and Remote Sensing Symposium. 25-29 July 2005. - Vol. 2. - P. 1349-1352. ↑
- C4196.** Mukhopadhyay P.K. FDTD modelling of a borehole radar wave propagation: a 3-D simulation study in conductive media. / Mukhopadhyay P.K., Inggs M.R., Wilkinson A.J. // 2005. IGARSS '05. Proceedings. 2005 IEEE International Geoscience and Remote Sensing Symposium. 25-29 July 2005. - Vol. 2. - P. 1353-1356. ↑
- C4197.** Lombardini F. Analysis of non-gaussian speckle statistics in high-resolution SAR images. 2005. IGARSS '05. Proceedings. 2005 IEEE International Geoscience and Remote Sensing Symposium. 25-29 July 2005. - Vol. 2. - P. 1337-1340. ↑
- C4198.** Awada A. Comparison between small slope approximation and two scale model in bistatic configuration. / Awada A., Khenchaf A., Coatanhay A., Ayari M.Y. // 2005. IGARSS '05. Proceedings. 2005 IEEE International Geoscience and Remote Sensing Symposium. 25-29 July 2005. - Vol. 2. - P. 1341-1344. ↑
- C4199.** Heezin Lee. Segmentation of ALSM point data and the prediction of subcanopy sunlight distribution. / Heezin Lee, Kampa K., Slatton K.C. // 2005. IGARSS '05. Proceedings. 2005 IEEE International Geoscience and Remote Sensing Symposium. 25-29 July 2005. - Vol. 1. - P. 4. ↑
- C4200.** Qiu Li. The application research on subsidence monitoring of coal mining area with D-InSAR. / Qiu Li, Lixin Wu, Baozheng Chen. // 2005. IGARSS '05. Proceedings. 2005 IEEE International Geoscience and Remote Sensing Symposium. 25-29 July 2005. - Vol. 7. - P. 5216-5218. ↑
- C4201.** Casu F. Large scale InSAR deformation time series: Phoenix and Houston case studies. / Casu F., Buckley S.M., Manzo M., Pepe A., Lanari R. // 2005. IGARSS '05. Proceedings. 2005 IEEE International Geoscience and Remote Sensing Symposium. 25-29 July 2005. - Vol. 7. - P. 5240-5243. ↑
- C4202.** Yamanokuchi T. Extracted grounding line of the Antarctic ice sheet from ERS-1/2 interferometric SAR data. / Yamanokuchi T., Koichiro Doi, Shibuya K. // 2005. IGARSS '05. Proceedings. 2005 IEEE International Geoscience and Remote Sensing Symposium. 25-29 July 2005. - Vol. 7. - P. 5190-5192. ↑
- C4203.** Dhont D. Detection of compression structures from SAR ERS imagery: example of the Central Japan seismic area. / Dhont D., Chorowicz J., Cadet J.-P. // 2005. IGARSS '05. Proceedings. 2005 IEEE International Geoscience and Remote Sensing Symposium. 25-29 July 2005. - Vol. 7. - P. 5204-5207. ↑
- C4204.** Parcharidis I.S. On the assessment of co-seismic InSAR images of different time span associated to Athens (Greece) 1999 earthquake. / Parcharidis I.S., Fomelis M. // 2005. IGARSS '05. Proceedings. 2005 IEEE International Geoscience and Remote Sensing Symposium. 25-29 July 2005. - Vol. 7. - P. 5251-5254. ↑
- C4205.** Jiun-Yee Yen. Temporal and spatial pattern of the 1997 Manyi Earthquake using differential InSAR. / Jiun-Yee Yen, Kun-Shan Chen, Chung-Pai Chang, Chih-Tien Wang. // 2005. IGARSS '05. Proceedings. 2005 IEEE International Geoscience and Remote Sensing Symposium. 25-29 July 2005. - Vol. 7. - P. 5308-5311. ↑
- C4206.** InSu Lee. Accuracy comparison of DEMs derived from multisource SAR images. / InSu Lee, Linlin Ge, Hsing-Chung Chang, YoungJin Lee. // 2005. IGARSS '05. Proceedings. 2005 IEEE International Geoscience and Remote Sensing Symposium. 25-29 July 2005. - Vol. 7. - P. 5312-5315. ↑
- C4207.** Hsing-Chung Chang. ERS tandem DInSAR: the change of ground surface in 24 hours. / Hsing-Chung Chang, Linlin Ge, Rizos C. // 2005. IGARSS '05. Proceedings. 2005 IEEE International Geoscience and Remote Sensing Symposium. 25-29 July 2005. - Vol. 7. - P. 5265-5267. ↑
- C4208.** Lixia Gong. Measuring mining induced subsidence with InSAR. / Lixia Gong, Jingfa Zhang, Zhanqiang Chang, Zhenhong Li, Qingshi Guo. // 2005. IGARSS '05. Proceedings. 2005 IEEE International Geoscience and Remote Sensing Symposium. 25-29 July 2005. - Vol. 7. - P. 5293-5295. ↑
- C4209.** Ngo M.T. Exploration of the lower atmosphere with millimeter-wave radar. / Ngo M.T., Linde G.J., Cheung W.J. // 2005. IGARSS '05. Proceedings. 2005 IEEE International Geoscience and Remote Sensing Symposium. 25-29 July 2005. - Vol. 7. - P. 5096-5099. ↑
- C4210.** Lim S. An improved attenuation correction algorithm using dual-polarization radar observations of precipitation. / Lim S., Chandrasekar V. // 2005. IGARSS '05. Proceedings. 2005 IEEE International Geoscience

and Remote Sensing Symposium. 25-29 July 2005. - Vol. 7. - P. 5100-5103. ↑

C4211. Yanting Wang. Performance of dual-polarization radar measurement in hybrid mode for precipitation. / Yanting Wang, Chandrasekar V. // 2005. IGARSS '05. Proceedings. 2005 IEEE International Geoscience and Remote Sensing Symposium. 25-29 July 2005. - Vol. 7. - P. 5084-5087. ↑

C4212. Nakagawa K. Field campaign of observing precipitation in the 2004 rainy season of Okinawa, Japan. / Nakagawa K., Kitamura Y., Hanado H., Iwanami K., Okamoto K. // 2005. IGARSS '05. Proceedings. 2005 IEEE International Geoscience and Remote Sensing Symposium. 25-29 July 2005. - Vol. 7. - P. 5088-5091. ↑

C4213. Nishimura K. Adaptive clutter suppression for multistatic observations with equatorial atmosphere radar. / Nishimura K., Gotoh E., Takai T., Sato T. // 2005. IGARSS '05. Proceedings. 2005 IEEE International Geoscience and Remote Sensing Symposium. 25-29 July 2005. - Vol. 7. - P. 5104-5107. ↑

C4214. Xiao Cheng. Glacier velocity measurements using differential interferometric SAR in Antarctic Grove Mountain. / Xiao Cheng, Yanmei Zhang. // 2005. IGARSS '05. Proceedings. 2005 IEEE International Geoscience and Remote Sensing Symposium. 25-29 July 2005. - Vol. 7. - P. 5171-5174. ↑

C4215. Xiao Cheng. Detecting ice motion with repeat-pass ENVISAT ASAR interferometry over Nunataks region in Grove Mountain, East Antarctic-the preliminary result. / Xiao Cheng, Yanmei Zhang. // 2005. IGARSS '05. Proceedings. 2005 IEEE International Geoscience and Remote Sensing Symposium. 25-29 July 2005. - Vol. 7. - P. 5186-5189. ↑

C4216. Yonghong Li. An improved autoregressive model for analysis of decadal elevation change time series over Antarctica. / Yonghong Li, Davis C.H. // 2005. IGARSS '05. Proceedings. 2005 IEEE International Geoscience and Remote Sensing Symposium. 25-29 July 2005. - Vol. 7. - P. 5153-5156. ↑

C4217. Scheuchl B. Analysis of the influence of NESZ variations on cross-polarized signatures of sea ice. / Scheuchl B., Cumming I. // 2005. IGARSS '05. Proceedings. 2005 IEEE International Geoscience and Remote Sensing Symposium. 25-29 July 2005. - Vol. 7. - P. 5157-5160. ↑

C4218. Geiser P. Picosecond mid-infrared LIDAR system. / Geiser P., Wilier U., Schade W. // 2005. QELS '05 Quantum Electronics and Laser Science Conference. 22-27 May 2005. - Vol. 3. - P. 1986-1987. ↑

C4219. Kona K.S. Dual-frequency dual-polarized sixteen-element stacked patch microstrip array antenna for soil moisture and sea surface salinity missions. / Kona K.S., Rahmat-Samii Y. // 2005 IEEE Antennas and Propagation Society International Symposium. 3-8 July 2005. - Vol. 1A. - P. 318-321. ↑

C4220. Frish M.B. Standoff sensing of natural gas leaks: evolution of the remote methane leak detector (RMLD). / Frish M.B., Wainner R.T., Stafford-Evans J., Green B.D., Allen M.G., Chancey S., Rutherford J., Midgley G., Wehnert P. // 2005. QELS '05 Quantum Electronics and Laser Science Conference. 22-27 May 2005. - Vol. 3. - P. 1941-1943. ↑

C4221. Geng J. A compact 100-km FMCW fiber laser radar. / Geng J., Spiegelberg C., Jiang S. // 2005. QELS '05 Quantum Electronics and Laser Science Conference. 22-27 May 2005. - Vol. 3. - P. 1983-1985. ↑

C4222. Smith J.R. The forward scattering surface interaction region. / Smith J.R., Mirotznik M.S. // 2005 IEEE Antennas and Propagation Society International Symposium. 3-8 July 2005. - Vol. 1A. - P. 384-387. ↑

C4223. de Ipina D.L. An architecture for sentient GPRS-enabled MicroBots. / de Ipina D.L., Vazquez J.I., de Garibay J.R., Sainz D. // 2005. CIRA 2005. Proceedings. 2005 IEEE International Symposium on Computational Intelligence in Robotics and Automation. 27-30 June 2005. - P. 145-150. ↑

C4224. El-Ocla H. Indirect method of RCS estimate of conducting target in random medium. 2005. Canadian Conference on Electrical and Computer Engineering. - Saskatoon, Sask., 1-4 May 2005. - P. 1194-1197. ↑

C4225. Toporkov J.V. Numerical study of wide-band low-grazing HF clutter from ocean-like surfaces. / Toporkov J.V., Sletten M.A. // 2005 IEEE Antennas and Propagation Society International Symposium. 3-8 July 2005. - Vol. 1A. - P. 388-391. ↑

C4226. Huang J. A wide-band dual-polarized VHF microstrip antenna for global sensing of sea ice thickness. / Huang J., Hussein Z., Petros A. // 2005 IEEE Antennas and Propagation Society International Symposium. 3-8

July 2005. - Vol. 2B. - P. 684-687. ↑

C4227. Hua Bo. SAR image segmentation based on immune algorithm. / Hua Bo, Fulong Ma, Baojun Han, Licheng Jiao. // 2005. ICCA '05. International Conference on Control and Automation. - Budapest, 29-29 June 2005. - Vol. 2. - P. 1279-1282. ↑

C4228. Alkhoul O. Gust front detection in weather radar images by entropy matched functional template. / Alkhoul O., DeBrunner V. // 2005. ICIP 2005. IEEE International Conference on Image Processing. 11-14 Sept. 2005. - Vol. 1. - P. I-645-8. ↑

C4229. Yanmei Zhang. Application of SRTM-DEM based two-pass SAR interferometry for detecting seismic deformation on high-altitude rugged terrain -- a case study in Kokoxili Ms8.1 Earthquake, 2001. / Yanmei Zhang, Xiao Cheng. // 2005. IGARSS '05. Proceedings. 2005 IEEE International Geoscience and Remote Sensing Symposium. 25-29 July 2005. - Vol. 7. - P. 5316-5319. ↑

C4230. Xian-Bin Wen. Classification of SAR imagery based on the multiscale stochastic process. / Xian-Bin Wen, Zheng Tian, Wei Lin. // 2005. Proceedings of 2005 International Conference on Machine Learning and Cybernetics. - Guangzhou, China, 18-21 Aug. 2005. - Vol. 9. - P. 5346-5349. ↑

C4231. Bovolo F. An adaptive multiscale approach to unsupervised change detection in multitemporal SAR images. / Bovolo F., Bruzzone L. // 2005. ICIP 2005. IEEE International Conference on Image Processing. 11-14 Sept. 2005. - Vol. 1. - P. I-665-8. ↑

C4232. Averill M.G. How to reconstruct the original shape of a radar signal?. / Averill M.G., Gang Xiang, Kreinovich V., Keller G.R., Starks S.A., Debroux P.S., Boehm J. // 2005. NAFIPS 2005. Annual Meeting of the North American Fuzzy Information Processing Society. 26-28 June 2005. - P. 717-721. ↑

C4233. Coyle D.B. A diode pumped, Nd:YAG, Q-switched unstable resonator developed for multi-billion shot, spaced based remote sensing applications. / Coyle D.B., Kay R.B., Stysley P.R., Poullos D. // 2005. QELS '05 Quantum Electronics and Laser Science Conference. 22-27 May 2005. - Vol. 2. - P. 850-852. ↑

C4234. Giordano F. Segmentation of coherence maps for flood damage assessment. / Giordano F., Goccia M., Dellepiane S. // 2005. ICIP 2005. IEEE International Conference on Image Processing. 11-14 Sept. 2005. - Vol. 2. - P. II-233-6. ↑

C4235. Munch J. Eye safe solid state lasers for remote sensing and coherent laser radar. / Munch J., Heintze M., Hamilton M., Manning S., Mao Y., Mudge D., Veitch P. // 2005. LEOS 2005. The 18th Annual Meeting of the IEEE Lasers and Electro-Optics Society. 22-28 Oct. 2005. - P. 187-188. ↑

C4236. Fornaro G. Advances in multipass SAR image registration. / Fornaro G., Manunta M., Serafino F., Berardino P., Sansosti E. // 2005. IGARSS '05. Proceedings. 2005 IEEE International Geoscience and Remote Sensing Symposium. 25-29 July 2005. - Vol. 7. - P. 4832-4835. ↑

C4237. Kersten P.R. A comparison of change detection statistics in POLSAR images. / Kersten P.R., Lee J.S., Ainsworth T.L. // 2005. IGARSS '05. Proceedings. 2005 IEEE International Geoscience and Remote Sensing Symposium. 25-29 July 2005. - Vol. 7. - P. 4836-4839. ↑

C4238. Xiaoli Ding. SAR interferogram filtering with 2D Vondrak filter. / Xiaoli Ding, Zhiwei Li, Dawei Zheng, Cheng Huang, Weibao Zou. // 2005. IGARSS '05. Proceedings. 2005 IEEE International Geoscience and Remote Sensing Symposium. 25-29 July 2005. - Vol. 7. - P. 4825-4828. ↑

C4239. Gao Li. Phase unwrapping based on network flow algorithm and divide and conquer strategy. / Gao Li, Wen Xiaoyang, Zhang Hong, Wang Chao. // 2005. IGARSS '05. Proceedings. 2005 IEEE International Geoscience and Remote Sensing Symposium. 25-29 July 2005. - Vol. 7. - P. 4829-4831. ↑

C4240. Lopez-Martinez C. A framework for the analysis of speckle noise effects in multidimensional SAR imagery. / Lopez-Martinez C., Pottier E. // 2005. IGARSS '05. Proceedings. 2005 IEEE International Geoscience and Remote Sensing Symposium. 25-29 July 2005. - Vol. 7. - P. 4840-4843. ↑

C4241. Neumann M. Data classification based on PolInSAR coherence shapes. / Neumann M., Reigber A., Ferro-Famil L. // 2005. IGARSS '05. Proceedings. 2005 IEEE International Geoscience and Remote Sensing Symposium. 25-29 July 2005. - Vol. 7. - P. 4852-4855. ↑

- C4242.** Honglei Chen. New blind source separation technique for removing vegetation bias in polarimetric SAR interferometer measurements. / Honglei Chen, Kasilingam D. // 2005. IGARSS '05. Proceedings. 2005 IEEE International Geoscience and Remote Sensing Symposium. 25-29 July 2005. - Vol. 7. - P. 4860-4862. ↑
- C4243.** Touzi R. A unified model for decomposition of coherent and partially coherent target scattering using polarimetric SARs. 2005. IGARSS '05. Proceedings. 2005 IEEE International Geoscience and Remote Sensing Symposium. 25-29 July 2005. - Vol. 7. - P. 4844-4847. ↑
- C4244.** Lee J.S. Applying polarimetric SAR interferometric data for forest classification. / Lee J.S., Papathanassiou K.P., Hajnsek I., Mette T., Grunes M.R., Ainsworth T., Ferro-Famil L. // 2005. IGARSS '05. Proceedings. 2005 IEEE International Geoscience and Remote Sensing Symposium. 25-29 July 2005. - Vol. 7. - P. 4848-4851. ↑
- C4245.** Lehner S.H. Wind field and ocean wave measurements in extreme weather situations. 2005. IGARSS '05. Proceedings. 2005 IEEE International Geoscience and Remote Sensing Symposium. 25-29 July 2005. - Vol. 7. - P. 4796-4798. ↑
- C4246.** Reigber A. Refined estimation of time-varying baseline errors in airborne SAR interferometry. / Reigber A., Prats P., Mallorqui J.J. // 2005. IGARSS '05. Proceedings. 2005 IEEE International Geoscience and Remote Sensing Symposium. 25-29 July 2005. - Vol. 7. - P. 4799-4802. ↑
- C4247.** Alpers W. The distribution of internal waves in the East China Sea and the Yellow Sea studied by multi-sensor satellite images. / Alpers W., Ming-Xia He, Kan Zeng, Ling-Fei Guo, Xiao-Ming Li. // 2005. IGARSS '05. Proceedings. 2005 IEEE International Geoscience and Remote Sensing Symposium. 25-29 July 2005. - Vol. 7. - P. 4784-4787. ↑
- C4248.** Snoeij P. Uniqueness of the ERS scatterometer for nowcasting and typhoon forecasting. / Snoeij P., Attema E., Hersbach H., Stoffelen A., Crapolicchio R., Lecomte P. // 2005. IGARSS '05. Proceedings. 2005 IEEE International Geoscience and Remote Sensing Symposium. 25-29 July 2005. - Vol. 7. - P. 4792-4795. ↑
- C4249.** Hong S.-H. Spaceborne radar interferometry for coastal DEM construction. / Hong S.-H., Lee C.-W., Won J.-S., Kwoun O.-I., Lu Z. // 2005. IGARSS '05. Proceedings. 2005 IEEE International Geoscience and Remote Sensing Symposium. 25-29 July 2005. - Vol. 7. - P. 4806-4808. ↑
- C4250.** Bai Jun. InSAR PS adaptive detection and its application in Beijing area. 2005. IGARSS '05. Proceedings. 2005 IEEE International Geoscience and Remote Sensing Symposium. 25-29 July 2005. - Vol. 7. - P. 4817-4820. ↑
- C4251.** Ma Debao. Quality assessment of SAR data available for SAR interferometry. / Ma Debao, Zheng Fang, Niu Chaoyang. // 2005. IGARSS '05. Proceedings. 2005 IEEE International Geoscience and Remote Sensing Symposium. 25-29 July 2005. - Vol. 7. - P. 4821-4824. ↑
- C4252.** Xiang Maosheng. Introduction on an experimental airborne InSAR system. / Xiang Maosheng, Wu Yirong, Li Shaoen, Wei Lideng. // 2005. IGARSS '05. Proceedings. 2005 IEEE International Geoscience and Remote Sensing Symposium. 25-29 July 2005. - Vol. 7. - P. 4809-4812. ↑
- C4253.** Raucoules D. InSAR unwrapping using pre-existent topographic information-Application to the DEM derivation on the test site of Marseille/Gardanne (France). / Raucoules D., Simonetto E., Souyris J.C., Pouthie N. // 2005. IGARSS '05. Proceedings. 2005 IEEE International Geoscience and Remote Sensing Symposium. 25-29 July 2005. - Vol. 7. - P. 4813-4816. ↑
- C4254.** Jae-Bin Lee. Segmentation and extraction of linear features for detecting discrepancies between LIDAR data strips. / Jae-Bin Lee, Ki-Yun Yu, Yong-II Kim, Habib A.F. // 2005. IGARSS '05. Proceedings. 2005 IEEE International Geoscience and Remote Sensing Symposium. 25-29 July 2005. - Vol. 7. - P. 4954-4957. ↑
- C4255.** Zhiqiang Xiao. Update of road network in GIS by fusing multi-sensor imagery. / Zhiqiang Xiao, Xiaoque Jiang, Guangshu Bao, Jixian Huang, Li Lu. // 2005. IGARSS '05. Proceedings. 2005 IEEE International Geoscience and Remote Sensing Symposium. 25-29 July 2005. - Vol. 7. - P. 4969-4971. ↑
- C4256.** Arakelyan A.K. Ka-band, short pulse, polarimetric, combined Doppler radar-radiometer system. / Arakelyan A.K., Hambaryan A.K., Smolin A.I., Karyan V.V., Pogosyan N.G., Manukyan M.R., Hovhannisyan G.G., Arakelyan A.A., Grigoryan M.L., Darbinyan S.A. // 2005. IGARSS '05. Proceedings. 2005 IEEE

International Geoscience and Remote Sensing Symposium. 25-29 July 2005. - Vol. 7. - P. 4910-4913. ↑

C4257. Arefi H. A hierarchical procedure for segmentation and classification of airborne LIDAR images. / Arefi H., Hahn M. // 2005. IGARSS '05. Proceedings. 2005 IEEE International Geoscience and Remote Sensing Symposium. 25-29 July 2005. - Vol. 7. - P. 4950-4953. ↑

C4258. Kyung-Won Park. Development of a precipitation algorithm optimized for the heavy rainfall using TRMM/TMI data. / Kyung-Won Park, Young-Seup Kim, Kyung-Soo Han, Joung-Min Yeom. // 2005. IGARSS '05. Proceedings. 2005 IEEE International Geoscience and Remote Sensing Symposium. 25-29 July 2005. - Vol. 7. - P. 5064-5067. ↑

C4259. Wanyu Li. Attenuation statistics for X band radar design. / Wanyu Li, Willie D., Chandrasekar V. // 2005. IGARSS '05. Proceedings. 2005 IEEE International Geoscience and Remote Sensing Symposium. 25-29 July 2005. - Vol. 7. - P. 5077-5080. ↑

C4260. Mega T. Melting layer observation by the broad band radar(BBR). / Mega T., Monden K., Ushio T., Okamoto K. // 2005. IGARSS '05. Proceedings. 2005 IEEE International Geoscience and Remote Sensing Symposium. 25-29 July 2005. - Vol. 7. - P. 5081-5083. ↑

C4261. Moralesa J. Ice water content (IWC) retrieval from cirrus clouds using millimeter-wave radar and in-situ ice crystal airborne data. / Moralesa J., Trabal J., Cruz-Pol S.L., Sekelsky S.M. // 2005. IGARSS '05. Proceedings. 2005 IEEE International Geoscience and Remote Sensing Symposium. 25-29 July 2005. - Vol. 7. - P. 5069-5072. ↑

C4262. Maeso J. DSD characterization and computations of expected reflectivity using data from a two-dimensional video disdrometer deployed in a tropical environment. / Maeso J., Bringi V.N., Cruz-Pol S., Chandrasekar V. // 2005. IGARSS '05. Proceedings. 2005 IEEE International Geoscience and Remote Sensing Symposium. 25-29 July 2005. - Vol. 7. - P. 5073-5076. ↑

C4263. Schwerdt M. TerraSAR-X: calibration concept of a multiple mode high resolution SAR. / Schwerdt M., Hounam D., Brautigam B., Alvarez-Perez J.-L. // 2005. IGARSS '05. Proceedings. 2005 IEEE International Geoscience and Remote Sensing Symposium. 25-29 July 2005. - Vol. 7. - P. 4874-4877. ↑

C4264. Mittermayer J. The system engineering and calibration segment of the TerraSAR-X ground segment. / Mittermayer J., Schulze D., Steinbrecher U., Marquez Martinez J. // 2005. IGARSS '05. Proceedings. 2005 IEEE International Geoscience and Remote Sensing Symposium. 25-29 July 2005. - Vol. 7. - P. 4878-4881. ↑

C4265. Kimura H. Polarization orientation effects in urban areas on SAR data. / Kimura H., Papathanassiou K.P., Hajnsek I. // 2005. IGARSS '05. Proceedings. 2005 IEEE International Geoscience and Remote Sensing Symposium. 25-29 July 2005. - Vol. 7. - P. 4863-4867. ↑

C4266. Roth A. Status of the TerraSAR-X Mission. / Roth A., Werninghaus R. // 2005. IGARSS '05. Proceedings. 2005 IEEE International Geoscience and Remote Sensing Symposium. 25-29 July 2005. - Vol. 7. - P. 4868-4869. ↑

C4267. Hajnsek I. TerraSAR-X: science exploration of polarimetric and interferometric SAR. / Hajnsek I., Eineder M. // 2005. IGARSS '05. Proceedings. 2005 IEEE International Geoscience and Remote Sensing Symposium. 25-29 July 2005. - Vol. 7. - P. 4882-4885. ↑

C4268. Lenz R. The TerraSAR-X ground calibration system and pattern estimation software. / Lenz R., Pontes J., Wiesbeck W. // 2005. IGARSS '05. Proceedings. 2005 IEEE International Geoscience and Remote Sensing Symposium. 25-29 July 2005. - Vol. 7. - P. 4894-4897. ↑

C4269. Arakelyan A.K. A complex of polarimetric, combined, short pulse radar-radiometers of S-, Ku, and Ka - band of frequencies for platform and vessel application. / Arakelyan A.K., Hambaryan A.K., Smolin A.I., Karyan V.V., Pogosyan N.G., Manukyan M.R., Hovhannisyan G.G., Arakelyan A.A., Darbinyan S., Grigoryan M.L. // 2005. IGARSS '05. Proceedings. 2005 IEEE International Geoscience and Remote Sensing Symposium. 25-29 July 2005. - Vol. 7. - P. 4898-4901. ↑

C4270. Schulz-Stellenfleth J. Use of TerraSAR-X for oceanography. / Schulz-Stellenfleth J., Lehner S., Horstmann J. // 2005. IGARSS '05. Proceedings. 2005 IEEE International Geoscience and Remote Sensing Symposium. 25-29 July 2005. - Vol. 7. - P. 4886-4889. ↑

- C4271.** Krieger G. TanDEM-X: mission concept and performance analysis. / Krieger G., Fiedler H., Hajnsek I., Eineder M., Werner M., Moreira A. // 2005. IGARSS '05. Proceedings. 2005 IEEE International Geoscience and Remote Sensing Symposium. 25-29 July 2005. - Vol. 7. - P. 4890-4893. ↑
- C4272.** Durham D. From VCL to Glory: the risk management approach to changing an existing spacecraft configuration. / Durham D., Itchkawich T.J. // 2005 IEEE Aerospace Conference. - Big Sky, MT, 5-12 March 2005. - P. 120-128. ↑
- C4273.** Schuler D.L. Utilization of fully polarimetric SAR data for improved measurement of directional ocean wave spectra. / Schuler D.L., Lee J.S., Kasilingam D., Pottier E. // 2005. Proceedings of MTS/IEEE OCEANS. 2005. - P. 55-57. ↑
- C4274.** Arakelyan A.K. Sea surface radar-radiometer joint image's natural origin signatures radio contrast and spatial size's distributions properties for various meteorology and seas. / Arakelyan A.K., Hambaryan A.K., Manukyan M.R., Arakelyan A.A. // 2005. Proceedings of MTS/IEEE OCEANS. 2005. - P. 301-307. ↑
- C4275.** Liye Liu. Study about the radiation properties of an antenna for ground-penetrating radar. / Liye Liu, Yi Su, Chunlin Huang, Junjie Mao. // 2005. MAPE 2005. IEEE International Symposium on Microwave, Antenna, Propagation and EMC Technologies for Wireless Communications. 8-12 Aug. 2005. - Vol. 1. - P. 391-394. ↑
- C4276.** Khamis N.H.H. Rainfall rate from meteorological radar data for microwave applications in Malaysia. / Khamis N.H.H., Din J., Rahman T.A. // 2005 13th IEEE International Conference on Networks, 2005. Jointly held with the 2005 IEEE 7th Malaysia International Conference on Communication. 16-18 Nov. 2005. - Vol. 2. - P. 3 ↑
- C4277.** Arakelyan A.K. C-band, narrow pulse, polarimetric Doppler-scatterometer for platform application. / Arakelyan A.K., Smolin A.I., Karyan V.V., Hambaryan A.K., Arakelyan A.A., Hakobyan I.K., Grigoryan M.L., Barksdale A.O.'N. // 2005. Proceedings of MTS/IEEE OCEANS. 2005. - P. 308-313. ↑
- C4278.** Ahmad K.A. QuikSCAT Radiometer (QRad) rain rates for wind vector quality control. / Ahmad K.A., Linwood Jones W., Kasparis T. // 2005. Proceedings of MTS/IEEE OCEANS. 2005. - P. 326-330. ↑
- C4279.** Bobak J.P. Satellite calibration and validation utilizing the Airborne Polarimetric Microwave Imaging Radiometer (APMIR). / Bobak J.P., Dowgiallo D.J., vonRenzell T.E., McGlothlin N.R. // 2005. Proceedings of MTS/IEEE OCEANS. 2005. - P. 352-354. ↑
- C4280.** Hambaryan A.K. A measuring complex of polarimetric, combined radar-radiometers of S-, and Ku-band of frequencies for vessel and airborne application. / Hambaryan A.K., Arakelyan A.K., Manukyan M.R., Darbinyan S.A., Arakelyan A.A. // 2005. Proceedings of MTS/IEEE OCEANS. 2005. - P. 314-319. ↑
- C4281.** Hambaryan A. Joint processing of the signals backscattered from and emitted by the sea surface. / Hambaryan A., Arakelyan A. // 2005. Proceedings of MTS/IEEE OCEANS. 2005. - P. 320-325. ↑
- C4282.** Khamis N.H.H. Analysis of rain cell size distribution from meteorological radar data for rain attenuation studies. / Khamis N.H.H., Din J., Rahman T.A. // 2005. APACE 2005. Asia-Pacific Conference on Applied Electromagnetics. 20-21 Dec. 2005. - P. 3 ↑
- C4283.** Kalmykov I.A. The using multifrequency airborne radar complex MARS for subsurface remote sensing. / Kalmykov I.A., Tsymbal V.N., Yefimov V.B. // 2005 European Microwave Conference. 4-6 Oct. 2005. - Vol. 3. - P. 4 ↑
- C4284.** Vanjari S.V. Information extraction from sensor nodes using air-borne radar and back-scatter modulation. / Vanjari S.V., Drogmeier J.V., Bell M.R. // 2005. MILCOM 2005. IEEE Military Communications Conference. - Atlantic City, NJ, 17-20 Oct. 2005. - P. 1421-1427. ↑
- C4285.** Sung-Hyun Kim. Dual-channel radiometers for Earth and atmosphere monitoring (DREAM) on micro satellite STSAT-2. / Sung-Hyun Kim, Ho-Jin Lee, Chun-Sik Chae, Hyuk Park, Seok-Hun Yun, Jong-Oh Park, Seung-Hun Lee, Eun-Sup Sim, De-Hai Zhang, Jing-Shan Jiang, Yong-Hoon Kim. // 2005. APMC 2005. Asia-Pacific Conference Proceedings Microwave Conference Proceedings. 4-7 Dec. 2005. - Vol. 1. - P. 3 ↑
- C4286.** Lenz R. A high accuracy calibration and receive instrument for TerraSAR-X ground calibration. / Lenz R., Pontes J., Wiesbeck W. // 2005 European Microwave Conference. 4-6 Oct. 2005. - Vol. 3. - P. 4 ↑

- C4287. Lin Hongwen. Design of delay mapping receiver for GPS remote sensing. / Lin Hongwen, Zhang Yiqiang, Zhang Qishan. // 2005. MAPE 2005. IEEE International Symposium on Microwave, Antenna, Propagation and EMC Technologies for Wireless Communications. - Beijing, 8-12 Aug. 2005. - Vol. 1. - P. 161-164. ↑
- C4288. Ya-Qiu Jin. Difference RCS of electromagnetic scattering from the target above a randomly rough surface. / Ya-Qiu Jin, Hongxia Ye. // 2005. MAPE 2005. IEEE International Symposium on Microwave, Antenna, Propagation and EMC Technologies for Wireless Communications. 8-12 Aug. 2005. - Vol. 1. - P. 169-172. ↑
- C4289. Roederer A.G. Antennas for Space: Some Recent European Developments and Trends. 2005. ICECom 2005. 18th International Conference on Applied Electromagnetics and Communications. - Dubrovnik, 12-14 Oct. 2005. - P. 1-8. ↑
- C4290. Lisheng Fan. A cross-entropy based parameter for ship detection from a polarimetric SAR image. / Lisheng Fan, Jian Yang, Ying Ning Peng. // 2005. MAPE 2005. IEEE International Symposium on Microwave, Antenna, Propagation and EMC Technologies for Wireless Communications. - Beijing, 8-12 Aug. 2005. - Vol. 1. - P. 6-9. ↑
- C4291. Laupattarakasem P. Calibration/validation of the SeaWinds radiometer rain rate algorithm. / Laupattarakasem P., Jones W.L., Ahmad K., Veleza S. // 2005. Proceedings of MTS/IEEE OCEANS. 2005. - P. 2601-2604. ↑
- C4292. Weissman D.E. Corrections to scatterometer wind vectors from the effects of rain, using high resolution NEXRAD radar collocations. / Weissman D.E., Bourassa M.A. // 2005. Proceedings of MTS/IEEE OCEANS. 2005. - P. 2012-2015. ↑
- C4293. Lucifredi I. Integrated Marine Mammal Monitoring and Protection System (IMAPS). / Lucifredi I., Stein P.J., Alix K.L., Herman J.C., Frankel A.S., Ellison W.T., Egnor D.E., Clark C.W., DeProspo D. // 2005. Proceedings of MTS/IEEE OCEANS. 2005. - P. 2634-2641. ↑
- C4294. Kearns T.A. A methodology for the efficient storage and processing of coastal point data. 2005. Proceedings of MTS/IEEE OCEANS. 2005. - P. 2625-2630. ↑
- C4295. Zhong Ping Lee. Bathymetry of shallow coastal regions derived from space-borne hyperspectral sensor. / Zhong Ping Lee, Casey B., Parsons R., Goode W., Weidemann A., Arnone R. // 2005. Proceedings of MTS/IEEE OCEANS. 2005. - P. 2160-2170. ↑
- C4296. Shi Zhenhua. The application of GPS to high frequency oceanic detecting radar. / Shi Zhenhua, Dong Peng, Shi Xinzh. // 2005. Proceedings of MTS/IEEE OCEANS. 2005. - P. 2093-2096. ↑
- C4297. Ebuchi N. Evaluation of marine surface winds observed by active and passive microwave sensors on ADEOS-II. 2005. Proceedings of MTS/IEEE OCEANS. 2005. - P. 2053-2056. ↑
- C4298. Bannoura W.J. NOAA Ocean Surface Topography Mission Jason-2 project overview. / Bannoura W.J., Wade A., Srinivas D.N. // 2005. Proceedings of MTS/IEEE OCEANS. 2005. - P. 2155-2159. ↑
- C4299. Adams I.S. Hurricane wind retrievals using the SeaWinds scatterometer on QuikSCAT. / Adams I.S., Jones W.L., Vasudevan S., Soisuvann S. // 2005. Proceedings of MTS/IEEE OCEANS. 2005. - P. 2148-2150. ↑
- C4300. Bellec R. Repeat-track SAS interferometry: feasibility study. / Bellec R., Legris M., Khenchaf A., Amate M., Hetet A. // 2005. Proceedings of MTS/IEEE OCEANS. 2005. - P. 748-754. ↑
- C4301. Holloway D. Seamless access to surface current vectors from the IOOS HF radar backbone. / Holloway D., Ullman D. // 2005. Proceedings of MTS/IEEE OCEANS. 2005. - P. 949-952. ↑
- C4302. Chandler R.C. A wavelet based method for the extraction of sea wave orientation. 2005. Proceedings of MTS/IEEE OCEANS. 2005. - P. 369-374. ↑
- C4303. Trizna D.B. Microwave and HF multi-frequency radars for dual-use coastal remote sensing applications. 2005. Proceedings of MTS/IEEE OCEANS. 2005. - P. 532-537. ↑
- C4304. Shen C.Y. Some Practical Ways to Determine Coastal Current's Vertical Structure. / Shen C.Y., Evans

T.E. // 2005. Proceedings of MTS/IEEE OCEANS. - Washington, DC, 17-23 Sept. 2005. - P. 1-8. ↑

C4305. Moisan T.A. Bio-physical Interactions in Ocean Margin Ecosystems (BIOME): understanding coastal dynamics in the Southern Mid-Atlantic Bight. / Moisan T.A., Atkinson L.P., Blanco J.L., Boicourt W., Hooker S., Maldnen C., Moisan J.R., Mannino A., Mitra M., Mulholland M., Nolan J., Russ M., Swift R.W., Tester P.A. // 2005. Proceedings of MTS/IEEE OCEANS. 2005. - P. 2830-2837. ↑

C4306. Torsekar V. Oceanic rain identification using multifractal analysis of QuikSCAT Sigma-0. / Torsekar V., Kasparis T., Jones W.L., Ahmad K., Long D.G. // 2005. Proceedings of MTS/IEEE OCEANS. 2005. - P. 2656-2663. ↑

C4307. Mingxin Nie. Ocean surface feature extraction and targets detection from SAR images using neural network. / Mingxin Nie, Ling Lu. // 2005. Proceedings of MTS/IEEE OCEANS. - Washington, DC, 17-23 Sept. 2005. - P. 1757-1760. ↑

C4308. Soisuvann S. A Novel Active and Passive Microwave Remote Sensing Technique for Measuring Ocean Surface Wind Vector. / Soisuvann S., Jones W.L., Jejenak Z. // 2005. Proceedings of MTS/IEEE OCEANS. - Washington, DC, 17-23 Sept. 2005. - P. 1-5. ↑

C4309. Fukagawa S. Simulation study for aerosol distribution retrieval from bistatic, imaging lidar data. / Fukagawa S., Kouga I., Kuze H., Takeuchi N., Sasaki M., Asaoka Y., Ogawa S. // 2005. CLEO/Pacific Rim 2005. Pacific Rim Conference on Lasers and Electro-Optics. 30-02 Aug. 2005. - P. 1261-1262. ↑

C4310. Boric-Lubecke O. Doppler radar sensing of multiple subjects in single and multiple antenna systems. / Boric-Lubecke O., Lubecke V.M., Host-Madsen A., Samardzija D., Cheung K. // 2005. 7th International Conference on Telecommunications in Modern Satellite, Cable and Broadcasting Services. 28-30 Sept. 2005. - Vol. 1. - P. 7-11. ↑

C4311. Gronlund R. Remote laser-induced fluorescence imaging for assessment of cultural heritage. / Gronlund R., Svanberg S., Hallstrom J., Barup K. // 2005. CLEO/Europe. 2005 Conference on Lasers and Electro-Optics Europe. - Munich, 17-17 June 2005. - P. 685. ↑

C4312. Chan Bong Park. Remote sensing and statistical analysis of Asian dust measured by 532/1064 nm Lidar during 2002-2005. / Chan Bong Park, Choo Hie Lee, Jin Hwan Kim. // 2005. CLEO/Pacific Rim 2005. Pacific Rim Conference on Lasers and Electro-Optics. 30-02 Aug. 2005. - P. 1256-1258. ↑

C4313. Korneev D. 3D imaging system based on FMCW millimeter wave radar. / Korneev D., Bogdanov L., Nalivkin A., Berezin S. // 2005. IRMMW-THz 2005. The Joint 30th International Conference on Infrared and Millimeter Waves and 13th International Conference on Terahertz Electronics. 19-23 Sept. 2005. - Vol. 2. - P. 367-368. ↑

C4314. Haykin S. Cognitive radar networks. 2005 1st IEEE International Workshop on Computational Advances in Multi-Sensor Adaptive Processing. 13-15 Dec. 2005. - P. 1-3. ↑

C4315. Shkvarko Y.V. Unified Bayesian-experiment design regularization technique for high-resolution reconstruction of the remote sensing imagery. / Shkvarko Y.V., Villalon-Turrubiates I.E. // 2005 1st IEEE International Workshop on Computational Advances in Multi-Sensor Adaptive Processing. - Puerto Vallarta, 13-13 Dec. 2005. - P. 165-172. ↑

C4316. Kobayashi T. Rayleigh-Mie lidar for accurate temperature profiling of the troposphere. / Kobayashi T., Dengxin Hua. // 2005. (CLEO). Conference on Lasers and Electro-Optics. 22-27 May 2005. - Vol. 3. - P. 1876-1878. ↑

C4317. {no data available}. 1st IEEE International Workshop on Computational Advances in Multi-Sensor Adaptive Processing (IEEE Cat. No.05EX1140C). 2005 1st IEEE International Workshop on Computational Advances in Multi-Sensor Adaptive Processing. 13-15 Dec. 2005. - {no data available}. ↑

C4318. Witzgall H.E. Exploiting fundamental properties of SAR data for compression of tactical SAR imagery. / Witzgall H.E., Goldstein J.S. // 2005 IEEE Aerospace Conference. - Big Sky, MT, 5-12 March 2005. - P. 1354-1362. ↑

C4319. Firdous S. Mueller matrix modeling of atmospheric scattering medium through polarized laser beam. /

Firdous S., Ikram M. // 2005 IEEE Aerospace Conference. - Big Sky, MT, 5-12 March 2005. - P. 1963-1971. ↑

C4320. Durham D. The story of Glory: Earth and solar science on one unique satellite. / Durham D., Itchkawich T. // 2005 IEEE Aerospace Conference. - Big Sky, MT, 5-12 March 2005. - P. 422-431. ↑

C4321. Perkovic D. An airborne pod-mounted dual beam interferometer. / Perkovic D., Frasier S.J., Tessier R., Sletten M.A., Toporkov J.V. // 2005 IEEE Aerospace Conference. - Big Sky, MT, 5-12 March 2005. - P. 1193-1201. ↑

C4322. Davis M.E. Space based radar technology challenges. 2005 IEEE Aerospace Conference. - Big Sky, MT, 5-12 March 2005. - P. 2154-2161. ↑

C4323. Parvin P. Remote element tracing of trans-uranium plumes using an interactive UV laser DIAL coupled with a phoswich detector. / Parvin P., Davoud-Abadi G.-R., Zamanipoor Z., Zangeneh H.-R., Jaleh B. // 2005. EQEC '05. European Quantum Electronics Conference. 12-17 June 2005. - P. 203. ↑

C4324. Gronlund R. Remote LIBS and Raman imaging for assessment of cultural heritage. / Gronlund R., Bengtsson M., Lundqvist M., Somesfalean G., Svanberg S. // 2005. CLEO/Europe. 2005 Conference on Lasers and Electro-Optics Europe. - Munich, 17-17 June 2005. - P. 684. ↑

C4325. Wong Ka Yan. An intelligent tropical cyclone eye fix system using motion field analysis. / Wong Ka Yan, Yip Chi Lap. // 2005. ICTAI 05. 17th IEEE International Conference on Tools with Artificial Intelligence. - Hong Kong, 16-16 Nov. 2005. - P. 5 P.-656. ↑

C4326. Zubkov A.N. Integrated dual spectral system of Earth surface monitoring. / Zubkov A.N., Smerklo L.M., Prudyus I.N., Andruschak R.V. // 2005 15th International Crimean Conference Microwave & Telecommunication Technology. - Sevastopol, Crimea, 16-16 Sept. 2005. - Vol. 2. - P. 948-949. ↑

C4327. Jager M. The distribution of interferometric phase differentials and a self-initialising PolInSAR classifier. / Jager M., Neumann M., Guillaso S., Reigber A. // 2005. EURAD 2005. European Radar Conference. - Paris, 6-7 Oct. 2005. - P. 181-184. ↑

C4328. Sauer S. Characterisation of buildings using polarimetric interferometric multiple track L-band SAR data. / Sauer S., Ferro-Famil L., Reigber A., Pettier E. // 2005. EURAD 2005. European Radar Conference. - Paris, 6-7 Oct. 2005. - P. 185-188. ↑

C4329. Martini A. Dry snow extent monitoring using multi-frequency and multi-temporal polarimetric indicators. / Martini A., Ferro-Famil L., Pottier E. // 2005. EURAD 2005. European Radar Conference. - Paris, 6-7 Oct. 2005. - P. 173-176. ↑

C4330. Allain S. New eigenvalue-based parameters for natural media characterization. / Allain S., Ferro-Famil L., Potier E. // 2005. EURAD 2005. European Radar Conference. - Paris, 6-7 Oct. 2005. - P. 177-180. ↑

C4331. Reigber A. Evaluating PolInSAR parameter estimation using tomographic imaging results. / Reigber A., Neumann M., Guillaso S., Sauer S., Ferro-Famil L. // 2005. EURAD 2005. European Radar Conference. - Paris, 6-7 Oct. 2005. - P. 189-192. ↑

C4332. Kalmykov I.A. The using multifrequency airborne radar complex MARS for subsurface remote sensing. / Kalmykov I.A., Tsymbal V.N., Yefimov V.B. // 2005. EURAD 2005. European Radar Conference. - Paris, 6-7 Oct. 2005. - P. 387-390. ↑

C4333. Lenz R. A high accuracy calibration and receive instrument for TerraSAR-X ground calibration. / Lenz R., Pontes J., Wiesbeck W. // 2005. EURAD 2005. European Radar Conference. - Paris, 6-7 Oct. 2005. - P. 411-414. ↑

C4334. Rovkin M.E. Radar system concept for simultaneous BSM of complicated and non-stable targets measurements. / Rovkin M.E., Khlusov V.A., Lighthart L.P., van der Zwan F. // 2005. EURAD 2005. European Radar Conference. - Paris, 6-7 Oct. 2005. - P. 221-223. ↑

C4335. Tokieda Y. High precision waterlevel gauge with an FMCW radar under limited bandwidth. / Tokieda Y., Sugawara H., Niimura S., Fujise T. // 2005. EURAD 2005. European Radar Conference. - Paris, 6-7 Oct. 2005. - P. 339-342. ↑

- C4336. {no data available}. EuRAD 2005 Sessions. 2005. EURAD 2005. European Radar Conference. 6-7 Oct. 2005. - P. 6. ↑
- C4337. Hamasaki T. Applications of polarimetric interferometric ground-based SAR (GB-SAR) system to environment monitoring and disaster prevention. / Hamasaki T., Ferro-Famil L., Pottier E., Sato M. // 2005. EURAD 2005. European Radar Conference. - Paris, 6-7 Oct. 2005. - P. 29-32. ↑
- C4338. Bolderheij F. A risk-based object-oriented approach to sensor management. / Bolderheij F., Absil F.G.J., van Genderen P. // 2005 8th International Conference on Information Fusion. 25-28 July 2005. - Vol. 1. - P. 8. ↑
- C4339. Yeary M. Spectral Signature Calculations for Remote Sensing. / Yeary M., Yu T.-Y., Nematifar S., Shapiro A. // 2005. IMTC 2005. Proceedings of the IEEE Instrumentation and Measurement Technology Conference. - Ottawa, Ont., 16-19 May 2005. - Vol. 3. - P. 2071-2075. ↑
- C4340. Tello M. A novel approach for the automatic detection of punctual isolated targets in a noisy background in SAR imagery. / Tello M., Lopez-Martinez C., Mallorqui J.J. // 2005. EURAD 2005. European Radar Conference. - Paris, 6-7 Oct. 2005. - P. 41-44. ↑
- C4341. Ferro-Famil L. Influence of acquisition conditions on forest classification using L-band Pol-inSAR data. / Ferro-Famil L., Pottier E. // 2005. EURAD 2005. European Radar Conference. - Paris, 6-7 Oct. 2005. - P. 113-116. ↑
- C4342. Lopez-Martinez C. Quantitative assessment of physical information retrieved via multidimensional radar systems. / Lopez-Martinez C., Pottier E. // 2005. EURAD 2005. European Radar Conference. - Paris, 6-7 Oct. 2005. - P. 117-120. ↑
- C4343. del Campo A.B. Vehicle control classification and identification through ISAR imaging. / del Campo A.B., Lopez A.A., Naranjo B.P.D., Menoyo J.G., Moran D.R., Duarte C.C. // 2005. EURAD 2005. European Radar Conference. - Paris, 6-7 Oct. 2005. - P. 65-68. ↑
- C4344. Kovalenko V. Effect of the data pre-processing on GPR mine detector performance. / Kovalenko V., Yarovoy A., Ligthart L.P. // 2005. EURAD 2005. European Radar Conference. - Paris, 6-7 Oct. 2005. - P. 73-76. ↑
- C4345. Baillarin-Ribbes F. Spot image / SARCOM: satellite imagery to reinforce maritime surveillance. / Baillarin-Ribbes F., Chikhi M., Campenon P. // 2005. IGARSS '05. Proceedings. 2005 IEEE International Geoscience and Remote Sensing Symposium. 25-29 July 2005. - Vol. 7. - P. 4781-4783. ↑
- C4346. Ji-Eun Kim. Investigation of physical characteristics of intertidal zone using NASA/JPL fully polarimetric AIRSAR data. / Ji-Eun Kim, Sang-Eun Park, Duk-jin Kim, Wooil M. Moon. // 2005. IGARSS '05. Proceedings. 2005 IEEE International Geoscience and Remote Sensing Symposium. 25-29 July 2005. - Vol. 3. - P. 2082-2085. ↑
- C4347. Czuchlewski K.R. New methods for landslide identification and mapping using SAR polarimetry obtained during the PacRim 2000 mission in Taiwan. / Czuchlewski K.R., Weissel J.K., Jong-Sen Lee. // 2005. IGARSS '05. Proceedings. 2005 IEEE International Geoscience and Remote Sensing Symposium. 25-29 July 2005. - Vol. 3. - P. 2086-2089. ↑
- C4348. Habib A.F. Comparative analysis of the performance of metric-analog cameras, amateur-digital cameras, and LIDAR. / Habib A.F., Ghanma M.S., Mitishita E.A., Machado A., Kim E.M., Kim C.J. // 2005. IGARSS '05. Proceedings. 2005 IEEE International Geoscience and Remote Sensing Symposium. 25-29 July 2005. - Vol. 3. - P. 2070-2073. ↑
- C4349. Pairman D. Forest detection in varying terrain using full-polarisation SAR data. / Pairman D., McNeill S.J., Belliss S.E. // 2005. IGARSS '05. Proceedings. 2005 IEEE International Geoscience and Remote Sensing Symposium. 25-29 July 2005. - Vol. 3. - P. 2078-2081. ↑
- C4350. Mitchell A.L. Sensitivity of radar backscatter to mangrove forest structure and AIRSAR imaging parameters. / Mitchell A.L., Lucas R.M., Proisy C., Melius A. // 2005. IGARSS '05. Proceedings. 2005 IEEE International Geoscience and Remote Sensing Symposium. 25-29 July 2005. - Vol. 3. - P. 2090-2093. ↑

- C4351.** Lucas R. The role of LiDAR data in understanding the relation between forest structure and SAR imagery. / Lucas R., Lee A., Williams M. // 2005. IGARSS '05. Proceedings. 2005 IEEE International Geoscience and Remote Sensing Symposium. 25-29 July 2005. - Vol. 3. - P. 2101-2104. ↑
- C4352.** Moser G. Generalized minimum-error thresholding for unsupervised change detection from SAR amplitude imagery. / Moser G., Serpico S.B. // 2005. IGARSS '05. Proceedings. 2005 IEEE International Geoscience and Remote Sensing Symposium. 25-29 July 2005. - Vol. 3. - P. 2121-2124. ↑
- C4353.** Lucas R.M. The contribution of PACRIM II to forest assessment in Queensland, Australia. / Lucas R.M., Antony, Milne K., Lee A.C., Moghaddam M., Cronin N., Witte C., Tickle P., Williams M. // 2005. IGARSS '05. Proceedings. 2005 IEEE International Geoscience and Remote Sensing Symposium. 25-29 July 2005. - Vol. 3. - P. 2094-2097. ↑
- C4354.** Anhua Chu. The interferometric data calibration for the AIRSAR PacRim II mission. / Anhua Chu, Yunjin Kim, van Zyl J., Yunling Lou, Chapman B. // 2005. IGARSS '05. Proceedings. 2005 IEEE International Geoscience and Remote Sensing Symposium. 25-29 July 2005. - Vol. 3. - P. 2098-2100. ↑
- C4355.** Alberga V. Comparison of methods for extracting and utilizing radar target characteristic parameters. / Alberga V., Staykova D., Krogager E., Danklmayer A., Chandra M. // 2005. IGARSS '05. Proceedings. 2005 IEEE International Geoscience and Remote Sensing Symposium. 25-29 July 2005. - Vol. 3. - P. 2019-2021. ↑
- C4356.** Monden K. Development and observation of the broad-band radar for meteorological application. / Monden K., Mega T., Ushio T., Okamoto K. // 2005. IGARSS '05. Proceedings. 2005 IEEE International Geoscience and Remote Sensing Symposium. 25-29 July 2005. - Vol. 3. - P. 2022-2025. ↑
- C4357.** Chandra M. AMPER: network on applied multiparameter environmental remote sensing: an EU sponsored research and training network. / Chandra M., Boerner W., Moreira A., Keydel W. // 2005. IGARSS '05. Proceedings. 2005 IEEE International Geoscience and Remote Sensing Symposium. 25-29 July 2005. - Vol. 3. - P. 2007-2011. ↑
- C4358.** Jian Yang. On the polarization entropy. / Jian Yang, Yilun Chen, Yingning Peng. // 2005. IGARSS '05. Proceedings. 2005 IEEE International Geoscience and Remote Sensing Symposium. 25-29 July 2005. - Vol. 3. - P. 2012-2014. ↑
- C4359.** Kobayashi S. Backscattering enhancement for Marshall-Palmer distributed rains for a W-band nadir-pointing radar with a finite beam width. / Kobayashi S., Tanelli S., Im E., Oguchi T. // 2005. IGARSS '05. Proceedings. 2005 IEEE International Geoscience and Remote Sensing Symposium. 25-29 July 2005. - Vol. 3. - P. 2026-2029. ↑
- C4360.** Yanting Wang. Application of cross-polar optimal polarizations for precipitation sensing. / Yanting Wang, Bringi V.N., Chandrasekar V. // 2005. IGARSS '05. Proceedings. 2005 IEEE International Geoscience and Remote Sensing Symposium. 25-29 July 2005. - Vol. 3. - P. 2042-2045. ↑
- C4361.** Donovan B.C. Principles and design considerations for short-range energy balanced radar networks. / Donovan B.C., McLaughlin D.J., Kurose J., Chandrasekar V. // 2005. IGARSS '05. Proceedings. 2005 IEEE International Geoscience and Remote Sensing Symposium. 25-29 July 2005. - Vol. 3. - P. 2058-2061. ↑
- C4362.** Junyent F. High resolution dual-polarization radar observation of tornados: implications for radar development and tornado detection. / Junyent F., Frasier S., McLaughlin D.J., Chandrasekar V., Bluestein H., French M. // 2005. IGARSS '05. Proceedings. 2005 IEEE International Geoscience and Remote Sensing Symposium. 25-29 July 2005. - Vol. 3. - P. 2034-2037. ↑
- C4363.** Santalla-del-Rio V. Polarimetric doppler measurements for weather radar applications. 2005. IGARSS '05. Proceedings. 2005 IEEE International Geoscience and Remote Sensing Symposium. 25-29 July 2005. - Vol. 3. - P. 2038-2041. ↑
- C4364.** Lai Xudong. The study of filter algorithm for Lidar intensity image. / Lai Xudong, Wan Youchuan. // 2005. IGARSS '05. Proceedings. 2005 IEEE International Geoscience and Remote Sensing Symposium. 25-29 July 2005. - Vol. 5. - P. 3285-3289. ↑
- C4365.** Qinyu Liu. Sea surface wind and cold tongue over the winter South China Sea. / Qinyu Liu, Xia Jiang, Shang-Ping Xie, Liu W.T. // 2005. IGARSS '05. Proceedings. 2005 IEEE International Geoscience and Remote

Sensing Symposium. 25-29 July 2005. - Vol. 5. - P. 3294-3297. ↑

C4366. Jingjue Jiang. Data segmentation for geometric feature extraction from lidar point clouds. / Jingjue Jiang, Zuxun Zhang, Ying Ming. // 2005. IGARSS '05. Proceedings. 2005 IEEE International Geoscience and Remote Sensing Symposium. 25-29 July 2005. - Vol. 5. - P. 3277-3280. ↑

C4367. Yi-Hsing Tseng. Automatic plane extraction from LIDAR data based on octree splitting and merging segmentation. / Yi-Hsing Tseng, Miao Wang. // 2005. IGARSS '05. Proceedings. 2005 IEEE International Geoscience and Remote Sensing Symposium. 25-29 July 2005. - Vol. 5. - P. 3281-3284. ↑

C4368. Xuetong Xie. A new fast wind vector retrieval algorithm for seawinds scatterometer. / Xuetong Xie, Yu Fang, Xiaoxiang Chen, Kehai Chen. // 2005. IGARSS '05. Proceedings. 2005 IEEE International Geoscience and Remote Sensing Symposium. 25-29 July 2005. - Vol. 5. - P. 3298-3301. ↑

C4369. Qulin Tan. An experiment for high resolution airborne SAR imaging based on phase gradient autofocus. / Qulin Tan, Zhou Fu, Zhengjun Liu, Jiping Hu. // 2005. IGARSS '05. Proceedings. 2005 IEEE International Geoscience and Remote Sensing Symposium. 25-29 July 2005. - Vol. 5. - P. 3322-3324. ↑

C4370. Kaizhi Wang. Auto-combination of sub-band for spotlight SAR imaging. / Kaizhi Wang, Xingzhao Li. // 2005. IGARSS '05. Proceedings. 2005 IEEE International Geoscience and Remote Sensing Symposium. 25-29 July 2005. - Vol. 5. - P. 3325-3328. ↑

C4371. Weissman D.E. Corrections to scatterometer wind vectors from the effects of rain, using high resolution NEXRAD radar collocations. / Weissman D.E., Bourassa M.A. // 2005. IGARSS '05. Proceedings. 2005 IEEE International Geoscience and Remote Sensing Symposium. 25-29 July 2005. - Vol. 5. - P. 3302-3305. ↑

C4372. {no data available}. Evaluation of microwave scatterometers and radiometers as satellite anemometers. 2005. IGARSS '05. Proceedings. 2005 IEEE International Geoscience and Remote Sensing Symposium. 25-29 July 2005. - Vol. 5. - P. 3310-3313. ↑

C4373. Jiancheng Shi. Estimation of bare surface soil moisture with L-band multi-polarization radar measurements. / Jiancheng Shi, Chen K.S. // 2005. IGARSS '05. Proceedings. 2005 IEEE International Geoscience and Remote Sensing Symposium. 25-29 July 2005. - Vol. 3. - P. 2191-2194. ↑

C4374. Jin-Young Hong. Examination of the semi-empirical polarimetric scattering model using field-measured data and existing theoretical models. / Jin-Young Hong, Yisok Oh. // 2005. IGARSS '05. Proceedings. 2005 IEEE International Geoscience and Remote Sensing Symposium. 25-29 July 2005. - Vol. 3. - P. 2211-2214. ↑

C4375. Wegmuller U. Monitoring of mining induced surface deformation using L-band SAR interferometry. / Wegmuller U., Spreckels V., Werner C., Strozzi T., Wiesmann A. // 2005. IGARSS '05. Proceedings. 2005 IEEE International Geoscience and Remote Sensing Symposium. 25-29 July 2005. - Vol. 3. - P. 2165-2168. ↑

C4376. Lixia Gong. Measure groundwater pumping induced subsidence with D-InSAR. / Lixia Gong, Jingfa Zhang, Qingshi Guo. // 2005. IGARSS '05. Proceedings. 2005 IEEE International Geoscience and Remote Sensing Symposium. 25-29 July 2005. - Vol. 3. - P. 2169-2171. ↑

C4377. Hung-Wei Lee. A comparisons of model based and image based surface parameters estimation from polarimetric SAR. / Hung-Wei Lee, Kun-Shan Chen, Jong-Sen Lee, Shi J.C., Tzong-Dar Wu, Hajnsek I. // 2005. IGARSS '05. Proceedings. 2005 IEEE International Geoscience and Remote Sensing Symposium. 25-29 July 2005. - Vol. 3. - P. 2215-2218. ↑

C4378. Daout F. Computation of bistatic RCS with NEC2 in a context of passive ISAR system. / Daout F., Schmitt F., Ginolhac G. // 2005. IGARSS '05. Proceedings. 2005 IEEE International Geoscience and Remote Sensing Symposium. 25-29 July 2005. - Vol. 5. - P. 3184-3187. ↑

C4379. Schott P. Different approximations to the computation of reflected and refracted angles thanks to snell-descartes laws and fresnel coefficients. / Schott P., Beaudoin L. // 2005. IGARSS '05. Proceedings. 2005 IEEE International Geoscience and Remote Sensing Symposium. 25-29 July 2005. - Vol. 5. - P. 3188-3191. ↑

C4380. Pottier E. PolSARpro v2.0: the polarimetric SAR data processing and educational toolbox. / Pottier E., Cloude S., Hajnsek I., Pearson T. // 2005. IGARSS '05. Proceedings. 2005 IEEE International Geoscience and Remote Sensing Symposium. 25-29 July 2005. - Vol. 5. - P. 3173-3176. ↑

- C4381. Wen Xiaoyang. Complex object's ISAR image simulation. / Wen Xiaoyang, Wang Chao, Zhang Hong. // 2005. IGARSS '05. Proceedings. 2005 IEEE International Geoscience and Remote Sensing Symposium. 25-29 July 2005. - Vol. 5. - P. 3181-3183. ↑
- C4382. Tzeng Y.C. Automatic detection of targets using fractal dimension. / Tzeng Y.C., Chu D.M., Wu M.F., Kun-Shan Chen. // 2005. IGARSS '05. Proceedings. 2005 IEEE International Geoscience and Remote Sensing Symposium. 25-29 July 2005. - Vol. 3. - P. 1713-1716. ↑
- C4383. Yongqiang Chen. Detection methods of submerged mobile using SAR images. / Yongqiang Chen, Jin Feng, Zhu Minhui. // 2005. IGARSS '05. Proceedings. 2005 IEEE International Geoscience and Remote Sensing Symposium. 25-29 July 2005. - Vol. 3. - P. 1717-1720. ↑
- C4384. Suvichakorn A. The application of cloud texture and motion derived from geostationary satellite images in rain estimation-a study on mid-latitude depressions. / Suvichakorn A., Tatnall A. // 2005. IGARSS '05. Proceedings. 2005 IEEE International Geoscience and Remote Sensing Symposium. 25-29 July 2005. - Vol. 3. - P. 1682-1685. ↑
- C4385. Huang Xiao-tao. A novel prescreening method for UWB SAR target detection using adaptive nonlinear filters. / Huang Xiao-tao, Wang Hong-gang, Yang Zhi-guo, Liu Xiang-jun. // 2005. IGARSS '05. Proceedings. 2005 IEEE International Geoscience and Remote Sensing Symposium. 25-29 July 2005. - Vol. 3. - P. 1709-1712. ↑
- C4386. Kidera S. A high-resolution imaging algorithm based on scattered waveform estimation for UWB pulse radar systems. / Kidera S., Sakamoto T., Sato T. // 2005. IGARSS '05. Proceedings. 2005 IEEE International Geoscience and Remote Sensing Symposium. 25-29 July 2005. - Vol. 3. - P. 1725-1728. ↑
- C4387. Hsing-Chung Chang. DInSAR for mine subsidence monitoring using multi-source satellite SAR images. / Hsing-Chung Chang, Linlin Ge, Rizos C. // 2005. IGARSS '05. Proceedings. 2005 IEEE International Geoscience and Remote Sensing Symposium. 25-29 July 2005. - Vol. 3. - P. 1742-1745. ↑
- C4388. Langemeyer S. Architecture of a flexible on-board real-time SAR-processor. / Langemeyer S., Simon-Klar C., Nolte N., Pirsch P. // 2005. IGARSS '05. Proceedings. 2005 IEEE International Geoscience and Remote Sensing Symposium. 25-29 July 2005. - Vol. 3. - P. 1746-1749. ↑
- C4389. Huang Chunlin. A new GPR calibration method for high accuracy thickness and permittivity measurement of multi-layered pavement. / Huang Chunlin, Su Yi. // 2005. IGARSS '05. Proceedings. 2005 IEEE International Geoscience and Remote Sensing Symposium. 25-29 July 2005. - Vol. 3. - P. 1729-1733. ↑
- C4390. Lei Wentai. A real-time back projection imaging algorithm for impulse surface penetrating radar. / Lei Wentai, Huang Chunlin, Su Yi. // 2005. IGARSS '05. Proceedings. 2005 IEEE International Geoscience and Remote Sensing Symposium. 25-29 July 2005. - Vol. 3. - P. 1734-1737. ↑
- C4391. Zhong-feng Qiu. Assimilating TOPEX/Poseidon data into an adjoint numerical tidal model in the East China Sea. / Zhong-feng Qiu, Yi-jun He. // 2005. IGARSS '05. Proceedings. 2005 IEEE International Geoscience and Remote Sensing Symposium. 25-29 July 2005. - Vol. 1. - P. 4. ↑
- C4392. {no data available}. IGARSS 2005. IEEE International Geoscience and Remote Sensing Symposium. 2005. IGARSS '05. Proceedings. 2005 IEEE International Geoscience and Remote Sensing Symposium. 25-29 July 2005. - Vol. 3. - {no data available}. ↑
- C4393. Dente L. Assimilation of ASAR data for wheat yield prediction: Matera case study. / Dente L., Rinaldi M., Mattia F., Satalino G. // 2005. IGARSS '05. Proceedings. 2005 IEEE International Geoscience and Remote Sensing Symposium. 25-29 July 2005. - Vol. 1. - P. 4. ↑
- C4394. Mironov V.L. Freeze-thaw processes radar remote sensing modeling and image processing. / Mironov V.L., Komarov S.A., Li S., Romanovsky V.E. // 2005. IGARSS '05. Proceedings. 2005 IEEE International Geoscience and Remote Sensing Symposium. 25-29 July 2005. - Vol. 1. - P. 4. ↑
- C4395. Burini A. SAR in agriculture: sensitivity of backscattering to grapes. / Burini A., Minchella A., Solimini D. // 2005. IGARSS '05. Proceedings. 2005 IEEE International Geoscience and Remote Sensing Symposium. 25-29 July 2005. - Vol. 3. - P. 1542-1545. ↑

- C4396.** Goodenough D.G. Multitemporal evaluation with ASAR of boreal forests. / Goodenough D.G., Hao Chen, Dyk A., Tian Han, Carey S. // 2005. IGARSS '05. Proceedings. 2005 IEEE International Geoscience and Remote Sensing Symposium. 25-29 July 2005. - Vol. 3. - P. 1662-1665. ↑
- C4397.** Hermawan E. The utilization of equatorial atmosphere radar (EAR) and global precipitation climatology project (GPCP) in indicating of rainfall intensity over Kototabang, West Sumatera, Indonesia. 2005. IGARSS '05. Proceedings. 2005 IEEE International Geoscience and Remote Sensing Symposium. 25-29 July 2005. - Vol. 3. - P. 1669-1673. ↑
- C4398.** Zhihui Li. Application of spatial information technology for emergency response in traffic accident. / Zhihui Li, Jingfa Zhang, Lixia Gong. // 2005. IGARSS '05. Proceedings. 2005 IEEE International Geoscience and Remote Sensing Symposium. 25-29 July 2005. - Vol. 3. - P. 1580-1582. ↑
- C4399.** Hsing-Chung Chang. InSAR and mathematical modelling for measuring surface deformation due to geothermal water extraction in New Zealand. / Hsing-Chung Chang, Linlin Ge, Rizos C. // 2005. IGARSS '05. Proceedings. 2005 IEEE International Geoscience and Remote Sensing Symposium. 25-29 July 2005. - Vol. 3. - P. 1587-1589. ↑
- C4400.** Palmer J. Sea surface effects on phase coherence in emulated bistatic radar systems. / Palmer J., Martorella M., Capria A., Littleton B., Homer J., Berizzi F. // 2005. IGARSS '05. Proceedings. 2005 IEEE International Geoscience and Remote Sensing Symposium. 25-29 July 2005. - Vol. 3. - P. 1975-1978. ↑
- C4401.** Pepe A. A space-time minimum cost flow phase unwrapping algorithm for the generation of DInSAR deformation time-series. / Pepe A., Lanari R. // 2005. IGARSS '05. Proceedings. 2005 IEEE International Geoscience and Remote Sensing Symposium. 25-29 July 2005. - Vol. 3. - P. 1979-1982. ↑
- C4402.** Weiss M. Determination of baseline and orientation of platforms for airborne bistatic radars. 2005. IGARSS '05. Proceedings. 2005 IEEE International Geoscience and Remote Sensing Symposium. 25-29 July 2005. - Vol. 3. - P. 1967-1970. ↑
- C4403.** Yuanyao Lu. Comparison on mitigating techniques to enhance bistatic STAP. / Yuanyao Lu, Ping Zhang. // 2005. IGARSS '05. Proceedings. 2005 IEEE International Geoscience and Remote Sensing Symposium. 25-29 July 2005. - Vol. 3. - P. 1971-1974. ↑
- C4404.** Blanco P. Application of the coherent pixels technique to the generation of deformation maps with ERS and ENVISAT data. / Blanco P., Mallorqui J.J., Navarrete D., Duque S., Prats P., Romero R., Dominguez J., Carrasco D. // 2005. IGARSS '05. Proceedings. 2005 IEEE International Geoscience and Remote Sensing Symposium. 25-29 July 2005. - Vol. 3. - P. 1983-1986. ↑
- C4405.** Danklmayer A. Application of principal component analysis in radar polarimetry. 2005. IGARSS '05. Proceedings. 2005 IEEE International Geoscience and Remote Sensing Symposium. 25-29 July 2005. - Vol. 3. - P. 1999-2002. ↑
- C4406.** Cloude S.R. On the status of bistatic polarimetry theory. 2005. IGARSS '05. Proceedings. 2005 IEEE International Geoscience and Remote Sensing Symposium. 25-29 July 2005. - Vol. 3. - P. 2003-2006. ↑
- C4407.** De Zan F. Coherent processing of long series of SAR images. / De Zan F., Rocca F. // 2005. IGARSS '05. Proceedings. 2005 IEEE International Geoscience and Remote Sensing Symposium. 25-29 July 2005. - Vol. 3. - P. 1987-1990. ↑
- C4408.** Boerner W. On the statistical aspects of radar polarimetry. / Boerner W., Morisaki J., Danklmayer A., Chandra M. // 2005. IGARSS '05. Proceedings. 2005 IEEE International Geoscience and Remote Sensing Symposium. 25-29 July 2005. - Vol. 3. - P. 1995-1998. ↑
- C4409.** Lei Wentai. Optimization based underground cylindrical objects position and electromagnetic parameters joint reversion. / Lei Wentai, Huang Chunlin, Su Yi. // 2005. IGARSS '05. Proceedings. 2005 IEEE International Geoscience and Remote Sensing Symposium. 25-29 July 2005. - Vol. 3. - P. 1772-1776. ↑
- C4410.** Lopez L. Oil spill detection using GLCM and MRF. / Lopez L., Moctezuma M., Parmiggiani F. // 2005. IGARSS '05. Proceedings. 2005 IEEE International Geoscience and Remote Sensing Symposium. 25-29 July 2005. - Vol. 3. - P. 1781-1784. ↑

- C4411.** Peng Chen. Comparison of ship detection algorithms in spaceborne SAR imagery. / Peng Chen, Weigen Huang, Jingsong Yang, Bin Fu, Xiulin Lou, Aiqing Shi. // 2005. IGARSS '05. Proceedings. 2005 IEEE International Geoscience and Remote Sensing Symposium. 25-29 July 2005. - Vol. 3. - P. 1750-1752. ↑
- C4412.** Losekoot M. Operational use of ship detection to combat illegal fishing in the Southern Indian Ocean. / Losekoot M., Schwab P. // 2005. IGARSS '05. Proceedings. 2005 IEEE International Geoscience and Remote Sensing Symposium. 25-29 July 2005. - Vol. 3. - P. 1767-1771. ↑
- C4413.** Hallikainen M. Feasibility of satellite Ku-band scatterometer data for retrieval of seasonal snow characteristics in Finland. / Hallikainen M., Lahtinen P., Yuanzhi Zhang, Takala M., Pulliainen J. // 2005. IGARSS '05. Proceedings. 2005 IEEE International Geoscience and Remote Sensing Symposium. 25-29 July 2005. - Vol. 3. - P. 1936-1939. ↑
- C4414.** Gleason S. An attempt to sense ocean winds and waves empirically using bi-static GNSS reflections in low Earth orbit. / Gleason S., Adjrad M. // 2005. IGARSS '05. Proceedings. 2005 IEEE International Geoscience and Remote Sensing Symposium. 25-29 July 2005. - Vol. 3. - P. 1959-1962. ↑
- C4415.** Ortiz A.M. Comparison of doppler centroid estimators in bistatic airborne SAR. / Ortiz A.M., Loffeld O., Knedlik S., Nies H., Natroshvili K. // 2005. IGARSS '05. Proceedings. 2005 IEEE International Geoscience and Remote Sensing Symposium. 25-29 July 2005. - Vol. 3. - P. 1963-1966. ↑
- C4416.** Anttila S. From EO data to snow covered area (SCA) end products using automated processing system. / Anttila S., Metsamaki S., Pulliainen J., Luojus K. // 2005. IGARSS '05. Proceedings. 2005 IEEE International Geoscience and Remote Sensing Symposium. 25-29 July 2005. - Vol. 3. - P. 1947-1950. ↑
- C4417.** Malnes E. Multi-sensor monitoring of snow parameters in Nordic mountainous areas. / Malnes E., Storvold R., Lauknes I., Solbo S., Solberg R., Amlien J., Koren H. // 2005. IGARSS '05. Proceedings. 2005 IEEE International Geoscience and Remote Sensing Symposium. 25-29 July 2005. - Vol. 3. - P. 1951-1954. ↑
- C4418.** Tang Li-bo. High resolution SAR imaging of moving ships. / Tang Li-bo, Li Dao-jing, Hong Wen, Cao Fang. // 2005. IGARSS '05. Proceedings. 2005 IEEE International Geoscience and Remote Sensing Symposium. 25-29 July 2005. - Vol. 5. - P. 3329-3332. ↑
- C4419.** Zhang Xiaoling. The analysis of time synchronization error in bistatic SAR system. / Zhang Xiaoling, Li Hongbo, Wang Jianguo. // 2005. IGARSS '05. Proceedings. 2005 IEEE International Geoscience and Remote Sensing Symposium. 25-29 July 2005. - Vol. 7. - P. 4619-4622. ↑
- C4420.** Rui-Feng Xue. Tomographic inverse scattering approach for radar imaging with multistatic acquisition. / Rui-Feng Xue, Bin Yuan, Junfa Mao, Ye Liu. // 2005. IGARSS '05. Proceedings. 2005 IEEE International Geoscience and Remote Sensing Symposium. 25-29 July 2005. - Vol. 7. - P. 4623-4625. ↑
- C4421.** Li Wei. A new jamming method on parasitic spaceborne SAR system. / Li Wei, Liang Diannong, Dong Zhen. // 2005. IGARSS '05. Proceedings. 2005 IEEE International Geoscience and Remote Sensing Symposium. 25-29 July 2005. - Vol. 7. - P. 4611-4614. ↑
- C4422.** Zeng Bin. Study of along track interferometric technology for the bistatic SAR. / Zeng Bin, Zhang Xiaoling, Huang Shunji. // 2005. IGARSS '05. Proceedings. 2005 IEEE International Geoscience and Remote Sensing Symposium. 25-29 July 2005. - Vol. 7. - P. 4615-4618. ↑
- C4423.** Ginolhac G. Narrowband multistatic ISAR imagery system. / Ginolhac G., Daout F., Schmitt F. // 2005. IGARSS '05. Proceedings. 2005 IEEE International Geoscience and Remote Sensing Symposium. 25-29 July 2005. - Vol. 7. - P. 4626-4629. ↑
- C4424.** Vesecky J.F. Using multifrequency HF radar to estimate ocean wind fields. / Vesecky J.F., Drake J., Laws K., Ludwig F.L., Teague C.C., Paduan J.D., Meadows L. // 2005. IGARSS '05. Proceedings. 2005 IEEE International Geoscience and Remote Sensing Symposium. 25-29 July 2005. - Vol. 7. - P. 4769-4772. ↑
- C4425.** Gleason S. Sea monitoring for detecting dangerous seas and tsunamis using space based GNSS bi-static radar technology. // 2005. IGARSS '05. Proceedings. 2005 IEEE International Geoscience and Remote Sensing Symposium. 25-29 July 2005. - Vol. 7. - P. 4773-4776. ↑
- C4426.** Wang Liang. Control sidelobes in UWB SAR images. / Wang Liang, Huang Xiaotao, Zhou Zhimin, Sun

Xiaokun. // 2005. IGARSS '05. Proceedings. 2005 IEEE International Geoscience and Remote Sensing Symposium. 25-29 July 2005. - Vol. 7. - P. 4630-4632. ↑

C4427. Shi Jun. Multi-target ISAR imaging method. / Shi Jun, Zhang Xiaoling, Huang Shuwei. // 2005. IGARSS '05. Proceedings. 2005 IEEE International Geoscience and Remote Sensing Symposium. 25-29 July 2005. - Vol. 7. - P. 4745-4748. ↑

C4428. Hua Zhang. The optimum selection of common master image for series of differential SAR processing to estimate long and slow ground deformation. / Hua Zhang, Qiming Zeng, Yihua Liu, Xiaofan Li, Liang Gao. // 2005. IGARSS '05. Proceedings. 2005 IEEE International Geoscience and Remote Sensing Symposium. 25-29 July 2005. - Vol. 7. - P. 4586-4589. ↑

C4429. Huanyin Yue. Land subsidence monitoring in city area by time series interferometric SAR data. / Huanyin Yue, Hanssen R., van Leijen F., Marinkovic P., Ketelaar G. // 2005. IGARSS '05. Proceedings. 2005 IEEE International Geoscience and Remote Sensing Symposium. 25-29 July 2005. - Vol. 7. - P. 4590-4592. ↑

C4430. Elmzoughi A. A "Real-like" polarimetric weather radar data generation using physical and statistical models. / Elmzoughi A., Abdelfattah R., Belhadj Z., Santalla Del Rio V. // 2005. ICECS 2005. 12th IEEE International Conference on Electronics, Circuits and Systems. - Gammarth, 11-14 Dec. 2005. - P. 1-4. ↑

C4431. Jung Hahn Chul. Observing coal mining subsidence from JERS-1 permanent scatterer analysis. / Jung Hahn Chul, Kyung-Duck Min. // 2005. IGARSS '05. Proceedings. 2005 IEEE International Geoscience and Remote Sensing Symposium. 25-29 July 2005. - Vol. 7. - P. 4578-4581. ↑

C4432. Pei Huaining. A new estimation method for DEM error by miscoregistration. / Pei Huaining, Ma Debao, Zheng Fang. // 2005. IGARSS '05. Proceedings. 2005 IEEE International Geoscience and Remote Sensing Symposium. 25-29 July 2005. - Vol. 7. - P. 4593-4595. ↑

C4433. Dehmollaian M. Polarization discrimination for improving foliage-camouflaged target detection. / Dehmollaian M., Sarabandi K. // 2005. IGARSS '05. Proceedings. 2005 IEEE International Geoscience and Remote Sensing Symposium. 25-29 July 2005. - Vol. 7. - P. 4604-4606. ↑

C4434. Li Wei. A new anti-jamming method for parasitic spaceborne SAR system. / Li Wei, Liang Diannong, Dong Zhen. // 2005. IGARSS '05. Proceedings. 2005 IEEE International Geoscience and Remote Sensing Symposium. 25-29 July 2005. - Vol. 7. - P. 4607-4610. ↑

C4435. Sang-Wook Kim. Comparison of FMCW and pulse type groundpenetrating radar(GPR) for water leakage detection. / Sang-Wook Kim, Se-Yun Kim. // 2005. IGARSS '05. Proceedings. 2005 IEEE International Geoscience and Remote Sensing Symposium. 25-29 July 2005. - Vol. 7. - P. 4596-4599. ↑

C4436. Komarov S.A. GPR signal simulations in the course of freeze/thaw process for a permafrost area. / Komarov S.A., Mironov V.L., Muzalevsky K.V. // 2005. IGARSS '05. Proceedings. 2005 IEEE International Geoscience and Remote Sensing Symposium. 25-29 July 2005. - Vol. 7. - P. 4600-4603. ↑

C4437. Liu Mingjun. DEM generation from radarsat stereo images in high relief areas. / Liu Mingjun, Zhang Jixian, Lin Zongjian, Yan Qin, Gao Wujun. // 2005. IGARSS '05. Proceedings. 2005 IEEE International Geoscience and Remote Sensing Symposium. 25-29 July 2005. - Vol. 7. - P. 4708-4711. ↑

C4438. Lei Pang. 3D positioning assessment for stereo configuration conditions of airborne SAR images in mountainous area. / Lei Pang, Li Zhang, Jixian Zhang, Guoman Huang, Mingbo Zhang, Jiankun Guo. // 2005. IGARSS '05. Proceedings. 2005 IEEE International Geoscience and Remote Sensing Symposium. 25-29 July 2005. - Vol. 7. - P. 4715-4717. ↑

C4439. Wei Jie. Refined extended chirp scaling algorithm for spaceborne ScanSAR imaging. / Wei Jie, Zhou Yinqing, Li Chunsheng. // 2005. IGARSS '05. Proceedings. 2005 IEEE International Geoscience and Remote Sensing Symposium. 25-29 July 2005. - Vol. 7. - P. 4677-4680. ↑

C4440. Xiaorong Xue. A new method of SAR image segmentation. / Xiaorong Xue, Qiming Zeng. // 2005. IGARSS '05. Proceedings. 2005 IEEE International Geoscience and Remote Sensing Symposium. 25-29 July 2005. - Vol. 7. - P. 4701-4703. ↑

C4441. Xiaorong Xue. A new method of SAR image target recognition based on SVM. / Xiaorong Xue, Qiming

Zeng, Rongchun Zhao. // 2005. IGARSS '05. Proceedings. 2005 IEEE International Geoscience and Remote Sensing Symposium. 25-29 July 2005. - Vol. 7. - P. 4718-4721. ↑

C4442. Zhang Bo. Segmentation and aspect estimation in SAR image of target chip. / Zhang Bo, Zhang Hong, Wang Chao. // 2005. IGARSS '05. Proceedings. 2005 IEEE International Geoscience and Remote Sensing Symposium. 25-29 July 2005. - Vol. 7. - P. 4737-4740. ↑

C4443. Kwang-Yong Kim. Implementation of the SAR data processing module based on component. / Kwang-Yong Kim, Kyung-Ok Kim. // 2005. IGARSS '05. Proceedings. 2005 IEEE International Geoscience and Remote Sensing Symposium. 25-29 July 2005. - Vol. 7. - P. 4741-4744. ↑

C4444. Zhaoying Han. Ship detection in SAR images using multi-polarimetric information. / Zhaoying Han, Jinsong Chong, Minhui Zhu. // 2005. IGARSS '05. Proceedings. 2005 IEEE International Geoscience and Remote Sensing Symposium. 25-29 July 2005. - Vol. 7. - P. 4729-4732. ↑

C4445. Xie Mei-hua. Nonlinear diffusion equation for speckle reducing and resolution enhancement. / Xie Mei-hua, Wang Zheng-ming. // 2005. IGARSS '05. Proceedings. 2005 IEEE International Geoscience and Remote Sensing Symposium. 25-29 July 2005. - Vol. 7. - P. 4733-4736. ↑

C4446. Zou Kun. Inversion of the low frequency UWB SAR. / Zou Kun, Liang Diannong. // 2005. IGARSS '05. Proceedings. 2005 IEEE International Geoscience and Remote Sensing Symposium. 25-29 July 2005. - Vol. 7. - P. 4637-4640. ↑

C4447. Xin Zhang. A real time autofocus algorithm for high resolution airborne SAR. / Xin Zhang, Xing-dong Liang, Chi-biao Ding, Yi-rong Wu. // 2005. IGARSS '05. Proceedings. 2005 IEEE International Geoscience and Remote Sensing Symposium. 25-29 July 2005. - Vol. 7. - P. 4641-4643. ↑

C4448. Dankert H. Wind measurements at FINO-I using marine radar-image sequences. / Dankert H., Horstmann J. // 2005. IGARSS '05. Proceedings. 2005 IEEE International Geoscience and Remote Sensing Symposium. 25-29 July 2005. - Vol. 7. - P. 4777-4780. ↑

C4449. Tian Jin. Man-made targets pose estimation using time-frequency distribution in UWB SAR. / Tian Jin, Zhimin Zhou, Wenge Chang, Xiaotao Huang. // 2005. IGARSS '05. Proceedings. 2005 IEEE International Geoscience and Remote Sensing Symposium. 25-29 July 2005. - Vol. 7. - P. 4633-4635. ↑

C4450. Yong Li. Automatic mosaicing for airborne SAR imaging based on subaperture processing. / Yong Li, Daiyin Zhu, Zhaoda Zhu, Ling Wang. // 2005. IGARSS '05. Proceedings. 2005 IEEE International Geoscience and Remote Sensing Symposium. 25-29 July 2005. - Vol. 7. - P. 4644-4647. ↑

C4451. Ling Wang. Range alignment for ISAR using genetic algorithms. / Ling Wang, Daiyin Zhu, Zhaoda Zhu. // 2005. IGARSS '05. Proceedings. 2005 IEEE International Geoscience and Remote Sensing Symposium. 25-29 July 2005. - Vol. 7. - P. 4666-4669. ↑

C4452. Wu Tao. Study on SAR image simulation based on SRTM DEM and landcover data. / Wu Tao, Wang Chao, Zhang Hong. // 2005. IGARSS '05. Proceedings. 2005 IEEE International Geoscience and Remote Sensing Symposium. 25-29 July 2005. - Vol. 7. - P. 4670-4672. ↑

C4453. Tang Yixian. General radar analysis and computation environment. / Tang Yixian, Wang Chao, Zhang Hong. // 2005. IGARSS '05. Proceedings. 2005 IEEE International Geoscience and Remote Sensing Symposium. 25-29 July 2005. - Vol. 7. - P. 4651-4654. ↑

C4454. Merryman Boncori J.P. Implementation of a co/decoding method in SAR processing based on time domain correlation: experimental validation. / Merryman Boncori J.P., Schwerdt M., Hounam D., Schiavon G. // 2005. IGARSS '05. Proceedings. 2005 IEEE International Geoscience and Remote Sensing Symposium. 25-29 July 2005. - Vol. 7. - P. 4655-4658. ↑

C4455. Okamoto K.i. The global satellite mapping of precipitation (GSMaP) project. / Okamoto K.i., Ushio T., Iguchi T., Takahashi N., Iwanami K. // 2005. IGARSS '05. Proceedings. 2005 IEEE International Geoscience and Remote Sensing Symposium. 25-29 July 2005. - Vol. 5. - P. 3414-3416. ↑

C4456. Shu Weiping. Computer simulation of wind measurements by increment's cumulant approach. / Shu Weiping, Zhao Zhengyu. // 2005. IGARSS '05. Proceedings. 2005 IEEE International Geoscience and Remote Sensing Symposium. 25-29 July 2005. - Vol. 7. - P. 4659-4662. ↑

Sensing Symposium. 25-29 July 2005. - Vol. 5. - P. 3417-3420. ↑

C4457. Zafar B. A methodology to study bright band structure on a global scale from TRMM precipitation radar. / Zafar B., Chandrasekar V. // 2005. IGARSS '05. Proceedings. 2005 IEEE International Geoscience and Remote Sensing Symposium. 25-29 July 2005. - Vol. 5. - P. 3400-3403. ↑

C4458. Takahashi N. Introduction of a melting layer model to a rain retrieval algorithm for microwave radiometers. / Takahashi N., Awaka J. // 2005. IGARSS '05. Proceedings. 2005 IEEE International Geoscience and Remote Sensing Symposium. 25-29 July 2005. - Vol. 5. - P. 3404-3409. ↑

C4459. Aguttes J.P. Low altitude flying for high resolution imaging satellite: comparison of low circular and elliptical orbits. / Aguttes J.P., Fernandez N., Foliard J. // 2005. IGARSS '05. Proceedings. 2005 IEEE International Geoscience and Remote Sensing Symposium. 25-29 July 2005. - Vol. 5. - P. 3421-3423. ↑

C4460. Jin K.-W. Improved physically-based AMSR-E oceanic rainfall algorithm. / Jin K.-W., Hong S.-W., Weitz R., Wilheit T. // 2005. IGARSS '05. Proceedings. 2005 IEEE International Geoscience and Remote Sensing Symposium. 25-29 July 2005. - Vol. 5. - P. 3462-3465. ↑

C4461. Yoong-Goog Cho. Signal processing architecture for a single radar node in a networked radar environment (NETRAD). / Yoong-Goog Cho, Bharadwaj N., Chandrasekar V., Zink M., Junyent F., Insanic E., McLaughlin D.J. // 2005. IGARSS '05. Proceedings. 2005 IEEE International Geoscience and Remote Sensing Symposium. 25-29 July 2005. - Vol. 5. - P. 3477-3480. ↑

C4462. Wilson J.J.W. Radiometric calibration of the advanced wind scatterometers carried on-board the METOP satellites. / Wilson J.J.W., Phillips P.L., Saldana J.F., Dumper K., Fiksel T. // 2005. IGARSS '05. Proceedings. 2005 IEEE International Geoscience and Remote Sensing Symposium. 25-29 July 2005. - Vol. 5. - P. 3436-3440. ↑

C4463. Rastogi M. Seawinds radiometer (SRad) on ADEOS-II brightness temperature calibration/validation. / Rastogi M., Jones W.L., Park J.D., Adams I. // 2005. IGARSS '05. Proceedings. 2005 IEEE International Geoscience and Remote Sensing Symposium. 25-29 July 2005. - Vol. 5. - P. 3441-3444. ↑

C4464. Liang Liao. Spaceborne dual-wavelength radar techniques for retrieval of hydrometeor profiles. / Liang Liao, Meneghini R. // 2005. IGARSS '05. Proceedings. 2005 IEEE International Geoscience and Remote Sensing Symposium. 25-29 July 2005. - Vol. 5. - P. 3396-3399. ↑

C4465. Blom M. VHF SAR image formation implemented on a GPU. / Blom M., Follo P. // 2005. IGARSS '05. Proceedings. 2005 IEEE International Geoscience and Remote Sensing Symposium. 25-29 July 2005. - Vol. 5. - P. 3352-3356. ↑

C4466. Cloude S.R. A framework for investigating space-borne polarimetric interferometry using the ALOS-PALSAR sensor. / Cloude S.R., Krieger G., Papathanassiou K.P. // 2005. IGARSS '05. Proceedings. 2005 IEEE International Geoscience and Remote Sensing Symposium. 25-29 July 2005. - Vol. 5. - P. 3361-3364. ↑

C4467. Hu Donghui. Correction method for saturated SAR data to improve radiometric accuracy. / Hu Donghui, Zhou Huanxue, Hong Wen. // 2005. IGARSS '05. Proceedings. 2005 IEEE International Geoscience and Remote Sensing Symposium. 25-29 July 2005. - Vol. 5. - P. 3344-3347. ↑

C4468. Shu Li. Improved beat frequency estimation in the MLBF Doppler ambiguity resolver. / Shu Li, Cumming I. // 2005. IGARSS '05. Proceedings. 2005 IEEE International Geoscience and Remote Sensing Symposium. 25-29 July 2005. - Vol. 5. - P. 3348-3351. ↑

C4469. Kimura H. Calibration of ALOS/PALSAR polarimetric data affected by faraday rotation. 2005. IGARSS '05. Proceedings. 2005 IEEE International Geoscience and Remote Sensing Symposium. 25-29 July 2005. - Vol. 5. - P. 3369-3372. ↑

C4470. Rose C.R. A GPM dual frequency DSD retrieval method based on linear model for DSD vertical profile. / Rose C.R., Chandrasekar V. // 2005. IGARSS '05. Proceedings. 2005 IEEE International Geoscience and Remote Sensing Symposium. 25-29 July 2005. - Vol. 5. - P. 3388-3391. ↑

C4471. Adhikari N.B. An assessment on the performance of GPM dual-frequency precipitation radar rain profiling methods through numerical simulation. / Adhikari N.B., Seto S., Iguchi T., Takahashi N., Satoh S.,

Hanado H. // 2005. IGARSS '05. Proceedings. 2005 IEEE International Geoscience and Remote Sensing Symposium. 25-29 July 2005. - Vol. 5. - P. 3392-3395. ↑

C4472. Isoguchi O. Research plans for developing a L-band wind retrieval model function by using ALOS/PALSAR. / Isoguchi O., Kawamura H., Shimada T. // 2005. IGARSS '05. Proceedings. 2005 IEEE International Geoscience and Remote Sensing Symposium. 25-29 July 2005. - Vol. 5. - P. 3373-3375. ↑

C4473. Iguchi T. Uncertainties in the rain retrieval algorithm for the GPM dual-frequency precipitation radar. / Iguchi T., Seto S., Takahashi N., Hanado H. // 2005. IGARSS '05. Proceedings. 2005 IEEE International Geoscience and Remote Sensing Symposium. 25-29 July 2005. - Vol. 5. - P. 3384-3387. ↑

C4474. Qulin Tan. Lake shoreline detection and tracing in SAR images using wavelet transform and ACM method. / Qulin Tan, Zhengjun Liu, Zhou Fu, Jiping Hu. // 2005. IGARSS '05. Proceedings. 2005 IEEE International Geoscience and Remote Sensing Symposium. 25-29 July 2005. - Vol. 5. - P. 3703-3706. ↑

C4475. Zhang Yanjie. A new interferogram generation method. 2005. IGARSS '05. Proceedings. 2005 IEEE International Geoscience and Remote Sensing Symposium. 25-29 July 2005. - Vol. 7. - P. 4557-4559. ↑

C4476. Han Chunming. Detection of the flood boundary in SAR image using texture. / Han Chunming, Guo Huadong, Shao Yun, Liao Jingjuan. // 2005. IGARSS '05. Proceedings. 2005 IEEE International Geoscience and Remote Sensing Symposium. 25-29 July 2005. - Vol. 5. - P. 3697-3699. ↑

C4477. Ulander L.M.H. Mapping of wind-thrown forests in Southern Sweden using space- and airborne SAR. / Ulander L.M.H., Smith G., Eriksson L., Folkesson K., Fransson J.E.S., Gustavsson A., Hallberg B., Joyce S., Magnusson M., Olsson H., Persson A., Walter F. // 2005. IGARSS '05. Proceedings. 2005 IEEE International Geoscience and Remote Sensing Symposium. 25-29 July 2005. - Vol. 5. - P. 3619-3622. ↑

C4478. Lv X. Monitoring flood using multi-temporal ENVISAT ASAR data. / Lv X., Ronggao Liu, Jiyuan Liu, Xianfang Song. // 2005. IGARSS '05. Proceedings. 2005 IEEE International Geoscience and Remote Sensing Symposium. 25-29 July 2005. - Vol. 5. - P. 3627-3629. ↑

C4479. Chih-Tien Wang. Deformation field over Western Taiwan Island using satellite InSAR. / Chih-Tien Wang, Kun-Shan Chen, Jiun-Yee Yen, Chung-Pai Chang. // 2005. IGARSS '05. Proceedings. 2005 IEEE International Geoscience and Remote Sensing Symposium. 25-29 July 2005. - Vol. 7. - P. 4570-4573. ↑

C4480. You Hongjian. Geo-referencing airborne interferometric SAR data. / You Hongjian, Xiang Maosheng, Ding Chibiao. // 2005. IGARSS '05. Proceedings. 2005 IEEE International Geoscience and Remote Sensing Symposium. 25-29 July 2005. - Vol. 7. - P. 4574-4577. ↑

C4481. Jingfa Zhang. Application of scatter-cluster InSAR in China country. / Jingfa Zhang, Lixia Gong. // 2005. IGARSS '05. Proceedings. 2005 IEEE International Geoscience and Remote Sensing Symposium. 25-29 July 2005. - Vol. 7. - P. 4567-4569. ↑


C4482. Bin Zou. An accurate co-registration method of spaceborne repeat-pass InSAR based on matrix transformation. / Bin Zou, Lin Hao, Xing Bao. // 2005. IGARSS '05. Proceedings. 2005 IEEE International Geoscience and Remote Sensing Symposium. 25-29 July 2005. - Vol. 7. - P. 4560-4563. ↑


C4483. Zhang Yanjie. An interferogram filtering method using wavelet transform. 2005. IGARSS '05. Proceedings. 2005 IEEE International Geoscience and Remote Sensing Symposium. 25-29 July 2005. - Vol. 7. - P. 4564-4566. ↑


C4484. Abdelfattah R. Analysis of the unbiased complex coherence estimation using varying ERS interferometric data. / Abdelfattah R., Nicolas J.-M. // 2005. IGARSS '05. Proceedings. 2005 IEEE International Geoscience and Remote Sensing Symposium. 25-29 July 2005. - Vol. 5. - P. 3522-3525. ↑


C4485. Inglada J. Fine registration of SPOT5 and Envisat/ASAR images and ortho-image production: a fully automatic approach. / Inglada J., Vadon H. // 2005. IGARSS '05. Proceedings. 2005 IEEE International Geoscience and Remote Sensing Symposium. 25-29 July 2005. - Vol. 5. - P. 3510-3512. ↑

C4486. Galland F. Registering of synthetic aperture radar and optical data. / Galland F., Tupin F., Nicolas J.-M., Roux M. // 2005. IGARSS '05. Proceedings. 2005 IEEE International Geoscience and Remote Sensing Symposium. 25-29 July 2005. - Vol. 5. - P. 3513-3516. ↑

C4487. Velloso M.L.F. Image fusion using fuzzy-nonparametric interpolation approach. / Velloso M.L.F., de Souza F.J. // 2005. IGARSS '05. Proceedings. 2005 IEEE International Geoscience and Remote Sensing Symposium. 25-29 July 2005. - Vol. 5. - P. 3530-3533. 

C4488. Eriksson L.E.B. Stem volume retrieval with spaceborne L-band repeat-pass coherence: multi-temporal combination for boreal forest. / Eriksson L.E.B., Askne J., Santoro M., Schmullius C., Wiesmann A. // 2005. IGARSS '05. Proceedings. 2005 IEEE International Geoscience and Remote Sensing Symposium. 25-29 July 2005. - Vol. 5. - P. 3591-3594. 

C4489. Heezin Lee. Detecting forest trails occluded by dense canopies using ALSM data. / Heezin Lee, Slatton K.C., Hojin Jhee. // 2005. IGARSS '05. Proceedings. 2005 IEEE International Geoscience and Remote Sensing Symposium. 25-29 July 2005. - Vol. 5. - P. 3587-3590. 

C4490. Barbot S. Phase unwrapping for DEM generation as an inverse problem. / Barbot S., Rudant J.-P., Briole P., Fruneau B. // 2005. IGARSS '05. Proceedings. 2005 IEEE International Geoscience and Remote Sensing Symposium. 25-29 July 2005. - Vol. 5. - P. 3538-3541. 

© В.И. Карнышев, 2011

Тематический реферативный сборник сгенерирован в автоматическом режиме
с использованием специализированного программного модуля (ПМО ТУСУР)